DETAILED CHEMICAL KINETIC MODELLING OF PROPULSION FUELS

by

Mark Lee Potter
BSc. (Hons.)

Thesis submitted for the degree of
Doctor of Philosophy
of the University of London
and for the Diploma of Membership of The Imperial College

Department of Mechanical Engineering,
Imperial College,
University of London

September 2003

BARL.
LONDON.
UNIV.

Abstract

Propulsion fuels such as kerosene and diesel feature complex mixtures of hydrocarbon compounds including alkane and aromatic molecules. The present study features the development of a detailed chemical kinetic model that can simulate the oxidation of both the individual components and the fuel blends found in typical samples of kerosene and diesel fuels.

The combustion of methyl – substituted aromatic components is investigated under Jet Stirred and Turbulent Flow Reactor conditions. The resulting toluene mechanism provides the basis for sub – mechanisms for m – xylene and 1 – methylnaphthalene.

The oxidation of other aromatics, phenylacetylene, naphthalene and n – propylbenzene are also investigated. The formation of PAH at intermediate temperatures is also explored under Turbulent Flow Reactor conditions.

The oxidation of kerosene is modelled on n – decane representing the alkane component, with the aromatic component being modelled on n – propylbenzene.

The result is a hierarchically constructed kinetic model that includes alkanes, alkenes, benzene, simple substituted aromatics (*e.g.* toluene, ethylbenzene, propylbenzene and phenylacetylene) and simple polycyclic aromatics (1 – methylnaphthalene, naphthalene and indene) molecules. The calculations performed with the detailed kinetic model are compared against experimental data for mechanism validation.

Acknowledgements

First and foremost, I would like to express my sincere debt and gratitude to my supervisor, Prof. R.P. Lindstedt. Without the aid of his phenomenal knowledge and understanding of combustion modelling, it would have been absolutely impossible to have completed this work. Moreover, his unique approach to the subject and endless encouragement and support has proved invaluable to me throughout my postgraduate studies. I would also like to thank him for aiding me with the arrangement of uninterrupted financial support from the Engineering and Physical Sciences Research Council, Nissan Motor Company (Japan) LTD, BP Chemicals LTD and Alstom Power LTD.

Furthermore, I would like to thank profusely Dr. M.P. Meyer, who acted as my second supervisor providing me with endless ideas, encouragement and above all, being a good friend. A special thanks also goes to my work partner Mr. K.-A. Rizos who has given me many enjoyable experiences of "meeting the deadline". Many thanks also go to my fellow work colleagues Drs. A. Kempf, S.A. Louloudi and N.A. Malik and Messrs F. Cerru, A. Jagtiani, T. S. Kuan, D. Luff and H. -C. Ozarovsky with whom I have had many pleasurable and intellectual discussions and helped keeping the mind focused on the goal in hand.

A special thanks goes to Profs. B.L. Davies and A.J. Kinloch for emotional and moral support and to Mrs. N. Jensen who helped manage my library account and being a supportive friend.

Last but not least, I wish to thank my parents who have given me their love and support throughout my postgraduate studies and beyond. My hope is that I stood up to their expectations.

Contents

Abstract i

Acknowledgements iii

Contents v

List of Figures ix

List of Tables xlvii

Nomenclature li

1 Introduction 1

1.1 Overview 1

1.2 The Constituents of Propulsive Fuels 2

1.3 Environmental Impact of Combustion 6

1.3.1 PAH and Soot Formation 7

1.4 Modelling of Combustion 9

1.4.1 Chemical Model 10
1.4.2 Mathematical Model 21
1.5 The Present Contribution 25
1.6 Outline of Thesis 26

2 Toluene and m – Xylene **29**

2.1 Introduction 29
2.2 A Detailed Mechanism for Toluene Combustion 29
2.2.1 The Pyrolysis of Toluene 30
2.2.2 The Oxidation of Toluene 37
2.2.3 Toluene Ignition Delay Times 64
2.2.4 The Oxidation of Toluene in a Turbulent Flow Reactor 68
2.3 The Oxidation of m – xylene 74
2.3.1 The Oxidation of m – xylene in a Turbulent Flow Reactor 74
2.4 Summary 85

3 Phenylacetylene and n – Propylbenzene **87**

3.1 Introduction 87
3.2 The Combustion of Phenylacetylene 88
3.2.1 Primary Reaction Paths for Phenylacetylene Oxidation 101
3.2.2 The Formation of Indene 106
3.2.3 The Formation of Naphthalene 109

3.2.4 The Formation of Phenanthrene and Anthracene 111

3.3 The Oxidation of n – Propylbenzene 113

3.3.1 The Oxidation of n – Propylbenzene at Low Pressure . 114

3.3.2 The Oxidation of n – Propylbenzene at High Pressure . 130

3.4 Summary 156

4 Naphthalene and 1 – Methylnaphthalene **159**

4.1 Introduction 159

4.2 The Oxidation of Naphthalene 160

4.2.1 The Oxidation of Naphthalene in a Turbulent Flow Reactor 160

4.3 The Oxidation of 1 – Methylnaphthalene 178

4.3.1 The Oxidation of 1 – methylnaphthalene 179

4.3.2 The Oxidation of 1 – methylnaphthalene in a Shock Tube 238

4.3.3 Discussion 241

4.4 The Formation of Acenaphthalene 242

4.5 Summary 246

5 The Oxidation of Kerosene Fuels **249**

5.1 Introduction 249

5.2 Background 249

5.3 The Oxidation of n – decane and n – propylbenzene 251

5.3.1 Test Case Details 251

5.3.2 Primary Reaction Paths for the Oxidation of the Paraffin Fuel Component under Jet Stirred Reactor conditions 272

5.4 Summary 284

6 Conclusions and Future Work **287**

6.1 Contributions of the Present Work 287

6.1.1 Toluene and m – Xylene 288

6.1.2 Phenylacetylene and n – Propylbenzene 288

6.1.3 Naphthalene and 1 – Methylnaphthalene 289

6.1.4 The Oxidation of Kerosene Fuels 291

6.2 Recommendations and Suggestions for Future Work 291

References **295**

A Reaction Mechanism **331**

B Thermodynamic Data **367**

C Species Structure **390**

List of Figures

1.1 Chemical composition of typical propulsion fuels [165]. 4

1.2 Typical classes of hydrocarbons found in propulsion fuels. . . . 5

1.3 Paraffin and aromatic constituents of typical propulsion fuels [182]. 6

1.4 Schematic diagram for soot formation in premixed flames [21]. 8

1.5 Possible addition sequences for PAH and soot formation [214]. 9

1.6 Hierarchial construction of a detailed chemical mechansim for propulsion fuels [182]. 11

1.7 Detailed chemical mechanism validation and verification procedure [182]. 22

2.1 Graph of H radical profile concentrations versus time for the pyrolysis of toluene in a Shock Tube. Experimental points are from Braun–Unkhoff *et al.* [26]. Lines are the computations from the detailed chemical mechanism. 33

2.2 Graph of intermediate species concentration profiles versus time for the pyrolysis of toluene in a Shock Tube. Experimental points are from Pamidimukkala *et al.* [199]. Lines are the computations from the detailed chemical mechanism. . . . 34

2.3 Graph of species profile concentrations versus temperature for the oxidation of toluene in a Jet Stirred Reactor. Experimental points are from Dagaut *et al.* [56] for a stoichiometry of ϕ = 0.5. Solid lines are the computations from the detailed chemical mechanism. 43

2.4 Graph of species profile concentrations versus temperature for the oxidation of toluene in a Jet Stirred Reactor. Experimental points are from Dagaut *et al.* [56] for a stoichiometry of ϕ = 0.5. Solid lines are the computations from the detailed chemical mechanism. 44

2.5 Graph of species profile concentrations versus temperature for the oxidation of toluene in a Jet Stirred Reactor. Experimental points are from Dagaut *et al.* [56] for a stoichiometry of ϕ = 0.5. Solid lines are the computations from the detailed chemical mechanism. 45

2.6 Graph of species profile concentrations versus temperature for the oxidation of toluene in a Jet Stirred Reactor. Experimental points are from Dagaut *et al.* [56] for a stoichiometry of ϕ = 0.5. Solid lines are the computations from the detailed chemical mechanism. 46

2.7 Graph of species profile concentrations versus temperature for the oxidation of toluene in a Jet Stirred Reactor. Experimental points are from Dagaut *et al.* [56] for a stoichiometry of ϕ = 0.5. Solid lines are the computations from the detailed chemical mechanism. 47

2.8 Graph of species profile concentrations versus temperature for the oxidation of toluene in a Jet Stirred Reactor. Experimental points are from Dagaut *et al.* [56] for a stoichiometry of ϕ = 1.5. Solid lines are the computations from the detailed chemical mechanism. 48

2.9 Graph of species profile concentrations versus temperature for the oxidation of toluene in a Jet Stirred Reactor. Experimental points are from Dagaut *et al.* [56] for a stoichiometry of ϕ = 1.5. Solid lines are the computations from the detailed chemical mechanism. 49

2.10 Graph of species profile concentrations versus temperature for the oxidation of toluene in a Jet Stirred Reactor. Experimental points are from Dagaut *et al.* [56] for a stoichiometry of ϕ = 1.5. Solid lines are the computations from the detailed chemical mechanism. 50

2.11 Graph of species profile concentrations versus temperature for the oxidation of toluene in a Jet Stirred Reactor. Experimental points are from Dagaut *et al.* [56] for a stoichiometry of ϕ = 1.5. Solid lines are the computations from the detailed chemical mechanism. 51

2.12 Graph of species profile concentrations versus temperature for the oxidation of toluene in a Jet Stirred Reactor. Experimental points are from Dagaut *et al.* [56] for a stoichiometry of ϕ = 1.5. Solid lines are the computations from the detailed chemical mechanism. 52

2.13 Diagram illustrating the consumption paths of the fuel toluene and it intermediate species in a Jet Stirred Reactor (T = 1180 K, P = 1 atm., ϕ = 1.5). Species in boxes are considered in subsequent pages. 60

2.14 Diagram illustrating the consumption paths of the fuel toluene and it intermediate species in a Jet Stirred Reactor (T = 1180 K, P = 1 atm., $\phi = 1.5$). Species in boxes are considered in subsequent pages. 61

2.15 Diagram illustrating the consumption paths of the fuel toluene and it intermediate species in a Jet Stirred Reactor (T = 1180 K, P = 1 atm., $\phi = 1.5$). Species in boxes are considered in subsequent pages. 62

2.16 Comparison of computed (lines) and measured (symbols) ignition delay times for lean ($\phi = 0.33$) toluene – oxygen – argon mixtures. Experimental points are from Burcat *et al.* [34]. . . 66

2.17 Comparison of computed (lines) and measured (symbols) ignition delay times for stoichiometric ($\phi = 1.0$) toluene – oxygen – argon mixtures. Experimental points are from Burcat *et al.* [34]. 67

2.18 Graph of species profile concentrations versus time for the oxidation of toluene in a Turbulent Flow Reactor. Experimental points are from Klotz *et al.* [148] for a stoichiometry of $\phi = 0.76$. Lines are the computations from the detailed chemical mechanism where the solid line represents $T_0 = 1173$ K and the dashed line represents $T_0 = 1200$ K. Both computations have been time shifted by 20 ms. 70

2.19 Graph of species profile concentrations versus time for the oxidation of toluene in a Turbulent Flow Reactor. Experimental points are from Klotz *et al.* [148] for a stoichiometry of $\phi = 0.76$. Lines are the computations from the detailed chemical mechanism where the solid line represents $T_0 = 1173$ K and the dashed line represents $T_0 = 1200$ K. Both computations have been time shifted by 20 ms. 71

2.20 Graph of temperature profile versus time for the oxidation of toluene in a Turbulent Flow Reactor. Lines are the computations from the detailed chemical mechanism and have been time shifted by 20 ms, where the solid line represents the initial conditions given by Klotz *et al.* [148] and the dashed line represents $T_0 = 1200$ K. 73

2.21 Graph of species profile concentrations versus time for the oxidation of m – xylene in a Turbulent Flow Reactor. Experimental points are from Emdee *et al.* [88] for a stoichiometry of $\phi = 1.0$. Solid lines are the computations from the detailed chemical mechanism and have been time shifted by 20 ms. . . 77

2.22 Graph of species profile concentrations versus time for the oxidation of m – xylene in a Turbulent Flow Reactor. Experimental points are from Emdee *et al.* [88] for a stoichiometry of $\phi = 1.0$. Solid lines are the computations from the detailed chemical mechanism and have been time shifted by 20 ms. . . 78

2.23 Graph of species profile concentrations versus time for the oxidation of m – xylene in a Turbulent Flow Reactor. Experimental points are from Emdee *et al.* [88] for a stoichiometry of $\phi = 1.0$. Solid lines are the computations from the detailed chemical mechanism and have been time shifted by 20 ms. . . 79

2.24 Diagram illustrating the consumption paths of the fuel m – xylene and its intermediate species in a Turbulent Flow Reactor at a reaction time of 50 ms. Species in boxes are considered in subsequent pages. 83

2.25 Diagram illustrating the consumption paths of the fuel m – xylene and its intermediate species in a Turbulent Flow Reactor at a reaction time of 50 ms. Species in boxes are considered in subsequent pages. 84

3.1 Graph of species profile concentrations versus time for the oxidation of phenylacetylene in a Turbulent Flow Reactor. Experimental points are from Shaddix [226]. Solid lines are the computations from the detailed chemical mechanism and have not been time shifted. 93

3.2 Graph of species profile concentrations versus time for the oxidation of phenylacetylene in a Turbulent Flow Reactor. Experimental points are from Shaddix [226]. Solid lines are the computations from the detailed chemical mechanism and have not been time shifted. 94

3.3 Graph of species profile concentrations versus time for the oxidation of phenylacetylene in a Turbulent Flow Reactor. Experimental points are from Shaddix [226]. Solid lines are the computations from the detailed chemical mechanism and have not been time shifted. 95

3.4 Graph of species profile concentrations versus time for the oxidation of phenylacetylene in a Turbulent Flow Reactor. Experimental points are from Shaddix [226]. Solid lines are the computations from the detailed chemical mechanism and have not been time shifted. 96

3.5 Graph of naphthalene species profile concentrations versus time for the oxidation of phenylacetylene in a Turbulent Flow Reactor. Experimental points are from Shaddix [226]. Solid lines are the computations from the detailed chemical mechanism and have not been time shifted. 97

3.6 Graph of phenanthrene species profile concentrations versus time for the oxidation of phenylacetylene in a Turbulent Flow Reactor. Experimental points are from Shaddix [226]. Solid lines are the computations from the detailed chemical mechanism and have not been time shifted. 98

3.7 Graph of anthracene species profile concentrations versus time for the oxidation of phenylacetylene in a Turbulent Flow Reactor. Experimental points are from Shaddix [226]. Solid lines are the computations from the detailed chemical mechanism and have not been time shifted. 99

3.8 Graph of temperature profile versus time for the oxidation of phenylacetylene in a Turbulent Flow Reactor. Experimental points are from Shaddix [226]. Solid lines are the computations from the detailed chemical mechanism and have not been time shifted. 100

3.9 Diagram illustrating the consumption paths of the fuel phenylacetylene and its intermediate species in a Turbulent Flow Reactor at a reaction time of 50 ms. Species in boxes are considered in subsequent pages. 104

3.10 Diagram illustrating the consumption paths of the fuel phenylacetylene and its intermediate species in a Turbulent Flow Reactor at a reaction time of 50 ms. Species in boxes are considered in subsequent pages. 105

3.11 Diagram illustrating the indene formation sequence for the oxidation of phenylacetylene in a Turbulent Flow Reactor. Species in boxes are considered in subsequent pages. 107

3.12 Diagram illustrating the indene formation sequence for the oxidation of phenylacetylene in a Turbulent Flow Reactor. Species in boxes are considered in subsequent pages. 108

3.13 Diagram illustrating the naphthalene formation sequence for the oxidation of phenylacetylene in a Turbulent Flow Reactor. 110

3.14 Diagram illustrating the phenanthrene formation sequence for the oxidation of phenylacetylene in a Turbulent Flow Reactor. 112

3.15 Diagram illustrating the anthracene formation sequence for the oxidation of phenylacetylene in a Turbulent Flow Reactor. 112

3.16 Graph of species profile concentrations versus time for the oxidation of n – propylbenzene in a Jet Stirred Reactor for a stoichiometry of $\phi = 0.5$ and a pressure of 1 atm. Experimental points are from Dagaut *et al.* [60]. Solid lines are the computations from the detailed chemical mechanism. 118

3.17 Graph of species profile concentrations versus time for the oxidation of n – propylbenzene in a Jet Stirred Reactor for a stoichiometry of $\phi = 0.5$ and a pressure of 1 atm. Experimental points are from Dagaut *et al.* [60]. Solid lines are the computations from the detailed chemical mechanism. 119

3.18 Graph of species profile concentrations versus time for the oxidation of n – propylbenzene in a Jet Stirred Reactor for a stoichiometry of $\phi = 0.5$ and a pressure of 1 atm. Experimental points are from Dagaut *et al.* [60]. Solid lines are the computations from the detailed chemical mechanism. 120

3.19 Graph of species profile concentrations versus time for the oxidation of n – propylbenzene in a Jet Stirred Reactor for a stoichiometry of $\phi = 0.5$ and a pressure of 1 atm. Experimental points are from Dagaut *et al.* [60]. Solid lines are the computations from the detailed chemical mechanism. 121

3.20 Graph of species profile concentrations versus time for the oxidation of n – propylbenzene in a Jet Stirred Reactor for a stoichiometry of $\phi = 1.0$ and a pressure of 1 atm. Experimental points are from Dagaut *et al.* [60]. Solid lines are the computations from the detailed chemical mechanism. 122

3.21 Graph of species profile concentrations versus time for the oxidation of n – propylbenzene in a Jet Stirred Reactor for a stoichiometry of $\phi = 1.0$ and a pressure of 1 atm. Experimental points are from Dagaut *et al.* [60]. Solid lines are the computations from the detailed chemical mechanism. 123

3.22 Graph of species profile concentrations versus time for the oxidation of n – propylbenzene in a Jet Stirred Reactor for a stoichiometry of $\phi = 1.0$ and a pressure of 1 atm. Experimental points are from Dagaut *et al.* [60]. Solid lines are the computations from the detailed chemical mechanism. 124

3.23 Graph of species profile concentrations versus time for the oxidation of n − propylbenzene in a Jet Stirred Reactor for a stoichiometry of $\phi = 1.0$ and a pressure of 1 atm. Experimental points are from Dagaut *et al.* [60]. Solid lines are the computations from the detailed chemical mechanism. 125

3.24 Graph of species profile concentrations versus time for the oxidation of n − propylbenzene in a Jet Stirred Reactor for a stoichiometry of $\phi = 1.5$ and a pressure of 1 atm. Experimental points are from Dagaut *et al.* [60]. Solid lines are the computations from the detailed chemical mechanism. 126

3.25 Graph of species profile concentrations versus time for the oxidation of n − propylbenzene in a Jet Stirred Reactor for a stoichiometry of $\phi = 1.5$ and a pressure of 1 atm. Experimental points are from Dagaut *et al.* [60]. Solid lines are the computations from the detailed chemical mechanism. 127

3.26 Graph of species profile concentrations versus time for the oxidation of n − propylbenzene in a Jet Stirred Reactor for a stoichiometry of $\phi = 1.5$ and a pressure of 1 atm. Experimental points are from Dagaut *et al.* [60]. Solid lines are the computations from the detailed chemical mechanism. 128

3.27 Graph of species profile concentrations versus time for the oxidation of n – propylbenzene in a Jet Stirred Reactor for a stoichiometry of $\phi = 1.5$ and a pressure of 1 atm. Experimental points are from Dagaut *et al.* [60]. Solid lines are the computations from the detailed chemical mechanism. 129

3.28 Graph of species profile concentrations versus time for the oxidation of n – propylbenzene in a Jet Stirred Reactor for a stoichiometry of $\phi = 0.5$ and a pressure of 10 atm. Experimental points are from Dagaut & Cathonnet [55]. Solid lines are the computations from the detailed chemical mechanism. . 135

3.29 Graph of species profile concentrations versus time for the oxidation of n – propylbenzene in a Jet Stirred Reactor for a stoichiometry of $\phi = 0.5$ and a pressure of 10 atm. Experimental points are from Dagaut & Cathonnet [55]. Solid lines are the computations from the detailed chemical mechanism. . 136

3.30 Graph of species profile concentrations versus time for the oxidation of n – propylbenzene in a Jet Stirred Reactor for a stoichiometry of $\phi = 0.5$ and a pressure of 10 atm. Experimental points are from Dagaut & Cathonnet [55]. Solid lines are the computations from the detailed chemical mechanism. . 137

3.31 Graph of species profile concentrations versus time for the oxidation of n − propylbenzene in a Jet Stirred Reactor for a stoichiometry of $\phi = 0.5$ and a pressure of 10 atm. Experimental points are from Dagaut & Cathonnet [55]. Solid lines are the computations from the detailed chemical mechanism. . 138

3.32 Graph of species profile concentrations versus time for the oxidation of n − propylbenzene in a Jet Stirred Reactor for a stoichiometry of $\phi = 1.0$ and a pressure of 10 atm. Experimental points are from Dagaut & Cathonnet [55]. Solid lines are the computations from the detailed chemical mechanism. . 139

3.33 Graph of species profile concentrations versus time for the oxidation of n − propylbenzene in a Jet Stirred Reactor for a stoichiometry of $\phi = 1.0$ and a pressure of 10 atm. Experimental points are from Dagaut & Cathonnet [55]. Solid lines are the computations from the detailed chemical mechanism. . 140

3.34 Graph of species profile concentrations versus time for the oxidation of n − propylbenzene in a Jet Stirred Reactor for a stoichiometry of $\phi = 1.0$ and a pressure of 10 atm. Experimental points are from Dagaut & Cathonnet [55]. Solid lines are the computations from the detailed chemical mechanism. . 141

3.35 Graph of species profile concentrations versus time for the oxidation of n – propylbenzene in a Jet Stirred Reactor for a stoichiometry of $\phi = 1.0$ and a pressure of 10 atm. Experimental points are from Dagaut & Cathonnet [55]. Solid lines are the computations from the detailed chemical mechanism. . 142

3.36 Graph of species profile concentrations versus time for the oxidation of n – propylbenzene in a Jet Stirred Reactor for a stoichiometry of $\phi = 1.5$ and a pressure of 10 atm. Experimental points are from Dagaut & Cathonnet [55]. Solid lines are the computations from the detailed chemical mechanism. . 143

3.37 Graph of species profile concentrations versus time for the oxidation of n – propylbenzene in a Jet Stirred Reactor for a stoichiometry of $\phi = 1.5$ and a pressure of 10 atm. Experimental points are from Dagaut & Cathonnet [55]. Solid lines are the computations from the detailed chemical mechanism. . 144

3.38 Graph of species profile concentrations versus time for the oxidation of n – propylbenzene in a Jet Stirred Reactor for a stoichiometry of $\phi = 1.5$ and a pressure of 10 atm. Experimental points are from Dagaut & Cathonnet [55]. Solid lines are the computations from the detailed chemical mechanism. . 145

3.39 Graph of species profile concentrations versus time for the oxidation of n – propylbenzene in a Jet Stirred Reactor for a stoichiometry of $\phi = 1.5$ and a pressure of 10 atm. Experimental points are from Dagaut & Cathonnet [55]. Solid lines are the computations from the detailed chemical mechanism. . 146

3.40 Graph of species profile concentrations versus time for the oxidation of n – propylbenzene in a Jet Stirred Reactor for a stoichiometry of $\phi = 2.0$ and a pressure of 10 atm. Experimental points are from Dagaut & Cathonnet [55]. Solid lines are the computations from the detailed chemical mechanism. . 147

3.41 Graph of species profile concentrations versus time for the oxidation of n – propylbenzene in a Jet Stirred Reactor for a stoichiometry of $\phi = 2.0$ and a pressure of 10 atm. Experimental points are from Dagaut *et al.* [60]. Solid lines are the computations from the detailed chemical mechanism. 148

3.42 Graph of species profile concentrations versus time for the oxidation of n – propylbenzene in a Jet Stirred Reactor for a stoichiometry of $\phi = 2.0$ and a pressure of 10 atm. Experimental points are from Dagaut *et al.* [60]. Solid lines are the computations from the detailed chemical mechanism. 149

3.43 Graph of species profile concentrations versus time for the oxidation of n – propylbenzene in a Jet Stirred Reactor for a stoichiometry of $\phi = 2.0$ and a pressure of 10 atm. Experimental points are from Dagaut *et al.* [60]. Solid lines are the computations from the detailed chemical mechanism. 150

3.44 Diagram illustrating the consumption paths of the fuel n – propylbenzene and its intermediate species in a Jet Stirred Reactor (T = 1060 K, P = 1 atm., $\phi = 1.5$). 155

4.1 Graph of species profile concentrations versus time for the oxidation of naphthalene in a Turbulent Flow Reactor. Experimental points are from Shaddix [226] for a stoichiometry of $\phi = 1.1$. Solid lines are the computations from the detailed chemical mechanism and have not been time shifted. 164

4.2 Graph of species profile concentrations versus time for the oxidation of naphthalene in a Turbulent Flow Reactor. Experimental points are from Shaddix [226] for a stoichiometry of $\phi = 1.1$. Solid lines are the computations from the detailed chemical mechanism and have not been time shifted. 165

4.3 Graph of species profile concentrations versus time for the oxidation of naphthalene in a Turbulent Flow Reactor. Experimental points are from Shaddix [226] for a stoichiometry of $\phi = 1.1$. Solid lines are the computations from the detailed chemical mechanism and have not been time shifted. 166

4.4 Graph of species profile concentrations versus time for the oxidation of naphthalene in a Turbulent Flow Reactor. Experimental points are from Shaddix [226] for a stoichiometry of $\phi = 1.1$. Solid lines are the computations from the detailed chemical mechanism and have not been time shifted. 167

4.5 Graph of temperature profile versus time for the oxidation of naphthalene in a Turbulent Flow Reactor. Experimental points are from Shaddix [226] for a stoichiometry of $\phi = 1.1$. Solid lines are the computations from the detailed chemical mechanism and have not been time shifted. 168

4.6 Diagram illustrating the consumption paths of the fuel naphthalene and its intermediate species in a Turbulent Flow Reactor at a reaction time of 75 ms. Species in boxes are considered in subsequent pages. 175

4.7 Diagram illustrating the consumption paths of the fuel naphthalene and its intermediate species in a Turbulent Flow Reactor at a reaction time of 75 ms. Species in boxes are considered in subsequent pages. 176

4.8 Diagram illustrating the consumption paths of the fuel naphthalene and its intermediate species in a Turbulent Flow Reactor at a reaction time of 75 ms. Species in boxes are considered in subsequent pages. 177

4.9 Graph of species profile concentrations versus temperature for the oxidation of 1 – methylnaphthalene in a Jet Stirred Reactor. Experimental points are from Dagaut [55] for a stoichiometry of $\phi = 0.5$. Solid lines are the computations from the detailed chemical mechanism. 184

4.10 Graph of species profile concentrations versus temperature for the oxidation of 1 – methylnaphthalene in a Jet Stirred Reactor. Experimental points are from Dagaut [55] for a stoichiometry of $\phi = 0.5$. Solid lines are the computations from the detailed chemical mechanism. 185

4.11 Graph of species profile concentrations versus temperature for the oxidation of 1 – methylnaphthalene in a Jet Stirred Reactor. Experimental points are from Dagaut [55] for a stoichiometry of $\phi = 0.5$. Solid lines are the computations from the detailed chemical mechanism. 186

4.12 Graph of species profile concentrations versus temperature for the oxidation of 1 – methylnaphthalene in a Jet Stirred Reactor. Experimental points are from Dagaut [55] for a stoichiometry of $\phi = 0.5$. Solid lines are the computations from the detailed chemical mechanism. 187

4.13 Graph of species profile concentrations versus temperature for the oxidation of 1 – methylnaphthalene in a Jet Stirred Reactor. Experimental points are from Dagaut [55] for a stoichiometry of $\phi = 1.0$. Solid lines are the computations from the detailed chemical mechanism. 188

4.14 Graph of species profile concentrations versus temperature for the oxidation of 1 – methylnaphthalene in a Jet Stirred Reactor. Experimental points are from Dagaut [55] for a stoichiometry of $\phi = 1.0$. Solid lines are the computations from the detailed chemical mechanism. 189

4.15 Graph of species profile concentrations versus temperature for the oxidation of 1 – methylnaphthalene in a Jet Stirred Reactor. Experimental points are from Dagaut [55] for a stoichiometry of $\phi = 1.0$. Solid lines are the computations from the detailed chemical mechanism. 190

4.16 Graph of species profile concentrations versus temperature for the oxidation of 1 – methylnaphthalene in a Jet Stirred Reactor. Experimental points are from Dagaut [55] for a stoichiometry of $\phi = 1.0$. Solid lines are the computations from the detailed chemical mechanism. 191

4.17 Graph of species profile concentrations versus temperature for the oxidation of 1 – methylnaphthalene in a Jet Stirred Reactor. Experimental points are from Dagaut [55] for a stoichiometry of $\phi = 1.5$. Solid lines are the computations from the detailed chemical mechanism. 192

4.18 Graph of species profile concentrations versus temperature for the oxidation of 1 – methylnaphthalene in a Jet Stirred Reactor. Experimental points are from Dagaut [55] for a stoichiometry of $\phi = 1.5$. Solid lines are the computations from the detailed chemical mechanism. 193

4.19 Graph of species profile concentrations versus temperature for the oxidation of 1 – methylnaphthalene in a Jet Stirred Reactor. Experimental points are from Dagaut [55] for a stoichiometry of $\phi = 1.5$. Solid lines are the computations from the detailed chemical mechanism. 194

4.20 Graph of species profile concentrations versus temperature for the oxidation of 1 – methylnaphthalene in a Jet Stirred Reactor. Experimental points are from Dagaut [55] for a stoichiometry of $\phi = 1.5$. Solid lines are the computations from the detailed chemical mechanism. 195

4.21 Graph of final temperature versus initial temperature for the oxidation of 1 – methylnaphthalene in a Jet Stirred Reactor for a stoichiometry of 1.0. 196

4.22 Graph of species profile concentrations versus time for the oxidation of 1 – methylnaphthalene in a Turbulent Flow Reactor. Experimental points are from Shaddix [226] for a stoichiometry of $\phi = 0.58$. Solid lines are the computations from the detailed chemical mechanism and have been time shifted by 32 ms. 203

4.23 Graph of species profile concentrations versus time for the oxidation of 1 – methylnaphthalene in a Turbulent Flow Reactor. Experimental points are from Shaddix [226] for a stoichiometry of $\phi = 0.58$. Solid lines are the computations from the detailed chemical mechanism and have been time shifted by 32 ms. 204

4.24 Graph of species profile concentrations versus time for the oxidation of 1 – methylnaphthalene in a Turbulent Flow Reactor. Experimental points are from Shaddix [226] for a stoichiometry of $\phi = 0.58$. Solid lines are the computations from the detailed chemical mechanism and have been time shifted by 32 ms. 205

4.25 Graph of species profile concentrations versus time for the oxidation of 1 – methylnaphthalene in a Turbulent Flow Reactor. Experimental points are from Shaddix [226] for a stoichiometry of $\phi = 0.58$. Solid lines are the computations from the detailed chemical mechanism and have been time shifted by 32 ms. 206

4.26 Graph of species profile concentrations versus time for the oxidation of 1 – methylnaphthalene in a Turbulent Flow Reactor. Experimental points are from Shaddix [226] for a stoichiometry of $\phi = 0.58$. Solid lines are the computations from the detailed chemical mechanism and have been time shifted by 32 ms. 207

4.27 Graph of temperature profile versus time for the oxidation of 1 – methylnaphthalene in a Turbulent Flow Reactor. Experimental points are from Shaddix [226] for a stoichiometry of $\phi = 0.58$. Solid lines are the computations from the detailed chemical mechanism and have been time shifted by 32 ms. . . 208

4.28 Graph of species profile concentrations versus time for the oxidation of 1 – methylnaphthalene in a Turbulent Flow Reactor. Experimental points are from Shaddix [226] for a stoichiometry of $\phi = 1.0$. Solid lines are the computations from the detailed chemical mechanism and have been time shifted by 32 ms. 209

4.29 Graph of species profile concentrations versus time for the oxidation of 1 – methylnaphthalene in a Turbulent Flow Reactor. Experimental points are from Shaddix [226] for a stoichiometry of $\phi = 1.0$. Solid lines are the computations from the detailed chemical mechanism and have been time shifted by 32 ms. 210

4.30 Graph of species profile concentrations versus time for the oxidation of 1 – methylnaphthalene in a Turbulent Flow Reactor. Experimental points are from Shaddix [226] for a stoichiometry of $\phi = 1.0$. Solid lines are the computations from the detailed chemical mechanism and have been time shifted by 32 ms. 211

4.31 Graph of species profile concentrations versus time for the oxidation of 1 – methylnaphthalene in a Turbulent Flow Reactor. Experimental points are from Shaddix [226] for a stoichiometry of $\phi = 1.0$. Solid lines are the computations from the detailed chemical mechanism and have been time shifted by 32 ms. 212

4.32 Graph of species profile concentrations versus time for the oxidation of 1 – methylnaphthalene in a Turbulent Flow Reactor. Experimental points are from Shaddix [226] for a stoichiometry of $\phi = 1.0$. Solid lines are the computations from the detailed chemical mechanism and have been time shifted by 32 ms. 213

4.33 Graph of temperature profile versus time for the oxidation of 1 – methylnaphthalene in a Turbulent Flow Reactor. Experimental points are from Shaddix [226] for a stoichiometry of $\phi = 1.0$. Solid lines are the computations from the detailed chemical mechanism and have been time shifted by 32 ms. . . 214

4.34 Graph of species profile concentrations versus time for the oxidation of 1 – methylnaphthalene in a Turbulent Flow Reactor. Experimental points are from Shaddix [226] for a stoichiometry of $\phi = 1.5$ for $T_0 = 1166$ K. Solid lines are the computations from the detailed chemical mechanism and have been time shifted by 32 ms. 215

4.35 Graph of species profile concentrations versus time for the oxidation of 1 – methylnaphthalene in a Turbulent Flow Reactor. Experimental points are from Shaddix [226] for a stoichiometry of $\phi = 1.5$ for $T_0 = 1166$ K. Solid lines are the computations from the detailed chemical mechanism and have been time shifted by 32 ms. 216

4.36 Graph of species profile concentrations versus time for the oxidation of 1 – methylnaphthalene in a Turbulent Flow Reactor. Experimental points are from Shaddix [226] for a stoichiometry of $\phi = 1.5$ for $T_0 = 1166$ K. Solid lines are the computations from the detailed chemical mechanism and have been time shifted by 32 ms. 217

4.37 Graph of species profile concentrations versus time for the oxidation of 1 – methylnaphthalene in a Turbulent Flow Reactor. Experimental points are from Shaddix [226] for a stoichiometry of $\phi = 1.5$ for $T_0 = 1166$ K. Solid lines are the computations from the detailed chemical mechanism and have been time shifted by 32 ms. 218

4.38 Graph of species profile concentrations versus time for the oxidation of 1 – methylnaphthalene in a Turbulent Flow Reactor. Experimental points are from Shaddix [226] for a stoichiometry of $\phi = 1.5$ for $T_0 = 1166$ K. Solid lines are the computations from the detailed chemical mechanism and have been time shifted by 32 ms. 219

4.39 Graph of temperature profile versus time for the oxidation of 1 – methylnaphthalene in a Turbulent Flow Reactor. Experimental points are from Shaddix [226] for a stoichiometry of $\phi = 1.5$ for $T_0 = 1166$ K. Solid lines are the computations from the detailed chemical mechanism and have been time shifted by 32 ms. 220

4.40 Graph of species profile concentrations versus time for the oxidation of 1 – methylnaphthalene in a Turbulent Flow Reactor. Experimental points are from Shaddix [226] for a stoichiometry of $\phi = 1.5$ for $T_0 = 1198$ K. Solid lines are the computations from the detailed chemical mechanism and have been time shifted by 32 ms. 221

4.41 Graph of species profile concentrations versus time for the oxidation of 1 – methylnaphthalene in a Turbulent Flow Reactor. Experimental points are from Shaddix [226] for a stoichiometry of $\phi = 1.5$ for $T_0 = 1198$ K. Solid lines are the computations from the detailed chemical mechanism and have been time shifted by 32 ms. 222

4.42 Graph of species profile concentrations versus time for the oxidation of 1 – methylnaphthalene in a Turbulent Flow Reactor. Experimental points are from Shaddix [226] for a stoichiometry of $\phi = 1.5$ for $T_0 = 1198$ K. Solid lines are the computations from the detailed chemical mechanism and have been time shifted by 32 ms. 223

4.43 Graph of species profile concentrations versus time for the oxidation of 1 – methylnaphthalene in a Turbulent Flow Reactor. Experimental points are from Shaddix [226] for a stoichiometry of $\phi = 1.5$ for $T_0 = 1198$ K. Solid lines are the computations from the detailed chemical mechanism and have been time shifted by 32 ms. 224

4.44 Graph of species profile concentrations versus time for the oxidation of 1 – methylnaphthalene in a Turbulent Flow Reactor. Experimental points are from Shaddix [226] for a stoichiometry of $\phi = 1.5$ for $T_0 = 1198$ K. Solid lines are the computations from the detailed chemical mechanism and have been time shifted by 32 ms. 225

4.45 Graph of temperature profile versus time for the oxidation of 1 – methylnaphthalene in a Turbulent Flow Reactor. Experimental points are from Shaddix [226] for a stoichiometry of $\phi = 1.5$ for $T_0 = 1198$ K. Solid lines are the computations from the detailed chemical mechanism and have been time shifted by 32 ms. 226

4.46 Diagram illustrating the consumption paths of the fuel 1 – methylnaphthalene and its intermediate species in a Jet Stirred Reactor (T = 1260 K, P = 1 atm., $\phi = 1.5$). Species in boxes are considered in subsequent pages. 234

4.47 Diagram illustrating the consumption paths of the fuel 1 – methylnaphthalene and its intermediate species in a Jet Stirred Reactor (T = 1260 K, P = 1 atm., $\phi = 1.5$). Species in boxes are considered in subsequent pages. 235

4.48 Diagram illustrating the consumption paths of the fuel 1 – methylnaphthalene and its intermediate species in a Jet Stirred Reactor (T = 1260 K, P = 1 atm., ϕ = 1.5). Species in boxes are considered in subsequent pages. 236

4.49 Diagram illustrating the consumption paths of the fuel 1 – methylnaphthalene and its intermediate species in a Jet Stirred Reactor (T = 1260 K, P = 1 atm., ϕ = 1.5). Species in boxes are considered in subsequent pages. 237

4.50 Comparison of computed (lines) and measured (symbols) ignition delay times for stoichiometric 1 – methylnaphthalene – air mixtures. Experimental points are from Pfahl *et al.* [202]. 239

4.51 Graph of acenaphthalene profile concentrations versus time for the oxidation of 1 – methylnaphthalene in a Turbulent Flow Reactor for the various stoichiometries. Experimental points are from Shaddix [226]. Solid lines are the computations from the detailed chemical mechanism and have been time shifted by 32 ms. 244

4.52 Graph of acenaphthalene profile concentrations versus time for the oxidation of naphthalene in a Turbulent Flow Reactor. Experimental points are from Shaddix [226]. Solid lines are the computations from the detailed chemical mechanism and have not been time shifted. 245

5.1 Graph of species profile concentrations versus temperature for the oxidation of n – decane and n – propylbenzene constituting the kerosene mix in a Jet Stirred Reactor. Experimental points are from Dagaut & Cathonnet [55] for a stoichiometry of $\phi = 0.75$. Solid lines are the computations from the detailed chemical mechanism. 256

5.2 Graph of species profile concentrations versus temperature for the oxidation of n – decane and n – propylbenzene constituting the kerosene mix in a Jet Stirred Reactor. Experimental points are from Dagaut & Cathonnet [55] for a stoichiometry of $\phi = 0.75$. Solid lines are the computations from the detailed chemical mechanism. 257

5.3 Graph of species profile concentrations versus temperature for the oxidation of n – decane and n – propylbenzene constituting the kerosene mix in a Jet Stirred Reactor. Experimental points are from Dagaut & Cathonnet [55] for a stoichiometry of $\phi = 0.75$. Solid lines are the computations from the detailed chemical mechanism. 258

5.4 Graph of species profile concentrations versus temperature for the oxidation of n – decane and n – propylbenzene constituting the kerosene mix in a Jet Stirred Reactor. Experimental points are from Dagaut & Cathonnet [55] for a stoichiometry of $\phi = 0.75$. Solid lines are the computations from the detailed chemical mechanism. 259

5.5 Graph of species profile concentrations versus temperature for the oxidation of n – decane and n – propylbenzene constituting the kerosene mix in a Jet Stirred Reactor. Experimental points are from Dagaut & Cathonnet [55] for a stoichiometry of $\phi = 1.0$. Solid lines are the computations from the detailed chemical mechanism. 260

5.6 Graph of species profile concentrations versus temperature for the oxidation of n – decane and n – propylbenzene constituting the kerosene mix in a Jet Stirred Reactor. Experimental points are from Dagaut & Cathonnet [55] for a stoichiometry of $\phi = 1.0$. Solid lines are the computations from the detailed chemical mechanism. 261

5.7 Graph of species profile concentrations versus temperature for the oxidation of n – decane and n – propylbenzene constituting the kerosene mix in a Jet Stirred Reactor. Experimental points are from Dagaut & Cathonnet [55] for a stoichiometry of $\phi = 1.0$. Solid lines are the computations from the detailed chemical mechanism. 262

5.8 Graph of species profile concentrations versus temperature for the oxidation of n – decane and n – propylbenzene constituting the kerosene mix in a Jet Stirred Reactor. Experimental points are from Dagaut & Cathonnet [55] for a stoichiometry of $\phi = 1.0$. Solid lines are the computations from the detailed chemical mechanism. 263

5.9 Graph of species profile concentrations versus temperature for the oxidation of n – decane and n – propylbenzene constituting the kerosene mix in a Jet Stirred Reactor. Experimental points are from Dagaut & Cathonnet [55] for a stoichiometry of $\phi = 1.5$. Solid lines are the computations from the detailed chemical mechanism. 264

5.10 Graph of species profile concentrations versus temperature for the oxidation of n – decane and n – propylbenzene constituting the kerosene mix in a Jet Stirred Reactor. Experimental points are from Dagaut & Cathonnet [55] for a stoichiometry of $\phi = 1.5$. Solid lines are the computations from the detailed chemical mechanism. 265

5.11 Graph of species profile concentrations versus temperature for the oxidation of n – decane and n – propylbenzene constituting the kerosene mix in a Jet Stirred Reactor. Experimental points are from Dagaut & Cathonnet [55] for a stoichiometry of $\phi = 1.5$. Solid lines are the computations from the detailed chemical mechanism. 266

5.12 Graph of species profile concentrations versus temperature for the oxidation of n – decane and n – propylbenzene constituting the kerosene mix in a Jet Stirred Reactor. Experimental points are from Dagaut & Cathonnet [55] for a stoichiometry of $\phi = 1.5$. Solid lines are the computations from the detailed chemical mechanism. 267

5.13 Graph of species profile concentrations versus temperature for the oxidation of n – decane and n – propylbenzene constituting the kerosene mix in a Jet Stirred Reactor. Experimental points are from Dagaut & Cathonnet [55] for a stoichiometry of $\phi = 2.0$. Solid lines are the computations from the detailed chemical mechanism. 268

5.14 Graph of species profile concentrations versus temperature for the oxidation of n – decane and n – propylbenzene constituting the kerosene mix in a Jet Stirred Reactor. Experimental points are from Dagaut & Cathonnet [55] for a stoichiometry of $\phi = 2.0$. Solid lines are the computations from the detailed chemical mechanism. 269

5.15 Graph of species profile concentrations versus temperature for the oxidation of n – decane and n – propylbenzene constituting the kerosene mix in a Jet Stirred Reactor. Experimental points are from Dagaut & Cathonnet [55] for a stoichiometry of $\phi = 2.0$. Solid lines are the computations from the detailed chemical mechanism. 270

5.16 Graph of species profile concentrations versus temperature for the oxidation of n – decane and n – propylbenzene constituting the kerosene mix in a Jet Stirred Reactor. Experimental points are from Dagaut & Cathonnet [55] for a stoichiometry of $\phi = 2.0$. Solid lines are the computations from the detailed chemical mechanism. 271

5.17 Diagram illustrating the consumption paths of the paraffin component of the kerosene mix (n – decane) and its intermediate species in a Jet Stirred Reactor (T = 1000 K, P = 10 atm, $\phi = 2.0$). Species in boxes are considered in subsequent pages. 279

5.18 Diagram illustrating the consumption paths of the paraffin component of the kerosene mix (n – decane) and its intermediate species in a Jet Stirred Reactor (T = 1000 K, P = 10 atm, $\phi = 2.0$). Species in boxes are considered in subsequent pages. 280

5.19 Diagram illustrating the consumption paths of the paraffin component of the kerosene mix (n – decane) and its intermediate species in a Jet Stirred Reactor (T = 1000 K, P = 10 atm, ϕ = 2.0). Species in boxes are considered in subsequent pages. 281

5.20 Diagram illustrating the consumption paths of the paraffin component of the kerosene mix (n – decane) and its intermediate species in a Jet Stirred Reactor (T = 1000 K, P = 10 atm, ϕ = 2.0). Species in boxes are considered in subsequent pages. 282

5.21 Diagram illustrating the consumption paths of the paraffin component of the kerosene mix (n – decane) and its intermediate species in a Jet Stirred Reactor (T = 1000 K, P = 10 atm, ϕ = 2.0). Species in boxes are considered in subsequent pages. 283

List of Tables

1.1 JP – 4 Fuel Constituents [84] 3

2.1 Summary of the Initial Conditions for the Pyrolysis of Toluene in a Shock Tube 31

2.2 Summary of the Initial Conditions for the Oxidation of Toluene in a Jet Stirred Reactor 37

2.3 Summary of the Initial Conditions for the Oxidation of Toluene in a Shock Tube 64

3.1 Summary of the Initial Conditions for the Oxidation of n – propylbenzene in a Jet Stirred Reactor at Low Pressure 114

3.2 Summary of the Initial Conditions for the Oxidation of n – propylbenzene in a Jet Stirred Reactor at High Pressure . . . 130

4.1 Summary of the Initial Conditions for the Oxidation of 1 – methylnaphthalene in a Jet Stirred Reactor 179

4.2 Summary of the initial conditions for the Oxidation of 1 – methylnaphthalene in a Turbulent Flow Reactor 197

5.1 Summary of the Initial Conditions for the Oxidation of the n – decane and n – propylbenzene kerosene fuel mixture in a Jet Stirred Reactor 251

A.1 Detailed Chemical Kinetic Mechanism 333

A.2 n – propylbenzene Detailed Kinetic Sub – Mechanism 358

A.3 n – butylbenzene Detailed Kinetic Sub – Mechanism 359

A.4 n – decane and do – decane Detailed Kinetic Sub Mechanism . 360

B.1 Thermodynamic Data 369

C.1 Species Structure and Thermodynamic Data. 390

l

Nomenclature

Roman Symbols

a	Parameter in F_c factor formulation
A	Pre–exponential factor
C_p	Heat capacity at constant pressure
E_a	Activation energy
F	Broadening factor
F_c	Parameter in broadening factor formulation
h_k	Enthalpy of species k
h_k^*	Enthalpy of species k at inlet
F	Broadening Factor
H^0	Mixture enthalpy
k	Rate constant
k_f	Rate constant

k_∞	High pressure limit
k_0	Low pressure limit
K_p	Equilibrium constant
m	Mass flow rate
M_k	Molecular weight of species k
N	Parameter in broadening factor formulation
n	Temperature dependancy
P	Pressure
S^0	Mixture enthalpy
R	Universal gas constant
R_k	Net rate of formation of species k
t	Time
T	Temperature

V_r	Reactor volume
Y_k	Mass fraction of species k
Y_k^*	Mass fraction of species k at intlet

Greek Symbols

Δ	Change of property
ν_k	Stoichiometric coefficient for species k
Ξ_{lk}	Stoichiometric coefficient of species k in reaction j
ξ^{lk}	Concentration dependence of species k in reaction j
ρ	Density
τ	Mean Residence Time
Φ_k	Molar concentration of species i

Chapter 1

Introduction

1.1 Overview

The past decade has seen a growing awareness of the impact of industry on the environment leading to a global commitment to reduce emissions as quickly and efficiently as possible. Although engines are becoming cleaner and quieter, there is still a great deal to accomplish. Thus, it is the desire of engineers who work in the design of engines to maximise the maintainability, reliability and efficiency as well as minimising the pollution and noise level output. The properties of different fuels and their propensity to generate pollutants is increasingly relevant in this context.

A propulsion fuel may be defined as a material from which energy can be liberated. In principle, a range of fuels can be utilised for propulsive purposes provided that financial or technological constraints are not limiting. It is therefore necessary to clarify the subject of this thesis given the broad background of the subject area of propulsion fuels. The focus of this work is on the modelling of the combustion chemistry for practical fuels which can be used for propulsive purposes such as in air breathing engines. Solid

rocket propellants are not investigated here. Additionally, the subject area of cryogenic fuels are also excluded from this study. Hence it may be considered that the term *propulsive fuels* used in this study is applicable to hydrocarbon fuels most commonly used in everyday transportation vehicles.

The modelling of the oxidation of propulsive fuels involves using detailed chemical kinetics which can give an understanding of the complex chemistry starting from the fuel and leading to the end products. An overview of how this is achieved is given below. Section 1.2 describes the initial difficulties in describing the constituents of typical propulsive fuels. Section 1.3 emphasises the environmental impact and the need for a deeper understanding into the combustion of propulsive fuels. Section 1.4 describes the role of chemical kinetics in developing an understanding of the complex combustion processes involved in the oxidation of propulsive fuels. Finally, Section 1.5 provides a brief overview of the current thesis.

1.2 The Constituents of Propulsive Fuels

The different types of propulsive fuels can be divided into many categories in terms of civilian transportation usage. The cases considered here are kerosene and diesel fuels. The type of fuel chosen will depend on the transportation method and hence the engine type. Kerosene fuels are mostly used by the aviation industry and diesel fuels are used in cars and buses. Kerosene and diesel fuels are obtained from crude oils from a process called *cracking* in a fractional distillation column [103]. Crude oils contain mixtures of many hundreds of types of hydrocarbons, each with their own discrete chemical and physical properties. Upon obtaining kerosene and diesel fuels from the cracking process, the number of different types of hydrocarbons present are still typically in the hundreds. Furthermore, the types of hydrocarbon molecules

present can vary according to the crude oil feed stocks and the cracking process [84]. Table 1.1 gives an example of the hydrocarbons found in a kerosene fuel sample, JP – 4. Further information on other propulsion fuel data is available in the literature (*e.g.* Edwards [84], Goodger & Vere [103], Hobson and Pohl [128] and Maurice [183]).

Table 1.1: JP – 4 Fuel Constituents [84]

Compound	Volume %
n – hexane	5.5
Cyclohexane	8.0
n – heptane	10.0
methylcyclohexane	10.0
toluene	10.0
n – octane	10.0
n – nonane	10.0
Cyclo – octane	8.0
n – decane	10.0
Decalin	5.0
Tetralin	1.0
n – docecane	10.0
1 – methylnaphthalene	0.5
n – tetradecane	10.0

The shear complexity of the constituents of typical aviation fuels is immediately apparent. To ascertain a better understanding of the chemical constituents of this sample of kerosene fuel, it is necessary to categorise the various hydrocarbon molecules into compound classes. The many types of hydrocarbon species found in the above fuel sample may be divided into three broad classes: Aromatics (about 20%), n – paraffins and iso – paraffins (about 60%) and cycloparaffins (about 20%) [183]. Figure 1.1 shows a detailed graph illustrating the various types of hydrocarbons found in three

typical kerosene samples used for different purposes where JP – 4, JP – 7 are military fuels, Jet – A a commercial fuel and DF2 is a diesel fuel.

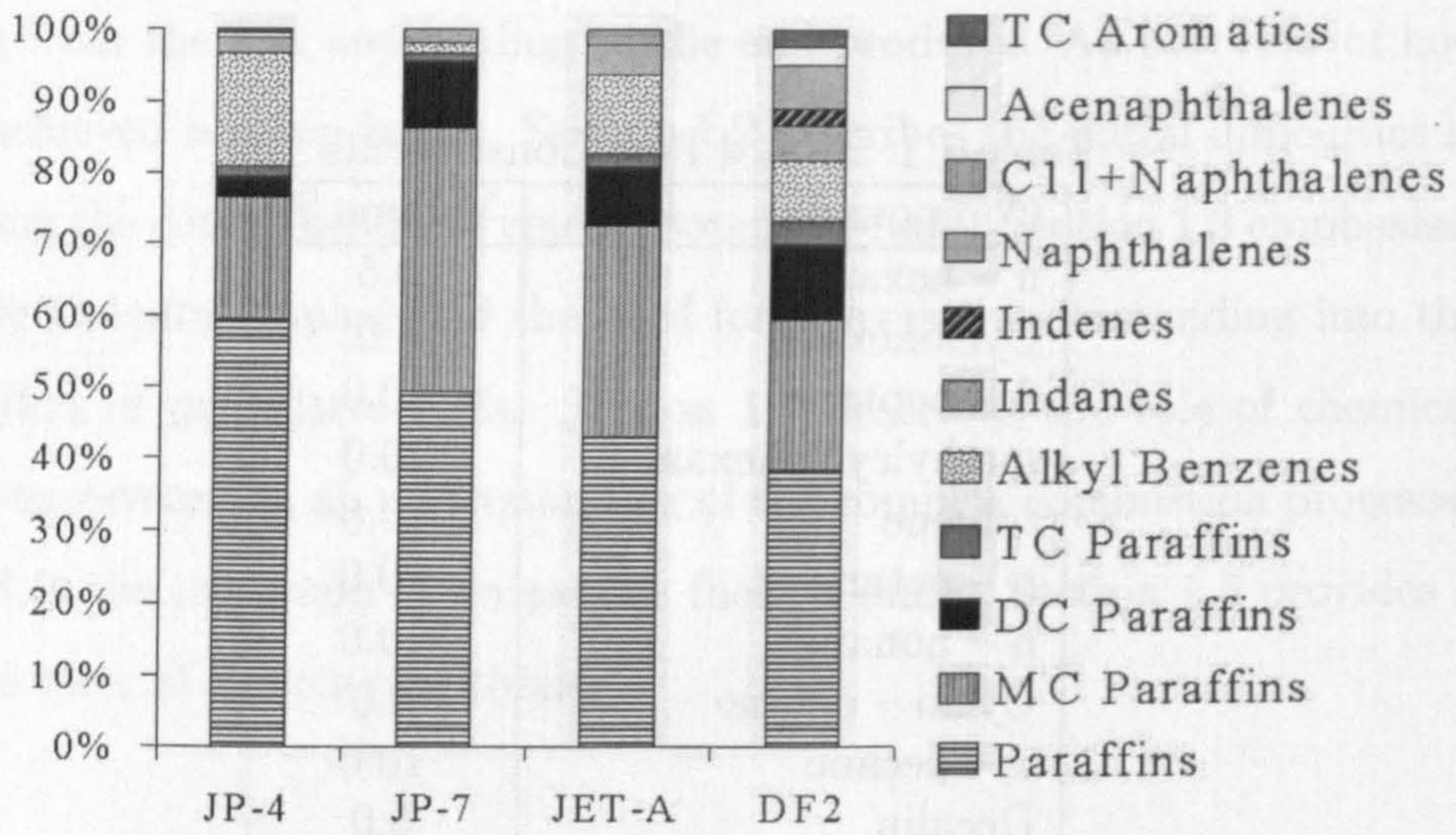


Figure 1.1: Chemical composition of typical propulsion fuels [165].

Paraffins are fully saturated compounds that may form straight chained, branched or cyclic structures. Examples of paraffins include decane and nonane. Aromatic compounds feature double bonded structures, the simplest being benzene which can form more complex compounds such as 1,4-diethylbenzene. Figure 1.2 illustrates some typical classes found in both kerosene and diesel fuels.

For combustion modelling purposes it is necessary to reduce the number of constituents found in both kerosene and diesel fuels as modelling the precise individual components is obviously impractical. Figure 1.3 illustrates

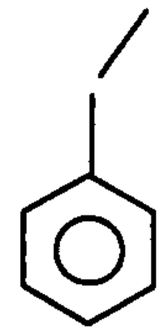
Compound Class	Name	Structure
n - paraffin	n - decane	CH_3-$(CH)_8$-CH_3
Mono-substituted aromatic	ethylbenzene	
alkene	1 - heptene	$CH_2CH4(CH_2)CH_3$

Figure 1.2: Typical classes of hydrocarbons found in propulsion fuels.

two constituent classes for four typical kerosene samples used for different purposes where JP - 4, JP - 5 and JP - 7 are military fuels. Jet - A a commercial aviation fuel and DF2 is a diesel fuel.

Diesel engine fuels typically contain an even more complex mixture of heavier hydrocarbons, typically in the range C_{10} to C_{22} compared to kerosene fuels which are typically in the range from C_1 to C_{12} [235]. Due to the higher range of paraffins, naphthenes, and aromatics, diesel fuel has a higher density than gasoline and contains over 10% more energy than the equivalent volume of gasoline. Hence, this higher energy content along with engine durability has led to diesel becoming a popular practical transportation fuel [39].

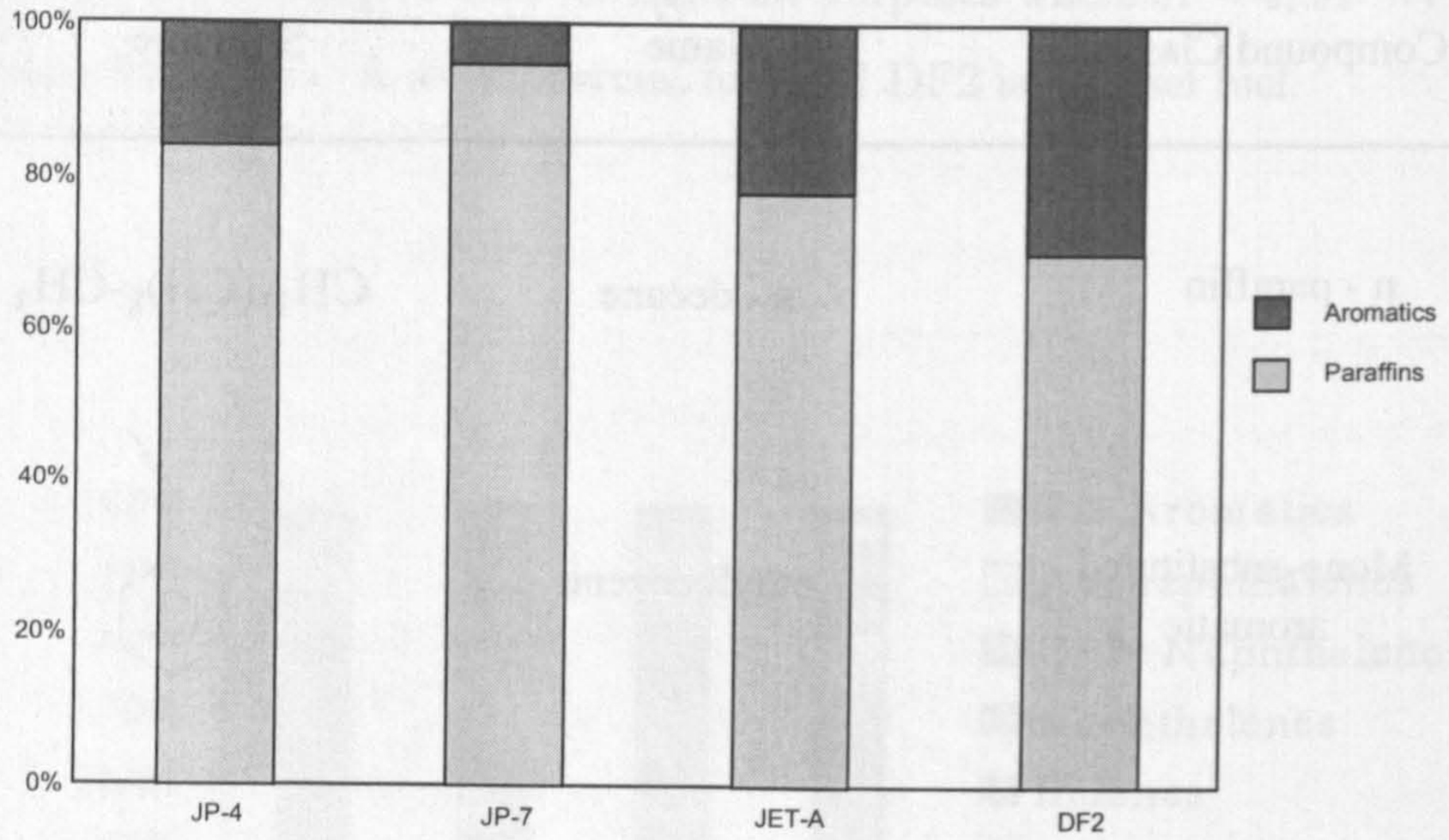


Figure 1.3: Paraffin and aromatic constituents of typical propulsion fuels [182].

1.3 Environmental Impact of Combustion

The combustion of hydrocarbon based propulsive fuels has led to several health hazards, such as respiratory diseases and fertility problems, as shown in numerous health studies (*e.g.* Dockery & Pope [78] and Dockery *et al.* [79]). Moreover, Kunzli *et al.* [155] conducted a study showing that air pollution from motorized traffic contributed to $\approx 3\%$ of the mortality rate in major European cities. Particulates form a family of polycyclic organic matter which include polycyclic aromatic compounds and heterocyclic compounds [154]. Their formation (see section 1.3.2) in exhaust fumes is due to the incomplete or partial combustion of the hydrocarbon fuel. The small size of the particles ($0.01 < d < 1\ \mu m$) makes them easily respirable and hence a key contributor to health effects such as lung cancer [1]. The trace elements present in hydrocarbon fuels can also cause health and environmental im-

pacts. For example, the production of SO_x is directly related to the amount of sulphur present in diesel which can contribute to the formation of acidic compounds in the atmosphere. Also, NO_x produced from the combustion of diesel can again react in the atmosphere producing photochemical smog. Carbon dioxide, produced from the combustion of all carbon based fuels, is a well known green house gas causing global climate change [160].

1.3.1 PAH and Soot Formation

There are many proposals aimed at explaining the origin of soot formation via ionic species [37] and polyacetylenes [131]. However, the majority opinion at present, with evidence from both experimental and theoretical areas of combustion science, embraces the fact that soot particles are initially formed from polycyclic aromatic hydrocarbons (PAH) [95].

As mentioned earlier, particulates are formed from the combustion of hydrocarbon fuels. There are many detailed reviews in the literature concerning soot that describe the basic mechanistic characteristics of particulate formation (*e.g.* Bockhorn [21], Frenklach [95, 96], Kohse – Höinghaus *et al.* [152], Longwell [176], Richter *et al.* [213], Richter & Howard [214] and Stanmore *et al.* [237]). Additionally, mechanistic models have been proposed under different fuels and conditions (*e.g.* Bohm & Jander [24], Cole *et al.* [47], D'Anna & Violi [68], Faravelli *et al.* [93], Hwang *et al.* [137], Miller & Melius [188], Mingming & Mulholland [192] and Roesler & De Tessan [221]).

The formation of soot may be defined as the conversion of a hydrocarbon fuel molecule containing a few carbon atoms into a carbonaceous agglomerate containing some millions of carbon atoms [21]. The transition from gas to solid phase encompasses physical and chemical processes. For example, the formation and growth of PAH and their transition to particles, the coagula-

tion of primary particles to larger aggregates, and finally the growth of solid particles by picking up growth components of the gas phase. Figure 1.4 illustrates the growth of soot from the individual hydrocarbon radical molecules during oxidation in a premixed flame [21].

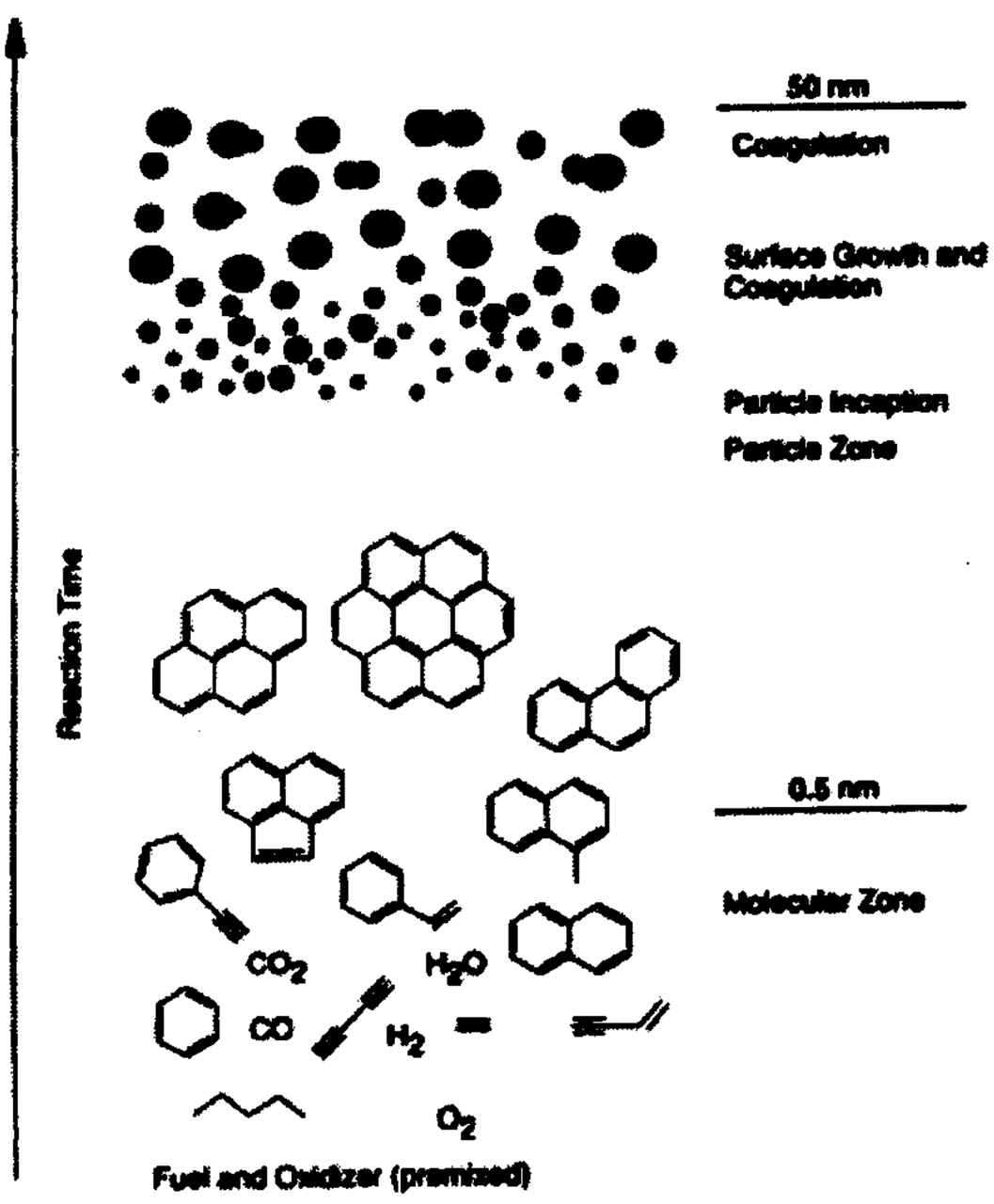
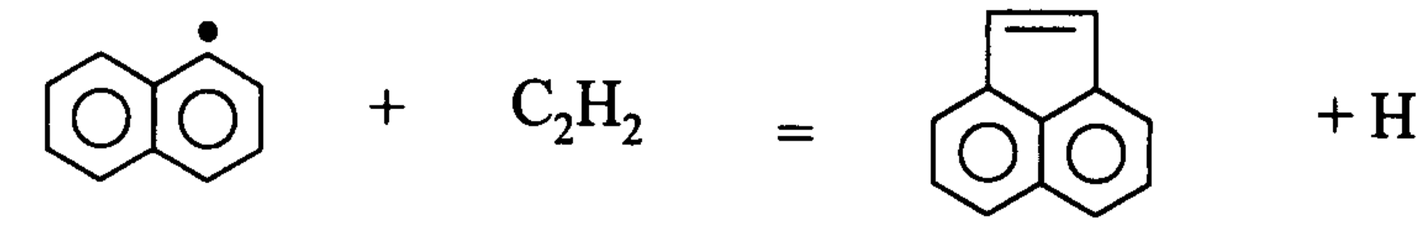


Figure 1.4: Schematic diagram for soot formation in premixed flames [21].

The growth of unsaturated rings containing a sufficiently large number of carbon atoms results from the interaction of stable species with radicals such as the reaction steps shown below in Figure 1.5

Further molecular growth of aromatics to form PAH's may proceed via the addition of other species such as methyl, propargyl and cyclopentadienyl (*e.g.* Colket & Seery [49], D'Anna & Violi [68], Lindstedt *et al.* [169], McEnally & Pfefferle [184], Melius *et al.* [186], Mingming & Mulholland [195] and Pope & Miller [206]).



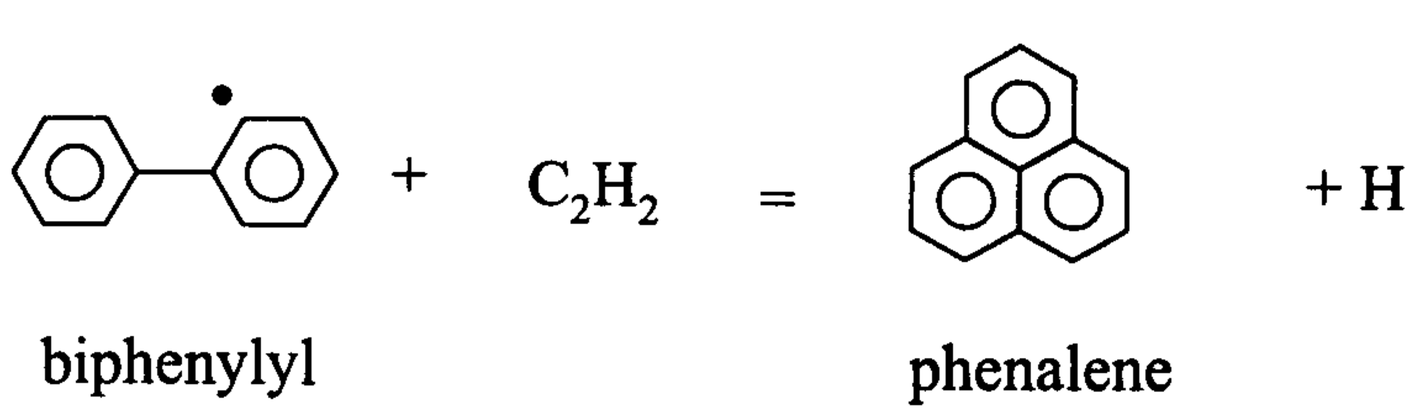


Figure 1.5: Possible addition sequences for PAH and soot formation [214].

Particle growth is initiated by the PAH structures coagulating to form soot particles. These soot particles pick up molecules from the gas phase for surface growth. Frenklach [95] comments that this is the least understood part of the soot formation process, partly due to the argument that stable species reactions are not fast enough to explain the formation of soot particles, hence other areas are explored as mentioned above.

Once soot particles are formed, they coalesce forming larger particles [214]. Experimental evidence has clarified that the particles look spherical and later acquire a fractal shape [109].

1.4 Modelling of Combustion

The modelling of the oxidation of the fuel compounds in the current work is evaluated using a computational fluid dynamics code (LAPREM). It uses an implicit solution procedure for the species transport equations. The method is based on a Newton linearisation of the source terms with the derivatives

evaluated analytically [141, 142]. The theory of the modelling may be considered in two parts; the chemical and mathematical models.

1.4.1 Chemical Model

The modelling of the combustion of propulsive hydrocarbon fuels utilises detailed chemical mechanisms involving elementary reaction steps [262]. The specific forward rate for each elementary reaction is typically expressed in a modified Arrhenius form (1.1)

$$k = AT^n exp(-E_a/RT) \tag{1.1}$$

Additionally, the thermodynamic and transport data of all the individual species are required. Detailed chemical mechanisms are developed in a logical and hierarchical manner. That is, the simplest hydrocarbon fuels are considered which are common intermediate species for higher based hydrocarbon fuels and subsequently, more complex fuels may be considered by the addition on new elementary reactions and species [262]. Figure 1.6 illustrates the hierarchical structure behind the construction of a detailed chemical mechanism for propulsion fuels.

By approaching the detailed chemical mechansim construction from a hierarchical perspective, it is possible to reduce the task of mechanism construction from the identification of primary reaction paths. Due to the gradual advances in combustion research, the experimental data for reaction rates are scarce for higher order hydrocarbons. Solutions to overcome this problem of the lack of experimental data include analogous reaction equivalents and quantum mechanical techniques such as QRRK theory [243].

Four distinct phases occur during typical combustion processes of hydrocarbons [101]. After ignition, the consumed fuel yields hydrogen atoms and

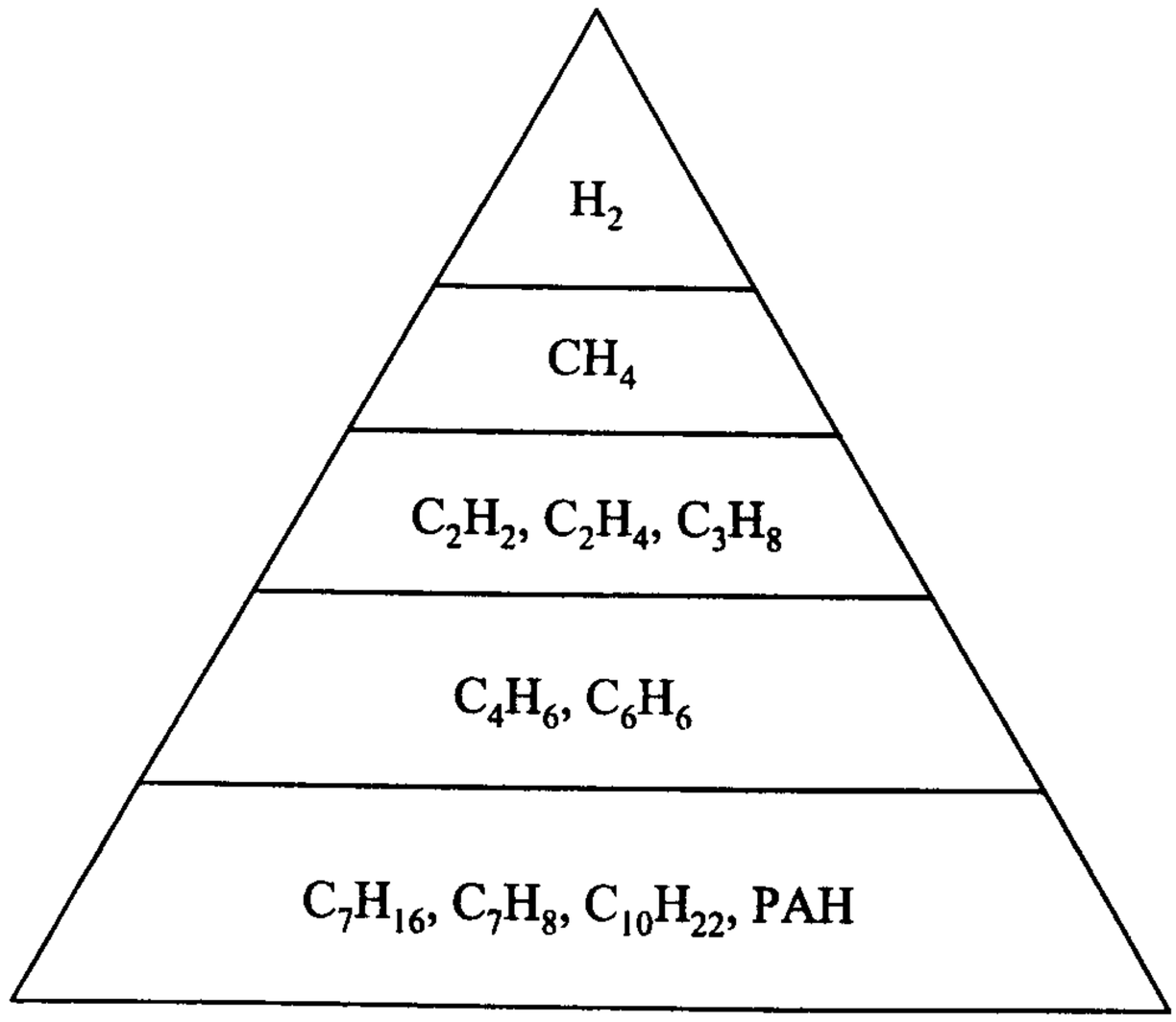


Figure 1.6: Hierarchial construction of a detailed chemical mechansim for propulsion fuels [182].

unsaturated hydrocarbons. In this initial phase almost no energy is released and only a small amount of hydrogen is oxidised. In the subsequent phase the unsaturated hydrocarbons and the hydrogen atom are oxidised to form carbon monoxide and water respectively. The main heat release occurs in the third phase when the carbon monoxide oxidises to form carbon dioxide. In the last phase, and given a sufficient high temperature, an equilibrium is established between the free radicals and the main combustion products water, carbon monoxide and dioxide. It can thus be concluded that the $H_2/CO/O_2$ system forms the fundamental building block for any detailed chemical kinetic mechanism. Historically [262], the H_2/O_2 was the first detailed chemical kinetic mechanism to be developed and has been thoroughly tested and validated in various experimental devices including Shock Tubes [108], Jet Stirred Reactors [140] and Laminar Flames [77].

The simplest hydrocarbon alkane component, methane is an important

intermediate for higher order hydrocarbon fuels [65] as well as the dominant ($\approx$ 90%) component in natural gas mixtures [52]. The modelling of methane combustion has been reviewed extensively in the literature (*e.g.* Barbe *et al.* [9], Dagaut *et al.* [65], Hidaka *et al.* [124], Hunter *et al.* [136], Reid *et al.* [209], Rota *et al.* [223], Sloane [233], Tan *et al.* [240] and Westbrook & Dryer [262]). The oxidation and combustion of methane can give arise to larger, more complex hydrocarbon structures such as ethane, ethylene and acetylene as a result of radical (*e.g.* methyl) recombination reactions [262]. Detailed mechanisms considering the formation and oxidation of these compounds have been formulated (*e.g.* Dagaut *et al.* [63, 64, 67], Gardiner *et al.* [100], Hidaka *et al.* [116, 122], Hunter *et al.* [135], Lindstedt & Skevis [172, 173], Marinov & Malte [180], Richter & Howard [215], Tan *et al.* [239], Volponi & Branch *et al.* [253], Wang & Frenklach [257] and Westbrook *et al.* [264]) under a variety of conditions.

The intermediate hydrocarbon chemistry has received considerable attention. Detailed chemical kinetic mechanisms have been formulated for C_3 hydrocarbons such as propane and propene under a variety of conditions (*e.g.* Atakan *et al.* [6], Cadman *et al.* [36], Dagaut *et al.* [61], Davis *et al.* [70], Heyberger *et al.* [115], Leung & Lindstedt [162], Warnatz [258] and Wilk *et al.* [267, 268]). The oxidation chemistry of butane and butene has been investigated (*e.g.* Chakir *et al.* [44, 45], Dagaut *et al.* [62], Kojima [153], Marinov *et al.* [181], Minetti *et al.* [190], Pitz *et al.* [205] and Warnatz *et al.* [259]) and mechanisms formulated for a broad range of devices including Jet Stirred Reactors, Shock Tubes and Premixed Laminar Flames.

The oxidation and pyrolysis chemistry of larger alkanes such as pentane, hexane and heptane has been the subject of substantial experimental and kinetic modelling analysis (*e.g.* Callahan *et al.* [38], Chakir *et al.* [43, 46],

Curran *et al.* [50, 51], Dagaut *et al.* [57], Glaude *et al.* [102], Ingemarsson *et al.* [139], Lindstedt & Maurice [166], Minetti *et al.* [191], Nehse *et al.* [198], Ribaucour *et al.* [211], Warnatz *et al.* [259] and Westbrook *et al.* [263, 265]). Detailed chemical mechanisms have been formulated for higher order paraffins, particularly n – decane. Bikas & Peters [18] computed the results of their detailed mechanism for a Premixed Laminar Flame and Shock Tube. The detailed mechanism for n – decane oxidation from Bikas and Peters [18] features a low temperature (under 1000 K) mechanism. Zeppieri *et al.* [272] developed a partially reduced skeletal chemical mechansim for the oxidation and pyrolysis of n – decane. The mechanism developed by Zeppieri *et al.* [272] was validated against experimental data from a Turbulent Flow Reactor ($T_{initial}$ = 1019 K, 1060 K, P = 1 atm., ϕ = 1.0), a Jet Stirred Reactor ($T_{initial}$ = 1033 K, P = 1 atm., ϕ = 1.0) and a Shock Tube (P = 3 atm., $T_{initial}$ = 1075 K, ϕ = 2.25). Zeppieri *et al.* [272] report that to simplify the mechanism in their study, it was assumed that the different isomers of a given alkyl radical are in partial equilibrium at each carbon number above the C_4 level result in only a single radical which is then used to represent all the isomers associated with it. The n – decane mechanism from Zeppieri *et al.* [272] is based on previous work on the oxidation of n – heptane.

Lindstedt & Maurice [167] developed an n – decane detailed chemical mechanism featuring 193 chemical species and 1085 elementary reactions. Additionally, the detailed mechanism of Lindstedt & Maurice [167] features isomerisation reactions of the five decyl radicals produced from n – decane oxidation with the rates based on the analogous equivalent for n – heptane [43]. Lindstedt & Maurice [167] comment that the emphasis of their study is on the chemical complexities at flame temperatures (>1000 K). The n – decane mechanism from Lindstedt & Maurice [167] has been validated and verified

against two rich n – decane Stabilized Laminar Premixed Flames. The first experimental data set comprised of a rich ($\phi = 1.7$) 3.2% n – decane/28.6% oxygen/68.2% nitrogen flame from Douté *et al.* [81] at atmospheric pressure. The second experimental data set was obtained from Delfau *et al.* [75] which comprised of a 5.1% n – decane/41.2% oxygen/53.7% argon flame at 0.06 atm. The experimental data sets from Douté *et al.* [81] and Delfau *et al.* [75] both feature major stable and radical species measurements. The calculations using the n – decane mechanism from Lindstedt & Maurice [167] show overall excellent agreement for both experimental data sets from Douté *et al.* [81] and Delfau *et al.* [75]. However, the calculations for the prediction of the H radical in the experimental data set from Delfau *et al.* [75] is under predicted by approximately 70%. Lindstedt & Maurice [167] report that this is due to uncertainties in the temperature profile since in increasing the imposed temperature by 100 K results in an over prediction of the H atom concentration. The results for benzene concentrations [167] are very encouraging in terms of trends when compared to the experimental data sets of Douté *et al.* [81] and Delfau *et al.* [75]. However the peak concentrations for benzene are underpredicted. Lindstedt & Maurice [167] comment that the primary producer for benzene is the propargyl radical recombination reaction which was found to be strongly partially equilibrated hence show a strong sensitivity to the temperature. Lindstedt and Maurice [167] demonstrate this by increasing the temperature profile by 100 K, which resulted in a more accurate concentration profile for benzene. The computations by Bikas & Peters [18] also agree with the experimental data from Douté *et al.* [81] and, interestingly, both studies [18, 167] agree that the primary production channel for benzene is via propargyl recombination reactions.

Nehse & Warnatz [198] developed a detailed chemical mechanism using

an automatic generator, LISP. The detailed mechanism takes into account low temperatures and has been validated against Shock Tube conditions (P = 13 atm., 630 – 1430 K. ϕ = 1.0, 2.0).

More recently, Battin-Leclerc *et al.* [11] developed a detailed chemical mechanism for n – decane focusing on the temperature range 550 – 1600 K, again using a detailed chemical mechanism generator computer package, EXGAS. It is interesting to note that the full detailed mechanism utilised in the study by Battin-Leclerc *et al.* [11] features 7920 reactions (low and high temperature) and 1216 species. The detailed mechanism from Battin-Leclerc *et al.* [11] has been validated under Jet Stirred Reactor ($T_{initial}$ = 922 K, 1030 K for ϕ = 0.2 and ϕ = 1.5 respectively, and T = 550 – 1025 K, ϕ = 1.0) and Stabilized Laminar Flame (ϕ = 1.9) conditions. The detailed n – decane chemical mechansim developed by Battin-Leclerc *et al.* [11] does not predict the experimental data profiles from Delfau *et al.* [75] as accurately as the study by Lindstedt & Maurice [167]. For example, inspection of the primary radical profile concentrations (H and OH) in the work of Battin-Leclerc *et al.* [11] clearly shows poor predictions in terms of magnitude and trends compared to the similar calculations performed by Lindstedt & Maurice [167]. Interestingly, Battin-Leclerc *et al.* [11] report that in the n – decane stabilized laminar premixed flame from Delfau *et al.* [75], the most significant production channel for benzene is via the recombination of propargyl with allyl radicals (68%), with the propargyl recombination route only contributing (32%). In contrast, Lindstedt & Maurice [167] report that the primary channel for benzene formation is via the propargyl recombination route. It should be noted that the predictions for benzene are far more accurate in terms of trends and magnitude in the study by Lindstedt & Maurice [167] than that conducted by Battin-Leclerc *et al.* [11].

The above mentioned n – decane chemical mechanisms all incorporate C - C cleavage of the decyl radicals yielding a a 1-olefin and a smaller alkyl radical. The C - C cleavage is favoured over C - H cleavage due to the lower bond energy [262]. Additionally, the detailed chemical mechanism for n – decane oxidation of Lindstedt & Maurice [167] features isomerisation of the five decyl radicals.

The aromatic component of hydrocarbon fuels is clearly a significant factor when modelling the combustion of practical fuels as outlined in Section 1.2. However, detailed investigations into the combustion of aromatic fuels have surprisingly not been the subject of extensive investigation. Benzene, the simplest of aromatic compounds has been studied experimentally under a variety of conditions including Shock Tubes (Burcat *et al.* [33]), Turbulent Flow Reactors, (Alzueta *et al.* [2], Brezinsky [29], Litzinger [174], Lyon [178] and Venkat *et al.* [252]) Jet Stirred Reactors (Chai & Pfefferle [42] and Ristori *et al.* [217]) and Flames (Bittner & Howard [20] and Shandross *et al.* [229]). Detailed chemical kinetic modelling schemes have been proposed to account for these experimental results (*e.g.* Alzueta *et al.* [2], Emdee *et al.* [89], Lindstedt & Skevis [171], Richter & Howard [215], Ristori *et al.* [217] and Tan & Frank [241]). Toluene has been investigated experimentally in Jet Stirred Reactors, Laminar Flames, Shock Tubes and Turbulent Flow Reactors (Emdee *et al.* [89], Litzinger [174] and Klotz *et al.* [148]), Shock Tubes (Burcat *et al.* [34]), Jet Stirred Reactors (Dagaut *et al.* [56]) and Laminar Flames (Davis *et al.* [69, 71]). Additionally, the pyrolysis of toluene has been investigated under Shock Tube conditions by workers Pamidimukkala *et al.* [199] and Braun–Unkhoff *et al.* [26]. The detailed kinetic modelling of toluene combustion has been attempted by Emdee *et al.* [89], Dagaut *et al.* [56], Klotz *et al.* [148] and Lindstedt & Maurice [168]. The study

of the combustion kinetics of more exotic MSA's such as ethylbenzene and phenylacetylene are not commonly found in any great depth in the literature. Shaddix [226] investigated experimentally the oxidation of phenylacetylene under flow reactor conditions (although there are some uncertainties in the initial conditions as discussed later). Dagaut *et al.* [60] investigated both the experimental and kinetic modelling aspects of n – propylbenzene oxidation under Jet Stirred Reactor conditions. Previously, Litzinger [174] investigated the experimental oxidation of n – propylbenzene, iso – propylbenzene, toluene and ethylbenzene under Turbulent Flow Reactor conditions. Emdee *et al.* [88] studied both the experimental and kinetic modelling of m – and p – xylene and o – xylene [87] under Turbulent Flow Reactor conditions. Emdee *et al.* [88] comment that the combustion chemistry of both m – and p – xylene is similar to that of toluene. Freund & Olmstead [97] studied the pyrolysis of n – butylbenzene in a Shock Tube.

Studies involving the combustion of PAH's are more of a rarity in the literature. Pfahl *et al.* [202] and Shaddix [226] investigated experimentally the oxidation of 1 – methylnaphthalene under Shock Tube and Turbulent Flow Reactor conditions respectively. Pitsch [203] proposed a detailed kinetic mechanism for both of the experimental studies. Additionally, Shaddix [226] studied the oxidation of naphthalene under Turbulent Flow Reactor conditions and Griesheimer & Homann [105] studied a naphthalene/oxygen/argon flame. Laskin & Lifshitz [157] studied both the experimental and kinetic modelling aspects of indene pyrolysis under Shock Tube conditions.

Attempts have been made to model the oxidation of practical fuels. Most recently, Dagaut [52] investigated the oxidation of natural gas, kerosene and diesel fuels. The natural gas fuel model proposed by Dagaut [52] consisted of methane, ethane and propane components and has been validated in a Jet

Stirred Reactor over a temperature range of 1100 – 1250 K, pressure of 1 atm. and a mean residence time of 0.14 s. The detailed natural gas mechanism developed by Dagaut [52] is primarily based upon the GRI 3.0 mechanism developed by Smith *et al.* [234]. In the past, studies such as Juchmann *et al.* [143] and Sick *et al.* [230] have shown that there are mechanistic uncertainties with respect to the oxidation of natural gas. For example, the modelling study by Juchmann *et al.* [143] of a CH_4/O_2 Stabilised Laminar Flame seeded with NO shows that the prediction of the CH_3 radical is $\approx 30\%$ higher than the measurements. Moreover, detailed chemical kinetic mechanisms from Sick *et al.* [230] and Warnatz *et al.* [261] have been applied to CH_4/O_2 Laminar Stabilised Flame seeded with NO by Juchmann *et al.* [143] and shown greater accuracy than the GRI mechanism from Smith *et al.* [234].

The kerosene fuel model proposed by Dagaut [52] consists of n – decane (74%), n – propylbenzene (15%) and propylcyclohexane (11%) in volume and was tested under atmospheric Jet Stirred Reactor conditions over temperature and stoichiometric ranges of 900 – 1300 K and $\phi = 0.5 - 2.0$ and with a residence time of 0.07 s. The diesel fuel model composition proposed by Dagaut [52] contained 0.025% n – hexadecane, 0.017% iso – octane, 0.014% n – propylcyclohexane and 0.0125% n – propylbenzene. The calculations were carried out under atmospheric Jet Stirred Reactor conditions over a temperature range of 1000 – 1250 K for fuel – lean, stoichiometric and fuel – rich conditions ($\phi = 0.5$, 1.0, 1.5). Dagaut [52] comments that the proposed detailed chemical mechansim for diesel fuels is not able to reproduce accurately the experimental data. Furthermore, Dagaut [52] reports that the diesel fuel model may be too simplistic and that the inclusion of PAH's could be necessary.

Lindstedt & Maurice [167] proposed a kerosene model containing n – de-

cane to represent the paraffin component and varied the aromatic component with benzene, toluene, ethylbenzene and ethylbenzene/naphthalene with a surrogate fuel blend consisting of 89% paraffins and 11% aromatics. The detailed chemical mechanism proposed by Lindstedt & Maurice [167] was tested against experimental data from Douté *et al.* [81] which composed of a rich ($\phi = 1.7$) 2.95% kerosene/28.65% oxygen/68.4% nitrogen Stabilised Laminar Flame. The calculations conducted by Lindstedt & Maurice [167] prove that benzene is a poor choice to represent the aromatic component in kerosene fuels and that a more complex structure is required. In contrast, the computations by Lindstedt & Maurice [167] show that the aromatic choices toluene and ethylbenzene can reproduce to a good degree of accuracy the predictions for benzene in the kerosene/oxygen/nitrogen Stabilised Laminar Flame from Douté *et al.* [81]. Lindstedt & Maurice [167] also report that the choice of aromatic component surprisingly does not affect the combustion chemistry of the paraffin component for surrogate fuel blends even though both components will obviously share the same radical pool. This argument is further reinforced in the current study. Additionally, Douté *et al.* [81] and Vovelle *et al.* [254] report of the similarities in the chemical flame structures of n – decane and kerosene flames.

Vovelle *et al.* [254] investigated experimentally the formation of aromatic compounds in n – decane and kerosene in a Stabilised Laminar Flame for rich ($\phi = 2.2$) conditions. The kerosene fuel blend was postulated to be composed of n – decane (90%) and toluene (10%). Vovelle *et al.* [254] report that the concentration of benzene is greater in the kerosene flame than in the n – decane flame. Vovelle *et al.* [254] comment that the aromatic hydrocarbons for n – decane are formed from acetylene whereas for the kerosene flame, the aromatic hydrocarbons are primarily formed from the aromatic component

of the fuel.

Dagaut *et al.* [58] investigated experimentally the oxidation of kerosene fuel in a Jet Stirred Reactor for a wide range of conditions covering low and high temperatures (550 – 1150 K, 10 – 40 atm., $\phi = 0.1 - 1.5$) with a mean residence time of 0.5 – 2.0 s. In this study, Dagaut *et al.* [58] identified a low temperature region (550 – 750 K) and observed a negative temperature coefficient behaviour. Above 750 K, Dagaut *et al.* [58] reported a rapid production of carbon monoxide and carbon dioxide as well as other saturated and unsaturated hydrocarbons indicating that the high temperature regime had been reached. A previous experimental and chemical kinetic modelling study by Dagaut *et al.* [59] on the oxidation of kerosene was performed in a Jet Stirred Reactor for the high temperature region (750 – 1150 K) over a pressure range of 10 – 40 atm. The focus of the work was on the paraffin component of the kerosene fuel blend (n – decane) as Dagaut *et al.* [59] report that Gureét *et al.* [107] developed a quasi–global model to reproduce the concentration profiles of the major chemical species for surrogate kerosene fuel blends. Dagaut *et al.* [59] comment that the validity of such quasi–global mechanisms cannot be extended to the whole operating conditions of engines and conclude that n – decane can reproduce most of the experimental data from the kerosene fuel. Nevertheless, an aromatic component must be considered to correctly predict the high concentrations of alkyl – substituted aromatics.

The detailed aromatic chemical mechanism developed in the present work features 1896 reactions and 324 species. The full detailed chemical mechanism takes into account both paraffin and aromatic components that constitute a typical sample of diesel fuel including MSA molecules (*e.g.* toluene, styrene) and PAH's (*e.g.* naphthalene, indene). The mechanism is based on

the previous modelling of simpler fuels by Lindstedt & Skevis [171], Leung & Lindstedt [162], Lindstedt & Maurice [166], Leung [161], Lindstedt & Skevis [172] and Lindstedt & Maurice [168]. A partial summary of earlier work is provided by Maurice [182]. Additionally, a low temperature detailed mechanism is included in this detailed reaction scheme developed by Rizos [218] for the smaller hydrocarbon compounds. The rate parameters not found in the literature have been based on analogous equivalent reactions with appropriate adjustments for collision frequencies and thermochemistry. A full listing can be found in Appendix A with a thorough discussion of reactions and reaction rate parameters found in the subsequent chapters. All reactions are treated as reversible, with the kinetic data for the reverse reactions evaluated from chemical equilibrium constants. The thermodynamic data for each species considered was obtained, when possible, from the literature (*e.g.* Burcat [32], Dagaut *et al.* [60], Kee *et al.* [144], Reid *et al.* [210], Richter & Howard [215], Rossini *et al.* [222] and Stull *et al.* [238]) with a full listing in Appendix B. However, for some species it was necassary to estimate the thermodynamic data using Benson's additivity method [16]. The estimation of thermodynamic data can sometimes lead to considerable uncertainties for certain reaction rates and caution is required in such cases.

1.4.2 Mathematical Model

The present procedure for detailed mechanism validation and verification involves a comparison of the calculations produced from the detailed chemical kinetic model with experimental measurements of primary, intermediate and free radical species concentrations. Reviews of the fundamentals of chemical kinetic modelling may be found in the literature (*e.g.* Cathonnet [41], Miller *et al.* [189] and Westbrook and Dryer [262]) with only a summary given

here.

As mentioned earlier, the process of mechanism validation and verification involves the comparison of calculated data against experimental measurements. Ideally, the validation and verification process should be carried out using experimental data from a variety of conditions and from several investigators. Unfortunately, in some published work this is not the case. Many detailed mechanisms have been produced with the calculations being compared to just one experimental case, and in the extreme the author(s) have modified the rates for individual reactions just to fit the data for that specific case. This can lead to inconclusive results such as missing elementary reaction steps or an incorrect reaction mechanism. Optimization based approaches featuring adjustment only within accepted uncertainty limits can guard against the latter only.

The validation and verification procedure is illustrated in Figure 1.7. Such a procedure involves iterative calculations with simple single point homogeneous systems such as Shock Tubes to 1 – D systems such as Stabilised Laminar Flames.

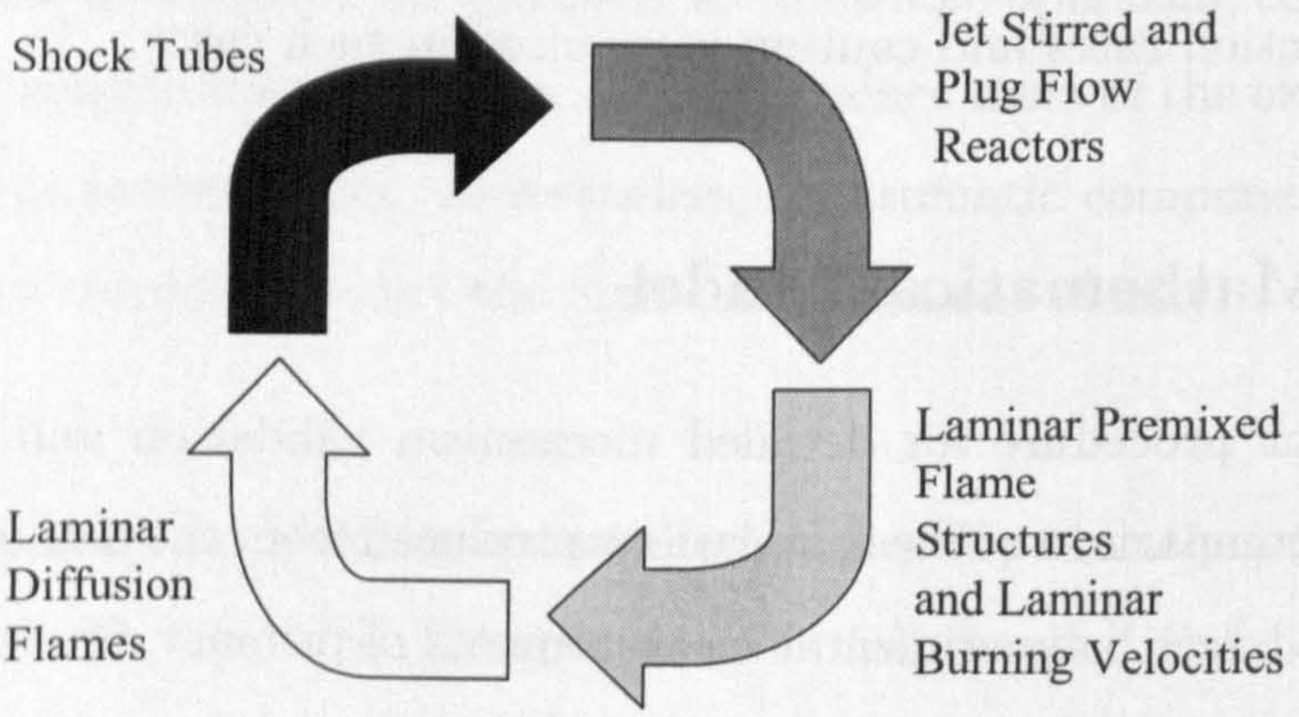


Figure 1.7: Detailed chemical mechanism validation and verification procedure [182].

In this study, only spatially homogeneous systems are considered (Shock Tubes, Turbulent Flow and Jet Stirred Reactors) as in Figure 1.7 with a summary of the physical characteristics given here. The more complicated systems which consider the transport of heat and mass, (Laminar Diffusion Flames, Freely Propagating and Stabilised Flames) are discussed elsewhere in the literature (*e.g.* Meyer [187], Miller *et al.* [189], Skevis [231], Warnatz *et al.* [260] and Westbrook & Dryer [262]).

The fundamental governing equations for the spatially homogeneous devices are readily derived from the Navier – Stokes equation found in texts such as Bird *et al.* [19] and Kuo [156]. However, the experimental devices require specific boundary conditions which have been discussed in detail by Jones & Lindstedt [141, 142] and Miller *et al.* [189].

Jet Stirred Reactors operate under highly turbulent conditions to enhance mixing of the reactants with the products to produce uniform conditions within the reactor. Moreover, in the modelling of a Jet Stirred Reactor, the mixing of the reactants is assumed to be instantaneous. Thus the reaction region may be assumed to be spatially homogeneous and hence diffusion effects can be ignored. Typical operating temperatures for a Jet Stirred Reactor are less than 1200 K and pressures of 1 – 10 atm. [189, 262]. The governing equations for the Jet Stirred Reactor are,

Conservation of Species

$$\frac{dY_k}{dt} = \frac{1}{\tau}\left(Y_k^* - Y_k\right) + \frac{R_k M_k}{\rho} \tag{1.2}$$

Conservation of Enthalpy

$$\frac{dh}{dt} = \frac{1}{\tau}\sum_{k=1}^{n_{sp}} Y_k^*\left(h_k^* - h_k\right) - \frac{1}{\rho}\sum_{k=1}^{n_{sp}} h_k R_k M_k \tag{1.3}$$

Species Source Term

$$R_k = \sum_{k=1}^{n_{reac}} \Xi_{jk} \left(k_j^f \prod_{i=1}^{n_{sp}} \phi_i{}^{\xi_{ji}^f} - k_j^r \prod_{i=1}^{n_{sp}} \phi_i{}^{\xi_{ji}^r} \right) \tag{1.4}$$

with time as the single independent variable. In the above equations, ρ represents the fluid density, h the mixture enthalpy, h_k is the specific enthalpy of species k , Y_k and M_k are the mass fraction and the molar mass of species k respectively. The subscript * indicates inlet conditions and τ is the mean residence time defined by

$$\tau = \frac{\rho V_R}{m} \tag{1.5}$$

with V_R the reactor volume, and m the mass flow rate through the reactor. The terms in the *Species Source Term* are: Ξ is the stoichiometric coefficient for species k in reaction j , ϕ is the molar concentration of species i , k^f and k^r are the forward and reverse rate constants for reaction j and ξ is the concentration dependence for species i in reaction j .

Turbulent Flow Reactors are characterized by high flow rates with negligible recirculation. The complete and rapid mixing of the fuel and oxidizer takes place at the inlet end of the reactor. Combustion typically takes place at atmospheric pressure over a temperature range of 900 – 1300 K. A major advantage of using a Turbulent Flow Reactor is the fact that the primary fuel is spread over a comparatively large region, typically 1 m making experimental access by optical or sampling techniques convenient. Due to the high flow rates in a Turbulent Flow Reactor, the time scales for mass and energy diffusion in the reactor are much larger than the residence time of the mixture, hence τ can be considered infinite [189, 262]. It follows that, the equations for the Turbulent Flow Reactor may be cast in the form,

Conservation of Species

$$\frac{dY_k}{dt} = \frac{R_k M_k}{\rho} \tag{1.6}$$

Conservation of Enthalpy

$$\frac{dh}{dt} = -\frac{1}{\rho}\sum_{k=1}^{n_{sp}} h_k R_k M_k \tag{1.7}$$

where the terms are described above as for the Jet Stirred Reactor.

Shock Tubes are a useful tool for studying combustion since they provide an insight into the initial stages of combustion. Hence, reactions such as molecular oxygen attack and thermal decomposition, which initiates the radical pool, can be investigated in detail via Shock Tube studies. Usually, experiments conducted in a Shock Tube are carried out at elevated temperatures and high pressures which can create difficulties in taking accurate measurements [262]. The equations solved for a Shock Tube are identical to that of the Turbulent Flow Reactor as discussed above.

1.5 The Present Contribution

The primary objective of this work is to develop, validate and verify a detailed chemical mechanism that can be used to accurately predict the oxidation of propulsive fuels for a wide range of conditions. Moreover, due to the vast variety of hydrocarbons found in practical fuels, a range of components are investigated. Additionally, the formation of PAH is analysed as a consequence of the environmental impact resulting from the usage of burning hydrocarbon fuels.

1.6 Outline of Thesis

The remainder of this study is divided up into five chapters; Chapter 2 focuses on the consolidation of the toluene sub – mechanism, previously investigated by Maurice and Lindstedt & Maurice [168] over a wide range of conditions. A delineation of the chemical reaction pathways is included along with a discussion of the rate parameters applied. The aromatic component m – xylene is also investigated under Turbulent Flow Reactor conditions.

Chapter 3 explores a sub – mechanism developed for PAH formation under intermediate temperatures. The formation of the three ringed structures anthracene, phenanthrene and acenaphthalene are investigated under Turbulent Flow Reactor conditions. Additionally, sub – mechanisms for phenylacetylene and n – propylbenzene are investigated, with a delineation of the chemical reaction pathways is included along with a discussion of the rate parameters applied.

Chapter 4 focuses on the oxidation of the PAH component found in diesel fuels, typically 1 – methylnaphthalene. This fuel component is studied for a variety of stoichiometric and experimental conditions; Jet Stirred Reactor, Turbulent Flow Reactor and Shock Tube. A delineation of the chemical reaction pathways is included along with a discussion of the rate parameters applied. Further, for mechanism validation and verification, the oxidation of naphthalene is investigated as it proves to be a significant primary intermediates during the combustion of 1 – methylnaphthalene.

Chapter 5 focuses on the combustion chemistry of kerosene fuels, which as discussed earlier, may have its components divided up into two categories, paraffins and alkyl – substituted aromatics. The kerosene model used here considers n – decane as the paraffin component whilst ethylbenzene and n – propylbenzene are used as the two alkyl – substituted aromatics.

Finally, conclusions of the present work are drawn with proposals for future work being recommended is given in Chapter 6.

Chapter 2

Toluene and m – Xylene

2.1 Introduction

Toluene is a significant constituent in practical fuels and is also readily formed from the oxidation of other hydrocarbons and commercial fuels. The present chapter consolidates the toluene sub – mechanism developed by Lindstedt & Maurice [168] and Maurice [182] by taking into account new kinetic data and a wider range of conditions. A path analysis is given and the major reaction channels outlined. A detailed sub – mechanism for m – xylene is subsequently developed from this basis.

2.2 A Detailed Mechanism for Toluene Combustion

Over the last few years, several experimental and numerical studies have reported results on the chemistry of toluene. The thermal decomposition has been investigated experimentally by Braun–Unkhoff *et al.* [26] and Pamidimukkala *et al.* [199]. The initial toluene concentrations and tem-

peratures in the experiments of Braun–Unkhoff *et al.* [26] ranged from 2 – 19 ppm and 1500 to 1700 K, while Pamidimukkala *et al.* [199] used an initial toluene concentration of 18000 ppm and varied the temperature between 1600 and 2100 K. Lindstedt & Maurice [168] have shown that the branching between the thermal decomposition reactions involving C – H and C – C cleavage, initially has a ratio of 3:1. Emdee *et al.* [89], Litzinger [174] and more recently Klotz *et al.* [148] studied the oxidation of toluene for temperatures around 1170 K in a Turbulent Flow Reactor for a variety of stoichiometries. Burcat *et al.* [34] investigated the oxidation of toluene in a Shock Tube over the temperature range 1300 – 1800 K for a variety of pressures and stoichiometric ratios. Recently, Dagaut *et al.* [56] studied the oxidation of toluene in a Jet Stirred Reactor over a temperature range of 1000 – 1350 K and for a range of stoichiometries (ϕ = 0.5, 1.0 and 1.5). Other studies of toluene oxidation include the work by Davis *et al.* [69, 71] who investigated toluene laminar burning velocities. A number of detailed chemical kinetic schemes have been constructed to model the combustion of toluene with varying degrees of success (*e.g.* Dagaut *et al.* [56], Emdee *et al.* [89], Klotz [148] and Lindstedt & Maurice [168]). The studies have shown that there are still many uncertainties and these are reviewed in the following sections.

2.2.1 The Pyrolysis of Toluene

The pyrolysis of toluene is considered under the experimental conditions of Braun–Unkhoff *et al.* [26] and Pamidimukkala *et al.* [199] in order to evaluate the branching ratio of reactions (1076) and (1077). Lindstedt & Maurice [168] previously explained these data sets and the topic is revisited as a result of other mechanistic changes.

$$C_7H_8 = C_6H_5 + CH_3 \quad (1076)$$

$$C_7H_8 = C_7H_7 + H \quad (1077)$$

Braun–Unkhoff *et al.* [26] measured the H radical concentrations as a function of time in argon mixtures containing 2.8 – 19.3 ppm of toluene, over a temperature range of 1555 – 1655 K and a pressure range of 1.86 – 1.89 atm. Pamidimukkala *et al.* [199] reported the time evolution of the stable species (CH_4, C_2H_2 and C_4H_2) in toluene – neon mixtures at a temperature of 1832 K and a pressure of 0.34 atm. The initial conditions for both pyrolysis experiments are summarized in Table 2.1

Table 2.1: Summary of the Initial Conditions for the Pyrolysis of Toluene in a Shock Tube

$[C_7H_8]$ ppm	T [K]	P [atm.]	Bath Gas	Source
2.8	1655	1.86	Ar	[26]
19.3	1555	1.89	Ar	[26]
18000.0	1832	0.34	Ne	[199]

The calculations for the H radical concentration profiles are shown in Figure 2.1. The profile for the H radical is well predicted for the 1655 K case as is the initial growth of H radicals in the 1555 K case. However, at later times (≥ 200 μs), the peak concentrations of the H radicals are under predicted as is evident in Figure 2.1. It is found that, in addition H attack on the fuel which contributes approximately 30 %, reactions (925) and (926)

$$C_6H_5 + H = C_6H_4 + H_2 \quad (925)$$

$$C_6H_5 + H = C_6H_6 \quad (926)$$

are the dominant reactions in consuming H radicals for T $\geq$ 200 μs contributing 25 % and 15 % respectively. The rate for reaction (925) stems from the work of Leung & Lindstedt [162]. The rate parameters for reaction (926) is obtained from Baulch *et al.* [13] as reported by Leung & Lindstedt [162]. It was found that a reduction in the frequency factor by a factor of 5 for reactions (925) and (926) significantly improved the results. However, such changes lead to difficulties in other systems. For example, in benzene flames reasonable levels of C_6H_4 are observed [218] and independent determination of the rates are necessary.

The study of CH_3 concentration profiles can delineate the rate parameters for the reaction involving C – C cleavage of the methyl group from the ring.

$$C_7H_8 \quad = \quad C_6H_5 + CH_3 \tag{1076}$$

However, direct measurements of CH_3 concentrations are presently not available. Nevertheless, it is possible to indirectly validate the branching ratio of the thermal decomposition reactions of toluene, by comparison with the experiments of Pamidimukkala *et al.* [199]. The detailed chemical kinetic mechanism in this study reproduces the concentration profiles of CH_4, C_2H_2 and C_2H_4 very well as is shown in Figure 2.2.

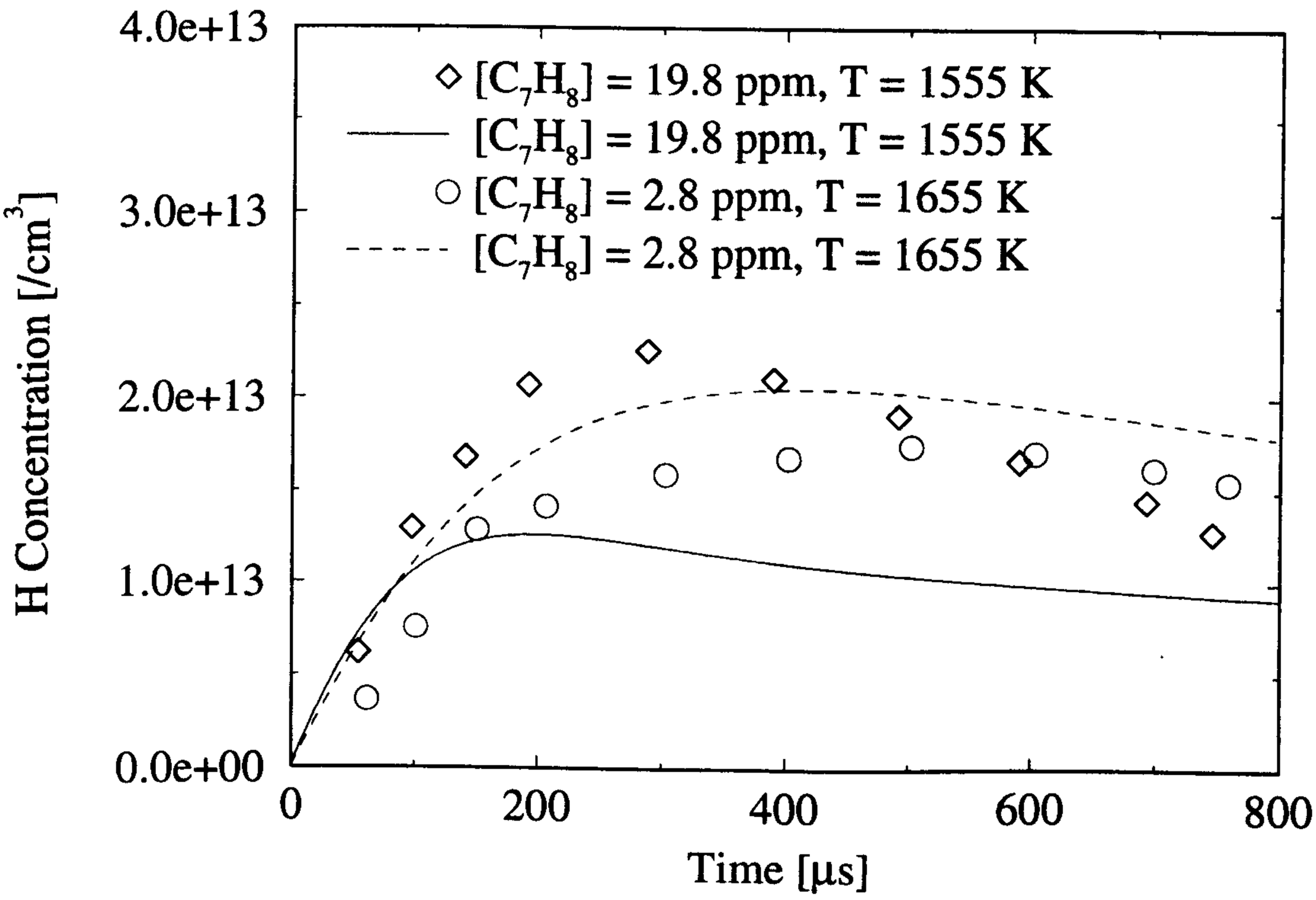


Figure 2.1: Graph of H radical profile concentrations versus time for the pyrolysis of toluene in a Shock Tube. Experimental points are from Braun–Unkhoff *et al.* [26]. Lines are the computations from the detailed chemical mechanism.

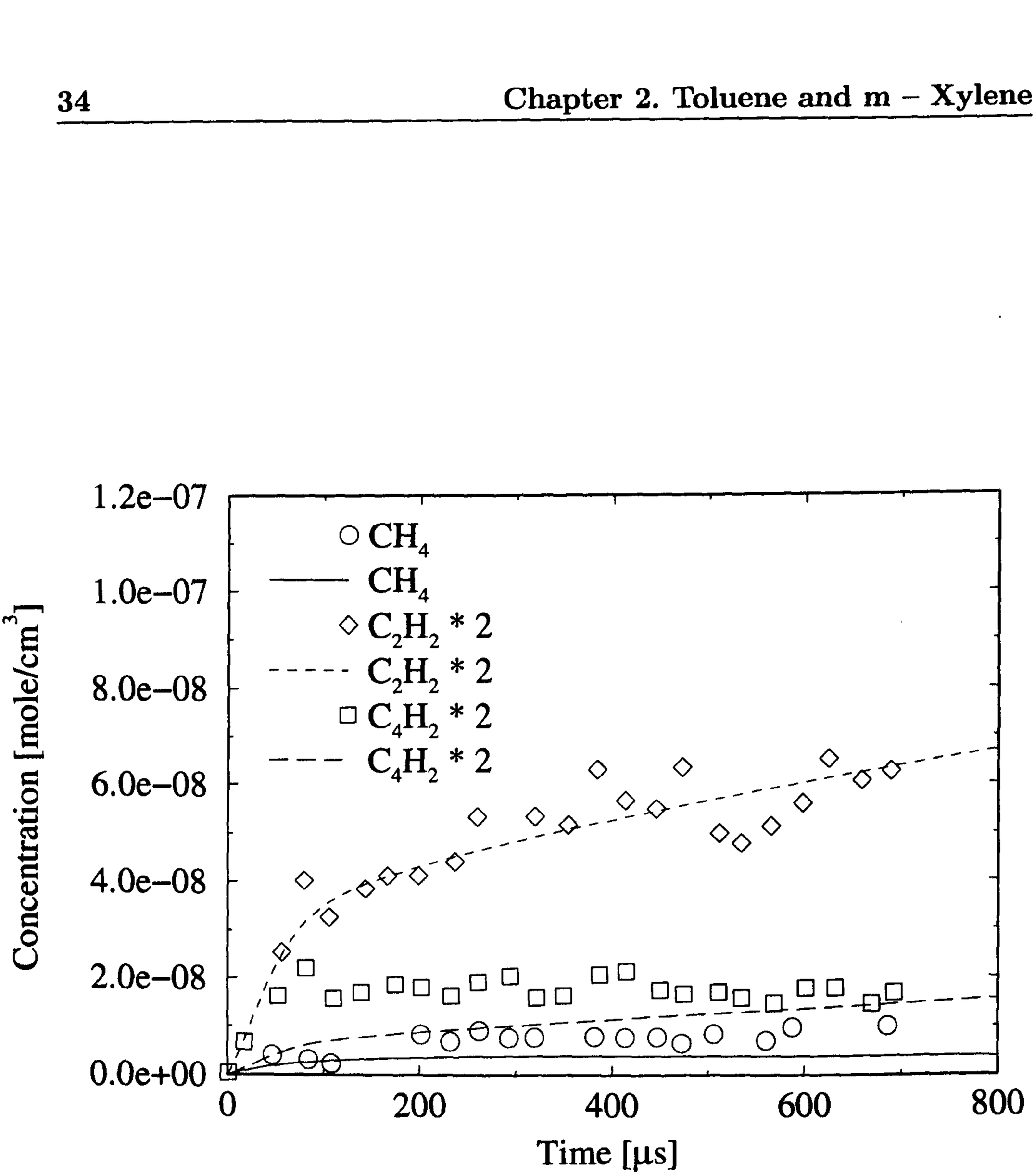


Figure 2.2: Graph of intermediate species concentration profiles versus time for the pyrolysis of toluene in a Shock Tube. Experimental points are from Pamidimukkala *et al.* [199]. Lines are the computations from the detailed chemical mechanism.

Primary Reaction Paths for the Pyrolysis of Toluene

The initial temporal evolution of the H radical concentration in the experiments of Braun–Unkhoff *et al.* [26] is strictly controlled by the C – H decomposition reaction from the methyl group (1077).

$$C_7H_8 \quad = \quad C_7H_7 + H \qquad (1077)$$

The rate adopted in this study for toluene thermal decomposition via C – H cleavage is a linear fit of experimental data (Astholz *et al.* [5], Brand *et al.* [25], Braun–Unkhoff *et al.* [26], Brooks *et al.* [30], Brouwer *et al.* [31], Hippler & Troe [127] and Muller-Markgraf & Troe [196]) as reported by Lindstedt & Maurice [168]. The formation of H radicals in the latter stages stems from the decomposition of benzyl radicals as well as other additional fragments. Reactions (1049), (1069) and (1077) summarize the primary H radical formation paths.

$$C_7H_7 \quad = \quad C_7H_7L \qquad (1049)$$

$$C_7H_7L \quad = \quad C_7H_6 + H \qquad (1069)$$

$$C_7H_8 \quad = \quad C_7H_7 + H \qquad (1077)$$

The reaction rate parameters for reactions (1049) and (1069) have been adopted from the study by Braun–Unkhoff *et al.* [27] of the thermal decomposition of benzyl radicals. Reactions (1049) and (1069) were proposed by Braun–Unkhoff *et al.* [27] from the analogous linearisation of the phenyl ring to explain the rapid formation of H radical atoms from benzyl molecules.

The initial ($\sim 1\ \mu$s) decomposition of toluene in the Shock Tube pyrolysis experiment of Pamidimukkala *et al.* [199] involves thermal decomposition via C – H cleavage and C – C cleavage (1076) and (1077).

$$C_7H_8 = C_6H_5 + CH_3 \quad (1076)$$

$$C_7H_8 = C_7H_7 + H \quad (1077)$$

It is found that the branching ratio between reactions (1076) and (1077) is 1:3 as also reported by Lindstedt & Maurice [168]. The rate parameters assigned to reaction (1076) are obtained from Pamidimukkala *et al.* [199] who investigated the pyrolysis of toluene over temperature and pressure ranges of 1550 – 2200 K and 0.2 – 0.5 atm. Pamidimukkala *et al.* [199] comment that the energy barrier for reaction (1076) is unusually low. The activation energy derived for this reaction is 303.9 kJ/mol, much lower than the heat of reaction (428.2 kJ/mol). Pamidimukkala *et al.* [199] used RRKM analysis to argue that it may be acceptable to use such a low energy barrier [199]. Rao & Skinner [208] have proposed rate constant parameters for reaction (1076) via measurements under Shock Tube conditions over a temperature range of 1450 – 1790 K and at a pressure of $\sim$ 0.4 atm. Pamidimukkala *et al.* [199] report that the use of the rate parameters from Rao & Skinner [208] in their toluene pyrolysis experiment, resulted in an under prediction of CH_4 by approximately a factor of 2. There are obvious discrepancies for the rate parameters for reaction (1076) and the associated problems are discussed below.

The formation of C_2H_2 from toluene is via the channel $C_7H_8 \rightarrow CH_3 \rightarrow C_2H_6 \rightarrow C_2H_5 \rightarrow C_2H_4 \rightarrow C_2H_3 \rightarrow C_2H_2$ and the formation of C_4H_2 is primarily from C_6H_5 linearising to C_6H_5(B) via reaction (924)

$$C_6H_5 = C_6H_5(B) \quad (924)$$

followed by thermal decomposition via C – C cleavage (950)

$$C_6H_5(B) = C_4H_3(I) + C_2H_2 \quad (950)$$

Diacetylene is formed from $C_4H_3(I)$ via reaction (522)

$$C_4H_3(I) + H \quad = \quad C_4H_2 + H_2 \tag{522}$$

The rates for the reactions discussed above have been thoroughly analysed in the study by Rizos [218].

2.2.2 The Oxidation of Toluene

The data sets used to validate and verify the toluene sub – mechanism under atmospheric Jet Stirred Reactor conditions have been obtained from Dagaut *et al.* [56]. The conditions considered here corresponds to $\phi = 0.5$ and 1.5 over an overall temperature range of 1000 – 1380 K and mean residence times of $\tau = 70$ and 120 ms respectively. Table 2.2 summarizes the initial conditions.

Table 2.2: Summary of the Initial Conditions for the Oxidation of Toluene in a Jet Stirred Reactor

Fuel	ϕ	T_0 [K]	Mean Residence Time [ms]	Pressure [atm.]
C_7H_8	0.5	1000 – 1300	70	1.0
C_7H_8	1.5	1080 – 1380	120	1.0

Overall the initial calculations using the detailed chemical mechanism agrees well with the experimental data from Dagaut *et al.* [56] as is illustrated in Figures 2.3 – 2.12. For the lean case ($\phi = 0.5$) ignition clearly occurs at approximately 1240 K as is evident in Figure 2.3. The sharp drop in the molecular oxygen concentration profile corresponds to a sharp rise in

the carbon dioxide concentration profile. The effect is captured by the computations. The fuel decay profile is perhaps too rapid at temperatures $\geq$ 1120 K. It is found that reaction (1079)

$$C_7H_8 + H \quad = \quad C_7H_7 + H_2 \tag{1079}$$

is the dominant channel in the fuel consumption at higher temperatures. The rate adopted for reaction (1079) is obtained from Baulch *et al.* [13] and follows an extensive literature survey. By contrast the detailed chemical kinetic sub – mechanisms for toluene oxidation by Dagaut *et al.* [56] and Emdee *et al.* [89] feature the rate parameters recommended by Hippler *et al.* [125]. It is found that at 1200 K, the rate recommended by Baulch *et al.* [13] is 10 % faster than that of Hippler *et al.* [125].

The generation of H radicals, which lead to H attack on the fuel (1079), is partly via ($\sim$ 10 %) by O ring substitution (1083).

$$C_7H_8 + O \quad = \quad OC_7H_7 + H \tag{1083}$$

The product of reaction (1083) eventually leads to C_6H_6 (this will be discussed in more detail in the path analysis section) which is somewhat over predicted as is evident in Figures 2.5 and 2.10 for the lean ($\phi = 0.5$) and rich ($\phi = 1.5$) cases respectively. It is found that this channel is the primary C_6H_6 formation channel ($\sim$ 40 %). The rate for reaction (1083) has been adopted from Hoffmann *et al.* [129] who considered a temperature range of 1100 – 1350 K at a pressure of 300 Pa. The over prediction of C_6H_6 may additionally stem from the somewhat too rapid fuel consumption.

The calculated concentration profiles for C_7H_6O are over predicted in both the lean ($\phi = 0.5$) and rich ($\phi = 1.5$) cases as is evident in Figures 2.5 and 2.10 respectively. It is found that for both the lean and the rich cases, the primary channel at 1160 K is reaction (1113).

$$C_7H_7O \quad = \quad C_7H_6O + H \qquad (1113)$$

The rate for reaction (1113) was estimated on the heat of reaction (~ 64 kJ/mol) plus an additional 4 kJ/mol and a frequency factor of 3.0E+12 m^3 $kmol^{-1}$ s^{-1} as recommended by Dean [73]. It is interesting to note that the detailed chemical mechanism of Dagaut *et al.* [56] features a rate expression, recommended by Brezinsky *et al.* [28], with a very high frequency factor (A = 1.3E+14 m^3 $kmol^{-1}$ s^{-1}) and very low barrier (E = 4.6 kJ/mol).

The computations reproduce C_8H_{10} well in terms of trends and magnitudes for both the lean ($\phi = 0.5$) and rich ($\phi = 1.5$) cases as is evident in Figures 2.5 and 2.10 respectively. It is found that the dominant channel for C_8H_{10} production in both the lean ($\phi = 0.5$) and rich ($\phi = 1.5$) cases is via C_7H_7 and CH_3 radical recombination (1061).

$$C_7H_7 + CH_3 \quad = \quad C_8H_{10} \qquad (1061)$$

The rate for reaction (1061) has been obtained from Maurice [182].

The levels of C_5H_6 are over predicted in both the lean ($\phi = 0.5$) and rich ($\phi = 1.5$) cases as is evident in Figures 2.6 and 2.11 respectively. The addition of H atoms onto the C_5H_5 ring (810),

$$C_5H_6 \quad = \quad C_5H_5 + H \qquad (810)$$

is the primary producer of C_5H_6 under both lean ($\phi = 0.5$) and rich ($\phi = 1.5$) conditions. The rate adopted for this reaction is obtained from Roy *et al.* [224] who studied the thermal decomposition via C – H cleavage (810) in a Shock Tube over temperature and pressure ranges of 1200 – 1600 K and 1 – 5 atm., respectively. A more in depth analysis of this reaction may be found in the study by Rizos [218]. In the study by Emdee *et al.* [89],

reaction (810) was written in reverse with an estimated frequency factor of 1.0E+11 m^3 $kmol^{-1}$ s^{-1}.

The predictions for CH_4 are in good agreement as shown in Figures 2.4 and 2.9. The high concentrations of CH_4 would indicate a direct route of formation from the fuel via the CH_3 radical and the primary CH_4 channel in the lean case is via H addition to methyl (61).

$$CH_3 + H = CH_4 \quad (61)$$

The rate for reaction (61) stems from the work of Baulch *et al.* [13].

For the rich case, the most significant channel (70 %) for CH_4 production is found to be CH_3 attack on the fuel leading to CH_4 and C_7H_7 (1094).

$$C_7H_8 + CH_3 = CH_4 + C_7H_7 \quad (1094)$$

The rate used for reaction (1094) has been adopted from Colket *et al.* [48]. Other primary channels for CH_4 formation is via reactions (78) and (1095) ($\sim$ 10 % each).

$$CH_4 + H = CH_3 + H_2 \quad (78)$$

$$C_7H_8 + CH_3 = C_7H_7P + CH_4 \quad (1095)$$

The rate for reaction (78) has been determined by Rabinowitz *et al.* [207] over a temperature and pressure range of 897 – 1729 K and 2000 – 4000 Pa using argon as a bath gas. The rate for reaction (1095) has been adopted from Colket *et al.* [48] as reported by Lindstedt & Maurice [168].

For temperatures $\geq$ 1220 K in the lean ($\phi = 0.5$) and 1260 K in the rich ($\phi = 1.5$) mixtures the prediction becomes poor for CH_4 as is evident in Figures 2.4 and 2.9. It is found that in both the lean and rich cases, the most significant reaction consuming CH_4 is via OH attack (80).

$$CH_4 + OH \quad = \quad CH_3 + H_2O \tag{80}$$

The rate for reaction (80) has been adopted from Baulch *et al.* [13] and a more detailed literature review of the rate parameters concerning the oxidation CH_4 can be found elsewhere (Rizos [218]).

The concentrations of C_2H_2 are reproduced well as shown in Figures 2.4 and 2.9. In both cases, the primary channel for C_2H_2 is the thermal decomposition of C_5H_5 radicals (787).

$$C_5H_5 + M \quad = \quad C_3H_3 + C_2H_2 + M \tag{787}$$

The rate for reaction (787) has been adopted from Ikeda *et al.* [138]. It is interesting to note that in the work of Dagaut *et al.* [56] the primary route for C_2H_2 is via C_2H_3 and that concentrations of C_2H_2 are heavily over predicted at lower temperatures.

The detailed chemical kinetic mechanism from Dagaut *et al.* [56] features the rate parameters as recommended by Emdee *et al.* [89] for the C – C cleavage of the CH_3 group from toluene yielding C_6H_5 and CH_3 (1076).

$$C_7H_8 \quad = \quad C_6H_5 + CH_3 \tag{1076}$$

Emdee *et al.* [89] adopted the expression from Rao & Skinner [208]. It is interesting to note that concentration profiles for CH_4, C_2H_6 and C_2H_4 are under predicted for lean conditions by Dagaut *et al.* [56]. A reaction route for the formation of these species is $C_7H_8 \rightarrow CH_3 \rightarrow C_2H_6 \rightarrow C_2H_5 \rightarrow C_2H_4$, which indicates the significance of reaction (1076).

Concentrations of C_4 species, (*e.g.* C_4H_6(T) and C_4H_4) are reproduced with a good level of accuracy as is evident in Figures 2.6 – 2.7 and Figures 2.11 – 2.12 for the lean and rich cases respectively. It is found that the primary route to C_4H_4 is via thermal decomposition of the C_5H_4O radical (900).

$$C_5H_4O = C_4H_4 + CO \quad (900)$$

The rate parameters assigned to reaction (900) has been obtained from Dagaut *et al.* [56] with the rate decreased by a factor of 4. The production of $C_4H_6(T)$ is primarily produced from the addition OH on the C_5 ring, followed by decomposition (794)

$$C_5H_5 + OH = C_4H_6(T) + CO \quad (794)$$

The rate for reaction (794) has also been adopted from Dagaut *et al.* [56].

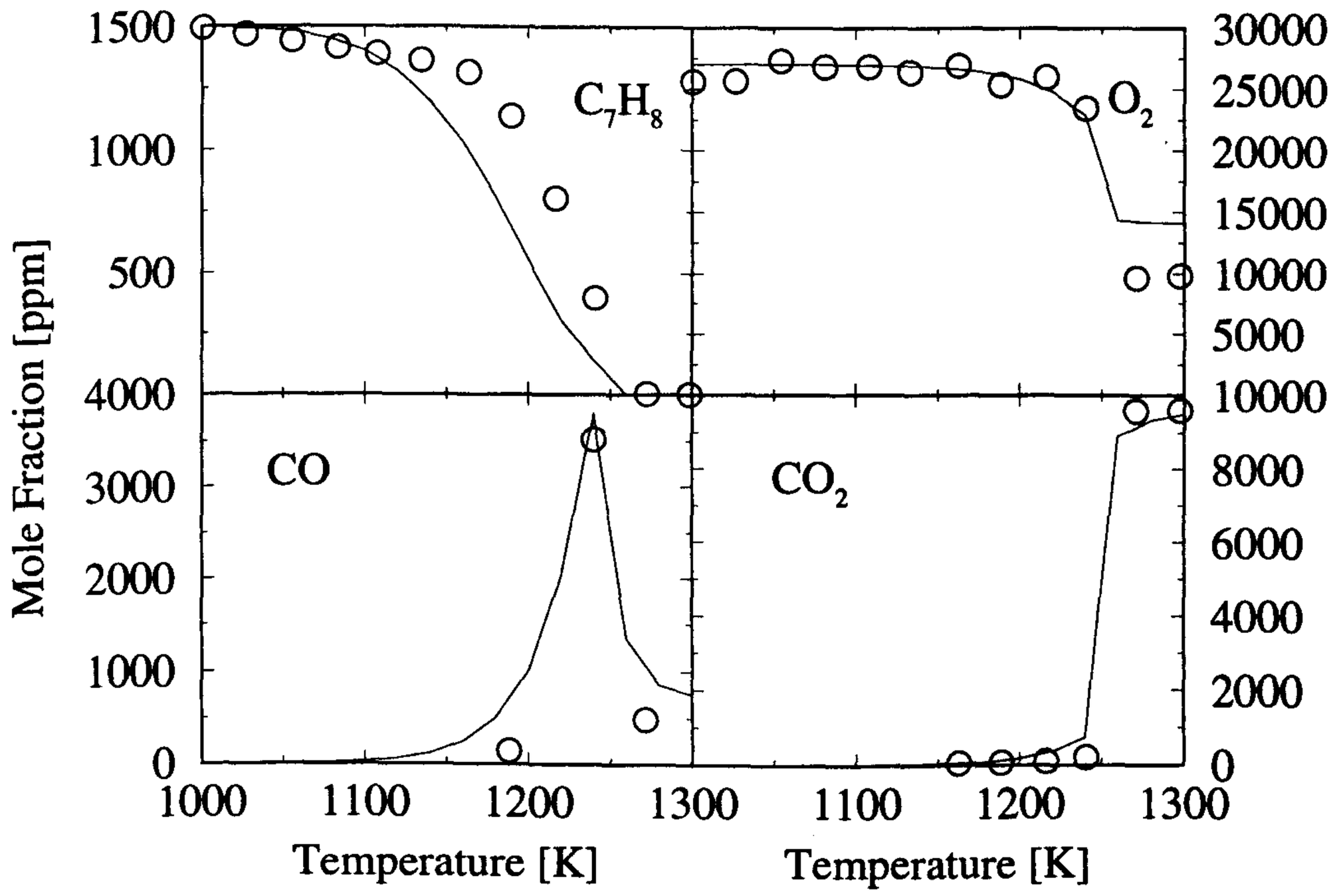


Figure 2.3: Graph of species profile concentrations versus temperature for the oxidation of toluene in a Jet Stirred Reactor. Experimental points are from Dagaut *et al.* [56] for a stoichiometry of $\phi = 0.5$. Solid lines are the computations from the detailed chemical mechanism.

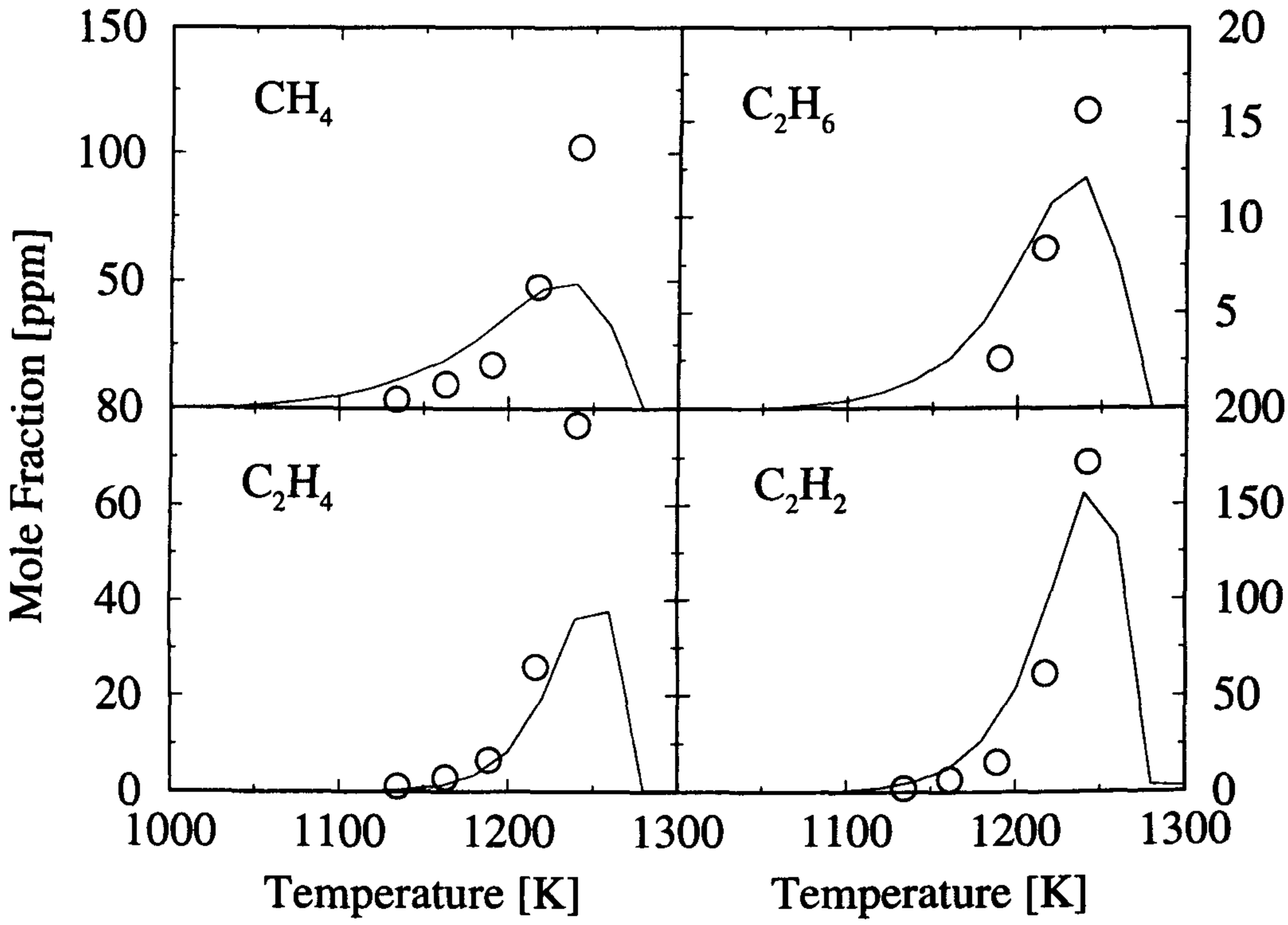


Figure 2.4: Graph of species profile concentrations versus temperature for the oxidation of toluene in a Jet Stirred Reactor. Experimental points are from Dagaut *et al.* [56] for a stoichiometry of $\phi = 0.5$. Solid lines are the computations from the detailed chemical mechanism.

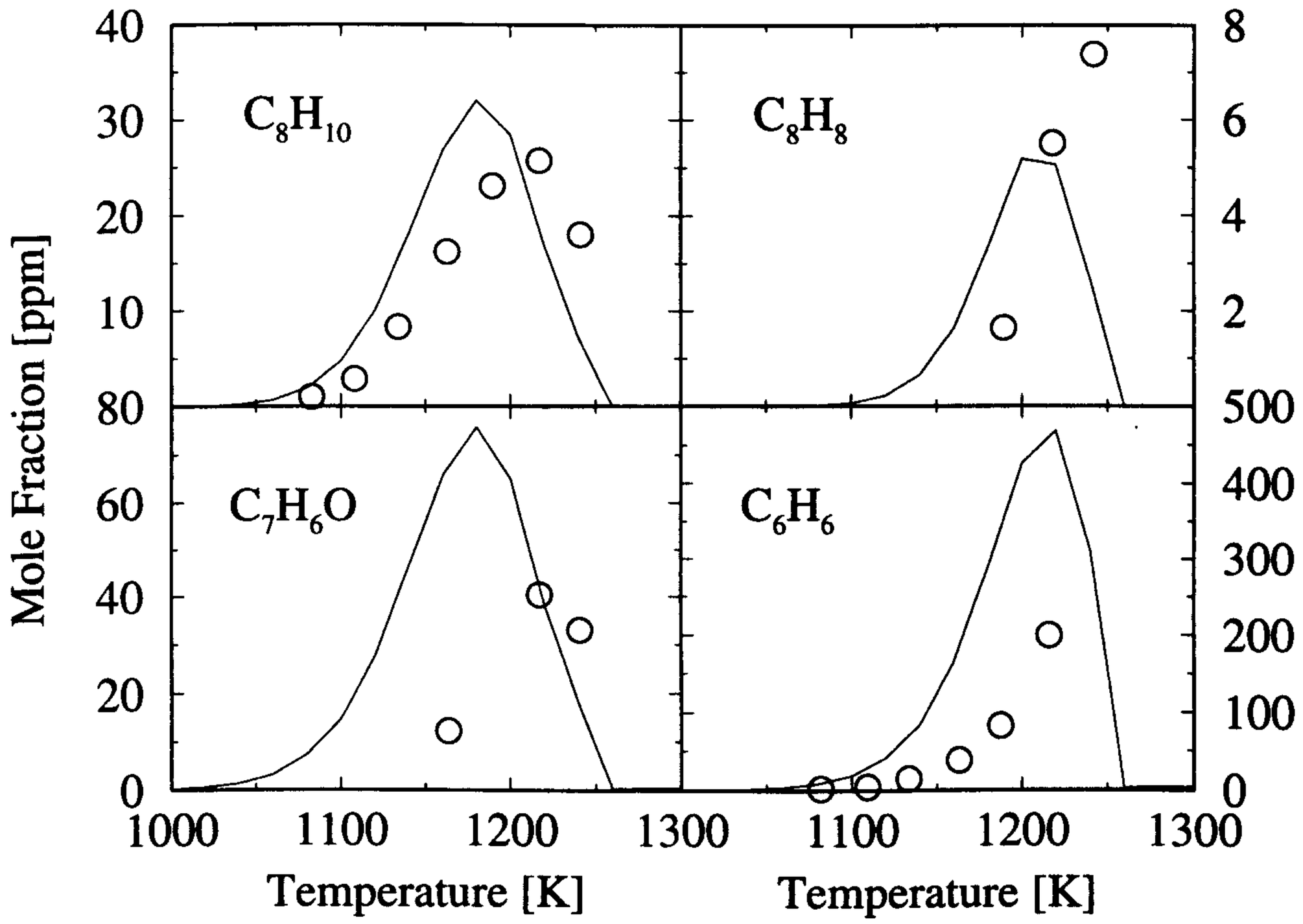


Figure 2.5: Graph of species profile concentrations versus temperature for the oxidation of toluene in a Jet Stirred Reactor. Experimental points are from Dagaut *et al.* [56] for a stoichiometry of $\phi = 0.5$. Solid lines are the computations from the detailed chemical mechanism.

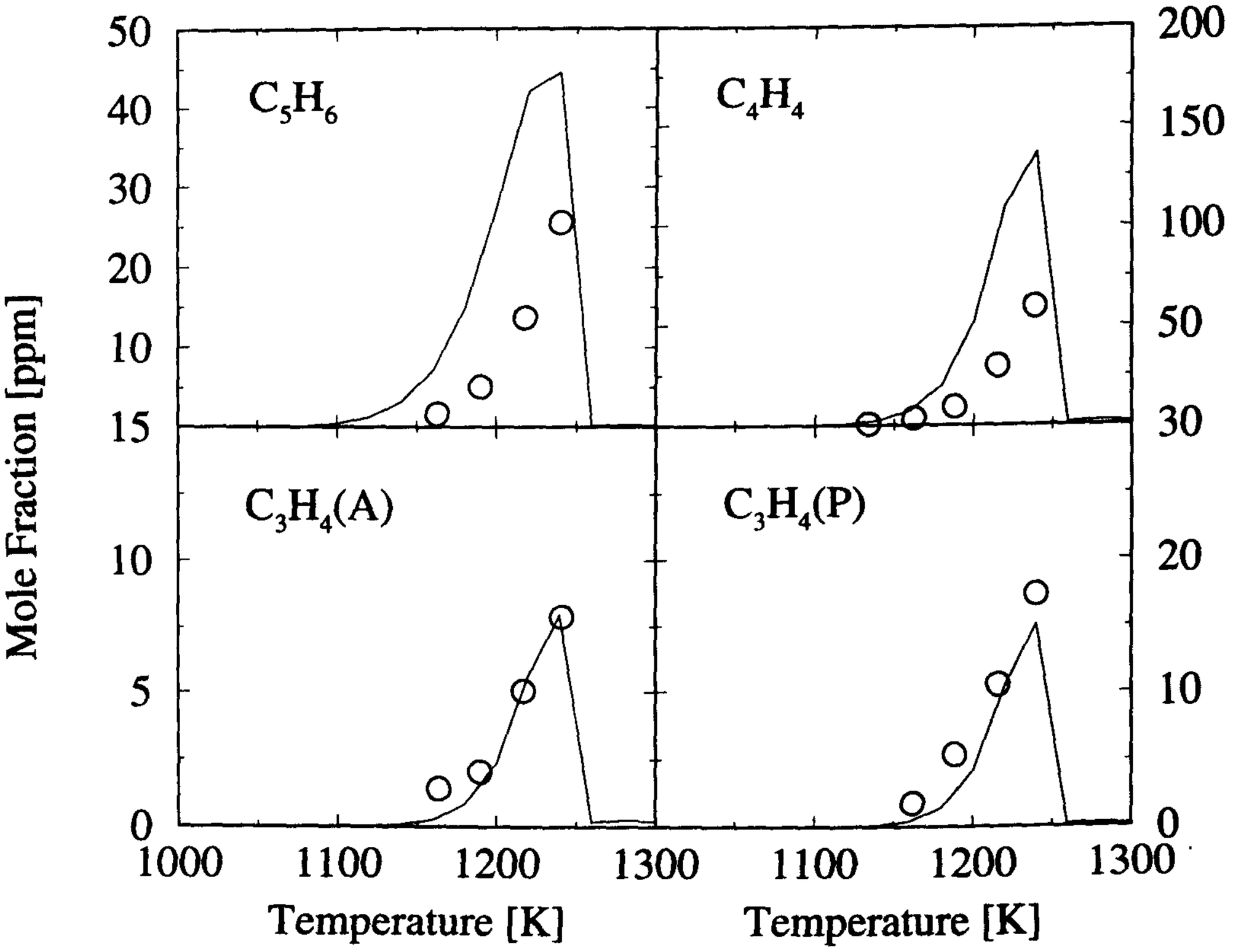


Figure 2.6: Graph of species profile concentrations versus temperature for the oxidation of toluene in a Jet Stirred Reactor. Experimental points are from Dagaut *et al.* [56] for a stoichiometry of $\phi = 0.5$. Solid lines are the computations from the detailed chemical mechanism.

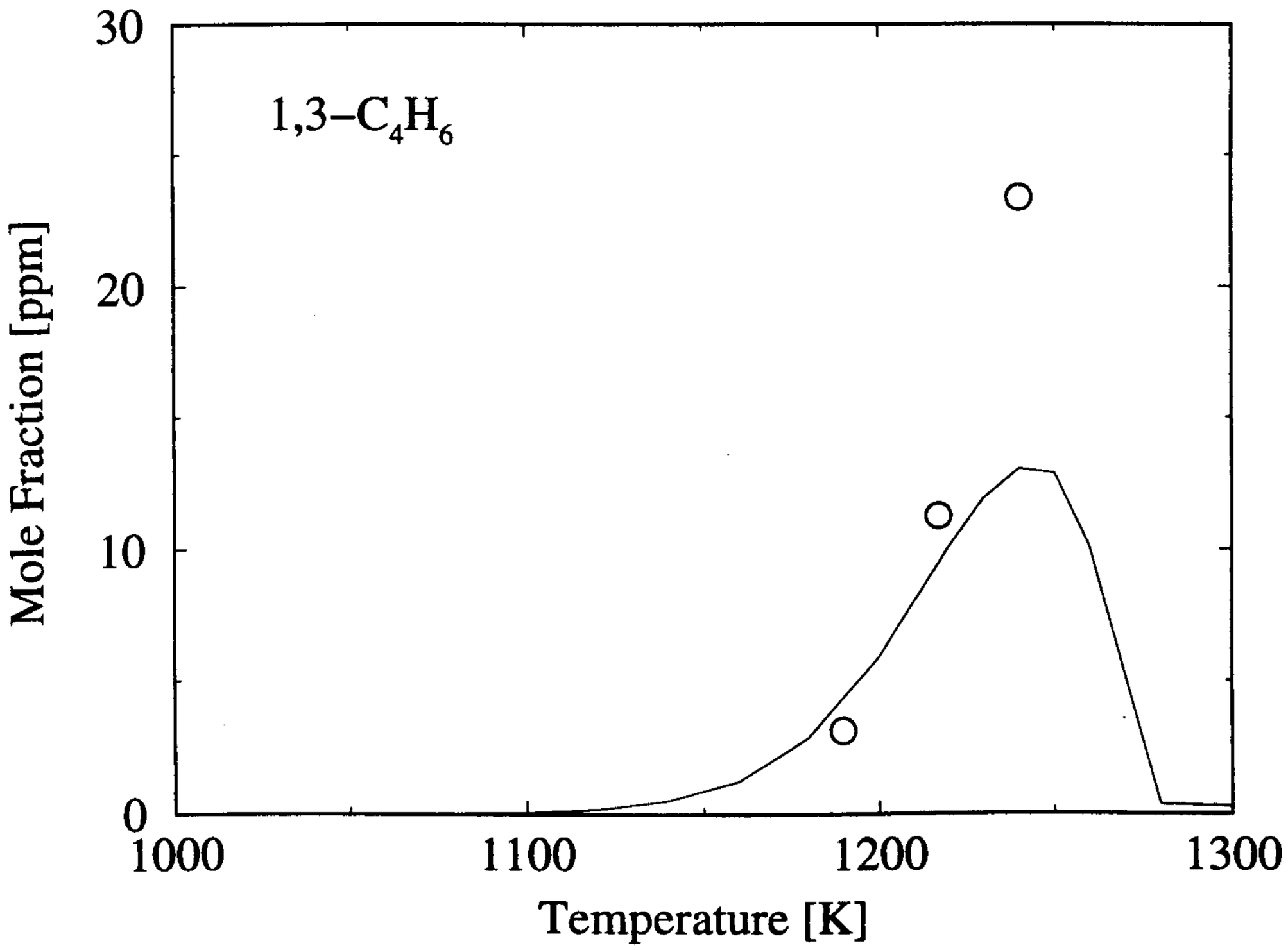


Figure 2.7: Graph of species profile concentrations versus temperature for the oxidation of toluene in a Jet Stirred Reactor. Experimental points are from Dagaut *et al.* [56] for a stoichiometry of $\phi = 0.5$. Solid lines are the computations from the detailed chemical mechanism.

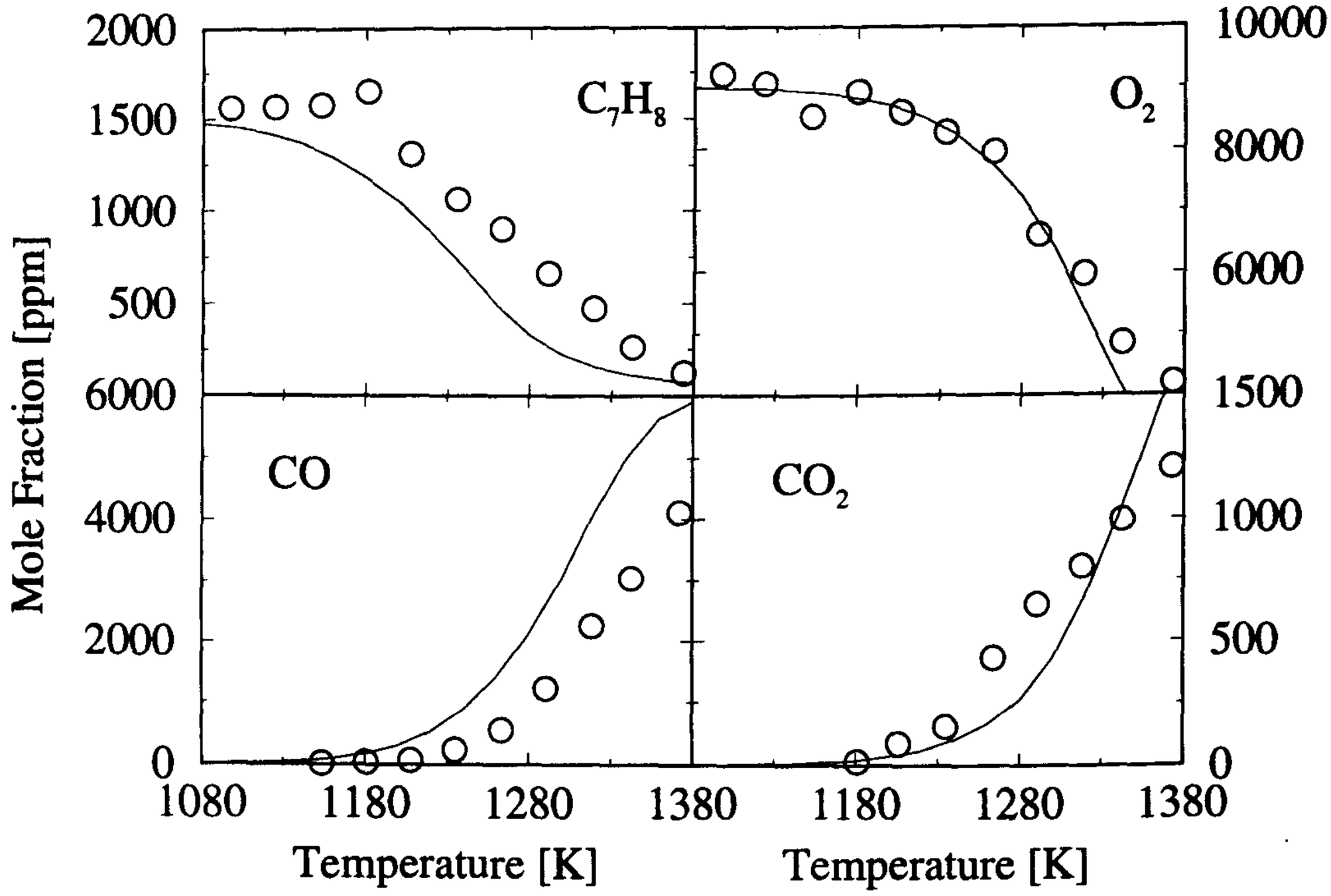


Figure 2.8: Graph of species profile concentrations versus temperature for the oxidation of toluene in a Jet Stirred Reactor. Experimental points are from Dagaut *et al.* [56] for a stoichiometry of $\phi = 1.5$. Solid lines are the computations from the detailed chemical mechanism.

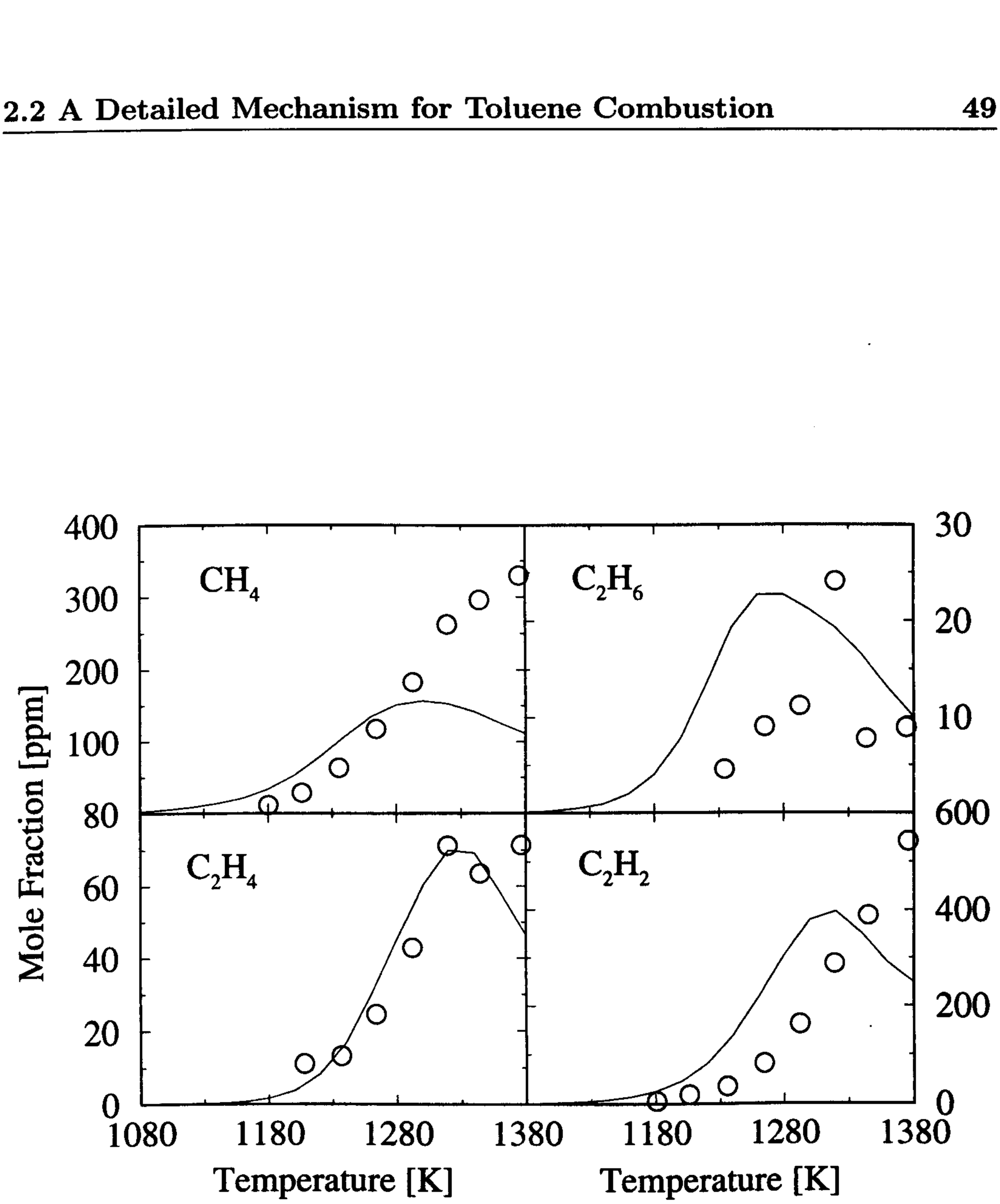


Figure 2.9: Graph of species profile concentrations versus temperature for the oxidation of toluene in a Jet Stirred Reactor. Experimental points are from Dagaut *et al.* [56] for a stoichiometry of $\phi = 1.5$. Solid lines are the computations from the detailed chemical mechanism.

BARL. LONDON. UNIV.

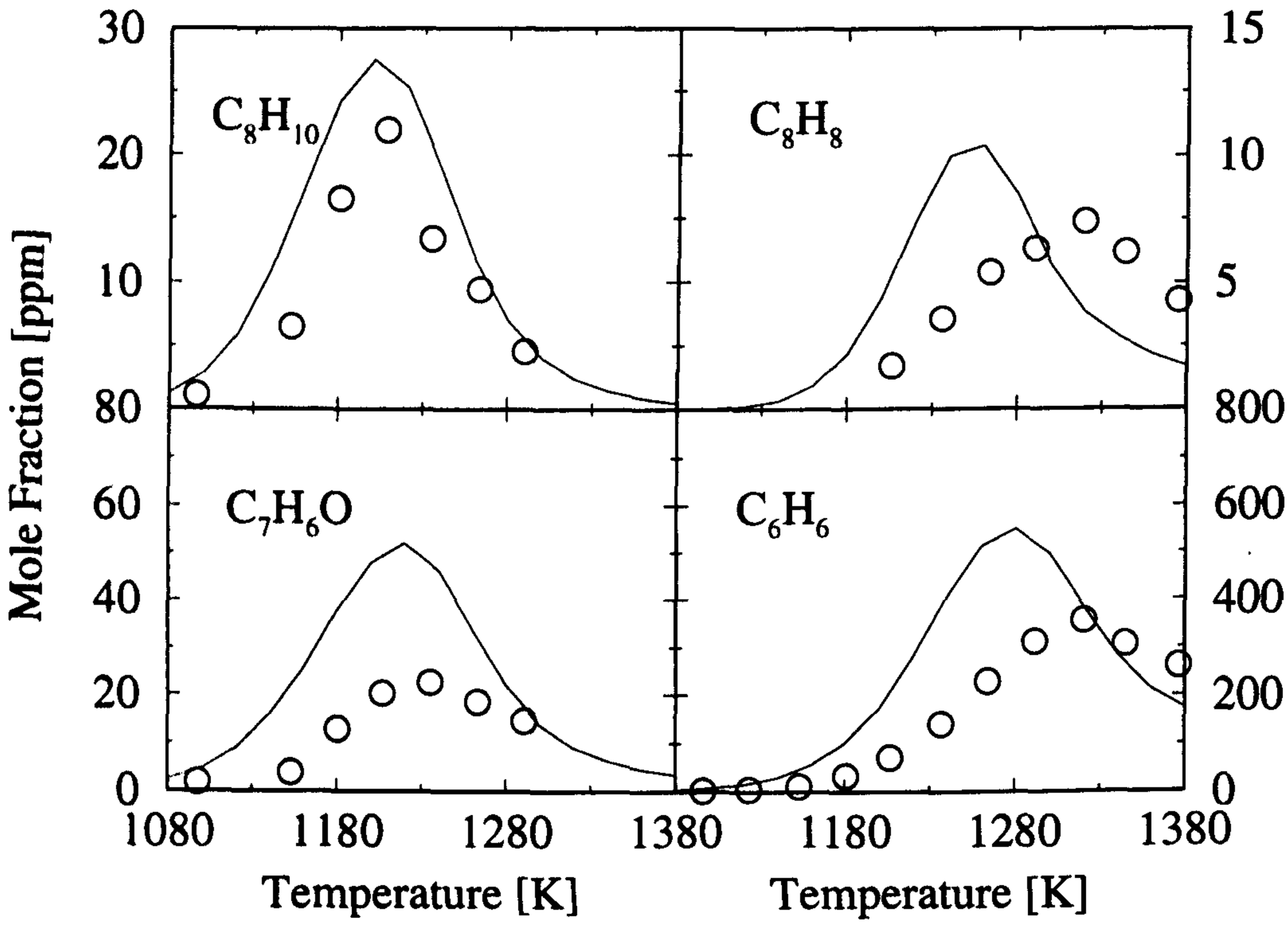


Figure 2.10: Graph of species profile concentrations versus temperature for the oxidation of toluene in a Jet Stirred Reactor. Experimental points are from Dagaut *et al.* [56] for a stoichiometry of $\phi = 1.5$. Solid lines are the computations from the detailed chemical mechanism.

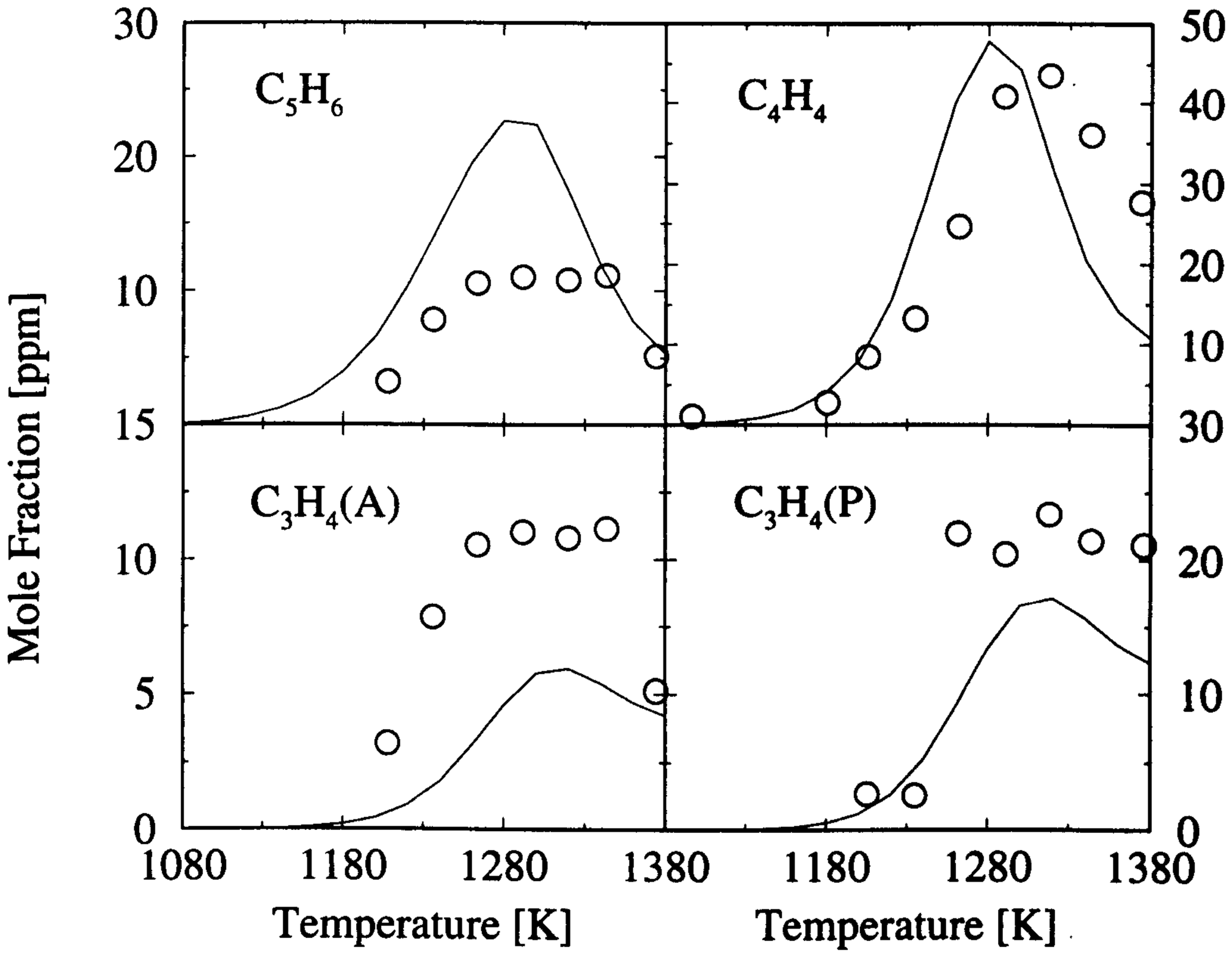


Figure 2.11: Graph of species profile concentrations versus temperature for the oxidation of toluene in a Jet Stirred Reactor. Experimental points are from Dagaut *et al.* [56] for a stoichiometry of $\phi = 1.5$. Solid lines are the computations from the detailed chemical mechanism.

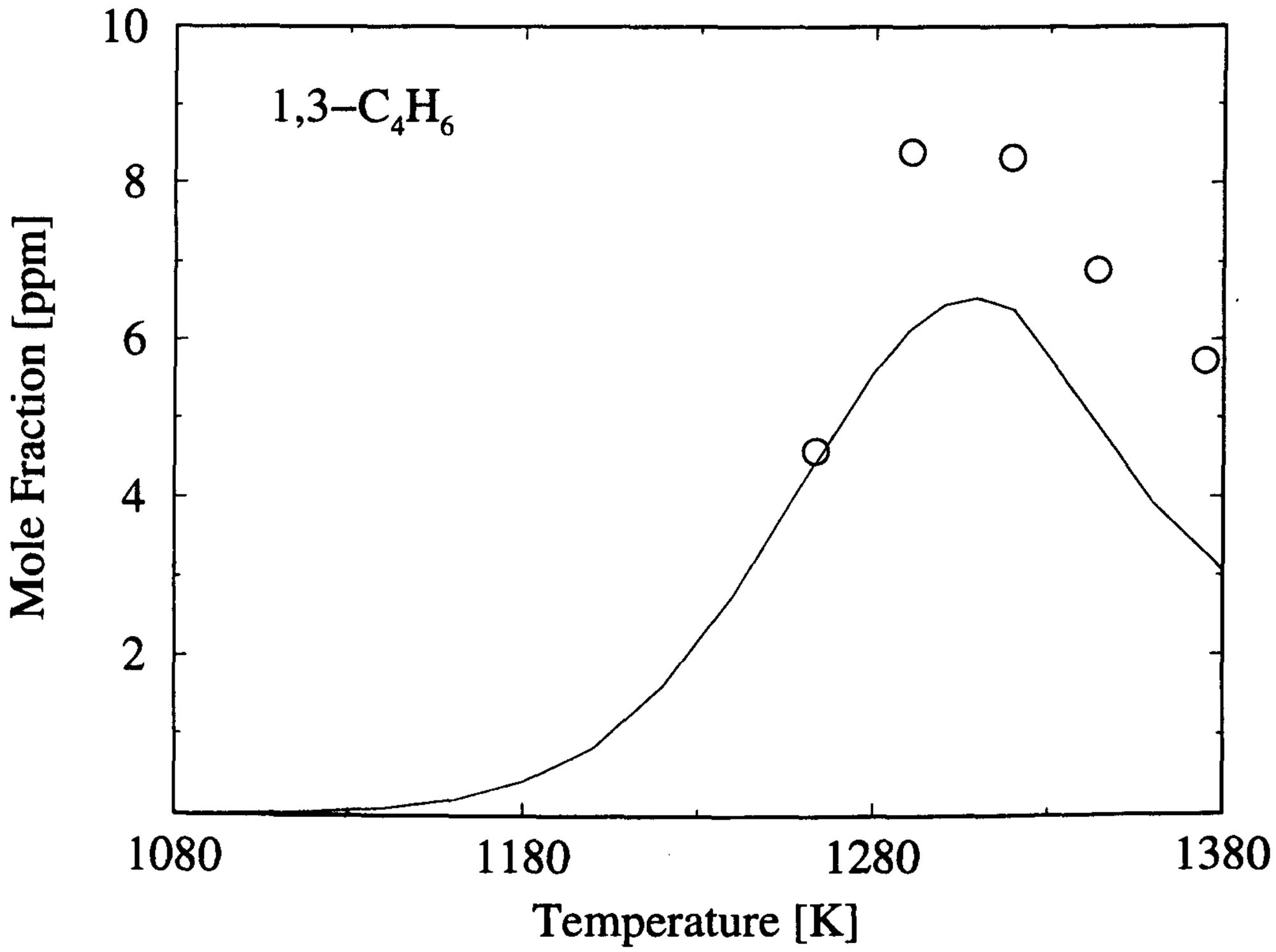


Figure 2.12: Graph of species profile concentrations versus temperature for the oxidation of toluene in a Jet Stirred Reactor. Experimental points are from Dagaut *et al.* [56] for a stoichiometry of $\phi = 1.5$. Solid lines are the computations from the detailed chemical mechanism.

Primary Reaction Paths for the Oxidation of Toluene

The oxidation of toluene Jet Stirred Reactor conditions proceeds through the reaction paths shown in Figures 2.13 – 2.15. The path analysis shown here applies to the rich case ($\phi = 1.5$) at a temperature of 1180 K.

The primary toluene consumption reactions under these conditions, is via C – C cleavage (10 %) of the CH_3 group (1076),

$$C_7H_8 = C_6H_5 + CH_3 \quad (1076)$$

and H attack on the CH_3 group yielding C_7H_7 and C_6H_6 (1078) and (1079).

$$C_7H_8 + H = C_6H_6 + CH_3 \quad (1078)$$
$$C_7H_8 + H = C_7H_7 + H_2 \quad (1079)$$

Reactions (1078) and (1079) contribute 10 % and 30 % respectively. The rate adopted for reaction (1078) has been obtained from Robaugh & Tsang [219] who considered a temperature and pressure range of 950 – 1100 K and 2.03 – 5.07 atm. using a thermal excitation technique. Baulch *et al.* [14] recommended a rate for reaction (1078) which is found to be 1.5 times faster than the rate recommended by Robaugh & Tsang [219] at 1200 K. The study of toluene oxidation in a JSR (Jet Stirred Reactor) by Dagaut *et al.* [56] features the rate expression of Robaugh & Tsang [219], with the frequency factor being increased by a factor of 2. In this study, it was not found necessary to adjust the frequency factor for reaction (1078).

Attack by OH radicals (1086) contribute a further 10 % and leads to C_7H_7.

$$C_7H_8 + OH = C_7H_7 + H_2O \quad (1086)$$

The rate implemented for reaction (1086) stems from the work of Baulch *et al.* [13]. An uncertainty factor of 2 is suggested.

The attack by CH_3 radicals on the methyl group of toluene (1094) contributes 5 % to fuel consumption and 70 % to CH_4 production.

$$C_7H_8 + CH_3 = CH_4 + C_7H_7 \quad (1094)$$

The substitution of O radicals onto the ring (1083) and side chain (1082) producing OC_7H_7, and C_7H_7O, contributes 15 % and 5 % respectively.

$$C_7H_8 + O = OC_7H_7 + H \quad (1083)$$

$$C_7H_8 + O = C_7H_7O + H \quad (1082)$$

The reaction rate parameters applied to reaction (1083) are assigned from the work of Hoffman *et al.* [129]. The detailed chemical mechanism by Dagaut *et al.* [56] does not feature O addition to the ring; only decomposition via attack/cleavage in the CH_3 group is considered. The rate for reaction (1082) has been assigned the rates parameters from Baulch *et al.* [13] who comment that there is an uncertainty factor of 3.2.

Benzyl produced from reactions (1079) and (1086) primarily undergoes H addition (40 %) as in the reverse of reaction (1077).

$$C_7H_8 = C_7H_7 + H \quad (1077)$$

A further 25 % of the C_7H_7 radical is consumed via O_2 (15 %) and HO_2 addition (10 %),

$$C_7H_7 + O_2 = C_7H_7O + O \quad (1056)$$

$$C_7H_7 + HO_2 = C_7H_7O + OH \quad (1057)$$

respectively. The rate for reaction (1056) is modelled on the analogous CH_3 radical attack on molecular oxygen (76),

$$CH_3 + O_2 \quad = \quad CH_3O + O \tag{76}$$

with the frequency factor adjusted accordingly. The rate for reaction (76) has been adopted from Baulch *et al.* [13]. The rate parameters for reaction (1057) stem from the recent work of Ellis *et al.* [86] who studied the reaction in a static/low – flow at a temperature of 773 K and a pressure of 0.658 atm. Ellis *et al.* [86] comment that the frequency factor in their work agrees well with that from other past studies. The detailed chemical kinetic mechanism formulated by Klotz *et al.* [148] features a frequency factor similar to that used in this work, however, the product distribution differs [148].

$$C_7H_7 + HO_2 = C_7H_6O + OH + H$$

Klotz *et al.* [148] highlight that the study of toluene oxidation in the Princeton Flow Reactor by Emdee *et al.* [89] features a high frequency factor (A = 2.5E+11 m^3 $kmol^{-1}$ s^{-1}) as suggested by Bartels *et al.* [10], even though the investigators were aware of the much lower value (A = 5.0E+09 m^3 $kmol^{-1}$ s^{-1}) suggested by Hippler *et al.* [126]. The reason for the selection of Emdee *et al.* [89] of a fast frequency factor was to explain the high concentrations of C_7H_6O found in the oxidation of toluene in their Princeton Flow Reactor. However, Klotz *et al.* [148] comment that in their study of toluene oxidation, more sensitive experimental apparatus was used, hence enabling a separation of C_7H_7OH and C_7H_6O. It was found that the concentrations of C_7H_6O are in fact lower than the measurements by Emdee *et al.* [89] suggest. For completeness, the detailed chemical mechanism from Dagaut *et al.* [56] features a frequency factor of 3.16E+09 m^3 $kmol^{-1}$ s^{-1} for reaction (1057) with the same product distribution as in the present study.

It is found that 15 % of the C_7H_7 radical is consumed through CH_3 addition to form ethylbenzene (1061).

$$C_7H_7 + CH_3 = C_8H_{10} \quad (1061)$$

The rate for reaction (1061) has been adopted from Colket *et al.* [48] as reported by Lindstedt & Maurice [168]. Ethylbenzene is consumed by thermal decomposition via C – H cleavage (30 %)

$$C_8H_{10} = C_8H_9 + H \quad (1207)$$

The rate assigned to reaction (1207) is adopted from Muller–Markgraf & Troe [197] who studied the pyrolysis of C_8H_{10}. Muller–Markgraf & Troe [197] comment that the rate parameters they recommend correspond to the high pressure limit.

Around 60 % of C_8H_{10} is consumed via H radical attack leading to C_8H_9 (30 %) and C_6H_6 (30 %) respectively.

$$C_8H_{10} + H = C_8H_9 + H_2 \quad (1209)$$

$$C_8H_{10} + H = C_6H_6 + C_2H_5 \quad (1208)$$

The rate for reaction (1209) is modelled on the reaction involving H attack on C_7H_8 (1079) [168].

$$C_7H_8 + H = C_7H_7 + H_2 \quad (1079)$$

The reaction involving H attack on the C – C bond linking the side chain to the aromatic as in reaction (1208) has been measured by Robaugh *et al.* [220] who studied the pyrolysis of C_8H_{10} in a Shock Tube for very low pressures over a temperature range of 1100 – 1300 K.

The C_8H_9 radical produced from reactions (1207) and (1209) is consumed by thermal decomposition (100 %) via C – H cleavage (1199).

$$C_8H_9 = C_8H_8 + H \quad (1199)$$

The rate for reaction (1199) stems from the work of Muller–Markgraf & Troe [197].

The consumption of C_8H_8 is via H (20 %) and OH (60 %) radical attack.

$$C_2H_4 + C_6H_5 = C_8H_8 + H \quad (935)$$

$$C_8H_8 + OH = C_7H_7 + CH_2O \quad (1195)$$

The rate of reaction (935) has been measured by Fahr & Stein [90] and (1195) has been estimated by Maurice [182].

The C_7H_7O radical produced from reactions (1056) and (1057) thermally decomposes via C – H (60 %) and C – C cleavage (40 %) via (1113) and (1111).

$$C_7H_7O = C_7H_6O + H \quad (1113)$$

$$C_7H_7O = C_6H_6 + CHO \quad (1111)$$

The rate for reaction has (1111) been estimated using the methodology of Dean [73].

Benzaldehyde is further consumed by thermal decomposition via C – H cleavage (15 %) as well as OH (10 %), H (25 %), CH_3 (10 %) and O (25 %) radical attack.

$$C_7H_6O = C_6H_5CO + H \quad (1101)$$

$$C_7H_6O + OH = C_6H_5CO + H_2O \quad (1106)$$

$$C_7H_6O + H = C_6H_5CO + H_2 \quad (1103)$$

$$C_7H_6O + CH_3 = C_6H_5CO + CH_4 \quad (1109)$$

$$C_7H_6O + O = C_6H_6 + CO_2 \quad (1104)$$

The rate for reaction (1101), featuring the thermal decomposition of C_7H_6O via C – H cleavage, is adopted from the study of Grela & Colussi [104].

The latter authors investigated the thermal decomposition of C_7H_6O in a Turbulent Flow Reactor over a temperature range of 1150 – 1250 K at very low pressures.

Reactions (1106), (1103) and (1109) have been adopted from the study of toluene oxidation in a Turbulent Flow Reactor by Emdee *et al.* [89]. Emdee *et al.* [89] comment that these reactions are based on analogy with CH_2O oxidation as reported by Lindstedt & Maurice [168]. The addition – decomposition reaction $C_7H_6O + O$ (1104) is assigned an estimated rate parameter of 2.0E+10 m^3 $kmol^{-1}$ s^{-1}.

The product (C_6H_5CO) of reactions (1101), (1106), (1103) and (1109) decomposes thermally via C – C cleavage to form C_6H_5 and CO (1099).

$$C_6H_5CO = C_6H_5 + CO \quad (1099)$$

The rate for reaction (1099) is assigned from Solly & Benson [236] who considered temperature and pressure ranges of 614 – 667 K and 3.20E+03 – 6.13E+04 Pa respectively.

The OC_7H_7 radical decomposes (80 %) via reaction (1120)

$$OC_7H_7 = C_5H_4CH_3 + CO \quad (1120)$$

The rate for reaction (1120) has been modelled on the analogous reaction (1001)

$$C_6H_5O = C_5H_5 + CO \quad (1001)$$

with the rate for reaction (1001) obtained from Frank *et al.* [94]. The detailed chemical mechanism of Emdee *et al.* [89] features a global step for reaction (1120) with the products assigned as $C_6H_6 + CO + H$. Emdee *et al.* [89] comment that these products can be derived directly from $C_5H_4CH_3$, and

this species indeed rapidly isomerises (80 %) to C_6H_6. However, in the study by Lindstedt & Rizos [170] it has been shown that $C_5H_4CH_3$ does stabilize, eventually forming C_6H_6 via C_6H_6(F).

In the current mechanism, $C_5H_4CH_3$ undergoes thermal decomposition via C – H cleavage (100 %) to form fulvene (910).

$$C_5H_4CH_3 \quad = \quad C_6H_6(F) + H \qquad (910)$$

The reaction step (910) has been proposed by Moskaleva *et al.* [193] who explored the possibilities of C_6H_6 formation from $C_5H_4CH_3$ radicals. Fulvene isomerises to C_6H_6 via reaction (985).

$$C_6H_6(F) + H \quad = \quad C_6H_6 + H \qquad (985)$$

The rate adopted for reaction (985) is adpoted from Marinov *et al.* [179] who comment that it is based on the work of Melius *et al.* [186].

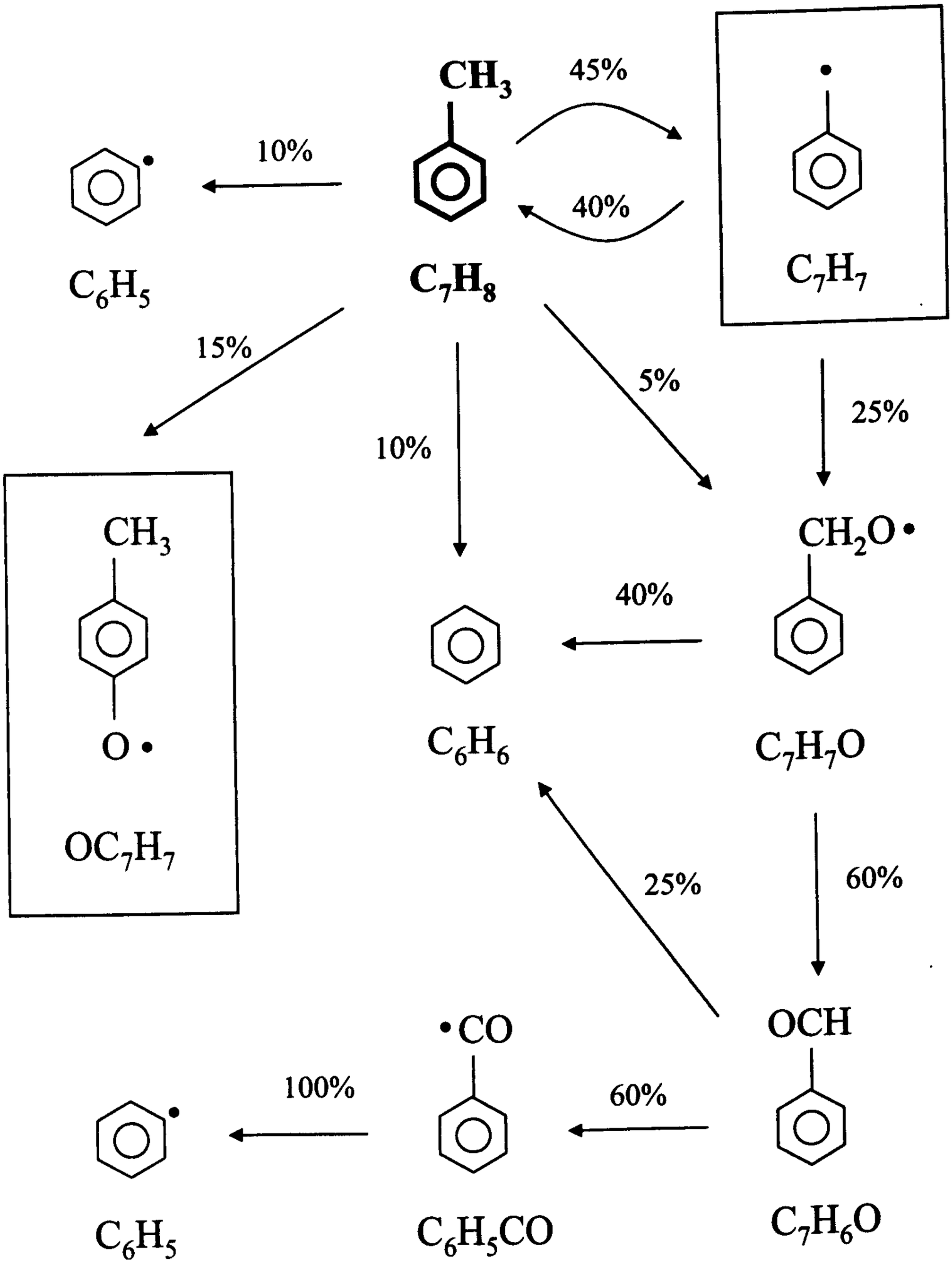


Figure 2.13: Diagram illustrating the consumption paths of the fuel toluene and it intermediate species in a Jet Stirred Reactor (T = 1180 K, P = 1 atm., $\phi = 1.5$). Species in boxes are considered in subsequent pages.

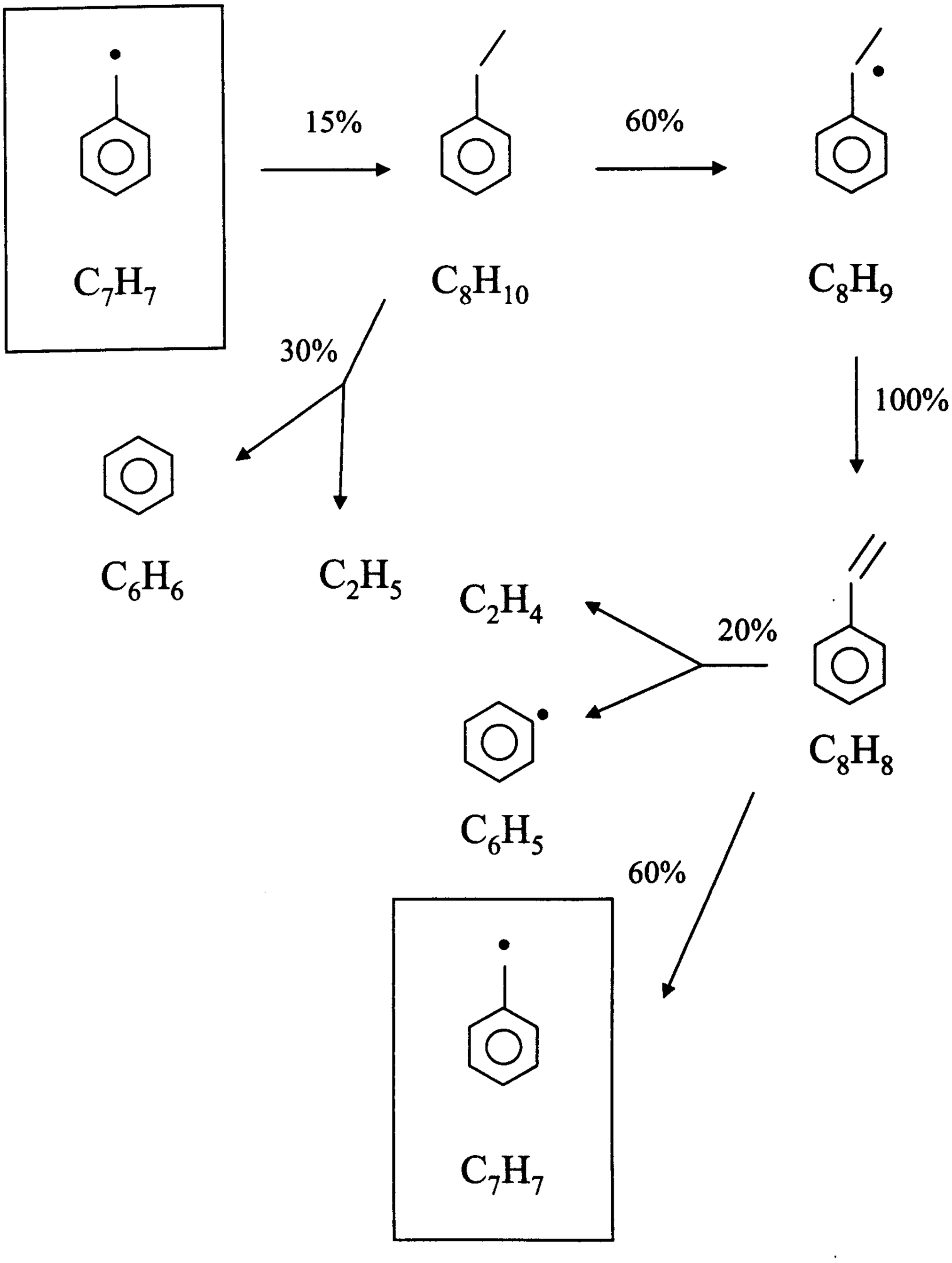


Figure 2.14: Diagram illustrating the consumption paths of the fuel toluene and it intermediate species in a Jet Stirred Reactor (T = 1180 K, P = 1 atm., $\phi = 1.5$). Species in boxes are considered in subsequent pages.

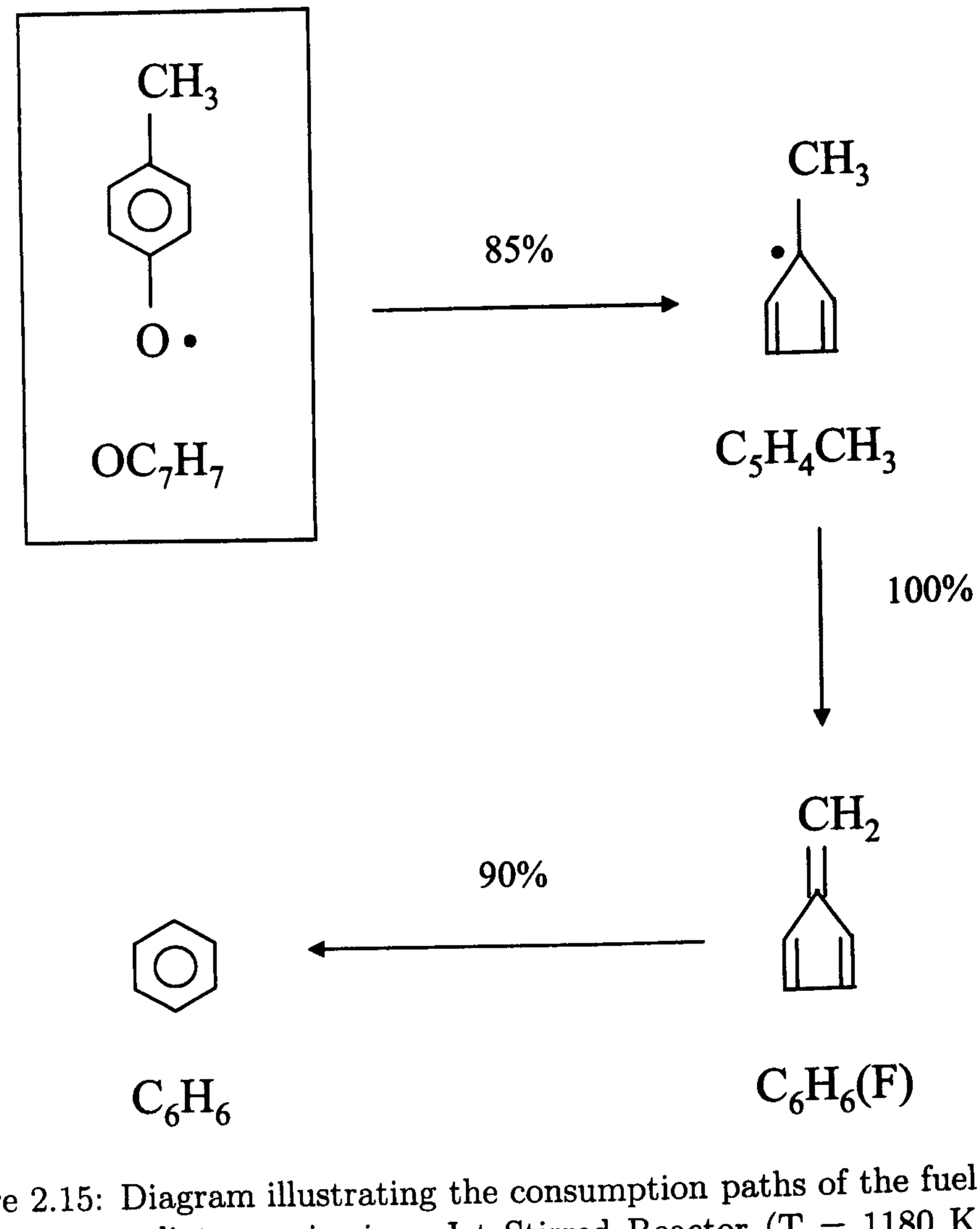


Figure 2.15: Diagram illustrating the consumption paths of the fuel toluene and it intermediate species in a Jet Stirred Reactor (T = 1180 K, P = 1 atm., $\phi = 1.5$). Species in boxes are considered in subsequent pages.

Discussion

A detailed chemical mechanism has been applied to the oxidation of toluene under JSR conditions for lean ($\phi = 0.5$) and rich ($\phi = 1.5$) conditions. In general, the detailed chemical mechanism performs very well.

It is evident that an evolution of the toluene detailed mechanism has taken place. In this study, global rate parameters have been omitted and replaced by more accurate elementary reaction steps. For example, one of the primary benzyl consumption reactions (1057)

$$C_7H_7 + HO_2 \quad = \quad C_7H_7O + O \qquad (1057)$$

has been reviewed and updated with the rate expression derived from Ellis *et al.* [86].

The consumption of the OC_7H_7 radical is another obvious reaction channel that has been reviewed and updated in this work. Emdee *et al.* [89] used a global reaction step,

$$OC_7H_7 \quad = \quad C_6H_6 + CO + H$$

bypassing the $C_5H_4CH_3$ radical. In this work, the global reaction step has been replaced by elementary reaction steps incorporating the formation and consumption of the $C_5H_4CH_3$ radical.

The present detailed chemical kinetic model can further be enhanced by the measurement of elementary reaction parameters such as that for the thermal decomposition of C_7H_7O (1113).

$$C_7H_7O \quad = \quad C_7H_6O + H \qquad (1113)$$

2.2.3 Toluene Ignition Delay Times

A comparative study of the oxidation of toluene under Shock Tube conditions provides further understanding of the detailed chemistry of initiation reactions. That is, the thermal decomposition reactions and the reactions between molecular oxygen and the fuel.

The experimental data sets used to validate the toluene sub – mechanism ignition reactions is obtained from Burcat *et al.* [34] for two cases using toluene – oxygen – argon mixtures. The first case considers lean ($\phi = 0.33$) conditions over a temperature range of 1330 – 1630 K and a pressure of 2.27 atm. The second case considers stoichiometric conditions over a temperature range of 1360 – 1760 K and a pressure of 2.28 atm. The ignition delay time is defined as the instant in time at which the sum of the CO and CO_2 concentration reaches 10 % of the final value. Table 2.3 summarizes the initial conditions.

Table 2.3: Summary of the Initial Conditions for the Oxidation of Toluene in a Shock Tube

Fuel	ϕ	T_0 [K]	Pressure [atm.]	Bath gas
C_7H_8	0.33	1330 – 1630	2.27	Ar
C_7H_8	1.0	1360 – 1760	2.28	Ar

Overall, the calculations agree well with the experimental data from Burcat *et al.* [34] as shown in Figures 2.16 and 2.17.

In the stoichiometric case and for lower temperatures $\leq$ 1480 K, the calculations begin to deviate away from the experimental points as is evident in Figure 2.17. However, for these low temperatures the experimental points are not linear. Experimental uncertainties may play a role though additional

low temperature reactions are perhaps more likely.

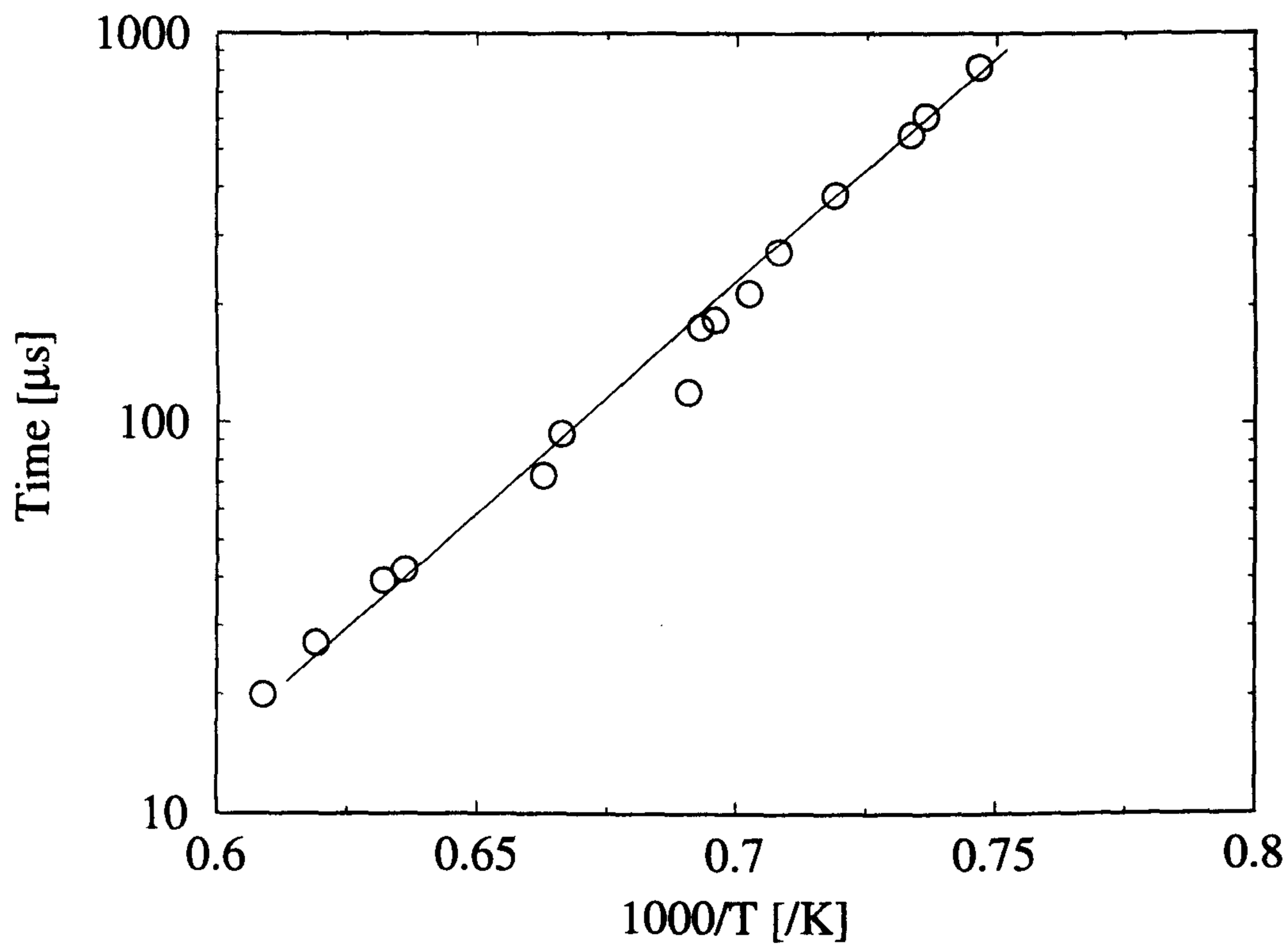


Figure 2.16: Comparison of computed (lines) and measured (symbols) ignition delay times for lean ($\phi = 0.33$) toluene – oxygen – argon mixtures. Experimental points are from Burcat *et al.* [34].

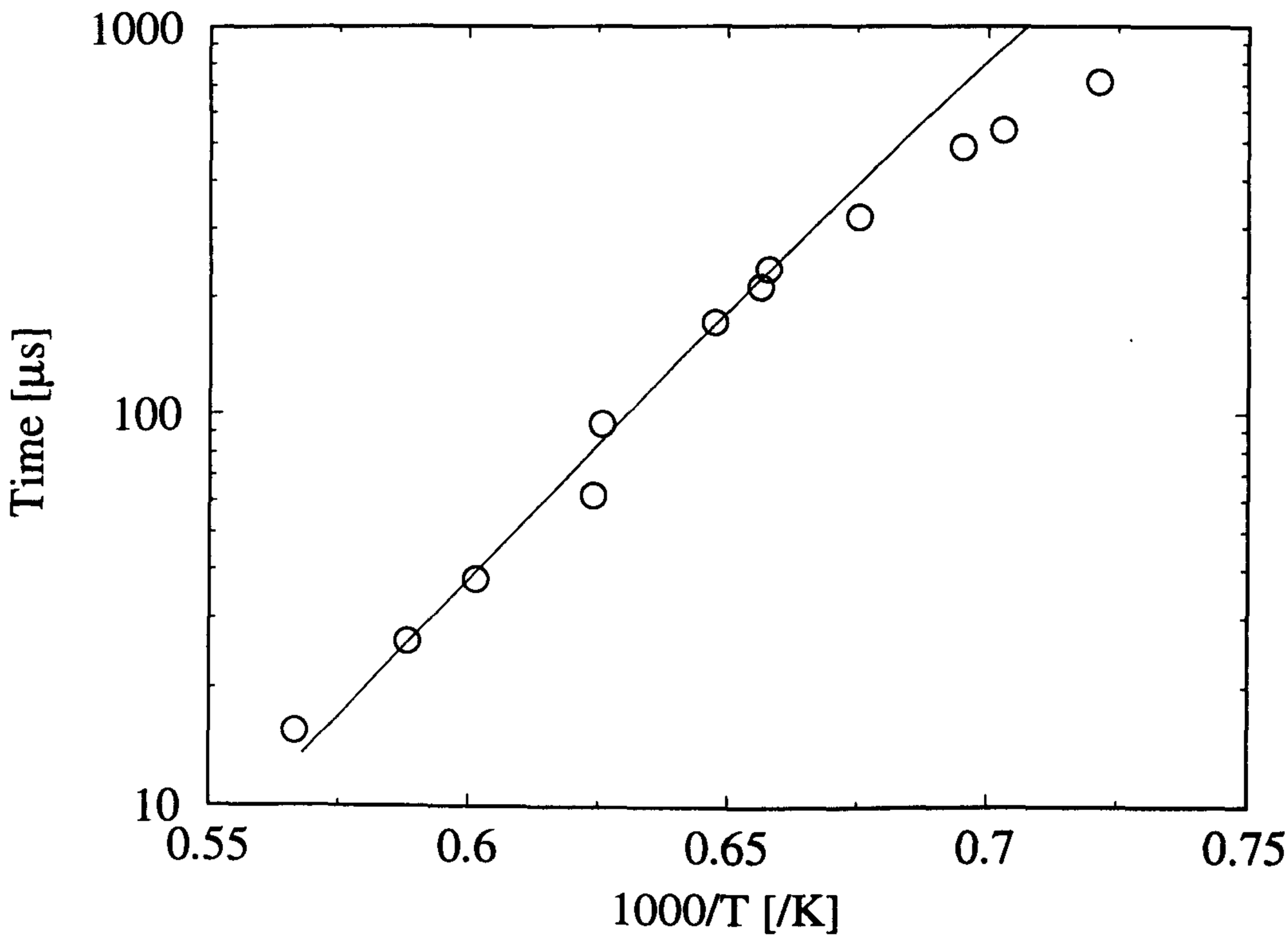


Figure 2.17: Comparison of computed (lines) and measured (symbols) ignition delay times for stoichiometric ($\phi = 1.0$) toluene – oxygen – argon mixtures. Experimental points are from Burcat *et al.* [34].

Primary Reaction Paths Determining the Ignition Delay Times

The primary consumption paths determining the ignition delay times of toluene are analysed for a temperature of 1560 K and stoichiometric conditions. For times ~ 1 μs, the initial radical pool is generated by the thermal decomposition of toluene via C – C and C – H cleavage (1077) and (1076).

$$C_7H_8 = C_7H_7 + H \quad (1077)$$

$$C_7H_8 = C_6H_5 + CH_3 \quad (1076)$$

It is found that reactions (1077) and (1076) contribute 60 % and 40 % respectively. Therefore it can be concluded that the initiation reaction (1091)

$$C_7H_8 + O_2 = C_7H_7 + HO_2 \quad (1091)$$

does not contribute in the generation of the initial radical pool. The rate adopted for reaction (1091) has been obtained from Baulch *et al.* [13]. The detailed chemical kinetic mechanisms from Dagaut *et al.* [56] features rate parameters proposed by Emdee *et al.* [89] who comment that reaction (1091) was fitted to the experimental results. It is found that the rate expression for reaction (1091) proposed by Emdee *et al.* [89] is approximately 40 times faster at 1200 K than that proposed by Baulch *et al.* [13].

2.2.4 The Oxidation of Toluene in a Turbulent Flow Reactor

The oxidation of toluene under Turbulent Flow Reactor conditions has also been investigated using the experimental data sets from Klotz *et al.* [148]. The data sets were acquired for a stoichiometric value of $\phi = 0.76$, at atmospheric pressure in a nitrogen bath gas and with an initial temperature

of 1173 K. Klotz *et al.* [148] report that there is a maximum uncertainty of 30 ms in the temporal evolution.

Comparisons between the experimental data sets from Klotz *et al.* [148] and the computations from the detailed chemical mechanism are shown in Figures 2.18 and 2.19 for a selection of species. The computations have been time shifted by 20 ms in accordance with suggestion of the experimental investigators [148].

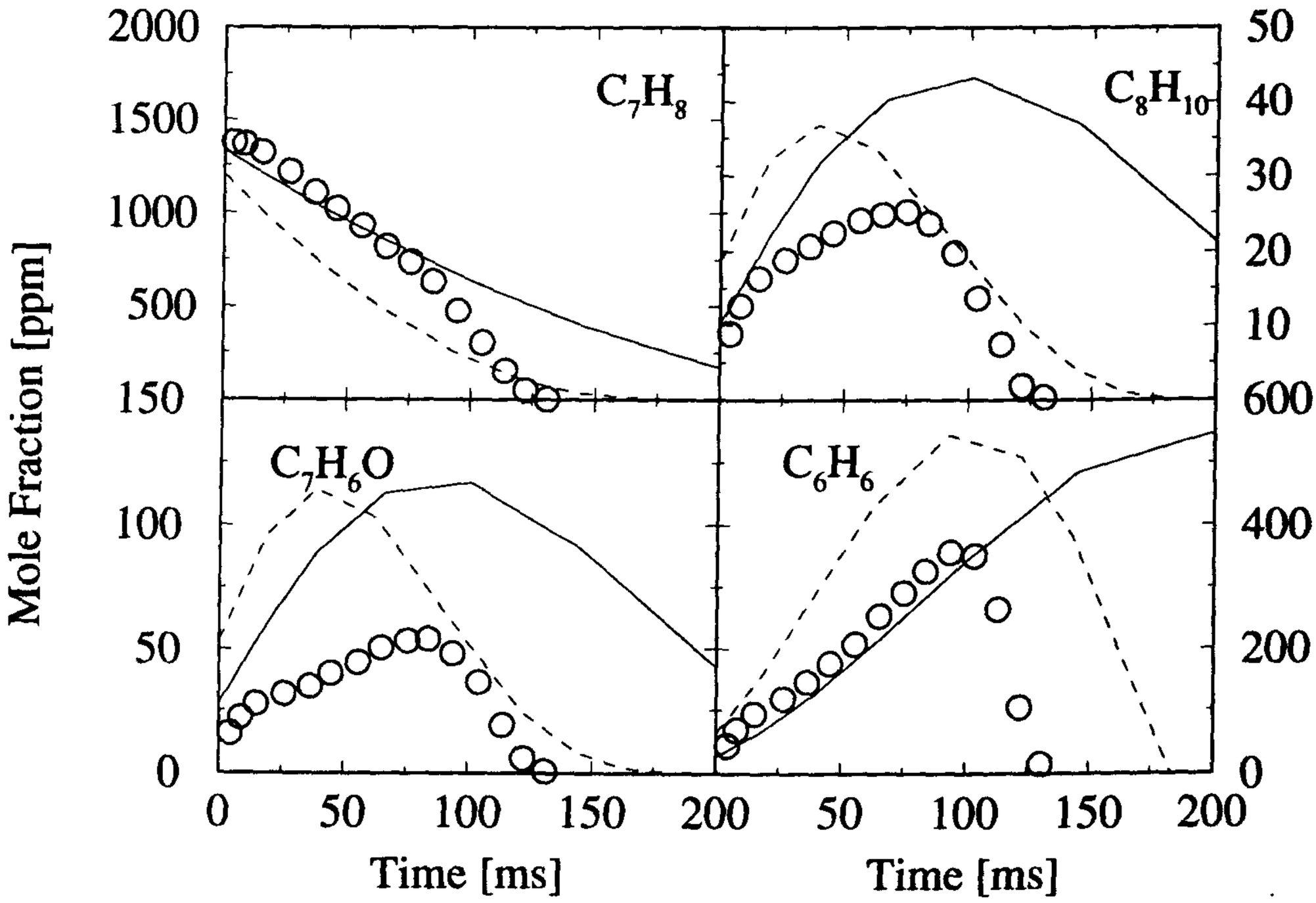


Figure 2.18: Graph of species profile concentrations versus time for the oxidation of toluene in a Turbulent Flow Reactor. Experimental points are from Klotz *et al.* [148] for a stoichiometry of $\phi = 0.76$. Lines are the computations from the detailed chemical mechanism where the solid line represents $T_0 = 1173$ K and the dashed line represents $T_0 = 1200$ K. Both computations have been time shifted by 20 ms.

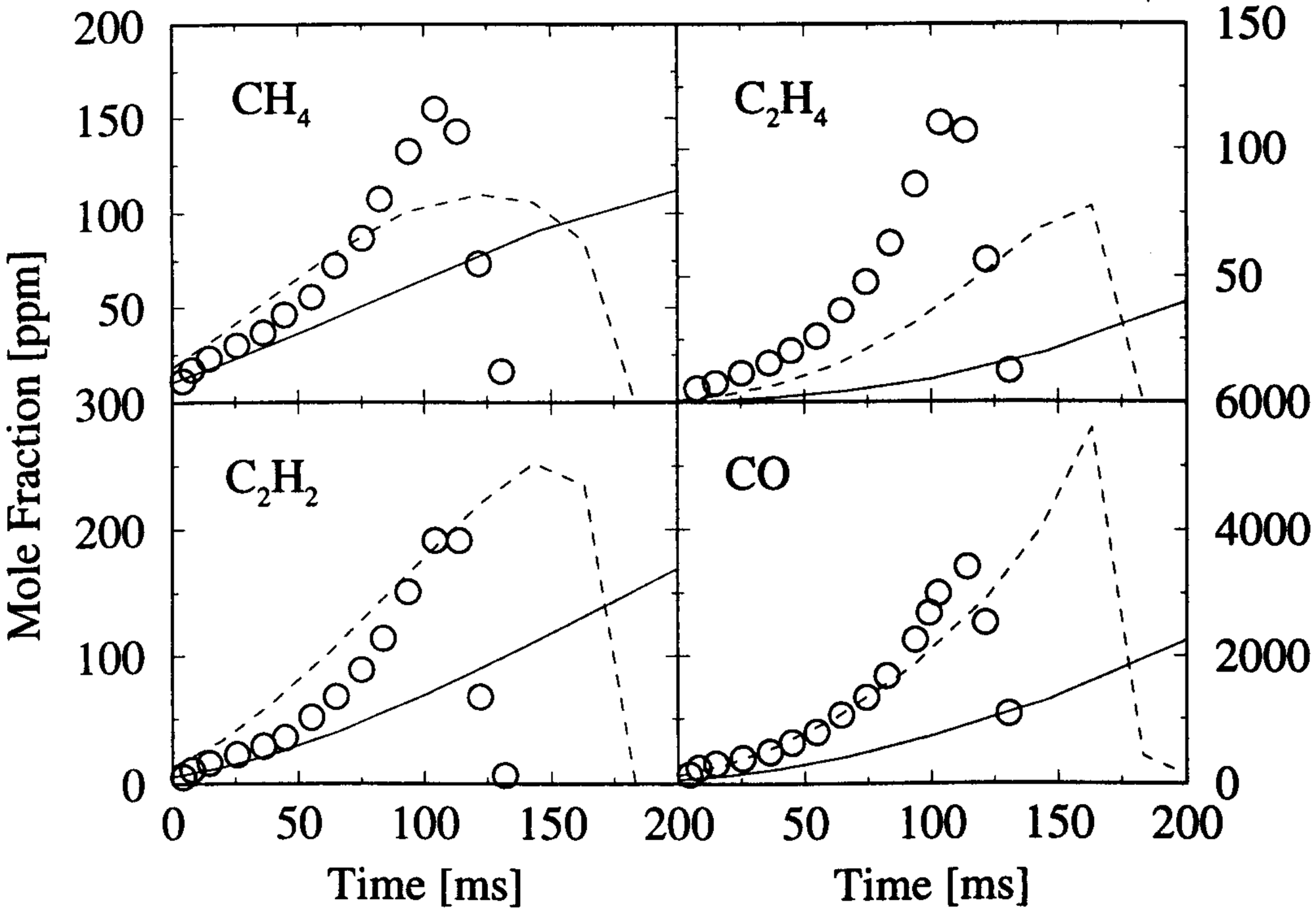


Figure 2.19: Graph of species profile concentrations versus time for the oxidation of toluene in a Turbulent Flow Reactor. Experimental points are from Klotz *et al.* [148] for a stoichiometry of $\phi = 0.76$. Lines are the computations from the detailed chemical mechanism where the solid line represents $T_0 = 1173$ K and the dashed line represents $T_0 = 1200$ K. Both computations have been time shifted by 20 ms.

Comparisons between the experimental data sets from Klotz *et al.* [148] and the calculations gives poor agreement. The calculations for the fuel decay line indicates that the concentration of radicals in the system may be too low due to the shallow gradient as is evident in Figure 2.18. For times $\geq$ 75 ms $\pm$ 30 ms an ignition phenomena would have to occur to explain drop in species concentrations. This may be further reinforced by analysis of the temperature, O_2 and CO_2 profiles which are unfortunately not included in the data sets from Klotz *et al.* [148]. Klotz *et al.* [148] suggest that in the latter stages of the toluene oxidation, the species profile concentrations are controlled by the $C_1 - C_4$ chemistry. However, the $C_1 - C_4$ chemistry used in the current mechanism has been thoroughly investigated in the work of Rizos [218] for a wide range of conditions and it may suggest that the experimental data from Klotz *et al.* [148] are subject to significant uncertainties. A test calculation is also shown where the initial temperature was raised to 1200 K. The species profiles have been clearly altered in terms of magnitudes and trends. Figure 2.20 shows a graph of the temperature profile versus time. The solid line represents the temperature profile for the initial conditions as given by Klotz *et al.* [148] and the dashed line represents the initial temperature at 1200 K. From Figure 2.20, it is evident that ignition occurs in the case where the initial temperature was set to 1200 K at an approximate time of 160 ms. The system is clearly very sensitive to small changes in the initial temperature. The current results are also inconsistent with the JSR data of Dagaut *et al.* [56] which suggest that the current mechanism may result in a somewhat too fast fuel decay.

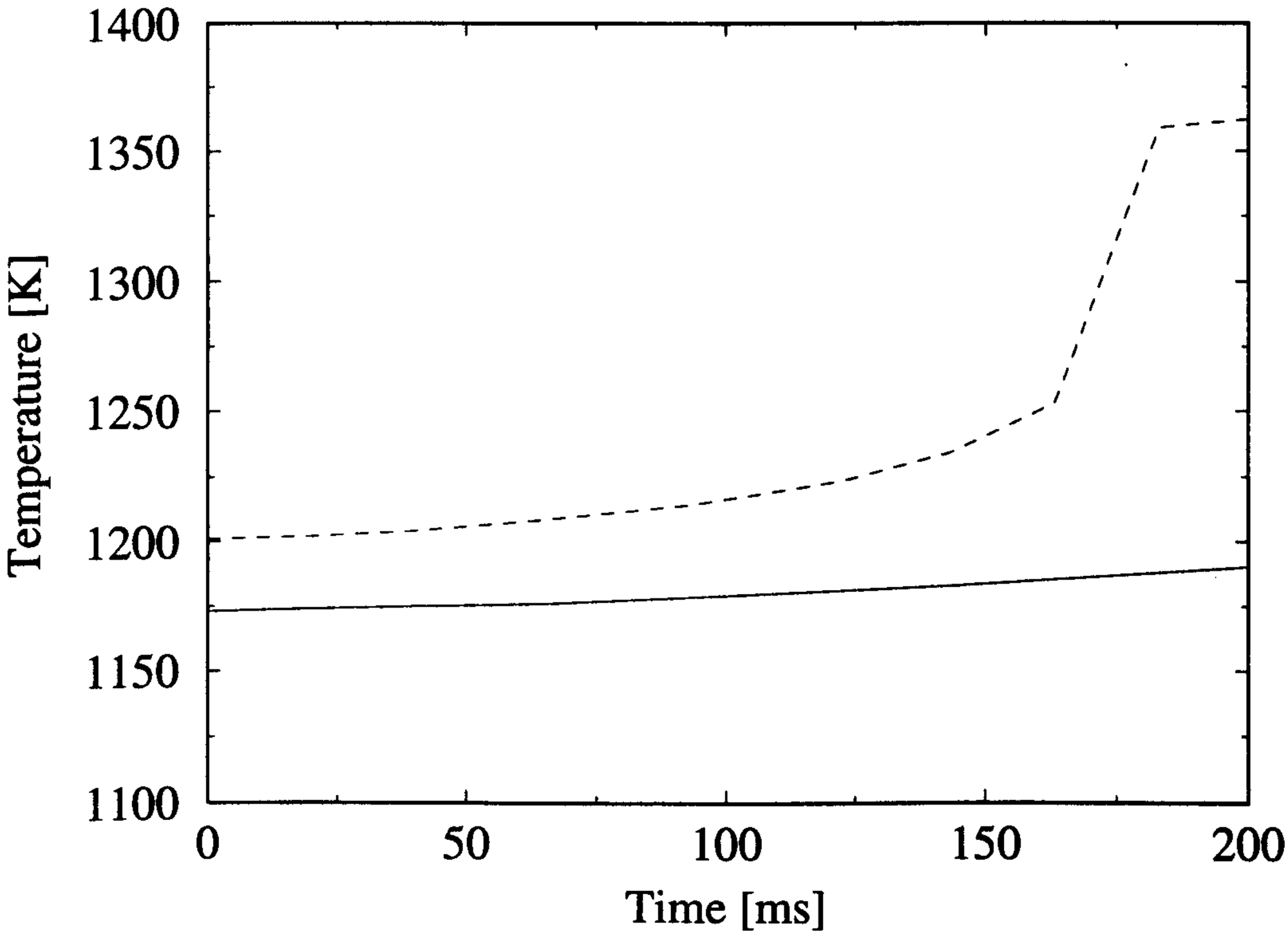


Figure 2.20: Graph of temperature profile versus time for the oxidation of toluene in a Turbulent Flow Reactor. Lines are the computations from the detailed chemical mechanism and have been time shifted by 20 ms, where the solid line represents the initial conditions given by Klotz *et al.* [148] and the dashed line represents $T_0 = 1200$ K.

2.3 The Oxidation of m – xylene

2.3.1 The Oxidation of m – xylene in a Turbulent Flow Reactor

The oxidation of m – xylene is here studied under the conditions of Emdee *et al.* [88] which correspond to a stoichiometry of $\phi = 1.0$, atmospheric pressure and an initial temperature of 1155 K. Emdee *et al.* [88] report that there is a maximum time shift of 20 ms.

The calculations for the oxidation of m – xylene and the intermediate products are shown in Figures 2.21 – 2.23. Overall, the detailed chemical mechanism performs well, reproducing the fuel and molecular oxygen profiles.

The high concentrations of CH_4 are well produced as is evident in Figures 2.22. It is found that at a reaction time of 75 ms reaction (1227)

$$C_8H_{10}(M) + CH_3 = C_8H_9(M) + CH_4 \quad (1227)$$

is the dominant reaction channel producing CH_4. The rate for reaction (1227) is modelled directly on reaction (1094)

$$C_7H_8 + CH_3 = CH_4 + C_7H_7 \quad (1094)$$

The levels of C_7H_6O are over predicted at later reaction times as is evident in Figure 2.22. At a reaction time of 75 ms, it is found that reactions (1113) and (1238)

$$C_7H_7O = C_7H_6O + H \quad (1113)$$
$$C_8H_8O(M) + H = C_7H_6O + CH_3 \quad (1238)$$

are the dominant channels, contributing ~ 50 % each. The rate for reaction (1238) is derived from reaction (1078).

$$C_7H_8 + H \quad = \quad C_6H_6 + CH_3 \tag{1078}$$

Concentration levels of $C_8H_8O(M)$ are over predicted at later reaction times ($\geq$ 25 ms) as illustrated in Figure 2.22. It is found that at a reaction time of 50 ms reaction (1253)

$$C_8H_9O(M) \quad = \quad C_8H_8O(M) + H \tag{1253}$$

is the main step for producing $C_8H_8O(M)$. The rate parameters adopted for reaction (1253) are modelled directly on the equivalent reaction

$$C_7H_7O \quad = \quad C_7H_6O + H \tag{1113}$$

The calculations for other single ring aromatics are illustrated in Figure 2.22. The predictions for C_6H_6 are excellent, with reaction (985) the main contributor.

$$C_6H_6(F) + H \quad = \quad C_6H_6 + H \tag{985}$$

Concentrations of C_7H_8 are somewhat over predicted as is evident in Figure 2.23.

$$C_8H_9O(M) \quad = \quad C_7H_8 + CHO \tag{1251}$$

Reaction (1251) is the dominant production channel for C_7H_6O. The rate parameters for reaction (1251) stem from the analogous reaction (1111).

$$C_7H_7O \quad = \quad C_6H_6 + CHO \tag{1111}$$

Levels of C_8H_8 are typically a factor of 3 under predicted. However, at a similar reaction time, the experimental concentration measurements for C_8H_{10} are 2 – 3 ppm lower than that for C_8H_8. In following the analogy

for toluene consumption, this conflicts with the mechanistic approach for the construction of the sub – mechanism for the oxidation of m – xylene. For example, in the experimental study of Dagaut *et al.* [56] featuring the oxidation of toluene under JSR conditions (Figure 2.10), the species concentrations of C_8H_{10} are typically 7 ppm whilst the concentrations of C_8H_8 are too low to be measured at 1155 K.

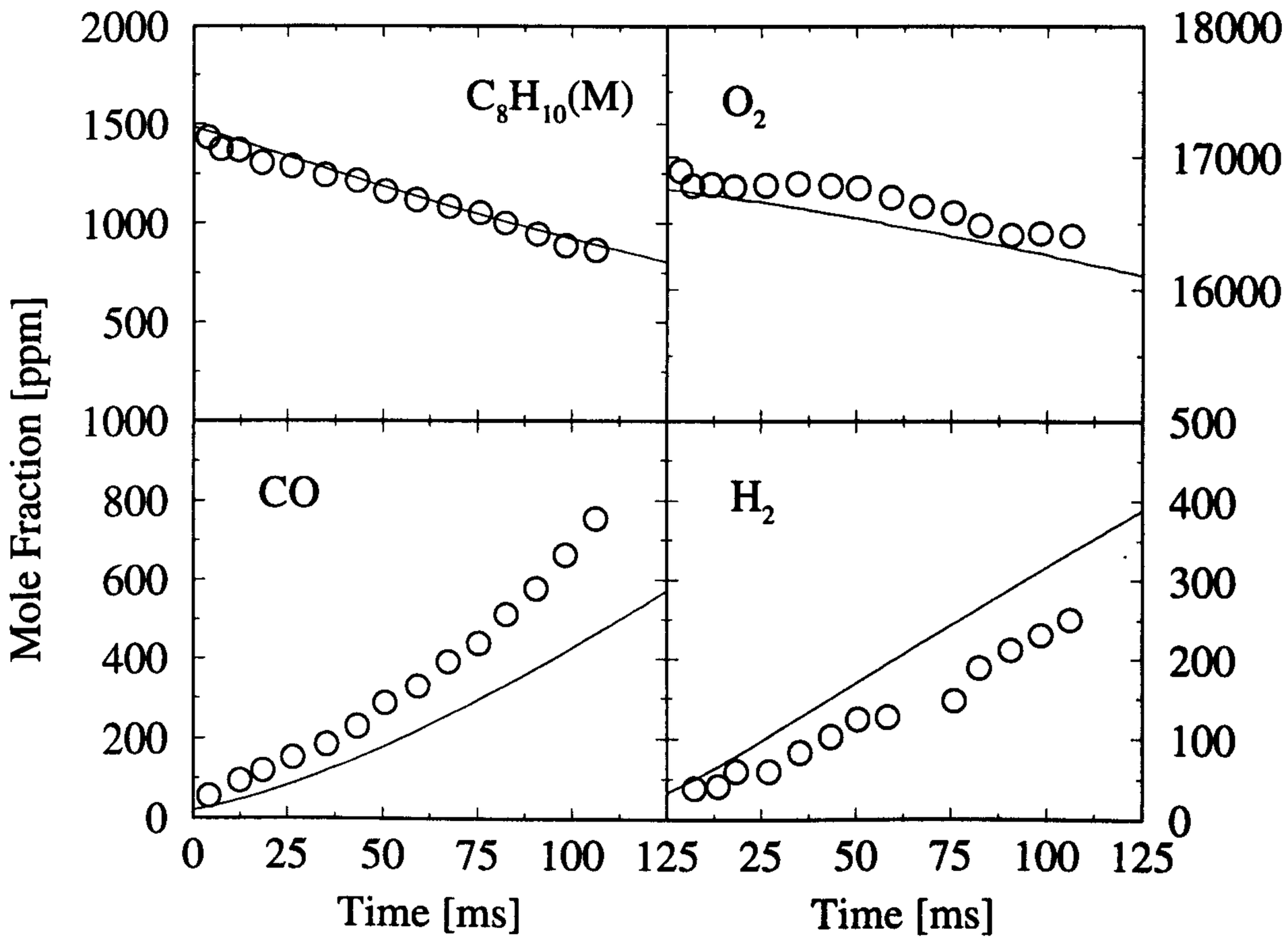


Figure 2.21: Graph of species profile concentrations versus time for the oxidation of m – xylene in a Turbulent Flow Reactor. Experimental points are from Emdee *et al.* [88] for a stoichiometry of $\phi = 1.0$. Solid lines are the computations from the detailed chemical mechanism and have been time shifted by 20 ms.

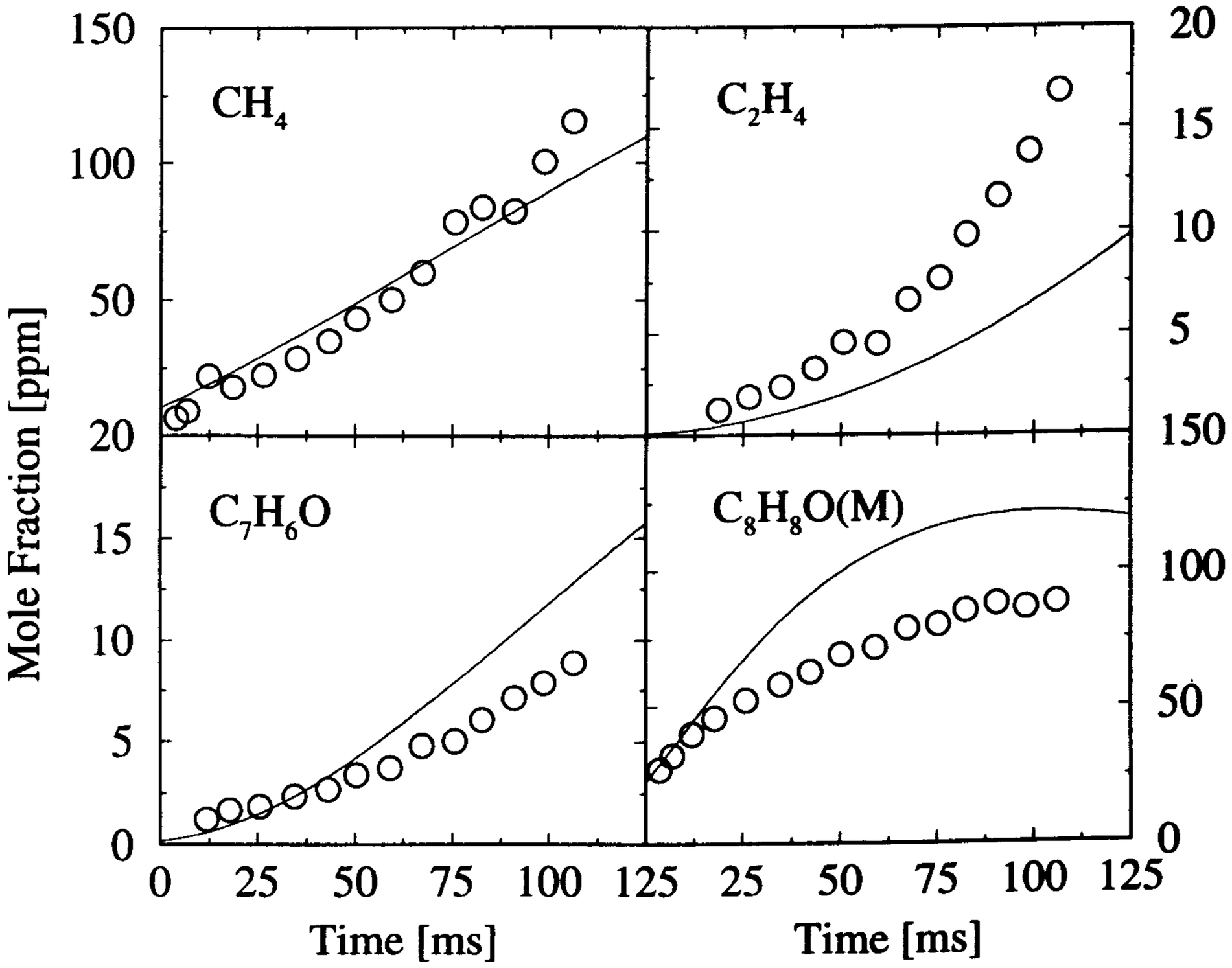


Figure 2.22: Graph of species profile concentrations versus time for the oxidation of m – xylene in a Turbulent Flow Reactor. Experimental points are from Emdee *et al.* [88] for a stoichiometry of $\phi = 1.0$. Solid lines are the computations from the detailed chemical mechanism and have been time shifted by 20 ms.

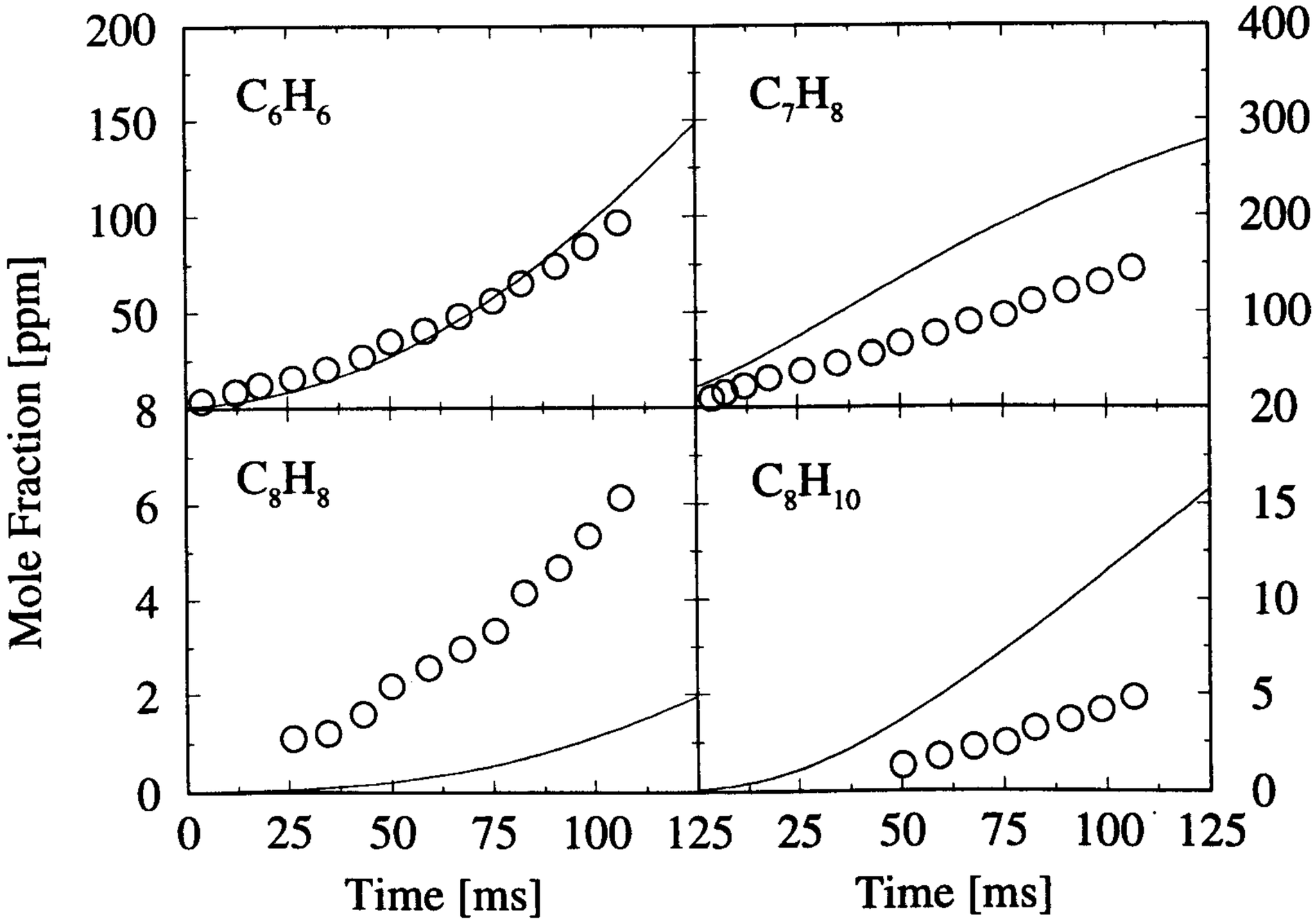


Figure 2.23: Graph of species profile concentrations versus time for the oxidation of m – xylene in a Turbulent Flow Reactor. Experimental points are from Emdee *et al.* [88] for a stoichiometry of $\phi = 1.0$. Solid lines are the computations from the detailed chemical mechanism and have been time shifted by 20 ms.

Primary Reaction Paths for the Oxidation of m – xylene under Turbulent Flow Reactor conditions

The oxidation of m – xylene proceeds through a number of chemical paths shown in Figures 2.24 – 2.25. The chemical kinetic rates applied in this study for the modelling of the oxidation of m – xylene are based on the oxidation of toluene which has been validated and evaluated in Section 2.2. The path analysis conducted here again applies to a reaction time of 75 ms.

The initial consumption of m – xylene is dominated by H radical attack (40 %) to form the m-C_8H_9 radical (1217).

$$C_8H_{10}(M) + H \quad = \quad C_8H_9(M) + H_2 \qquad (1217)$$

The rate parameters for reaction (1217) are assigned from the analogous reaction for toluene oxidation (1079).

$$C_7H_8 + H \quad = \quad C_7H_7 + H_2 \qquad (1079)$$

A further reaction channel for the fuel consumption is via OH radical attack (25 %).

$$C_8H_{10}(M) + OH \quad = \quad C_8H_9(M) + H_2O \qquad (1221)$$

The rate parameters for reaction (1221) are modelled directly on reaction (1086).

$$C_7H_8 + OH \quad = \quad C_7H_7 + H_2O \qquad (1086)$$

A further 10 % of the fuel is consumed via the substitution reaction (1220),

$$C_8H_{10}(M) + O \quad = \quad C_8H_9O(M) + H \qquad (1220)$$

with the rate for reaction (1220) being obtained from reaction (1082).

$$C_7H_8 + O = C_7H_7O + H \quad (1082)$$

The $C_8H_9(M)$ radical undergoes H addition (30 %) to reform the fuel, molecular oxygen attack (25 %) and HO_2 radical attack (20 %).

$$C_8H_{10}(M) = C_8H_9(M) + H \quad (1215)$$
$$C_8H_9(M) + O_2 = C_8H_9O(M) + O \quad (1204)$$
$$C_8H_9(M) + HO_2 = C_8H_9O(M) + OH \quad (1205)$$

The rate parameters for reactions (1215), (1204) and (1205) are modelled directly on the equivalent reactions (1077), (1056) and (1057).

$$C_7H_8 = C_7H_7 + H \quad (1077)$$
$$C_7H_7 + O_2 = C_7H_7O + O \quad (1056)$$
$$C_7H_7 + HO_2 = C_7H_7O + OH \quad (1057)$$

The $C_8H_9O(M)$ radical thermally decomposes via C – C and C – H cleavage (1251) and (1253),

$$C_8H_9O(M) = C_7H_8 + CHO \quad (1251)$$
$$C_8H_9O(M) = C_8H_8O(M) + H \quad (1253)$$

with reaction (1251) contributing 35 % and reaction (1253) 65 %. The rates for reactions (1251) and (1253) are modelled on the analogous equivalent reactions (1111) and (1113).

$$C_7H_7O = C_6H_6 + CHO \quad (1111)$$
$$C_7H_7O = C_7H_6O + H \quad (1113)$$

The $C_8H_8O(M)$ intermediate under goes a variety of radical attacks (1244), (1239), (1242), (1247) and (1241) which contribute 15 %, 20 %, 30 %, 10 % and 10 % respectively.

$$C_8H_8O(M) + OH = C_7H_7CO + H_2O \quad (1244)$$

$$C_8H_8O(M) + H = C_7H_7CO + H_2 \quad (1239)$$

$$C_8H_8O(M) + O = C_7H_8 + CO_2 \quad (1242)$$

$$C_8H_8O(M) + CH_3 = C_7H_7CO + CH_4 \quad (1247)$$

$$C_8H_8O(M) + O = OC_7H_7 + CHO \quad (1241)$$

The C_7H_7CO radical undergoes thermal decomposition via C – C bond cleavage (100 %) (1234).

$$C_7H_7CO = C_7H_7P + CO \quad (1234)$$

The rate (1234) has been adopted from the analogous equivalent reaction (1099).

$$C_6H_5CO = C_6H_5 + CO \quad (1099)$$

The consumption of the smaller compounds have been discussed earlier in the text and also in the study by Rizos [218].

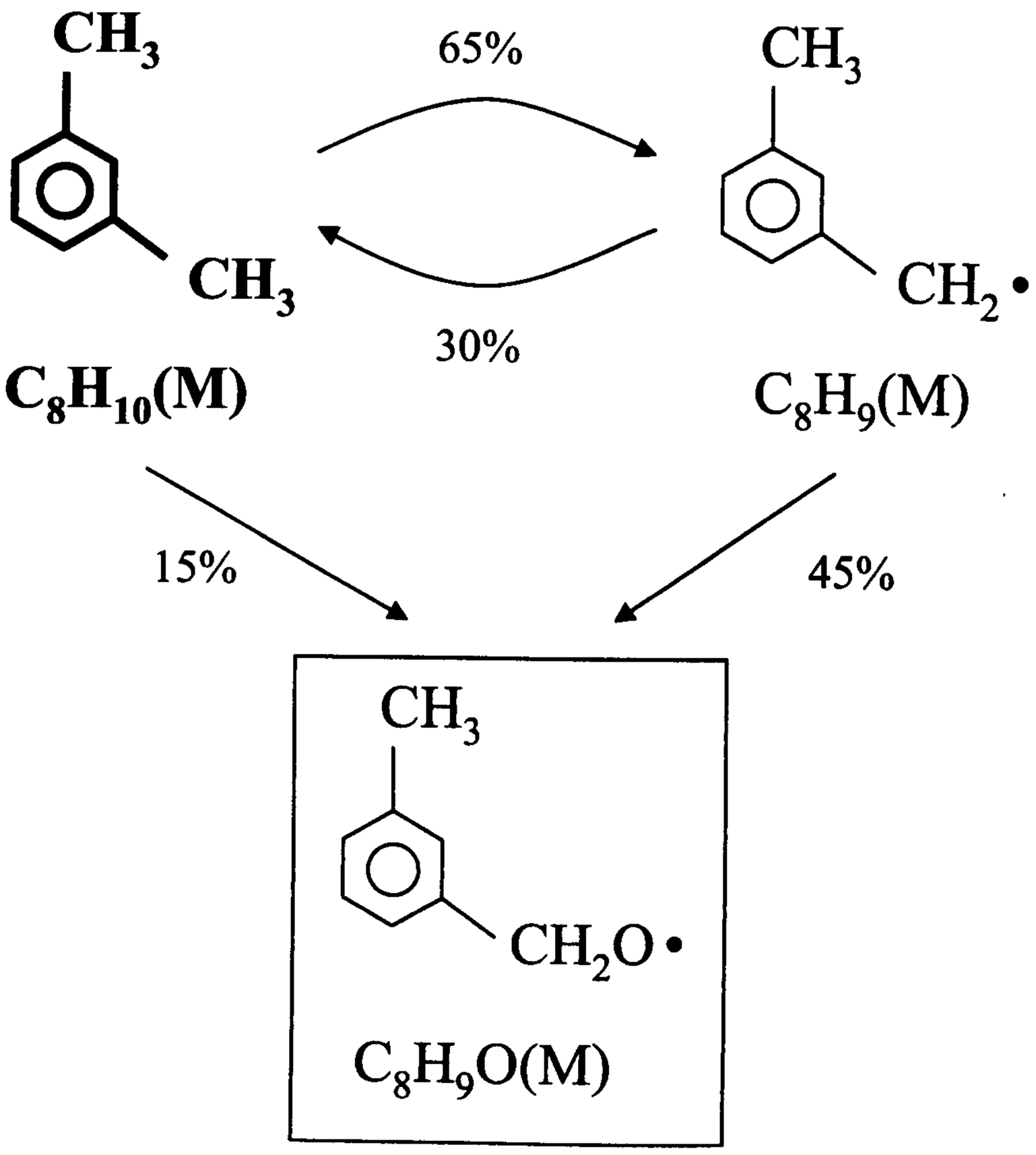


Figure 2.24: Diagram illustrating the consumption paths of the fuel m – xylene and its intermediate species in a Turbulent Flow Reactor at a reaction time of 50 ms. Species in boxes are considered in subsequent pages.

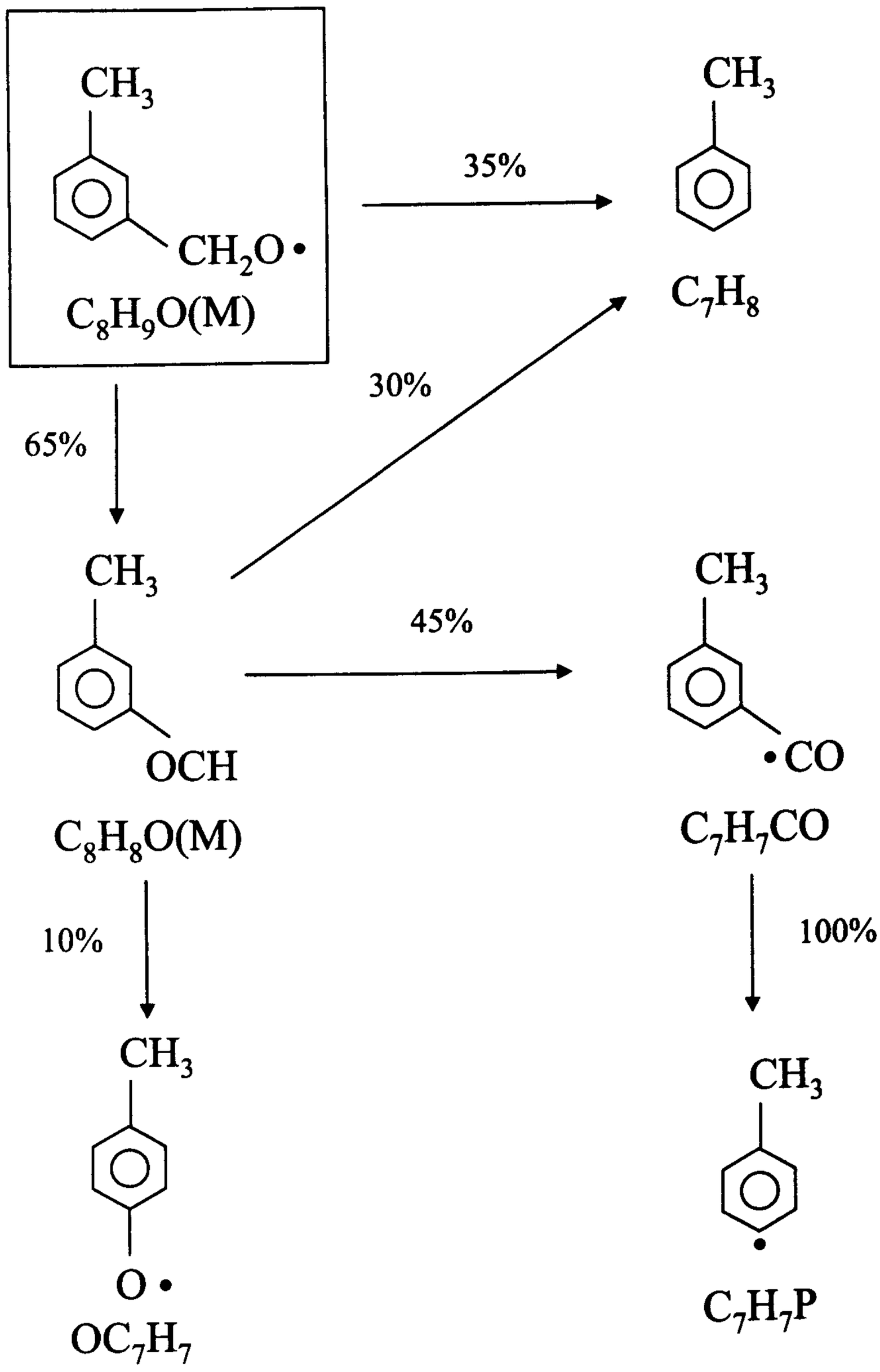


Figure 2.25: Diagram illustrating the consumption paths of the fuel m – xylene and its intermediate species in a Turbulent Flow Reactor at a reaction time of 50 ms. Species in boxes are considered in subsequent pages.

2.4 Summary

In the present chapter, a comprehensive detailed reaction mechanism for the inclusion of methyl – substituted aromatics representing components commonly found in diesel fuels has been developed and verified against a variety of experimental data. Overall, the detailed chemical kinetic mechanism has been found to perform well. However, there are issues that require further clarification in order to support the development of accurate detailed chemical kinetic mechanisms. The cleavage of the CH_3 group from the ring needs to have the thermodynamic issues resolved as discussed by Pamidimukkala *et al.* [199] and Rao & Skinner [208]. It is found that in all cases considered in this study, there is an under prediction for the concentration profiles regarding CH_4 which may stem from the unresolved issues in the rate parameters for reaction (1076).

$$C_7H_8 = C_6H_5 + CH_3 \quad (1076)$$

The analogy used for developing a comprehensive detailed chemical kinetic mechanism for m – xylene based on the oxidation of toluene has been shown to work well. However, common problems were also found. For example, the concentrations of C_7H_6O and C_8H_8O(M) were consistently over predicted for the various fuels. The reactions responsible are (1113) and (1253) for the toluene and m – xylene fuels respectively.

$$C_7H_7O = C_7H_6O + H \quad (1113)$$
$$C_8H_9O(M) = C_8H_8O(M) + H \quad (1253)$$

The over predictions may thus stem from the uncertainties in the estimation of reaction (1113) and the absence of fall off curves.

Problems were encountered in some of the experimental data used for mechanism validation. Further detailed mechanism validation and verification is still required to cover as large a variety of conditions as possible.

Various elementary reaction steps in the toluene sub – mechanism have been updated in this study. For example the rate parameters for the reaction regarding HO_2 attack on C_7H_7 radicals, as in reaction (1057)

$$C_7H_7 + HO_2 \quad = \quad C_7H_7O + OH \tag{1057}$$

utilises the recent work of Ellis *et al.* [86]. Naturally, these updated reaction rate parameters have been applied to the sub – mechanism of m – xylene.

Chapter 3

Phenylacetylene and n – Propylbenzene

3.1 Introduction

As discussed in Chapter 1, the formation of PAH is of particular importance to combustion modelling. Many reviews have been published (*e.g.* Bockhorn [21], Frenklach [95, 96], Kohse – Höinghaus *et al.* [152], Longwell [176], Richter *et al.* [213], Richter & Howard [214] and Stanmore *et al.* [237]) correlating PAH channels with soot formation.

Many studies, both experimental and detailed chemical kinetic mechanisms have been published (*e.g.* Bohm & Jander [24], Cole *et al.* [47], D'Anna & Violi [68], Faravelli *et al.* [93], Hwang *et al.* [137], Miller & Melius [188], Mingming & Mulholland [192] and Roesler & De Tessan [221]) concerning the formation of PAH's. However the focus of their work are for flame temperatures which are typically $\geq$ 1800 K. The present study focuses on the formation of PAH's under Turbulent Flow Reactor conditions which are typically 1170 K and thus much lower than flame temperatures. The

detailed kinetic mechanisms involved in the formation of PAH may be significantly different to that at flame temperatures. The practical aspect of PAH formation for temperatures typically 1170 K may be the boundary layer near the walls of a combustion engine since temperatures here will be significantly lower than in the centre.

Additionally a sub – mechanism for the oxidation of n – propylbenzene is explored. This alkyl – substituted aromatic is a useful component in representing the aromatic constituent in kerosene fuels. Hence, its combustion chemistry is of interest to engineers.

3.2 The Combustion of Phenylacetylene

Detailed chemical kinetic studies involving the combustion of phenylacetylene have not been found in the literature at present. However experimental data is available. Phenylacetylene is a key intermediate species in the formation and oxidation of MSA and PAH.

The experimental data set considered here is from Shaddix [226]. Phenylacetylene is combusted under Turbulent Flow Reactor conditions at atmospheric pressure and an initial temperature of 1172 K. It should be noted that an amendment was made to the initial conditions in this study. The growth of C_8H_8 is extremely rapid as is evident in Figure 3.2 and the species behaves as a secondary fuel. It would accordingly appear possible that some pre – combustion and/or cracking of the fuel did occur. This suspicion of error led to the following adjustment for the initial conditions. Accordingly, initial concentrations of CO, CO_2, C_8H_8 and H_2O with values of 750, 1000, 45, and 660 ppm respectively is given to these species. Additionally, the fuel was reduced by 220 ppm corresponding to the amount required to produce 1000 and 750 ppm of CO_2 and CO respectively. Shaddix reports an uncertainty

of 32 ms in the temporal evolution.

A comparison of the results produced from the detailed chemical kinetic mechanism and the experimental data from Shaddix [226] is illustrated in Figures 3.1 – 3.8. Overall the detailed chemical mechanism performs well given the experimental uncertainties in the initial fuel mixture. The fuel decay profile along with molecular oxygen, CO and CO_2 are well produced by the detailed chemical mechanism as is evident in Figure 3.1.

The first PAH mass growth species indene, is well produced by the detailed chemical kinetic mechanism as is evident in Figure 3.2 and formation paths are discussed below.

The concentrations for C_7H_6O are under predicted although the trends are accurate as is evident in Figure 3.2. It is found that at a reaction time of 2.5 ms, the initial growth of C_7H_6O is controlled by reaction (1041)

$$C_6H_5CH + O_2 \quad = \quad C_7H_6O + O \tag{1041}$$

with the rate for reaction being modelled on the analogous equivalent reaction (56).

$$^3CH_2 + O_2 \quad = \quad CH_2O + O \tag{56}$$

The rate parameters for reaction (56) have been discussed by Rizos [218]. It may be concluded that uncertainties in the rate parameters in the modelling of reaction (1041) may play a pivitol role in improving the computations for C_7H_6O.

Levels of C_7H_8 are well produced by the detailed chemical kinetic mechanism as illustrated in Figure 3.2. Reaction (1077) is found to be the dominant channel for C_7H_8 and contributes 80 %.

$$C_7H_8 \quad = \quad C_7H_7 + H \tag{1077}$$

The rate parameters applied to reaction (1077) have been discussed in Chapter 2.

Given the uncertainties in the initial fuel mixture the levels of C_8H_8 are well produced with respect to the experimental data from Shaddix [226]. The dominant formation path is via reaction (1199)

$$C_8H_9 = C_8H_8 + H \quad (1199)$$

The rate parameters applied to reaction (1199) have been discussed in Chapter 2.

The calculations for C_6H_5OH are poor in terms of magnitudes and trends as shown in Figure 3.3, although experimental data is missing for the first 50 ms. In the first 2 ms, reaction (1002) is the dominant channel leading to C_6H_5OH.

$$C_6H_5O + H = C_6H_5OH \quad (1002)$$

The rate adopted is from Baulch *et al.* [13] as reported by Maurice [182].

Levels of C_6H_6 are excellent as is evident in Figure 3.3. Reaction (985) is found to be the dominant route to C_6H_6.

$$C_6H_6(F) + H = C_6H_6 + H \quad (985)$$

The calculations for $C_4H_6(T)$ and C_5H_6 are reproduced well in terms of magnitude but not in terms of trends. Both species are derived from C_5H_5.

$$C_5H_5 + OH = C_4H_6(T) + CO \quad (794)$$
$$C_5H_6 = C_5H_5 + H \quad (810)$$

It can tentatively be concluded that uncertainties for the formation of the C_5H_5 radical may be responsible for the poor trend agreement. The rates for reactions (794) and (810) have been discussed in the text of Rizos [218].

Levels of smaller species such as C_2H_2, C_2H_4, C_4H_4 and C_3 species are well reproduced as illustrated in Figure 3.4. The dominant channel for C_2H_2 is found to be (932).

$$C_6H_5 + C_2H_2 \quad = \quad C_8H_6 + H \qquad (932)$$

The high concentrations of C_2H_2 would suggest a very direct channel from the fuel. This is evident as shown above. The rate adopted for reaction (932) is from the work of Richter *et al.* [216] who used theoretical calculations to evaluate the rate parameters over temperature and pressure ranges of 300 – 2100 K and 1 – 10 atm. Herzler & Frank [113] have also investigated the rate for reaction (932) under Shock – Tube conditions over a temperature range of 1600 – 1900 K and a pressure of 2.3 atm. It is found that at 1200 K, the rate parameters proposed by Herzler & Frank [113] is 20 times faster than that proposed by Richter *et al.* [216].

The calculations for C_2H_4 are very good as is evident in Figure 3.4. It is found that reaction (935) is the main channel.

$$C_2H_4 + C_6H_5 \quad = \quad C_8H_8 + H \qquad (935)$$

The rate stems from Fahr & Stein [91] as reported by Maurice [182].

The concentrations for C_4H_4 are well produced, with reaction (568) the dominant channel.

$$C_4H_5(T) + O_2 \quad = \quad C_4H_4 + HO_2 \qquad (568)$$

The rate parameters applied to reaction (568) are discussed by Rizos [218].

Levels of anthracene and phenanthrene are well produced in terms of trends. However, concentrations are under predicted in terms of magnitudes as is evident in Figures 3.6 and Figures 3.7 respectively. Consideration must however, be given to the experimental uncertainties for these minor species.

The temporal evolution of the temperature profile is shown in Figure 3.8. The trend produced by the detailed chemical kinetic mechanism is very acceptable.

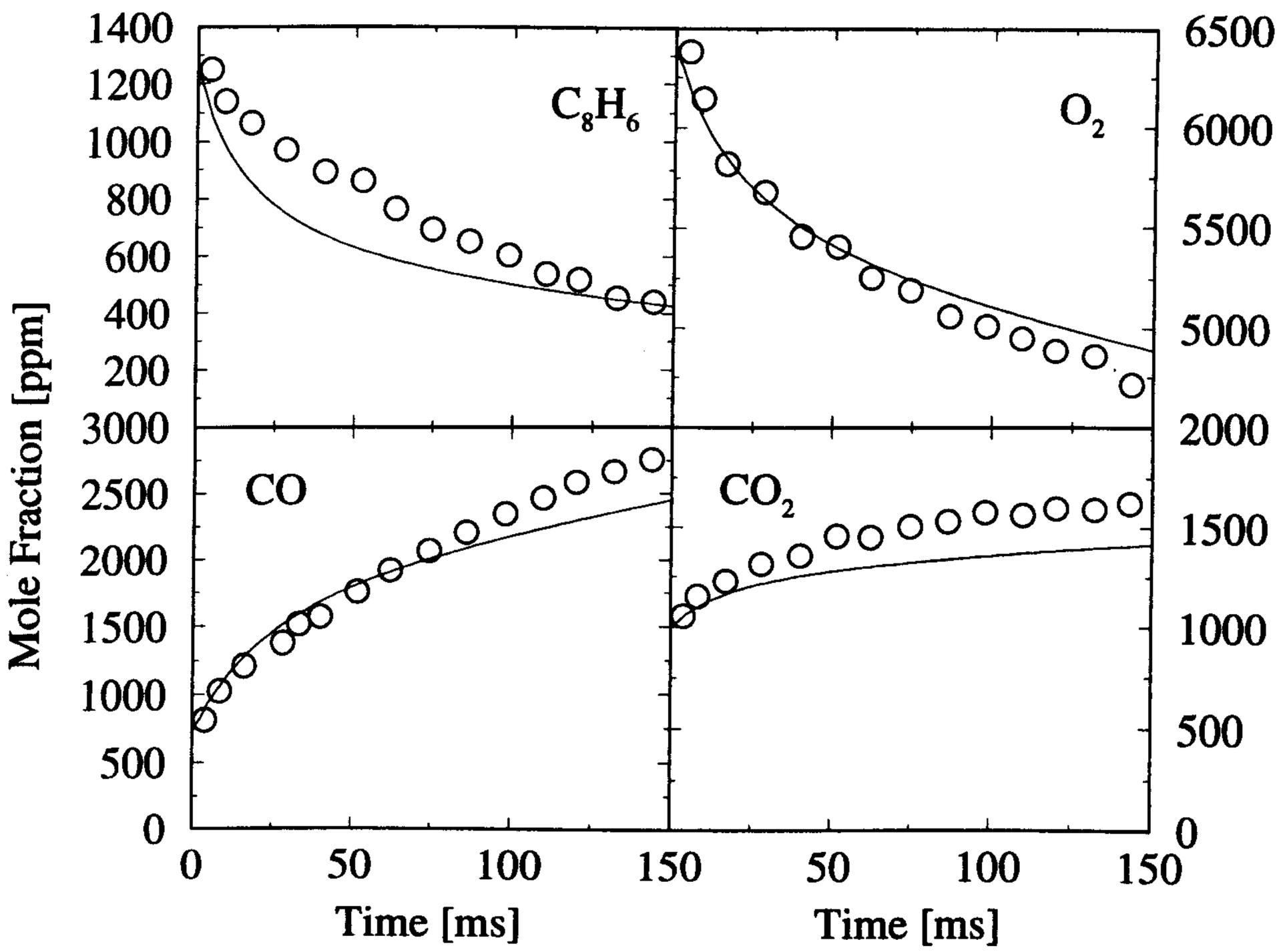


Figure 3.1: Graph of species profile concentrations versus time for the oxidation of phenylacetylene in a Turbulent Flow Reactor. Experimental points are from Shaddix [226]. Solid lines are the computations from the detailed chemical mechanism and have not been time shifted.

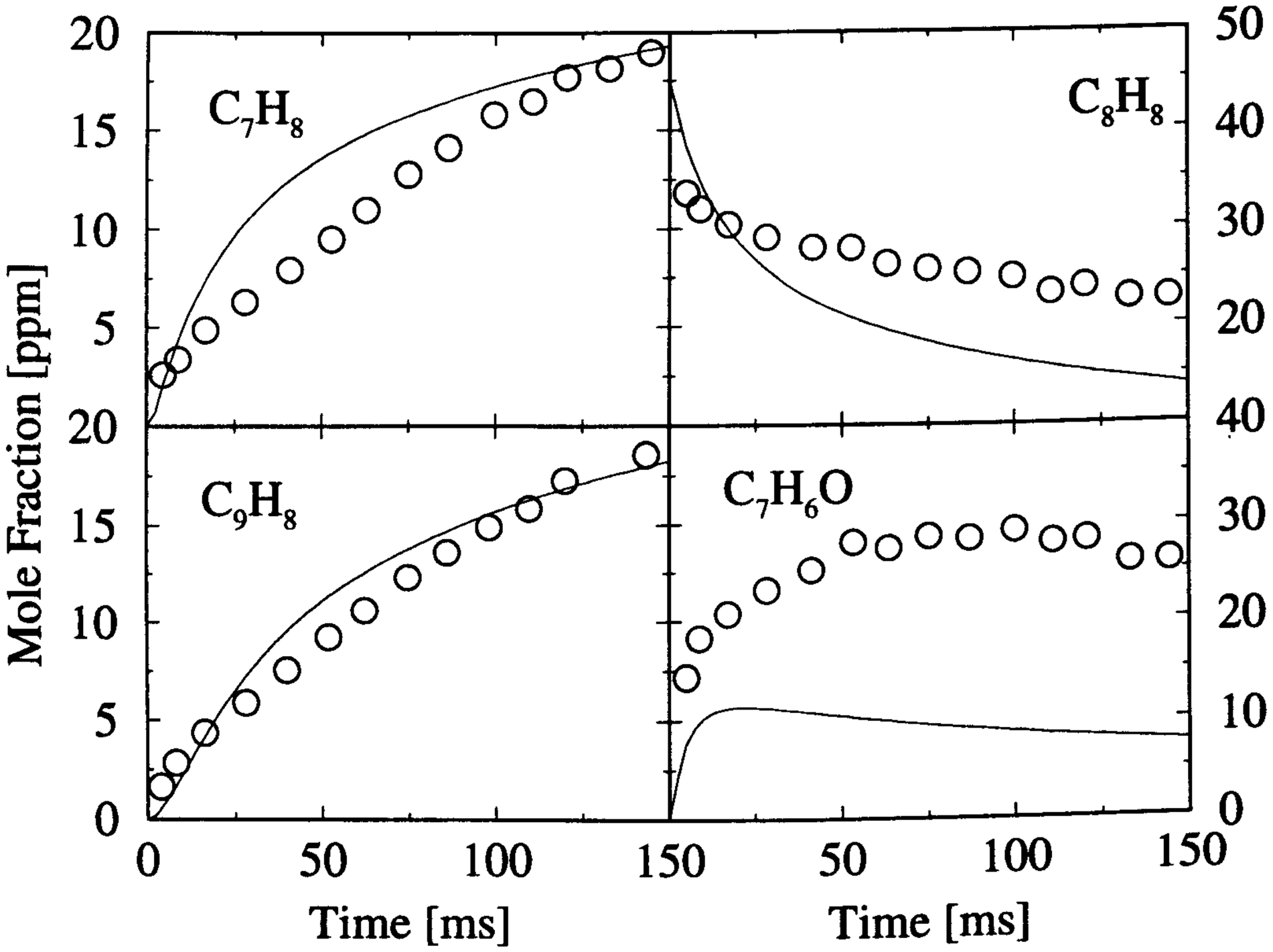


Figure 3.2: Graph of species profile concentrations versus time for the oxidation of phenylacetylene in a Turbulent Flow Reactor. Experimental points are from Shaddix [226]. Solid lines are the computations from the detailed chemical mechanism and have not been time shifted.

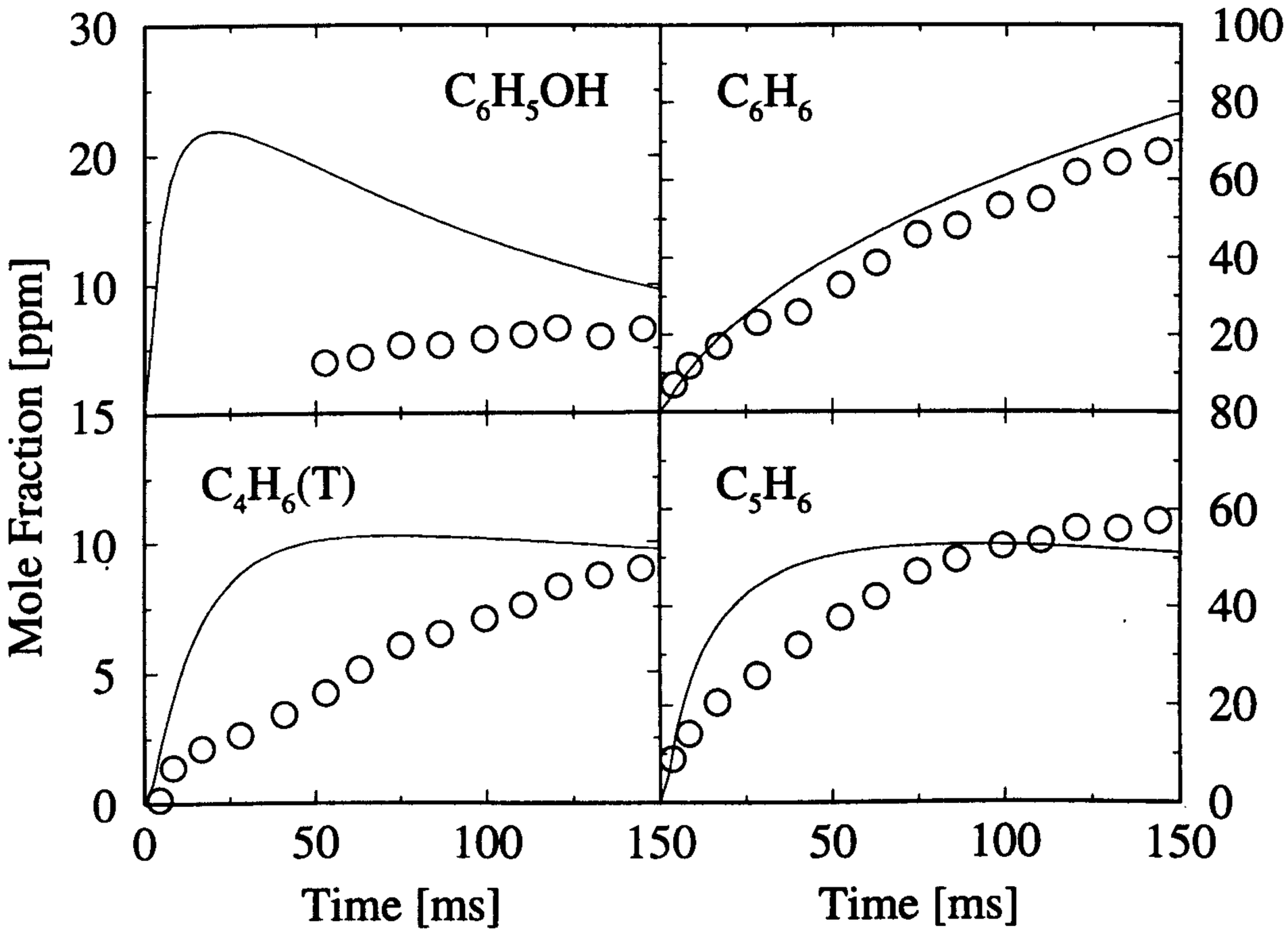


Figure 3.3: Graph of species profile concentrations versus time for the oxidation of phenylacetylene in a Turbulent Flow Reactor. Experimental points are from Shaddix [226]. Solid lines are the computations from the detailed chemical mechanism and have not been time shifted.

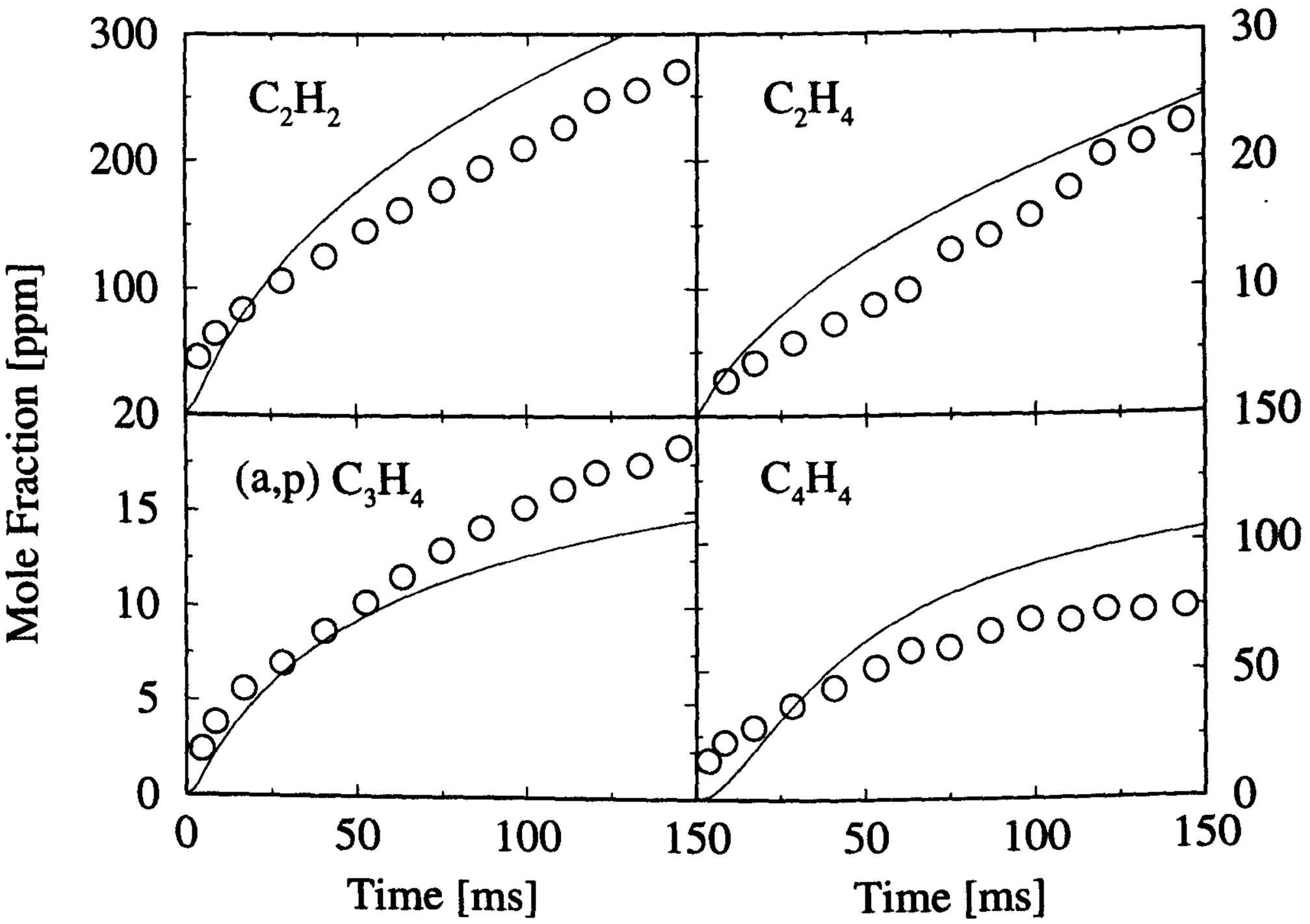


Figure 3.4: Graph of species profile concentrations versus time for the oxidation of phenylacetylene in a Turbulent Flow Reactor. Experimental points are from Shaddix [226]. Solid lines are the computations from the detailed chemical mechanism and have not been time shifted.

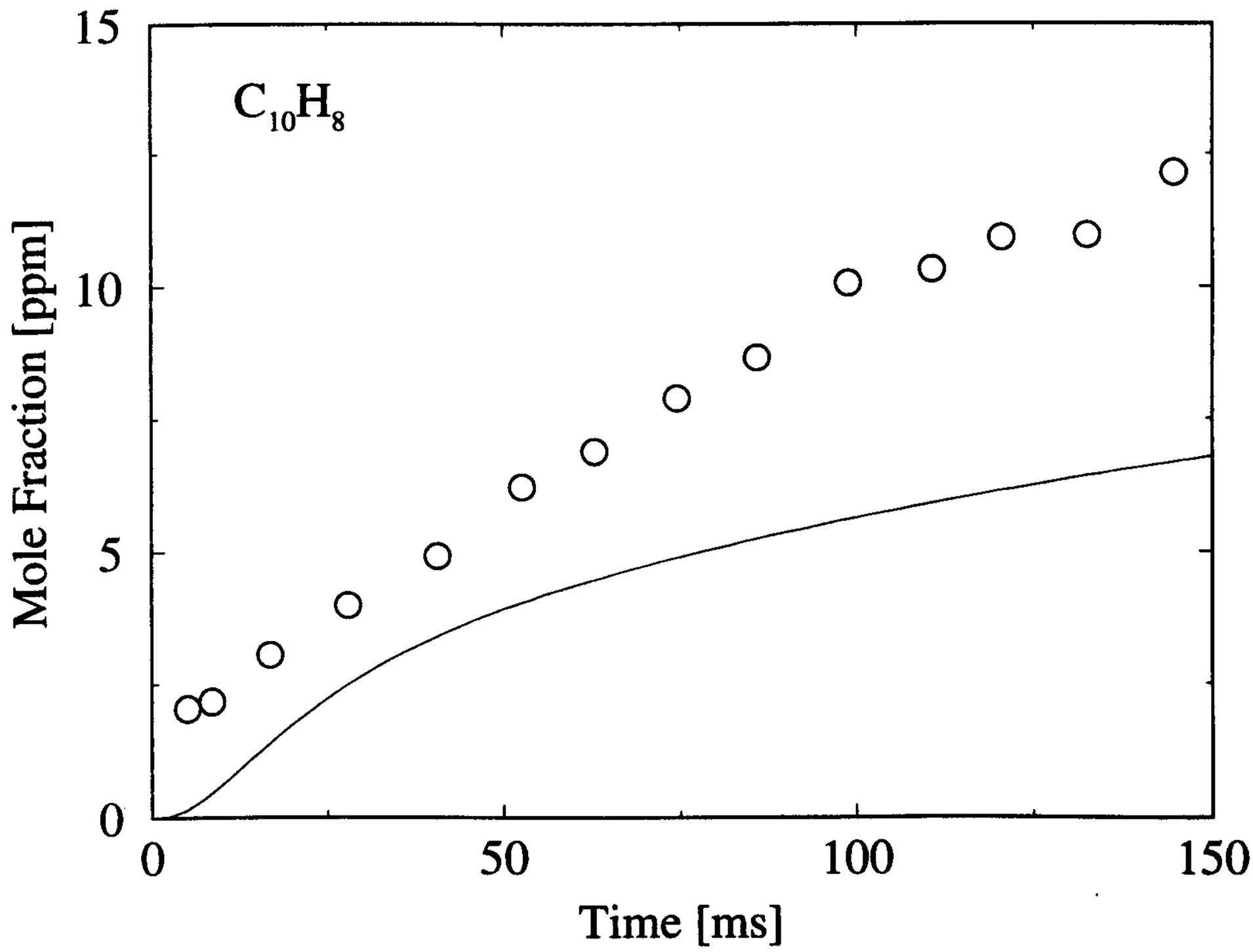


Figure 3.5: Graph of naphthalene species profile concentrations versus time for the oxidation of phenylacetylene in a Turbulent Flow Reactor. Experimental points are from Shaddix [226]. Solid lines are the computations from the detailed chemical mechanism and have not been time shifted.

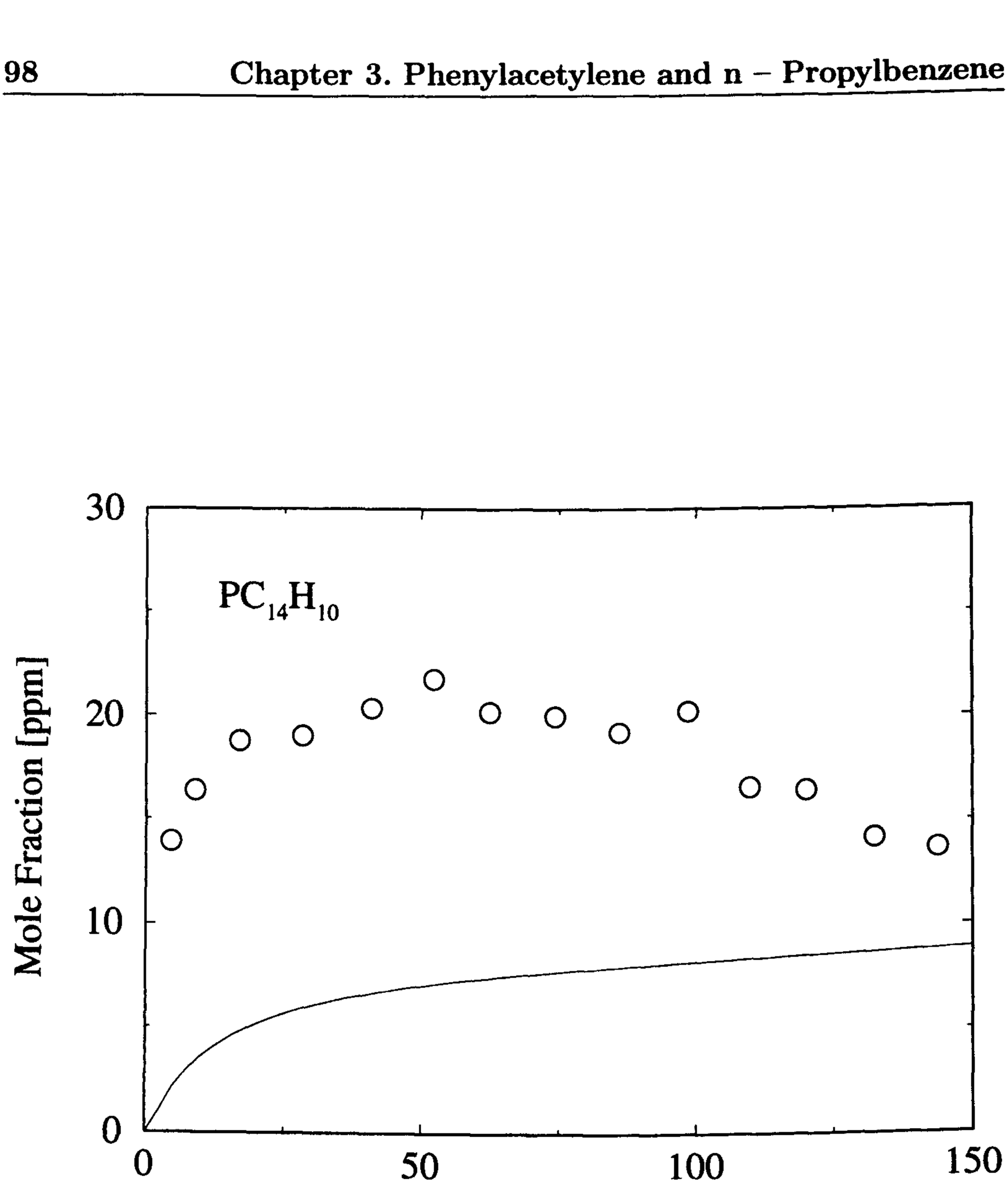


Figure 3.6: Graph of phenanthrene species profile concentrations versus time for the oxidation of phenylacetylene in a Turbulent Flow Reactor. Experimental points are from Shaddix [226]. Solid lines are the computations from the detailed chemical mechanism and have not been time shifted.

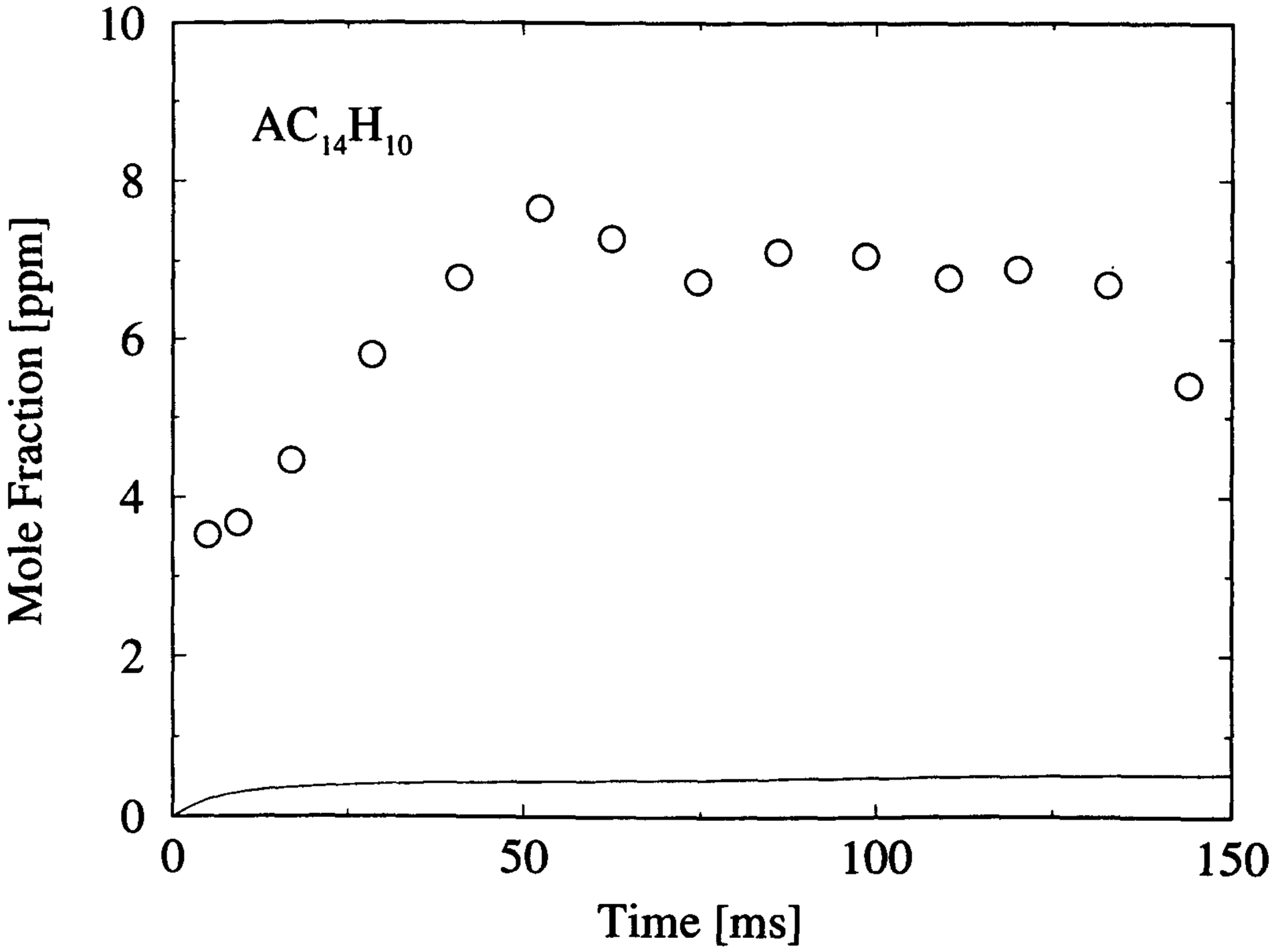


Figure 3.7: Graph of anthracene species profile concentrations versus time for the oxidation of phenylacetylene in a Turbulent Flow Reactor. Experimental points are from Shaddix [226]. Solid lines are the computations from the detailed chemical mechanism and have not been time shifted.

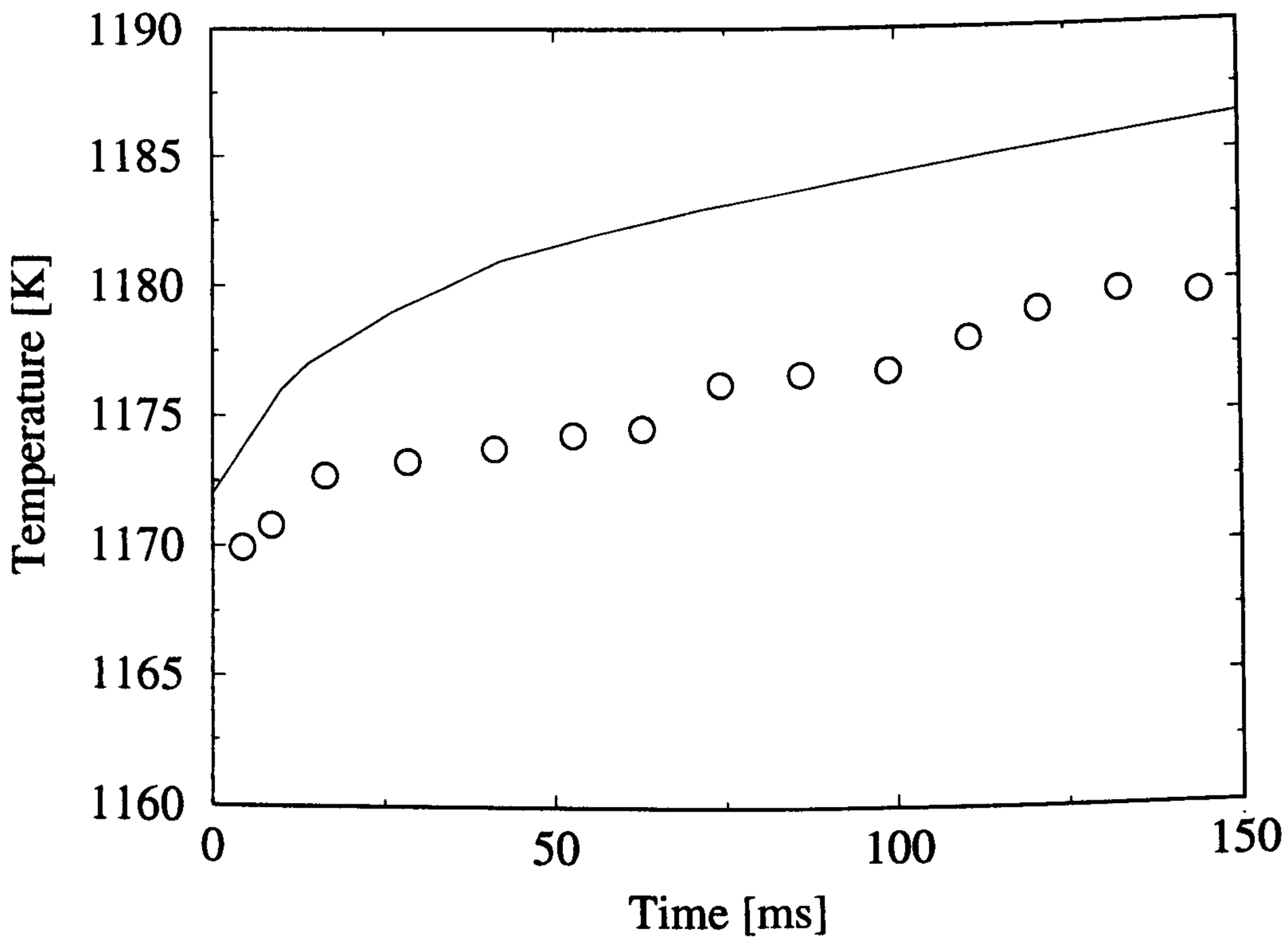


Figure 3.8: Graph of temperature profile versus time for the oxidation of phenylacetylene in a Turbulent Flow Reactor. Experimental points are from Shaddix [226]. Solid lines are the computations from the detailed chemical mechanism and have not been time shifted.

3.2.1 Primary Reaction Paths for Phenylacetylene Oxidation

The oxidation of phenylacetylene proceeds through a number of chemical paths as shown in Figures 3.9 – 3.10. The general modelling approach for developing a phenylacetylene sub – mechanism is to model the side chain reactions on acetylene. The acetylene sub – mechanism has been reviewed in the study by Rizos [218] and follows the work of Lindstedt & Skevis [172]. Ring attack is also considered with the rates modelled on benzene reactions. The major reaction path analysis is conducted at a reaction time of 50 ms.

Radical attack on the fuel is governed by O and OH attack with reaction (1160) contributing 35 % and reactions (1154), (1155) and (1151) 15 % each.

$$C_8H_6 + OH = C_8H_5 + H_2O \quad (1160)$$

$$C_8H_6 + O = C_6H_5C_2O + H \quad (1154)$$

$$C_8H_6 + O = C_8H_5O + H \quad (1155)$$

$$C_8H_6 + O = C_6H_5 + C_2HO \quad (1151)$$

The rate for reaction (1160) has been adopted from Frenklach & Wang [96].

The rate for reaction (1154), involving O radical attack on the side chain, is modelled on reaction (146).

$$C_2H_2 + O = C_2HO + H \quad (146)$$

The rate adopted for reaction (1155) has been modelled on the analogous reaction (959) with rate parameters as discussed in Chapter 2.

$$C_6H_6 + O = C_6H_5O + H \quad (959)$$

Reaction (1151) has been modelled on the analogous reaction (146).

$$C_2H_2 + O = C_2HO + H \quad (146)$$

The C_8H_5 radical undergoes O_2 attack on to the ring (75 %) via (1142).

$$C_8H_5 + O_2 = C_8H_5OO \quad (1142)$$

The rate for reaction (1142) is based on the analogous equivalent reaction with the rate parameters as discussed in Chapter 4.

$$C_6H_5 + O_2 = C_6H_5OO \quad (931)$$

A further 25 % of the C_8H_5 radical is consumed via reaction (1141) with the rate modelled on reaction (930).

$$C_8H_5 + O_2 = C_8H_5O + O \quad (1141)$$
$$C_6H_5 + O_2 = C_6H_5O + O \quad (930)$$

The C_8H_5OO radical thermally decomposes with reactions (1233) and (1232) contributing 55 % and 45 % respectively.

$$C_8H_5OO = C_8H_5O + O \quad (1233)$$
$$C_8H_5OO = C_7H_5 + CO_2 \quad (1232)$$

The rates for reactions (1233) and (1232) have been modelled on reactions (1008) and (1006).

$$C_6H_5OO = C_6H_5O + O \quad (1008)$$
$$C_6H_5OO = C_5H_5 + CO_2 \quad (1006)$$

The C_8H_5O radical also decomposes to the C_7H_5 radical via reaction (1231).

$$C_8H_5O = C_7H_5 + CO \quad (1231)$$

The C_7H_5 radical undergoes H attack with the dominant reaction (1029) contributing (80 %).

$$C_7H_6 + H = C_7H_5 + H_2 \quad (1029)$$

The rate for reaction (1029) is modelled on reaction (812) as discussed by Lindstedt & Rizos [170].

$$C_5H_6 + H = C_5H_5 + H_2 \quad (812)$$

The C_7H_6 compound undergoes H and O radical attack via reactions (1069), (1028) and (1032).

$$C_7H_7L = C_7H_6 + H \quad (1069)$$
$$C_7H_6 + H = C_5H_5 + C_2H_2 \quad (1028)$$
$$C_7H_6 + O = C_7H_5 + OH \quad (1032)$$

The rates for reactions (1069) and (1028) are adopted from Braun–Unkhoff *et al.* [27] as reported by Maurice [182].

The rates for reaction (1032) is obtained from the analogous reaction

$$C_5H_6 + O = C_5H_5 + OH \quad (814)$$

which has been discussed in the text of Lindstedt & Rizos [170] along with the consumption of the smaller species.

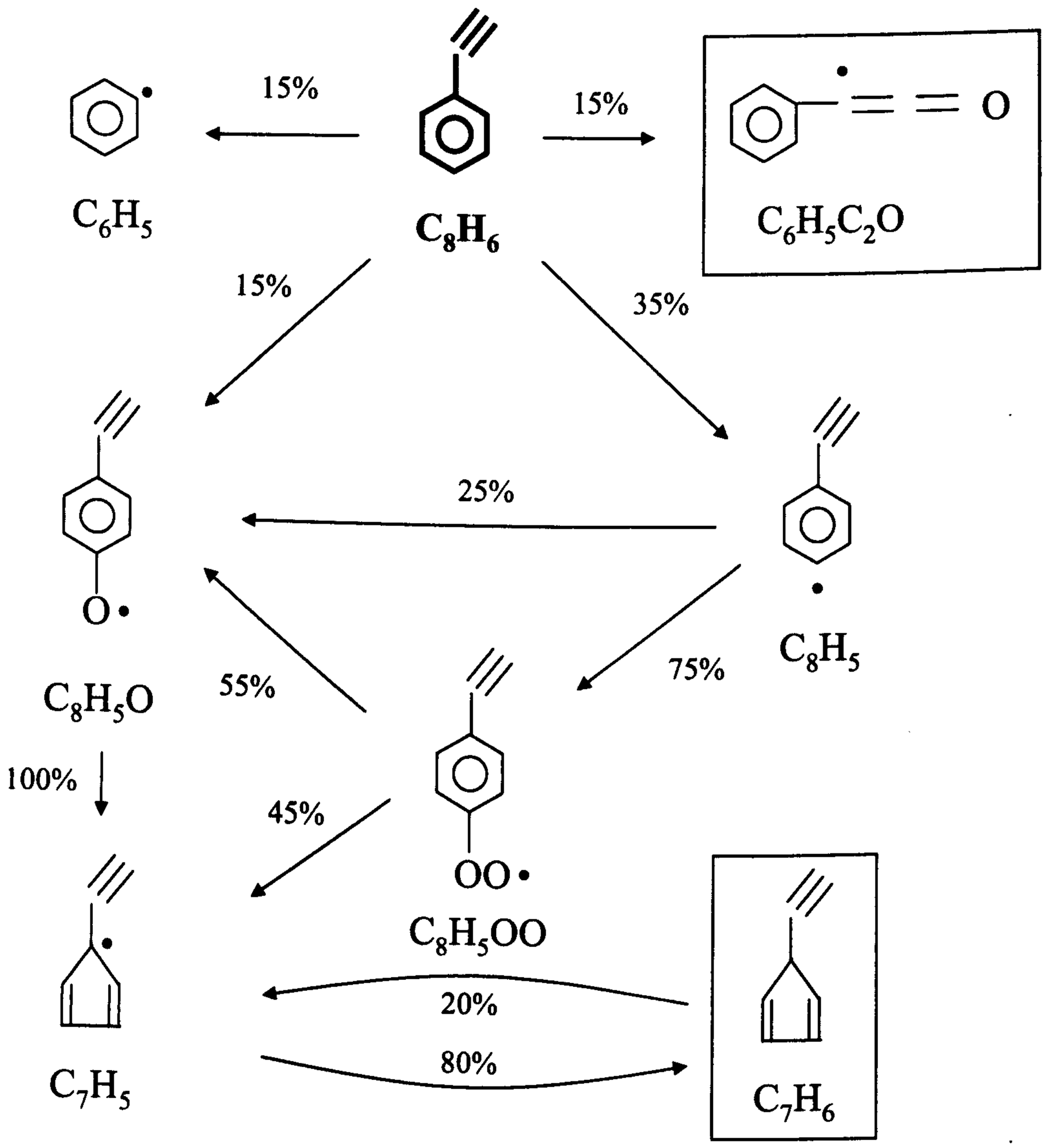


Figure 3.9: Diagram illustrating the consumption paths of the fuel phenylacetylene and its intermediate species in a Turbulent Flow Reactor at a reaction time of 50 ms. Species in boxes are considered in subsequent pages.

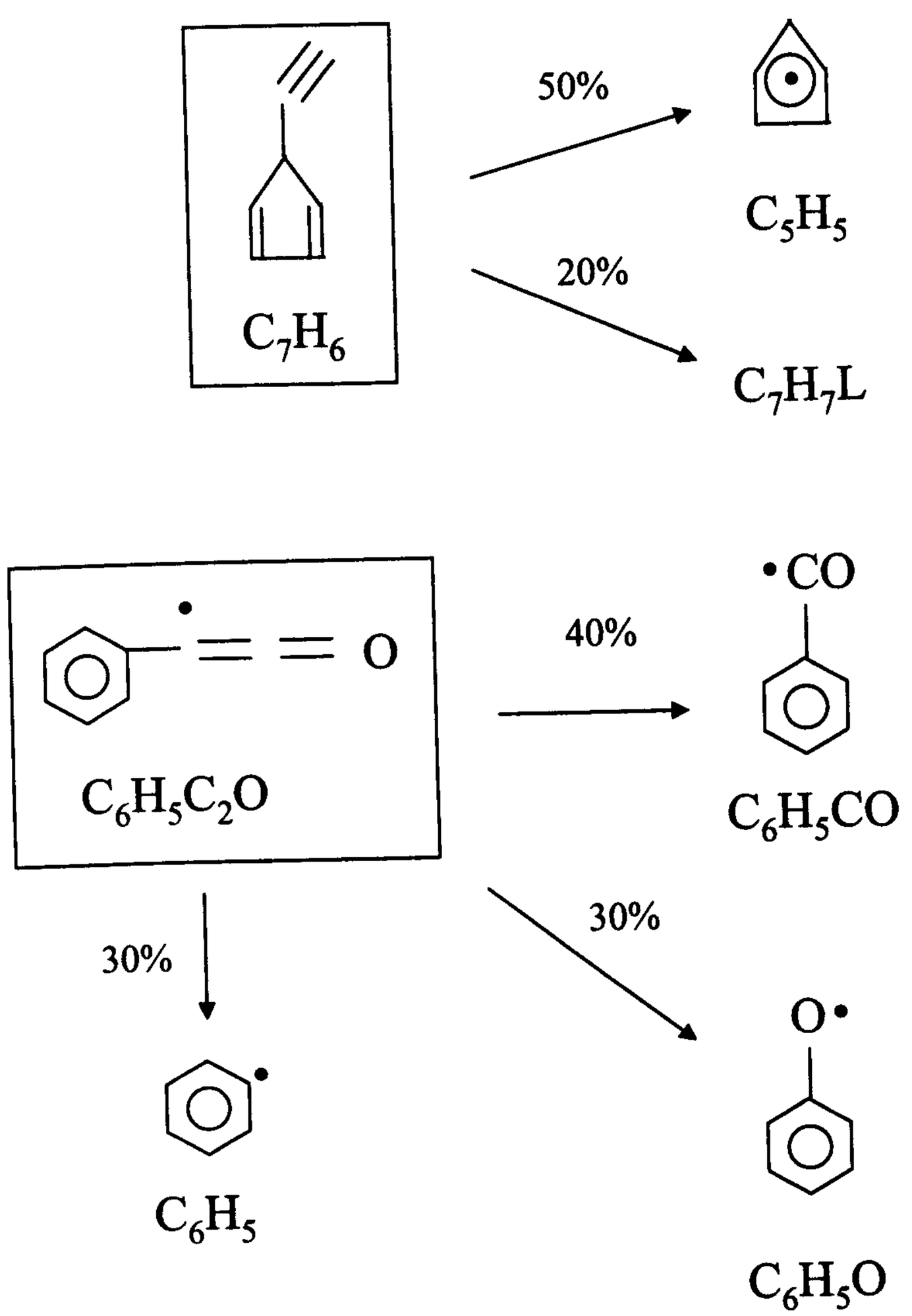


Figure 3.10: Diagram illustrating the consumption paths of the fuel phenylacetylene and its intermediate species in a Turbulent Flow Reactor at a reaction time of 50 ms. Species in boxes are considered in subsequent pages.

3.2.2 The Formation of Indene

Indene concentration profiles are shown in Figure 3.2. It is evident that the model produces very good agreement with the experimental data from Shaddix [226]. The key features of indene formation have been presented in the work of Lindstedt *et al.* [169] and a summary is given here. Figures 3.11 and 3.12 show schematic diagrams for the indene formation sequence.

The sequence is initiated by the formation of $C_9H_8(T)$ via reaction steps (1047) and (1165) contributing $\sim$ 50 % each.

$$C_6H_5CH + C_2H_2 = C_9H_8(T) \quad (1047)$$

$$C_8H_6 + {}^3CH_2 = C_9H_8(T) \quad (1165)$$

The rate for reaction (1047) is estimated whilst the rate for reaction (1165) is adopted from Lindstedt *et al.* [169].

The $C_9H_8(T)$ formed then undergoes H addition via (1291) with the rate obtained from Lindstedt *et al.* [169].

$$C_9H_9(I) = C_9H_8(T) + H \quad (1291)$$

It is found that reaction (1291) is the rate limiting step in this indene formation sequence.

The $C_9H_9(I)$ radical then goes through the isomerisation sequences described by (1292), (1293) and (1295)

$$C_9H_9(I) = C_9H_9(N) \quad (1292)$$

$$C_9H_9(N) = C_9H_9(S) \quad (1293)$$

$$C_9H_9(S) = C_9H_8 + H \quad (1295)$$

Indene is finally produced from the thermal decomposition via C – H cleavage (1295). The rates have been adopted from Lindstedt *et al.* [169].

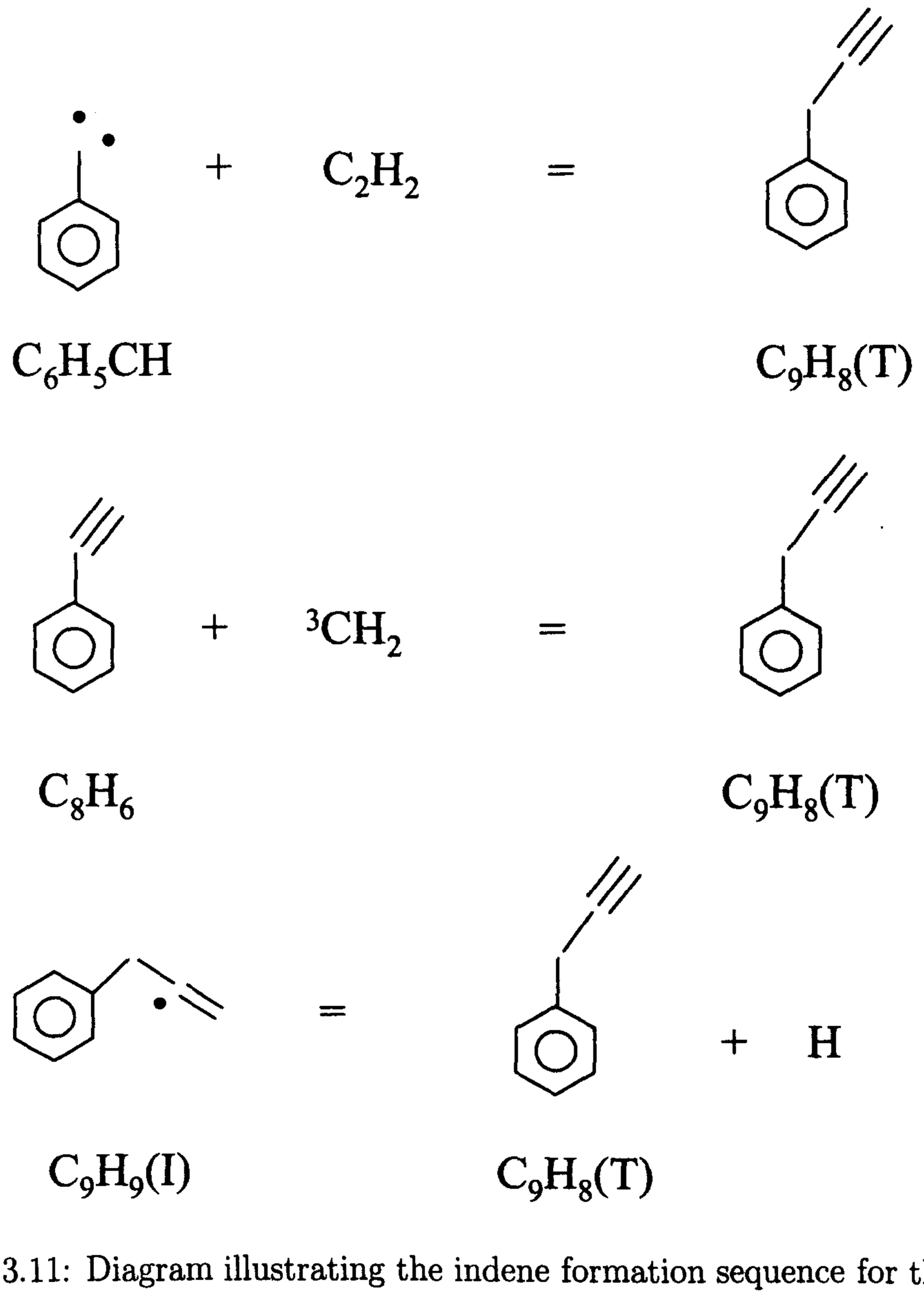
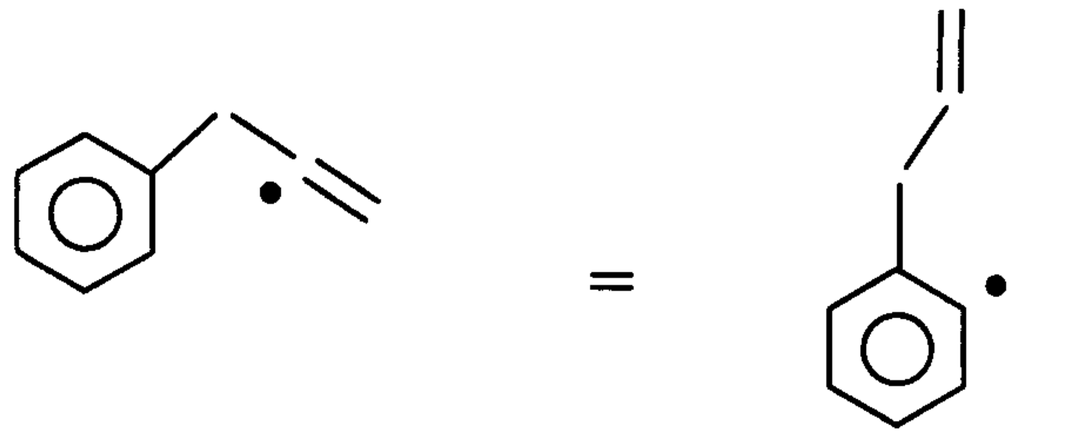
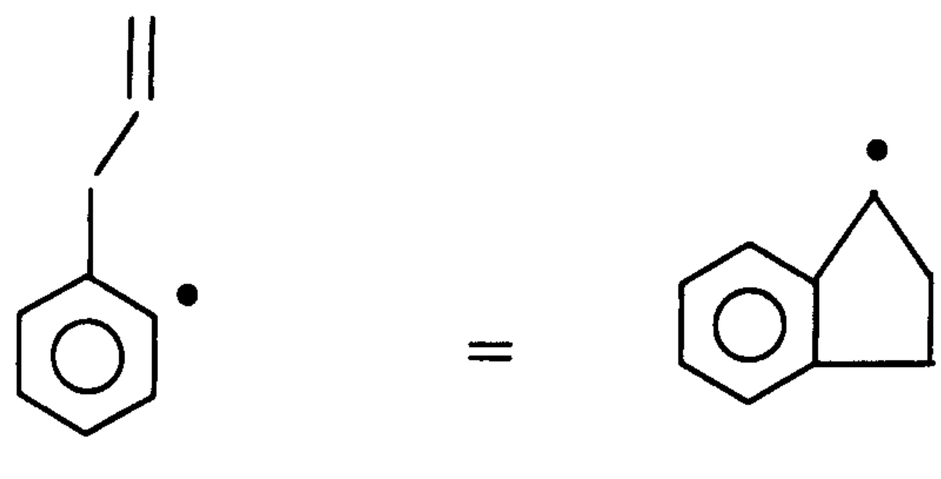


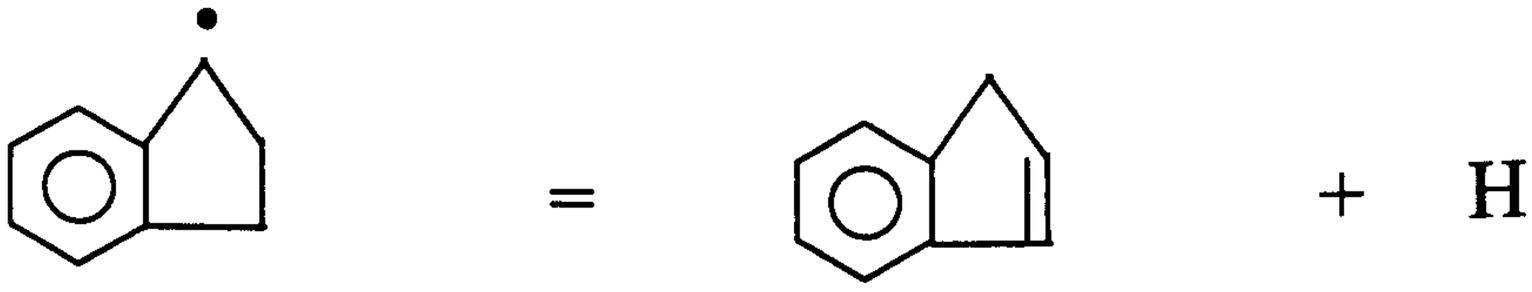
Figure 3.11: Diagram illustrating the indene formation sequence for the oxidation of phenylacetylene in a Turbulent Flow Reactor. Species in boxes are considered in subsequent pages.



$C_9H_9(I)$ $C_9H_9(N)$



$C_9H_9(N)$ $C_9H_9(S)$



$C_9H_9(S)$ C_9H_8 + H

Figure 3.12: Diagram illustrating the indene formation sequence for the oxidation of phenylacetylene in a Turbulent Flow Reactor. Species in boxes are considered in subsequent pages.

3.2.3 The Formation of Naphthalene

Naphthalene concentration profiles are illustrated in Figure 3.5. It is evident that the model produces good agreement with the experimental data from Shaddix [226]. The key features of naphthalene formation have been presented in the work of Lindstedt *et al.* [169], with a summary given here. Figure 3.13 shows a schematic diagram for the formation of naphthalene.

The sequence is initiated by the radical $C_8H_7(P)$ undergoing C_2H_2 addition to form the radical $C_{10}H_9P$ as in reaction (1189) with the rate adopted from Lindstedt *et al.* [169].

$$C_8H_7P + C_2H_2 \quad = \quad C_{10}H_9P \tag{1189}$$

It is found that reaction (1189) is the rate limiting step in the naphthalene formation sequence.

The $C_{10}H_9P$ radical formed then isomerises to the $C_{10}H_9T$ radical via reaction (1347) with the rate being adopted from Lindstedt *et al.* [169].

$$C_{10}H_9P \quad = \quad C_{10}H_9T \tag{1347}$$

The $C_{10}H_9T$ radical thermally decomposes via C – H cleavage (1318) producing naphthalene and H radicals. The rate stems from the work of Lindstedt *et al.* [169].

$$C_{10}H_8 + H \quad = \quad C_{10}H_9T \tag{1318}$$

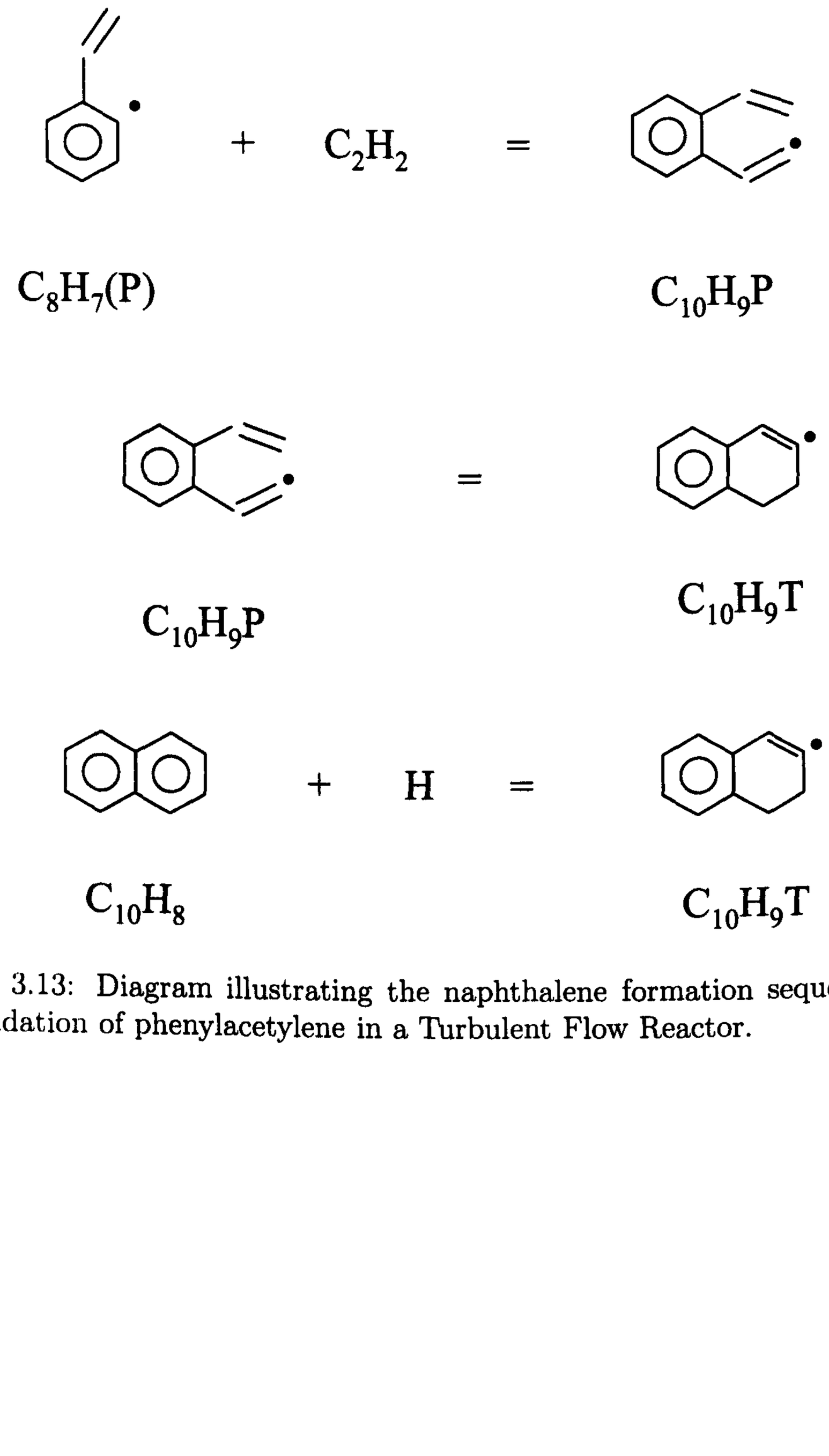


Figure 3.13: Diagram illustrating the naphthalene formation sequence for the oxidation of phenylacetylene in a Turbulent Flow Reactor.

3.2.4 The Formation of Phenanthrene and Anthracene

Species concentration profiles for the three ringed structures phenanthrene and anthracene are shown Figures 3.6 and 3.7 respectively. As mentioned before, although the trends are good, the magnitudes are low. The relative sequences leading to the formation of phenanthrene and anthracene are discussed below with schematic diagrams for the formation sequences given in Figures 3.14 and 3.15 respectively.

A direct path leads to the formation of phenanthrene via reaction (1465).

$$C_8H_6 + C_6H_5 \quad = \quad PC_{14}H_{10} + H \qquad (1465)$$

A frequency factor of 2.0E+10 and a barrier of 40 kJ/mol is implemented to take into account a H transfer.

The formation of anthracene is governed by three sequences as discussed below. The isomerisation of phenanthrene to anthracene via the reverse of reaction (1464) contributes 25 %.

$$AC_{14}H_{10} \quad = \quad PC_{14}H_{10} \qquad (1464)$$

The rate has been obtained from Richter & Howard [215]. Anthracene is also formed by the global steps (1466) and (1467)

$$C_8H_6 + C_6H_5CH \quad = \quad AC_{14}H_{10} + {}^3CH_2 \qquad (1466)$$

$$C_6H_5CH + C_6H_5CH = \quad AC_{14}H_{10} + H_2 \qquad (1467)$$

Reaction (1466) has a barrier of 80 kJ/mol to take into account two hydrogen transfers. Reaction (1467) has been estimated. It is found that reaction (1466) and (1467) contribute 25 % and 75 % respectively.

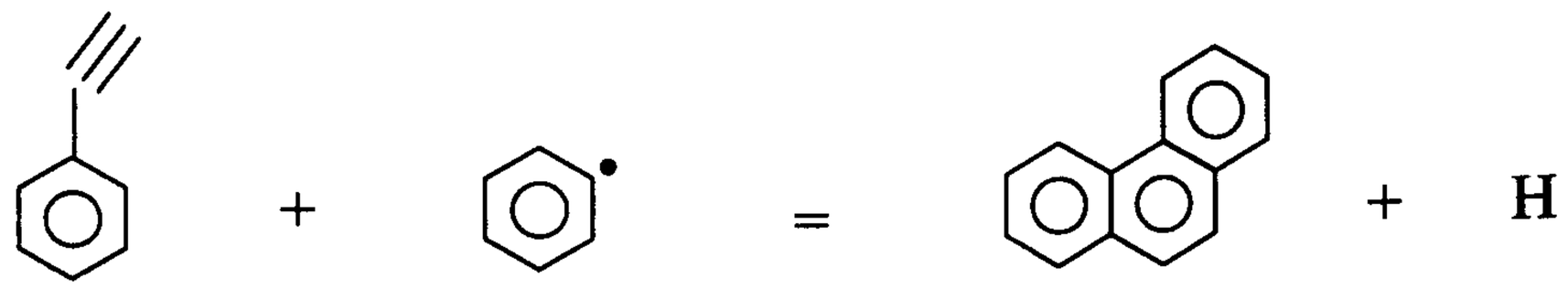
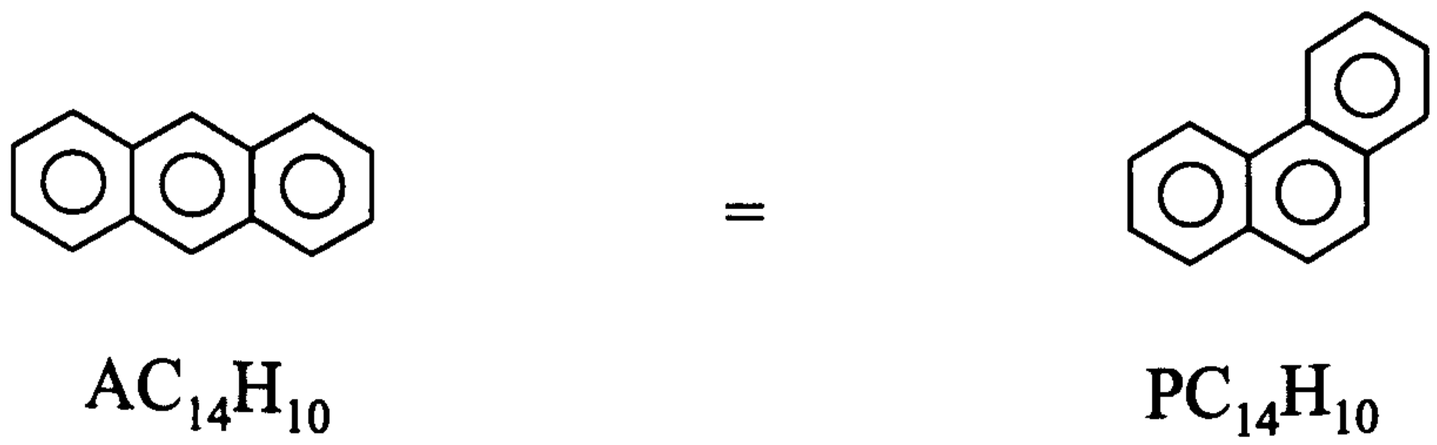


Figure 3.14: Diagram illustrating the phenanthrene formation sequence for the oxidation of phenylacetylene in a Turbulent Flow Reactor.



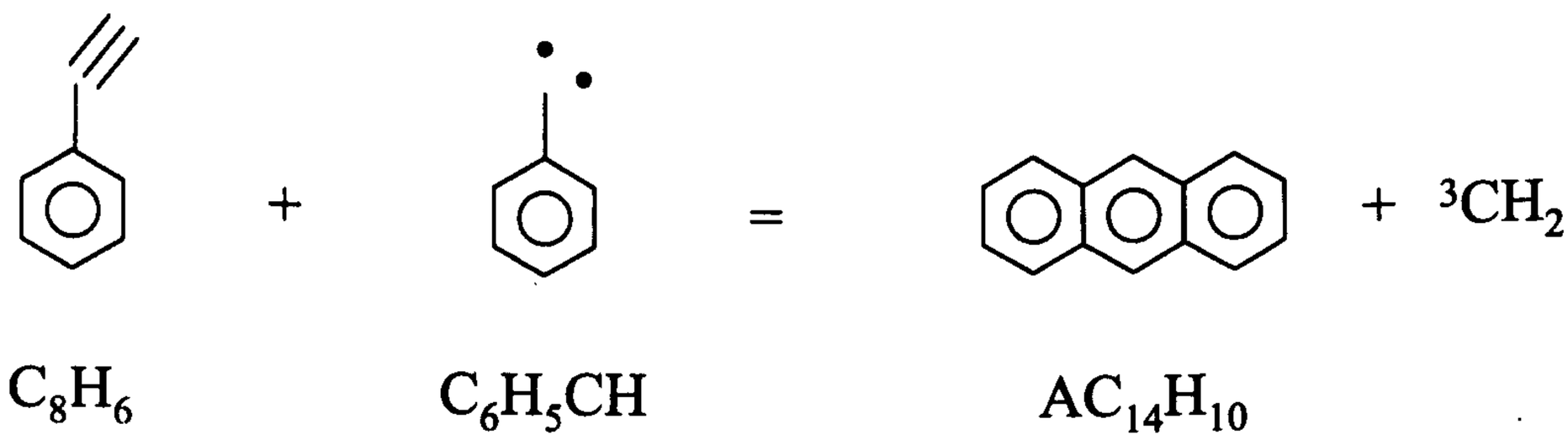


Figure 3.15: Diagram illustrating the anthracene formation sequence for the oxidation of phenylacetylene in a Turbulent Flow Reactor.

3.3 The Oxidation of n – Propylbenzene

The choice of the aromatic component for the constituents of kerosene fuels is further broadened with the study of the oxidation of propylbenzene. The complexity is high enough to be selected for representing the monocyclic alkyl – aromatic content of practical fuels [60]. Litzinger [174] studied the oxidation of n – propylbenzene in a Turbulent Flow Reactor for low fuel conversion at a temperature of approximately of 1060 K for stoichiometric ratios of $\phi = 0.65$, 1.0 and 1.5 at a pressure of 1 atm. A variety of species profiles were measured and a conceptual mechanistic interpretation was presented. However, due to the low fuel conversion no CO profiles were reported. More recently, Dagaut *et al.* [60] carried out the oxidation of n – propylbenzene under Jet Stirred Reactor conditions for low to high fuel conversion for a variety of stoichiometries ($\phi = 0.5$, 1.0 and 1.5) over a temperature range of 950 – 1250 K and a pressure of 1 atm. Additionally, Dagaut *et al.* [60] proposed a detailed chemical kinetic mechanism to model the experimental data of Dagaut *et al.* [60]. Interestingly, both Litzinger [174] and Dagaut *et al.* [60] reported low concentration levels of propene in the experiments conducted for the oxidation of n – propylbenzene. The unexpected small formation of propene was attributed to the isomerisation of 1 – phenyl – 2 – propyl to 2 – phenyl – 1 – propyl which thermally decomposes via C – C cleavage to methyl radicals and styrene.

3.3.1 The Oxidation of n – Propylbenzene at Low Pressure

Test Case Details

The data sets used to validate and verify the n – propylbenzene sub – mechanism under Jet Stirred Reactor condition is obtained from Dagaut *et al.* [60]. The data utilised here consists of three cases, where $\phi = 0.5$, 1.0, and 2.0 over an overall temperature range of 900 – 1250 K for a mean residence time of $\tau = 70$ ms at atmospheric pressure. Table 3.1 summarizes the initial conditions for the oxidation of n – propylbenzene in a Jet Stirred Reactor.

Table 3.1: Summary of the Initial Conditions for the Oxidation of n – propylbenzene in a Jet Stirred Reactor at Low Pressure

Fuel	ϕ	T_0 [K]	Mean Residence Time [ms]	Pressure [atm.]
C_9H_{12}	0.5	900 – 1200	70	1.0
C_9H_{12}	1.0	950 – 1250	70	1.0
C_9H_{12}	2.0	950 – 1250	70	1.0

The results of the calculations are compared to the experimental data sets from Dagaut *et al.* [60] in Figures 3.16 – 3.27. Overall the detailed chemical mechanism performs well in reproducing the species concentration profiles as is evident in Figures 3.16 – 3.27. The fuel decay profile is reproduced accurately for all stoichiometries as is evident in Figures 3.16, 3.20 and 3.24. However, the O_2, CO and CO_2 profiles are less well reproduced which is somewhat surprising given that intermediate hydrocarbon levels are in good agreement with the exception of C_2H_6. Unfortunately, phenol concentrations are not given for the rich case. It is interesting to note that in the lean case, ignition occurs (~1180 K) as is evident in Figure 3.16 due to sharp drop

in the concentrations of molecular oxygen and carbon dioxide, leading to a sharp rise in the carbon dioxide concentrations. This is encountered in both the calculations and the experimental data.

The trends for styrene are well produced by the detailed chemical mechanism for all stoichiometries as is evident in Figures 3.19, 3.23 and 3.27. In all cases it is found that reaction (1199) is the dominant channel (~80 %).

$$C_8H_9 = C_8H_8 + H \quad (1199)$$

The species concentration profiles for styrene were further improved by a reduction in the rate parameter by a factor of 3 for reaction (1195).

$$C_8H_8 + OH = C_7H_7 + CH_2O \quad (1195)$$

Benzene calculations are in good agreement with the experimental data from Dagaut *et al.* [60] as shown in Figures 3.19, 3.23 and 3.27. The primary production channel (75 %) for benzene is via

$$C_9H_{12} + H = C_3H_7(N) + C_6H_6 \quad (1486)$$

for all cases at 1060 K. The rate for reaction (1486) has been obtained from Dagaut *et al.* [60].

Toluene and ethylbenzene are well produced for all cases as shown in Figures 3.19, 3.23 and 3.27 and Figures 3.18, 3.22 and 3.26 respectively. It is found that the dominant channels for C_7H_8 and C_8H_{10} are via reactions (1077) and (1061).

$$C_7H_8 = C_7H_7 + H \quad (1077)$$

$$C_7H_7 + CH_3 = C_8H_{10} \quad (1061)$$

Again, the reduction in the frequency factor for reaction (1195) significantly improved the calculations for these species due to the concentrations of benzyl being reduced in the system.

The concentrations of C_7H_6O are well produced in all cases as is evident in Figures 3.18, 3.22 and 3.26. It is found that for all conditions

$$C_7H_7O \quad = \quad C_7H_6O + H \tag{1113}$$

is the dominant channel.

The low concentrations of C_3H_6 are well reproduced by the detailed chemical mechanism. It is found that at 990 K the dominant formation channel is via reaction (353)

$$C_3H_5(A) + H \quad = \quad C_3H_6 \tag{353}$$

with the rate parameters being discussed in the text of Rizos [218]. Dagaut [60] comment that the unexpected small concentrations of propene is attributed to an isomerisation of the $2C_9H_{11}$ radical, which then thermally decomposes to C_8H_8 and CH_3 radicals. This reaction sequence was implemented in the current detailed chemical kinetic mechanism. It was found that C_8H_8 was heavily over predicted in all cases. Furthermore, the isomerisation step [60] created a large concentration of CH_3 radicals which led to CH_4 and C_2H_6 being heavily over predicted at low temperatures.

The concentrations of C_2H_6 are over predicted, especially for the stoichiometric and rich cases as is evident in Figures 3.18, 3.22 and 3.26. It is found that in all cases that reaction (74)

$$CH_3 + CH_3 \quad = \quad C_2H_6 \tag{74}$$

is the dominant channel (~90 %) for C_2H_6 production. The rate for reaction (74) has been discussed by Baulch *et al.* [14].

Concentration profiles for C_2H_4 are well reproduced for all cases as is evident in Figures 3.17, 3.21 and 3.25. The dominant reactions for the creation of C_2H_4 are (188) and (1509) which contribute ~35 % each.

$$C_2H_4 + H = C_2H_5 \quad (188)$$

$$1C_9H_{11} = C_7H_7 + C_2H_4 \quad (1509)$$

The rate parameters for reaction (188) have been discussed by Rizos [218] and the rate for reaction (1509) has been modelled on the work of Dean [73].

Other smaller species (C_2H_2 and CH_2O) are also well reproduced by the detailed chemical mechanism as shown in Figures 3.17, 3.21 and 3.25.

The concentrations of CH_4 are over predicted at low temperatures and under predicted at high temperatures for the lean case as shown in Figure 3.17. At 1000 K it is found that

$$C_9H_{12} + CH_3 = 3C_9H_{11} + CH_4 \quad (1479)$$

is the dominant channel for CH_4 production (~50 %). The rate of Dagaut *et al.* [60] has been used. At higher temperatures (1140 K), reaction

$$CH_3 + HO_2 = CH_4 + O_2 \quad (84b)$$

is the dominant channel (~50 %) for methane production for the lean case. The rate for reaction (84b) has been adopted from Tsang & Hampson [249] who report an uncertainty factor of 5. The rate has been increased by a factor of 3 in this study, well within the uncertainty band. However, for the stoichiometric and rich cases, the concentration levels of methane are well predicted as is evident in Figures 3.21 and 3.25. It is found that at 1060 K, the dominant channel for methane production is reaction (1479).

$$C_9H_{12} + CH_3 = 3C_9H_{11} + CH_4 \quad (1479)$$

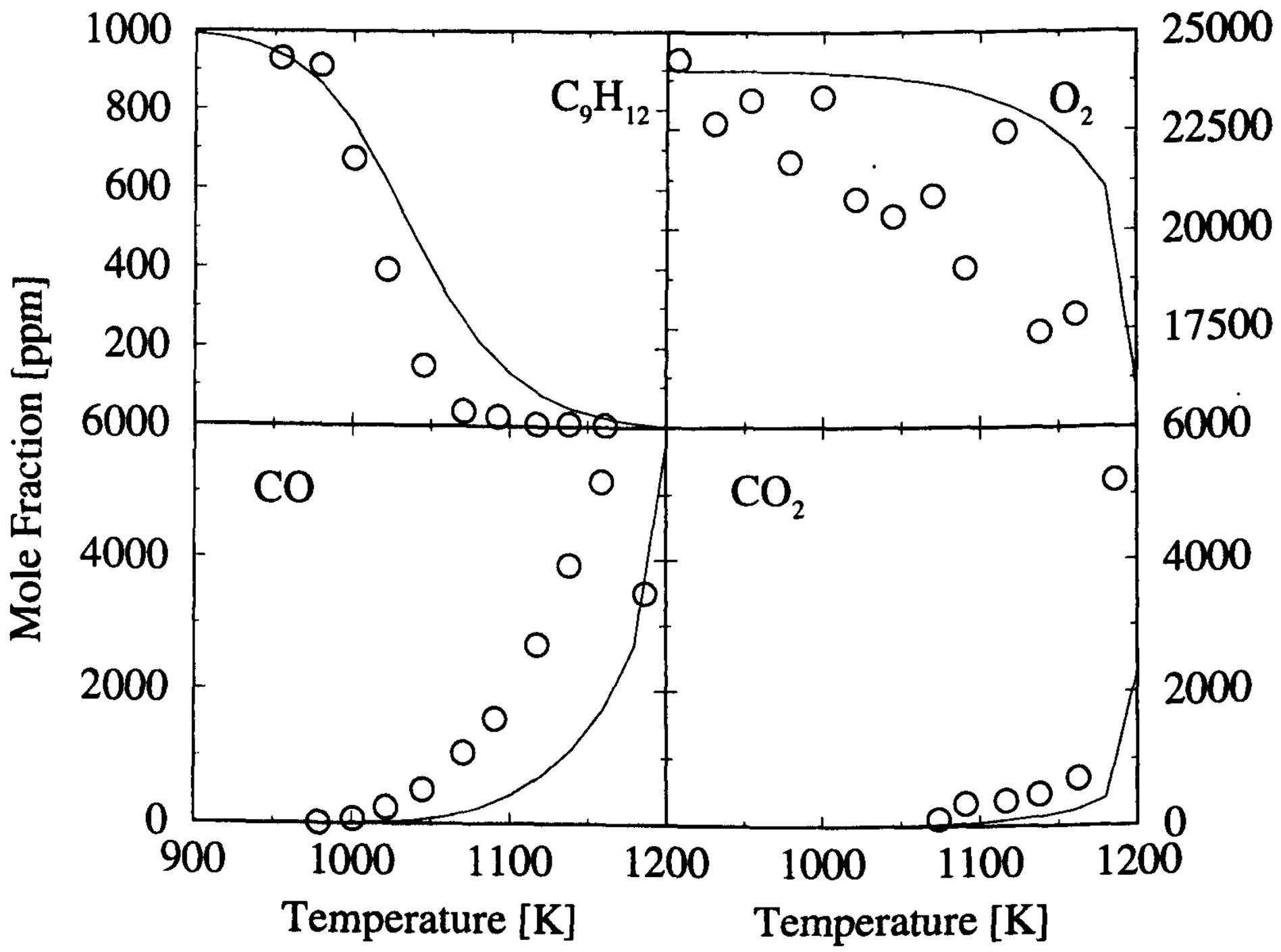


Figure 3.16: Graph of species profile concentrations versus time for the oxidation of n – propylbenzene in a Jet Stirred Reactor for a stoichiometry of $\phi = 0.5$ and a pressure of 1 atm. Experimental points are from Dagaut *et al.* [60]. Solid lines are the computations from the detailed chemical mechanism.

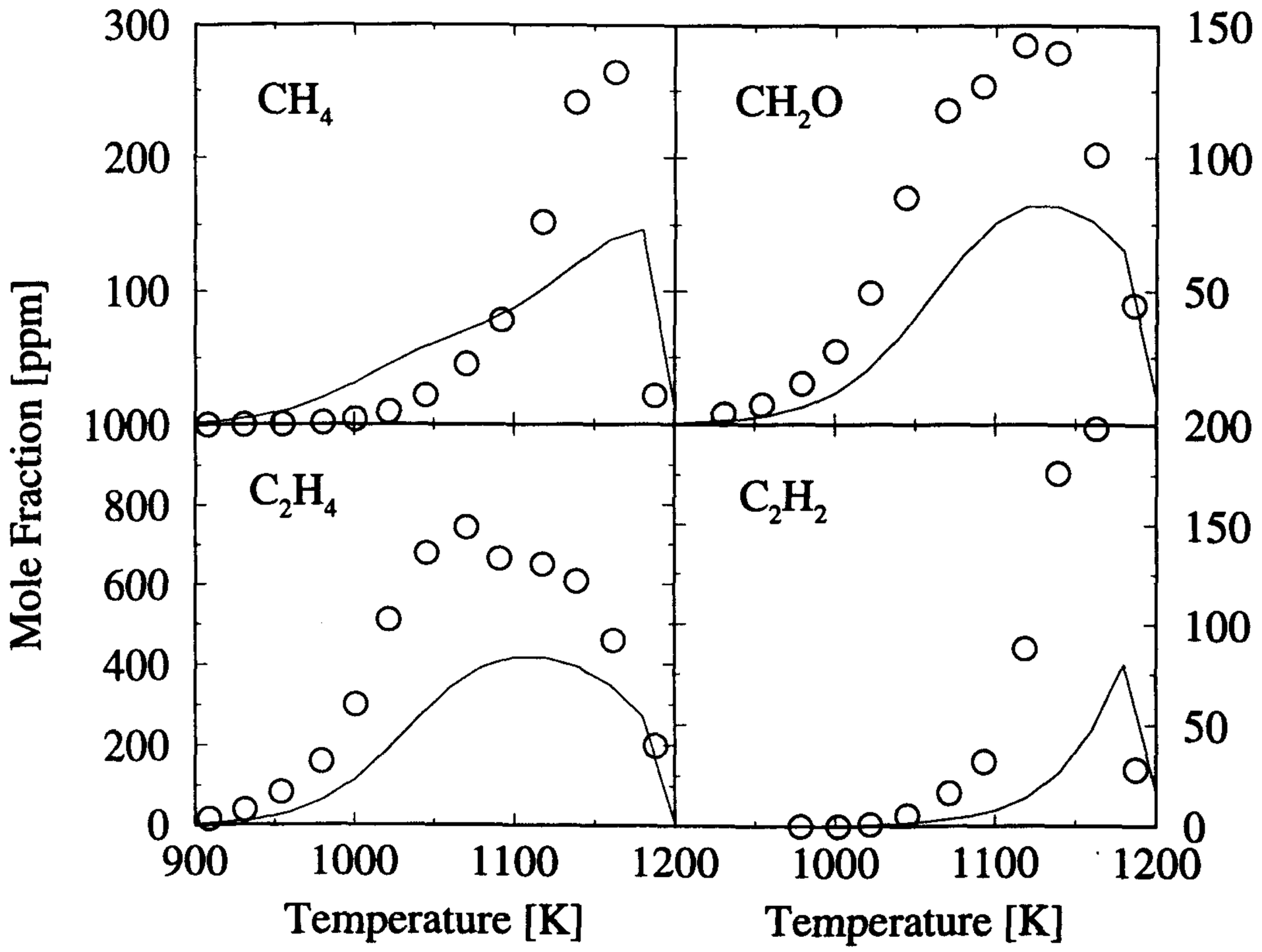


Figure 3.17: Graph of species profile concentrations versus time for the oxidation of n – propylbenzene in a Jet Stirred Reactor for a stoichiometry of $\phi = 0.5$ and a pressure of 1 atm. Experimental points are from Dagaut *et al.* [60]. Solid lines are the computations from the detailed chemical mechanism.

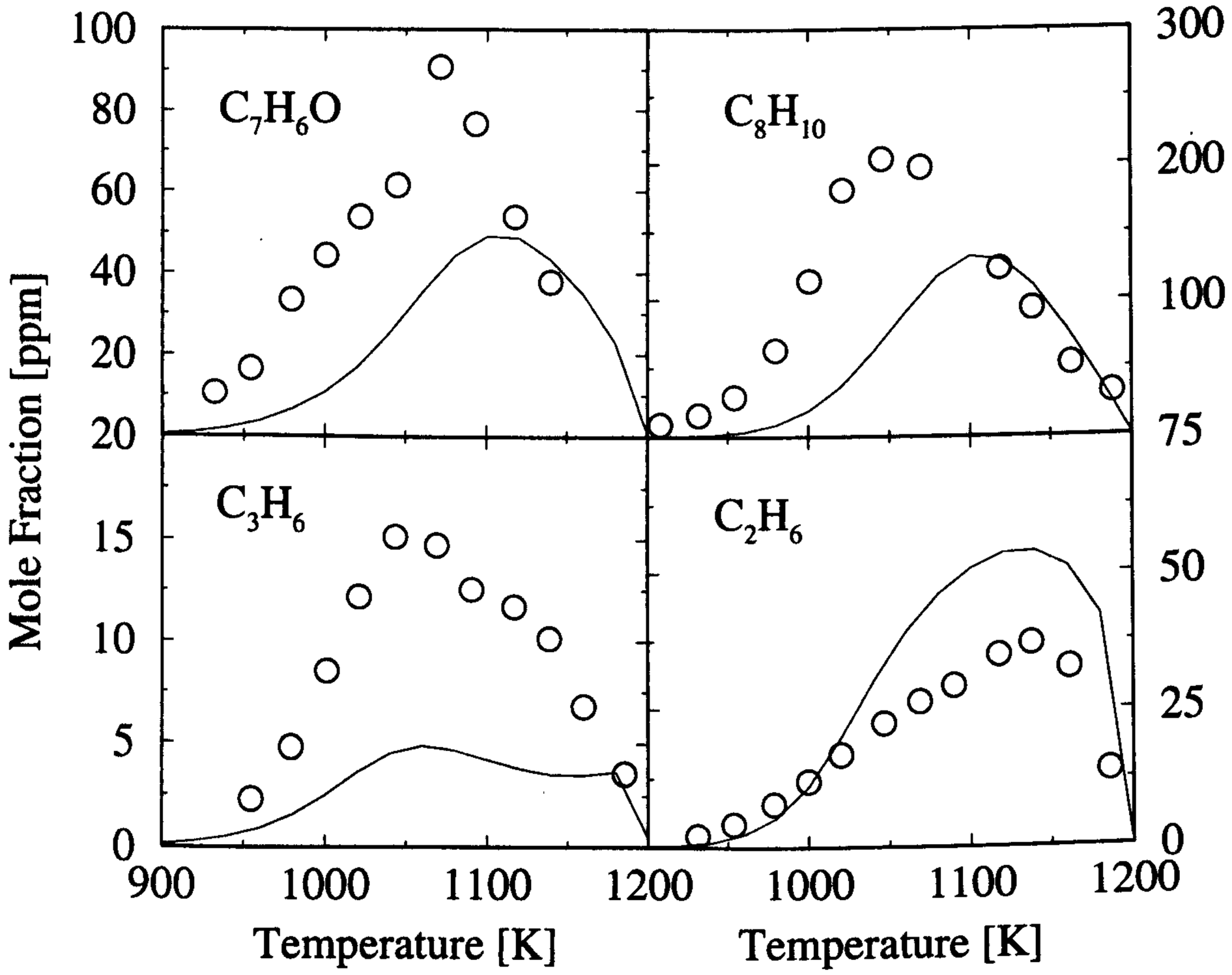


Figure 3.18: Graph of species profile concentrations versus time for the oxidation of n – propylbenzene in a Jet Stirred Reactor for a stoichiometry of $\phi = 0.5$ and a pressure of 1 atm. Experimental points are from Dagaut *et al.* [60]. Solid lines are the computations from the detailed chemical mechanism.

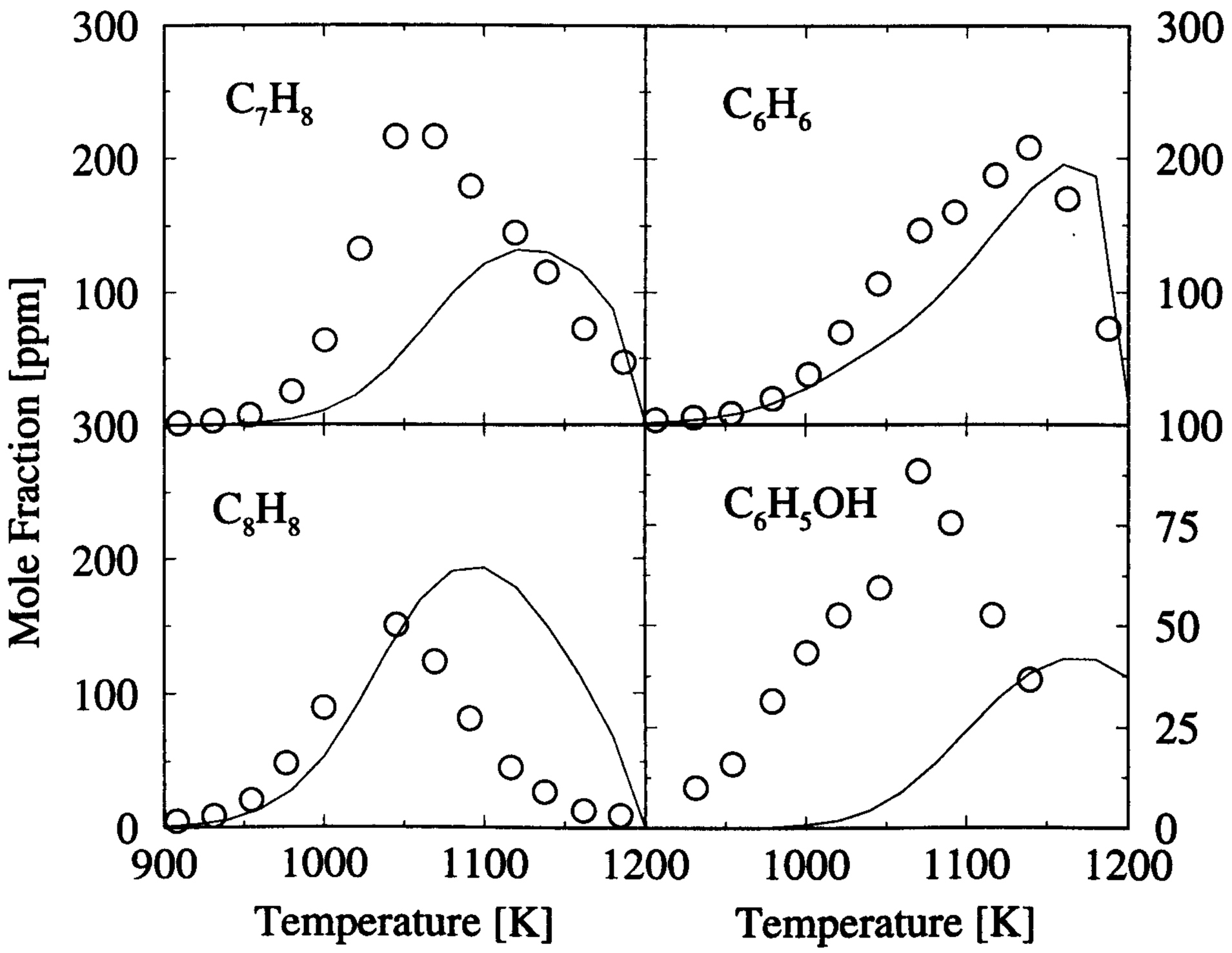


Figure 3.19: Graph of species profile concentrations versus time for the oxidation of n – propylbenzene in a Jet Stirred Reactor for a stoichiometry of $\phi = 0.5$ and a pressure of 1 atm. Experimental points are from Dagaut *et al.* [60]. Solid lines are the computations from the detailed chemical mechanism.

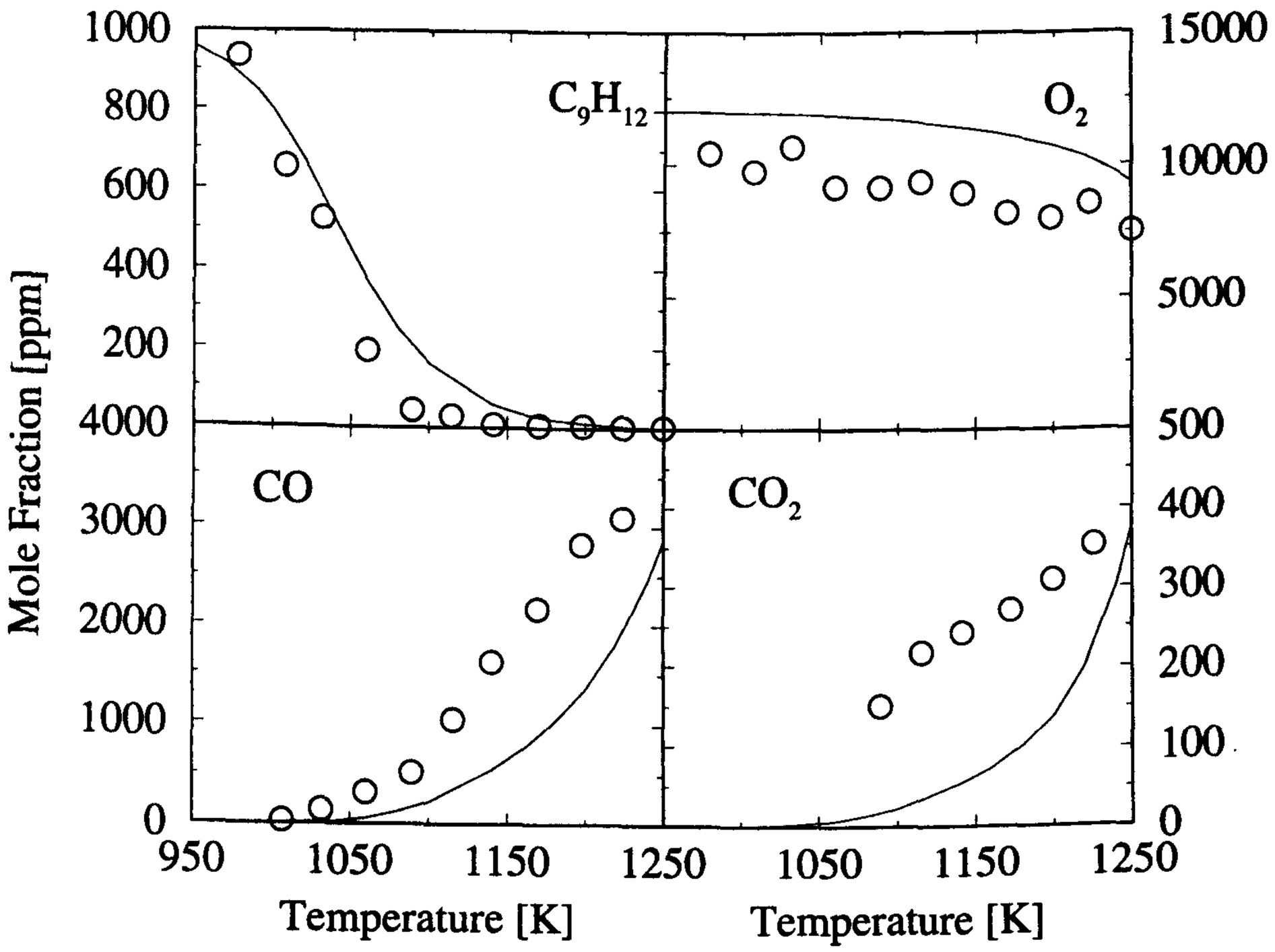


Figure 3.20: Graph of species profile concentrations versus time for the oxidation of n – propylbenzene in a Jet Stirred Reactor for a stoichiometry of $\phi = 1.0$ and a pressure of 1 atm. Experimental points are from Dagaut *et al.* [60]. Solid lines are the computations from the detailed chemical mechanism.

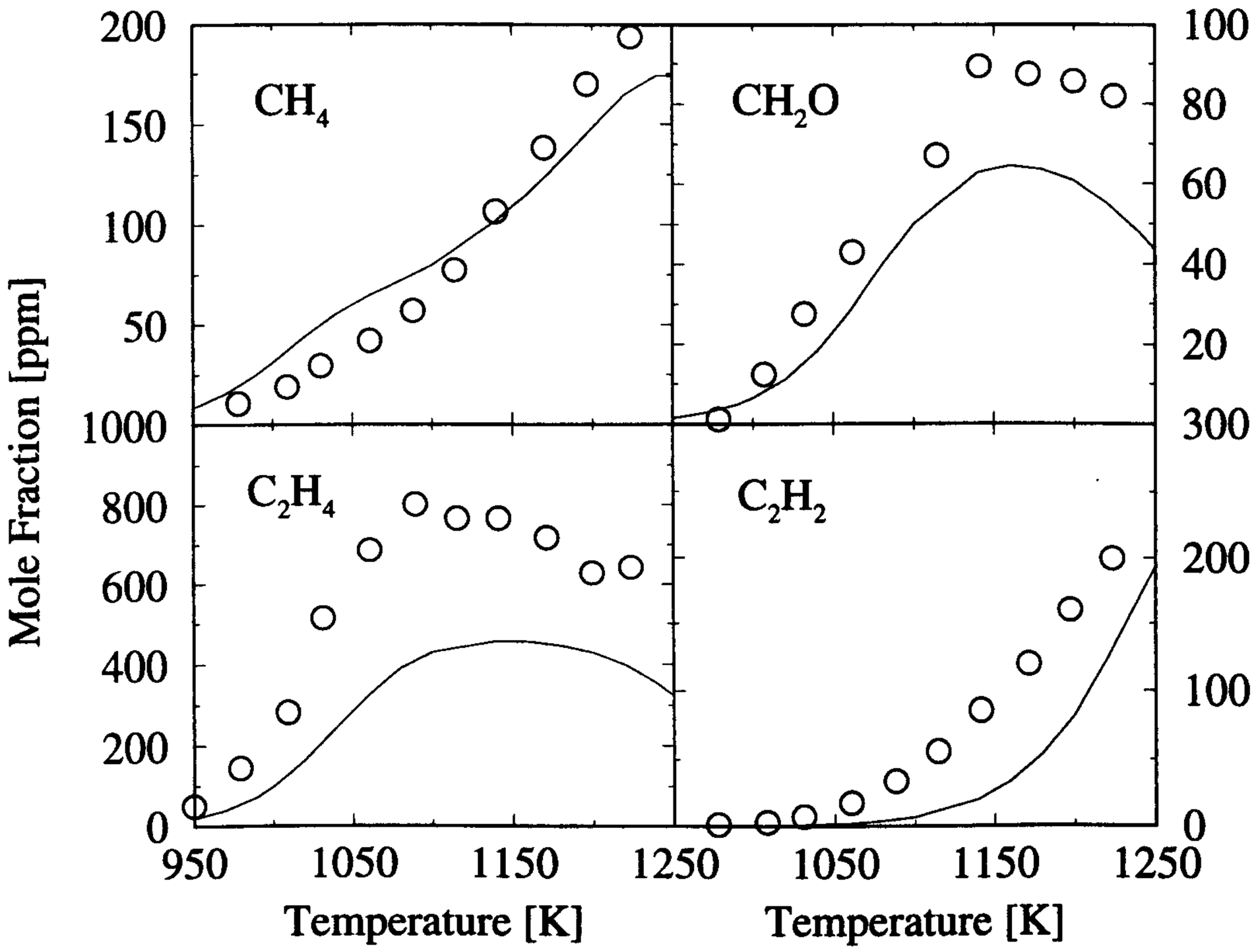


Figure 3.21: Graph of species profile concentrations versus time for the oxidation of n – propylbenzene in a Jet Stirred Reactor for a stoichiometry of $\phi = 1.0$ and a pressure of 1 atm. Experimental points are from Dagaut *et al.* [60]. Solid lines are the computations from the detailed chemical mechanism.

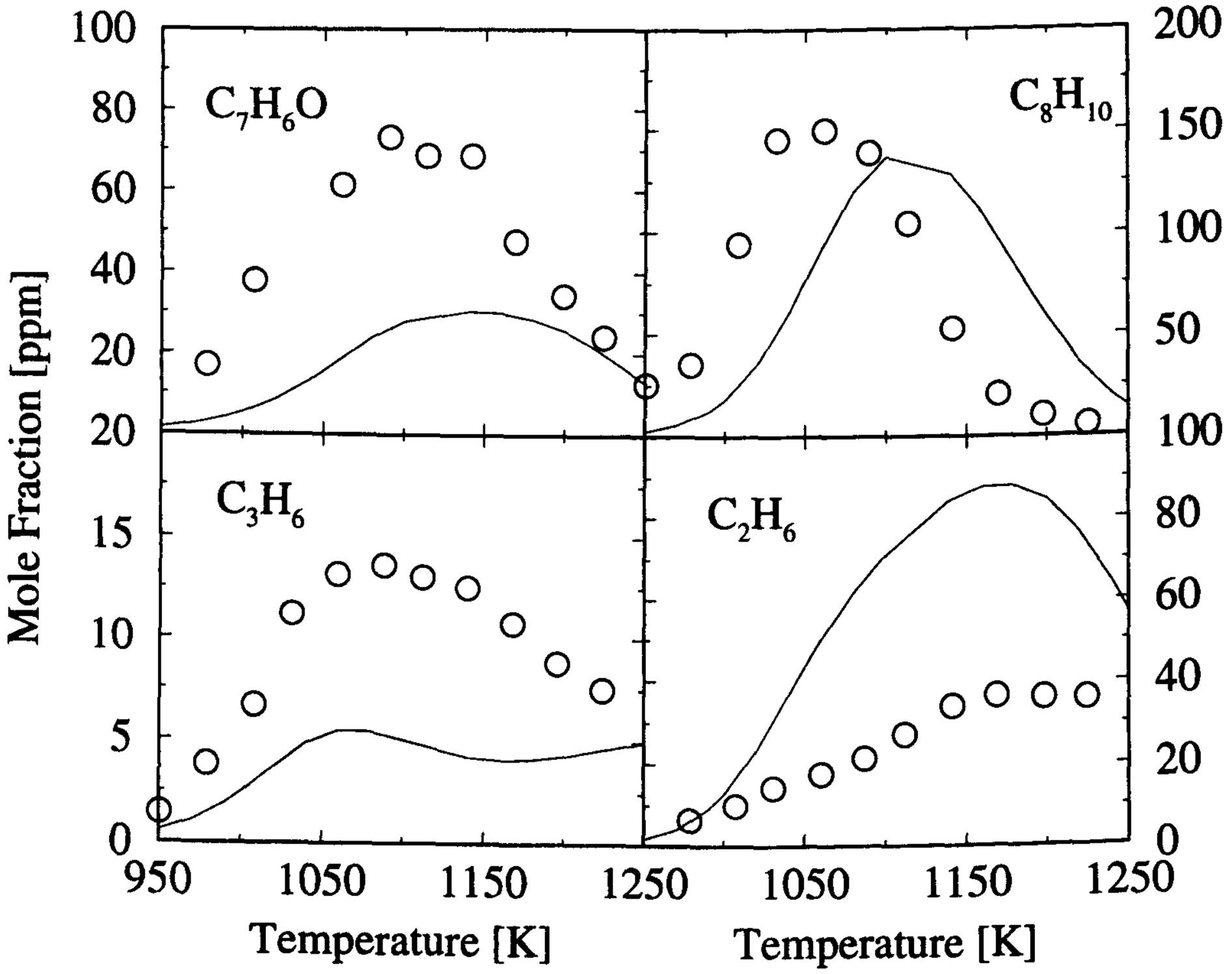


Figure 3.22: Graph of species profile concentrations versus time for the oxidation of n – propylbenzene in a Jet Stirred Reactor for a stoichiometry of $\phi = 1.0$ and a pressure of 1 atm. Experimental points are from Dagaut *et al.* [60]. Solid lines are the computations from the detailed chemical mechanism.

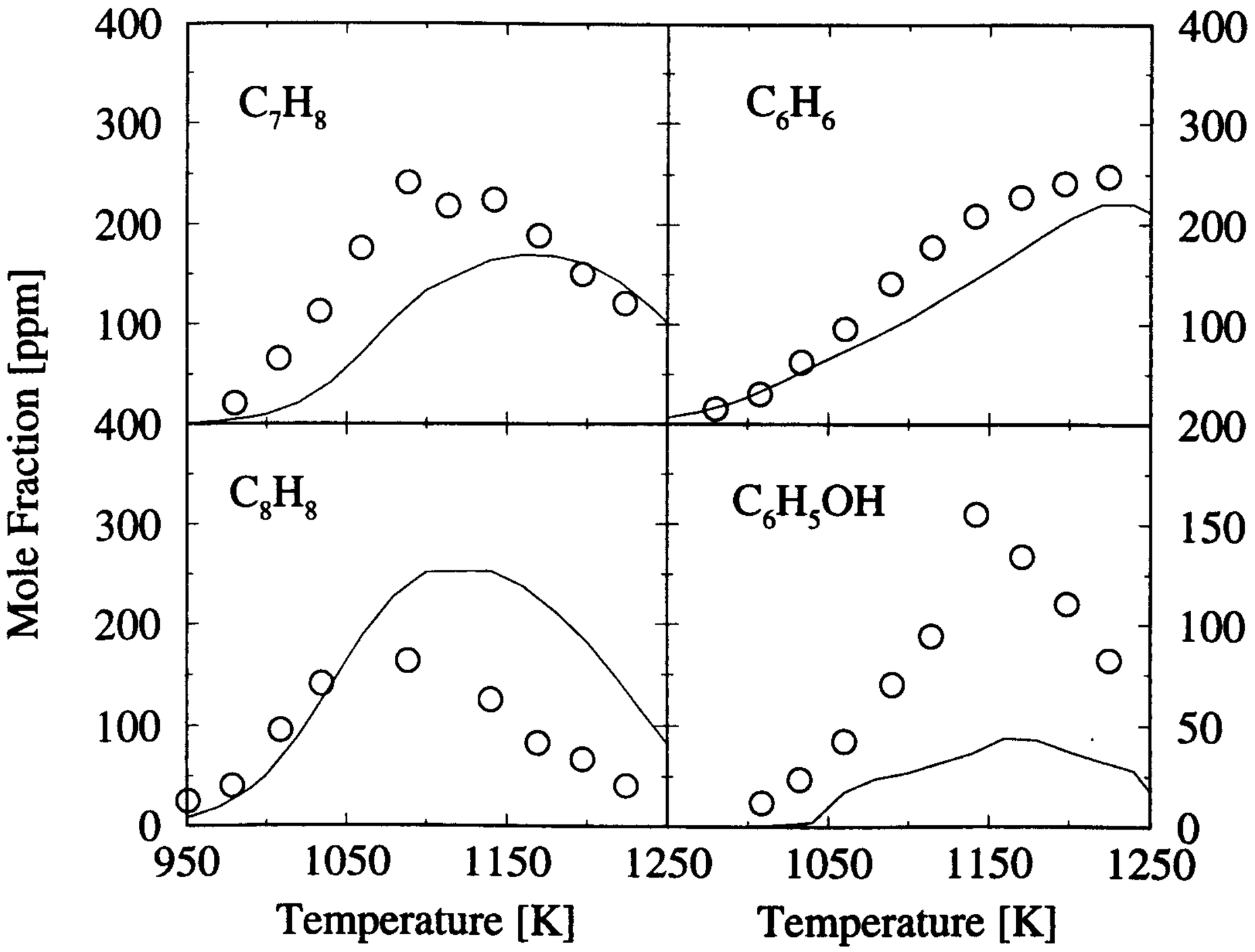


Figure 3.23: Graph of species profile concentrations versus time for the oxidation of n – propylbenzene in a Jet Stirred Reactor for a stoichiometry of $\phi = 1.0$ and a pressure of 1 atm. Experimental points are from Dagaut *et al.* [60]. Solid lines are the computations from the detailed chemical mechanism.

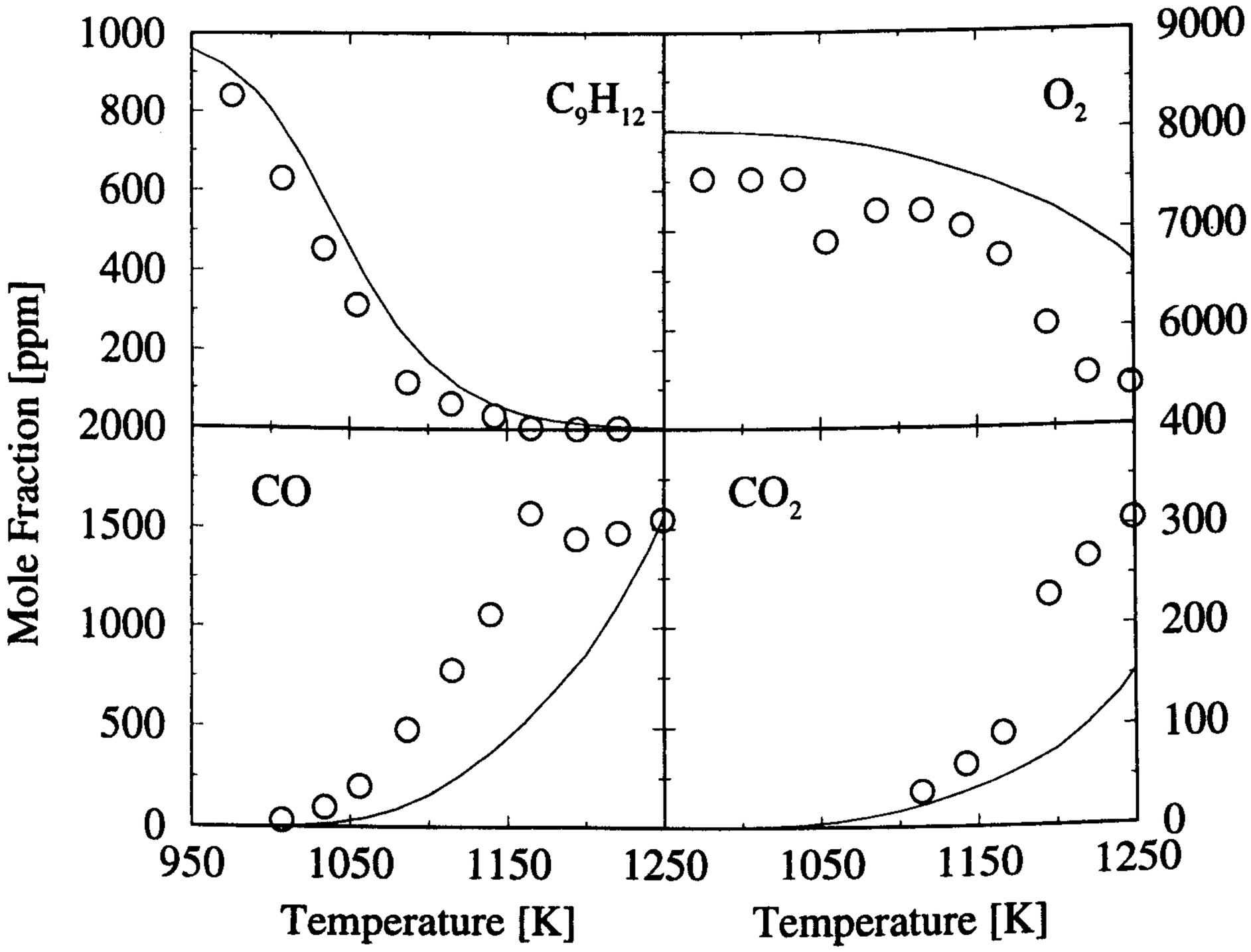


Figure 3.24: Graph of species profile concentrations versus time for the oxidation of n – propylbenzene in a Jet Stirred Reactor for a stoichiometry of $\phi = 1.5$ and a pressure of 1 atm. Experimental points are from Dagaut *et al.* [60]. Solid lines are the computations from the detailed chemical mechanism.

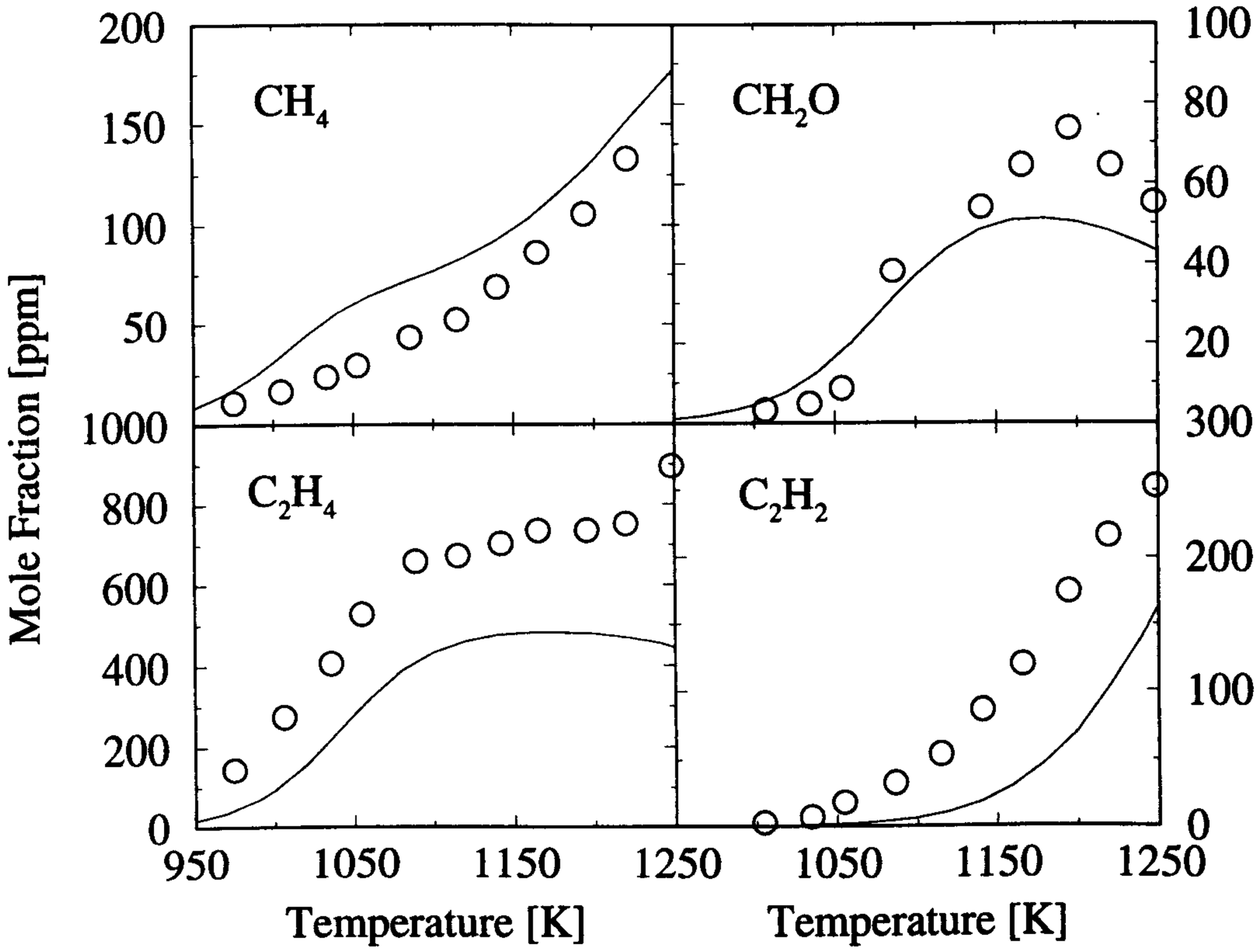


Figure 3.25: Graph of species profile concentrations versus time for the oxidation of n – propylbenzene in a Jet Stirred Reactor for a stoichiometry of $\phi = 1.5$ and a pressure of 1 atm. Experimental points are from Dagaut *et al.* [60]. Solid lines are the computations from the detailed chemical mechanism.

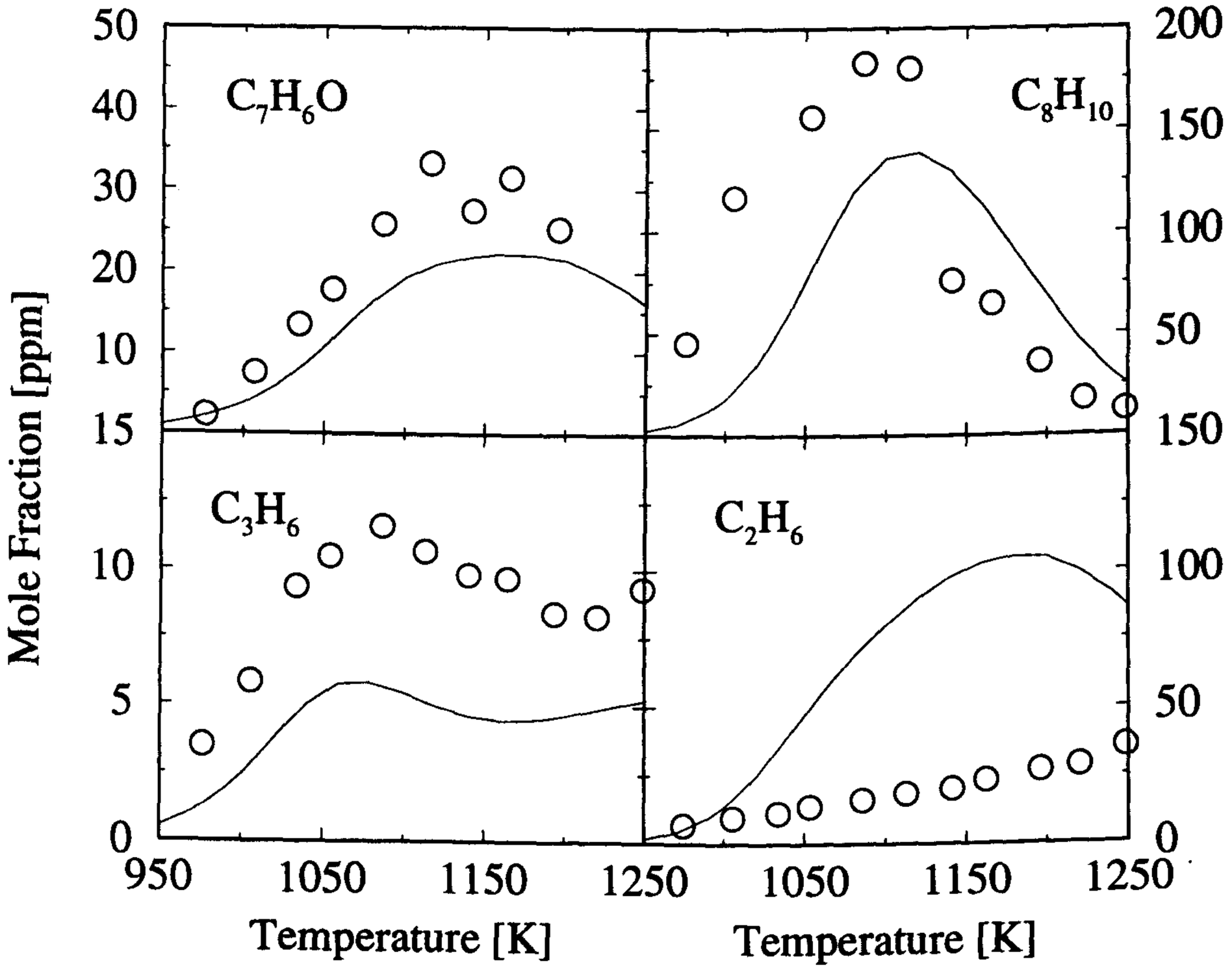


Figure 3.26: Graph of species profile concentrations versus time for the oxidation of n – propylbenzene in a Jet Stirred Reactor for a stoichiometry of $\phi = 1.5$ and a pressure of 1 atm. Experimental points are from Dagaut *et al.* [60]. Solid lines are the computations from the detailed chemical mechanism.

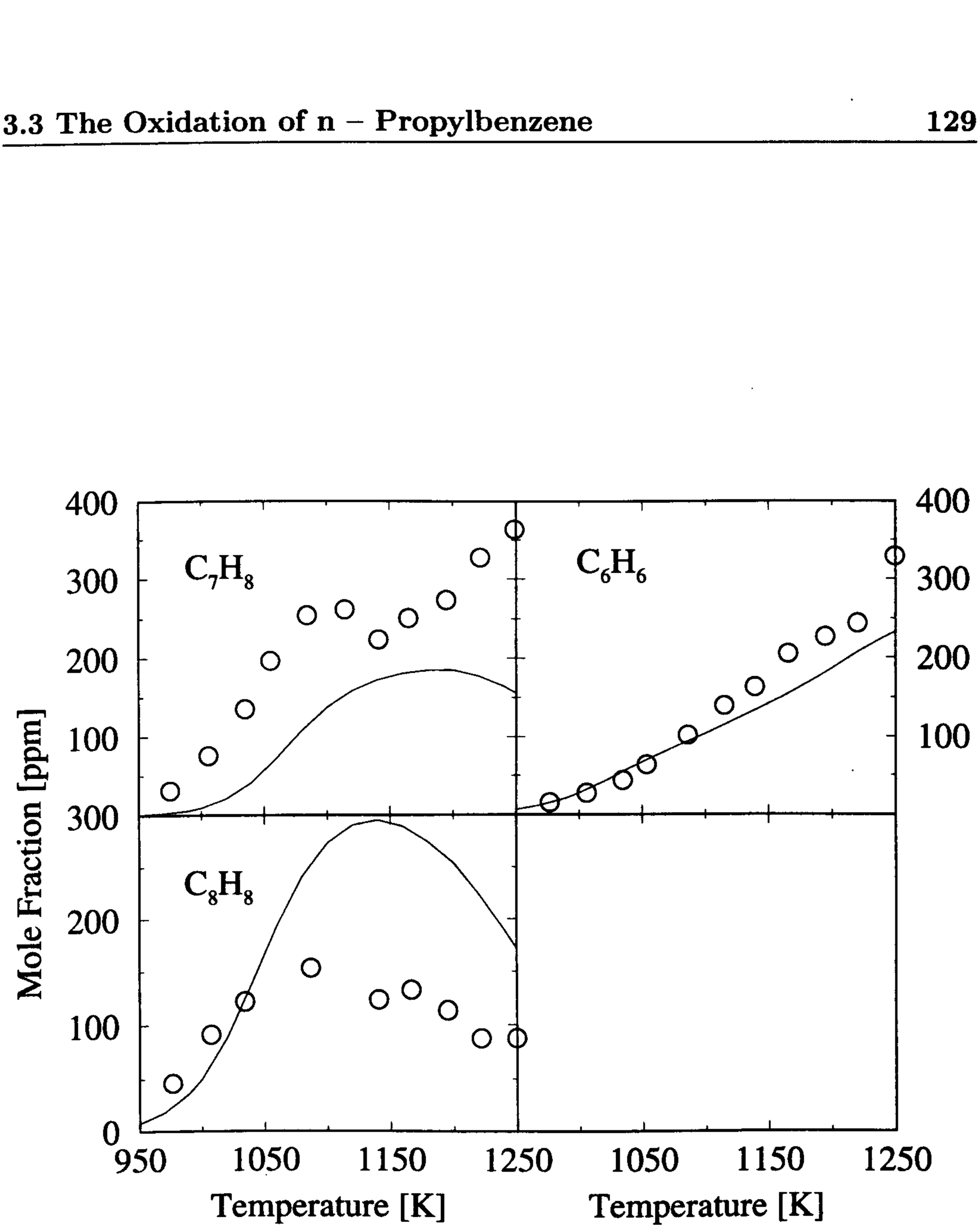


Figure 3.27: Graph of species profile concentrations versus time for the oxidation of n – propylbenzene in a Jet Stirred Reactor for a stoichiometry of $\phi = 1.5$ and a pressure of 1 atm. Experimental points are from Dagaut *et al.* [60]. Solid lines are the computations from the detailed chemical mechanism.

3.3.2 The Oxidation of n – Propylbenzene at High Pressure

Test Case Details

Computations have also been performed for a variety of stoichiometries under Jet Stirred Reactor conditions at a pressure of 10 atm. The data consists of four cases, with $\phi = 0.5$, 1.0, 1.5 and 2.0, an overall temperature range of 900 – 1200 K and a mean residence time of $\tau = 500$ ms obtained from Dagaut & Cathonnet [55]. Table 3.2 summarizes the initial conditions for the oxidation of n – propylbenzene in a Jet Stirred Reactor.

Table 3.2: Summary of the Initial Conditions for the Oxidation of n – propylbenzene in a Jet Stirred Reactor at High Pressure

Fuel	ϕ	T_0 [K]	Mean Residence Time [ms]	Pressure [atm.]
C_9H_{12}	0.5	900 – 1200	500	10.0
C_9H_{12}	1.0	900 – 1200	500	10.0
C_9H_{12}	1.5	900 – 1200	500	10.0
C_9H_{12}	2.0	900 – 1200	500	10.0

The calculations for the oxidation of n – propylbenzene and the intermediate and final products are shown in Figures 3.28 – 3.43. Overall, the calculations predict the fuel profile trends and intermediate species. However, in the lean case, the fuel consumption is under predicted leading to an under prediction of O_2 consumption and CO and CO_2 production as is evident in Figure 3.28. This is contradictory to the low pressure lean case where an accurate fuel profile is produced by the detailed chemical mechanism as illustrated in Figure 3.20. Moreover, ignition is found to occur at a temperature of approximately of 1040 K. This is also evident in the experi-

mental data from Dagaut & Cathonnet [55], most notably shown by the drop in CO concentration at approximately 1020 K (Figure 3.28). Additionally, ignition phenomena also occurs in the stoichiometric case as is evident in Figure 3.32 shown by the drop in the molecular oxygen and carbon dioxide profiles at approximately a temperature of 1080 K. Similarly, ignition occurs in the experimental data for this case at 1080 K. The under prediction of the fuel consumption for the lean and stoichiometric cases may stem from the uncertainties in reaction (1489),

$$C_9H_{12} = C_8H_9 + CH_3 \quad (1489)$$

since fall off may need to be taken into account. However, if this were the case, then the fuel profiles for the the two rich cases would exhibit the same behaviour and this is not the case as is evident in Figures 3.36 and 3.40.

The concentration profiles for C_8H_8 are reproduced well in all cases as is evident in Figures 3.31, 3.35, 3.39 and 3.43 for stoichiometries of $\phi = 0.5$, 1.0, 1.5 and 2.0 respectively. However, the peak for this species is shifted to higher temperatures for all cases by approximately 100 K. This may indicate uncertainties in the estimation of the energy barrier for the dominant production channel,

$$C_9H_{12} = C_8H_9 + CH_3 \quad (1489)$$

since the consumption path is via $C_9H_{12} \rightarrow C_8H_9 \rightarrow C_8H_8$ for all cases. The calculations for the high pressure case again highlights the problem encountered for accurate C_8H_8 prediction. Again, it is found that to improve predictions of styrene, it is necessary to reduce the frequency factor by a factor of 3 for reaction (1195).

$$C_8H_8 + OH = C_7H_7 + CH_2O \quad (1195)$$

As the stoichiometry changes from lean to rich, the agreement for C_6H_6 improves. This is contradictory to the low pressure cases where accurate benzene concentration profiles are produced by the detailed chemical mechanism as is evident in Figures 3.19, 3.23 and 3.27 for all cases.

It is found for the lean case at 1000 K, reaction

$$C_7H_6O + O = C_6H_6 + CO_2 \quad (1104)$$

is the dominant production channel (60 %) for benzene whilst reaction (1487)

$$C_9H_{12} + H = C_6H_6 + C_3H_7(N) \quad (1487)$$

contributes (10 %). For the rich case ($\phi = 1.5$), reaction (1104) contributes (35 %) and reaction (1487) contributes (20 %).

Additionally, the concentrations of C_7H_8 are over predicted at $\geq$ 1000 K for all cases as is evident in Figures 3.31, 3.35, 3.39 and 3.43, although the trends are very accurate. It is found that the dominant benzyl production channel is

$$C_8H_8 + OH = C_7H_7 + CH_2O \quad (1195)$$

which explains the over prediction of toluene since $C_7H_7 \rightarrow C_7H_8$.

The high concentrations of C_7H_7 in the system, generated by reaction (1195), additionally leads to an over prediction of C_8H_{10}, formed via (1061), in all cases as is evident in Figures 3.30, 3.34, 3.38 and 3.42.

$$C_7H_7 + CH_3 = C_8H_{10} \quad (1061)$$

The species concentration profiles for C_7H_6O are well reproduced for all cases as shown in Figures 3.30, 3.34, 3.38 and 3.42. It is found that reaction (1113) is the dominant channel (80 %) in generating C_7H_6O.

$$C_7H_7O \quad = \quad C_7H_6O + H \tag{1113}$$

Levels of C_2H_6 are poorly reproduced as is evident in Figures 3.30, 3.34, 3.38 and 3.42. Again, it is found that reaction (74) is the dominant channel in all cases.

$$CH_3 + CH_3 \quad = \quad C_2H_6 \tag{74}$$

The C_3H_6 species concentration profiles are reasonably well predicted in terms of trends for the lean and stoichiometric case as is evident in Figures 3.30, 3.34 respectively. At a temperature of 920 K, it is found that reaction (432) is the dominant production channel (~75 %) for the lean and stoichiometric case.

$$C_3H_7(N) + O_2 \quad = \quad C_3H_6 + HO_2 \tag{432}$$

The rate parameters are discussed in the text of Rizos [218]. However for the two rich cases, the trends are poor as is evident in Figures 3.38 and 3.42, and at a temperature of 1000 K it is found that reaction (395) is the dominant channel.

$$C_3H_6 + H \quad = \quad C_3H_7(N) \tag{395}$$

The concentrations of smaller species are reproduced well as shown in Figures 3.29, 3.33, 3.37 and 3.41. For example, the computations for C_2H_4 are in good agreement with the experimental data in terms of trends and magnitudes. It is found that in all cases reaction (1509) is the single most dominant channel for C_2H_4 creation, contributing 40 % in the lean case and 50 % in the rich ($\phi = 1.5$) case at a temperature of 950 K.

$$1C_9H_{11} \quad = \quad C_7H_7 + C_2H_4 \tag{1509}$$

The computations for CH_4 are predicted well as illustrated in Figures 3.29, 3.33, 3.37 and 3.41 for stoichiometries of $\phi = 0.5$, 1.0, 1.5 and 2.0 respectively. The detailed chemical mechanism is able to reproduce the change in trends in passing from lean to rich stoichiometries. At a temperature of 980 K, it is found that reaction (84b) is the dominant channel for all stoichiometries.

$$CH_3 + HO_2 \quad = \quad CH_4 + O_2 \tag{84b}$$

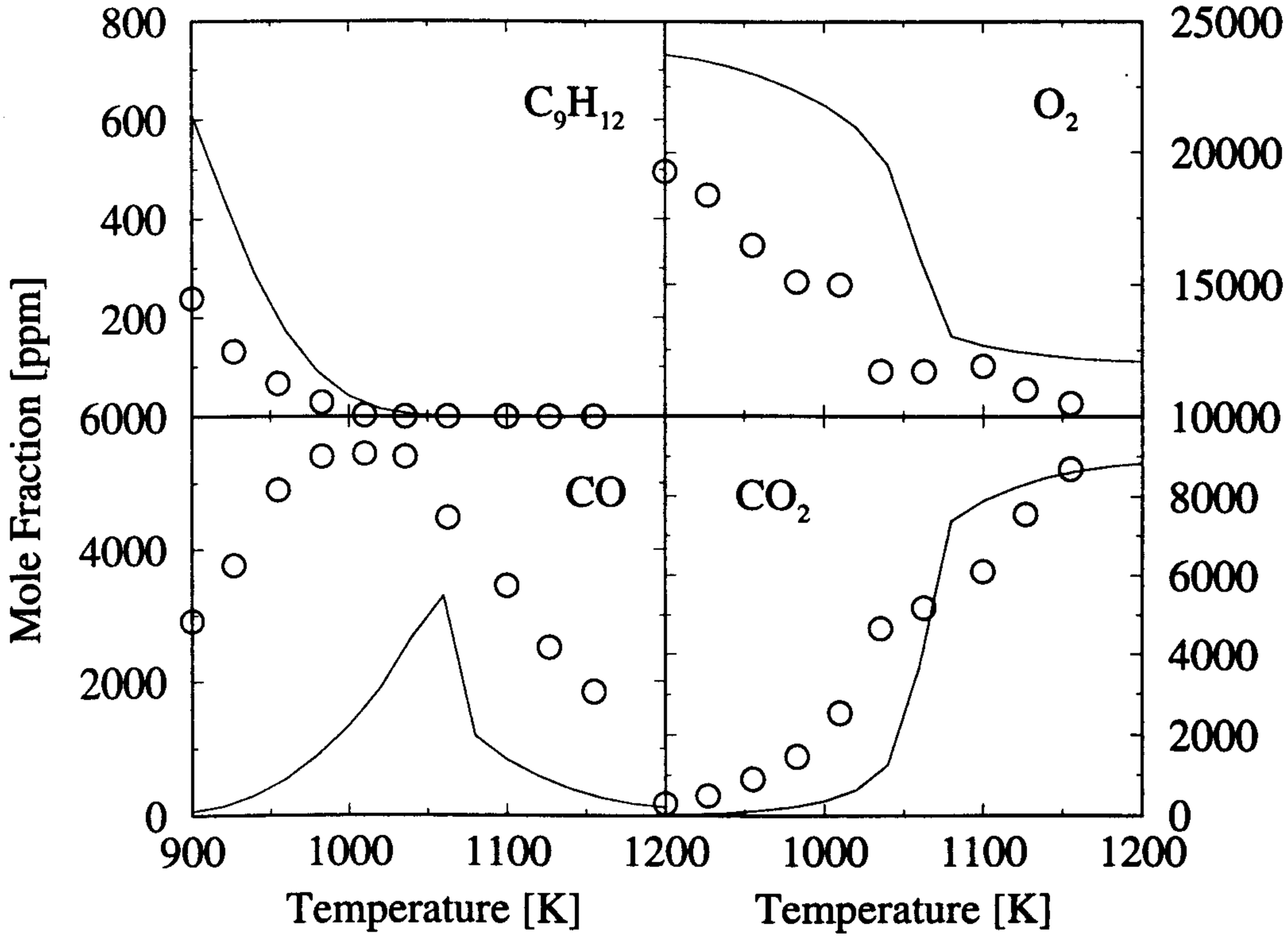


Figure 3.28: Graph of species profile concentrations versus time for the oxidation of n – propylbenzene in a Jet Stirred Reactor for a stoichiometry of $\phi = 0.5$ and a pressure of 10 atm. Experimental points are from Dagaut & Cathonnet [55]. Solid lines are the computations from the detailed chemical mechanism.

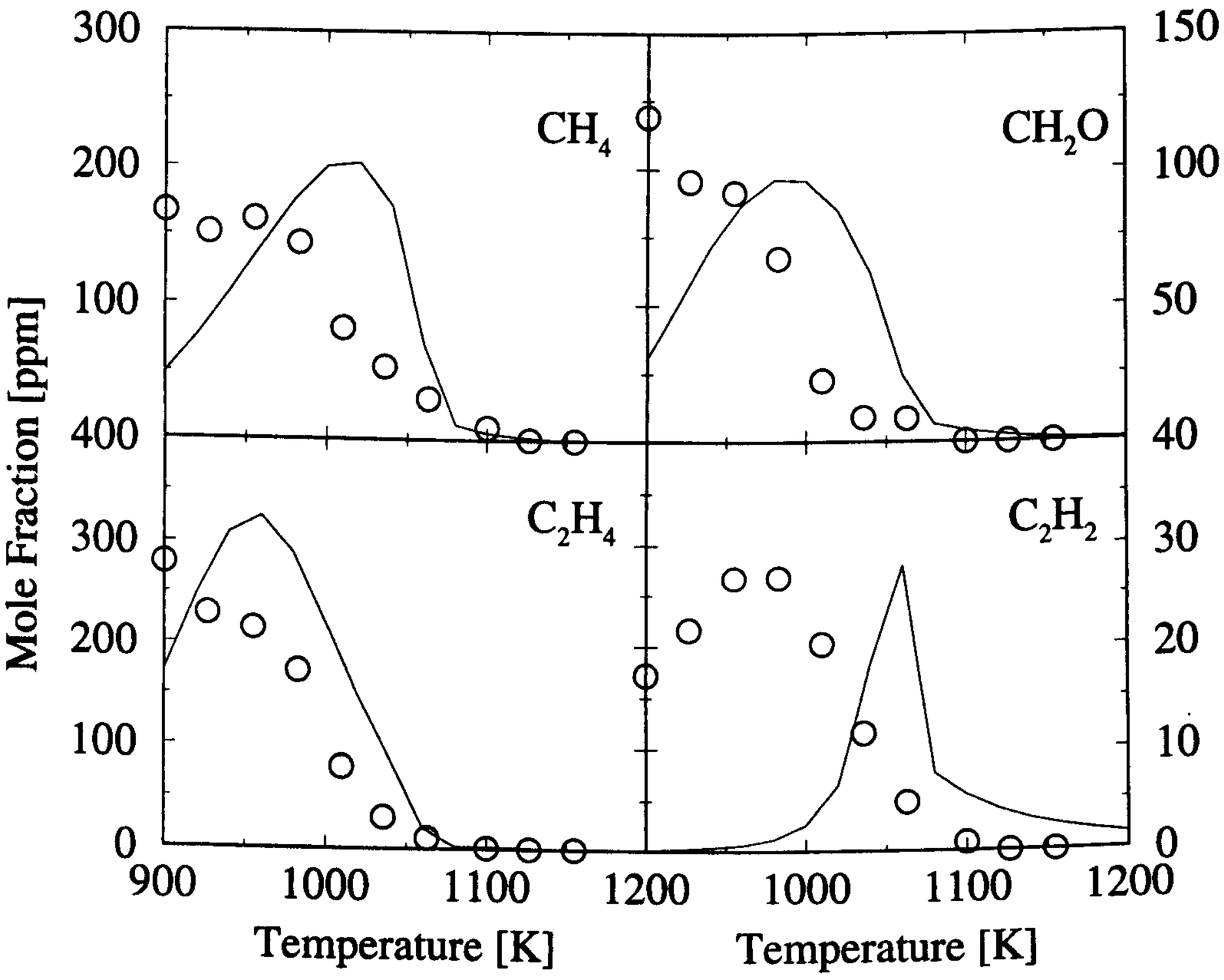


Figure 3.29: Graph of species profile concentrations versus time for the oxidation of n – propylbenzene in a Jet Stirred Reactor for a stoichiometry of $\phi = 0.5$ and a pressure of 10 atm. Experimental points are from Dagaut & Cathonnet [55]. Solid lines are the computations from the detailed chemical mechanism.

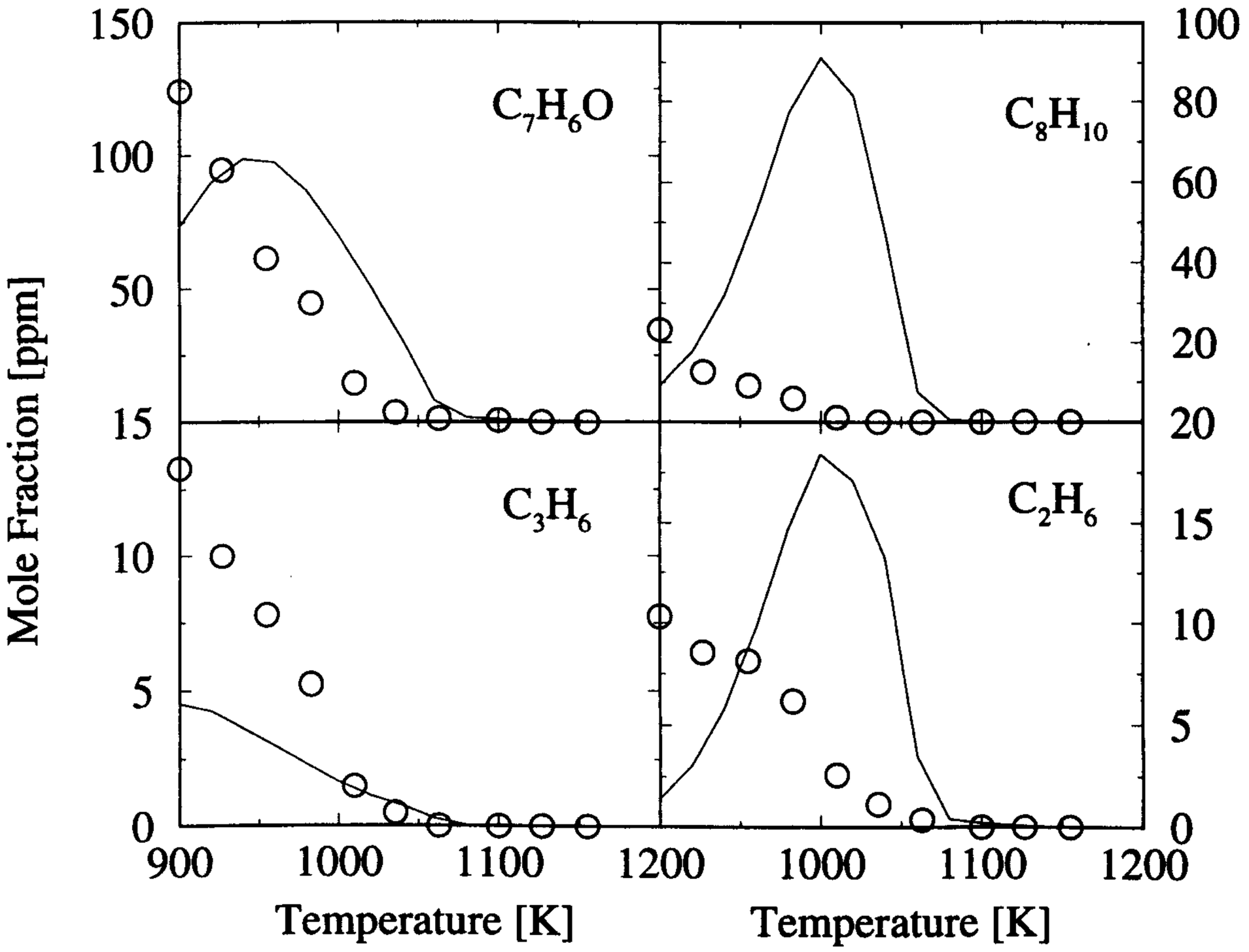


Figure 3.30: Graph of species profile concentrations versus time for the oxidation of n – propylbenzene in a Jet Stirred Reactor for a stoichiometry of $\phi = 0.5$ and a pressure of 10 atm. Experimental points are from Dagaut & Cathonnet [55]. Solid lines are the computations from the detailed chemical mechanism.

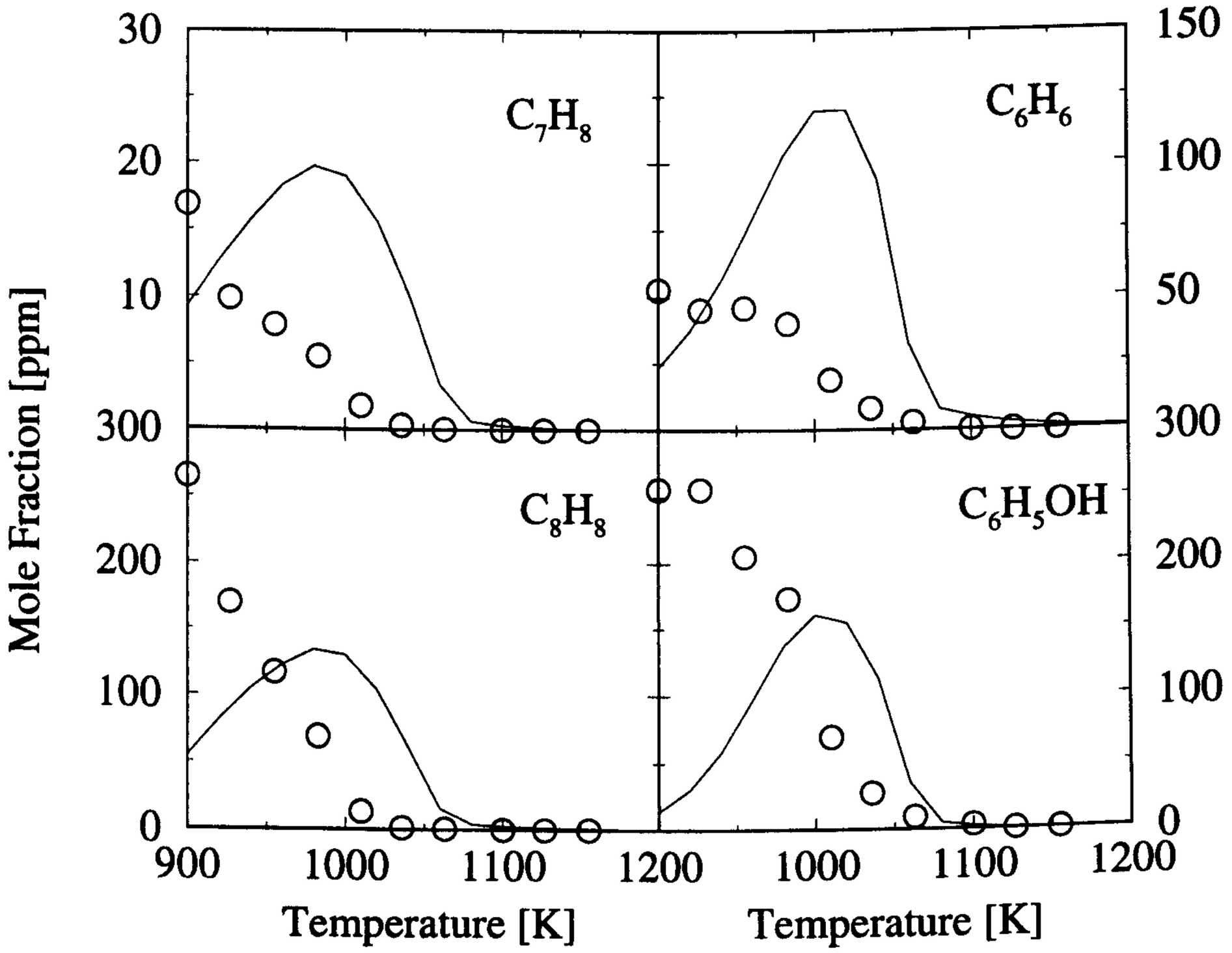


Figure 3.31: Graph of species profile concentrations versus time for the oxidation of n – propylbenzene in a Jet Stirred Reactor for a stoichiometry of $\phi = 0.5$ and a pressure of 10 atm. Experimental points are from Dagaut & Cathonnet [55]. Solid lines are the computations from the detailed chemical mechanism.

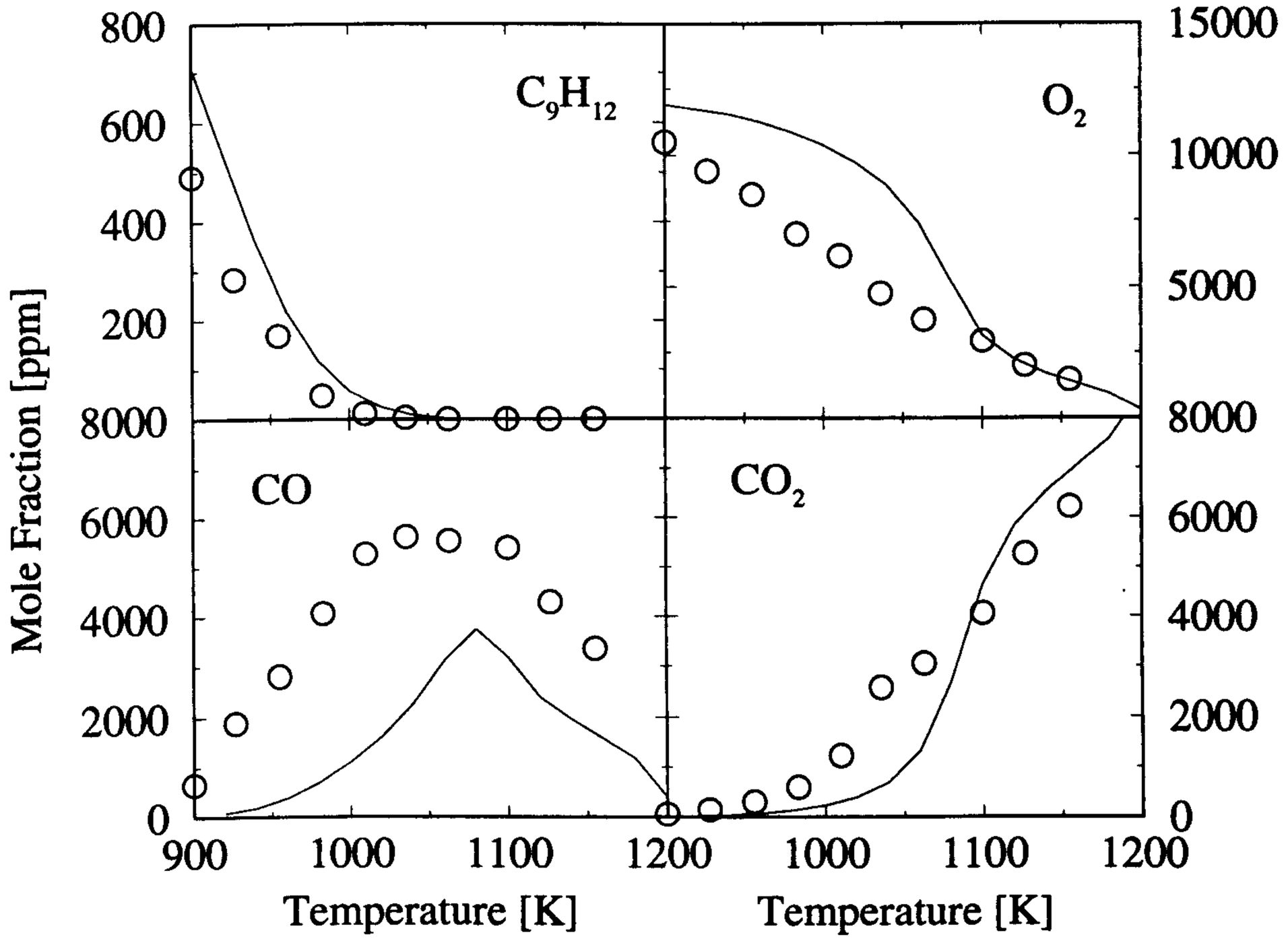


Figure 3.32: Graph of species profile concentrations versus time for the oxidation of n – propylbenzene in a Jet Stirred Reactor for a stoichiometry of $\phi = 1.0$ and a pressure of 10 atm. Experimental points are from Dagaut & Cathonnet [55]. Solid lines are the computations from the detailed chemical mechanism.

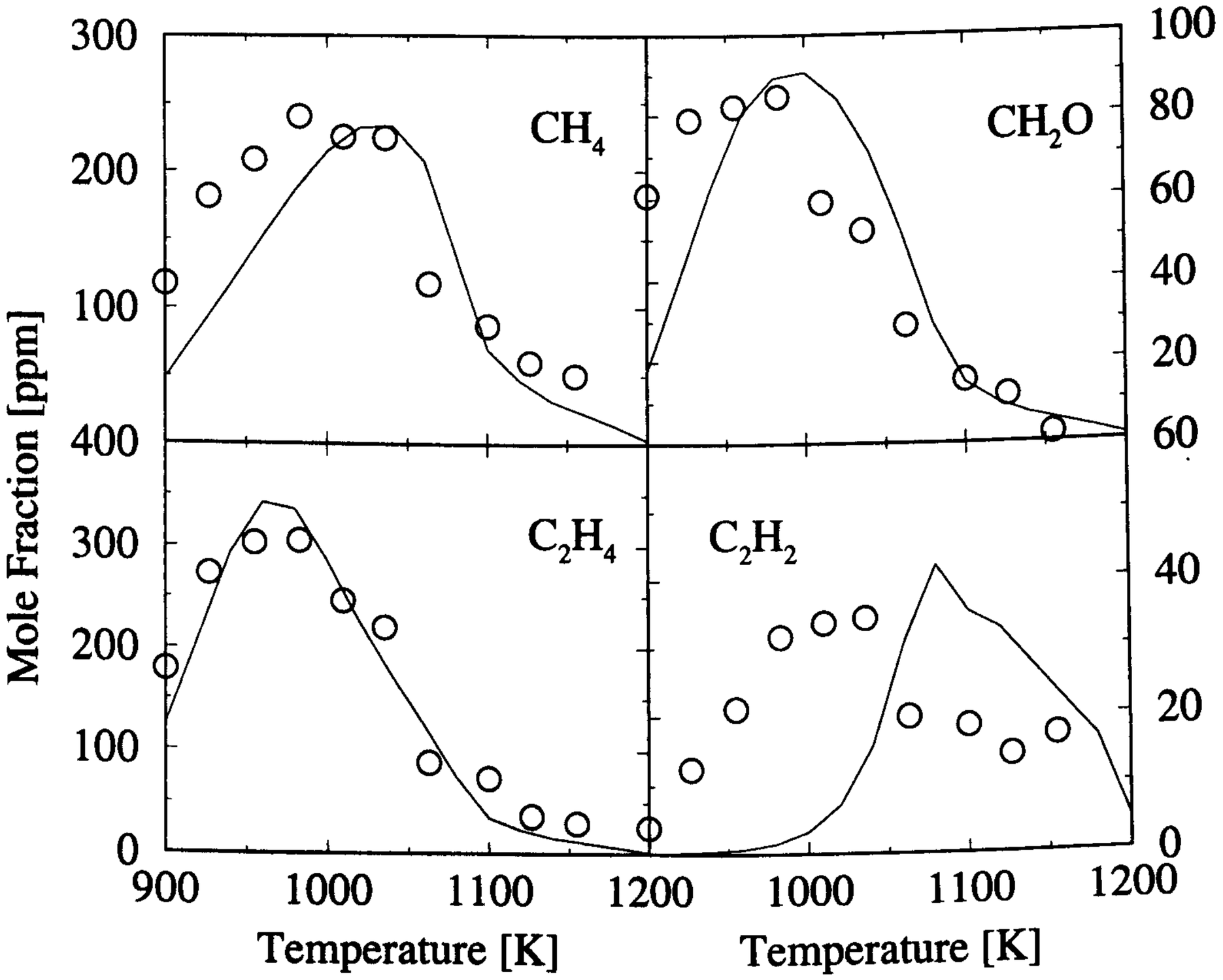


Figure 3.33: Graph of species profile concentrations versus time for the oxidation of n – propylbenzene in a Jet Stirred Reactor for a stoichiometry of $\phi = 1.0$ and a pressure of 10 atm. Experimental points are from Dagaut & Cathonnet [55]. Solid lines are the computations from the detailed chemical mechanism.

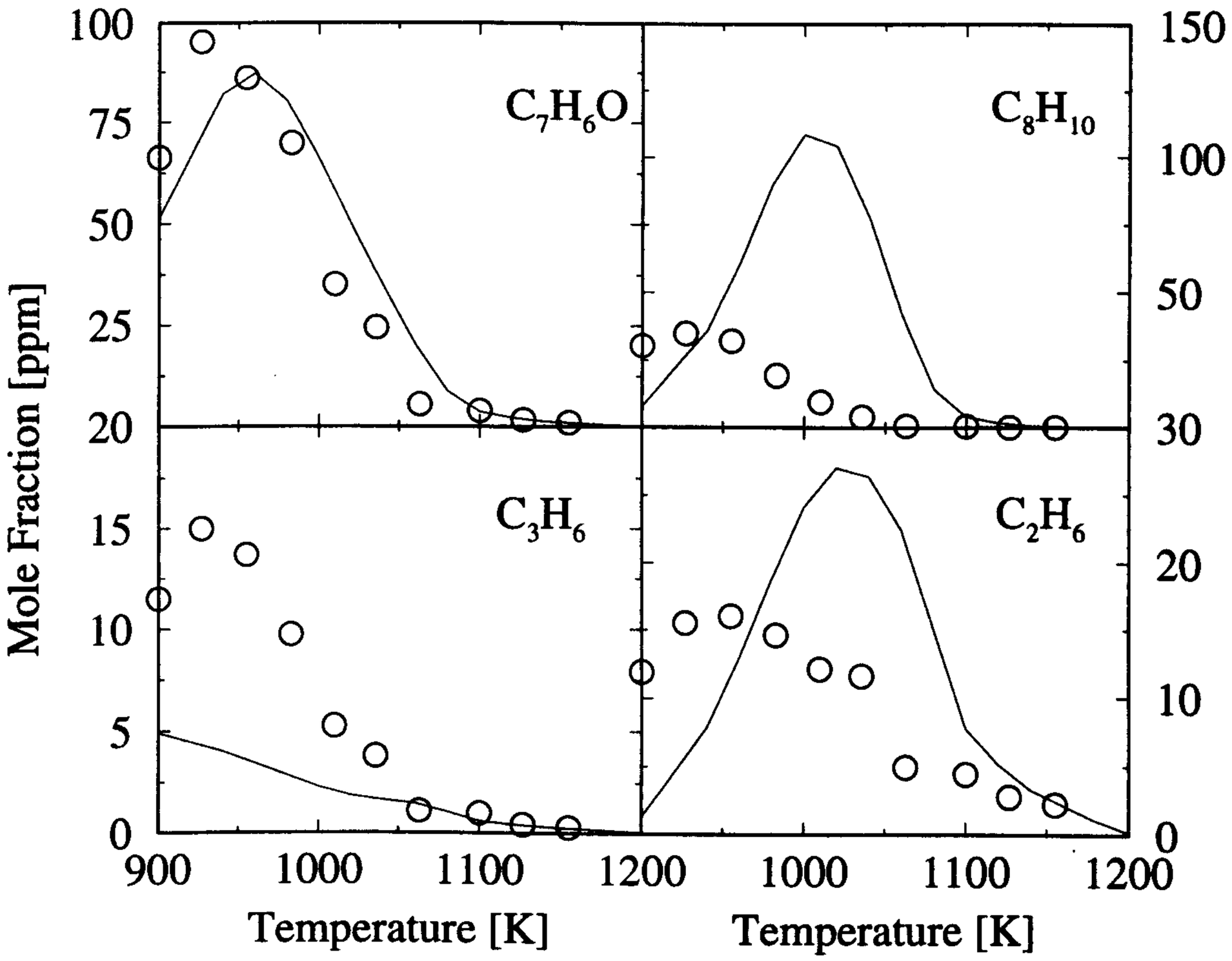


Figure 3.34: Graph of species profile concentrations versus time for the oxidation of n – propylbenzene in a Jet Stirred Reactor for a stoichiometry of $\phi = 1.0$ and a pressure of 10 atm. Experimental points are from Dagaut & Cathonnet [55]. Solid lines are the computations from the detailed chemical mechanism.

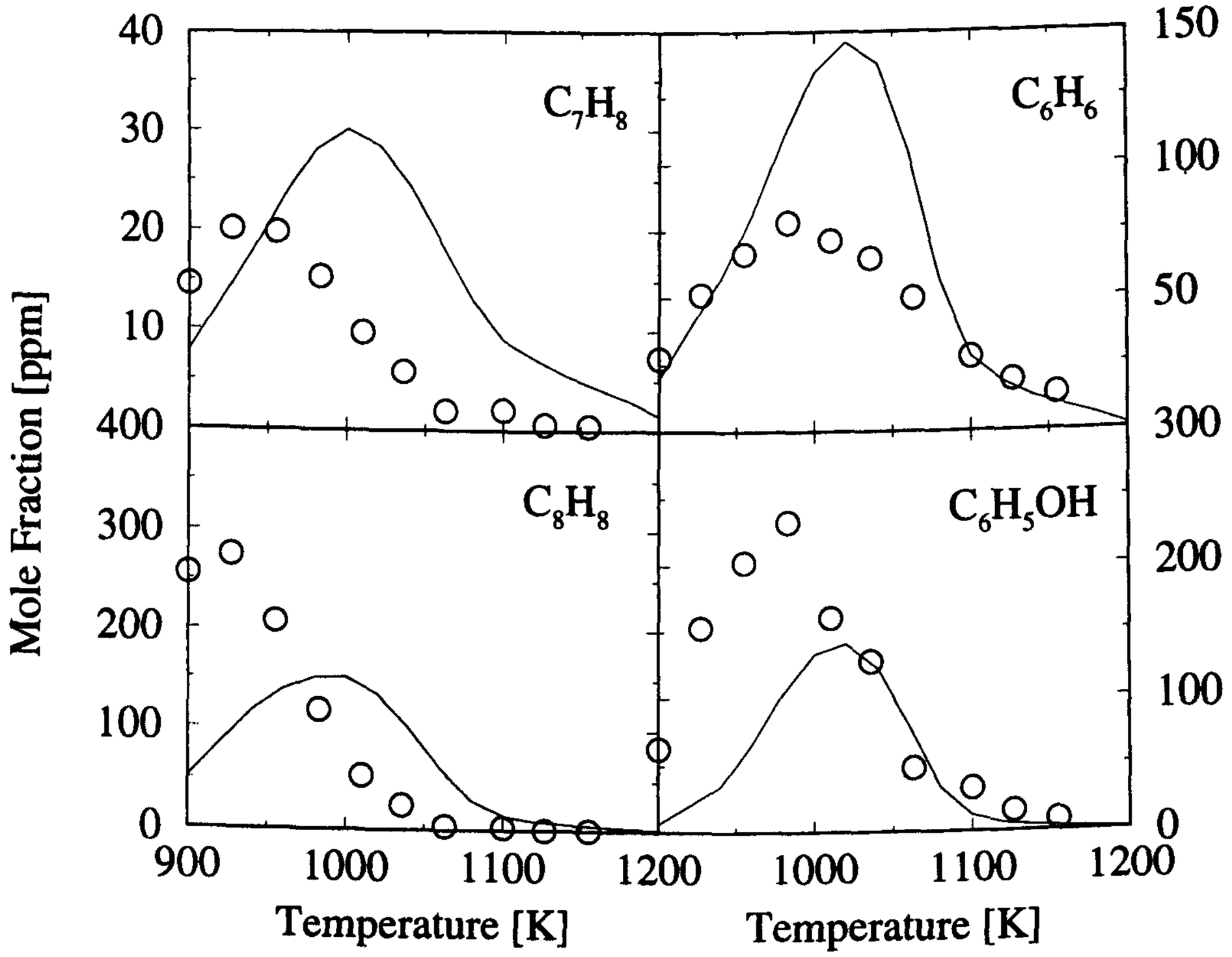


Figure 3.35: Graph of species profile concentrations versus time for the oxidation of n – propylbenzene in a Jet Stirred Reactor for a stoichiometry of $\phi = 1.0$ and a pressure of 10 atm. Experimental points are from Dagaut & Cathonnet [55]. Solid lines are the computations from the detailed chemical mechanism.

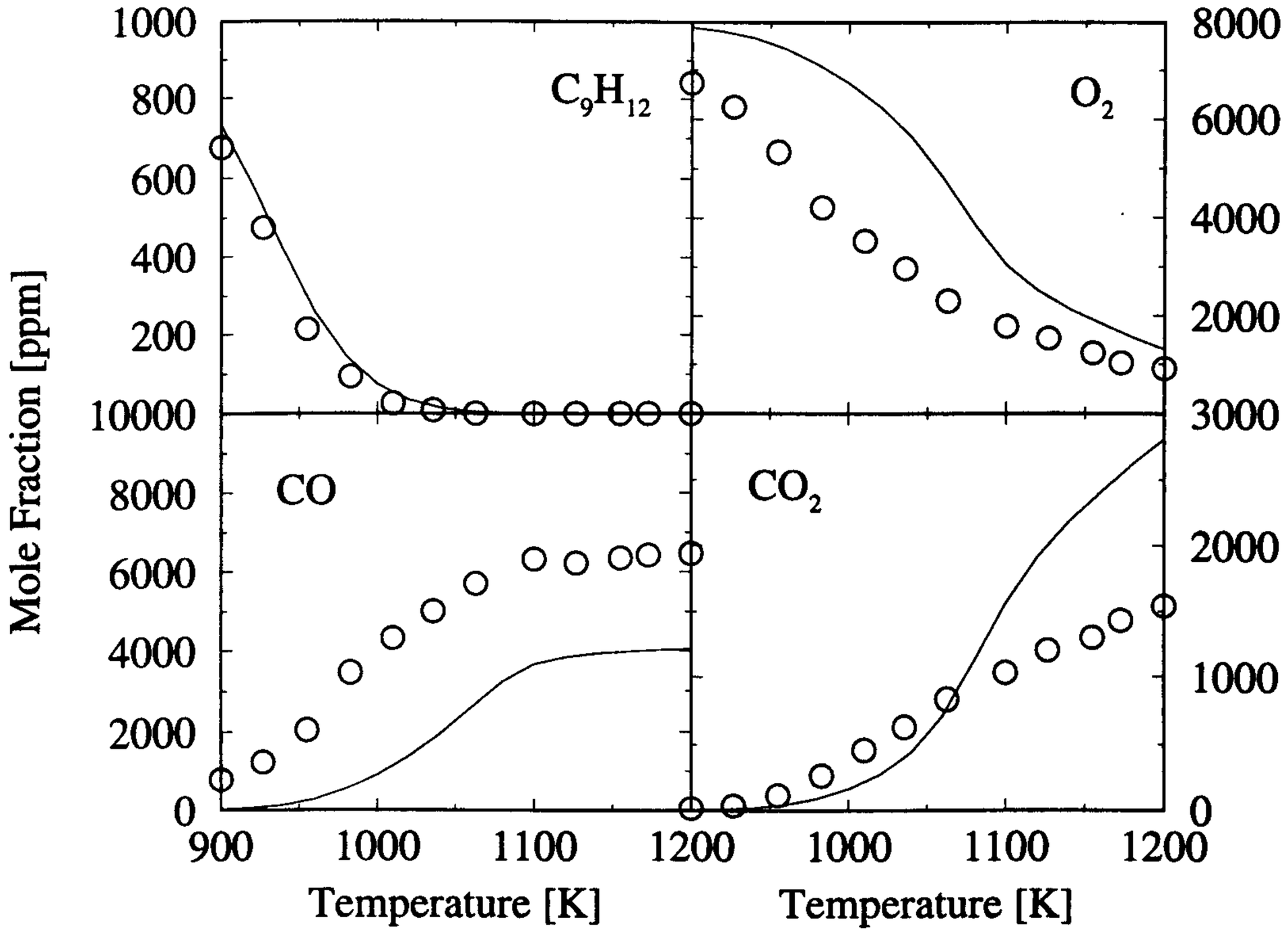


Figure 3.36: Graph of species profile concentrations versus time for the oxidation of n – propylbenzene in a Jet Stirred Reactor for a stoichiometry of $\phi = 1.5$ and a pressure of 10 atm. Experimental points are from Dagaut & Cathonnet [55]. Solid lines are the computations from the detailed chemical mechanism.

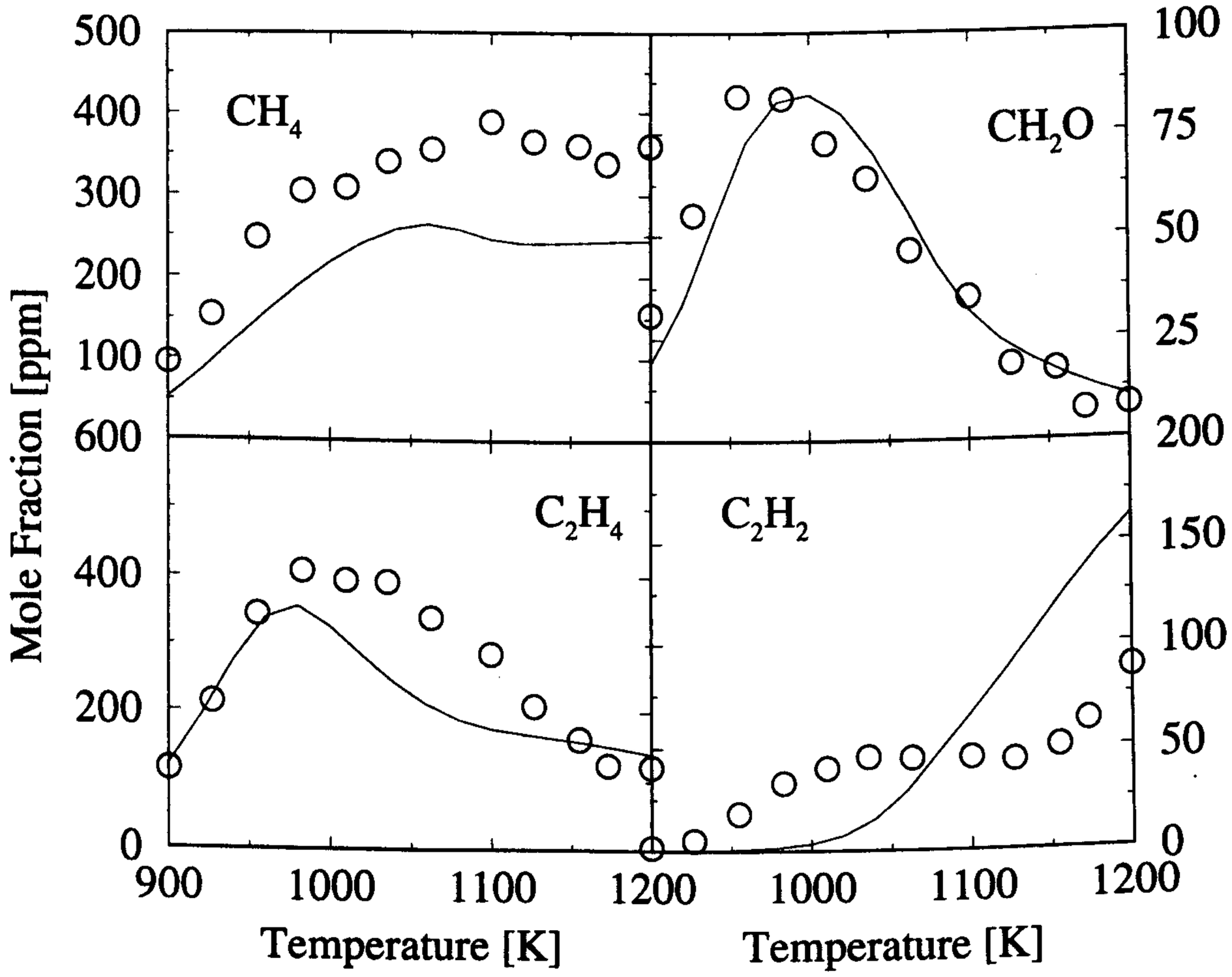


Figure 3.37: Graph of species profile concentrations versus time for the oxidation of n – propylbenzene in a Jet Stirred Reactor for a stoichiometry of $\phi = 1.5$ and a pressure of 10 atm. Experimental points are from Dagaut & Cathonnet [55]. Solid lines are the computations from the detailed chemical mechanism.

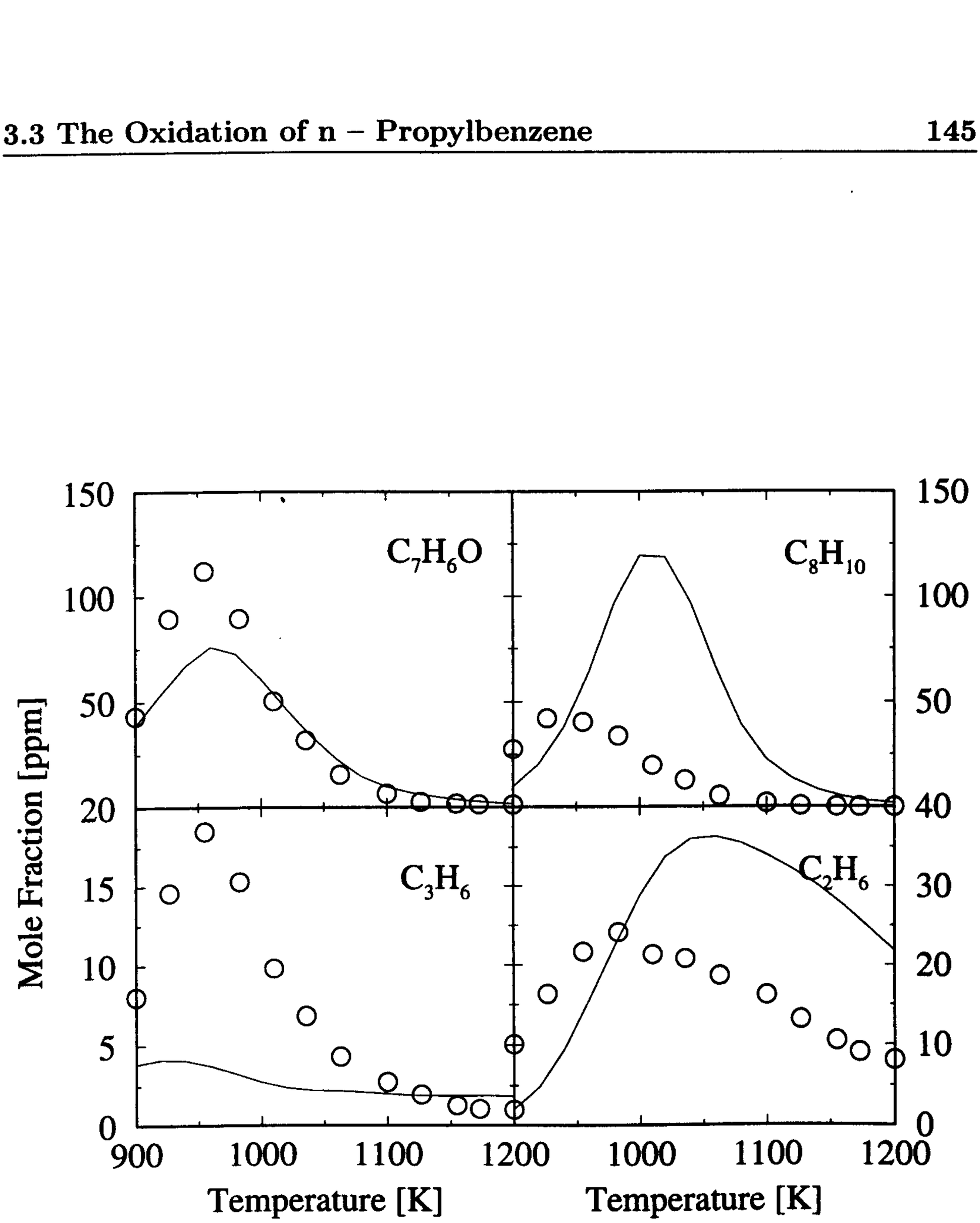


Figure 3.38: Graph of species profile concentrations versus time for the oxidation of n – propylbenzene in a Jet Stirred Reactor for a stoichiometry of $\phi = 1.5$ and a pressure of 10 atm. Experimental points are from Dagaut & Cathonnet [55]. Solid lines are the computations from the detailed chemical mechanism.

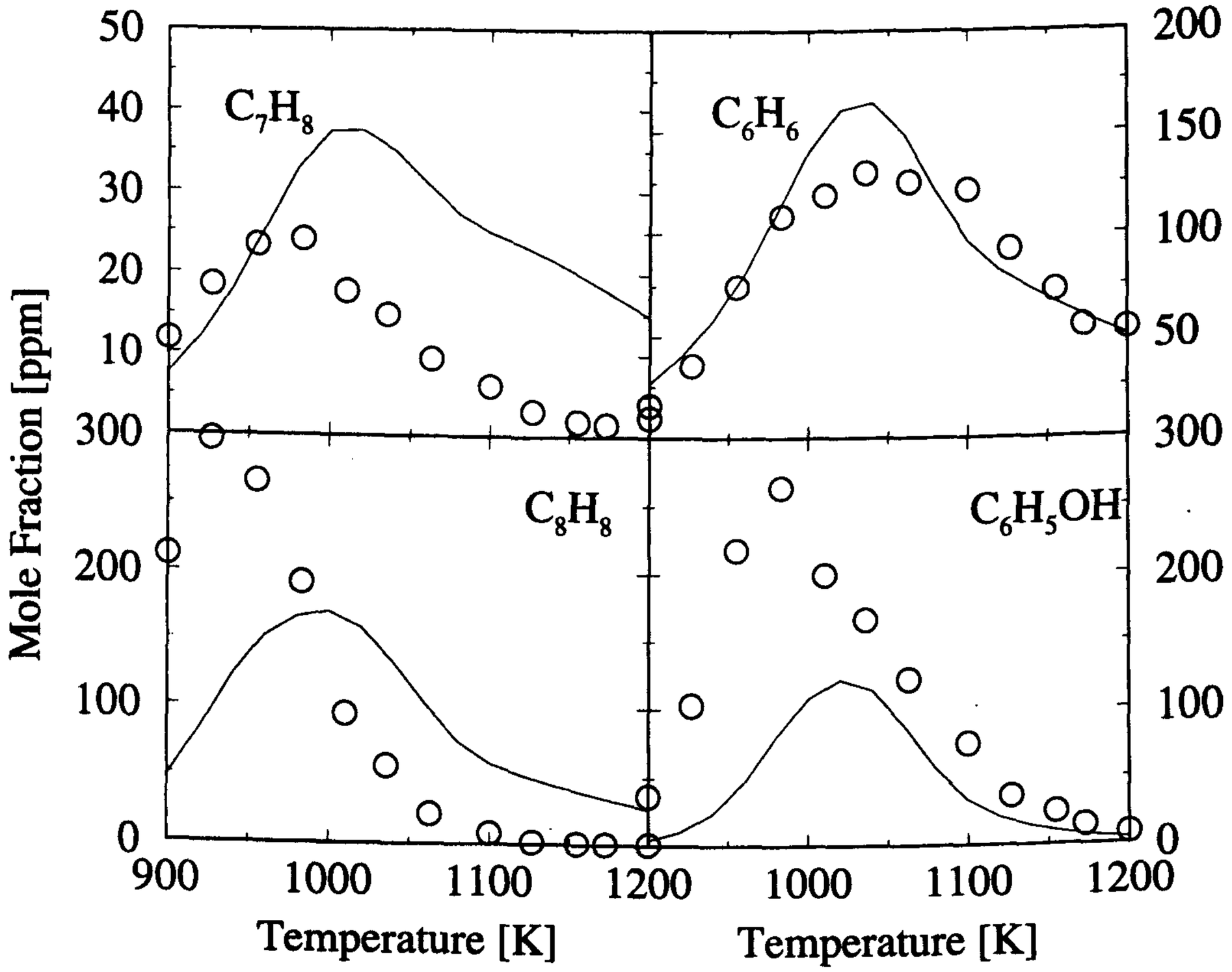


Figure 3.39: Graph of species profile concentrations versus time for the oxidation of n – propylbenzene in a Jet Stirred Reactor for a stoichiometry of $\phi = 1.5$ and a pressure of 10 atm. Experimental points are from Dagaut & Cathonnet [55]. Solid lines are the computations from the detailed chemical mechanism.

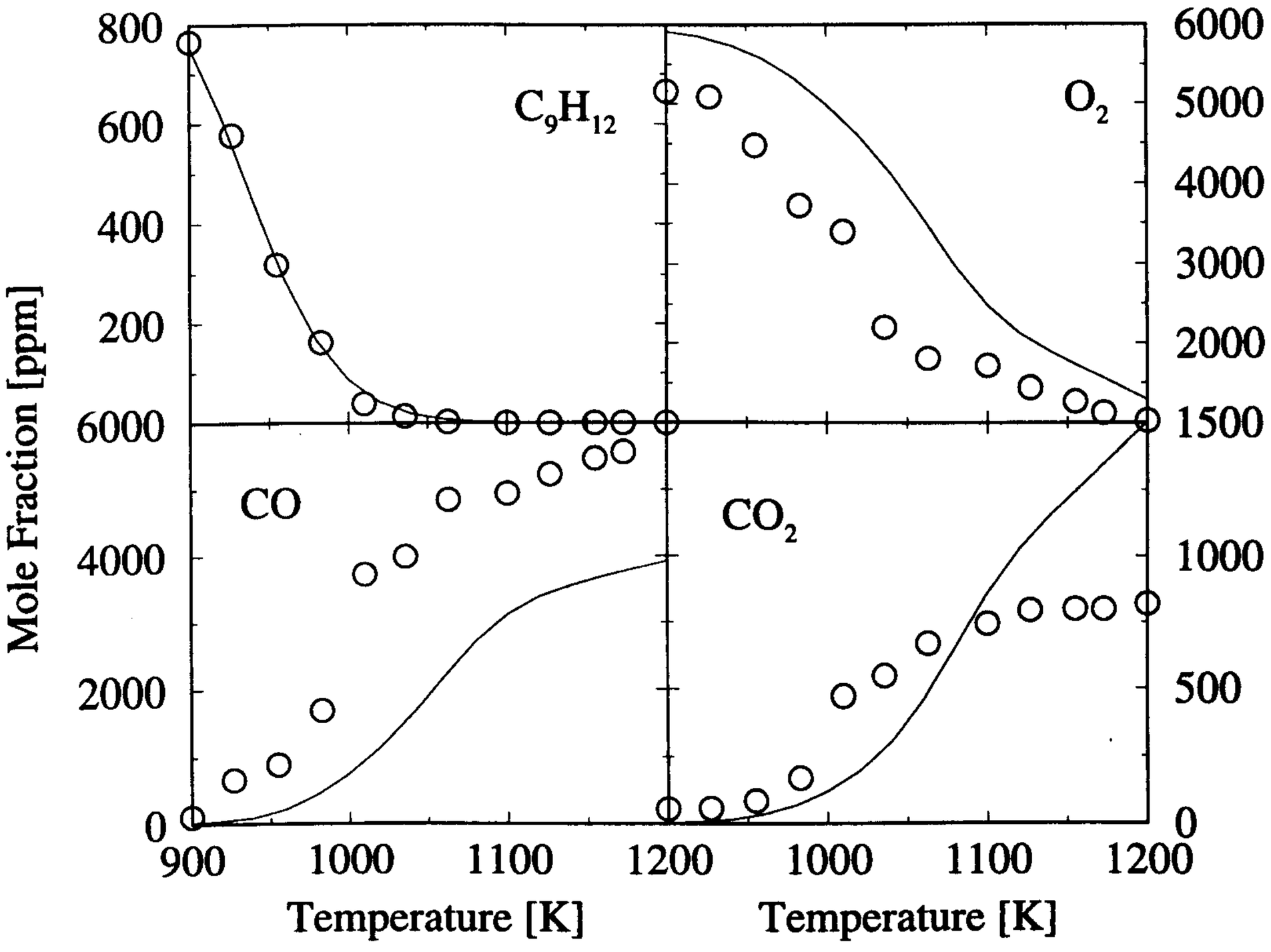


Figure 3.40: Graph of species profile concentrations versus time for the oxidation of n – propylbenzene in a Jet Stirred Reactor for a stoichiometry of $\phi = 2.0$ and a pressure of 10 atm. Experimental points are from Dagaut & Cathonnet [55]. Solid lines are the computations from the detailed chemical mechanism.

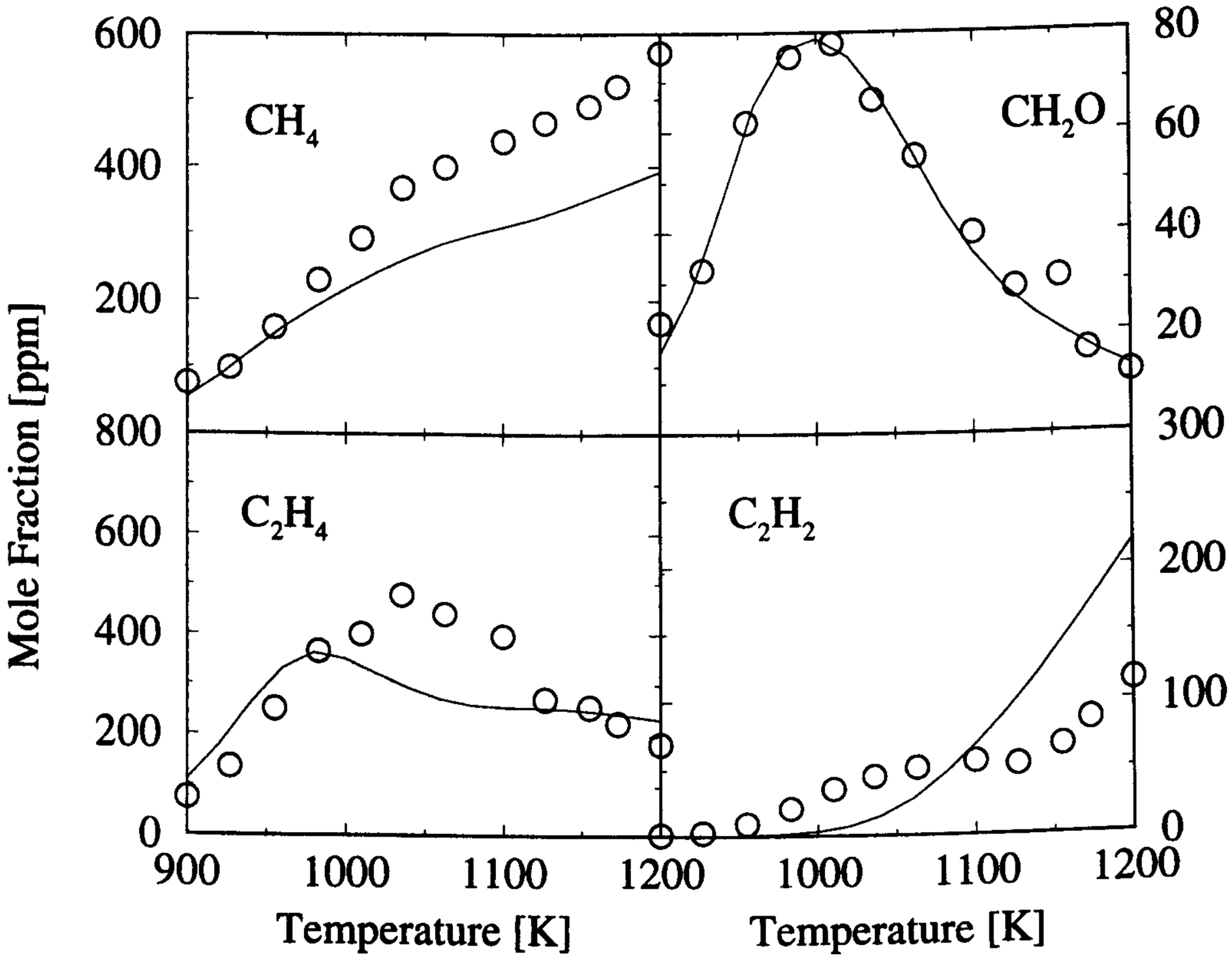


Figure 3.41: Graph of species profile concentrations versus time for the oxidation of n – propylbenzene in a Jet Stirred Reactor for a stoichiometry of $\phi = 2.0$ and a pressure of 10 atm. Experimental points are from Dagaut *et al.* [60]. Solid lines are the computations from the detailed chemical mechanism.

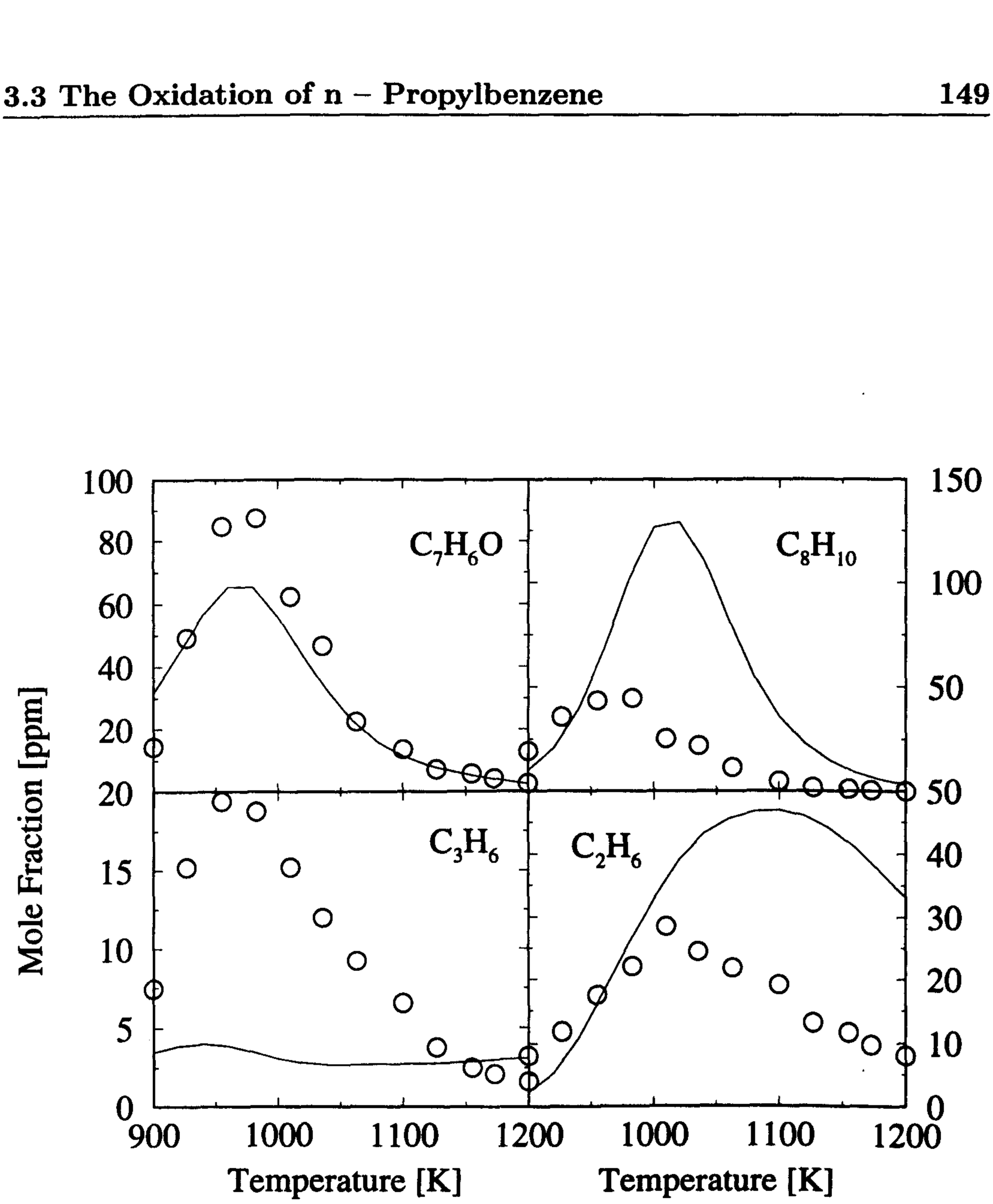


Figure 3.42: Graph of species profile concentrations versus time for the oxidation of n – propylbenzene in a Jet Stirred Reactor for a stoichiometry of $\phi = 2.0$ and a pressure of 10 atm. Experimental points are from Dagaut *et al.* [60]. Solid lines are the computations from the detailed chemical mechanism.

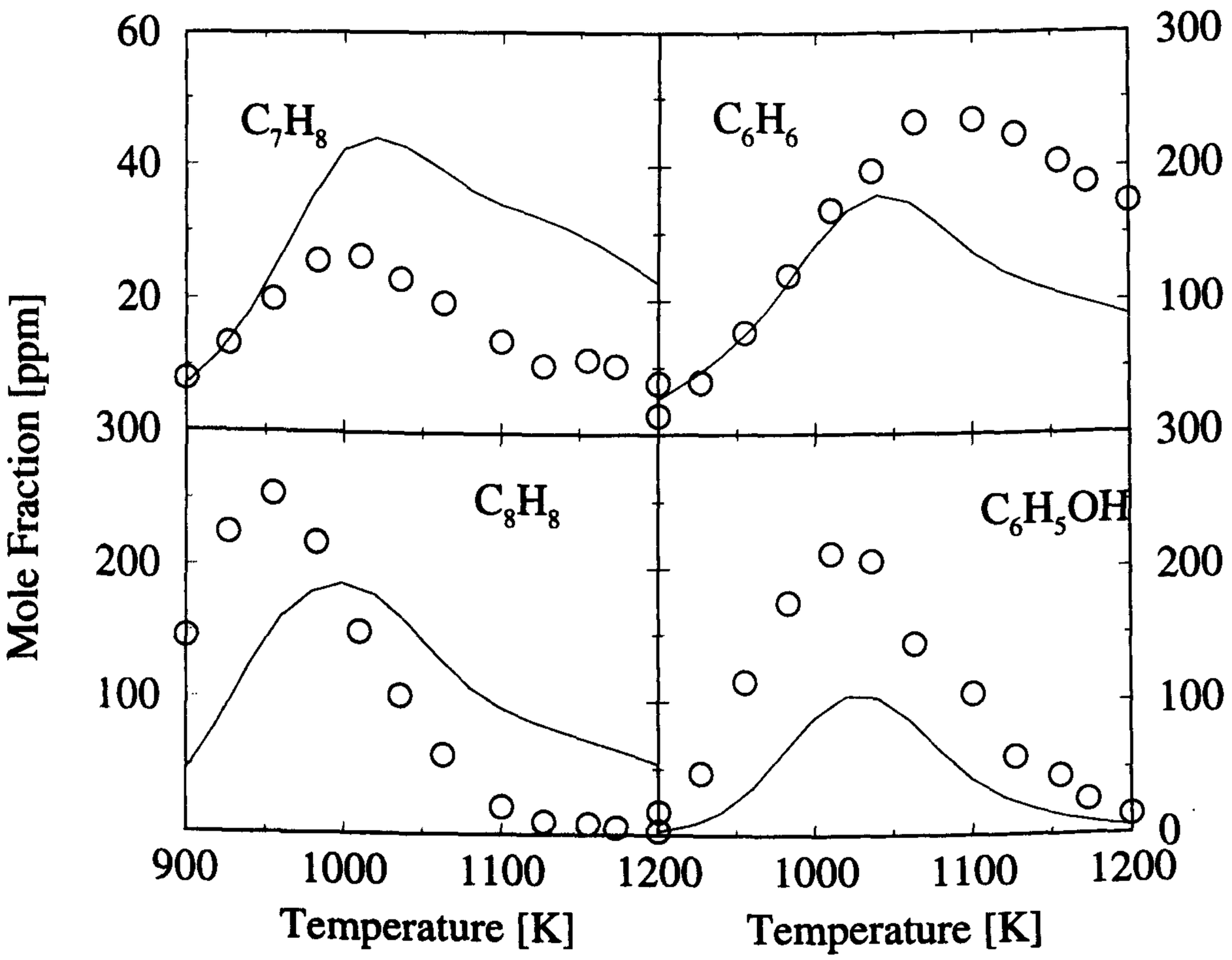


Figure 3.43: Graph of species profile concentrations versus time for the oxidation of n – propylbenzene in a Jet Stirred Reactor for a stoichiometry of $\phi = 2.0$ and a pressure of 10 atm. Experimental points are from Dagaut *et al.* [60]. Solid lines are the computations from the detailed chemical mechanism.

Primary Reaction Paths for the Oxidation of n – propylbenzene

The oxidation of n – propylbenzene under Jet Stirred Reactor conditions proceeds through the reaction paths shown in Figure 3.44. The path analysis shown here applies to the rich case ($\phi = 1.5$) at a temperature of 1060 K for the case of atmospheric pressure.

The initial consumption of C_9H_{12} involves thermal decomposition via C – C with (1489) cleavage contributing (35 %)

$$C_9H_{12} = C_8H_9 + CH_3 \quad (1489)$$

The energy barrier has been modelled on the heat of reaction (~320.6 kJ/mol), with an additional 20 kJ/mol added (which is within the uncertainty limits as recommended by Dean [73]) and the frequency factor has been adopted from the work of Dagaut *et al.* [60].

A further 20 % is consumed by thermal decomposition via C – C cleavage through the channel

$$C_9H_{12} = C_7H_7 + C_2H_4 \quad (1488)$$

The energy barrier has been modelled on the heat of reaction (~326.7 kJ/mol) and the frequency factor has been adopted from the work of Dagaut *et al.* [60].

The $1C_9H_{11}$ radical is formed from H and OH attack on the fuel with reactions (1468) and (1474) contributing 5 % each.

$$C_9H_{12} + H = 1C_9H_{11} + H_2 \quad (1468)$$
$$C_9H_{12} + OH = 1C_9H_{11} + H_2O \quad (1474)$$

The rate for H radical attack on the fuel has been obtained from Dagaut *et al.* [60]. The rate for OH radical attack has been based on the analogous reaction

$$C_3H_8 + OH \quad = \quad C_3H_7(I) + H_2O \tag{439}$$

with the rate parameters being discussed by Rizos [218].

The $1C_9H_{11}$ radical, thermally decomposes via C – C cleavage leading to C_7H_7 and C_2H_4.

$$1C_9H_{11} \quad = \quad C_7H_7 + C_2H_4 \tag{439}$$

The rate parameters have been modelled on the work of Dean [73].

The $2C_9H_{11}$ radical is formed from H and OH attack on the fuel with reactions (1469) and (1475) contributing 5 % each.

$$C_9H_{12} + H \quad = \quad 2C_9H_{11} + H_2 \tag{1469}$$
$$C_9H_{12} + OH \quad = \quad 2C_9H_{11} + H_2O \tag{1475}$$

The rate for H radical attack on the fuel has been obtained from Dagaut *et al.* [60]. The rate for OH radical attack has been based on the analogous reaction (439).

$$C_3H_8 + OH \quad = \quad C_3H_7(I) + H_2O \tag{439}$$

The $2C_9H_{11}$ radical is consumed by C – H bond cleavage via reactions (55 % and 45 % respectively)

$$2C_9H_{11} \quad = \quad 1C_9H_{10} + H \tag{1512}$$
$$2C_9H_{11} \quad = \quad 2C_9H_{10} + H \tag{1514}$$

with the rates modelled on reaction (418).

$$C_3H_7(I) \quad = \quad C_3H_6 + H \tag{418}$$

The frequency factor for reactions (1512) and (1514) have been halved to take into account the branching ratio to $1C_9H_{10}$ and $2C_9H_{10}$ with the rate for (418) being obtained from Leung & Lindstedt [162].

The $1C_9H_{10}$ compound formed from reaction (1512) undergoes H addition to form $1C_9H_{11}$ via the reverse of reaction

$$1C_9H_{11} = C_9H_{10} + H \quad (1508)$$

The rate for reaction (1508) has been modelled on reaction (418).

$$C_3H_7(I) = C_3H_6 + H \quad (418)$$

The $2C_9H_{10}$ compound produced from reaction (1514) undergoes H radical attack

$$2C_9H_{10} + H = C_7H_7 + C_2H_4 \quad (1524)$$

forming benzyl and ethylene. The rate for reaction (1524) is modelled directly on the analogous reaction (1518).

$$1C_9H_{10} + H = C_8H_8 + CH_3 \quad (1518)$$

The rate parameters for (1518) has been adopted from Tsang & Walker [251].

The $3C_9H_{11}$ radical is formed from H and OH attack on the fuel with (1470) and (1476) contributing 5 % each.

$$C_9H_{12} + H = 3C_9H_{11} + H_2 \quad (1470)$$
$$C_9H_{12} + OH = 3C_9H_{11} + H_2O \quad (1476)$$

The rate for H radical attack on the fuel has been obtained from Dagaut *et al.* [60]. The rate for OH radical attack is based on the analogous reaction (440), discussed by Rizos [218].

$$C_3H_8 + OH \quad = \quad C_3H_7(N) + H_2O \tag{440}$$

The $3C_9H_{11}$ radical thermally decomposes via C – C cleavage (1516) with the rate being derived from the work of Dean [73]. An additional barrier of 40 kJ/mol is added to take into account a hydrogen transfer.

$$3C_9H_{11} \quad = \quad C_8H_8 + CH_3 \tag{1516}$$

The consumption of the smaller species has been discussed in Chapter 2 and in the study by Rizos [218].

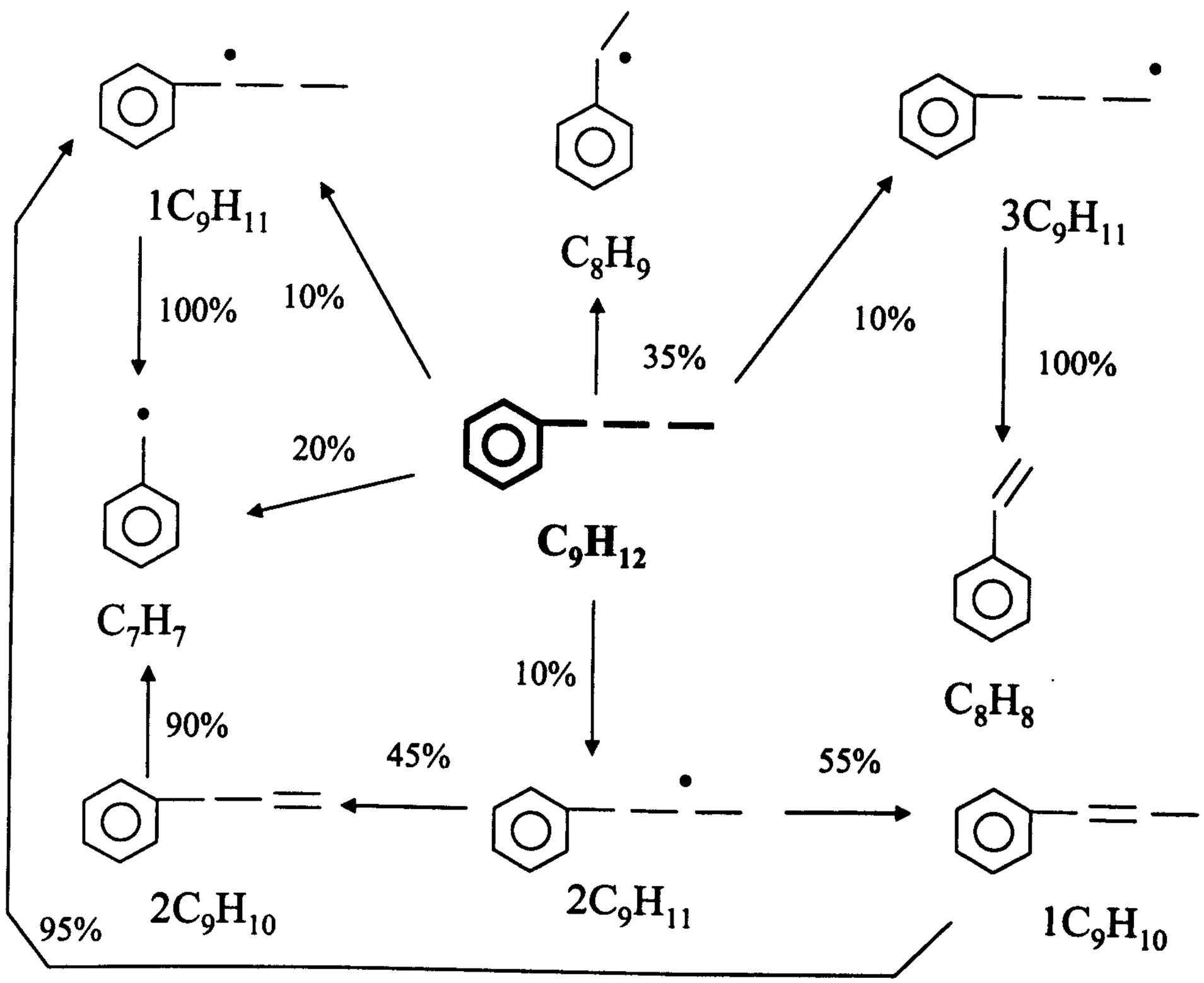


Figure 3.44: Diagram illustrating the consumption paths of the fuel n – propylbenzene and its intermediate species in a Jet Stirred Reactor (T = 1060 K, P = 1 atm., $\phi = 1.5$).

3.4 Summary

In the present Chapter, the detailed chemical kinetic mechanism has been applied to the oxidation of phenylacetylene under Turbulent Flow Reactor conditions. The general modelling approach is such that the side chain and ring reactions are modelled on the analogous equivalent reactions of acetylene and benzene respectively. It has been found that there are significant experimental uncertainties in the data sets of Shaddix [226]. The amendment to the initial conditions led to good predictions for the initial, intermediate and end products. However, caution should be given over the validity of the detailed mechanism. Further investigations into a wide range of experimental data sets is required to reassure the accuracy of the detailed chemical kinetic mechanism.

Additionally, global reaction steps involving ring – ring reactions have been applied to predict the formation of the three ring structures phenanthrene, anthracene and acenaphthalene. It was discovered that typical reaction steps as found in the literature and involving the formation of a radical site on the ring and followed by addition reactions are too slow. At these intermediate temperatures, O_2 addition plays an influential role, hence reaction steps as those mentioned above are too slow to be able to compete with molecular oxygen reactions. The formation of the three ring structures was found to be via ring – ring reactions. However, no experimental data was found in the literature regarding these type of reaction steps. This work therefore demonstrates the significance, and the lack of knowledge and understanding of this type of chemistry. It can be concluded that, for future purposes, a thorough investigation into the formation of various PAH structures be carried out at intermediate temperatures with ring – ring reaction steps acting as the dominant formation channel for PAH formation, particu-

larly three ringed structures.

The oxidation of n – propylbenzene has been investigated under Jet Stirred Reactor conditions for pressures of 1 and 10 atm. Overall, the detailed chemical mechanism can reproduce fuel and intermediate species profiles with some degree of accuracy. However, problems have been encountered with the C_8H_8 and C_6H_6 species concentration profiles. It was found that reaction (1195)

$$C_8H_8 + OH \quad = \quad C_7H_7 + CH_2O \tag{1195}$$

is the dominant channel and by reducing the frequency factor by a factor of 3 significantly improved the results for these species. It is therefore necessary to fully validate and verify the styrene sub – mechanism over a wide range of conditions. However, this is made difficult due to the lack of experimental data available in the literature. Overall, the role of low temperature chemistry also needs to be further explored.

The isomerisation step utilised by Dagaut *et al.* [60] on the $2C_9H_{11}$ radical was not used to compute the current set of results in this study due to the high level of methyl generated which lead to C_2H_6 being heavily over predicted in all cases. Interestingly, the low concentrations of C_3H_6 encountered under these set of conditions are still reproduced reasonably well.

Chapter 4

Naphthalene and 1 – Methylnaphthalene

4.1 Introduction

The complex mixtures constituting practical fuels diesel fuels have been discussed in Chapter 1. It has been suggested in previous studies (*e.g.* Dagaut [52], Pfahl *et al.* [202], Pitsch [203]) that the inclusion of PAH and alkyl – substituted PAH molecules to represent the aromatic component of diesel fuels is necessary and analysis of practical fuel compositions support this proposal. Therefore, the main focus of the present chapter is to discuss the extension of the systematically constructed detailed chemical mechanism to PAH compounds. The oxidation of naphthalene and 1 – methylnaphthalene is here investigated under a variety of conditions.

4.2 The Oxidation of Naphthalene

Many PAH formation reviews (*e.g.* Frenklach [95], Kohse – Höinghaus *et al.* [152], Longwell [176], Richter *et al.* [213], and Richter & Howard [214]) have shown that naphthalene is a key soot precursor and hence the formation and destruction of this compound is of particular importance to combustion modelling. Furthermore, naphthalene is one of the key intermediate species produced in the oxidation of 1 – methylnaphthalene. Therefore the naphthalene sub – mechanism is of critical importance.

Currently, no detailed chemical mechanisms describing the oxidation of naphthalene have been produced, although the inclusion of naphthalene reactions have been implemented in various detailed chemical mechanisms involving the formation of PAH (*e.g.* Faravelli *et al.* [93], Lindstedt *et al.* [169], Richter *et al.* [212], and D'Anna & Violi [68]). The sub – mechanism developed in this study for the oxidation of naphthalene is primarily based on benzene due to the similarities in structure.

4.2.1 The Oxidation of Naphthalene in a Turbulent Flow Reactor

The experimental data set used to validate and verify the naphthalene sub – mechanism under Turbulent Flow Reactor conditions is obtained from Shaddix [226]. The conditions correspond to a stoichiometric ratio of $\phi = 1.1$ at atmospheric pressure and with an initial temperature of 1197 K. Shaddix [226] reports an uncertainty of 32 ms in the temporal evolution of the experimental data.

The calculations for the oxidation of naphthalene and the intermediate and final products are shown in Figures 4.1 – 4.4. Overall, the calculations

are in very good agreement with the exception of $C_{10}H_7OH$ as illustrated in Figure 4.2. Due to the scatter in the experimental data for the fuel profile of naphthalene, shown in Figure 4.1, the focus was to produce an accurate O_2 decay profile. Shaddix [226] reports that the scatter in the fuel profile of naphthalene is caused by condensation of the fuel.

The calculations reproduce indene concentrations as is evident in Figure 4.2. It is found that the primary channel is H addition on to the C_9H_7 radical (1258), and the accurate prediction of C_9H_8 is encouraging.

$$C_9H_7 + H \quad = \quad C_9H_8 \qquad (1258)$$

The agreement between the computations and the experimental data for C_8H_8 is excellent as is evident in Figure 4.2. It is found at a reaction time of 75 ms the primary source for this species is via reaction (1185).

$$C_8H_7P + H \quad = \quad C_8H_8 \qquad (1185)$$

The rate for reaction (1185) has been estimated as reported by Maurice [182] and is modelled on the analogous reaction involving H addition to C_6H_5 (926).

$$C_6H_5 + H \quad = \quad C_6H_6 \qquad (926)$$

The rate for reaction (926) has been obtained from Baulch *et al.* [13].

The calculated levels of C_8H_6 are in good agreement with the experimental data of Shaddix [226] as is evident in Figure 4.2. It is found that reactions (1170) and (1297) constitute the most important formation channels and contribute approximately 50 % each.

$$C_8H_7 \quad = \quad C_8H_6 + H \qquad (1170)$$

$$C_9H_6O \quad = \quad C_8H_6 + CO \qquad (1297)$$

Other aromatics such as C_7H_8, C_7H_6O, C_6H_6 and C_5H_6 are also well reproduced as is evident in Figure 4.3. It is found that the primary channel for C_7H_8 formation is via H addition to the C_7H_7 radical (1077).

$$C_7H_8 = C_7H_7 + H \quad (1077)$$

The formation of C_7H_6O is of particular interest since it results from the rupture of the first C_9H_7 ring. At later times ($\geq$ 100 ms) the concentration profile shows a curvature similar to that of C_9H_8. This is due to C_7H_6O being derived from C_9H_7 due to the addition of molecular oxygen, followed by the decomposition to form C_7H_6O and C_2HO via the exothermic (-160 kJ/mol) reaction (1265).

$$C_9H_7 + O_2 = C_7H_6O + C_2HO \quad (1265)$$

The rate adopted is estimated and as activation barrier of 10 kJ/mol has been added to account for the initial adduct formation.

The computations for C_6H_6 produce good agreement as shown in Figure 4.3. It is found that reactions (1104) and (985) are the primary channels

$$C_7H_6O + O = C_6H_6 + CO_2 \quad (1104)$$

$$C_6H_6(F) + H = C_6H_6 + H \quad (985)$$

The production of C_5H_6 is via the reverse of reaction (810) with good agreement being obtained between the computations and the experimental data from Shaddix [226] as is evident in Figure 4.3.

$$C_5H_6 = C_5H_5 + H \quad (810)$$

Other smaller species are well predicted as illustrated in Figure 4.4. The production of C_4H_4 is via reaction (900)

$$C_5H_4O \quad = \quad C_4H_4 + CO \qquad (900)$$

The concentrations of the C_3 species, although low, are well reproduced and the same also applies to C_2 species.

A graph of the evolution of temperature versus time is illustrated in Figure 4.5. The detailed mechanism performs well and predicts the small temperature rise experienced from the oxidation of $C_{10}H_8$.

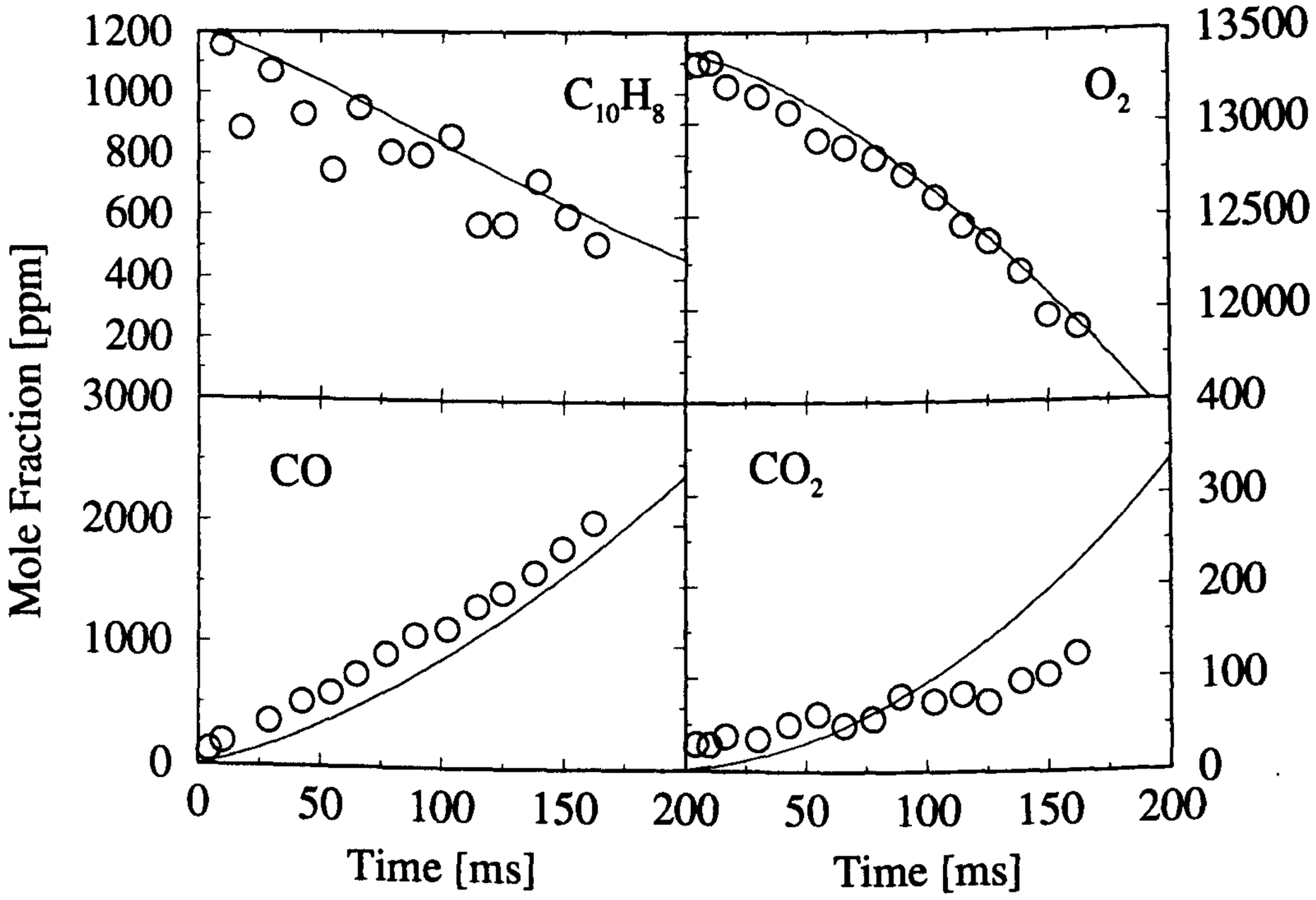


Figure 4.1: Graph of species profile concentrations versus time for the oxidation of naphthalene in a Turbulent Flow Reactor. Experimental points are from Shaddix [226] for a stoichiometry of $\phi = 1.1$. Solid lines are the computations from the detailed chemical mechanism and have not been time shifted.

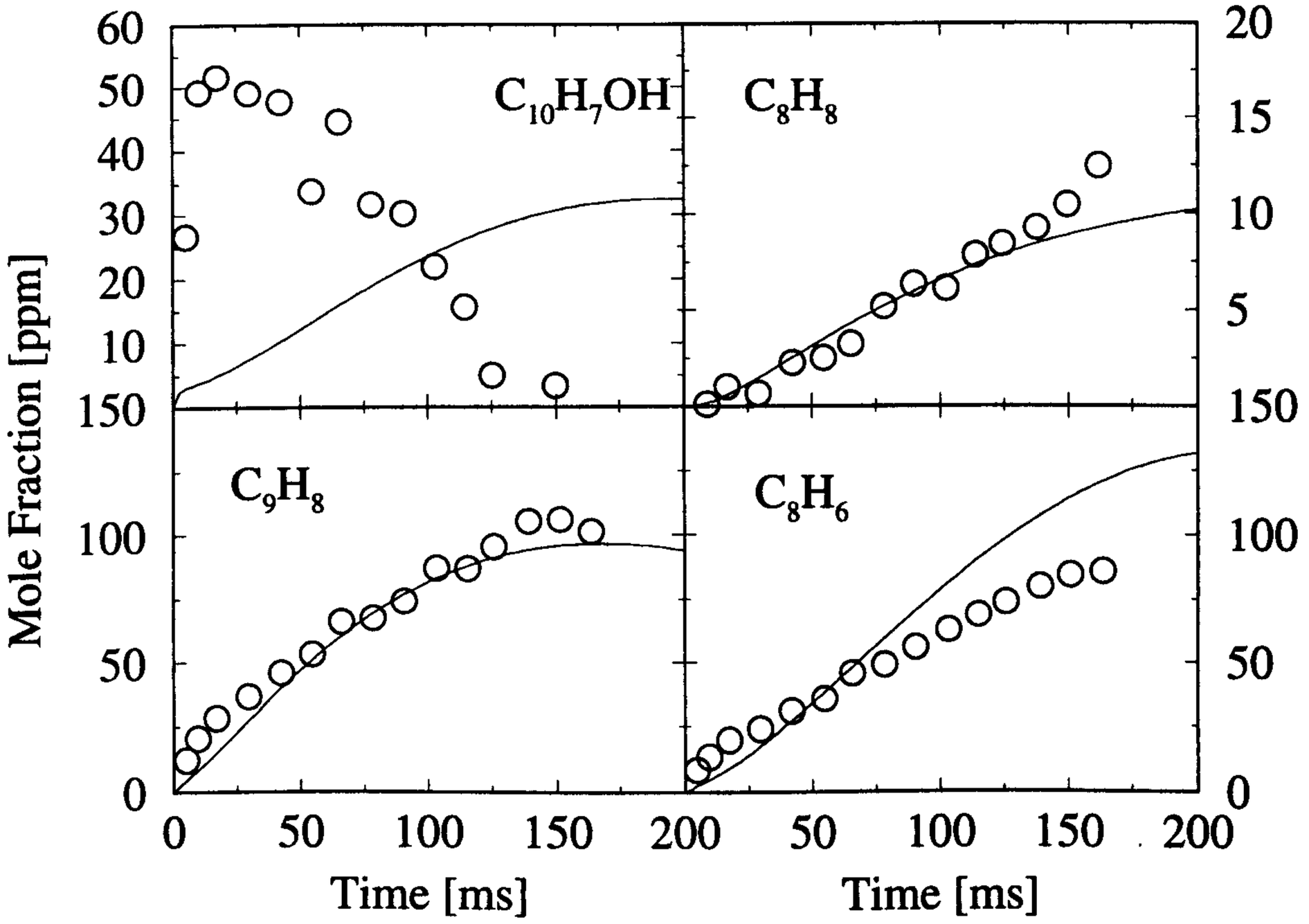


Figure 4.2: Graph of species profile concentrations versus time for the oxidation of naphthalene in a Turbulent Flow Reactor. Experimental points are from Shaddix [226] for a stoichiometry of $\phi = 1.1$. Solid lines are the computations from the detailed chemical mechanism and have not been time shifted.

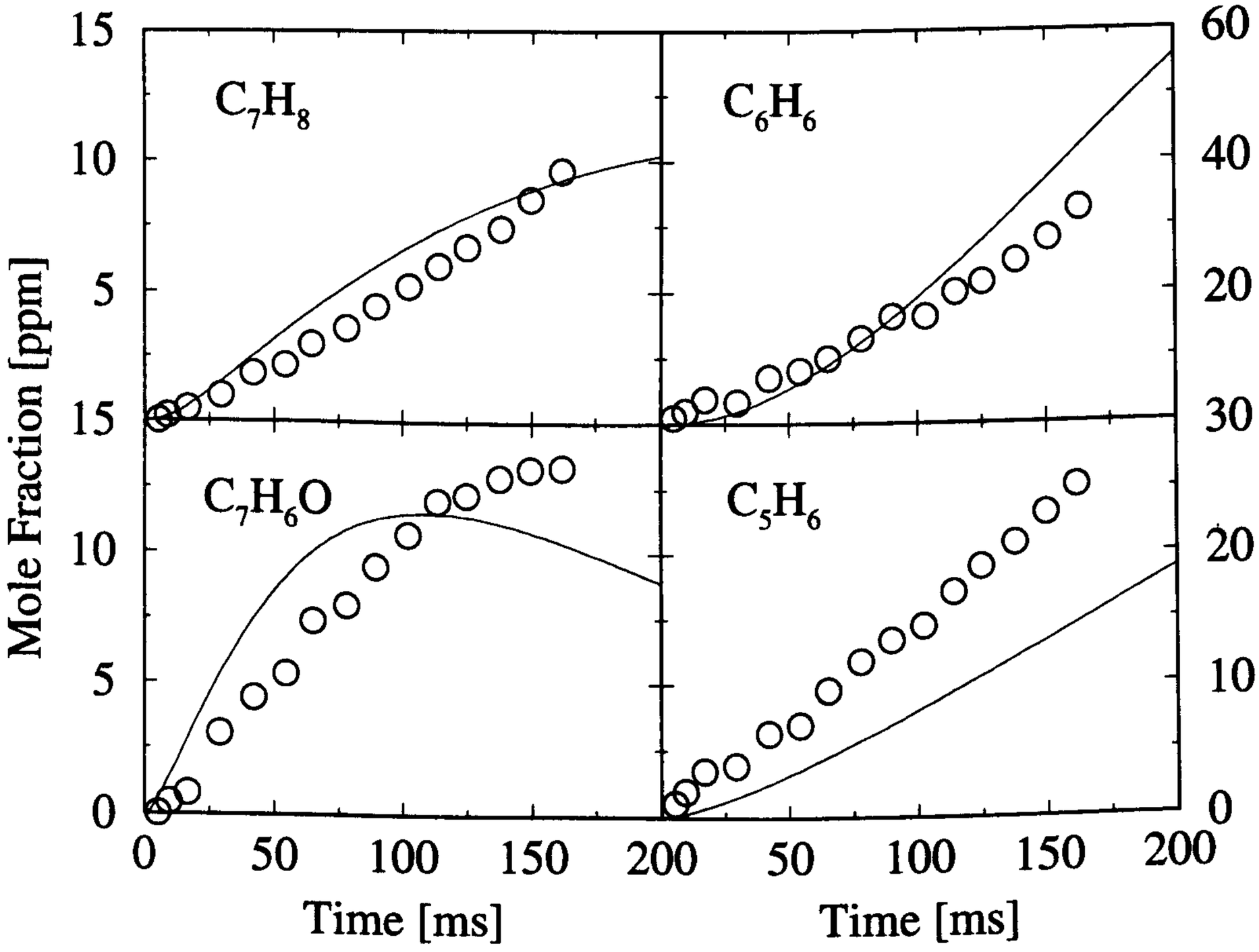


Figure 4.3: Graph of species profile concentrations versus time for the oxidation of naphthalene in a Turbulent Flow Reactor. Experimental points are from Shaddix [226] for a stoichiometry of $\phi = 1.1$. Solid lines are the computations from the detailed chemical mechanism and have not been time shifted.

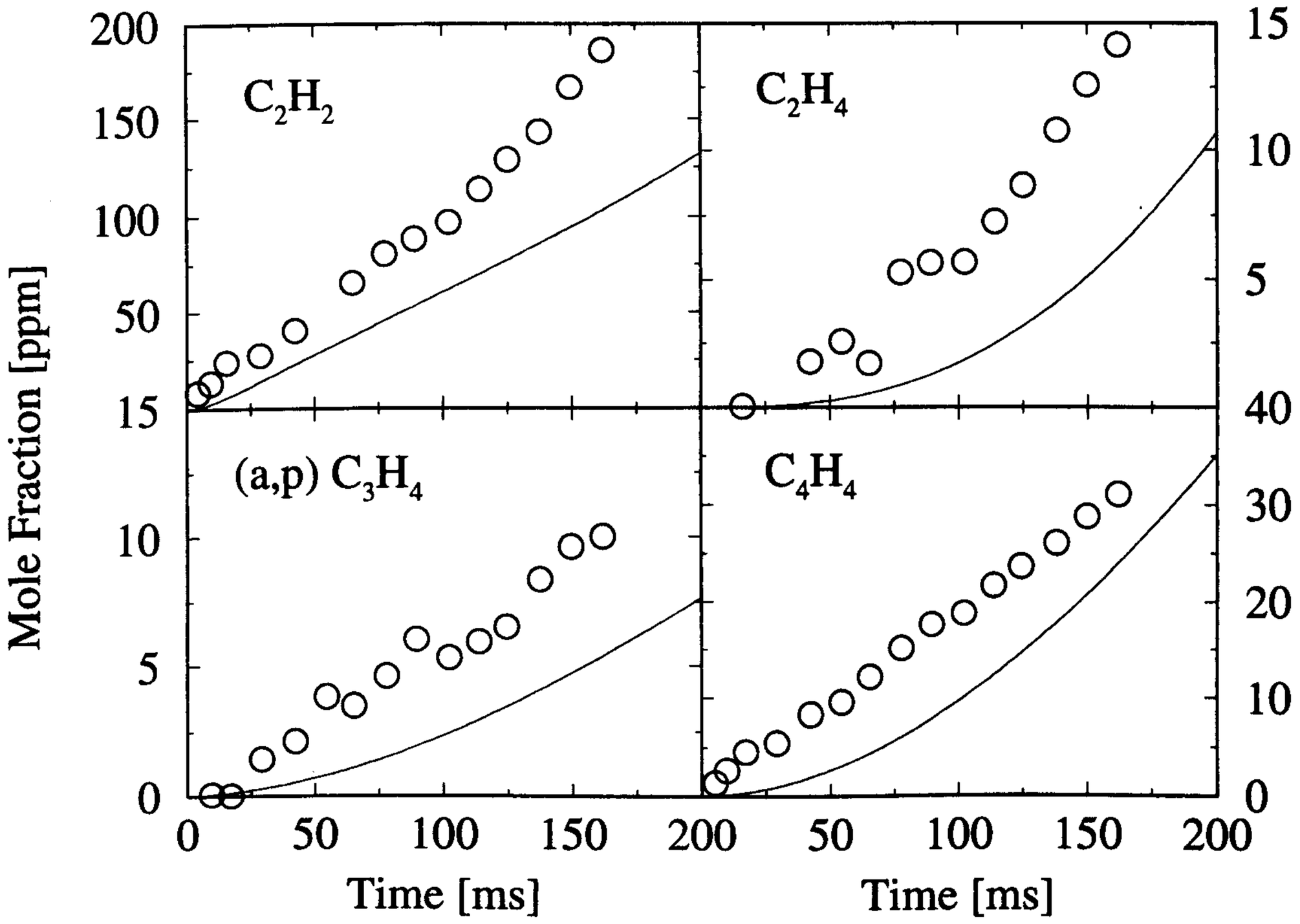


Figure 4.4: Graph of species profile concentrations versus time for the oxidation of naphthalene in a Turbulent Flow Reactor. Experimental points are from Shaddix [226] for a stoichiometry of $\phi = 1.1$. Solid lines are the computations from the detailed chemical mechanism and have not been time shifted.

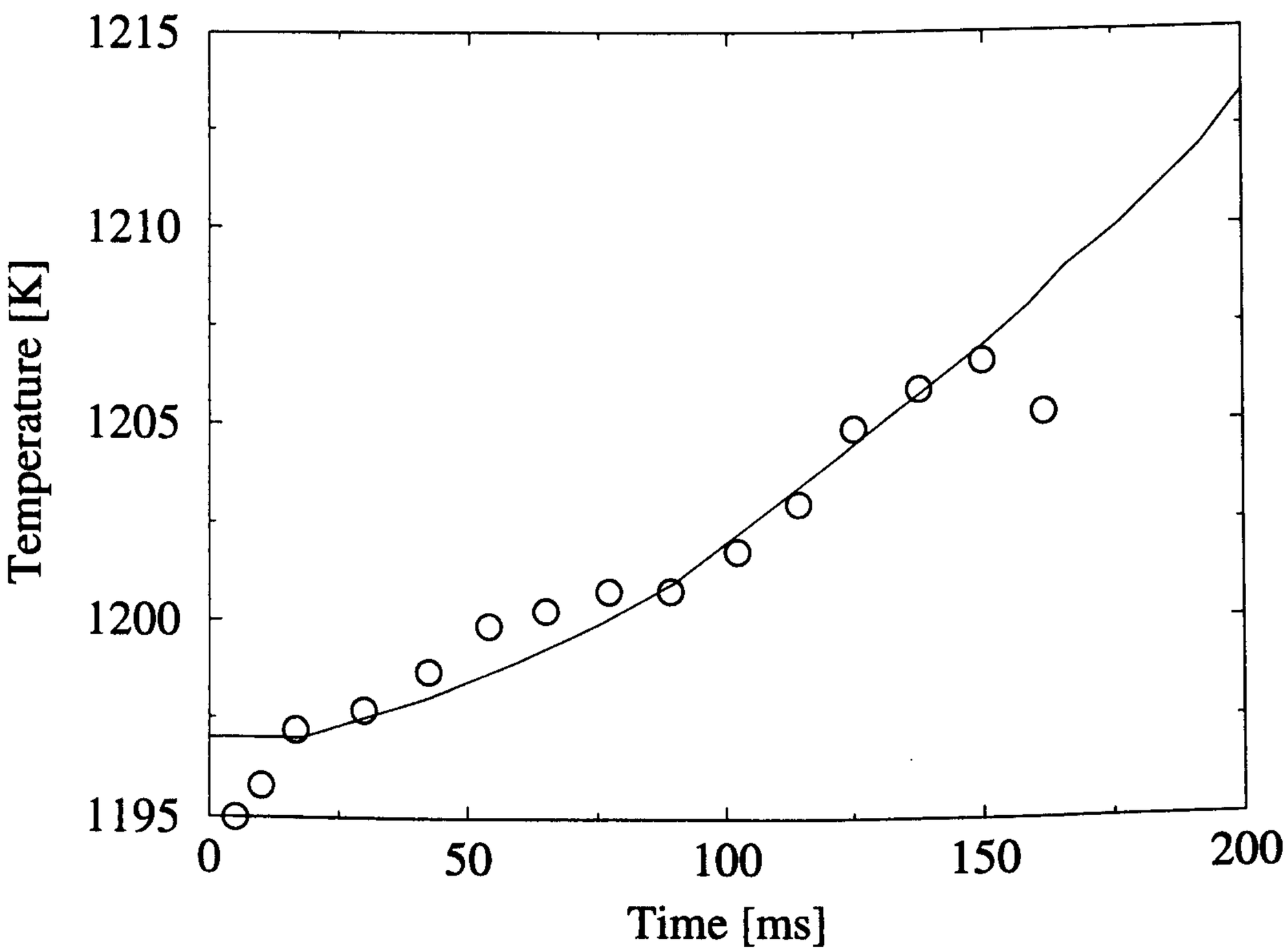


Figure 4.5: Graph of temperature profile versus time for the oxidation of naphthalene in a Turbulent Flow Reactor. Experimental points are from Shaddix [226] for a stoichiometry of $\phi = 1.1$. Solid lines are the computations from the detailed chemical mechanism and have not been time shifted.

Primary Reaction Paths for the Oxidation of Naphthalene

The oxidation of naphthalene proceeds through a number of chemical paths as shown in Figures 4.6 – 4.8. As previously mentioned, the general conceptual modelling approach is based on the similarity to benzene oxidation where possible. The chemical kinetic rates which constitute the benzene sub – mechanism have been thoroughly validated in the study by Rizos [218]. The frequency factor have naturally been adjusted for molecular size differences. The major reactions in the oxidation of naphthalene are discussed below with the path analysis conducted at a reaction time of 75 ms.

The initial attack on the fuel, is via by H radical attack (1305) which contributes 15 %.

$$C_{10}H_7 + H_2 \quad = \quad C_{10}H_8 + H \qquad (1305)$$

The rate parameters for reaction (1305) are based on the analogous reaction for C_6H_6 (956).

$$C_6H_6 + H \quad = \quad C_6H_5 + H_2 \qquad (956)$$

The reaction has been measured by Kiefer *et al.* [147] under Shock Tube conditions over a temperature range of 300 – 5000 K and a pressure of 0.2 – 1.0 atm. The rate for reaction (1305) has also been studied by Alzueta *et al.* [2] and Mebel *et al.* [185].

$$C_6H_5 + H_2 \quad = \quad C_6H_6 + H$$

The latter investigators used QRRK analysis over a temperature range of 500 – 800 K and suggested that the rate is approximately 2.5 times faster at 1200 K than proposed by Kiefer *et al.* [147].

Attack by O radicals contributes a further 40 % to the consumption of $C_{10}H_8$ (1320)

$$C_{10}H_8 + O \quad = \quad C_{10}H_7O + H \tag{1320}$$

with the rate being modelled directly on the analogous reaction for C_6H_6 (959)

$$C_6H_6 + O \quad = \quad C_6H_5O + H \tag{959}$$

The rate for reaction (959) is obtained from Baulch *et al.* [13].

A further 40 % is consumed via OH radical attack (1321)

$$C_{10}H_8 + OH \quad = \quad C_{10}H_7 + H_2O \tag{1321}$$

with the rate (1321) being modelled on the analogous reaction (960).

$$C_6H_6 + OH \quad = \quad C_6H_5 + H_2O \tag{960}$$

The rate is again adopted from Baulch *et al.* [13].

The $C_{10}H_7$ radical, produced from reactions (1305) and (1321), undergoes O_2 addition (1306) and (1307)

$$C_{10}H_7 + O_2 \quad = \quad C_{10}H_7O + O \tag{1306}$$

$$C_{10}H_7 + O_2 \quad = \quad C_{10}H_7OO \tag{1307}$$

with the former contributing 70 % and the latter 30 %. The rates have been modelled on the analogous reactions (930) and (931).

$$C_6H_5 + O_2 \quad = \quad C_6H_5O + O \tag{930}$$

$$C_6H_5 + O_2 \quad = \quad C_6H_5OO \tag{931}$$

The rate for reaction (930) has been assigned from Frank *et al.* [94] who measured the rate over temperature and pressure ranges of 900 – 1800 K and 1.32 – 2.53 atm. The rate for reaction (931) is based on the work on C_6H_5

reactions with molecular oxygen from Yu & Lin [271] at a temperature and pressure range of 297 – 500 K and 2.63E-02 – 1.1E-01 atm. respectively.

The $C_{10}H_7OO$ radical thermally decomposes via two routes (1369) and (1368) with a 1:1 branching ratio.

$$C_{10}H_7OO = C_{10}H_6O_2 + H \quad (1369)$$

$$C_{10}H_7OO = C_9H_7 + CO_2 \quad (1368)$$

The rate for reaction (1369) has been modelled on the analogous reaction

$$C_6H_5OO = C_6H_4O_2 + H \quad (1007)$$

which has been obtained from the work of DiNaro *et al.* [76]. The reaction has uncertainties in the rate parameters and may be treated as adjustable [76].

The rate adopted for reaction (1368) is modelled directly on the analogous reaction (1006)

$$C_6H_5OO = C_5H_5 + CO_2 \quad (1006)$$

with the rate parameters adopted from DiNaro *et al.* [76]. Additionally, DiNaro *et al.* [76] reports that reaction (1006) is significant for CO_2 production, as also found in this study for the equivalent $C_{10}H_7OO$ reactions. However, there are still uncertainties in the rate parameters for the consumption paths of C_6H_5OO [76].

The C_9H_7 radical formed is consumed by H addition to form C_9H_8 (35 %), and addition/decomposition reactions via HO_2 radical attack (15 %), O radical attack (15 %) and O_2 attack (15 %).

$$C_9H_7 + H = C_9H_8 \quad (1258)$$

$$C_9H_7 + HO_2 = C_9H_7O + OH \quad (1269)$$

$$C_9H_7 + O = C_9H_6O + H \quad (1260)$$

$$C_9H_7 + O_2 = C_6H_5O + C_3H_2O \quad (1263)$$

The rate for reaction (1258), which involves H addition to the C_9H_7 radical to form C_9H_8, has the frequency factor set to 2.0E+11 as reported by Lindstedt *et al.* [169]. The HO_2 attack on the C_9H_7 radical (1269) is modelled on reaction (798).

$$C_5H_5 + HO_2 = C_5H_5O + OH \quad (798)$$

The rate for reaction (798) is obtained from Zhong & Bozzelli [274] who used QRRK analysis at atmospheric pressure over a temperature range of 900 – 1300 K. The rate for reaction (1260) is modelled on the analogous equivalent reaction (789).

$$C_5H_5 + O = C_5H_4O + H \quad (789)$$

The rate for reaction (789) adopted from the work of Zhong & Bozzelli [274].

Indene is recycled back to the C_9H_7 radical via reactions (1276), (1277) and (1278).

$$C_9H_8 + H = C_9H_7 + H_2 \quad (1276)$$

$$C_9H_8 + O = C_9H_7 + OH \quad (1277)$$

$$C_9H_8 + OH = C_9H_7 + H_2O \quad (1278)$$

The H radical contributes 55 %, O radical 15 % and OH attack 30 % to the consumption. The rates for reactions (1276), (1277) and (1278) have been modelled on the analogous reactions for H, O and OH attack on C_5H_6 (812), (814) and (815).

$$C_5H_6 + H = C_5H_5 + H_2 \quad (812)$$
$$C_5H_6 + O = C_5H_5 + OH \quad (814)$$
$$C_5H_6 + OH = C_5H_5 + H_2O \quad (815)$$

The rates for the above reactions have been obtained from Zhong & Bozzelli [274].

The C_9H_7O radical produced from reaction (1269) thermally decomposes (100 %) via reaction (1301) leading to ring opening.

$$C_9H_7O = C_8H_7 + CO \quad (1301)$$

The rate used is consistent with the study on 1 – methylnaphthalene oxidation by Pitsch [203].

The C_8H_7 radical produced from reaction (1301) thermally decomposes (100 %) via C – H cleavage (1170).

$$C_8H_7 = C_8H_6 + H \quad (1170)$$

The C_9H_6O, formed from reaction (1260), decomposes (100 %) via reaction (1297) which also provides a phenylacetylene formation channel.

$$C_9H_6O = C_8H_6 + CO \quad (1297)$$

The $C_{10}H_6O_2$ adduct (1369) further thermally decomposes or undergoes H radical attack with reactions (1363) and (1364) contributing approximately 60 % and 40 % respectively.

$$C_{10}H_6O_2 = C_9H_6O + CO \quad (1363)$$
$$C_{10}H_6O_2 + H = C_9H_7O + CO \quad (1364)$$

The rate for reaction (1363) is modelled directly on reaction (995) with the rate parameters being adopted from Frank *et al.* [94].

$$C_6H_4O_2 \quad = \quad C_5H_4O + CO \tag{995}$$

The other major consumption route involves H attack on $C_{10}H_6O_2$ (1364) and is modelled on reaction (996). The rate for this reaction has been adopted from Alzueta *et al.* [3].

$$C_6H_4O_2 + H \quad = \quad C_5H_5O + CO \tag{996}$$

The $C_{10}H_7O$ radical, formed with reactions (1320) and (1306), thermally decomposes via reaction (1365).

$$C_{10}H_7O \quad = \quad C_9H_7 + CO \tag{1365}$$

The rate for reaction (1365) is modelled on reaction (1001) which has been adopted from Lin & Lin [164] who measured the rate under Shock Tube conditions over a temperature and pressure range of 1000 – 1500 K and 4.05E+04 – 9.12E+04 Pa respectively.

$$C_6H_5O \quad = \quad C_5H_5 + CO \tag{1001}$$

The consumption of C_8H_6 and its intermediates have been discussed in Chapter 3.

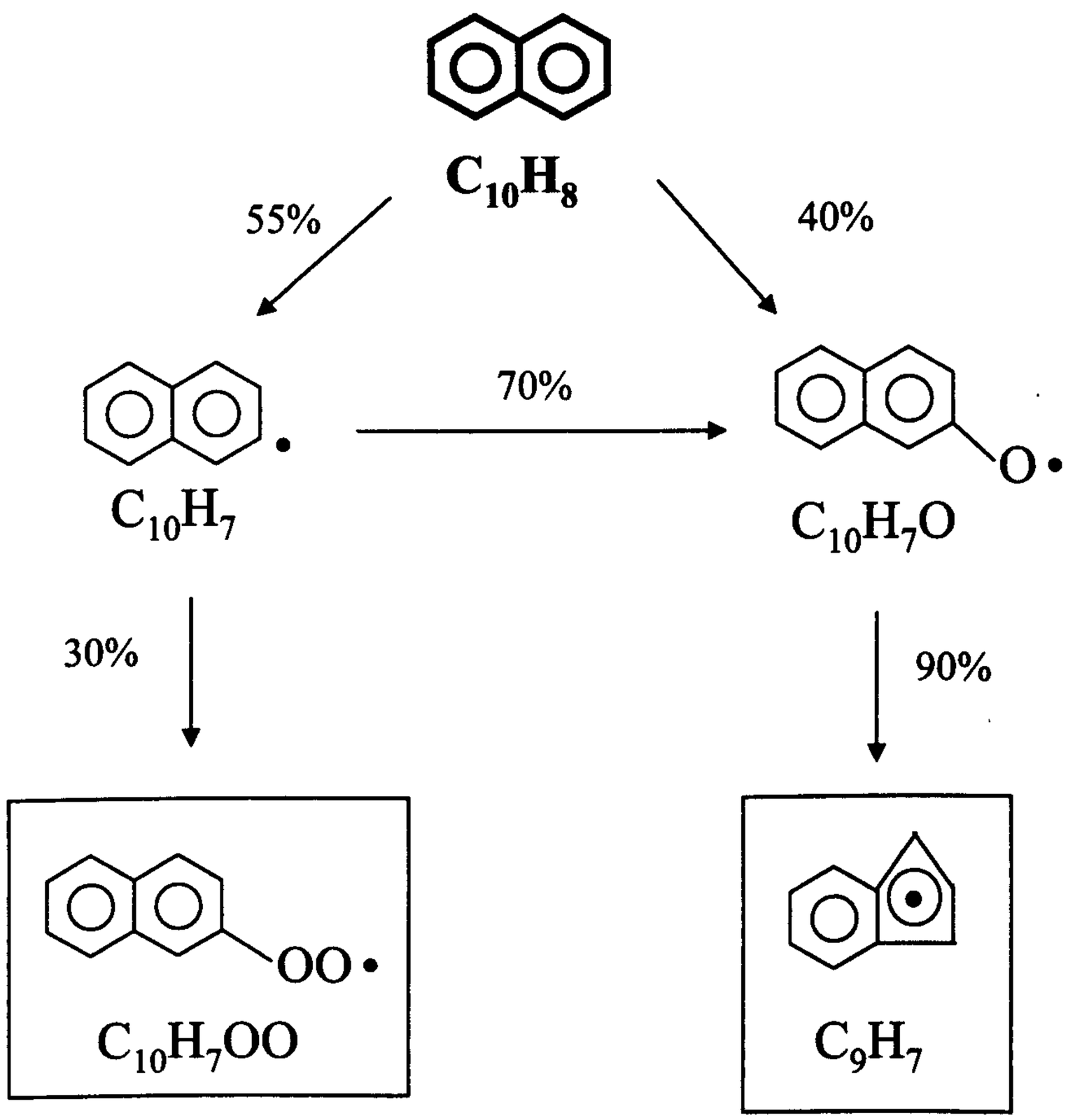


Figure 4.6: Diagram illustrating the consumption paths of the fuel naphthalene and its intermediate species in a Turbulent Flow Reactor at a reaction time of 75 ms. Species in boxes are considered in subsequent pages.

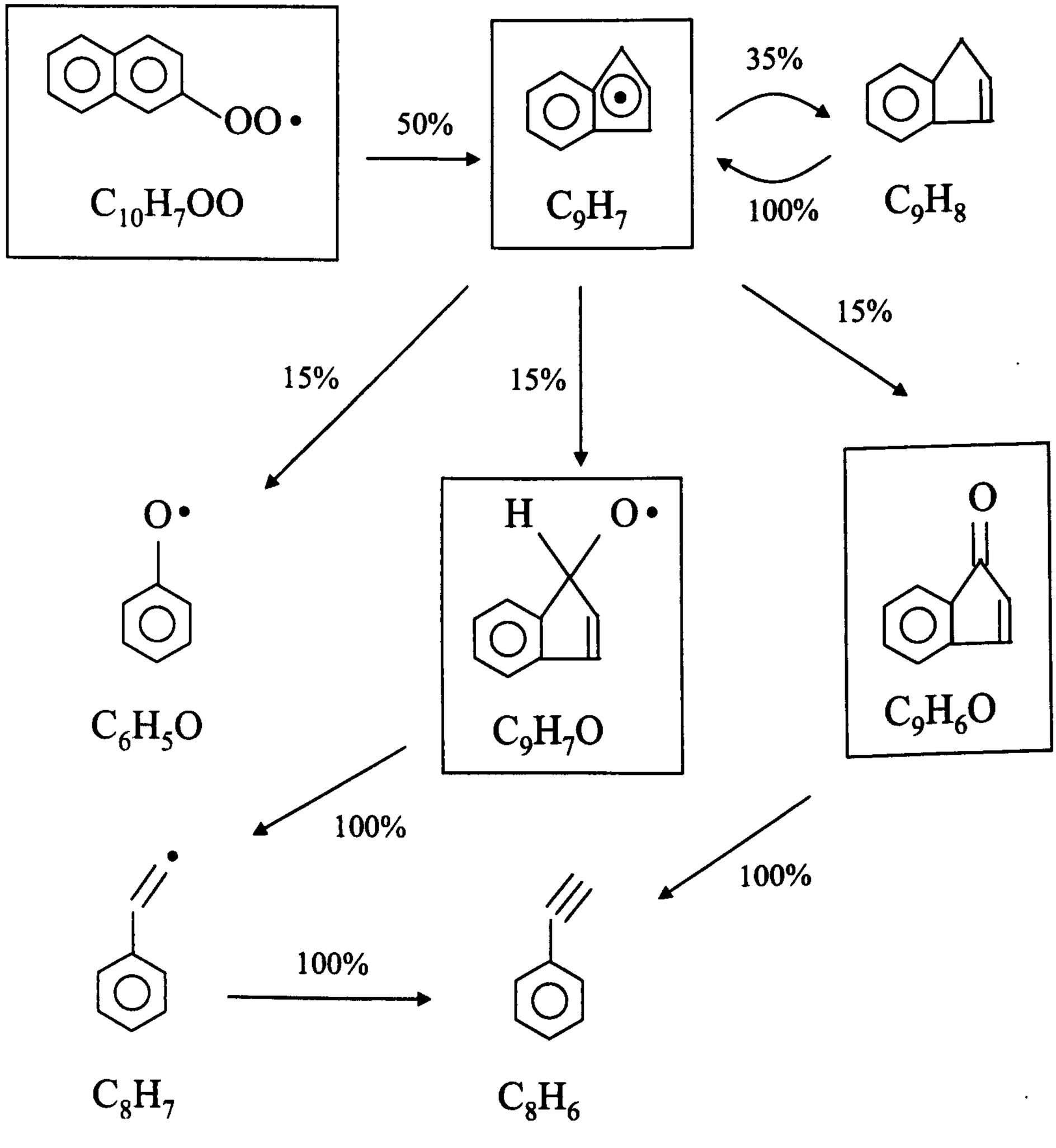


Figure 4.7: Diagram illustrating the consumption paths of the fuel naphthalene and its intermediate species in a Turbulent Flow Reactor at a reaction time of 75 ms. Species in boxes are considered in subsequent pages.

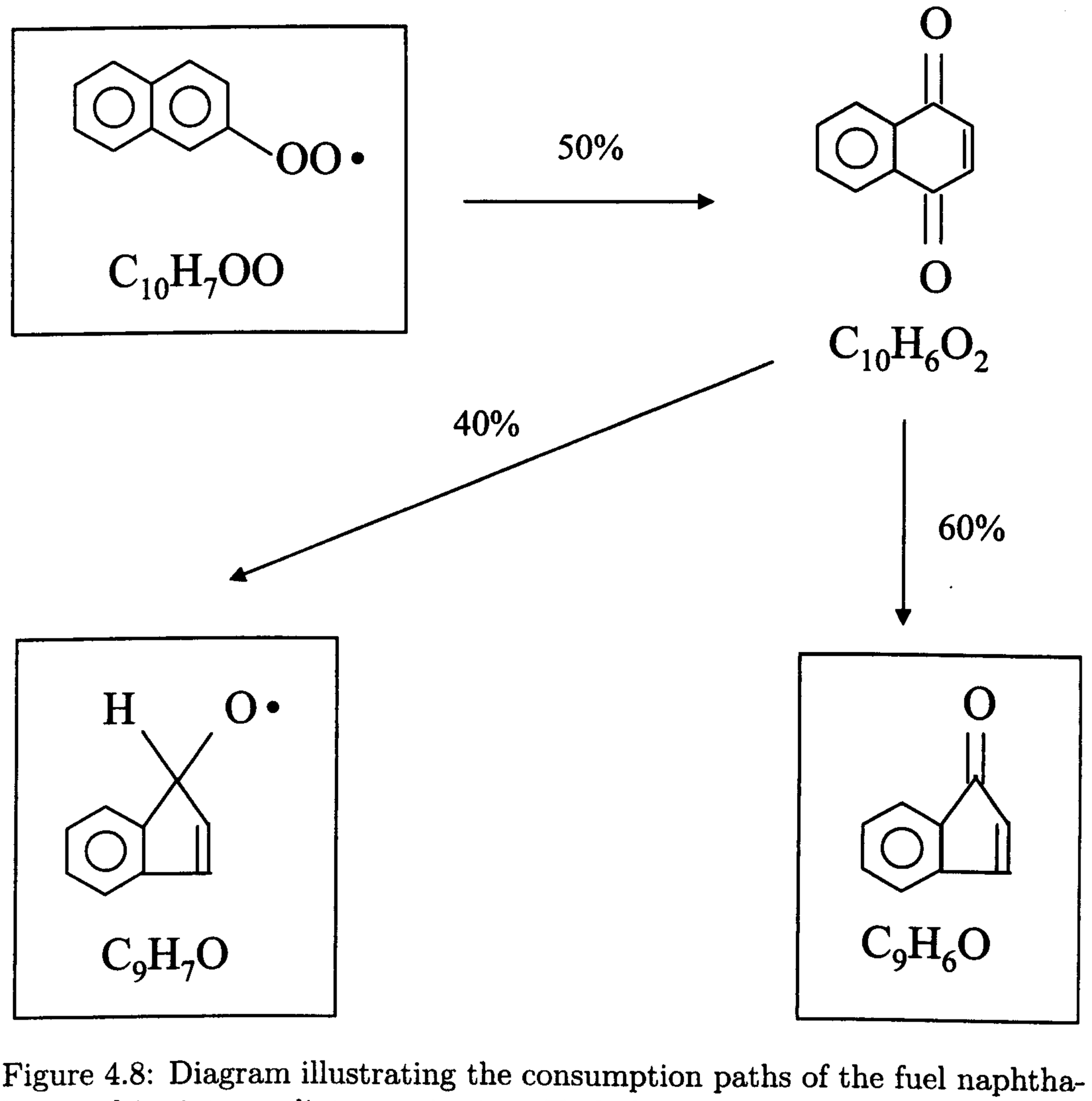


Figure 4.8: Diagram illustrating the consumption paths of the fuel naphthalene and its intermediate species in a Turbulent Flow Reactor at a reaction time of 75 ms. Species in boxes are considered in subsequent pages.

4.3 The Oxidation of 1 – Methylnaphthalene

The detailed chemical kinetic mechanism for the oxidation of 1 – methylnaphthalene developed here is fundamentally based on the analogous oxidation of toluene. Shaddix *et al.* [227] noted the structural, as well as the thermochemical, similarities of the major intermediates with respect to those previously observed for toluene [228]. To date, the only detailed chemical kinetic modelling study for 1 – methylnaphthalene found in the literature is from Pitsch [203] who based his work on experimental data from Shaddix *et al.* [227] for a stoichiometry of $\phi = 0.58$. The detailed chemical mechanism from Pitsch [203] only features consumption via decomposition/radical attack on the methyl group of 1 – methylnaphthalene. Shaddix *et al.* [227] proposed a conceptual reaction mechanism for the oxidation of 1 – methylnaphthalene at a temperature approximately of 1170 K based upon data obtained from the Princeton Flow Reactor.

The oxidation of 1 – methylnaphthalene has also been investigated by Pfahl *et al.* [202] under Shock Tube conditions for stoichiometric 1 – methylnaphthalene – air mixtures over a temperature range of 940 – 1300 K and at a pressure of 13 atm. Pfahl *et al.* [202] comment that over the entire temperature range investigated, the self ignition process begins with a deflagration. Furthermore, Pfahl *et al.* [202] report that the deflagrative inhomogeneous self ignition appears to originate from hot spots or foreign particles present in the test mixture. The deflagration leads to a significant pressure and temperature rise within the unburned gas and a shortening of the ignition delay time. Despite the obvious uncertainties in the data, Pitsch [203] developed a detailed chemical kinetic mechanism which was validated against the experimental data from Pfahl *et al.* [202].

4.3.1 The Oxidation of 1 – methylnaphthalene

The data sets used to validate and verify the 1 – methylnaphthalene sub – mechanism under JSR condition were obtained by Dagaut [55]. The data utilised here consists of three cases, with $\phi = 0.5$, 1.0 and 1.5 over an overall temperature range of 1090 – 1440 K for a mean residence time of $\tau = 100$ ms and a pressure of 1 atm. Table 4.1 summarizes the initial conditions.

Table 4.1: Summary of the Initial Conditions for the Oxidation of 1 – methylnaphthalene in a Jet Stirred Reactor

Fuel	ϕ	T_0 [K]	Mean Residence Time [ms]	Pressure [atm.]
$C_{11}H_{10}$	0.5	1090 – 1290	100	1.0
$C_{11}H_{10}$	1.0	1090 – 1380	100	1.0
$C_{11}H_{10}$	1.5	1140 – 1440	100	1.0

The results of the calculations compared to the experimental data from Dagaut [55] are encouraging as illustrated in Figures 4.9 – 4.20. For example, the general trend of O_2 consumption increasing with temperature is captured, along with the corresponding species having orders of magnitude 1000 ppm, 100 ppm, 10 ppm and 1.0 ppm.

The calculations for the stoichiometric case shows a rapid drop in the molecular oxygen concentration profile for temperatures greater than 1280 K as is evident in Figure 4.13. The sharp drop in molecular oxygen corresponds to a rapid rise in CO_2 concentration as is evident in Figure 4.13. It can therefore be proposed that ignition may have occurred for temperatures greater than 1280 K. Figure 4.21 illustrates a graph of initial temperature against final temperature and reveals that ignition does occur for temperatures greater than 1280 K.

The fuel decay curve for the lean case ($\phi = 0.5$) is perhaps too rapid with respect to the experimental data from Dagaut [55] as is evident in Figure 4.9. This leads to the over prediction of species concentrations high up the chain such as $C_{11}H_8O$, $C_{10}H_8$ and C_9H_8 as illustrated in Figure 4.12. It is found that reaction (1401)

$$C_{11}H_{10} + OH \quad = \quad C_{11}H_9 + H_2O \tag{1401}$$

is the most significant fuel consumption reaction at 1170 K. The rate for reaction (1401) has been modelled on the analogous reaction (1086) with the frequency factor adjusted for molecular size differences.

$$C_7H_8 + OH \quad = \quad C_7H_7 + H_2O \tag{1086}$$

In all cases, the concentrations of $C_{11}H_8O$ are over predicted as is evident in Figures 4.12, 4.16 and 4.20. It is found that reaction (1427), featuring the thermal decomposition of $C_{11}H_9O$ via C – H cleavage, is the primary channel ($\sim$ 80 %).

$$C_{11}H_9O \quad = \quad C_{11}H_8O + H \tag{1427}$$

The rate for reaction (1427) has been modelled on the analogous reaction (1113).

$$C_7H_7O \quad = \quad C_7H_6O + H \tag{1113}$$

By contrast, in the detailed kinetic modelling study by Pitsch [203] it is found that reaction (1378) is the primary route to $C_{11}H_8O$.

$$C_{11}H_9 + O \quad = \quad C_{11}H_8O + H \tag{1378}$$

The rate adopted for reaction (1378) is modelled on the analogous reaction (1052).

$$C_7H_7 + O \quad = \quad C_7H_6O + H \tag{1052}$$

The rate for reaction (1052) is adopted from Hippler *et al.* [126] as reported by Lindstedt & Maurice [168]. Hippler *et al.* [126] studied the oxidation of C_7H_7 radicals over a temperature range of 1200 – 1500 K. The detailed chemical kinetic mechanism proposed by Pitsch [203] features rate parameters proposed by Emdee *et al.* [89] to fit the data. The rate proposed is ~ 5 times faster than that determined by Hippler *et al.* [126].

The calculations for the $C_{10}H_8$ concentration profiles show better agreement with increasing stoichiometry as is evident in Figures 4.12, 4.16 and 4.20. It is found that for the lean case ($\phi = 0.5$) the dominant channel is via reaction (1425) featuring the thermal decomposition of $C_{11}H_9O$ via C – C cleavage.

$$C_{11}H_9O \quad = \quad C_{10}H_8 + CHO \tag{1425}$$

The rate assigned to reaction (1425) is modelled directly on the analogous equivalent as in reaction (1111).

$$C_7H_7O \quad = \quad C_6H_6 + CHO \tag{1111}$$

For the stoichiometric and rich ($\phi = 1.5$) cases the primary source (~ 35 %) for $C_{10}H_8$ formation is via reaction (1332) featuring hydrogen assisted isomerisation.

$$C_9H_6CH_2 + H \quad = \quad C_{10}H_8 + H \tag{1332}$$

The rate of Laskin & Lifshitz [157], who studied the thermal decomposition of C_9H_8 under Shock Tube conditions over a temperature range of 1150 – 1900 K has been assigned. Reaction step (1332) may be compared with reaction (985) which considers the formation of benzene from fulvene.

$$C_6H_6(F) + H \quad = \quad C_6H_6 + H \tag{985}$$

The concentration profiles for C_9H_8 are reproduced well for all cases as is evident in Figures 4.12, 4.16 and 4.20. It is found that reaction (1258)

$$C_9H_7 + H \quad = \quad C_9H_8 \tag{1258}$$

is the dominant channel (95 %) leading to C_9H_8 in all cases. The rate for reaction (1258) has been assigned a frequency factor of 2.0E+11 as reported by Lindstedt *et al.* [169].

The species concentration profiles for C_8H_6 are over predicted for all cases as is evident in Figures 4.11, 4.15 and 4.19. It is found that the most significant routes leading to C_8H_6 are reactions (1170) and (1297).

$$C_8H_7 \quad = \quad C_8H_6 + H \tag{1170}$$

$$C_9H_6O \quad = \quad C_8H_6 + CO \tag{1297}$$

The branching ratio is approximately 1:1 in the stoichiometric case at 1190 K. The rate for reaction (1170) has been adopted from Wang & Frenklach [256]. The rate for reaction (1297) has been modelled on the analogous reaction (1001).

$$C_6H_5O \quad = \quad C_5H_5 + CO \tag{1001}$$

The uncertainties involved in the rate parameters for the thermal decomposition of C_9H_6O is a key issue in the over prediction of the concentrations for C_8H_6.

The aromatics C_7H_8, C_6H_6 and C_5H_6 are comparatively well reproduced as is evident in Figures 4.11, 4.15 and 4.19.

The calculations for C_7H_8 for the lean ($\phi = 0.5$) and rich ($\phi = 1.5$) are, however, poor at higher temperatures. It is found that reactions (1079) and

(1083) are the dominant C_7H_8 consumption channels for the lean case at 1220 K. For the rich case at 1390 K reaction (1086) is the dominant reaction in consuming C_7H_8. The reactions are well established and it is likely that the dominant uncertainties can be found in the formation channels.

$$C_7H_8 + H = C_7H_7 + H_2 \quad (1079)$$
$$C_7H_8 + O = OC_7H_7 + H \quad (1083)$$
$$C_7H_8 + OH = C_7H_7 + H_2O \quad (1086)$$

The concentrations of some smaller species (C_2H_4, C_2H_2, and CH_2O) are all well reproduced as is evident in Figures 4.10, 4.14 and 4.18. However, levels of CH_4 are under predicted for the stoichiometric and rich cases as is evident in Figure 4.14 and 4.18. It is found that the most significant reactions for the production of CH_4 are

$$C_{11}H_{10} + CH_3 = C_{11}H_9 + CH_4 \quad (1410)$$
$$C_{11}H_{10} + CH_3 = C_{11}H_9P + CH_4 \quad (1410b)$$

contributing 60 % and 20 % respectively. The rate adopted for reactions (1410) and (1410b) are modelled directly on the toluene analogous equivalent as in reactions

$$C_7H_8 + CH_3 = CH_4 + C_7H_7 \quad (1094)$$
$$C_7H_8 + CH_3 = C_7H_7P + CH_4 \quad (1095)$$

with the rate parameters being discussed in Chapter 2.

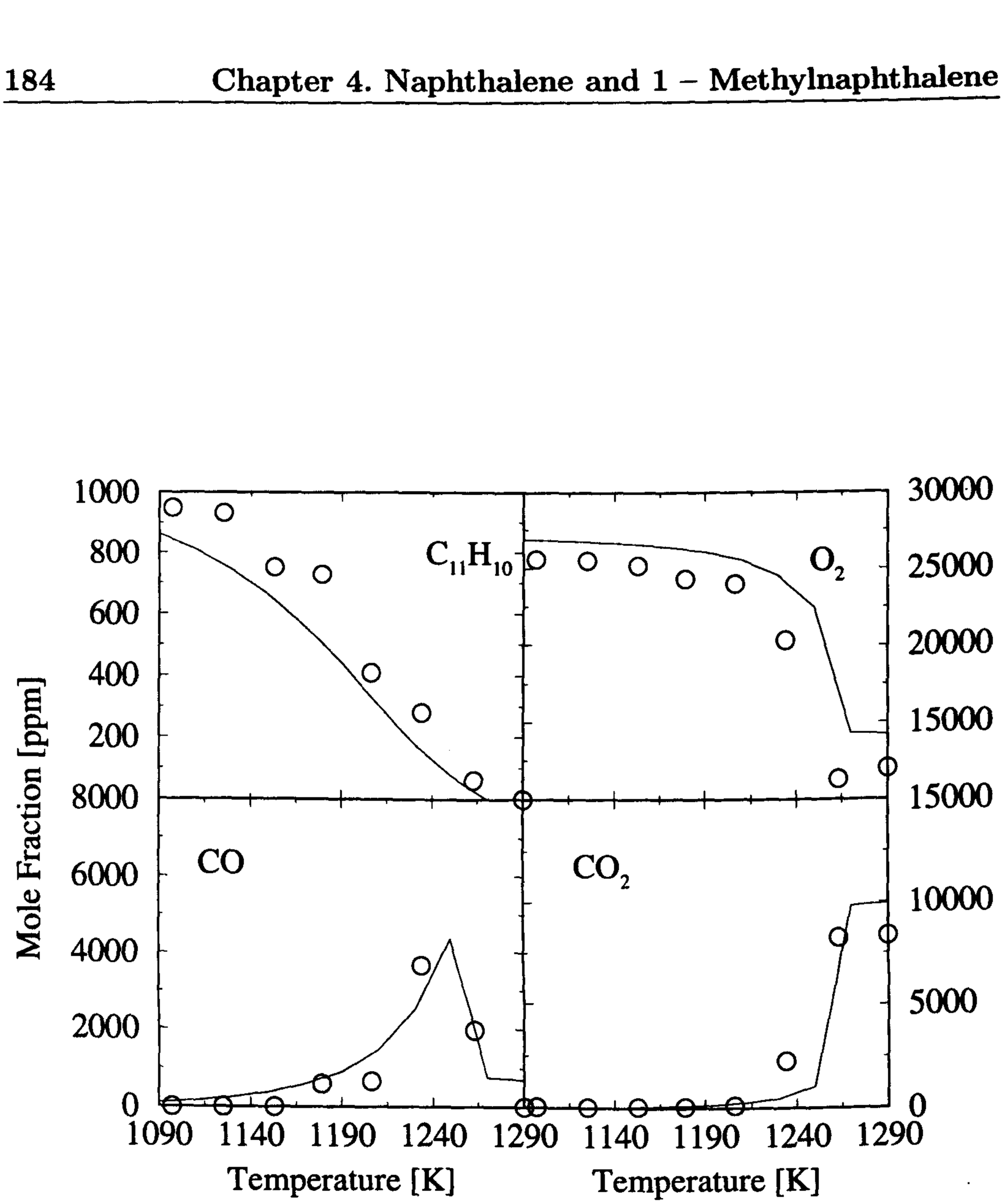


Figure 4.9: Graph of species profile concentrations versus temperature for the oxidation of 1 – methylnaphthalene in a Jet Stirred Reactor. Experimental points are from Dagaut [55] for a stoichiometry of $\phi = 0.5$. Solid lines are the computations from the detailed chemical mechanism.

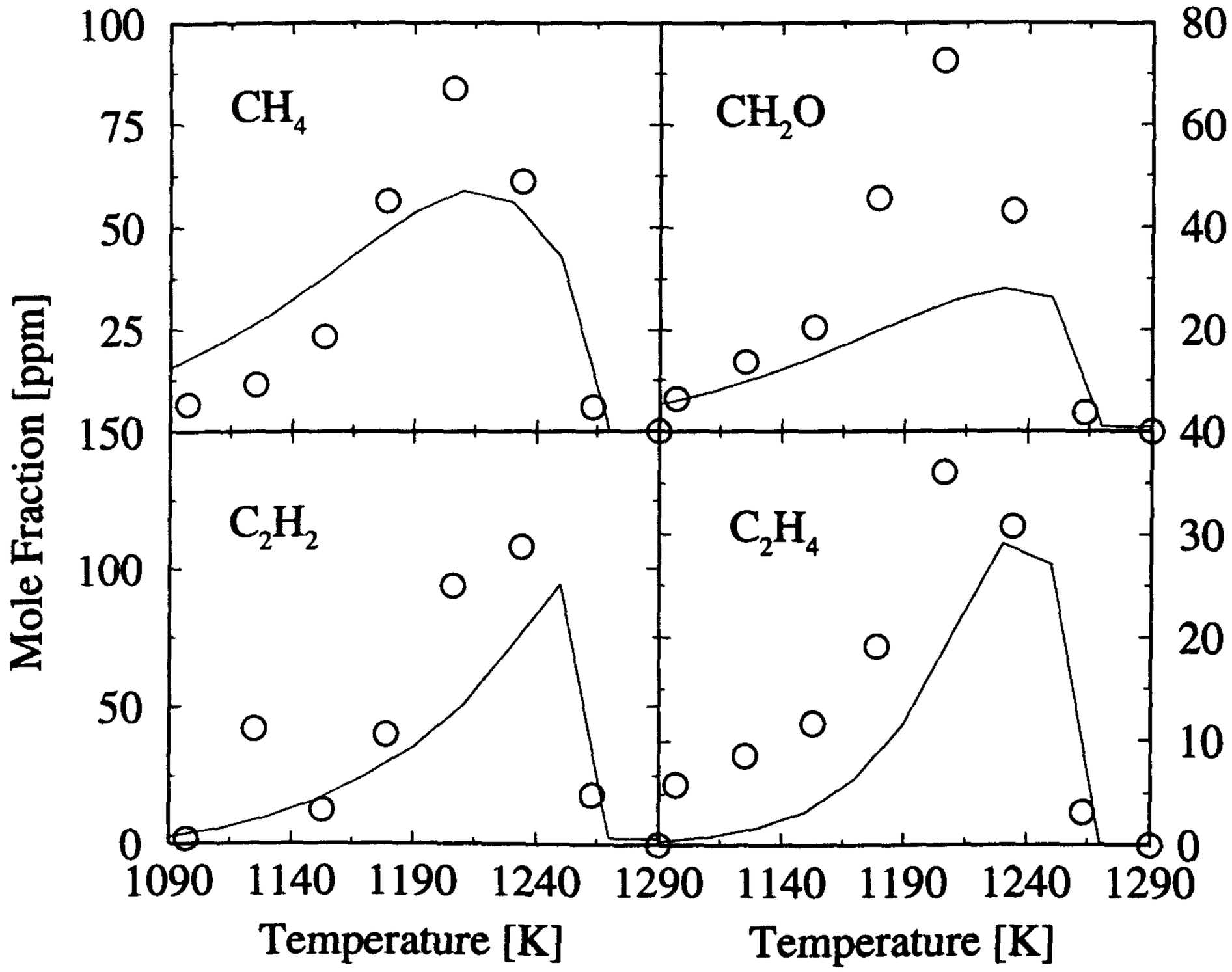


Figure 4.10: Graph of species profile concentrations versus temperature for the oxidation of 1 – methylnaphthalene in a Jet Stirred Reactor. Experimental points are from Dagaut [55] for a stoichiometry of $\phi = 0.5$. Solid lines are the computations from the detailed chemical mechanism.

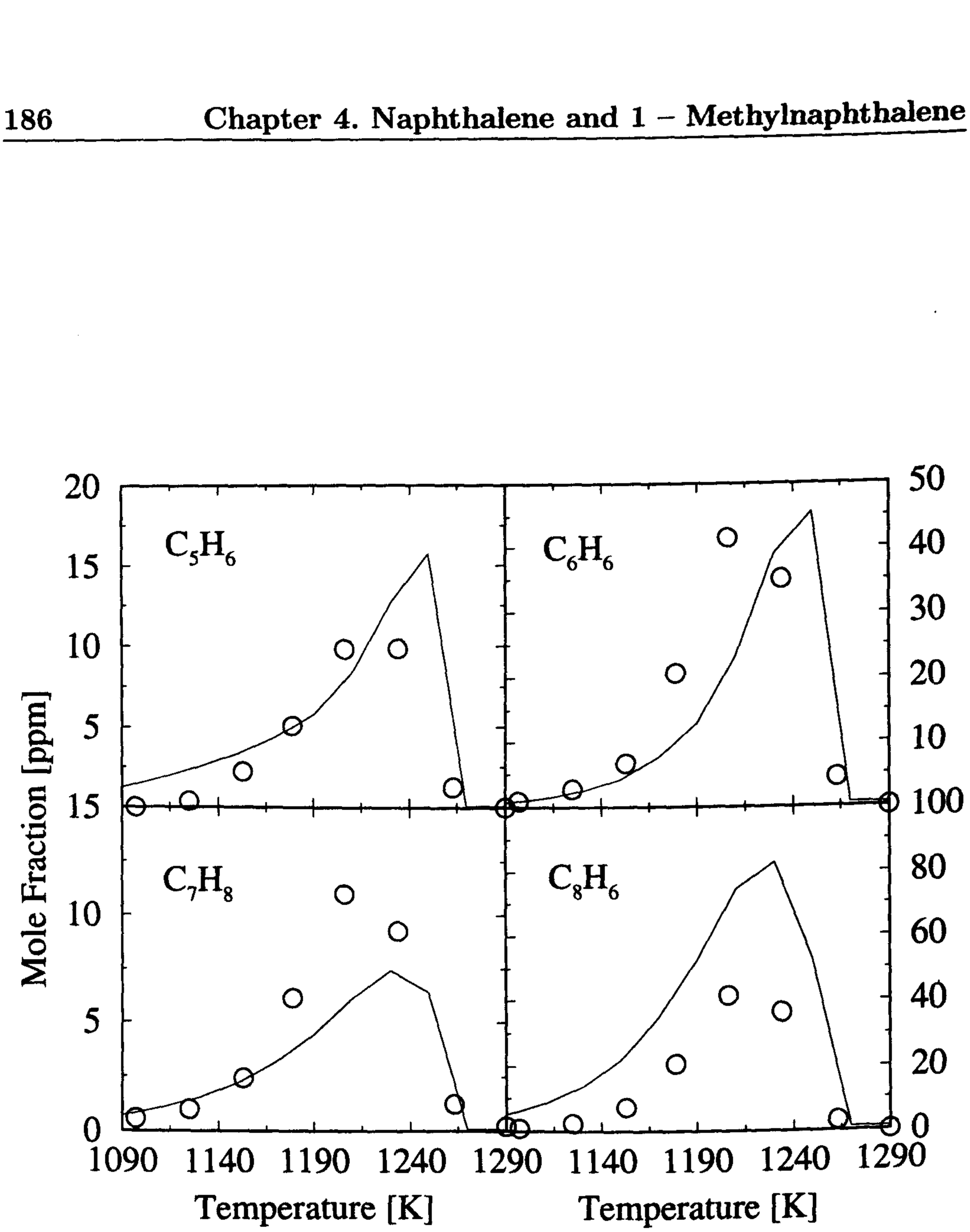


Figure 4.11: Graph of species profile concentrations versus temperature for the oxidation of 1 – methylnaphthalene in a Jet Stirred Reactor. Experimental points are from Dagaut [55] for a stoichiometry of $\phi = 0.5$. Solid lines are the computations from the detailed chemical mechanism.

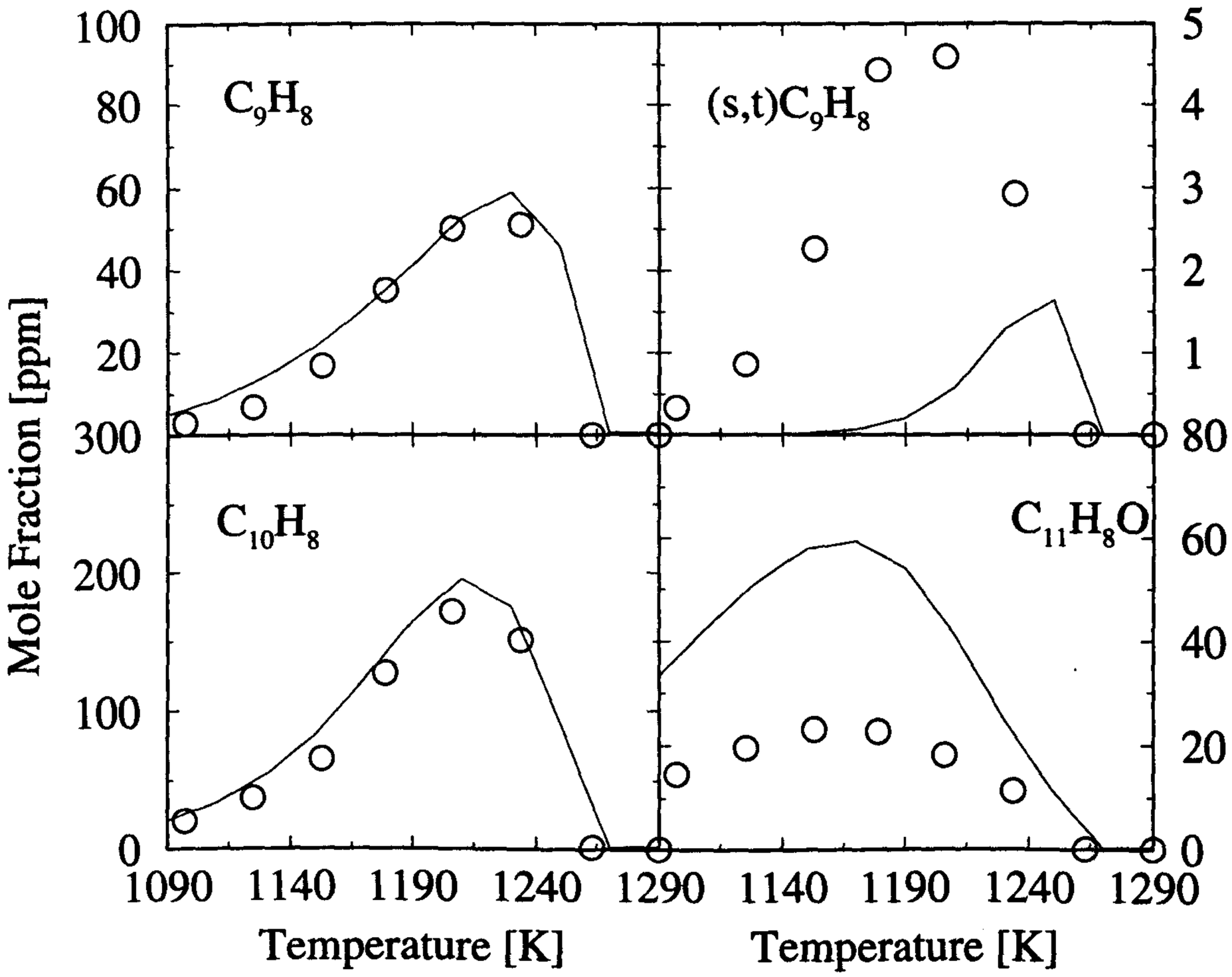


Figure 4.12: Graph of species profile concentrations versus temperature for the oxidation of 1 – methylnaphthalene in a Jet Stirred Reactor. Experimental points are from Dagaut [55] for a stoichiometry of $\phi = 0.5$. Solid lines are the computations from the detailed chemical mechanism.

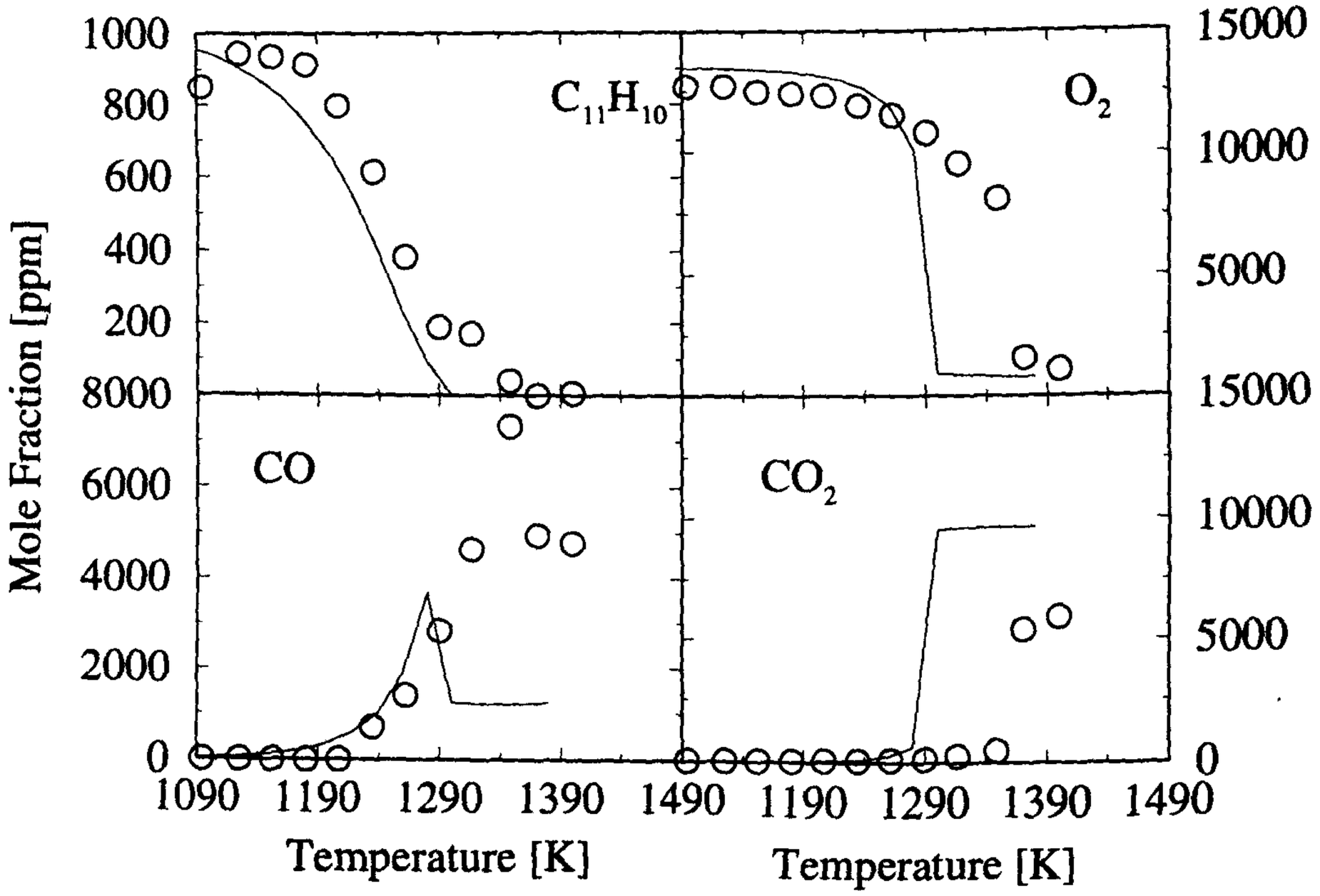


Figure 4.13: Graph of species profile concentrations versus temperature for the oxidation of 1 – methylnaphthalene in a Jet Stirred Reactor. Experimental points are from Dagaut [55] for a stoichiometry of $\phi = 1.0$. Solid lines are the computations from the detailed chemical mechanism.

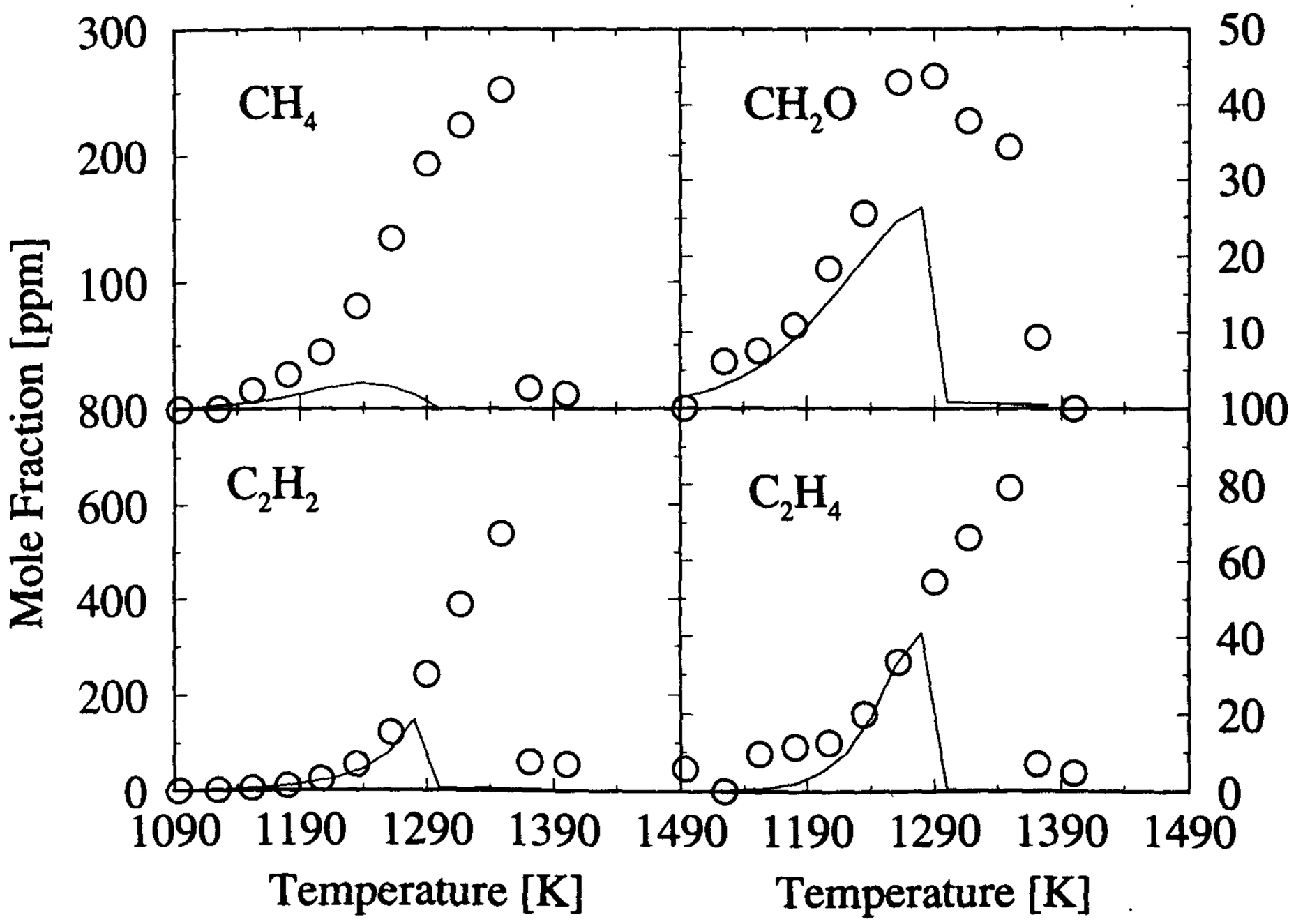


Figure 4.14: Graph of species profile concentrations versus temperature for the oxidation of 1 – methylnaphthalene in a Jet Stirred Reactor. Experimental points are from Dagaut [55] for a stoichiometry of $\phi = 1.0$. Solid lines are the computations from the detailed chemical mechanism.

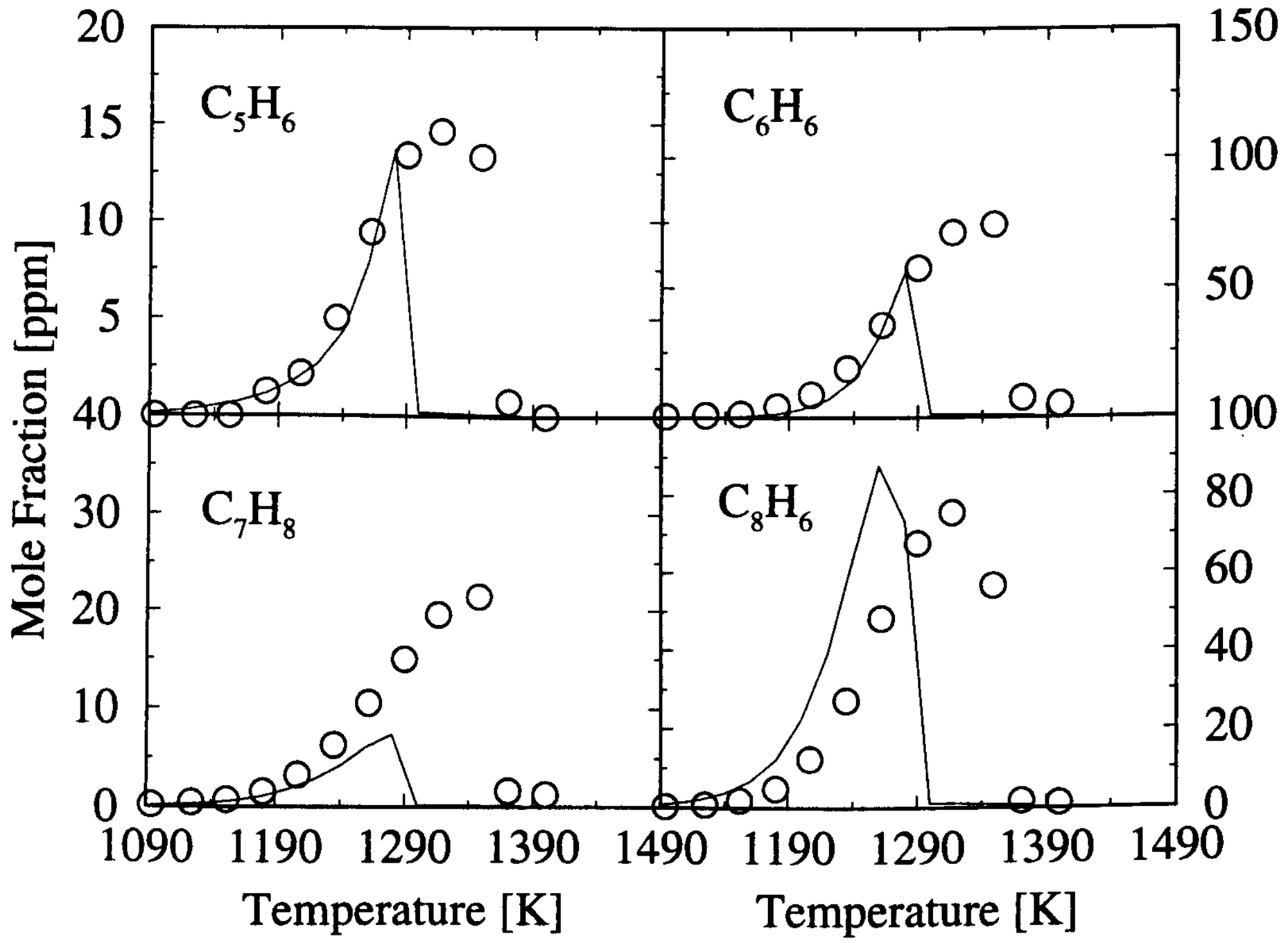


Figure 4.15: Graph of species profile concentrations versus temperature for the oxidation of 1 – methylnaphthalene in a Jet Stirred Reactor. Experimental points are from Dagaut [55] for a stoichiometry of $\phi = 1.0$. Solid lines are the computations from the detailed chemical mechanism.

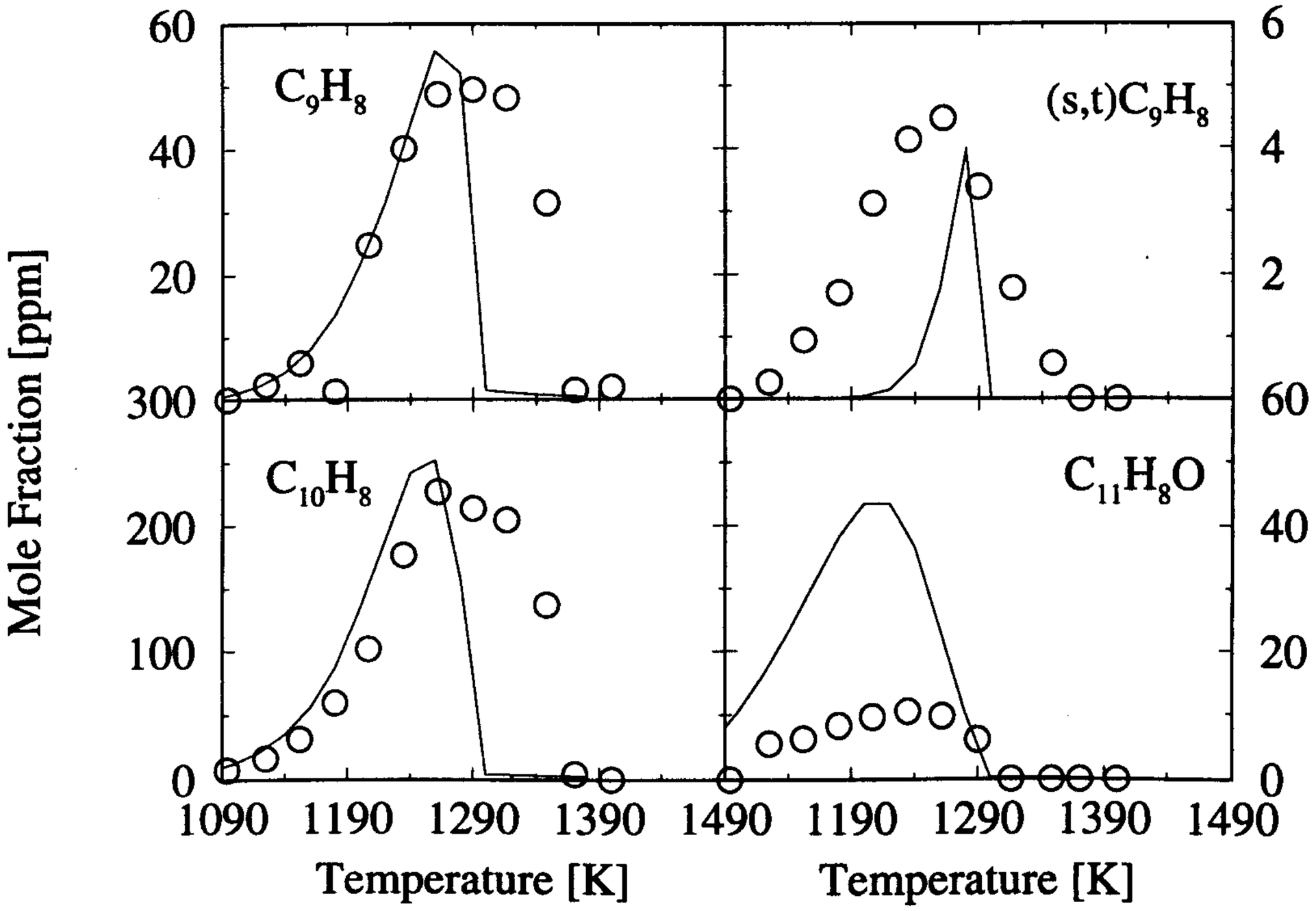


Figure 4.16: Graph of species profile concentrations versus temperature for the oxidation of 1 – methylnaphthalene in a Jet Stirred Reactor. Experimental points are from Dagaut [55] for a stoichiometry of $\phi = 1.0$. Solid lines are the computations from the detailed chemical mechanism.

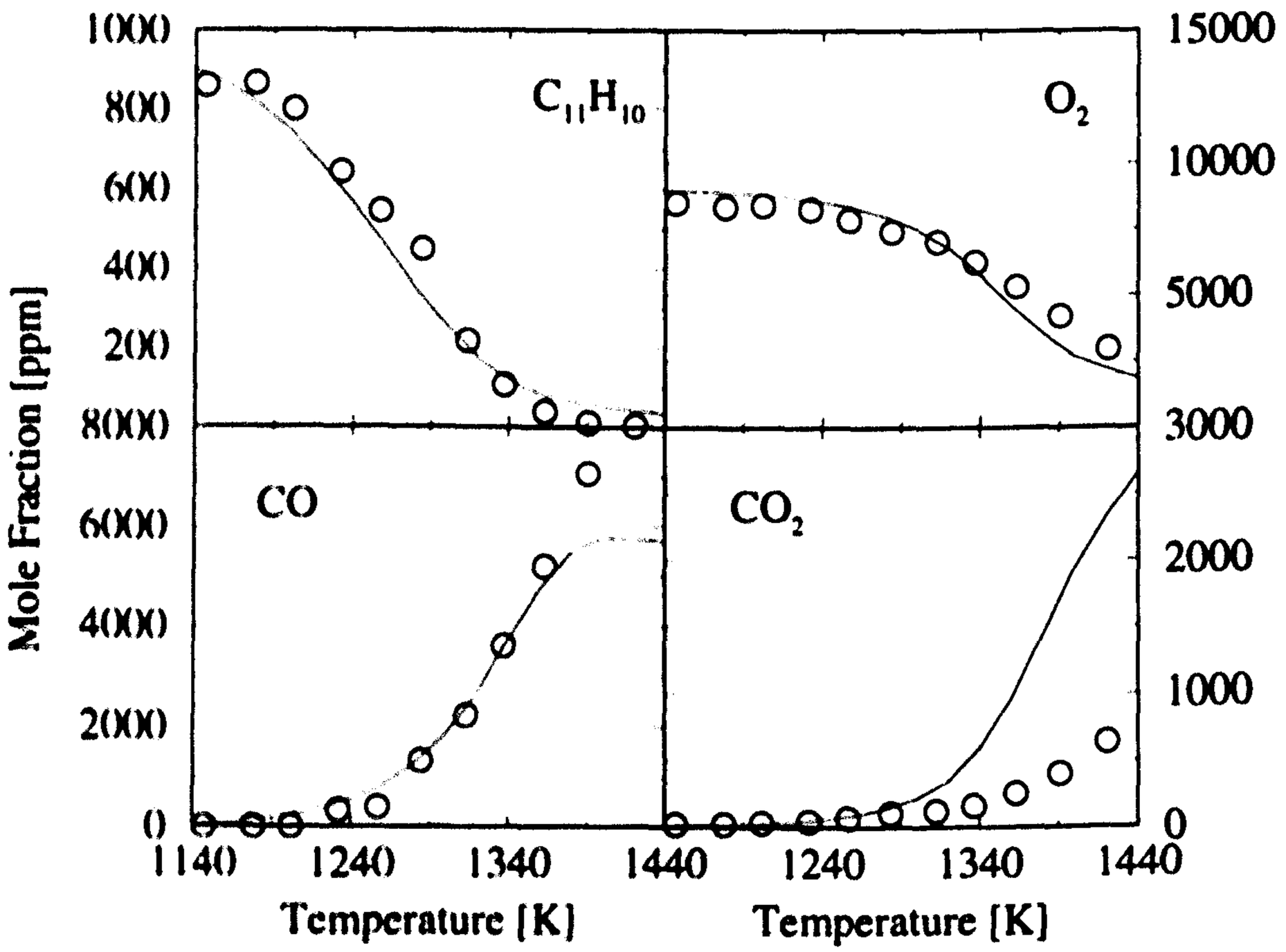


Figure 4.17: Graph of species profile concentrations versus temperature for the oxidation of 1 – methylnaphthalene in a Jet Stirred Reactor. Experimental points are from Dagaut [55] for a stoichiometry of $\phi = 1.5$. Solid lines are the computations from the detailed chemical mechanism.

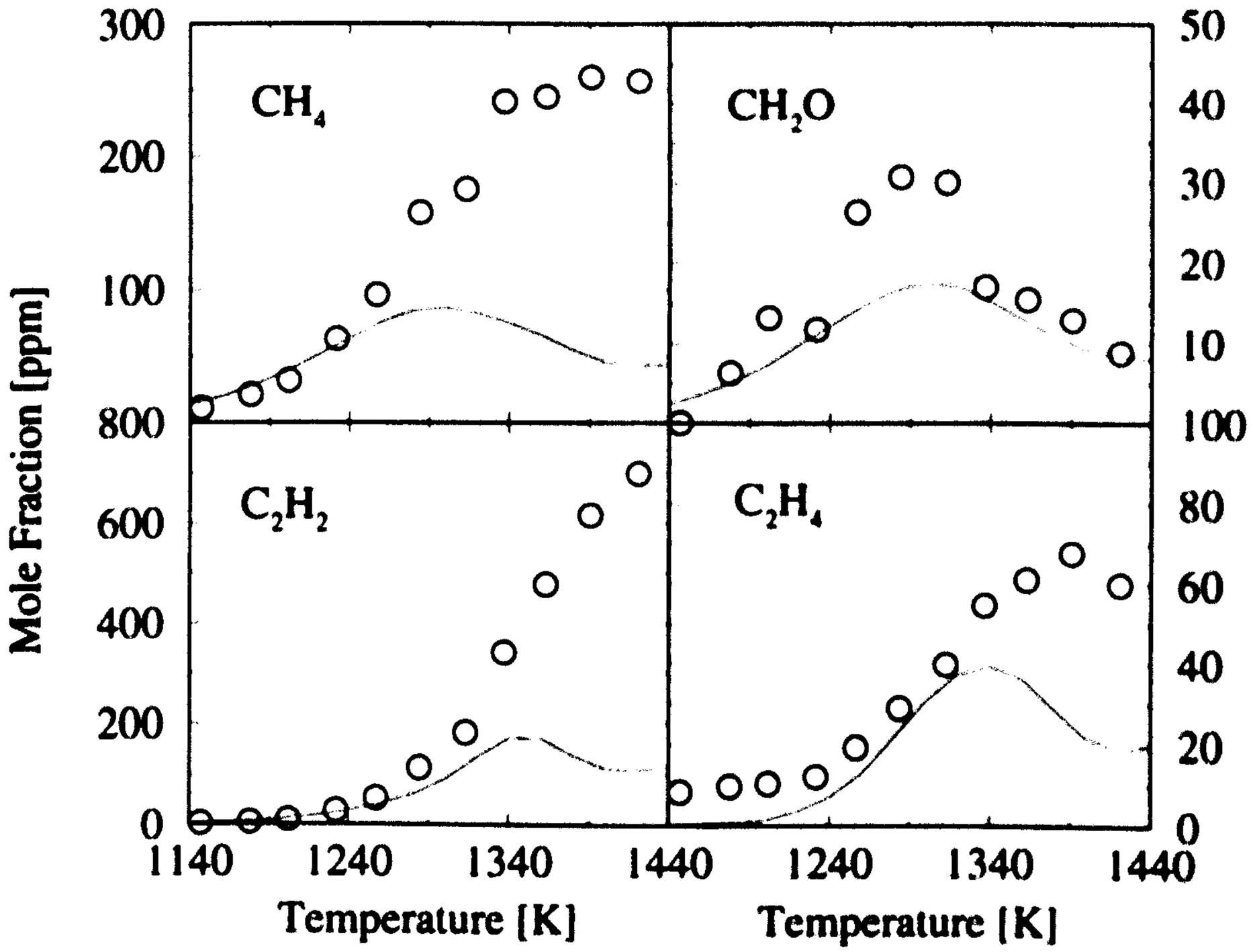


Figure 4.18: Graph of species profile concentrations versus temperature for the oxidation of 1 – methylnaphthalene in a Jet Stirred Reactor. Experimental points are from Dagaut [55] for a stoichiometry of $\phi = 1.5$. Solid lines are the computations from the detailed chemical mechanism.

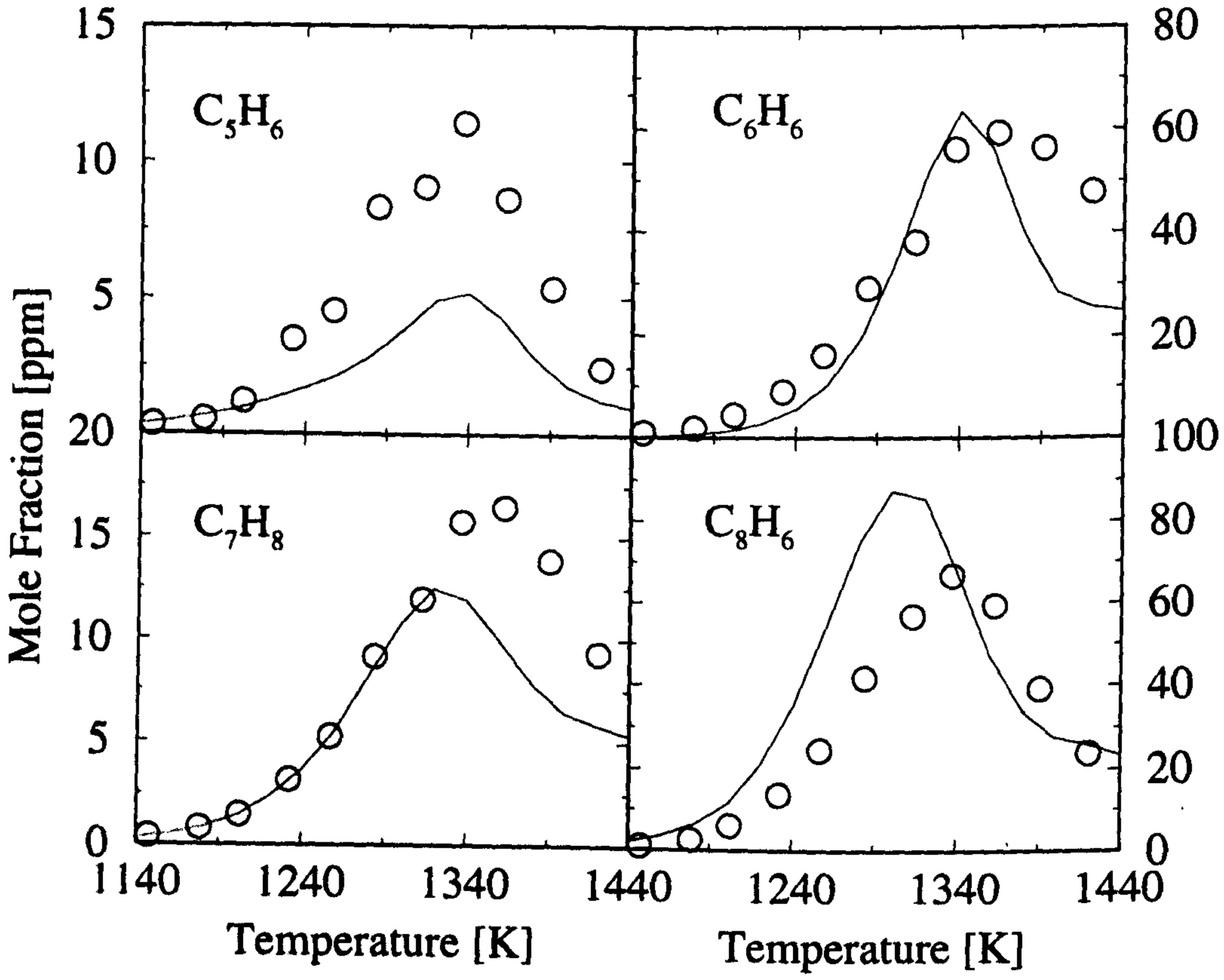


Figure 4.19: Graph of species profile concentrations versus temperature for the oxidation of 1 – methylnaphthalene in a Jet Stirred Reactor. Experimental points are from Dagaut [55] for a stoichiometry of $\phi = 1.5$. Solid lines are the computations from the detailed chemical mechanism.

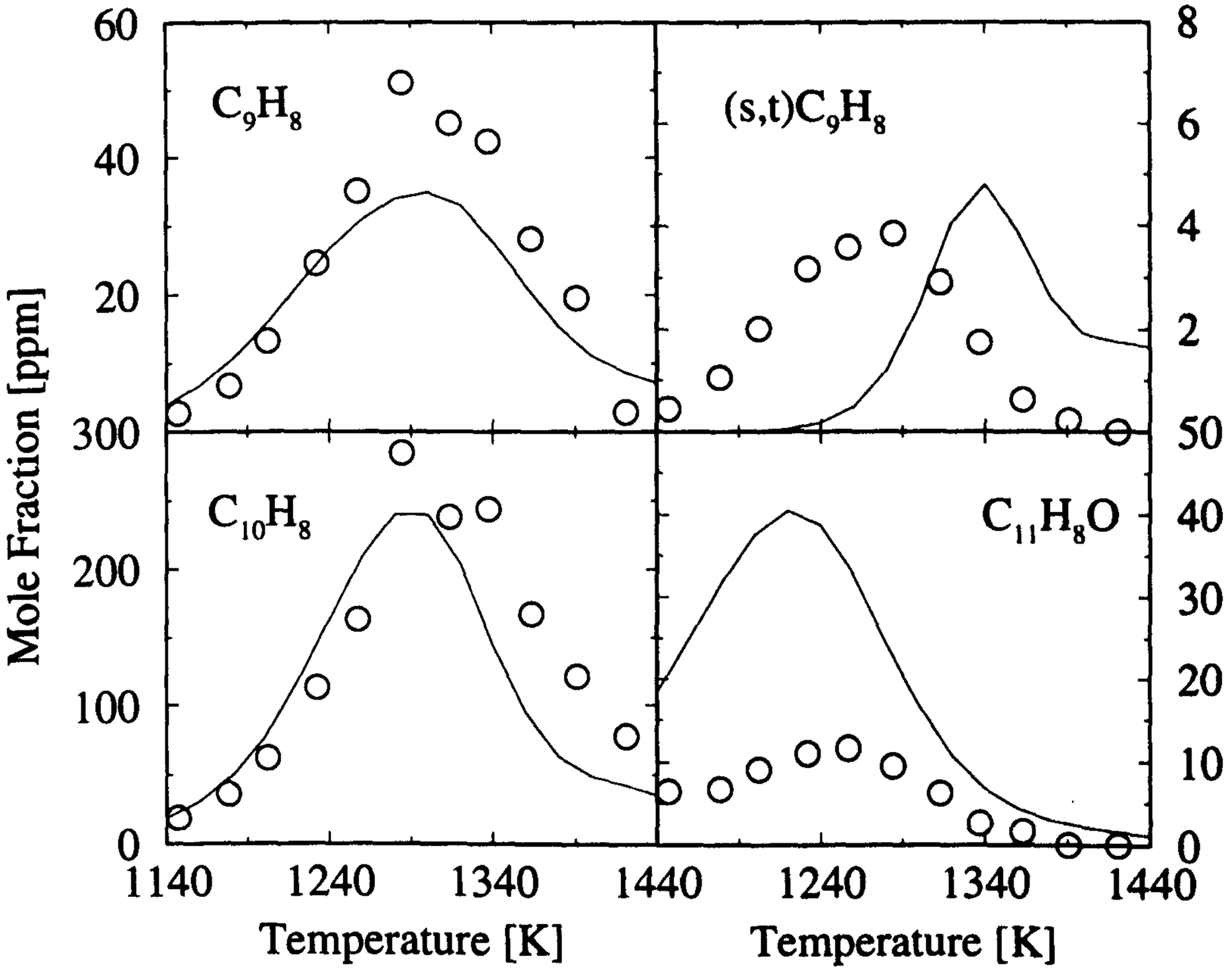


Figure 4.20: Graph of species profile concentrations versus temperature for the oxidation of 1 – methylnaphthalene in a Jet Stirred Reactor. Experimental points are from Dagaut [55] for a stoichiometry of $\phi = 1.5$. Solid lines are the computations from the detailed chemical mechanism.

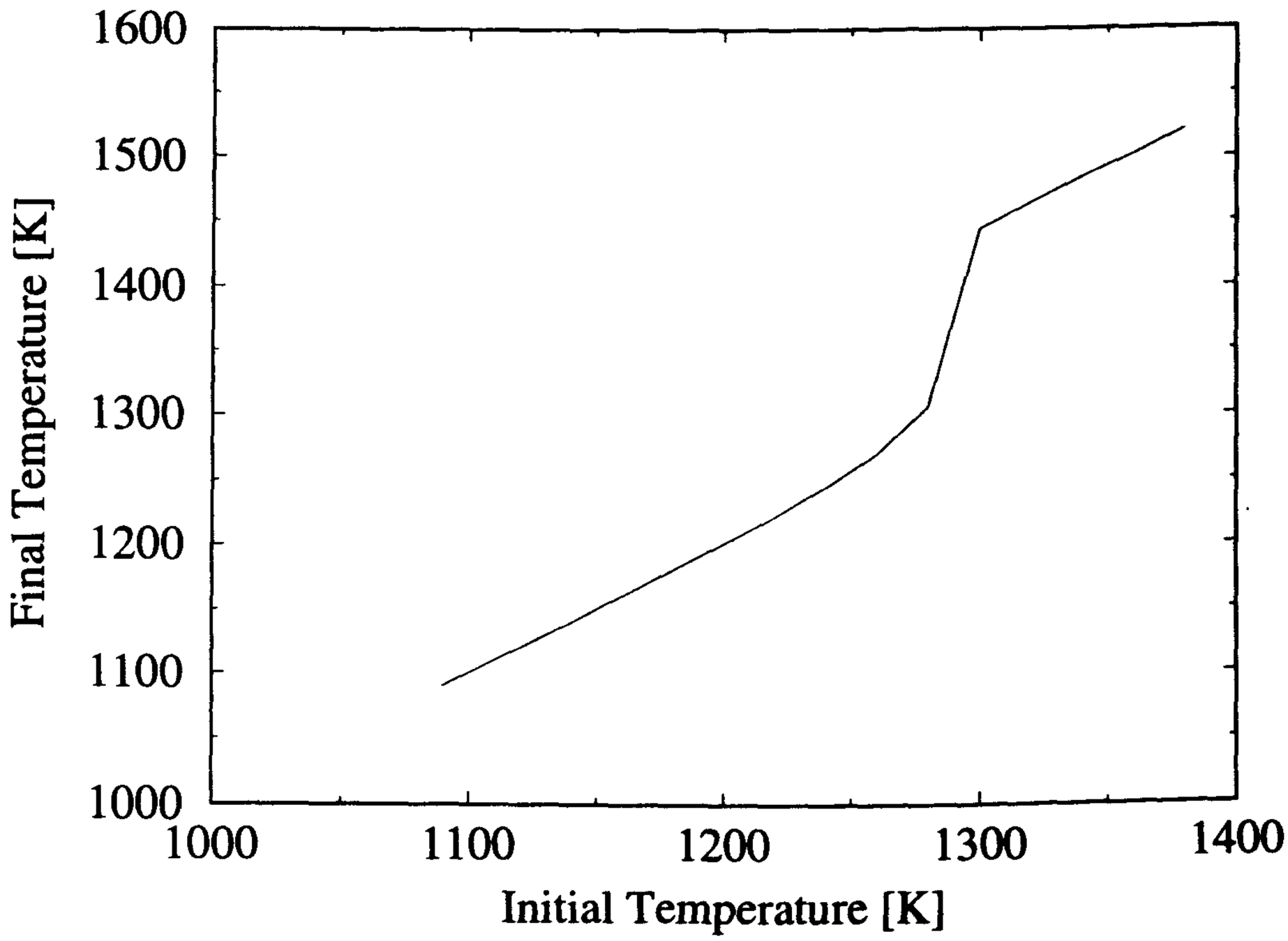


Figure 4.21: Graph of final temperature versus initial temperature for the oxidation of 1 – methylnaphthalene in a Jet Stirred Reactor for a stoichiometry of 1.0.

The oxidation of 1 – methylnaphthalene is additionally studied in the Princeton Turbulent Flow Reactor (PFR) configuration. The experimental data sets are obtained from Shaddix [226] and consist of three stoichiometries, $\phi = 0.58$, 1.0 and 1.5 representing lean to rich conditions. The pressure and initial temperature is set to atmospheric pressure and $\sim$ 1170 K respectively. However, for the second rich case, ($\phi = 1.5$) the initial temperature is raised to 1198 K to show the sensitivity of the consumption reactions of 1 – methylnaphthalene in the context of the CH_3 group. Shaddix [226] reports that an uncertainty of 32 ms in the experimental time evolution. Table 4.2 summarizes the initial conditions for the oxidation of 1 – methylnaphthalene in the PFR as reported by Shaddix [226].

Table 4.2: Summary of the initial conditions for the Oxidation of 1 – methylnaphthalene in a Turbulent Flow Reactor

Fuel	ϕ	T_0 [K]	Residence Time [ms]	Pressure [atm.]
$C_{11}H_{10}$	0.58	1170	150	1.0
$C_{11}H_{10}$	1.0	1169	150	1.0
$C_{11}H_{10}$	1.5	1166	150	1.0
$C_{11}H_{10}$	1.5	1198	150	1.0

The computations featuring the detailed mechanism are compared with the experimental data for the oxidation of 1 – methylnaphthalene from Shaddix [226] in Figures 4.22 – 4.45. Overall, the detailed chemical mechanism performs reasonably well in reproducing overall trends for species having orders of magnitude 1000 ppm, 100 ppm, 10 ppm, 1.0 ppm. However, in all cases the rate of fuel consumption is too slow, hence leading to a shallow gradient as is evident in Figures 4.22, 4.28, 4.34 and 4.40. This is in direct

contrast to the JSR data of Dagaut *et al.* [56] and it has not proved possible to reconcile the data sets further. The PFR data also indicates a measure of "pre – combustion" which may have affected the temporal evolution as discussed below.

Shaddix [226] comments that in the lean case ($\phi = 0.58$), partial CO $\rightarrow$ CO_2 conversion occurs in the last 40 ms leading to rapid molecular oxygen consumption and significant heat release, hence a large temperature rise, not usually occurring for Turbulent Flow Reactor conditions. These events are illustrated in Figures 4.22 and 4.27. This effect of ignition is captured in the calculations. However, there is approximately a 60 ms delay for this effect to occur, and given the overall uncertainties no further effort was made to address this issue.

It may be proposed that pre – combustion is occurring in the study of the oxidation of 1 – methylnaphthalene by Shaddix [226]. In Figures 4.28, 4.34, and 4.40 concerning the stoichiometric and the two rich cases for $T_0 = 1166$ K and 1198 K respectively, the initial production of the CO_2 concentration profiles is rapid for approximately 25 ms, then thereafter, the gradient drops slightly, indicating a drop in the rate of production of CO_2. Additionally, in all cases the concentration species profiles for C_2H_4 are higher initially than that for C_2H_6. Typically, the profile concentrations for C_2H_4 and C_2H_6 are 8 and 2 ppm respectively at a time of 3 ms as is evident in Figures 4.23, 4.29, 4.35 and 4.41. It would be expected that the most direct production path for C_2H_4 would be $C_{11}H_{10} \rightarrow CH_3 \rightarrow C_2H_6 \rightarrow C_2H_5 \rightarrow C_2H_4$, hence the species profile concentrations for C_2H_6 could be expected to rise more than for C_2H_4. It is also found that the concentrations of $C_{11}H_8O$ are significantly higher than that for the analogous equivalent in the oxidation of toluene (C_7H_6O). For example, the concentrations of C_7H_6O in the oxidation of toluene for the

rich case in a Jet Stirred Reactor are typically $\sim$ 10 ppm, as is evident in Figure 2.10 and as reported by Dagaut *et al.* [56]. For similar mean residence times, temperatures and stoichiometry in the study by Shaddix [226], the concentrations of $C_{11}H_8O$ are typically an order of magnitude higher as is evident in Figures 4.37 and 4.43 respectively. The species concentration profiles of $C_{11}H_8O$ in the Turbulent Flow Reactor study from Shaddix [226] may also be compared to that of the Jet Stirred Reactor Study from Dagaut [55]. The experimental values for the concentrations of $C_{11}H_8O$ in the data sets from Dagaut [55] do not exceed 20 ppm (lean case as illustrated in Figure 4.12) for any of the cases considered. By comparison, at 100 ms (which is the mean residence time of the Jet Stirred Reactor study from Dagaut [55]) for any given case from Shaddix [226], the concentrations for $C_{11}H_8O$ are approximately an order of magnitude higher indicating incompatibilities between the experimental data sets from Dagaut [55] and Shaddix [226].

Furthermore, the rapid formation of the alcohol $C_{10}H_7OH$ indicates that precombustion has occurred since the concentrations, for this species are suspiciously high relative to the concentrations of $C_{10}H_8$ as is evident in Figures 4.25, 4.31, 4.37 and 4.43 for lean, stoichiometric, and rich (T_0 = 1166 K and 1198 K) cases respectively.

The calculations for $C_{10}H_8$ are over predicted in all cases as is evident in Figures 4.25, 4.31, 4.37 and 4.43 for the lean, stoichiometric and the two rich cases for T_0 = 1166 K and 1198 K, respectively. It is found that in all cases the most significant channel leading to $C_{10}H_8$ are reactions (1425) and (1332).

$$C_{11}H_9O = C_{10}H_8 + CHO \quad (1425)$$

$$C_9H_6CH_2 + H = C_{10}H_8 + H \quad (1332)$$

Interestingly, with the over prediction of $C_{10}H_8$ as discussed above, the calcu-

lations for C_9H_8 are under predicted in all cases as is evident in Figures 4.25, 4.31, 4.37 and 4.43. Since the production of C_9H_8 follows closely that of the consumption of $C_{10}H_8$, and given that $C_{10}H_8$ is over predicted it seems logical to suggest that C_9H_8 should be over predicted as well.

The computations for the species profile concentrations for C_8H_6 have produced mixed results. Excellent agreement is achieved for the stoichiometric and the lower temperature rich case (T_0 = 1166 K) as is evident in Figures 4.30 and 4.36 respectively. However, there are discrepancies for the lean and rich case (T_0 = 1198 K) with an over prediction for the former and under prediction for the latter of the species concentration profiles for C_8H_6 as illustrated in Figures 4.24 and 4.42. It is found that for the lean case, reaction (1170) is the single most dominant reaction producing C_8H_6,

$$C_8H_7 = C_8H_6 + H \quad (1170)$$

$$C_9H_6O = C_8H_6 + CO \quad (1297)$$

whilst in the rich case (T_0 = 1198 K) both reactions (1170) and (1297) are of equal importance.

Other aromatic species such as C_8H_8, C_6H_6, C_7H_8 are predicted with reasonable accuarcy as is evident in Figures 4.24, 4.30, 4.36 and 4.42 for the lean, stoichiometric and the two rich cases for T_0 = 1166 K and 1198 K. The calculations for C_6H_6 are low for all cases. It is found that reactions (1111), (1104) and (985)

$$C_7H_7O = C_6H_6 + CHO \quad (1111)$$

$$C_7H_6O + O = C_6H_6 + CO_2 \quad (1104)$$

$$C_6H_6(F) + H = C_6H_6 + H \quad (985)$$

are the most significant channels for C_6H_6 and contribute approximately 30 %, 20 % and 17 % respectively.

The calculations for C_7H_6O are acceptable for all cases as is evident in Figures 4.26, 4.32, 4.38 and 4.44. However, for the rich (T_0 = 1198 K) case, there appears to be a problem regarding the measurements. Until approximately 50 ms, the experimental data does not register the presence of C_7H_6O, in which case at the time mentioned, C_7H_6O suddenly appears.

Levels for the smaller species CH_4, C_2H_6, C_2H_4 and C_2H_2 are illustrated in Figures 4.23, 4.29, 4.35 and 4.41 for the lean, stoichiometric and the two rich cases for T_0 = 1166 K and 1198 K, respectively. The calculations for C_2H_6 are well reproduced. However, the concentrations for CH_4 concentrations are under predicted in all cases. It may again be suggested that perhaps the rate expression for reaction (1410)

$$C_{11}H_{10} + CH_3 \quad = \quad C_{11}H_9 + CH_4 \tag{1410}$$

is too slow since in all cases, it is found to be the dominant production channel for CH_4. The rate for reaction (1410) is modelled on the analogous in reaction (1094).

$$C_7H_8 + CH_3 \quad = \quad C_7H_7 + CH_4 \tag{1094}$$

The C_3 species computations are not well reproduced as shown in Figures 4.26, 4.32, 4.38 and 4.44. The oxidation of C_3, as well as other small species, have been thoroughly investigated in the work of Rizos [218]. The low concentration of the C_3 species may also lead to greater experimental uncertainties.

Levels of $C_{12}H_{12}$ are well produced for all cases as is evident in Figures 4.26, 4.32, 4.38 and 4.44. Reaction (1386) is the dominant channel.

$$C_{11}H_9 + CH_3 \quad = \quad C_{12}H_{12} \tag{1386}$$

The rate is modelled on reaction (1061)

$$C_7H_7 + CH_3 \quad = \quad C_8H_{10} \tag{1061}$$

with the rates parameters being discussed earlier in the text.

The temperature profiles for the stoichiometric and the two rich cases for T_0 = 1166 K and 1198 K, indicate an absence of ignition phenomena as is evident in Figures 4.27, 4.33, 4.39 and 4.45.

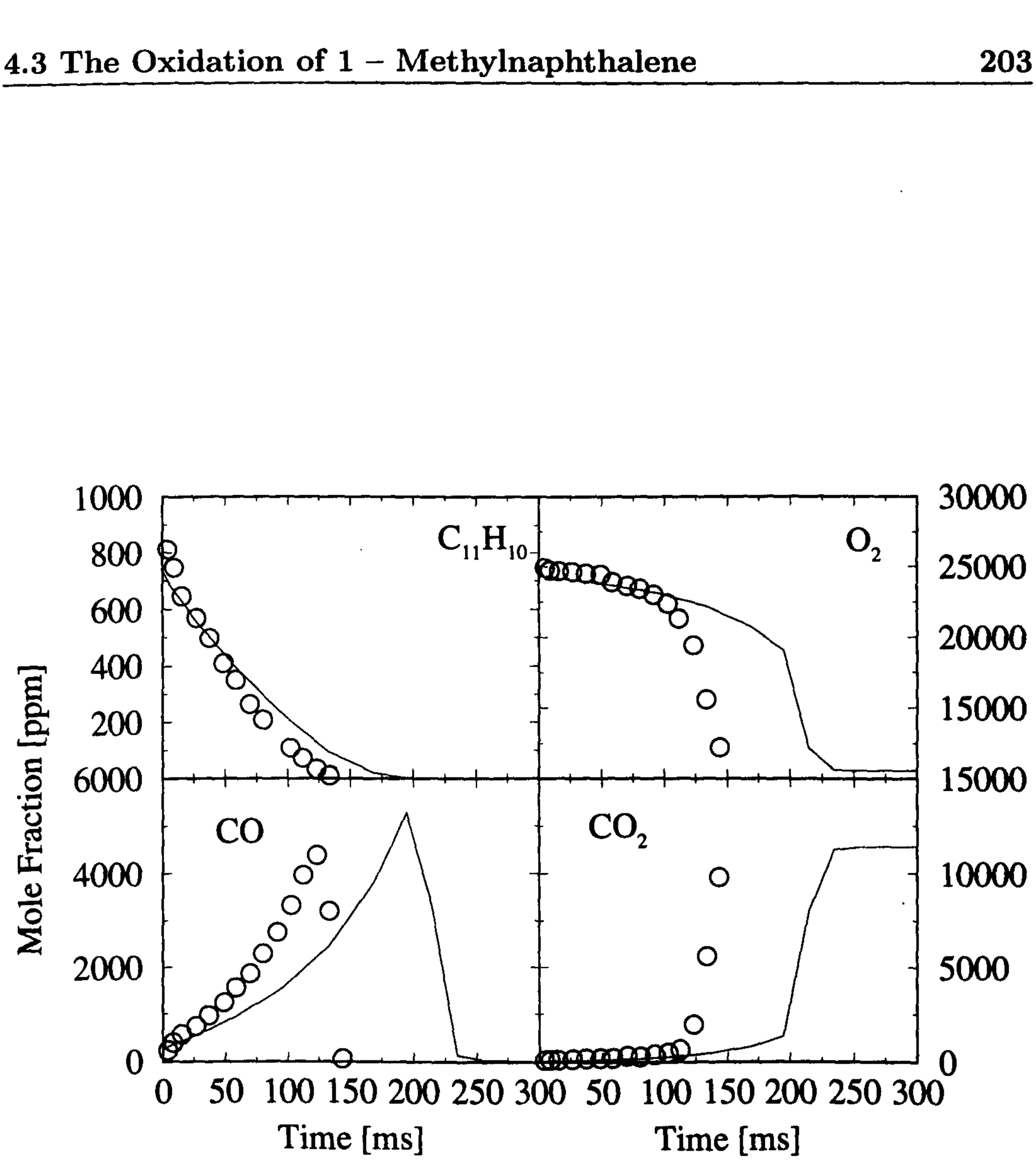


Figure 4.22: Graph of species profile concentrations versus time for the oxidation of 1 – methylnaphthalene in a Turbulent Flow Reactor. Experimental points are from Shaddix [226] for a stoichiometry of $\phi = 0.58$. Solid lines are the computations from the detailed chemical mechanism and have been time shifted by 32 ms.

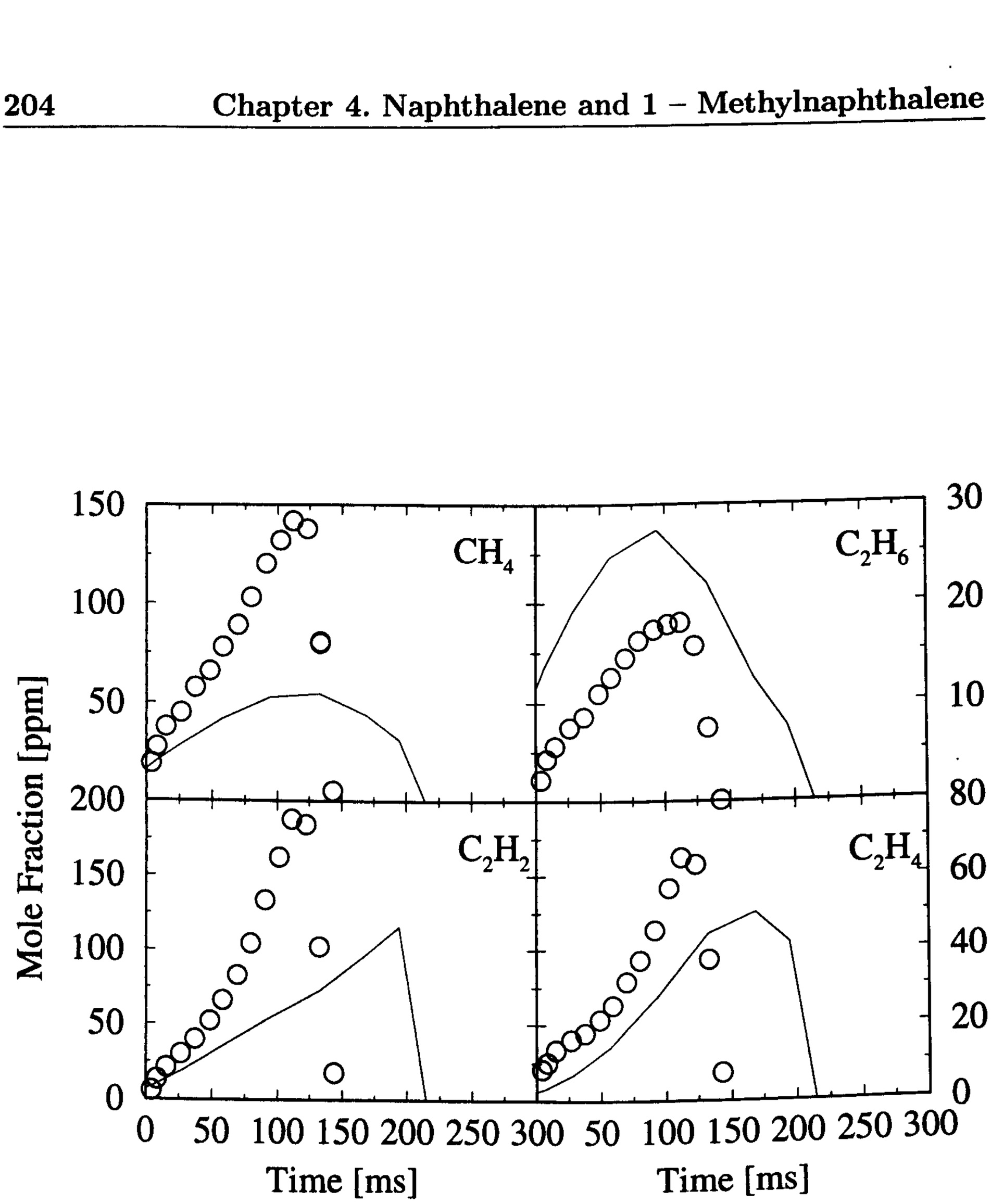


Figure 4.23: Graph of species profile concentrations versus time for the oxidation of 1 – methylnaphthalene in a Turbulent Flow Reactor. Experimental points are from Shaddix [226] for a stoichiometry of $\phi = 0.58$. Solid lines are the computations from the detailed chemical mechanism and have been time shifted by 32 ms.

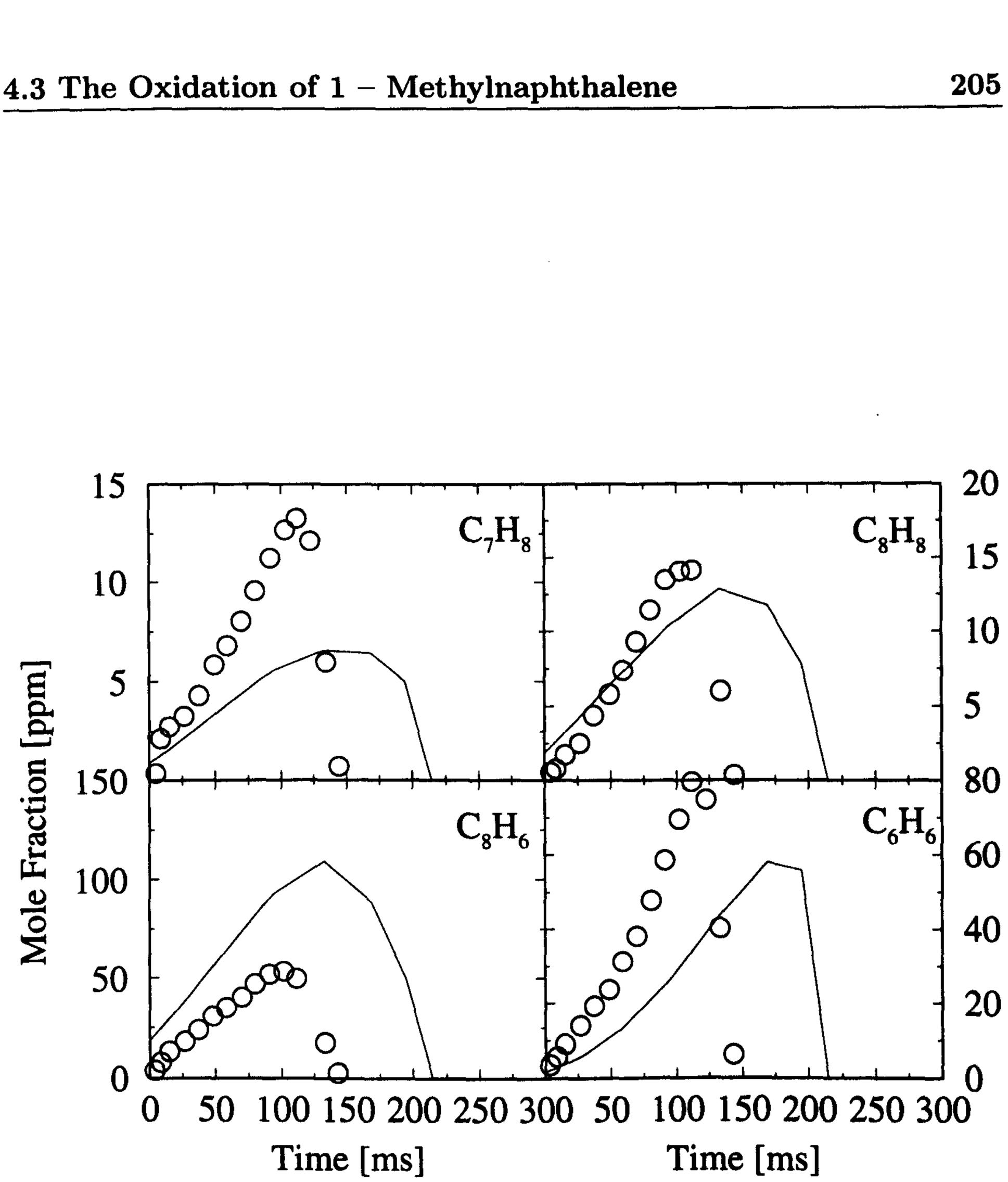


Figure 4.24: Graph of species profile concentrations versus time for the oxidation of 1 – methylnaphthalene in a Turbulent Flow Reactor. Experimental points are from Shaddix [226] for a stoichiometry of $\phi = 0.58$. Solid lines are the computations from the detailed chemical mechanism and have been time shifted by 32 ms.

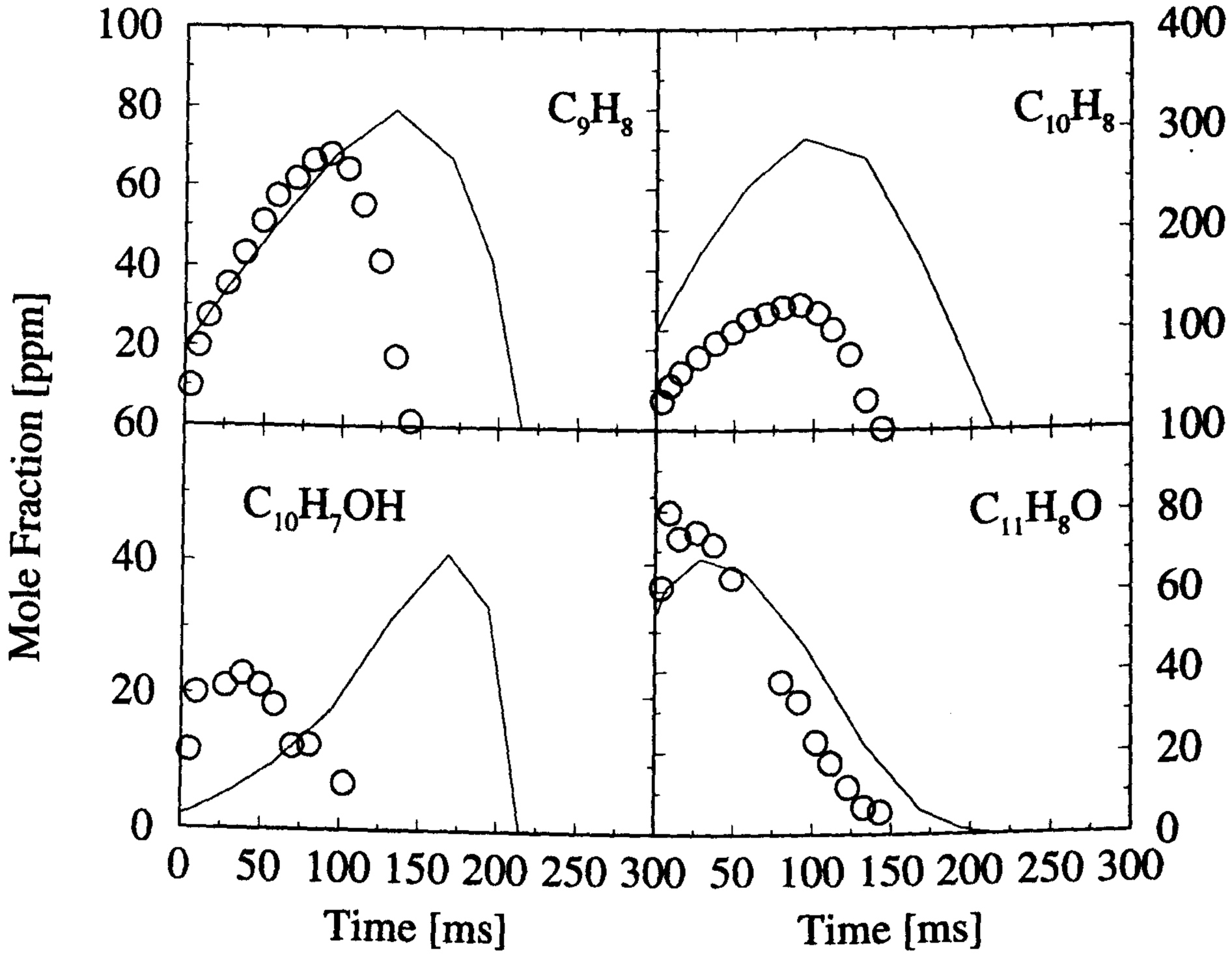


Figure 4.25: Graph of species profile concentrations versus time for the oxidation of 1 – methylnaphthalene in a Turbulent Flow Reactor. Experimental points are from Shaddix [226] for a stoichiometry of $\phi = 0.58$. Solid lines are the computations from the detailed chemical mechanism and have been time shifted by 32 ms.

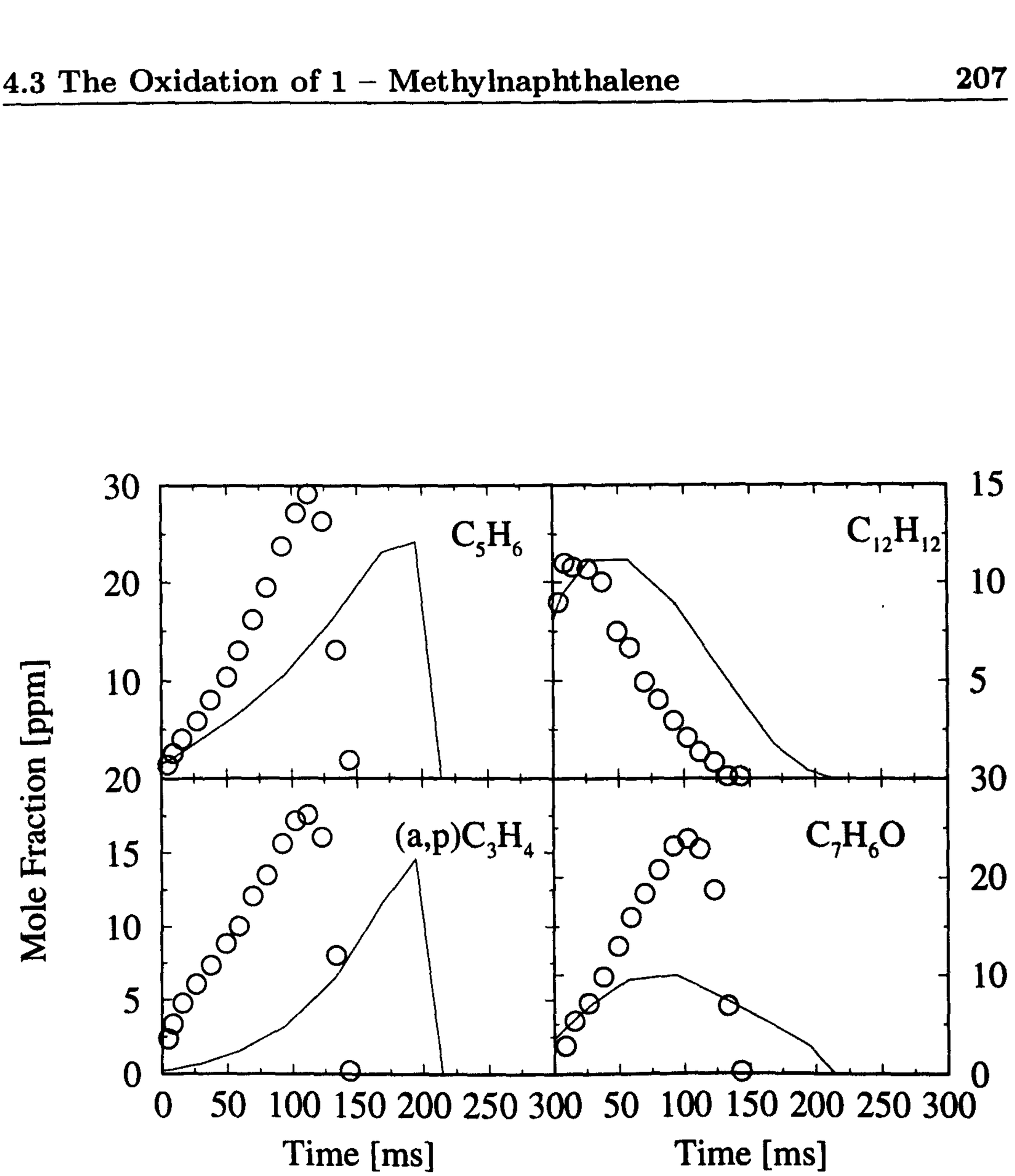


Figure 4.26: Graph of species profile concentrations versus time for the oxidation of 1 – methylnaphthalene in a Turbulent Flow Reactor. Experimental points are from Shaddix [226] for a stoichiometry of $\phi = 0.58$. Solid lines are the computations from the detailed chemical mechanism and have been time shifted by 32 ms.

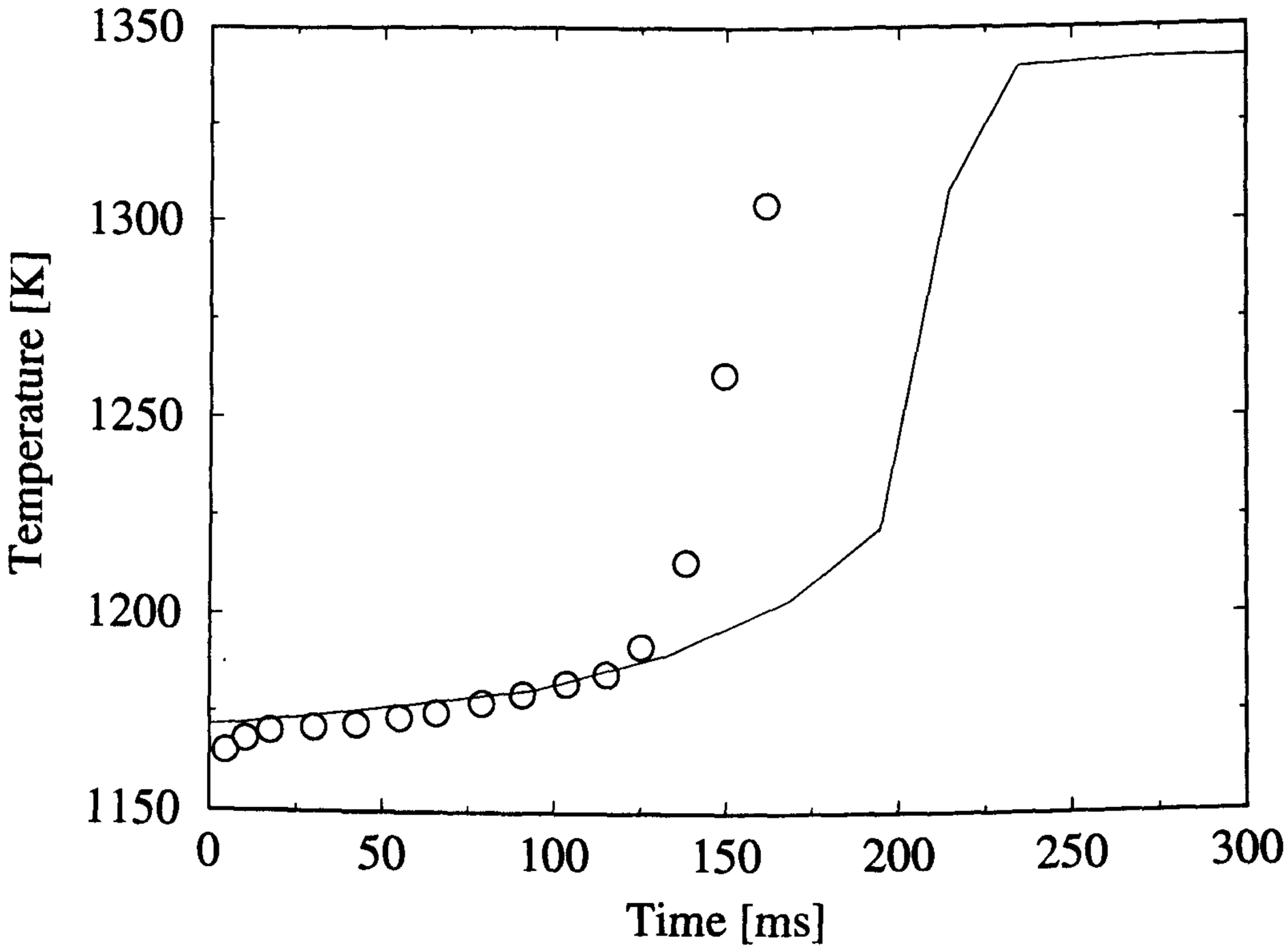


Figure 4.27: Graph of temperature profile versus time for the oxidation of 1 – methylnaphthalene in a Turbulent Flow Reactor. Experimental points are from Shaddix [226] for a stoichiometry of $\phi = 0.58$. Solid lines are the computations from the detailed chemical mechanism and have been time shifted by 32 ms.

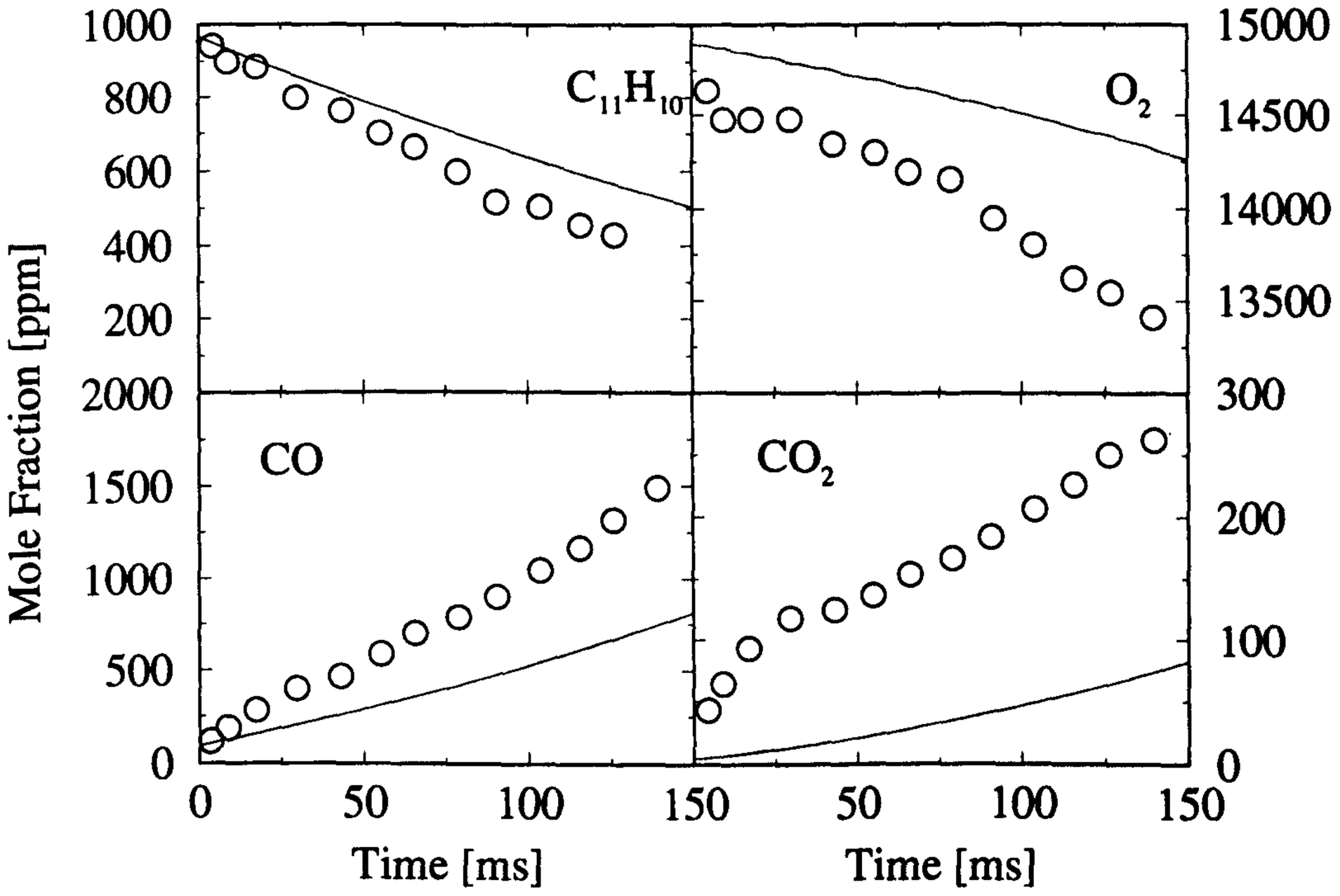


Figure 4.28: Graph of species profile concentrations versus time for the oxidation of 1 – methylnaphthalene in a Turbulent Flow Reactor. Experimental points are from Shaddix [226] for a stoichiometry of $\phi = 1.0$. Solid lines are the computations from the detailed chemical mechanism and have been time shifted by 32 ms.

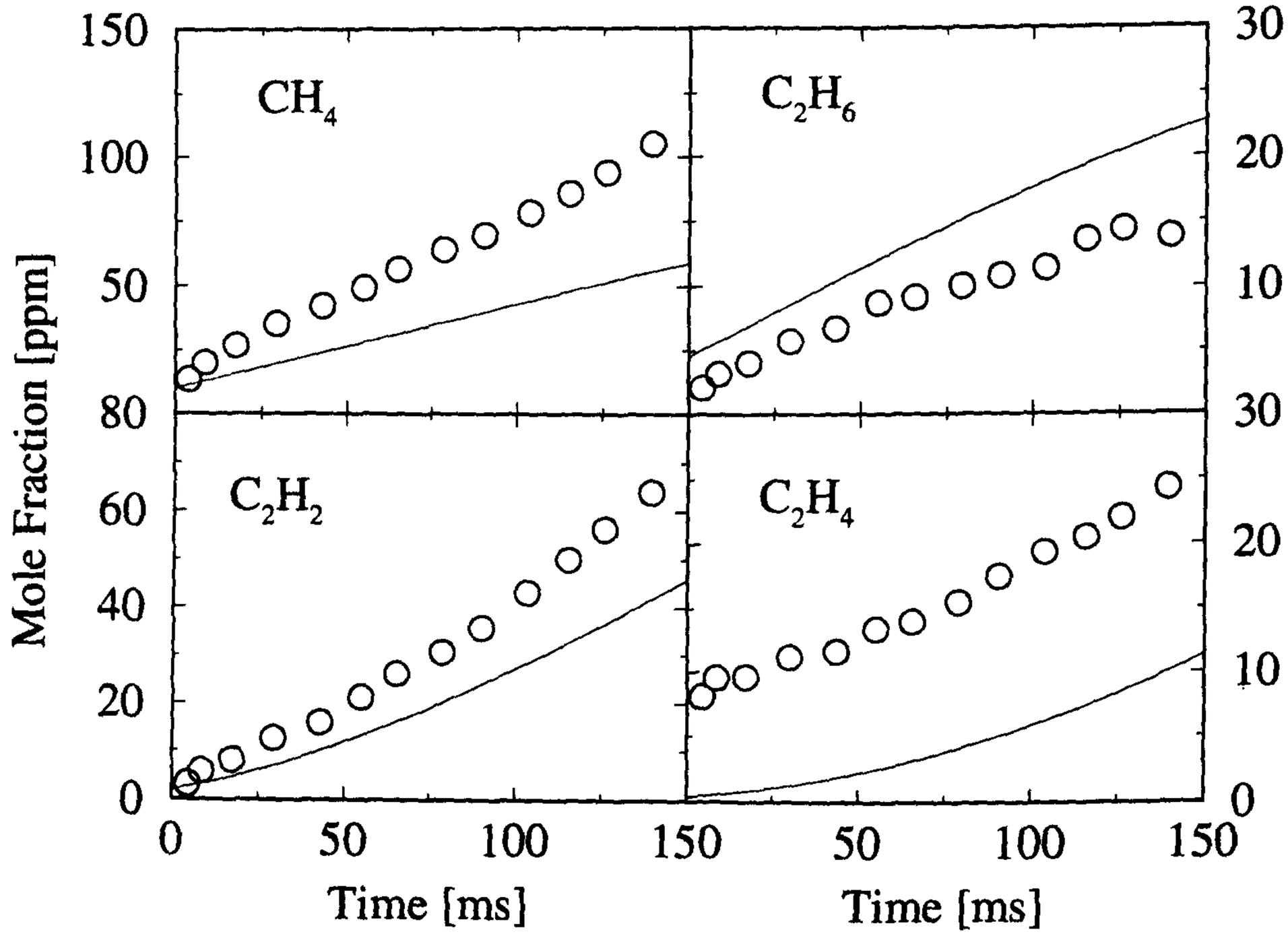


Figure 4.29: Graph of species profile concentrations versus time for the oxidation of 1 – methylnaphthalene in a Turbulent Flow Reactor. Experimental points are from Shaddix [226] for a stoichiometry of $\phi = 1.0$. Solid lines are the computations from the detailed chemical mechanism and have been time shifted by 32 ms.

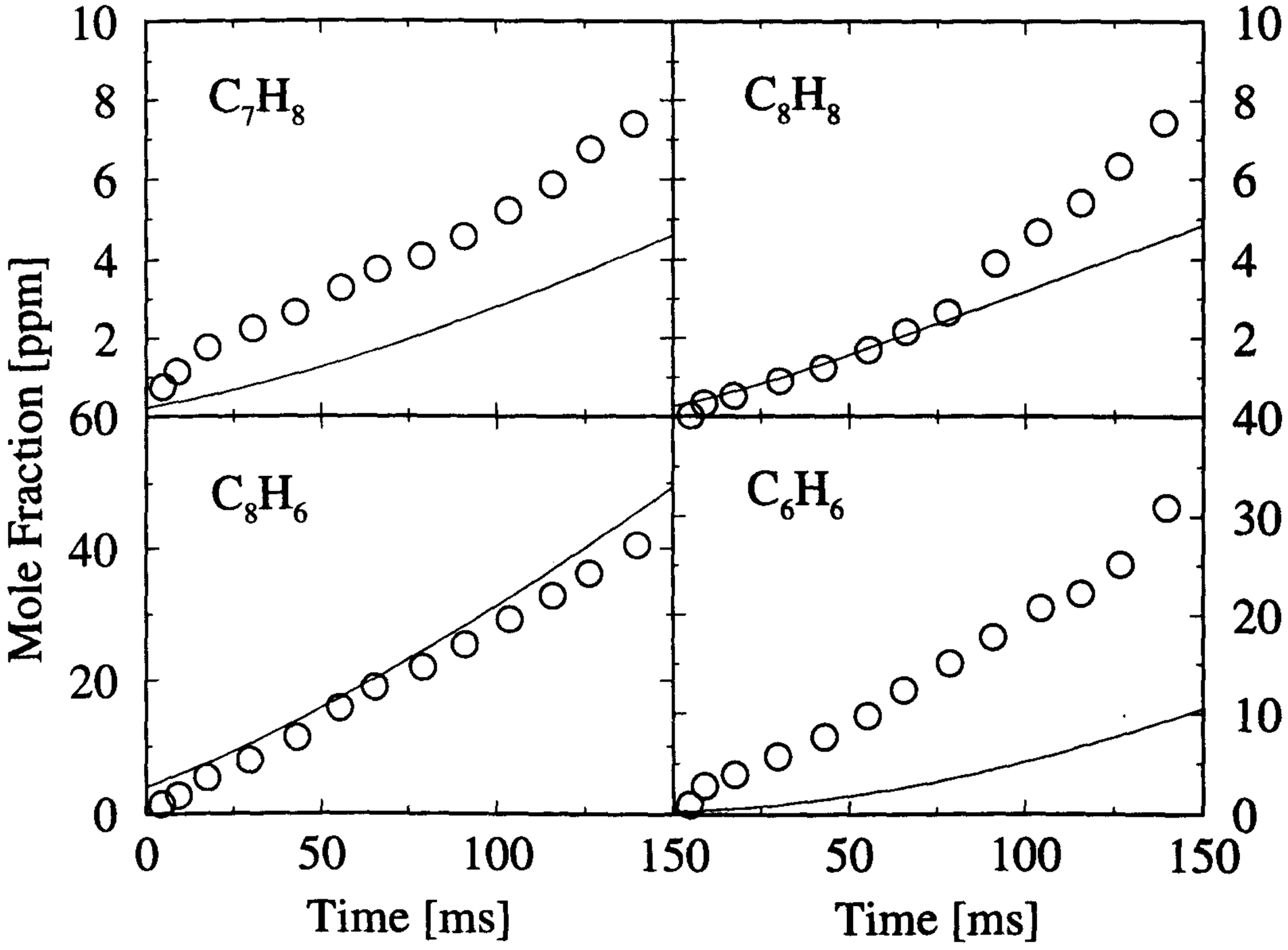


Figure 4.30: Graph of species profile concentrations versus time for the oxidation of 1 – methylnaphthalene in a Turbulent Flow Reactor. Experimental points are from Shaddix [226] for a stoichiometry of $\phi = 1.0$. Solid lines are the computations from the detailed chemical mechanism and have been time shifted by 32 ms.

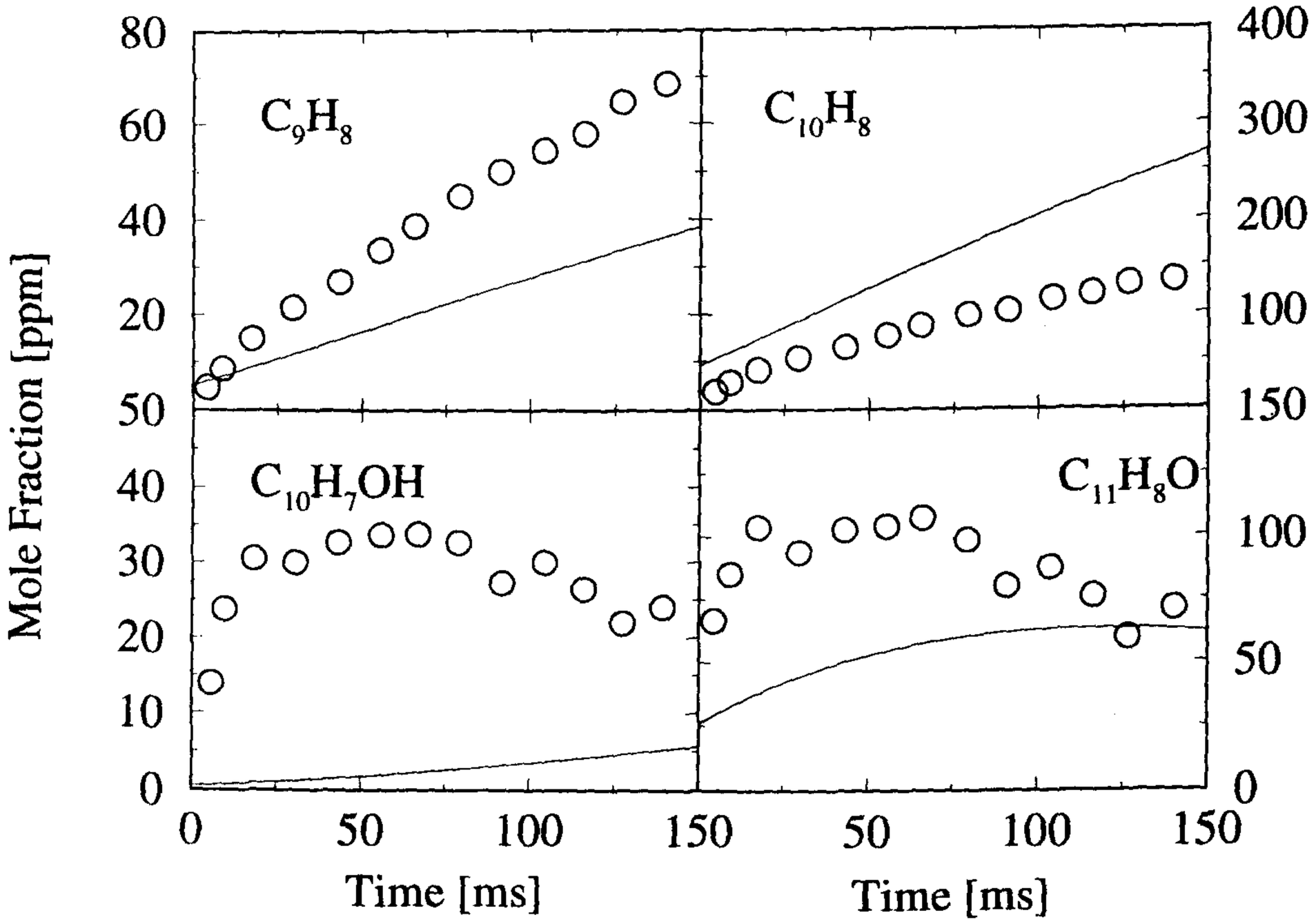


Figure 4.31: Graph of species profile concentrations versus time for the oxidation of 1 – methylnaphthalene in a Turbulent Flow Reactor. Experimental points are from Shaddix [226] for a stoichiometry of $\phi = 1.0$. Solid lines are the computations from the detailed chemical mechanism and have been time shifted by 32 ms.

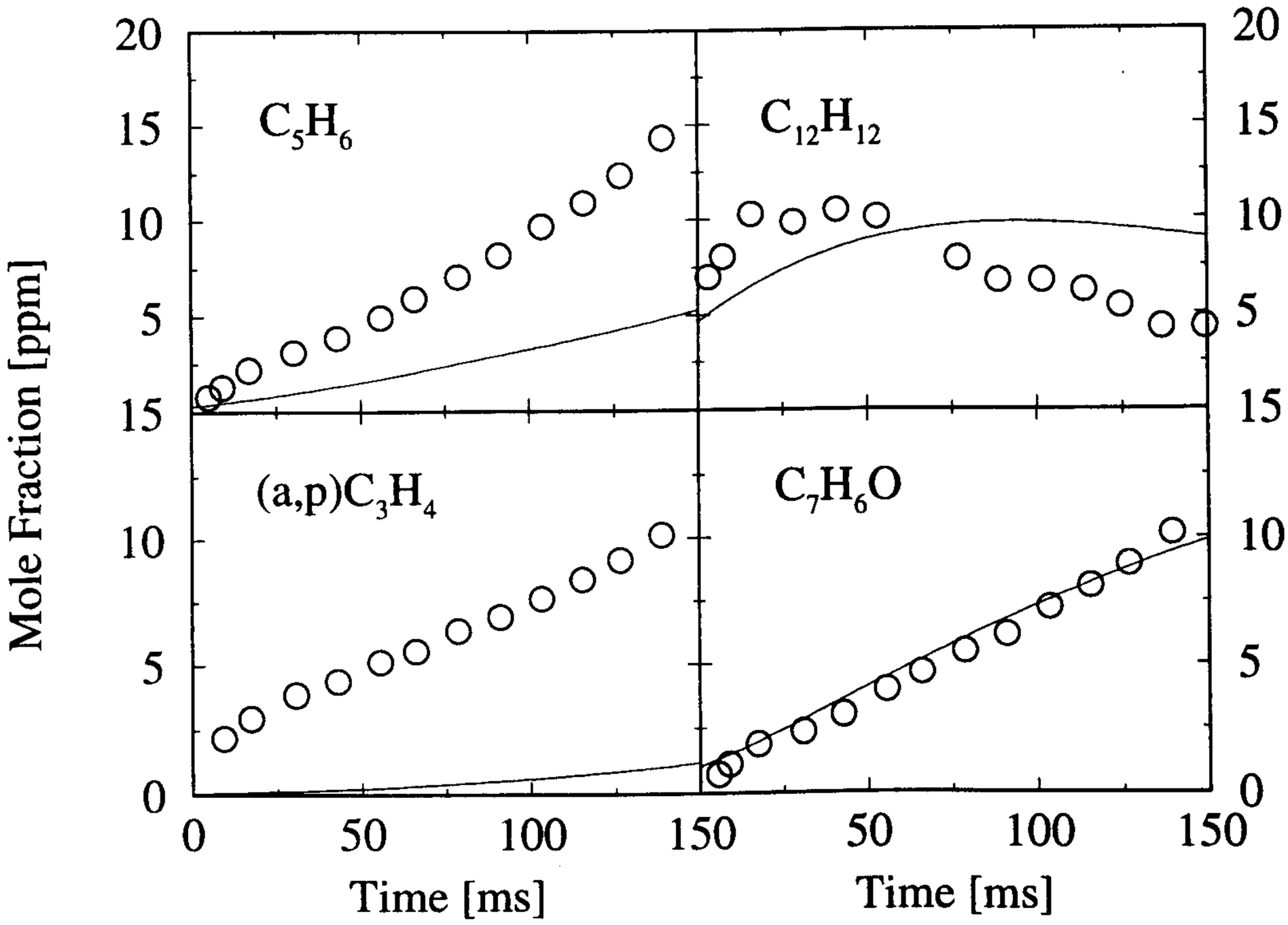


Figure 4.32: Graph of species profile concentrations versus time for the oxidation of 1 – methylnaphthalene in a Turbulent Flow Reactor. Experimental points are from Shaddix [226] for a stoichiometry of $\phi = 1.0$. Solid lines are the computations from the detailed chemical mechanism and have been time shifted by 32 ms.

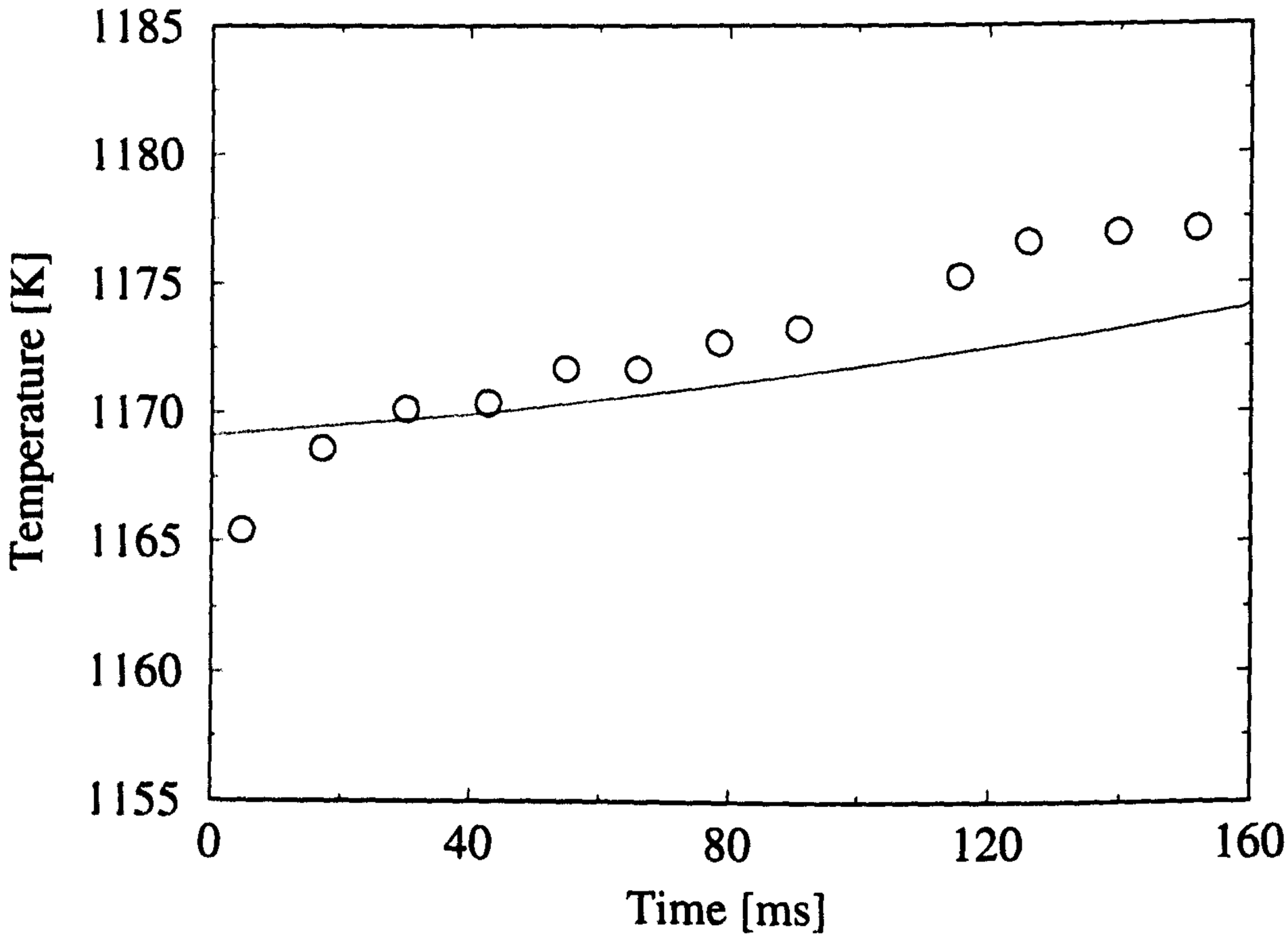


Figure 4.33: Graph of temperature profile versus time for the oxidation of 1 methylnaphthalene in a Turbulent Flow Reactor. Experimental points are from Shaddix [226] for a stoichiometry of $\phi = 1.0$. Solid lines are the computations from the detailed chemical mechanism and have been time shifted by 32 ms.

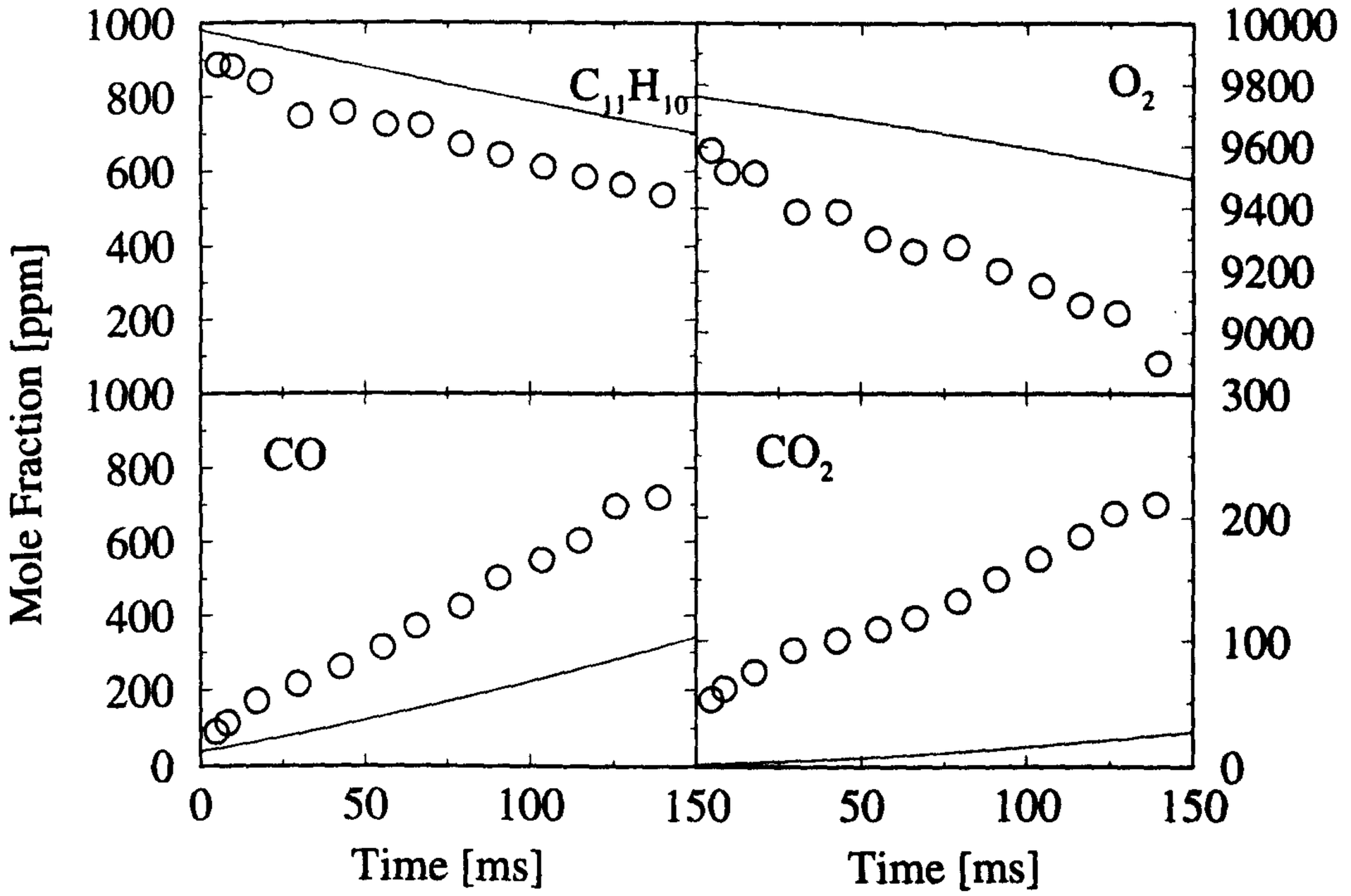


Figure 4.34: Graph of species profile concentrations versus time for the oxidation of 1 – methylnaphthalene in a Turbulent Flow Reactor. Experimental points are from Shaddix [226] for a stoichiometry of $\phi = 1.5$ for $T_0 = 1166$ K. Solid lines are the computations from the detailed chemical mechanism and have been time shifted by 32 ms.

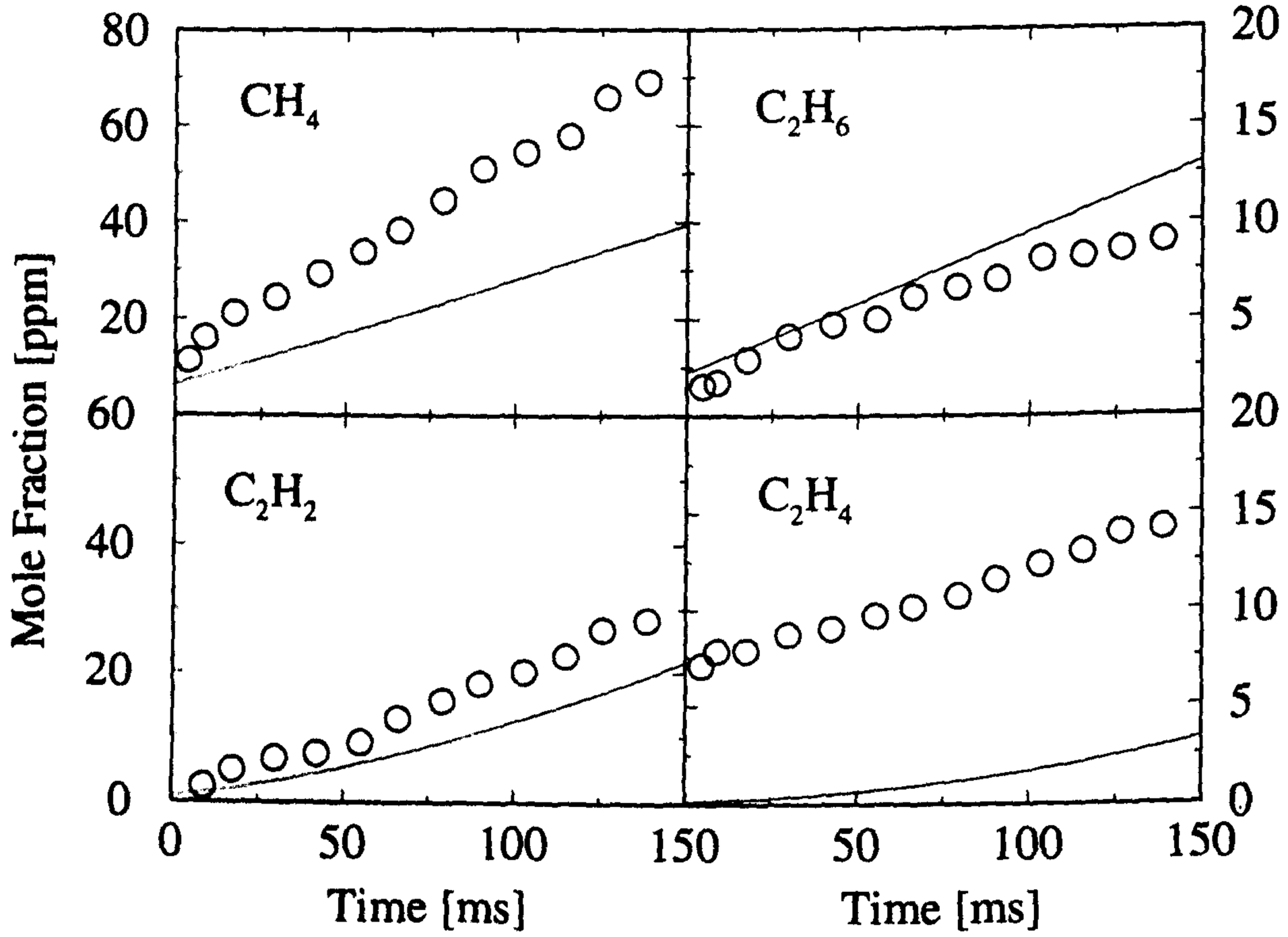


Figure 4.35: Graph of species profile concentrations versus time for the oxidation of 1 – methylnaphthalene in a Turbulent Flow Reactor. Experimental points are from Shaddix [226] for a stoichiometry of $\phi = 1.5$ for $T_0 = 1166$ K. Solid lines are the computations from the detailed chemical mechanism and have been time shifted by 32 ms.

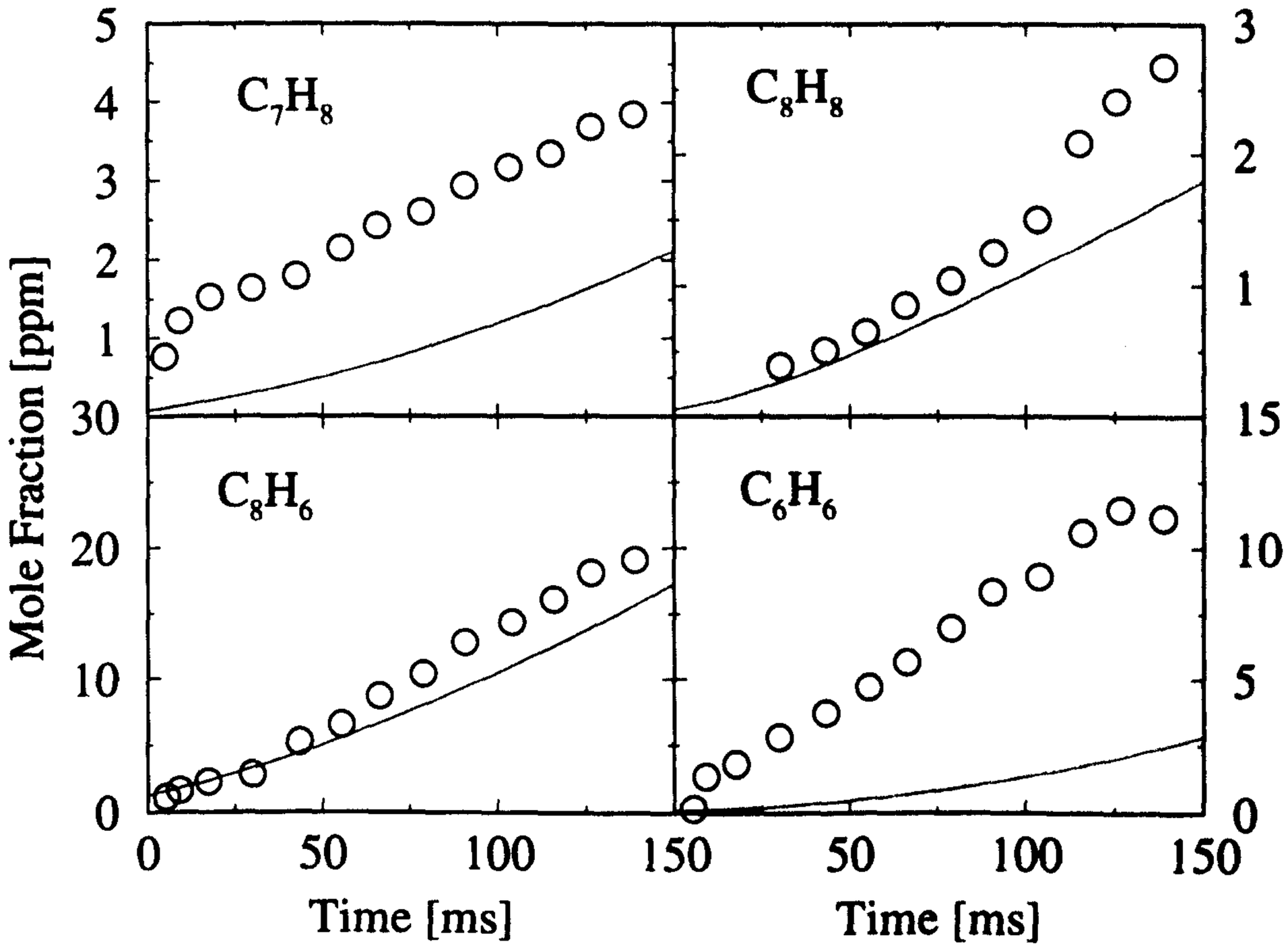


Figure 4.36: Graph of species profile concentrations versus time for the oxidation of 1 – methylnaphthalene in a Turbulent Flow Reactor. Experimental points are from Shaddix [226] for a stoichiometry of $\phi = 1.5$ for $T_0 = 1166$ K. Solid lines are the computations from the detailed chemical mechanism and have been time shifted by 32 ms.

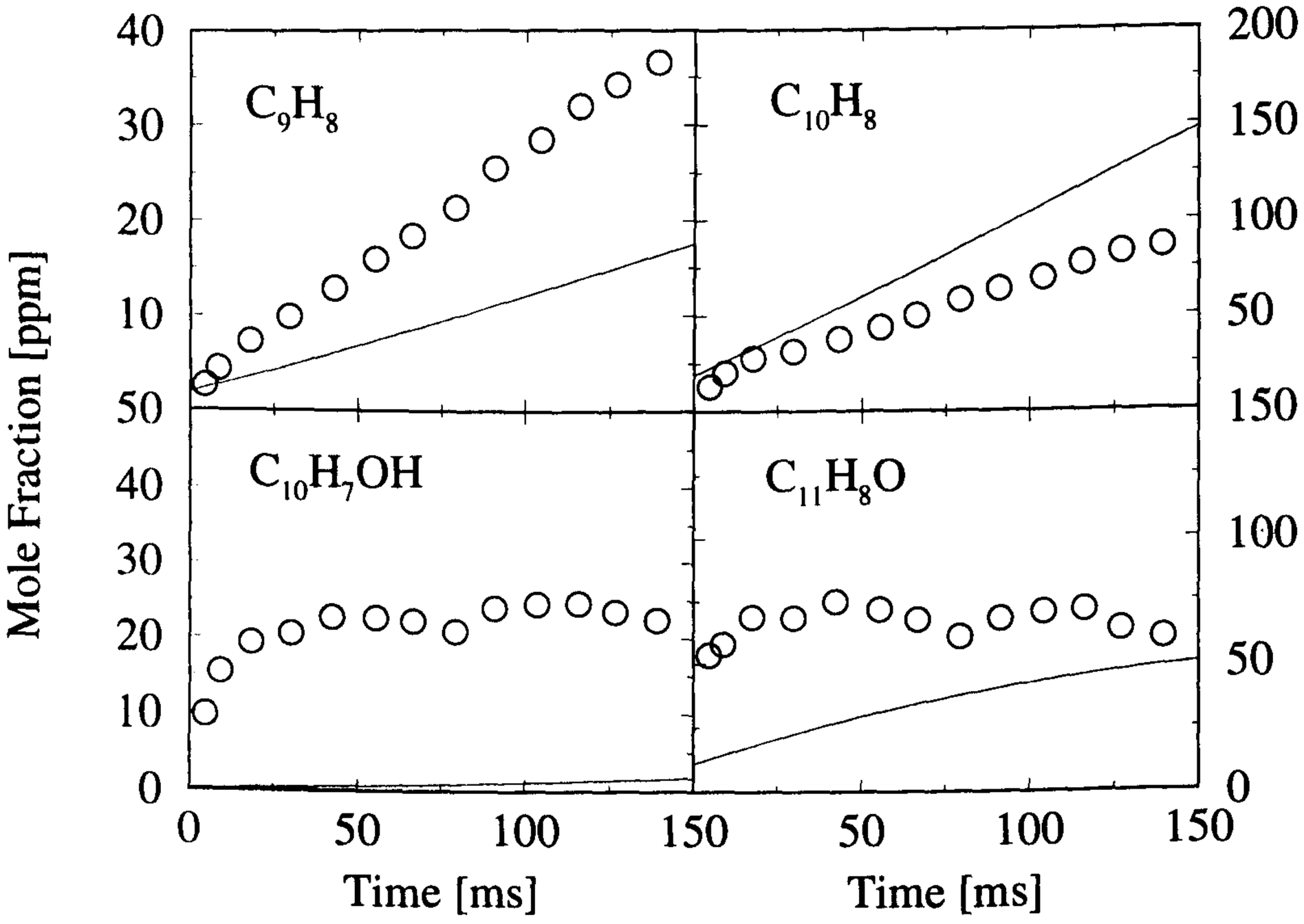


Figure 4.37: Graph of species profile concentrations versus time for the oxidation of 1 – methylnaphthalene in a Turbulent Flow Reactor. Experimental points are from Shaddix [226] for a stoichiometry of $\phi = 1.5$ for $T_0 = 1166$ K. Solid lines are the computations from the detailed chemical mechanism and have been time shifted by 32 ms.

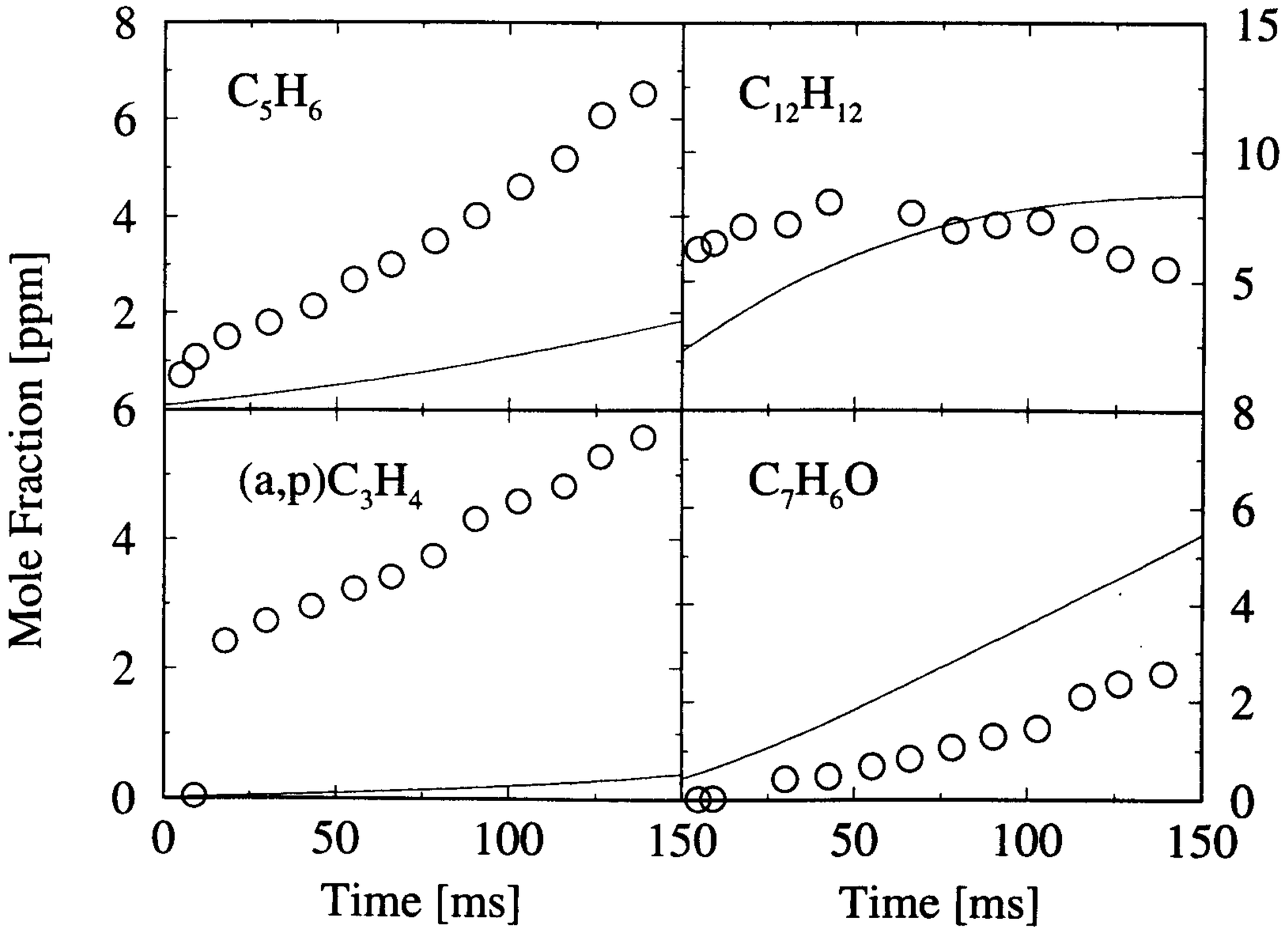


Figure 4.38: Graph of species profile concentrations versus time for the oxidation of 1 – methylnaphthalene in a Turbulent Flow Reactor. Experimental points are from Shaddix [226] for a stoichiometry of $\phi = 1.5$ for $T_0 = 1166$ K. Solid lines are the computations from the detailed chemical mechanism and have been time shifted by 32 ms.

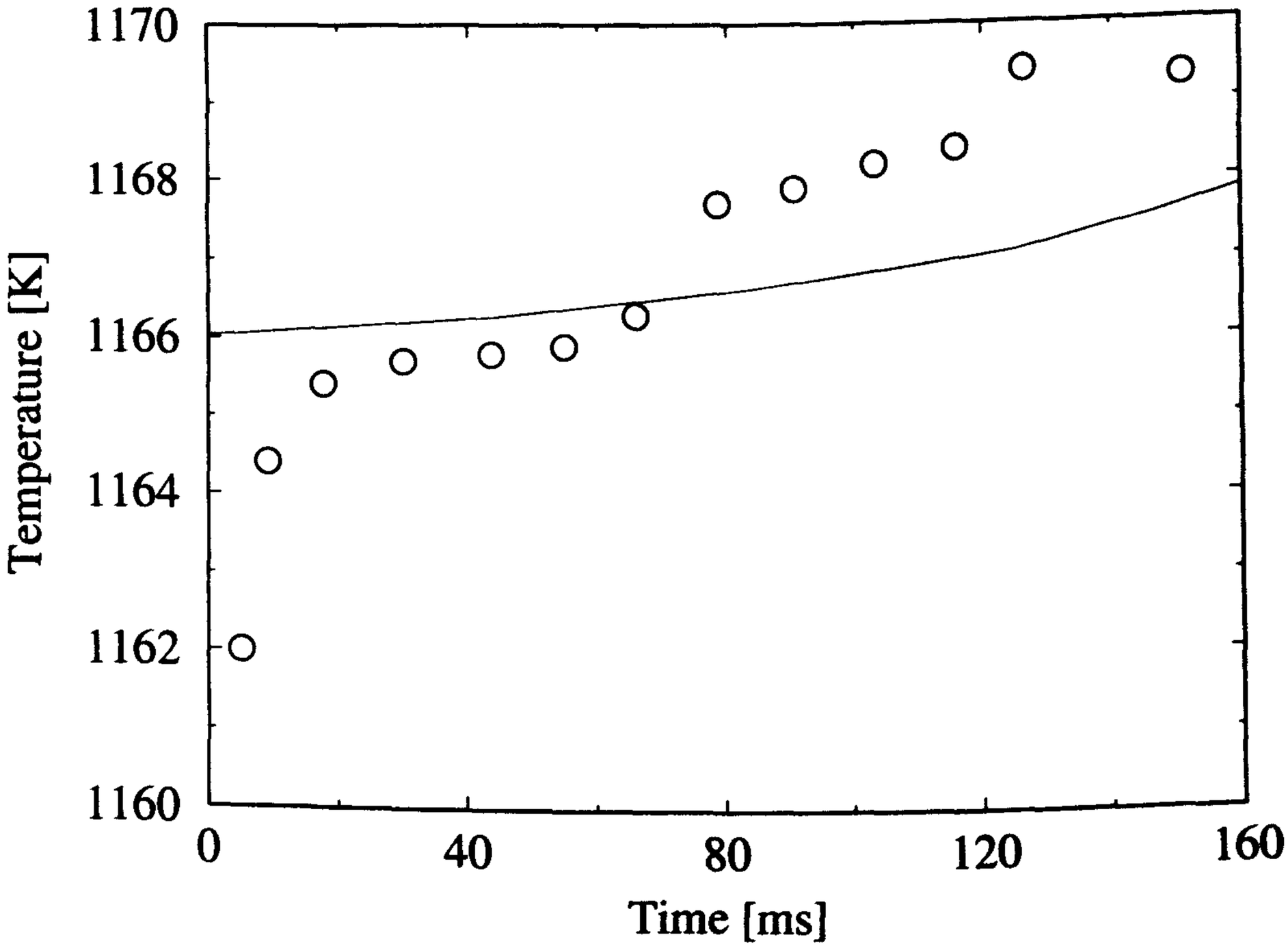


Figure 4.39: Graph of temperature profile versus time for the oxidation of 1 – methylnaphthalene in a Turbulent Flow Reactor. Experimental points are from Shaddix [226] for a stoichiometry of $\phi = 1.5$ for $T_0 = 1166$ K. Solid lines are the computations from the detailed chemical mechanism and have been time shifted by 32 ms.

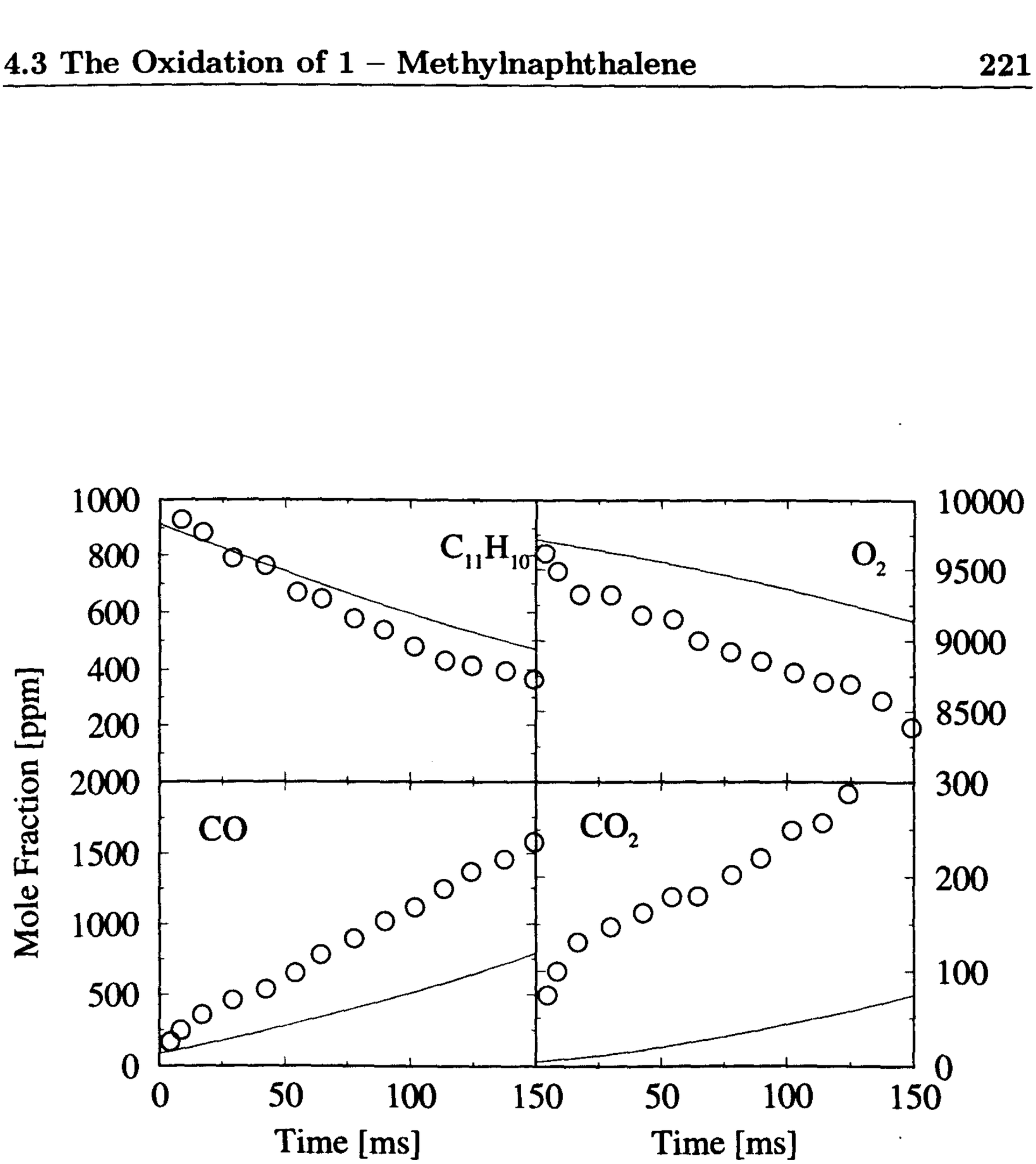


Figure 4.40: Graph of species profile concentrations versus time for the oxidation of 1 – methylnaphthalene in a Turbulent Flow Reactor. Experimental points are from Shaddix [226] for a stoichiometry of $\phi = 1.5$ for $T_0 = 1198$ K. Solid lines are the computations from the detailed chemical mechanism and have been time shifted by 32 ms.

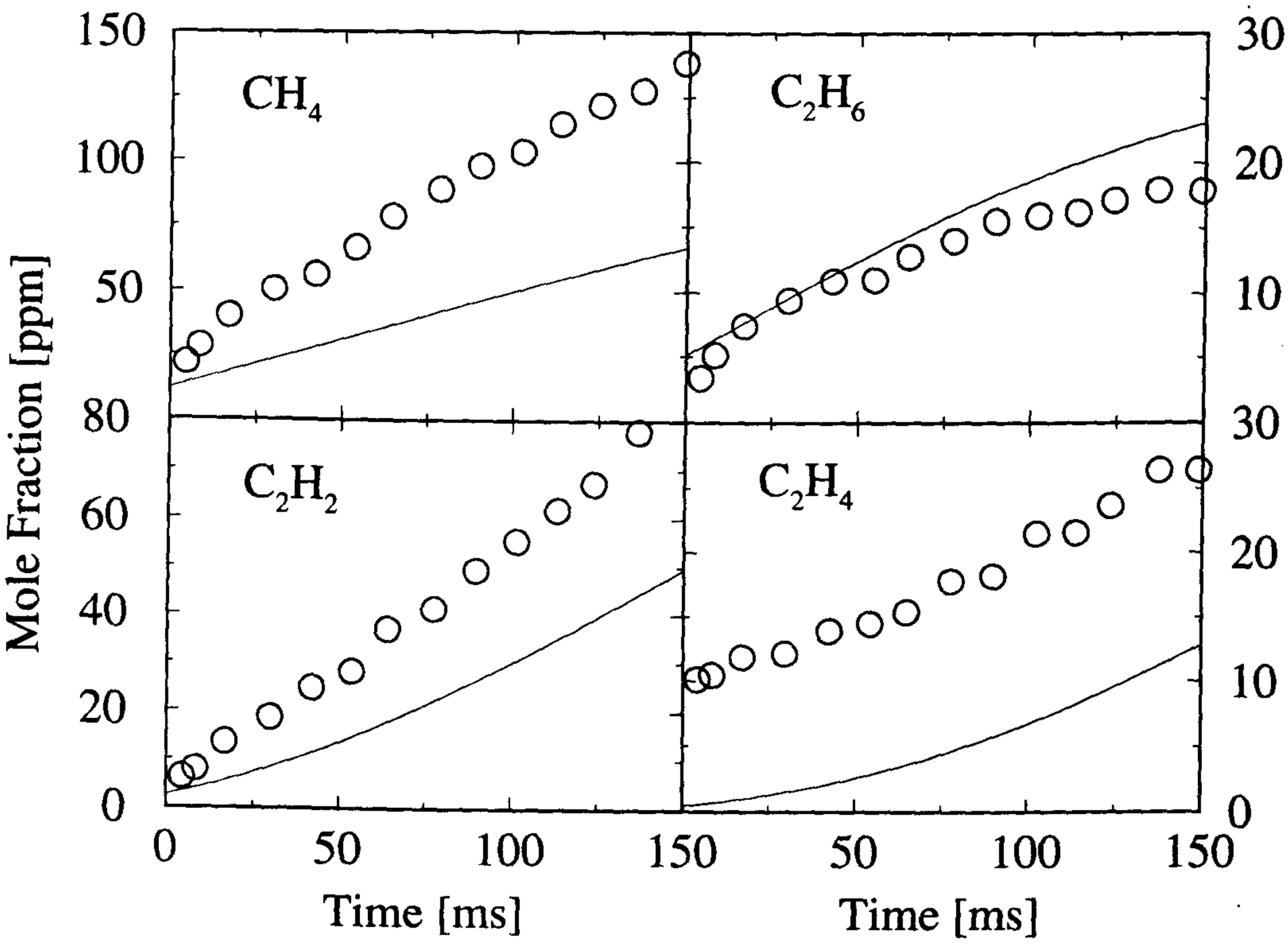


Figure 4.41: Graph of species profile concentrations versus time for the oxidation of 1 – methylnaphthalene in a Turbulent Flow Reactor. Experimental points are from Shaddix [226] for a stoichiometry of $\phi = 1.5$ for $T_0 = 1198$ K. Solid lines are the computations from the detailed chemical mechanism and have been time shifted by 32 ms.

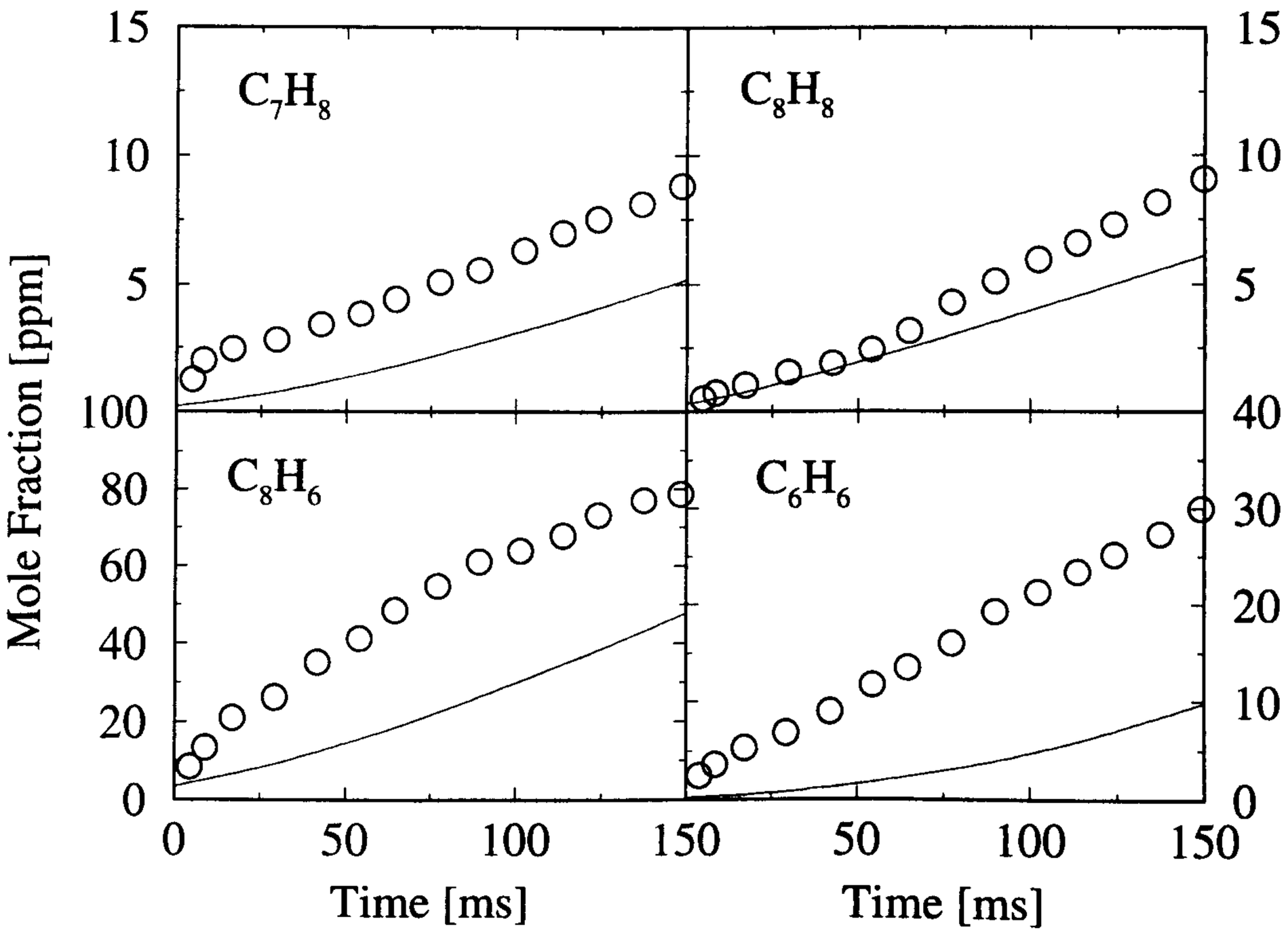


Figure 4.42: Graph of species profile concentrations versus time for the oxidation of 1 – methylnaphthalene in a Turbulent Flow Reactor. Experimental points are from Shaddix [226] for a stoichiometry of $\phi = 1.5$ for $T_0 = 1198$ K. Solid lines are the computations from the detailed chemical mechanism and have been time shifted by 32 ms.

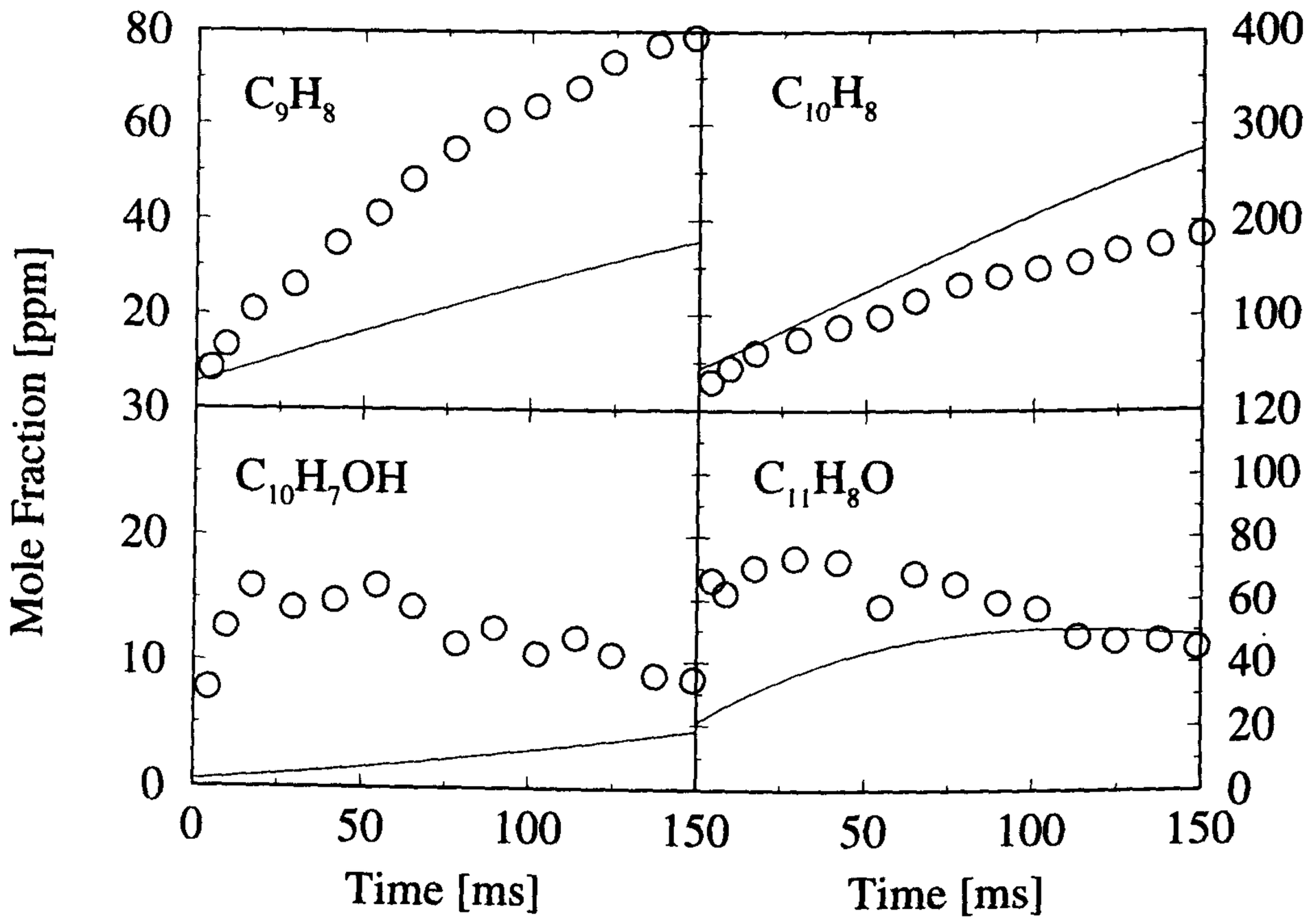


Figure 4.43: Graph of species profile concentrations versus time for the oxidation of 1 – methylnaphthalene in a Turbulent Flow Reactor. Experimental points are from Shaddix [226] for a stoichiometry of $\phi = 1.5$ for $T_0 = 1198$ K. Solid lines are the computations from the detailed chemical mechanism and have been time shifted by 32 ms.

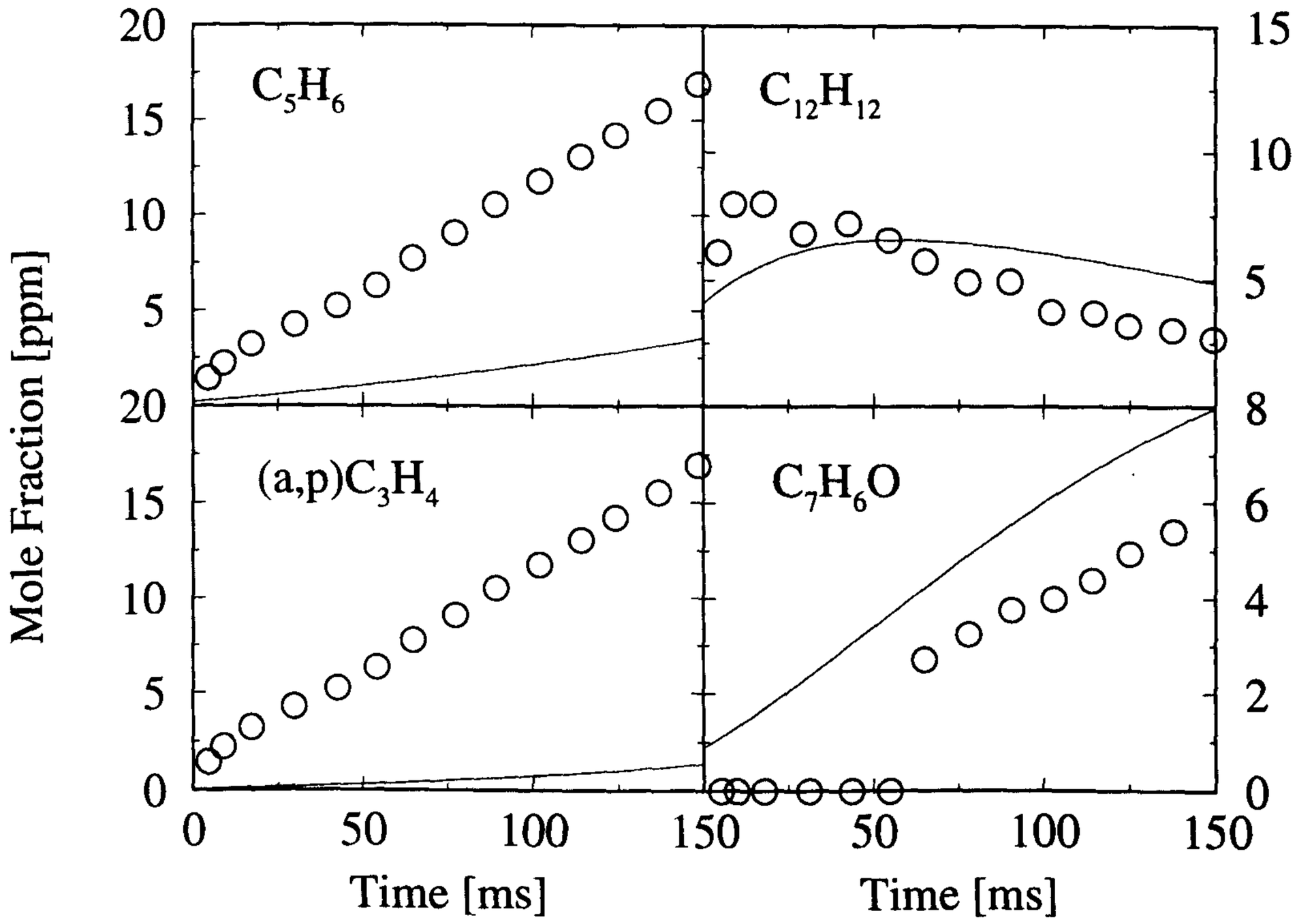


Figure 4.44: Graph of species profile concentrations versus time for the oxidation of 1 – methylnaphthalene in a Turbulent Flow Reactor. Experimental points are from Shaddix [226] for a stoichiometry of $\phi = 1.5$ for $T_0 = 1198$ K. Solid lines are the computations from the detailed chemical mechanism and have been time shifted by 32 ms.

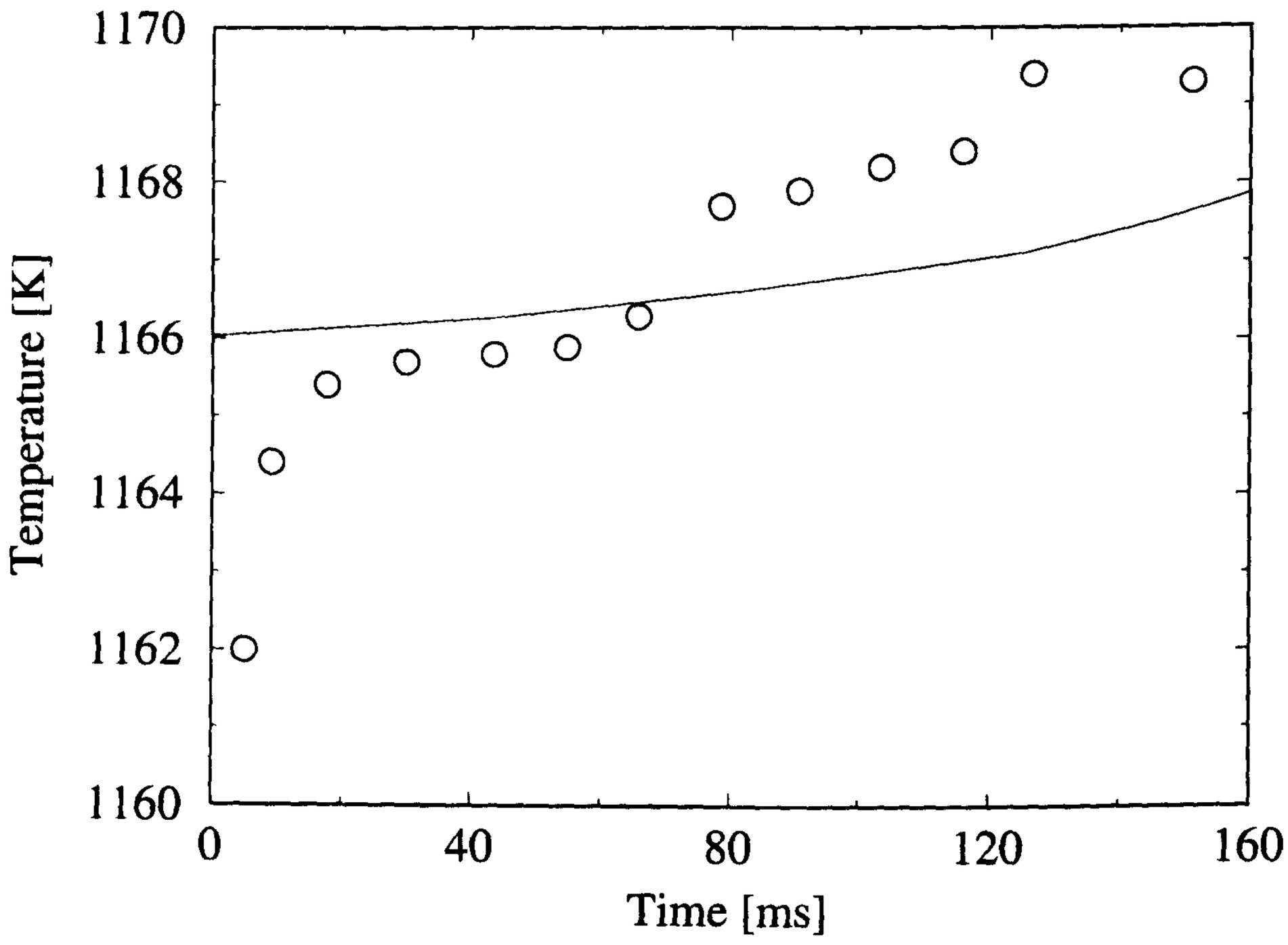


Figure 4.45: Graph of temperature profile versus time for the oxidation of 1 – methylnaphthalene in a Turbulent Flow Reactor. Experimental points are from Shaddix [226] for a stoichiometry of $\phi = 1.5$ for $T_0 = 1198$ K. Solid lines are the computations from the detailed chemical mechanism and have been time shifted by 32 ms.

Primary Reaction Paths for the Oxidation of 1 – methylnaphthalene

The oxidation of 1 – methylnaphthalene in a Jet Stirred Reactor proceeds through a number of chemical paths shown in Figures 4.46 – 4.49. The path analysis conducted here applies to the rich case ($\phi = 1.5$) and a temperature of 1260 K.

As mentioned earlier, the general modelling approach for the oxidation of 1 – methylnaphthalene is based on similarity to that of toluene. The chemical kinetic rates applied in this study for the modelling of the oxidation of 1 – methylnaphthalene are therefore based on the study of toluene oxidation in Section 2.2. The frequency factors have naturally been adjusted for molecular size differences.

The thermal decomposition via C – C cleavage (1393) contributes ~ 10 % under the current conditions.

$$C_{11}H_{10} = C_{10}H_7 + CH_3 \quad (1393)$$

The reaction has been modelled on the analogous toluene reaction (1076).

$$C_7H_8 = C_6H_5 + CH_3 \quad (1076)$$

The detailed chemical kinetic mechanism from Pitsch [203] features the rate parameters from Rao & Skinner [208]. Attack by OH radicals on the fuel contributes a further 15 % (1401)

$$C_{11}H_{10} + OH = C_{11}H_9 + H_2O \quad (1401)$$

The rate parameters for reaction (1401) has been modelled on the analogous reaction (1086).

$$C_7H_8 + OH = C_7H_7 + H_2O \quad (1086)$$

The dominant fuel consumption channel (30 %) is via H radical attack, (1396).

$$C_{11}H_{10} + H \quad = \quad C_{11}H_9 + H_2 \tag{1396}$$

The rate parameters assigned to reaction (1396) have been modelled directly on the analogous reaction (1079).

$$C_7H_8 + H \quad = \quad C_7H_7 + H_2 \tag{1079}$$

The study of 1 – methylnaphthalene oxidation in a Turbulent Flow Reactor by Pitsch [203] features the rate parameters as recommended by Hippler *et al.* [125] as discussed previously in the text.

Additionally, H radical attack contributes a further 10 % via attack on the methyl group (1395).

$$C_{11}H_{10} + H \quad = \quad C_{10}H_8 + CH_3 \tag{1395}$$

The rate assigned to reaction (1395) is modelled on the analogous reaction (1078).

$$C_7H_8 + H \quad = \quad C_6H_6 + CH_3 \tag{1078}$$

The rate parameters implemented for reaction (1078) have been obtained from Robaugh & Tsang [219] as discussed above.

The O radical attack on the ring results in the expulsion of H radicals (1400) and contributes 15 % to the consumption of the fuel.

$$C_{11}H_{10} + O \quad = \quad OC_{11}H_9 + H \tag{1400}$$

The rate (1400) is modelled on reaction (1083).

$$C_7H_8 + O \quad = \quad OC_7H_7 + H \tag{1083}$$

A further 10 % is consumed via ring attack by OH radicals abstracting an H atom (1402).

$$C_{11}H_{10} + OH = C_{11}H_9P + H_2O \quad (1402)$$

The rate for reaction (1402) has been modelled on the equivalent toluene reaction (1090).

$$C_7H_8 + OH = C_7H_7P + H_2O \quad (1090)$$

The rate for reaction (1090) is in turn modelled on reaction (960)

$$C_6H_6 + OH = C_6H_5 + H_2O \quad (960)$$

with the rate adopted from the work of Baulch *et al.* [13].

The $C_{11}H_9$ radical produced from reactions (1401) and (1396) undergoes H addition (60 %) to form $C_{11}H_{10}$ (1394).

$$C_{11}H_{10} = C_{11}H_9 + H \quad (1394)$$

The rate for reaction (1394) has been modelled directly on the analogous reaction (1077).

$$C_7H_8 = C_7H_7 + H \quad (1077)$$

Additionally, O_2 and OH attack contribute 10 % and 15 % respectively, to the consumption of $C_{11}H_9$ via (1383) and (1380).

$$C_{11}H_9 + O_2 = C_{11}H_9O + O \quad (1383)$$
$$C_{11}H_9 + OH = C_{11}H_9O + H \quad (1380)$$

The rates for reactions (1383) and (1380) have been modelled on the following analogous reactions.

$$CH_3 + O_2 = CH_3O + O \quad (76)$$
$$CH_3 + OH = CH_3O + H \quad (66)$$

The rates for reactions (76) and (66) have been adopted from the studies by Dean & Westmoreland [74] and Baulch *et al.* [13] respectively [162]. By contrast, the detailed chemical mechanism from Pitsch [203] features a global step for reaction (1383) with the following product distribution [203],

$$C_{11}H_9 + O_2 = C_{11}H_8O + O + H$$

The estimated rate parameters for the above reaction were obtained from Brezinksy *et al.* [28].

The $C_{11}H_9O$ radical produced from reactions (1383) and (1380) is further decomposed thermally via C – H cleavage and C – C cleavage with reactions (1427) and (1425) contributing 60 % and 40 % respectively.

$$C_{11}H_9O = C_{11}H_8O + H \quad (1427)$$
$$C_{11}H_9O = C_{10}H_8 + CHO \quad (1425)$$

The rates for reactions (1427) and (1425) have been modelled on the analogous reactions given below.

$$C_7H_7O = C_7H_6O + H \quad (1113)$$
$$C_7H_7O = C_6H_6 + CHO \quad (1111)$$

The $C_{11}H_8O$ formed in reaction (1427) is consumed (25 %) through thermal decomposition via C – H cleavage (1415), while radical attack via OH (1420) contributes 15 %, the H radical (1417) 20 %, the O radical (1418) 25 %.

$$C_{11}H_8O = C_{11}H_7O + H \quad (1415)$$
$$C_{11}H_8O + OH = C_{11}H_7O + H_2O \quad (1420)$$
$$C_{11}H_8O + H = C_{11}H_7O + H_2 \quad (1417)$$
$$C_{11}H_8O + O = C_{10}H_8 + CO_2 \quad (1418)$$

Reactions (1415), (1420) and (1417) feature consumption of the side chain and reaction (1418) is a side chain addition – decomposition reaction. The rate parameters adopted for reactions (1415), (1417), (1418) and (1420) are modelled on analogous reactions.

$$C_7H_6O = C_6H_5CO + H \quad (1101)$$
$$C_7H_6O + OH = C_6H_5CO + H_2O \quad (1106)$$
$$C_7H_6O + H = C_6H_5CO + H_2 \quad (1103)$$
$$C_7H_6O + O = C_6H_6 + CO_2 \quad (1104)$$

The $C_{11}H_7O$ radical, formed in reactions (1415), (1420), and (1417), is consumed (100 %) via thermal decomposition (1413).

$$C_{11}H_7O = C_{10}H_7 + CO \quad (1413)$$

The rate assigned to reaction (1413) is obtained from the analogous reaction (1099).

$$C_6H_5CO = C_6H_5 + CO \quad (1099)$$

The product ($OC_{11}H_9$) of reaction (1400), decomposes (100 %) via reaction (1434) with the rate being obtained from the analogous reaction (1120).

$$OC_{11}H_9 = C_9H_6CH_3 + CO \quad (1434)$$
$$OC_7H_7 = C_5H_4CH_3 + CO \quad (1120)$$

The $C_9H_6CH_3$ radical undergoes thermal decomposition (75 %) via C – H cleavage (1349).

$$C_9H_6CH_3 = C_9H_6CH_2 + H \quad (1349)$$

The rate for reaction (1349) has been estimated by Laskin and Lifshitz [157] who comment that it is modelled on analogy with the reaction pathway in the context of C_5H_5 and CH_3 radicals. A further 25 % is consumed via H addition to form $C_9H_7CH_3$ (1362)

$$C_9H_7CH_3 = C_9H_6CH_3 + H \quad (1362)$$

with the rate for reaction (1362) obtained from Laskin and Lifshitz [157]. The $C_9H_7CH_3$ radical formed from the reverse of reaction (1362), thermally decomposes via C – C cleavage (100 %) forming C_9H_7 and CH_3 (1272).

$$C_9H_7 + CH_3 = C_9H_7CH_3 \quad (1272)$$

The rate for reaction (1272) has been obtained from Laskin and Lifshitz [157]. The $C_9H_6CH_2$ isomer forms $C_{10}H_8$ via reactions (1332) and (1331), which contribute 70 % and 30 % respectively. The rate for reaction (1331) has been adopted from Laskin and Lifshitz [157].

$$C_9H_6CH_2 + H = C_{10}H_8 + H \quad (1332)$$
$$C_9H_6CH_2 = C_{10}H_8 \quad (1331)$$

The $C_{11}H_9P$ radical formed in reaction (1402), undergoes O_2 addition with (1391) and (1392) contributing 70 % and 30 % respectively.

$$C_{11}H_9P + O_2 = OC_{11}H_9 + O \quad (1391)$$
$$C_{11}H_9P + O_2 = C_{11}H_9OOP \quad (1392)$$

The rate for reaction (1391) is obtained from the analogous reaction (930) studied by Frank *et al.* [94].

$$C_6H_5 + O_2 \quad = \quad C_6H_5O + O \tag{930}$$

The O_2 addition reaction (1392) is modelled on reaction (931).

$$C_6H_5 + O_2 \quad = \quad C_6H_5OO \tag{931}$$

The rate for reaction (931) was evaluated by DiNaro *et al.* [76] and is based on the work on C_6H_5 reactions with molecular oxygen by Yu and Lin [271] who considered a temperature and pressure range of 297 – 500 K and 2.63E-02 – 1.1E-01 atm. The product of reaction (931) decomposes (100 %) via reaction (1450) with the rate assigned from the analogous reaction (1008) obtained by DiNaro *et al.* [76].

$$OOC_{11}H_9P \quad = \quad OC_{11}H_9 + O \tag{1450}$$

$$C_6H_5OO \quad = \quad C_6H_5O + O \tag{1008}$$

DiNaro *et al.* [76] comment that reaction (1008) has been evaluated by QRRK analysis, and there are still uncertainties in the rate parameters for the consumption paths of C_6H_5OO [76]. The $OC_{11}H_9$ radical is consumed via reaction (1434) as discussed previously.

The consumption paths of $C_{10}H_8$ and $C_{10}H_7$ have been discussed in the previous section which considers the oxidation of naphthalene in a Turbulent Flow Reactor.

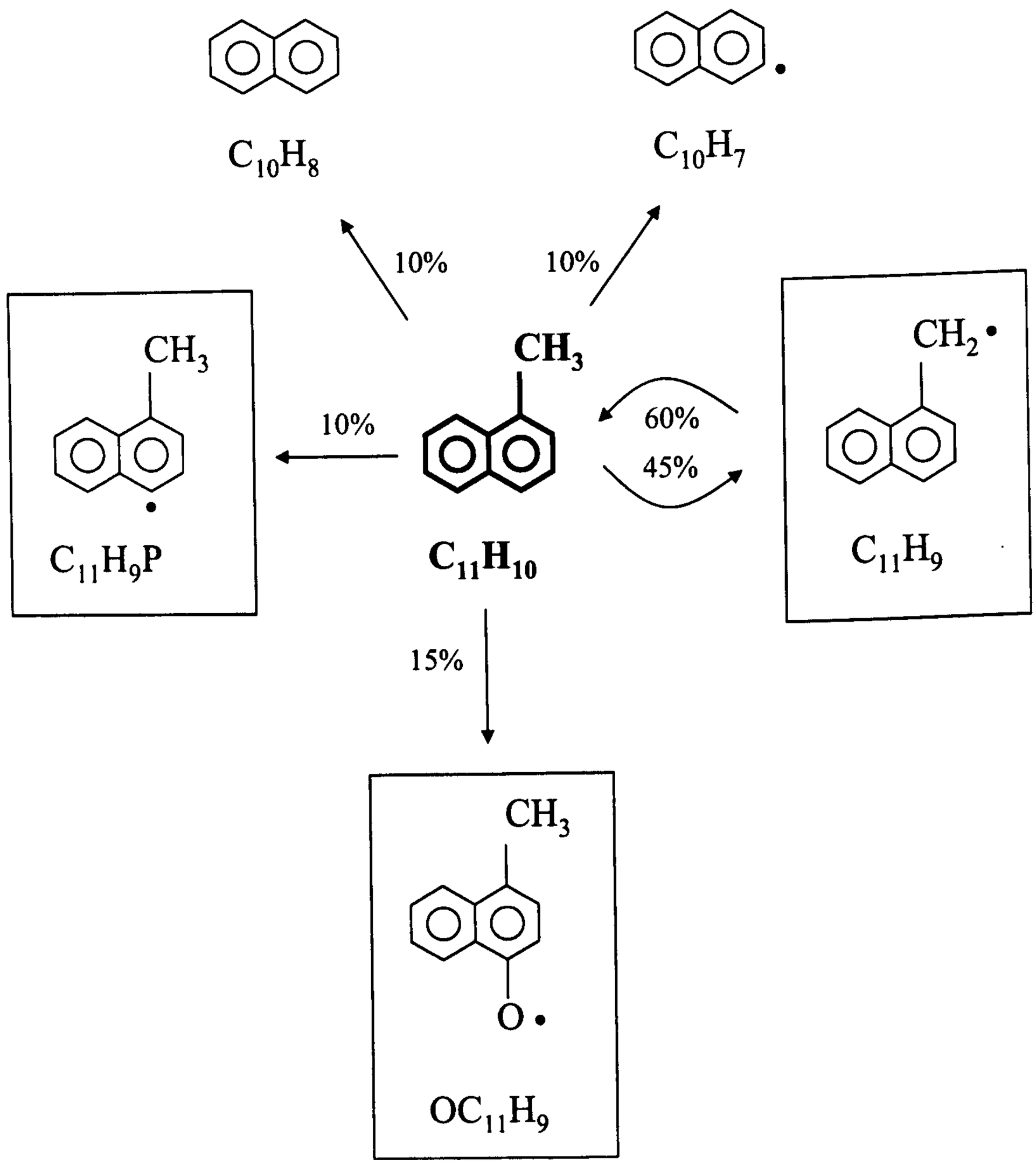


Figure 4.46: Diagram illustrating the consumption paths of the fuel 1 – methylnaphthalene and its intermediate species in a Jet Stirred Reactor (T = 1260 K, P = 1 atm., ϕ = 1.5). Species in boxes are considered in subsequent pages.

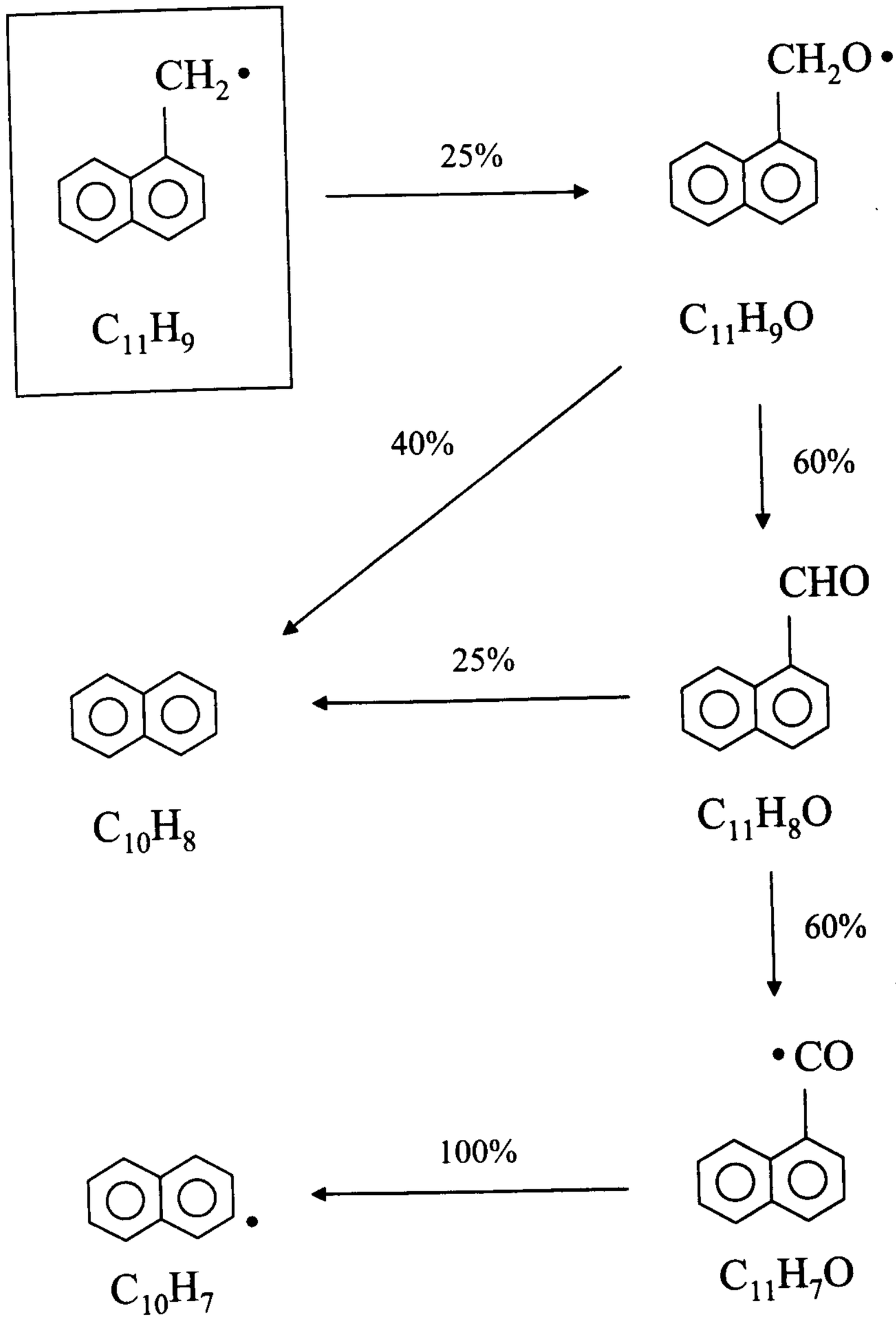


Figure 4.47: Diagram illustrating the consumption paths of the fuel 1 – methylnaphthalene and its intermediate species in a Jet Stirred Reactor (T = 1260 K, P = 1 atm., ϕ = 1.5). Species in boxes are considered in subsequent pages.

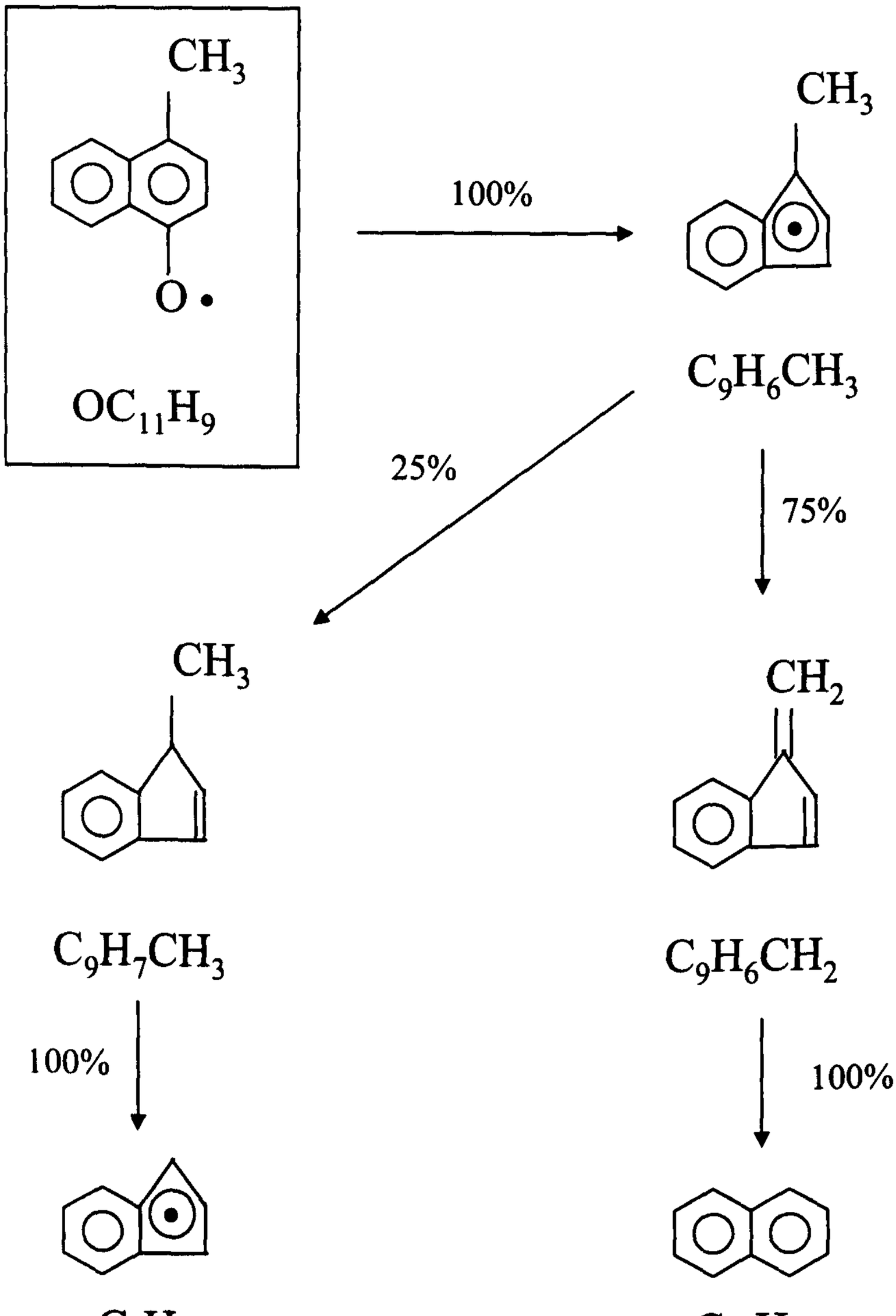


Figure 4.48: Diagram illustrating the consumption paths of the fuel 1 – methylnaphthalene and its intermediate species in a Jet Stirred Reactor (T = 1260 K, P = 1 atm., ϕ = 1.5). Species in boxes are considered in subsequent pages.

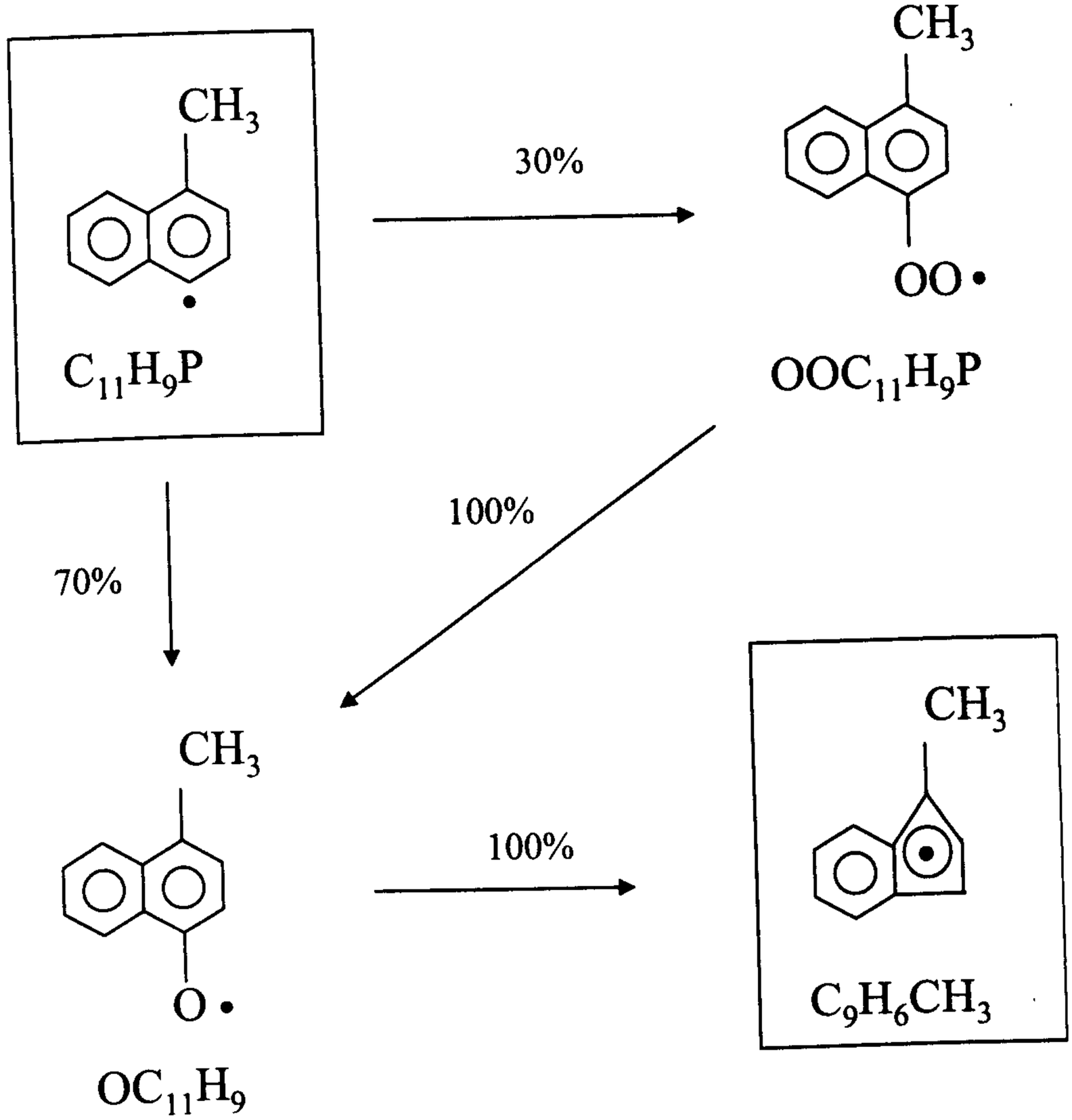


Figure 4.49: Diagram illustrating the consumption paths of the fuel 1 – methylnaphthalene and its intermediate species in a Jet Stirred Reactor (T = 1260 K, P = 1 atm., ϕ = 1.5). Species in boxes are considered in subsequent pages.

4.3.2 The Oxidation of 1 – methylnaphthalene in a Shock Tube

Ignition delay times have been studied using the data from Pfahl *et al.* [202]. The experimental set up considers 1 – methylnaphthalene – air mixtures for a stoichiometry of $\phi = 1.0$ at pressure of 13 atm. and a temperature range of 940 – 1300 K. Pfahl *et al.* [202] comment that the ignition delay time is defined as the time between the reflection of the shock wave and the first pressure rise. However, for the calculations the maximum temporal derivative of the temperature is chosen to indicate the ignition time [203]. Figure 4.50 illustrates the computations from the detailed chemical mechanism with the experimental data from Pfahl *et al.* [202].

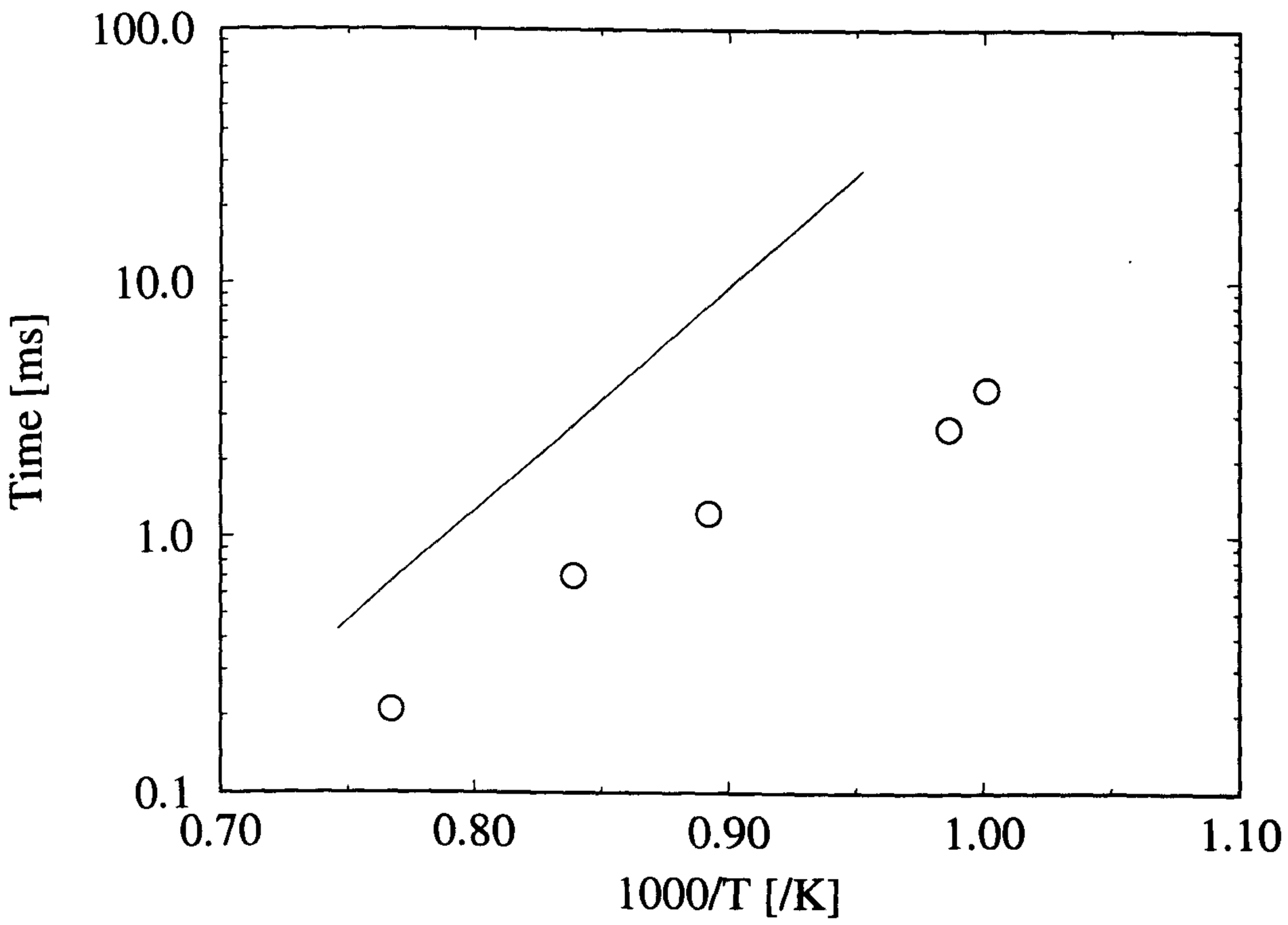


Figure 4.50: Comparison of computed (lines) and measured (symbols) ignition delay times for stoichiometric 1 – methylnaphthalene – air mixtures. Experimental points are from Pfahl *et al.* [202].

The detailed chemical mechanism fails to predict accurately the ignition delay times as shown in Figure 4.50. However, it has been reported by Pfahl *et al.* [202] that flame kernels have been observed in the Shock Tube prior to detonation. The propagating flames led to an additional compression of the unburned mixture which therefore implies that the corresponding ignition delay times are reduced, hence the experimental points obtained from Pfahl *et al.* [202] may be considered to be a lower limit.

In the study by Pitsch [203], the predictions of the experimental data are of reasonable accuracy. However, the reactions constituting the 1 – methylnaphthalene detailed sub – mechanism from Pitsch [203] are primarily based on the toluene oxidation study by Emdee *et al.* [89]. It has been discussed previously that the reaction rate parameters used by Emdee *et al.* [89] for reactions such as

$$\begin{aligned} C_7H_8 + O_2 &= C_7H_7 + HO_2 \\ C_7H_7 + HO_2 &= C_7H_6O + OH + H \end{aligned} \tag{1091}$$

with the 1 – methylnaphthalene analogous equivalent being

$$\begin{aligned} C_{11}H_{10} + O_2 &= C_{11}H_9 + HO_2 \\ C_{11}H_9 + HO_2 &= C_{11}H_8O + OH + H \end{aligned} \tag{1406}$$

are inaccurate.

At a temperature of 1200 K and a reaction time of ~ 10 μs, the radical pool is generated by the initiation reaction (1406)

$$C_{11}H_{10} + O_2 = C_{11}H_9 + HO_2 \tag{1406}$$

which is in agreement with the detailed chemical mechanism from Pitsch [203]. Further attack on the fuel proceeds via the consumption of the HO_2 radicals produced from reaction (1406) as in reaction (1408)

$$C_{11}H_{10} + HO_2 \quad = \quad C_{11}H_9 + H_2O_2 \tag{1408}$$

also in agreement with the study by Pitsch [203]. The rate for reaction (1408) is modelled on the direct analogous equivalent reaction (1092)

$$C_7H_8 + HO_2 \quad = \quad C_{11}H_9 + H_2O_2 \tag{1092}$$

where the rate for reaction (1092) is obtained from Baulch *et al.* [14]. The H_2O_2 produced from reaction (1092) goes on to further chain branching via reaction (16)

$$H_2O_2 + M \quad = \quad OH + OH + M \tag{16}$$

again in agreement with Pitsch [203].

4.3.3 Discussion

A sub – mechanism describing the oxidation of 1 – methylnaphthalene has been incorporated into a hierachally constructed detailed chemical mechanism for hydrocarbon combustion. The mechanism has been systematically evaluated by quantitative comparisons under JSR conditions with the experimental data obtained from Dagaut [55]. The data covers an overall temperature range of 1090 – 1440 K for a variety of stoichiometries (ϕ = 0.5, 1.0 and 1.5). The overall performance of the detailed mechanism is encouraging with regards to the computations for a large variety of species both high up and low down the chain. As mentioned previously, the 1 – methylnaphthalene sub – mechanism has been based on the toluene sub – mechanism. In contrast to the current study the detailed chemical kinetic mechanism for 1 – methylnaphthalene from Pitsch [203] does not feature ring attack. New formation paths in the context of C_5H_5 and CH_3 radicals regarding $C_{10}H_8$

formation have also been investigated here. Additionally, the detailed chemical kinetic mechanism for 1 – methylnaphthalene from Pitsch [203] features many global reaction steps as well as adjustments to the rate parameters to produce more accurate calculations with respect to the experimental data. These have been replaced by elementary reaction steps in this study, with the application of legitimate rate parameters.

The species profile concentrations for the stoichiometric case was found to be poor for temperatures $\geq$ 1280 K as is evident in Figures 4.13 – 4.16. It was found that an ignition phenomena had occured resulting in a rapid rise in the final temperature as illustrated in Figure 4.21.

4.4 The Formation of Acenaphthalene

The formation of acenaphthalene during the oxidation of 1– methylnaphthalene has also been considered under Turbulent Flow Reactor conditions.

The acenaphthalene concentration profiles are illustrated in Figure 4.51 for lean, stoichiometric and both rich cases. Although the trends are good, the magnitudes are under predicted. It is evident that in the lean case, consumption of acenaphthalene occurs at later reaction times and such steps are not considered in this mechanism.

The primary reaction path for acenaphthalene is via the interaction of indenyl and propargyl radicals in the global reaction step of (1463) and the rate for this reaction is estimated.

$$C_9H_7 + C_3H_3 \quad = \quad AC_{12}H_8 + H_2 \tag{1463}$$

The formation of acenaphthalene in naphthalene fuels is also considered. Figure 4.52 illustrates the species concentration profile for acenaphthalene.

The initial growth within the fist 30 ms is predicted well. However for later reaction times consumption of acenaphthalene takes place which is not considered within this detailed chemical mechanism. Reaction (1463) is again found to be the major reaction path for acenaphthalene formation.

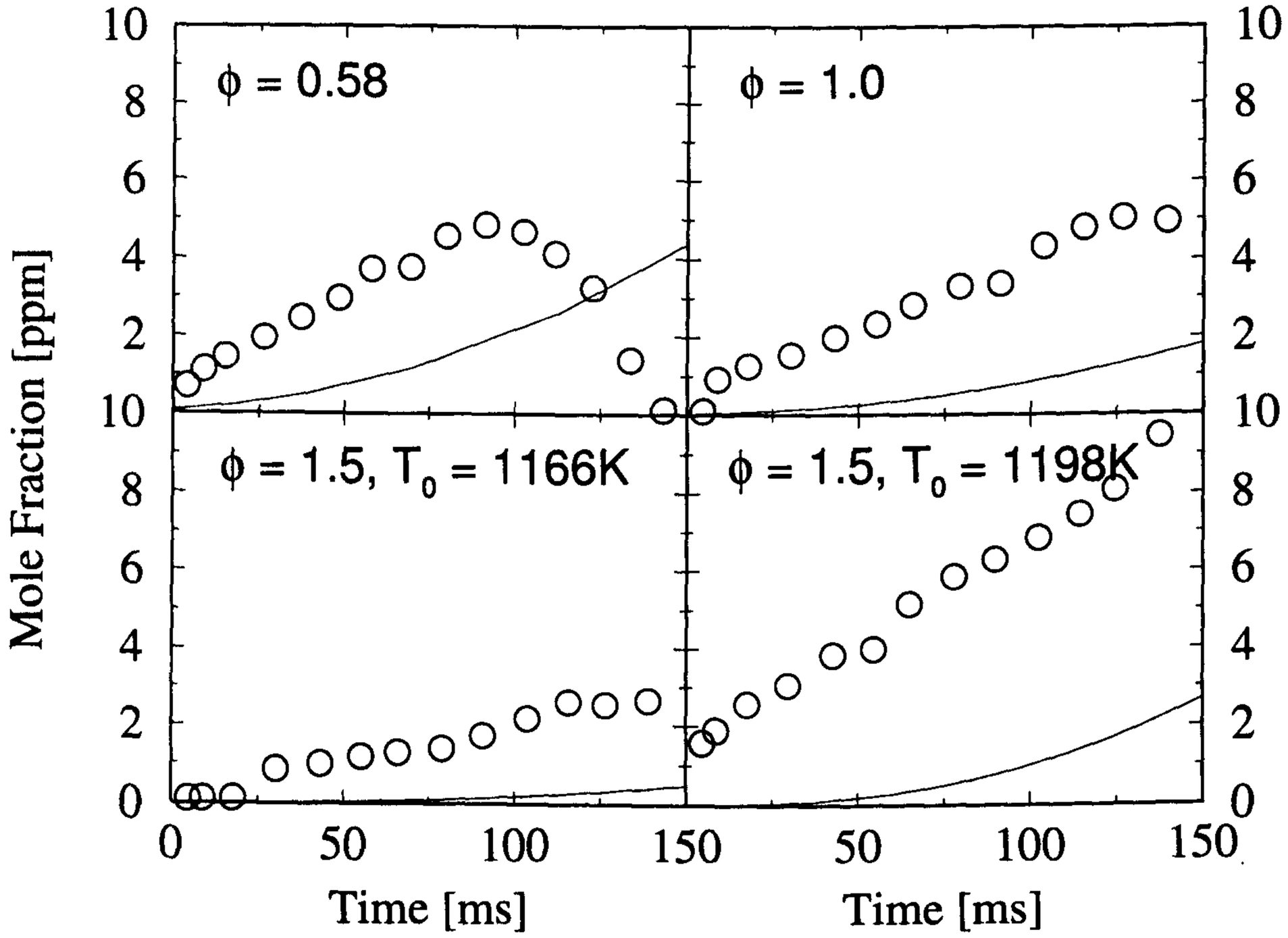


Figure 4.51: Graph of acenaphthalene profile concentrations versus time for the oxidation of 1 – methylnaphthalene in a Turbulent Flow Reactor for the various stoichiometries. Experimental points are from Shaddix [226]. Solid lines are the computations from the detailed chemical mechanism and have been time shifted by 32 ms.

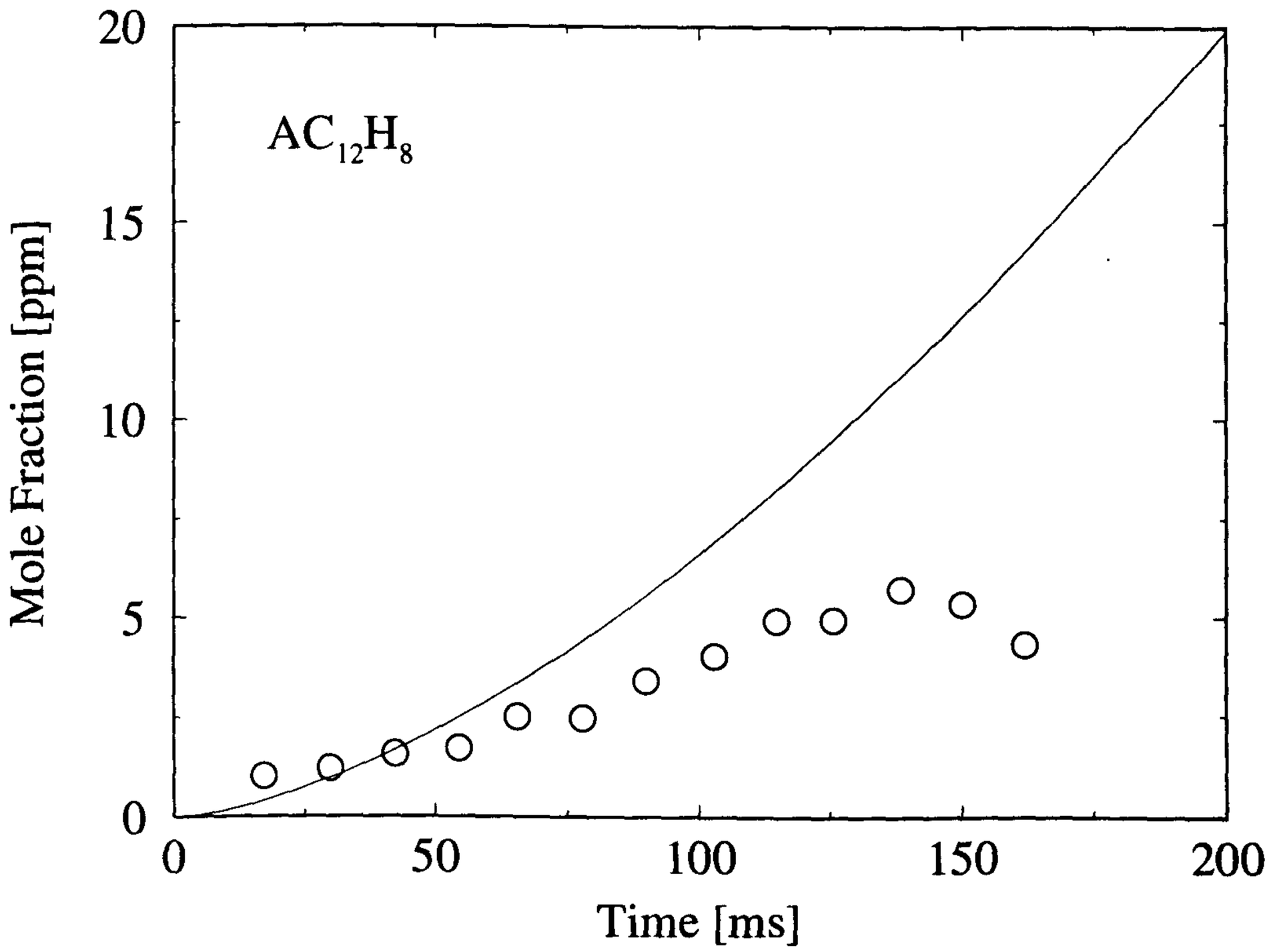


Figure 4.52: Graph of acenaphthalene profile concentrations versus time for the oxidation of naphthalene in a Turbulent Flow Reactor. Experimental points are from Shaddix [226]. Solid lines are the computations from the detailed chemical mechanism and have not been time shifted.

4.5 Summary

In the present Chapter, a comprehensive detailed reaction mechanism for the oxidation of naphthalene and 1 – methylnaphthalene has been developed and validated against a variety of experimental datas and fuels. Overall, the detailed chemical kinetic mechanism has been found to perform well. However, there are issues that require further clarification in order to support the development of more accurate detailed chemical kinetic mechanisms. The cleavage of the CH_3 group from the ring needs to have the thermodynamic issues resolved as discussed by Pamidimukkala *et al.* [199] and Rao & Skinner [208]. It is found that in all cases considered in this study, there is an under prediction for the concentration profiles regarding CH_4 which may stem from the unresolved issues in the rate parameters for reaction (1077)

$$C_{11}H_{10} = C_{10}H_7 + CH_3 \quad (1077)$$

The analogy used for developing a comprehensive detailed chemical kinetic mechanism for 1 – methylnaphthalene based on the oxidation of toluene has been shown to work well. However, common problems were also found. For example, the calculations for C_7H_6O and $C_{11}H_8O$ were consistently over predicted for the various fuels. The reactions responsible are (1113), and (1427) for the toluene and 1 – methylnaphthalene and fuels respectively.

$$C_7H_7O = C_7H_6O + H \quad (1113)$$

$$C_{11}H_9O = C_{11}H_8O + H \quad (1427)$$

The over predictions may stem from the uncertainties in the estimation of reaction (1113) and the need to determine fall off curves.

Problems were encountered in some of the experimental data used for mechanism validation as outlined above, and further detailed data is still required to cover as large a variety of conditions as possible.

A comparison of the sub – mechanism for 1 – methylnaphthalene oxidation used in this study with that of Pitsch [203] clearly shows the replacement of fast global reaction steps with elementary reaction sequences improves agreement with the experimental data.

Furthermore, a naphthalene sub – mechanism has been developed based on the analogy with benzene. Low temperature channels have been incorporated from the work of DiNaro *et al.* [76]. Such a mechanism is important, not only for the significance of this species in PAH formation but also due to the high concentration levels encountered in the oxidation of 1 – methylnaphthalene. The performance of the naphthalene sub – mechanism is encouraging, however, additional experimental studies are required for mechanism validation and verification purposes.

Chapter 5

The Oxidation of Kerosene Fuels

5.1 Introduction

The complexities of practical fuels such as kerosene have been outlined in Chapter 1. Due to the composition of kerosene fuels being a mixture of alkanes and alkyl – substituted aromatics, a simplified kerosene fuel blend model is proposed. The alkane component is modelled on n – decane with n – propylbenzene selected as the alkyl – substituted aromatic component. The pure case of n – propylbenzene is investigated in Chapter 3.

5.2 Background

The kerosene fuel blend model used in this study consists of decane and n – propylbenzene representing the paraffin and alkyl – substituted aromatic respectively. A number of experimental and numerical studies have been presented in the past for the paraffin component. Experimental studies suitable

for the validation and verification of the decane sub – mechanism include those of Delfau *et al.* [75], Douté *et al.* [81] and Vovelle *et al.* [254]. The study by Delfau *et al.* [75] features a 5.1% n – decane/41.2% oxygen/53.7% argon flame at a pressure of 0.06 atm. The study by Douté *et al.* [81] comprised a rich ($\phi = 1.7$) 3.2% n – decane/28.6% oxygen/68.2% nitrogen flame at atmospheric pressure. Finally, the experimental data set from Vovelle *et al.* [254] features a rich ($\phi = 2.2$), 8.0% n – decane/56.4% oxygen/35.6% argon, burner stabilised laminar flame. Several detailed kinetic studies have been published using the experimental data from Delfau *et al.* [75], Douté *et al.* [81] and Vovelle *et al.* [254] resulting in varying degrees of accuracy (*e.g.* Battin–Leclerc *et al.* [11], Bikas & Peters [18], Douté *et al.* [82], and Lindstedt & Maurice [167]). Of particular interest is the study by Lindstedt & Maurice [167] who modelled the experimental data of Douté *et al.* [81], consisting of a rich ($\phi = 1.7$) 2.95% kerosene/28.65% oxygen/68.4% nitrogen, burner stabilized laminar flame at atmospheric pressure. Lindstedt & Maurice [167] comment that the fuel model was composed of 89 % n – decane and 11 % aromatics with the aromatic component is varied between benzene, toluene and ethylbenzene. It is interesting to note that Lindstedt & Maurice [167] comment that the consumption paths for the paraffin component, n – decane are unaffected by the presence of the aromatic component, hence different aromatic components will not affect the consumption paths for the paraffin component. Additionally, Douté *et al.* [81] and Vovelle *et al.* [254] report the similarities in the flame structures for n – decane and kerosene flames. The current work builds on that of Lindstedt & Maurice [167] and considers an extension to low and intermediate temperatures.

5.3 The Oxidation of n – decane and n – propylbenzene

5.3.1 Test Case Details

In Chapter 3, the mechanistic validation and verification of the mechanisms for n – propylbenzene, representing a possible monocyclic alkyl – aromatic choice for kerosene fuels, was considered. The next logical step is to study the oxidation of a kerosene fuel mix with n – decane and n – propylbenzene representing the paraffin and monocyclic aromatic components respectively.

The data sets used to validate and verify the n – decane and n – propylbenzene sub – mechanism under Jet Stirred Reactor conditions is obtained from Dagaut & Cathonnet [55]. The model for the kerosene fuel was proposed to consist of 70% n – decane and 30% n – propylbenzene (by weight). The pressure was set to 10 atmospheres and a variety of stoichiometries were selected ($\phi = 0.75$, 1.0, 1.5 and 2.0), with a mean residence time (τ) of 500 ms over a temperature range of 800 – 1100 K. Table 5.1 summarizes the initial conditions for the oxidation of the n – decane and n – propylbenzene kerosene mixture in a Jet Stirred Reactor.

Table 5.1: Summary of the Initial Conditions for the Oxidation of the n – decane and n – propylbenzene kerosene fuel mixture in a Jet Stirred Reactor

ϕ	T_0 [K]	Mean Residence Time [ms]	Pressure [atm.]
0.75	800 – 1100	500	10
1.0	800 – 1100	500	10
1.5	800 – 1100	500	10
2.0	800 – 1100	500	10

Overall the initial calculations for both test cases agree well with the experimental data from Dagaut & Cathonnet [55] as shown in Figures 5.1 – 5.16. For example, the general trend of O_2 consumption increasing with temperature having the order of magnitude of 10,000 ppm is captured, along with the corresponding species predictions having orders of magnitude 1000 ppm, 100 ppm, 10 ppm, 1.0 ppm and 0.1 ppm. The kerosene model may seem somewhat inaccurate as shown by the decane fuel curves at low temperature for the different stoichiometries. However, the complexity of a real fuel mixture must be taken into account. Furthermore, low temperatures establish conditions which are not typical of gas turbine engines and open up additional channels which are only partly considered here. Prediction of the intermediate species and end products are, however, typically well within order of magnitude accuracy, hence providing some justification for the model.

The experimental fuel profiles change to a shallower decay curve with increasing stoichiometry as is evident in Figures 5.1, 5.5, 5.9 and 5.13. This effect is captured by the calculations.

The concentrations for large alkanes, such as $C_4H_8(N)$, $1C_5H_{10}$ and $1C_6H_{12}$, are well predicted for all stoichiometries as is evident in Figures 5.4, 5.8, 5.12 and 5.16. The peak concentrations of $C_4H_8(N)$ are over predicted for all stoichiometries and do not change with temperature. The primary reactions involved in the production of $C_4H_8(N)$ are (702), (1608) and (1744) which contribute 40 %, 15 % and 35 % respectively.

$$C_4H_9(N) + O_2 = C_4H_8(N) + HO_2 \quad (702)$$

$$3C_{10}H_{21} = 1C_6H_{13} + C_4H_8(N) \quad (1608)$$

$$C_7H_{13} = C_3H_5(A) + C_4H_8(N) \quad (1744)$$

The rate parameters adopted for reaction (702) have been discussed in detail by Rizos [218]. The reaction rate parameters applied to reaction (1608)

have been estimated by Maurice [182]. The rate utilised for reaction (1744) stems from the work of Chakir *et al.* [43] as reported by Maurice [182]. The calculations for $1C_6H_{12}$ are respectable in terms of trends. However, in all cases they are over predicted at higher temperatures with the dominant channel being reaction (1611).

$$5C_{10}H_{21} = C_4H_9(N) + 1C_6H_{12} \quad (1611)$$

Predictions for propene are good in terms of trends as shown in Figures 5.4, 5.8, 5.12 and 5.16. However, the magnitudes are approximately 100 ppm too low. It may be postulated that the source for this lack of propene stems from the propyl group chemistry associated with the n – propylbenzene component of the kerosene mix. However, as was noted by Dagaut *et al.* [60] and Litzinger [174] (see discussion in Chapter 3) the levels of propene are surprisingly low for a pure n – propylbenzene fuel. From this it may be concluded that the source of the lack of propene is from the n – decane component of the kerosene mix and not from n – propylbenzene. Due to the high concentrations of this species, it may be postulated that there is a further direct channel.

Styrene concentration levels are reproduced of similar quality to that found in the high pressure n – propylbenzene case (Section 3.3.2) such that the peak is shifted to approximately 100 K higher than for the experimental data as illustrated in Figures 5.3, 5.7, 5.11 and 5.15. Again, uncertainties in the rate parameters and fall off may need to be taken into account for reaction (1189)

$$C_9H_{12} = C_8H_9 + CH_3 \quad (1489)$$

since C_8H_9 thermally decomposes to C_8H_8 via C – H cleavage.

Computations for benzene agree well for all cases as is evident in Figures 5.3, 5.7, 5.11 and 5.15. It is found that for the lean case reaction

$$C_7H_6O + O \quad = \quad C_6H_6 + CO_2 \tag{1104}$$

is the dominant production channel (50 %) whilst reaction (1487)

$$C_9H_{12} + H \quad = \quad C_6H_6 + C_3H_7(N) \tag{1487}$$

contributes (15 %). For the rich case ($\phi = 1.5$), reaction (1104) and (1487) contribute (30 %) each. For the lean and stoichiometric cases at higher temperatures ($\geq$ 980 K), benzene is over predicted. This may be due to ignition phenomena since the growth of the concentration profiles is accurately predicted by the detailed chemical kinetic mechanism.

The trends for phenol are well produced by the detailed chemical kinetic mechanism as illustrated in Figures 5.3, 5.7, 5.11, and 5.15. However, as for the pure n – propylbenzene case investigated in Chapter 3, levels are under predicted. Reaction (1002) is found to be the dominant channel for phenol production with the rate adopted from Baulch *et al.* [13].

$$C_6H_5O + H \quad = \quad C_6H_5OH \tag{1002}$$

Similar to the case for pure n – propylbenzene, the trends for C_7H_6O are well produced. However, the concentration profile for this species are under predicted typically by a factor of 2.5. In all cases it is found that reaction (1113) is the dominant producer of C_7H_6O.

$$C_7H_7O \quad = \quad C_7H_6O + H \tag{1113}$$

Concentrations for C_2H_4 are well reproduced in terms of trend and magnitudes for all cases as is evident in Figures 5.2, 5.6, 5.10 and 5.14. Arguably,

in the lean and stoichiometric case the concentrations are slightly over predicted. At 1000 K, for the lean case it is found that reaction (207) is the dominant channel (35 %).

$$C_2H_5 + O_2 \quad = \quad C_2H_4 + HO_2 \qquad (207)$$

Levels of C_2H_2 are also well produced as shown in Figures 5.2, 5.6, 5.10 and 5.14. It is found that (172) is the dominant channel for production, contributing 70 % and 50 % for the lean ($\phi = 0.75$) and rich ($\phi = 2.0$) cases respectively.

$$C_2H_3 + O_2 \quad = \quad C_2H_2 + HO_2 \qquad (172)$$

The rate for reaction (172) has been reviewed by Rizos [218].

Concentration profiles for CH_2O shown in Figures 5.2, 5.6, 5.10 and 5.14. Reaction (109) contributes 30 % in the lean case and 35 % in the rich case.

$$CH_3O + M \quad = \quad CH_2O + H + M \qquad (109)$$

Methane is predicted well in all cases as is evident in Figures 5.2, 5.6, 5.10 and 5.14. Reaction (84b) contributes 60 % of production in the rich ($\phi = 2.0$) case and 50 % in the lean ($\phi = 0.75$) case.

$$CH_3 + HO_2 \quad = \quad CH_4 + O_2 \qquad (84b)$$

The rate for reaction (84b) has been adopted from Tsang & Hampson [249] who report an uncertainty factor of 5. The rate has been increased by a factor of 3 in this study, well within the uncertainty band. Due to the methyl radical primarily being derived from the alkane component of the fuel via reaction (426) (contributing 40 %) the problem of the methane trends experienced in the pure case of Chapter 3 does not occur in the kerosene mix. The rate for (426) has been discussed by Rizos [218].

$$C_3H_7(N) \quad = \quad C_2H_4 + CH_3 \qquad (426)$$

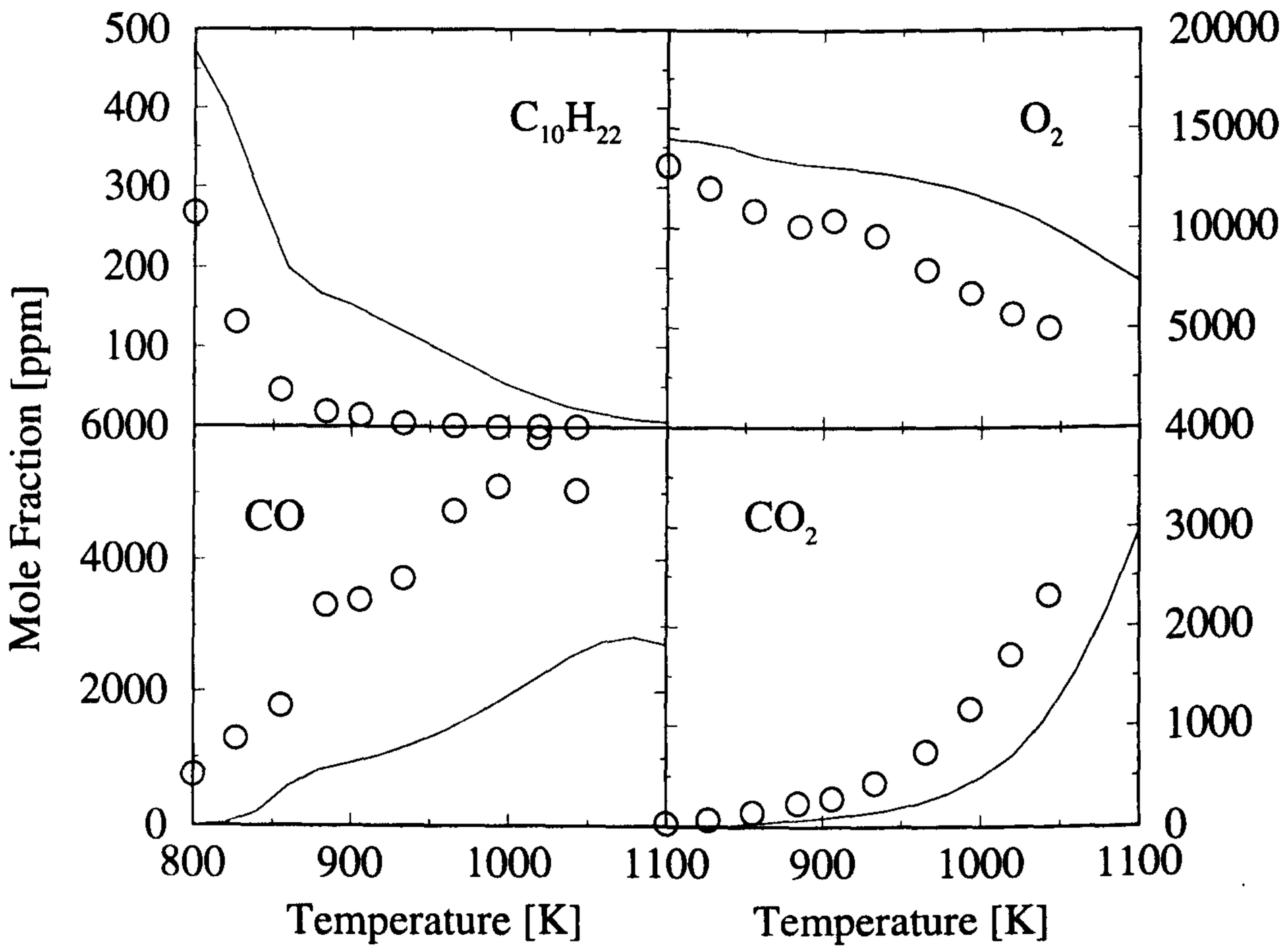


Figure 5.1: Graph of species profile concentrations versus temperature for the oxidation of n – decane and n – propylbenzene constituting the kerosene mix in a Jet Stirred Reactor. Experimental points are from Dagaut & Cathonnet [55] for a stoichiometry of $\phi = 0.75$. Solid lines are the computations from the detailed chemical mechanism.

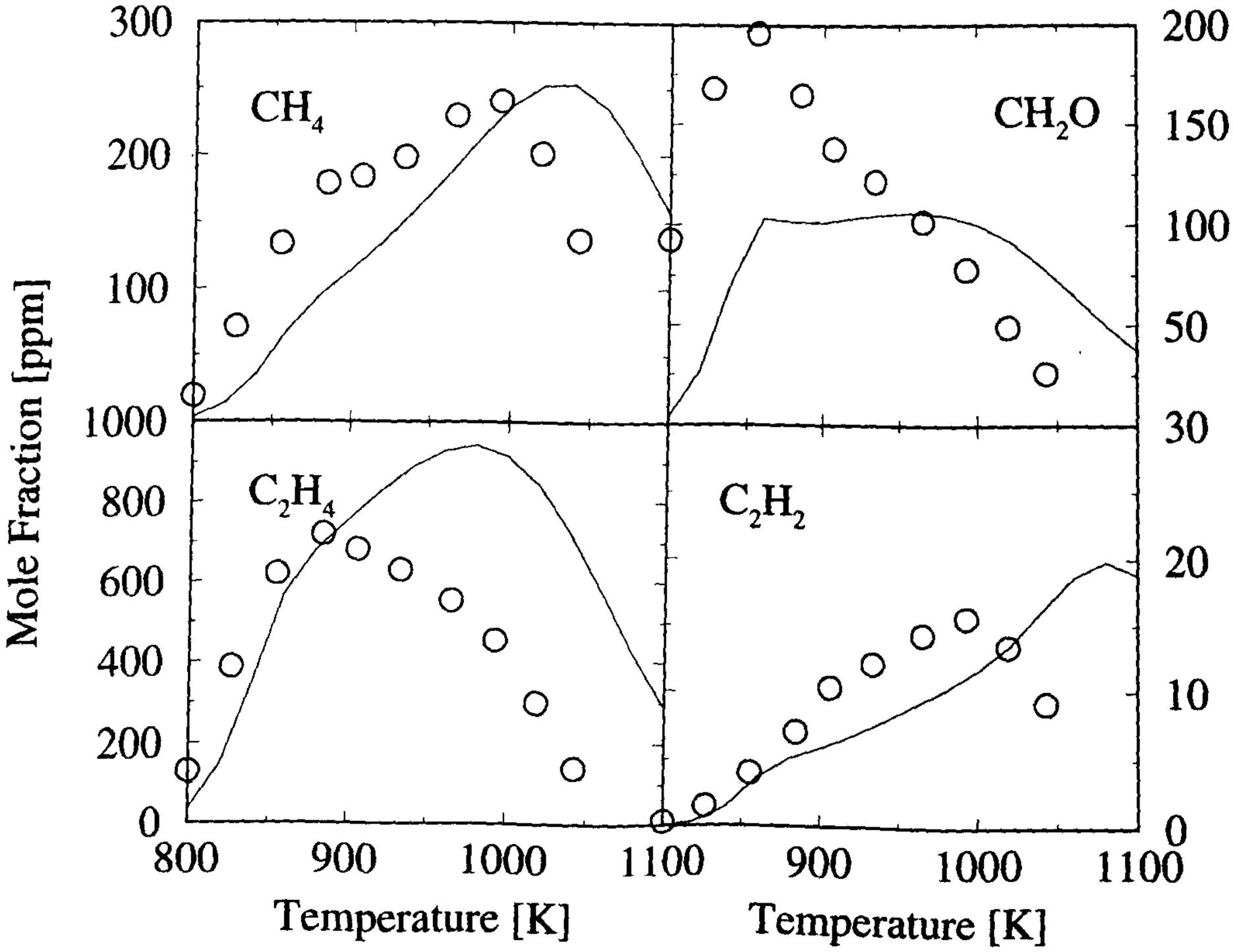


Figure 5.2: Graph of species profile concentrations versus temperature for the oxidation of n – decane and n – propylbenzene constituting the kerosene mix in a Jet Stirred Reactor. Experimental points are from Dagaut & Cathonnet [55] for a stoichiometry of $\phi = 0.75$. Solid lines are the computations from the detailed chemical mechanism.

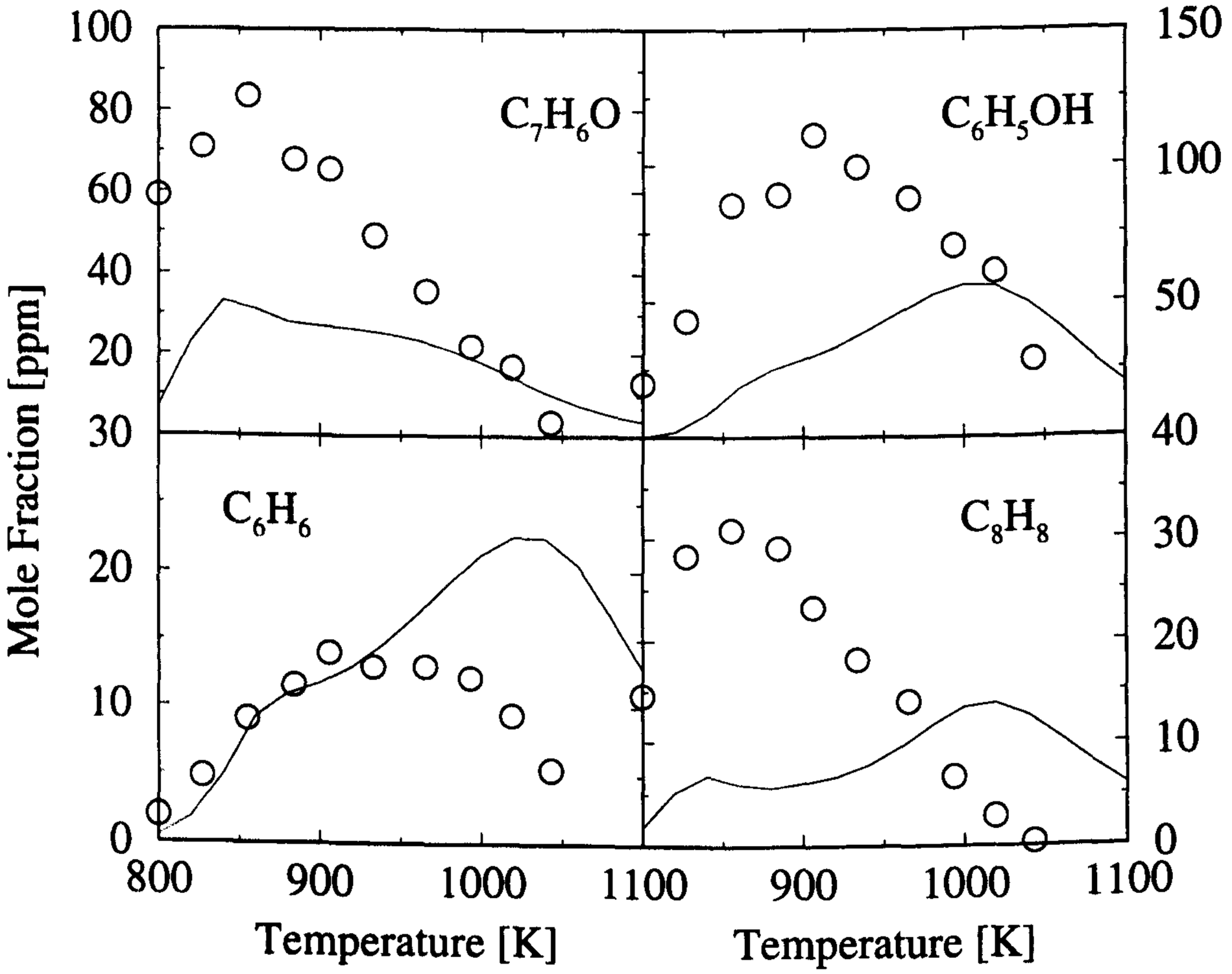


Figure 5.3: Graph of species profile concentrations versus temperature for the oxidation of n – decane and n – propylbenzene constituting the kerosene mix in a Jet Stirred Reactor. Experimental points are from Dagaut & Cathonnet [55] for a stoichiometry of $\phi = 0.75$. Solid lines are the computations from the detailed chemical mechanism.

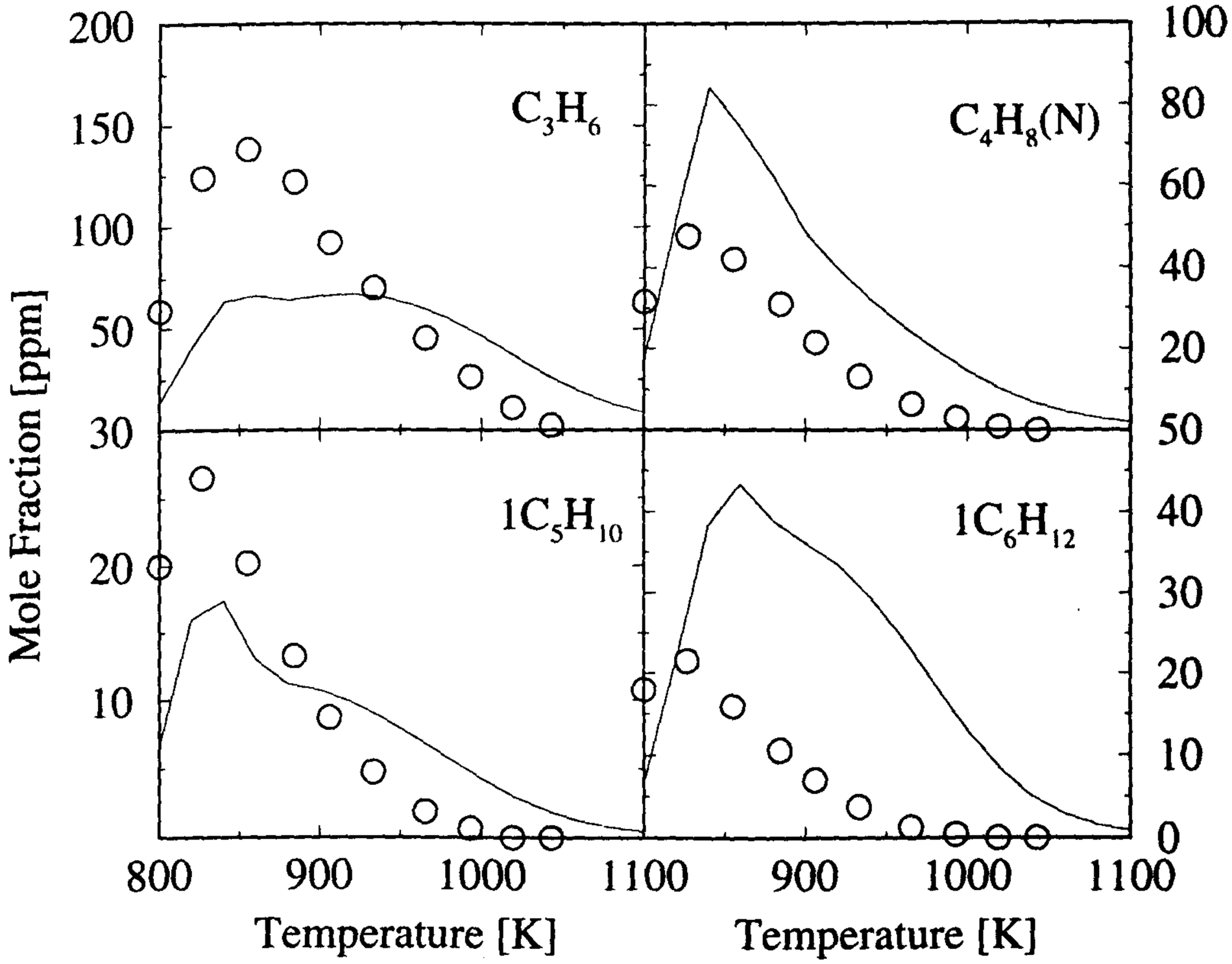


Figure 5.4: Graph of species profile concentrations versus temperature for the oxidation of n – decane and n – propylbenzene constituting the kerosene mix in a Jet Stirred Reactor. Experimental points are from Dagaut & Cathonnet [55] for a stoichiometry of $\phi = 0.75$. Solid lines are the computations from the detailed chemical mechanism.

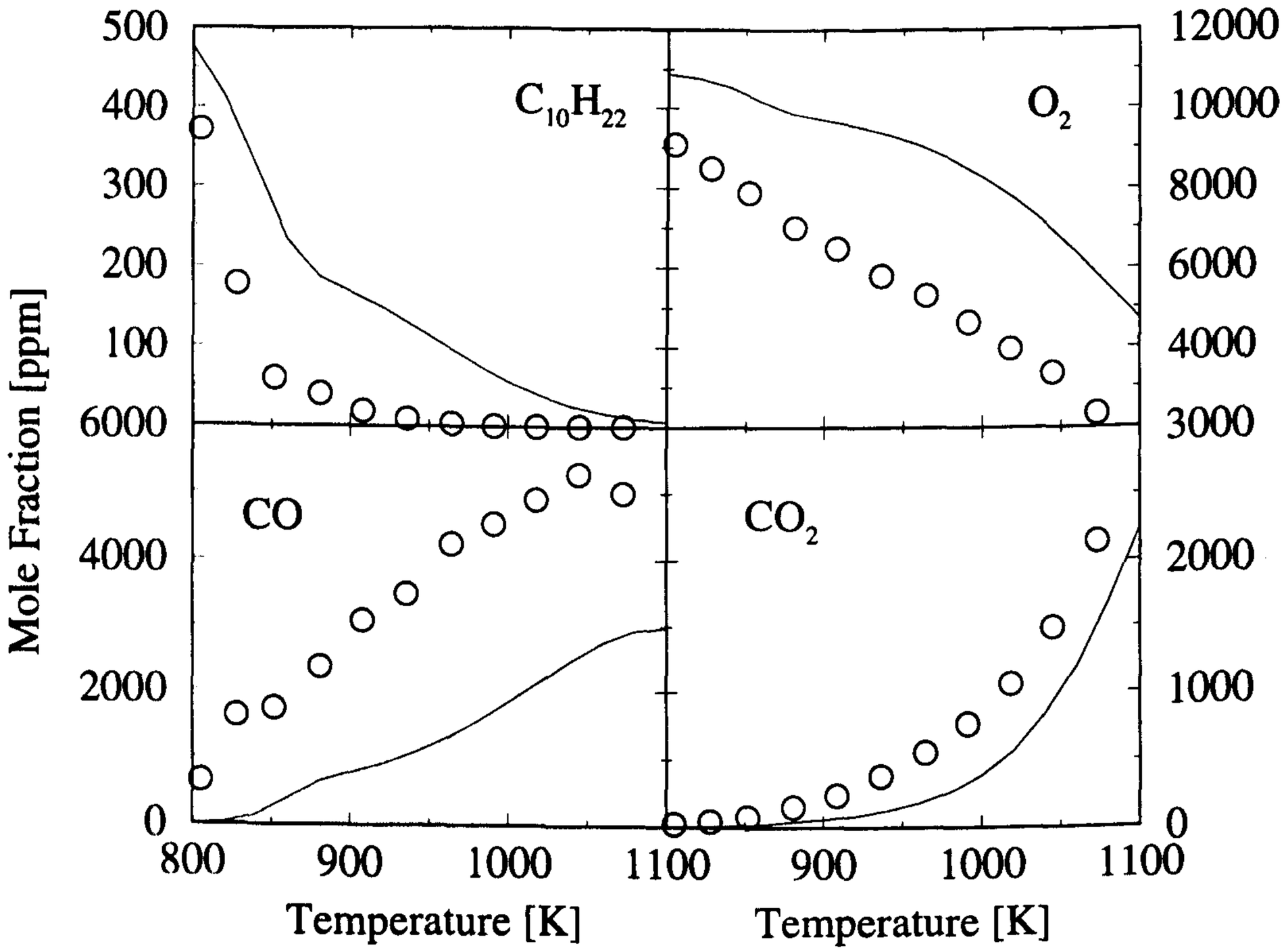


Figure 5.5: Graph of species profile concentrations versus temperature for the oxidation of n – decane and n – propylbenzene constituting the kerosene mix in a Jet Stirred Reactor. Experimental points are from Dagaut & Cathonnet [55] for a stoichiometry of $\phi = 1.0$. Solid lines are the computations from the detailed chemical mechanism.

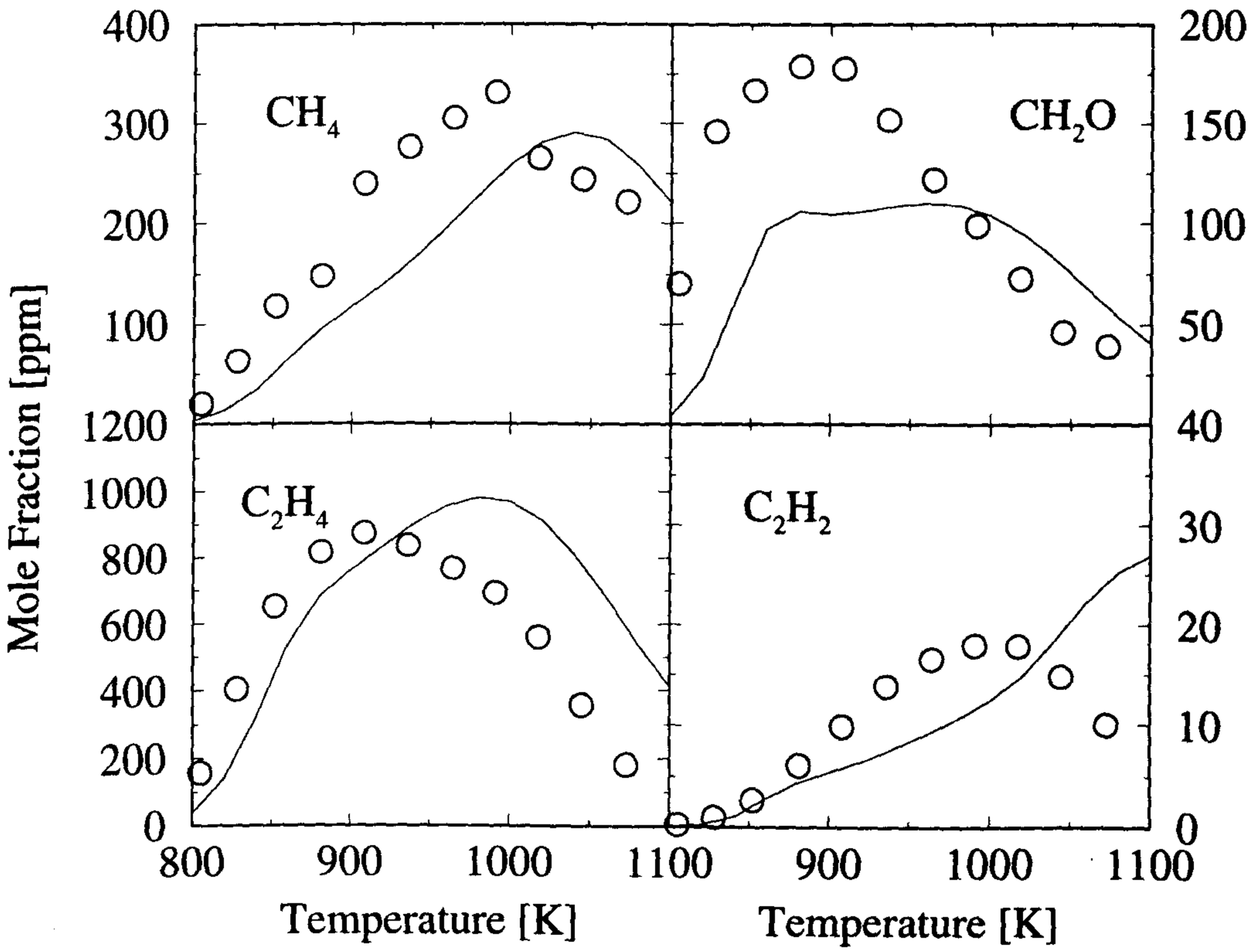


Figure 5.6: Graph of species profile concentrations versus temperature for the oxidation of n – decane and n – propylbenzene constituting the kerosene mix in a Jet Stirred Reactor. Experimental points are from Dagaut & Cathonnet [55] for a stoichiometry of $\phi = 1.0$. Solid lines are the computations from the detailed chemical mechanism.

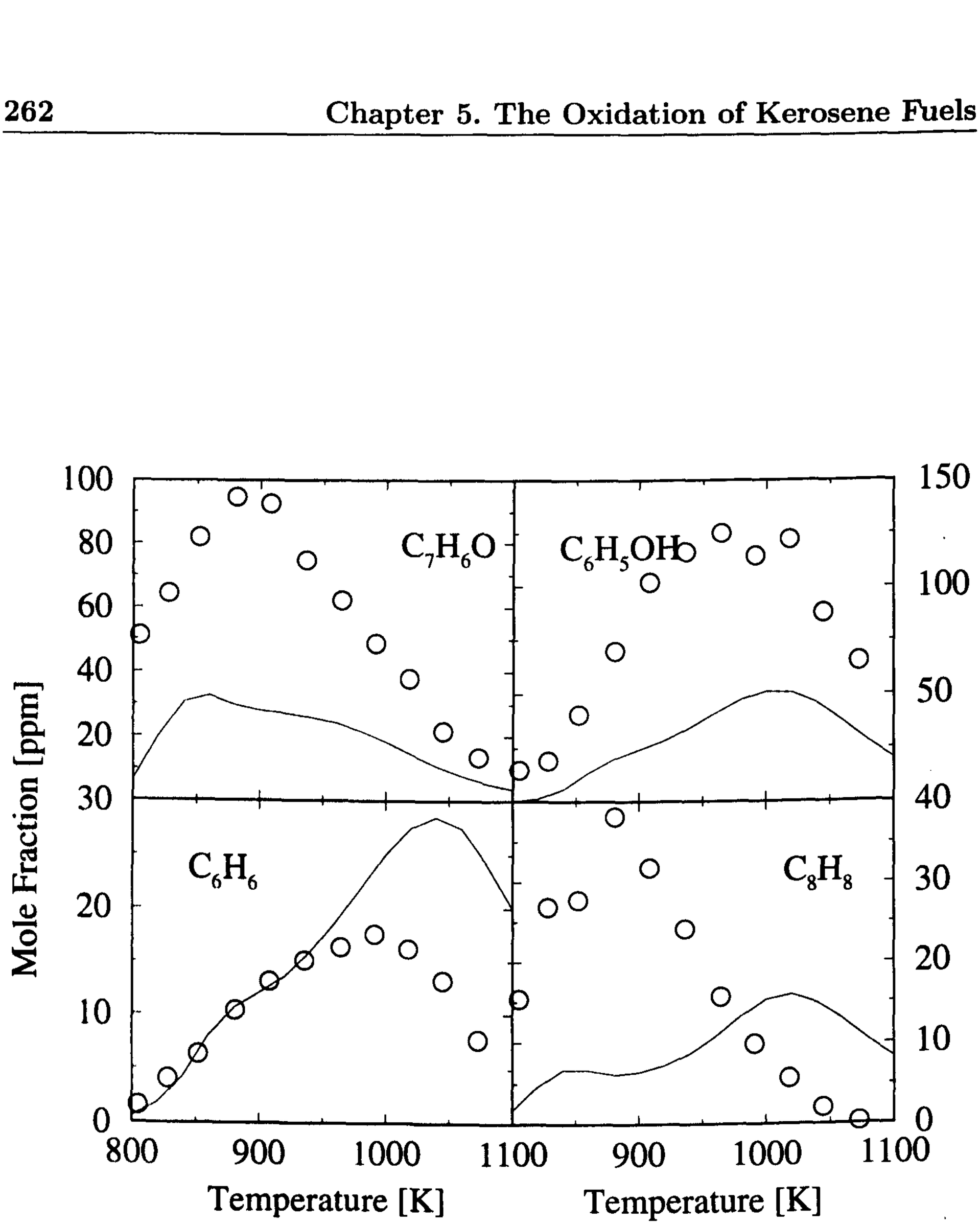


Figure 5.7: Graph of species profile concentrations versus temperature for the oxidation of n – decane and n – propylbenzene constituting the kerosene mix in a Jet Stirred Reactor. Experimental points are from Dagaut & Cathonnet [55] for a stoichiometry of $\phi = 1.0$. Solid lines are the computations from the detailed chemical mechanism.

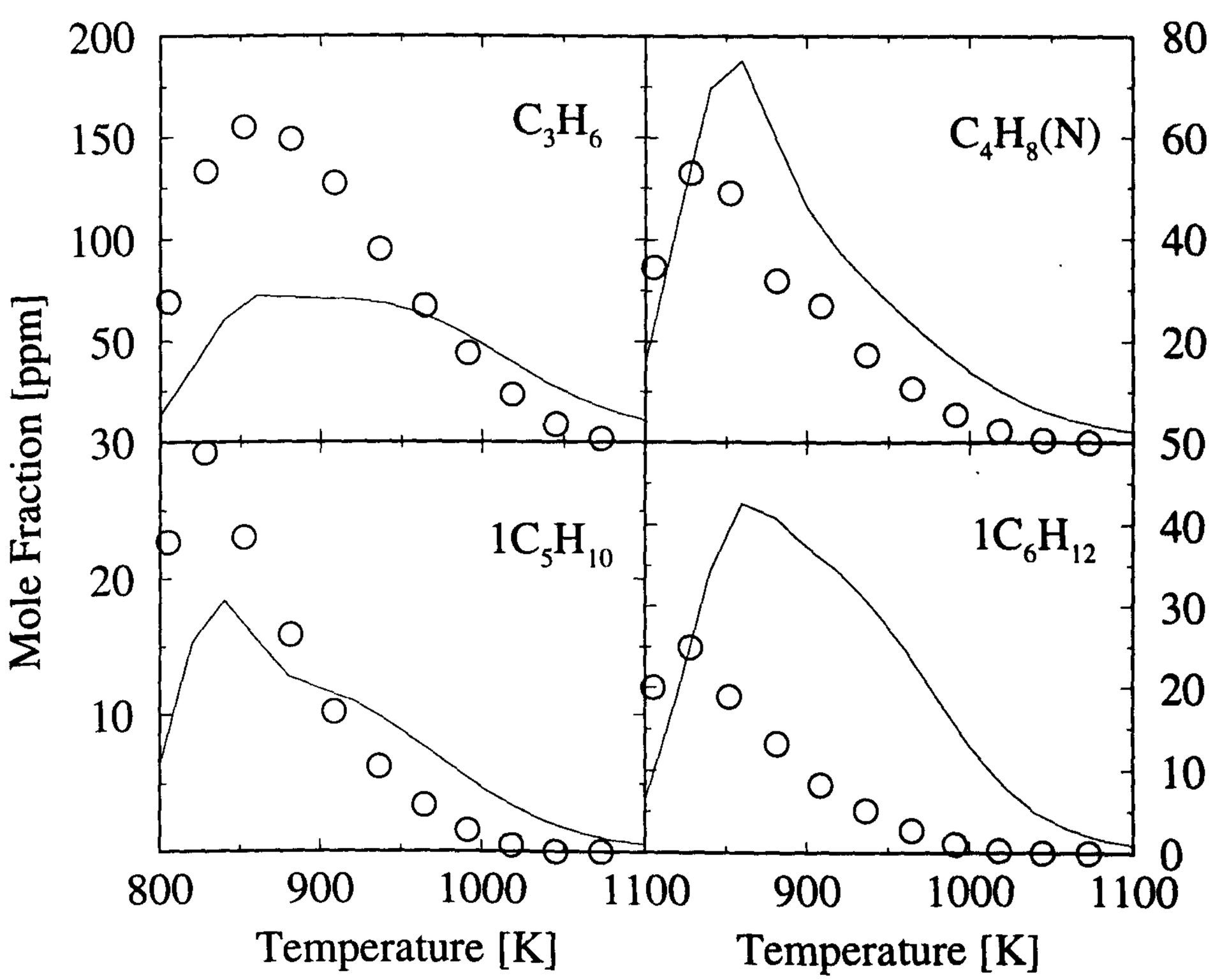


Figure 5.8: Graph of species profile concentrations versus temperature for the oxidation of n – decane and n – propylbenzene constituting the kerosene mix in a Jet Stirred Reactor. Experimental points are from Dagaut & Cathonnet [55] for a stoichiometry of $\phi = 1.0$. Solid lines are the computations from the detailed chemical mechanism.

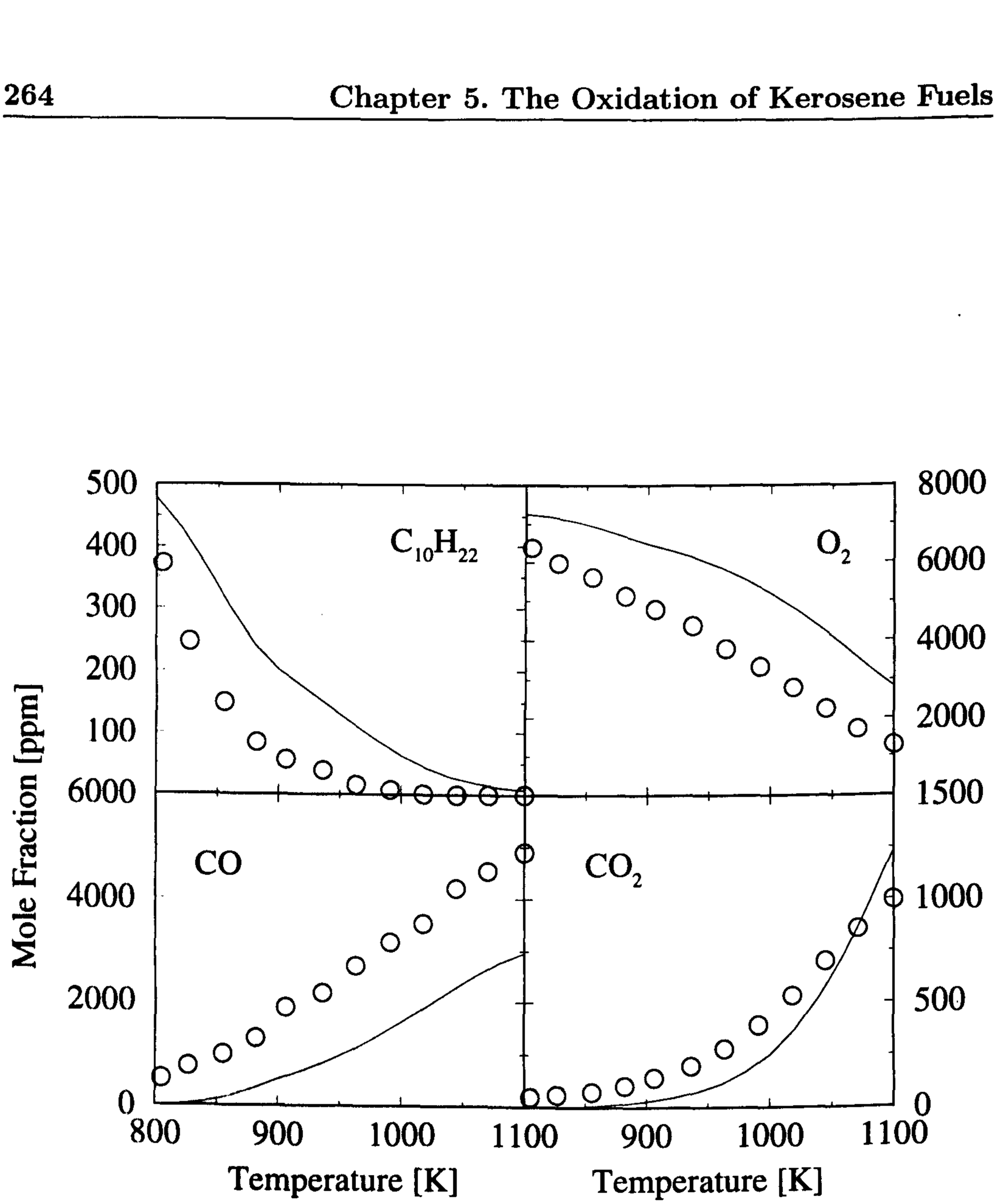


Figure 5.9: Graph of species profile concentrations versus temperature for the oxidation of n – decane and n – propylbenzene constituting the kerosene mix in a Jet Stirred Reactor. Experimental points are from Dagaut & Cathonnet [55] for a stoichiometry of $\phi = 1.5$. Solid lines are the computations from the detailed chemical mechanism.

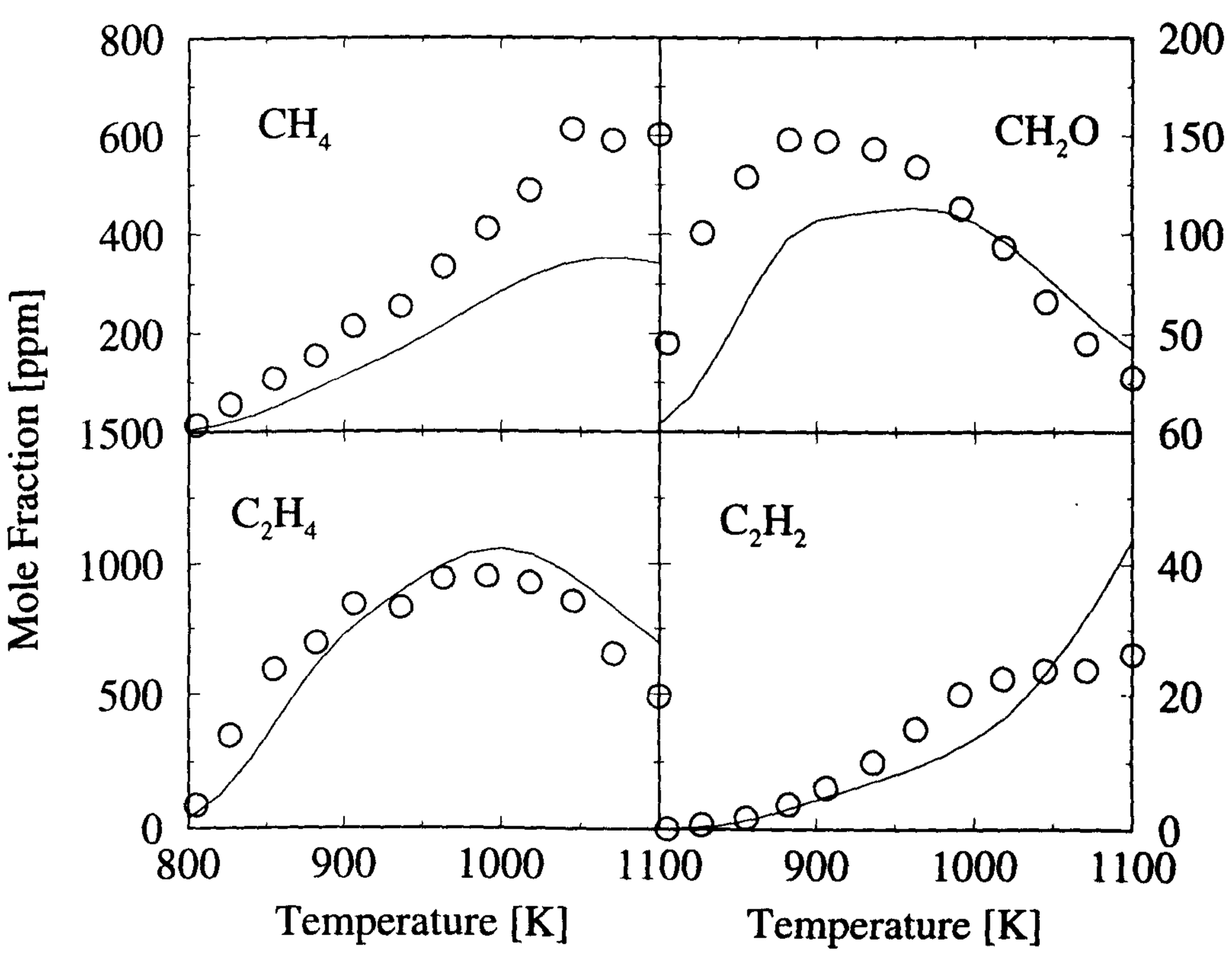


Figure 5.10: Graph of species profile concentrations versus temperature for the oxidation of n – decane and n – propylbenzene constituting the kerosene mix in a Jet Stirred Reactor. Experimental points are from Dagaut & Cathonnet [55] for a stoichiometry of $\phi = 1.5$. Solid lines are the computations from the detailed chemical mechanism.

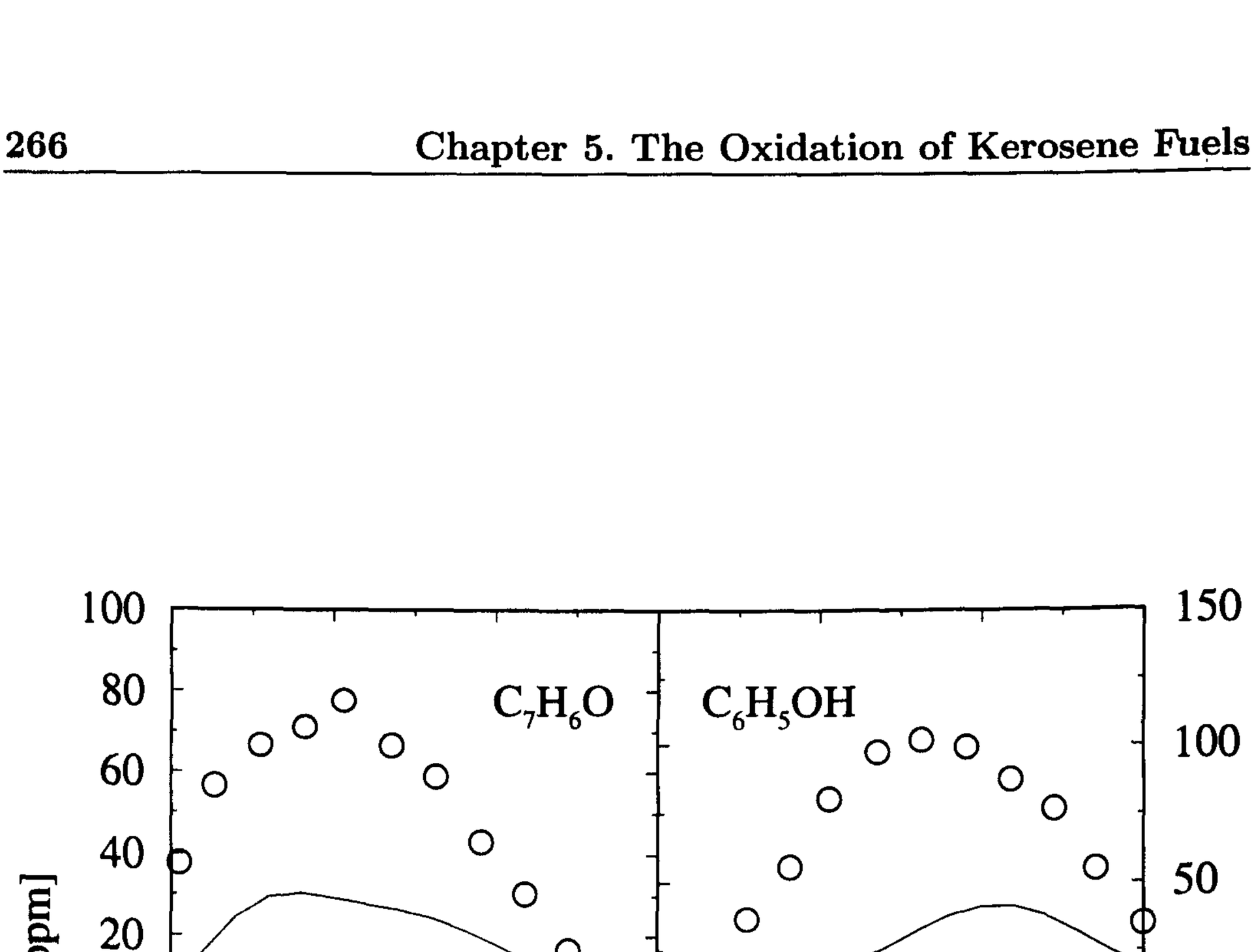


Figure 5.11: Graph of species profile concentrations versus temperature for the oxidation of n – decane and n – propylbenzene constituting the kerosene mix in a Jet Stirred Reactor. Experimental points are from Dagaut & Cathonnet [55] for a stoichiometry of $\phi = 1.5$. Solid lines are the computations from the detailed chemical mechanism.

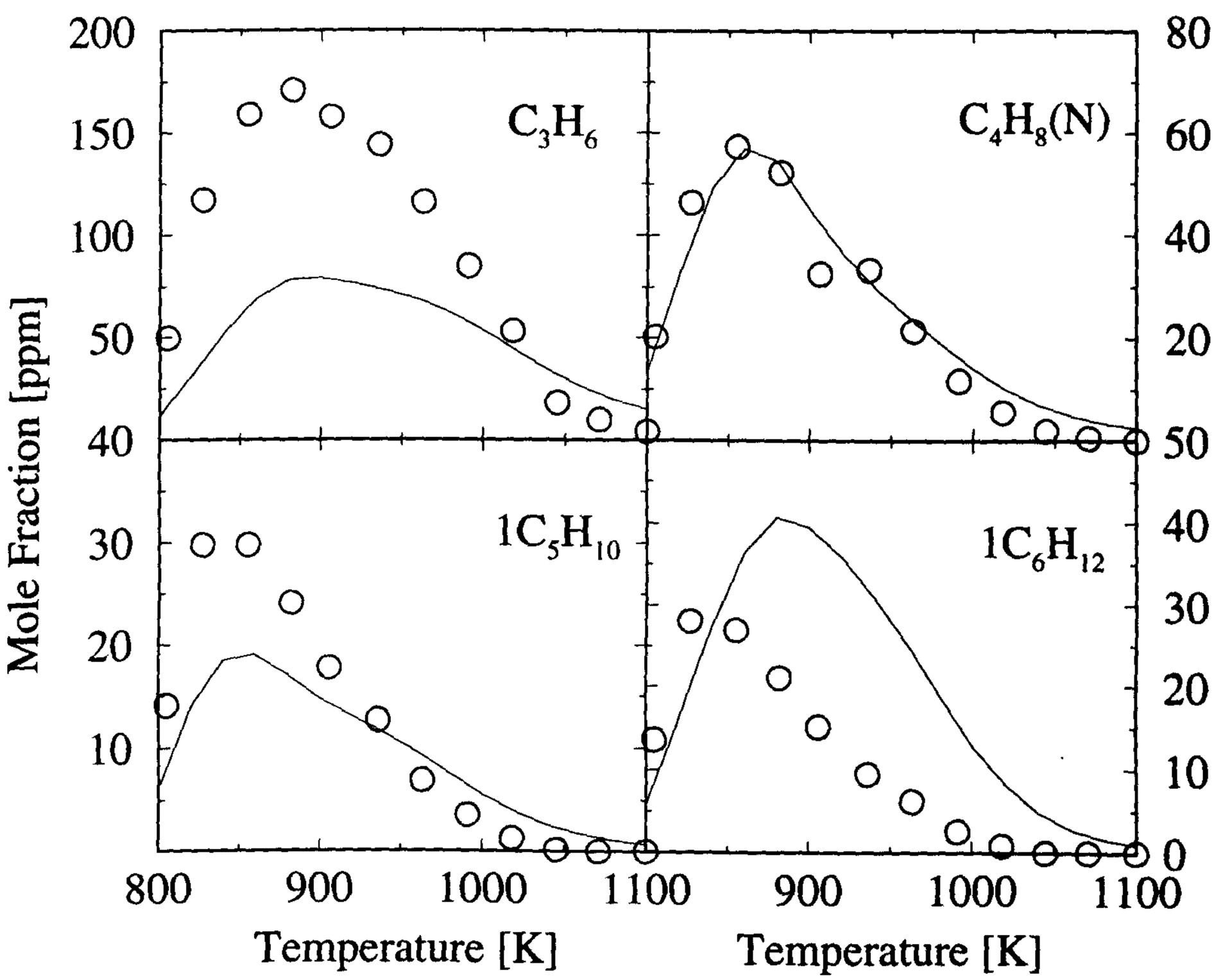


Figure 5.12: Graph of species profile concentrations versus temperature for the oxidation of n – decane and n – propylbenzene constituting the kerosene mix in a Jet Stirred Reactor. Experimental points are from Dagaut & Cathonnet [55] for a stoichiometry of $\phi = 1.5$. Solid lines are the computations from the detailed chemical mechanism.

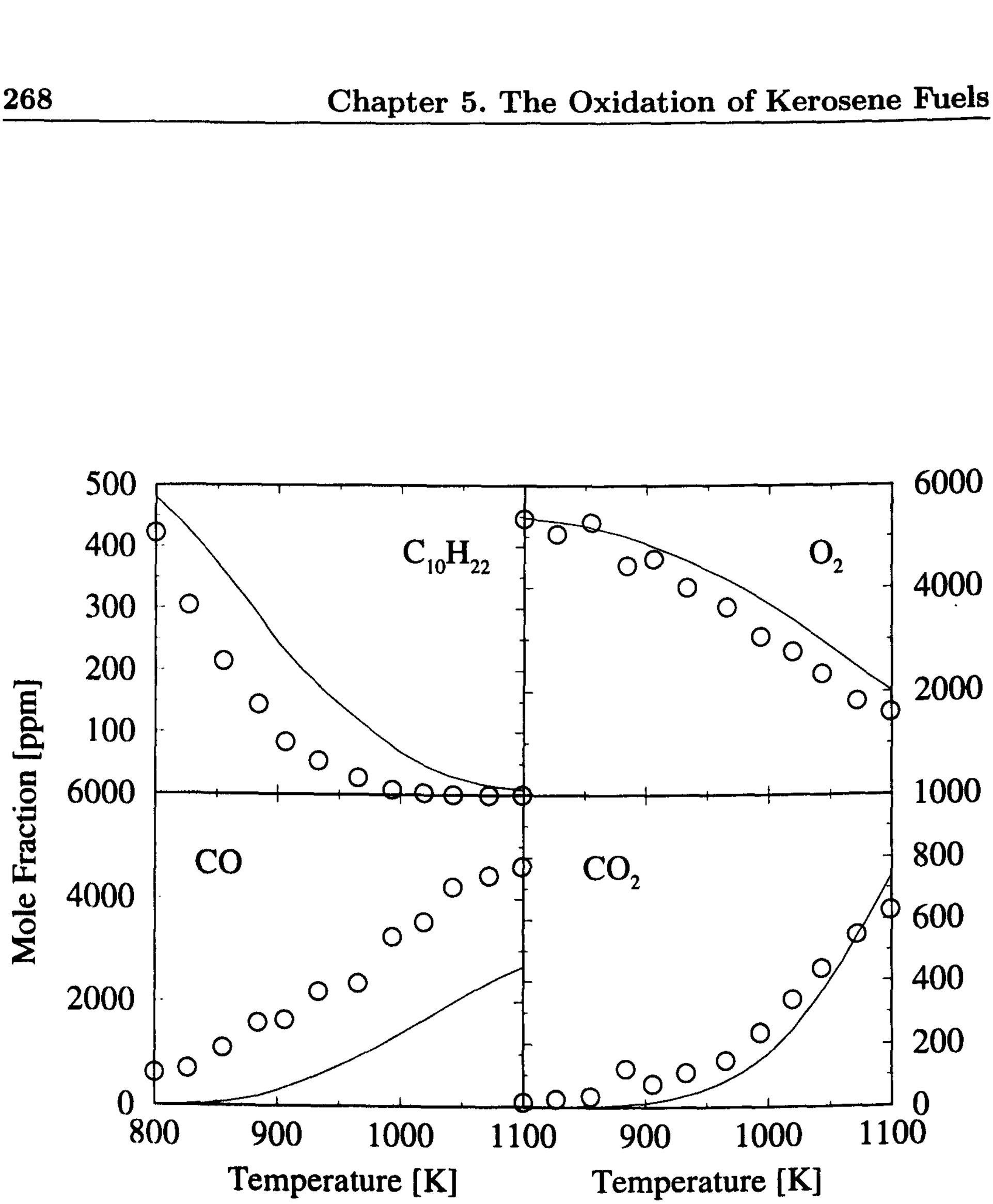


Figure 5.13: Graph of species profile concentrations versus temperature for the oxidation of n – decane and n – propylbenzene constituting the kerosene mix in a Jet Stirred Reactor. Experimental points are from Dagaut & Cathonnet [55] for a stoichiometry of $\phi = 2.0$. Solid lines are the computations from the detailed chemical mechanism.

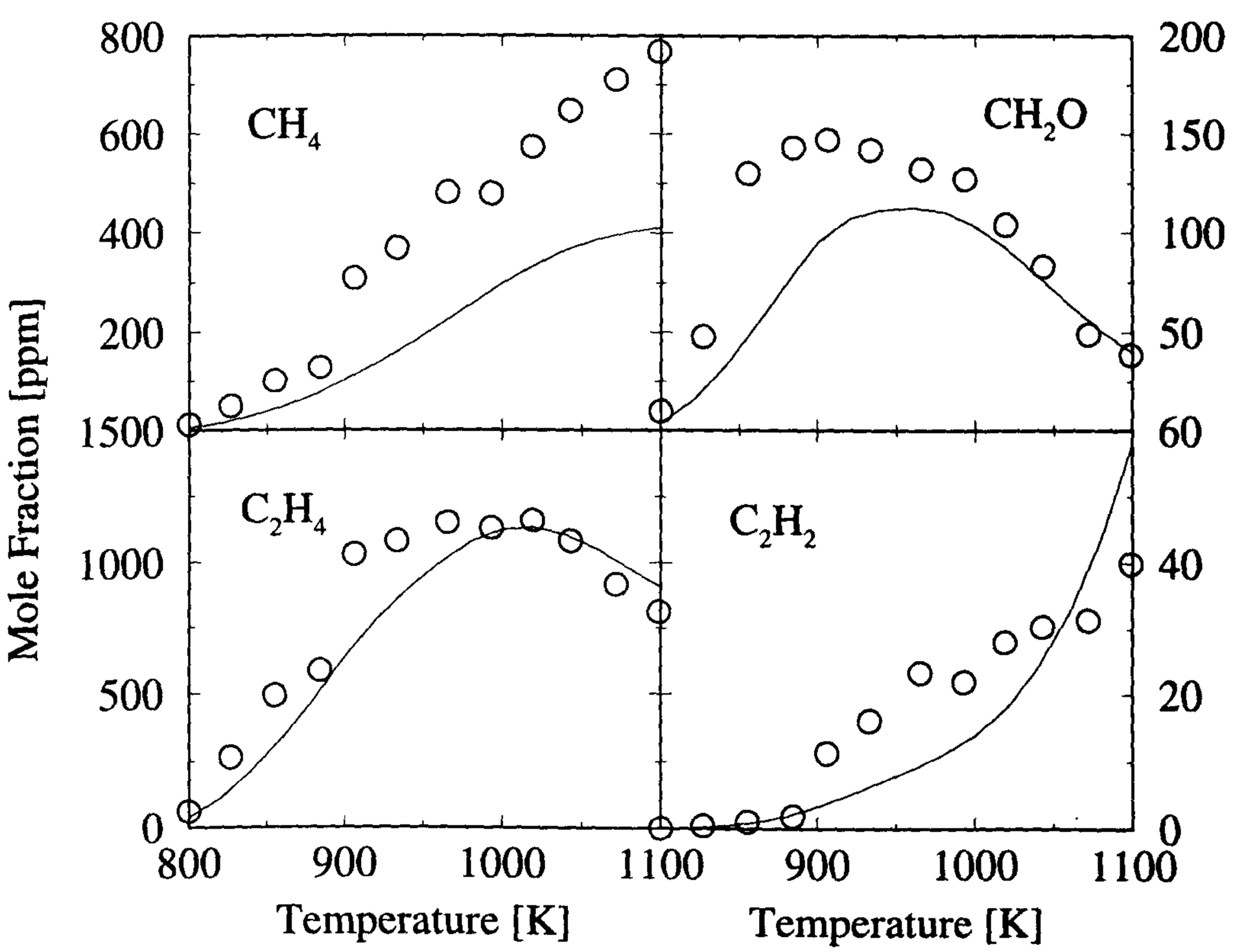


Figure 5.14: Graph of species profile concentrations versus temperature for the oxidation of n – decane and n – propylbenzene constituting the kerosene mix in a Jet Stirred Reactor. Experimental points are from Dagaut & Cathonnet [55] for a stoichiometry of $\phi = 2.0$. Solid lines are the computations from the detailed chemical mechanism.

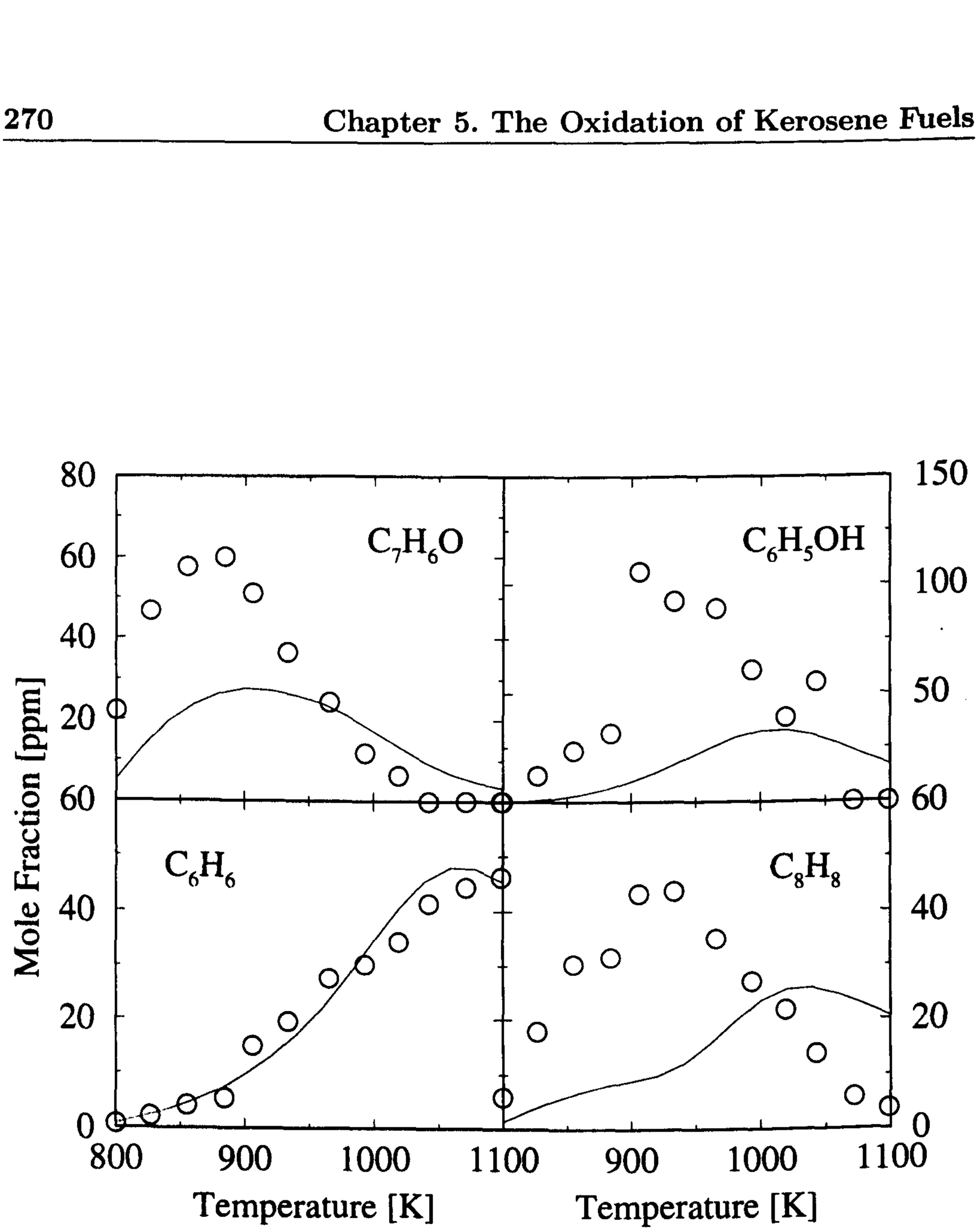


Figure 5.15: Graph of species profile concentrations versus temperature for the oxidation of n – decane and n – propylbenzene constituting the kerosene mix in a Jet Stirred Reactor. Experimental points are from Dagaut & Cathonnet [55] for a stoichiometry of $\phi = 2.0$. Solid lines are the computations from the detailed chemical mechanism.

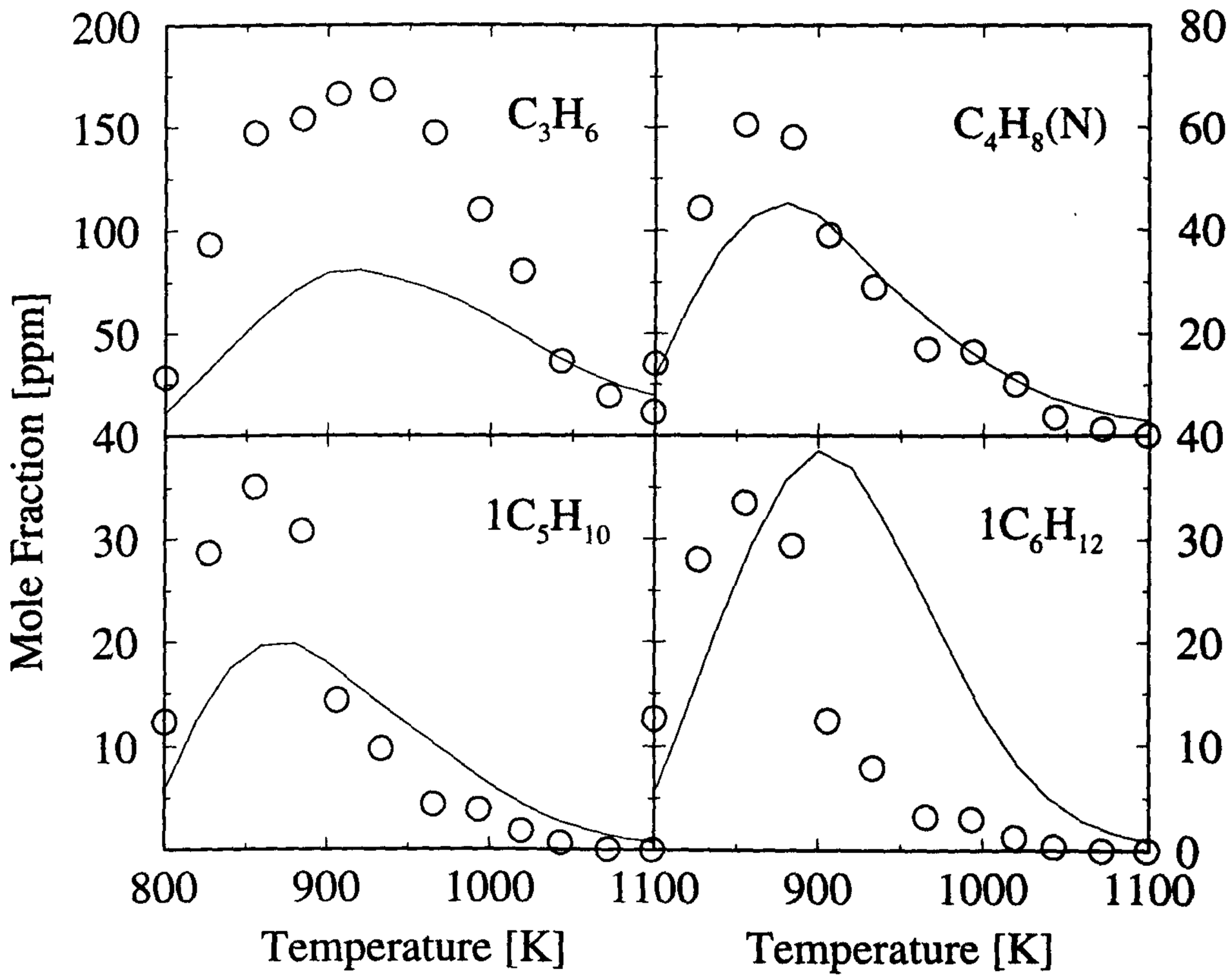


Figure 5.16: Graph of species profile concentrations versus temperature for the oxidation of n – decane and n – propylbenzene constituting the kerosene mix in a Jet Stirred Reactor. Experimental points are from Dagaut & Cathonnet [55] for a stoichiometry of $\phi = 2.0$. Solid lines are the computations from the detailed chemical mechanism.

5.3.2 Primary Reaction Paths for the Oxidation of the Paraffin Fuel Component under Jet Stirred Reactor conditions

The primary constituent (n – decane) of the fuel mixture is consumed through various chemical paths as shown in Figures 5.17 – 5.21. The current path analysis is conducted at 1000 K for the rich ($\phi = 2.0$) case. The major reactions in the consumption of decane are discussed below. The initial path taken by the decane fuel is to form 5 decyl radicals; $1C_{10}H_{21}$, $2C_{10}H_{21}$, $3C_{10}H_{21}$, $4C_{10}H_{21}$ and $5C_{10}H_{21}$ as a result of radical attack on the fuel.

The first decyl radical, $1C_{10}H_{21}$ is formed from of H and OH radical attack on the fuel with reactions (1573) and (1578) contributing 5 % and 10 % respectively.

$$C_{10}H_{22} + H = 1C_{10}H_{21} + H_2 \quad (1573)$$

$$C_{10}H_{22} + OH = 1C_{10}H_{21} + H_2O \quad (1578)$$

The rate parameters for reactions (1573) and (1578) are modelled on the corresponding n – heptane reactions.

$$C_7H_{16} + H = 1C_7H_{15} + H_2 \quad (1666)$$

$$C_7H_{16} + OH = 1C_7H_{15} + H_2O \quad (1674)$$

The rates for reactions (1666) and (1674) have been adopted from the work of Chakir *et al.* [43] as reported by Maurice [182]. The $1C_{10}H_{21}$ radical formed from reactions (1573) and (1578) is mostly consumed by thermal decomposition via C – C (70 %) cleavage (1606) with the rate adopted from Maurice [182].

$$1C_{10}H_{21} = C_8H_{17} + C_2H_4 \quad (1606)$$

Additionally, the $1C_{10}H_{21}$ radical undergoes isomerisation to form $2C_{10}H_{21}$ and $5C_{10}H_{21}$ with reactions (1613) and (1615) contributing 15 % each.

$$1C_{10}H_{21} = 4C_{10}H_{21} \quad (1613)$$

$$1C_{10}H_{21} = 5C_{10}H_{21} \quad (1615)$$

The rates for reactions (1613) and (1615) stem from the work of Maurice [182]. The C_8H_{17} radical thermally decomposes via C – C cleavage through three reaction channels with (1640), (1641) and (1645) contributing 15 %, 30 % and 40 % respectively.

$$C_8H_{17} = 1C_7H_{14} + CH_3 \quad (1640)$$

$$C_8H_{17} = 1C_5H_{11} + C_3H_6 \quad (1641)$$

$$C_8H_{17} = 1C_6H_{13} + C_2H_4 \quad (1645)$$

The rates for reactions (1640), (1641) and (1645) are obtained from the study by Westbrook [265] as reported by Maurice [182].

Heptene ($1C_7H_{14}$) produced from reaction (1640) undergoes HO_2 radical attack as in reaction (1723) leading to the C_7H_{13} radical.

$$1C_7H_{14} + HO_2 = C_7H_{13} + H_2O_2 \quad (1723)$$

The rate for reaction (1723) is obtained from Chakir *et al.* [43] as reported by Maurice [182].

The C_7H_{13} radical is further consumed with thermal decomposition with reactions (1744) and (1745) contributing 65 % and 25 % respectively.

$$C_7H_{13} = C_3H_5(A) + C_4H_8(N) \quad (1744)$$

$$C_7H_{13} = C_3H_4(A) + C_4H_9(N) \quad (1745)$$

The rates for reactions (1744) and (1745) are obtained from Chakir *et al.* [43] as reported by Maurice [182].

The $1C_5H_{11}$ radical produced from reaction (1641) thermally decomposes via C – C cleavage (1769) with the rate adopted from Maurice [182].

$$1C_5H_{11} = C_3H_7(N) + C_2H_4 \quad (1769)$$

The $1C_6H_{13}$ radical produced from reaction (1699) thermally decomposes via C – C cleavage (1748) with the rate obtained from Westbrook [265] as reported by Maurice [182].

$$1C_6H_{13} = C_2H_4 + C_4H_9(N) \quad (1748)$$

The $2C_{10}H_{21}$ decyl radical is formed from H and OH attack on the fuel with reactions (1574) and (1579) contributing 5 % and 10 % each.

$$C_{10}H_{22} + H = 2C_{10}H_{21} + H_2 \quad (1574)$$
$$C_{10}H_{22} + OH = 2C_{10}H_{21} + H_2O \quad (1579)$$

The rates adopted for reactions (1574) and (1579) are modelled on reactions (1667) and (1675) with the rates being obtained from Chakir *et al.* [43] as reported by Maurice [182].

$$C_7H_{16} + H = 2C_7H_{15} + H_2 \quad (1667)$$
$$C_7H_{16} + OH = 2C_7H_{15} + H_2O \quad (1675)$$

The $2C_{10}H_{21}$ radical thermally decomposes via C – C cleavage (1607) forming $1C_7H_{15}$ and C_3H_6. The rate for reaction (1607) is estimated as reported by Maurice [182].

$$2C_{10}H_{21} = 1C_7H_{15} + C_3H_6 \quad (1607)$$

The $1C_7H_{15}$ radical further thermally decomposes via C – C cleavage via reaction (1686) (contributing 40 %) and isomerisation (1697) (contributing 50 %)

$$1C_7H_{15} = C_2H_4 + 1C_5H_{11} \quad (1686)$$

$$1C_7H_{15} = 2C_7H_{15} \quad (1697)$$

The rates for reactions (1686) and (1697) have been adopted from Westbrook [265] and Chakir *et al.* [43] as reported by Maurice [182].

The $2C_7H_{15}$ radical thermally decomposes via C – C cleavage (1687) with the rate adopted from Maurice [182].

$$2C_7H_{15} = C_3H_6 + C_4H_9(N) \quad (1687)$$

The $3C_{10}H_{21}$ radical is formed from H and OH attack on the fuel and reactions (1575) and (1580) contribute 5 % and 10 % each.

$$C_{10}H_{22} + H = 3C_{10}H_{21} + H_2 \quad (1575)$$

$$C_{10}H_{22} + OH = 3C_{10}H_{21} + H_2O \quad (1580)$$

The rates for reactions (1575) and (1580) have been modelled on reactions (1668) and (1676) with the rates being adopted from Chakir *et al.* [43] as reported by Maurice [182].

$$C_7H_{16} + H = 3C_7H_{15} + H_2 \quad (1668)$$

$$C_7H_{16} + OH = 3C_7H_{15} + H_2O \quad (1676)$$

The $3C_{10}H_{21}$ radical thermally decomposes via C – C cleavage as in reaction (1608) with the rate stemming from the work of Maurice [182].

$$3C_{10}H_{21} = 1C_6H_{13} + C_4H_8(N) \quad (1608)$$

The $4C_{10}H_{21}$ radical is produced from H and OH attack on the fuel via reactions (1576) and (1581) which contribute 5 % and 10 % each.

$$C_{10}H_{22} + H = 4C_{10}H_{21} + H_2 \quad (1576)$$

$$C_{10}H_{22} + OH = 4C_{10}H_{21} + H_2O \quad (1581)$$

The rate parameters for reactions (1576) and (1581) are modelled on reactions

$$C_7H_{16} + H = 3C_7H_{15} + H_2 \quad (1669)$$

$$C_7H_{16} + OH = 3C_7H_{15} + H_2O \quad (1677)$$

The rates for reactions (1669) and (1677) are obtained from Chakir *et al.* [43] as reported by Maurice [182]. The $4C_{10}H_{21}$ radical then thermally decomposes via C – C cleavage with reactions (1609) and (1610) contributing 50 % each.

$$4C_{10}H_{21} = 1C_5H_{11} + 1C_5H_{10} \quad (1609)$$

$$4C_{10}H_{21} = C_8H_{16} + C_2H_5 \quad (1610)$$

The rates have been adopted from Maurice [182]. Octene formed in reaction (1610), undergoes H addition as in the reverse of reaction (1643).

$$C_8H_{17} = C_8H_{16} + H \quad (1643)$$

The rate for reaction (1643) has been adopted from Maurice [182]. The pentene formed in reaction (1609) also predominantly undergoes H addition with the reverse of reaction (1770) contributing 20 % to the consumption of $1C_5H_{10}$.

$$1C_5H_{11} = 1C_5H_{10} + H \quad (1770)$$

The rate for reaction (1770) has been adopted from Maurice [182]. Additionally, a total of 60 % is consumed through OH radical attack via reactions (1781) and (1784) contributing 40 % and 20 % respectively.

$$1C_5H_{10} + OH = C_5H_9 + H_2O \quad (1781)$$

$$1C_5H_{10} + OH = C_3H_5(S) + C_2H_4 + H_2O \quad (1784)$$

The rates for reactions (1781) and (1784) have been adopted from Westbrook [265] and Maurice [182] respectively.

The $5C_{10}H_{21}$ radical is produced from H and OH radical attack on the fuel as in reactions (1577) and (1582) contributing 5 % and 10 % each.

$$C_{10}H_{22} + H = 5C_{10}H_{21} + H_2 \quad (1577)$$

$$C_{10}H_{22} + OH = 5C_{10}H_{21} + H_2O \quad (1582)$$

The rates for reactions (1577) and (1582) have been modelled on reactions (1669) and (1677).

$$C_7H_{16} + H = 4C_7H_{15} + H_2 \quad (1669)$$

$$C_7H_{16} + OH = 4C_7H_{15} + H_2O \quad (1677)$$

The $5C_{10}H_{21}$ radical is consumed via thermal decomposition by C – C cleavage with reactions (1611) and (1612) contributing 50 % each.

$$5C_{10}H_{21} = C_4H_9(N) + 1C_6H_{12} \quad (1611)$$

$$5C_{10}H_{21} = C_3H_7(N) + 1C_7H_{14} \quad (1612)$$

Hexene is further consumed by thermal decomposition via C – C cleavage as well as H and OH radical attack, with reactions (1750), (1752), (1762), and (1763) contributing 20%, 15 %, 15 % and 15 % respectively.

$$1C_6H_{12} = C_3H_7(N) + C_3H_5(A) \quad (1750)$$

$$1C_6H_{12} + H = C_6H_{11} + H_2 \quad (1752)$$

$$1C_6H_{12} + OH = C_2H_3 + C_4H_8(N) + H_2O \quad (1762)$$

$$1C_6H_{12} + OH = C_3H_5(A) + C_3H_6 + H_2O \quad (1763)$$

The rates have been adopted from Chakir *et al.* [43] as reported by Maurice [182]. The C_6H_{11} radical thermally decomposes via C – C cleavage with the rate adopted from Chakir *et al.* [43] as reported by Maurice [182].

$$C_6H_{11} = C_3H_6 + C_3H_5(A) \quad (1767)$$

The consumption of n – propylbenzene has been discussed in Chapter 3.

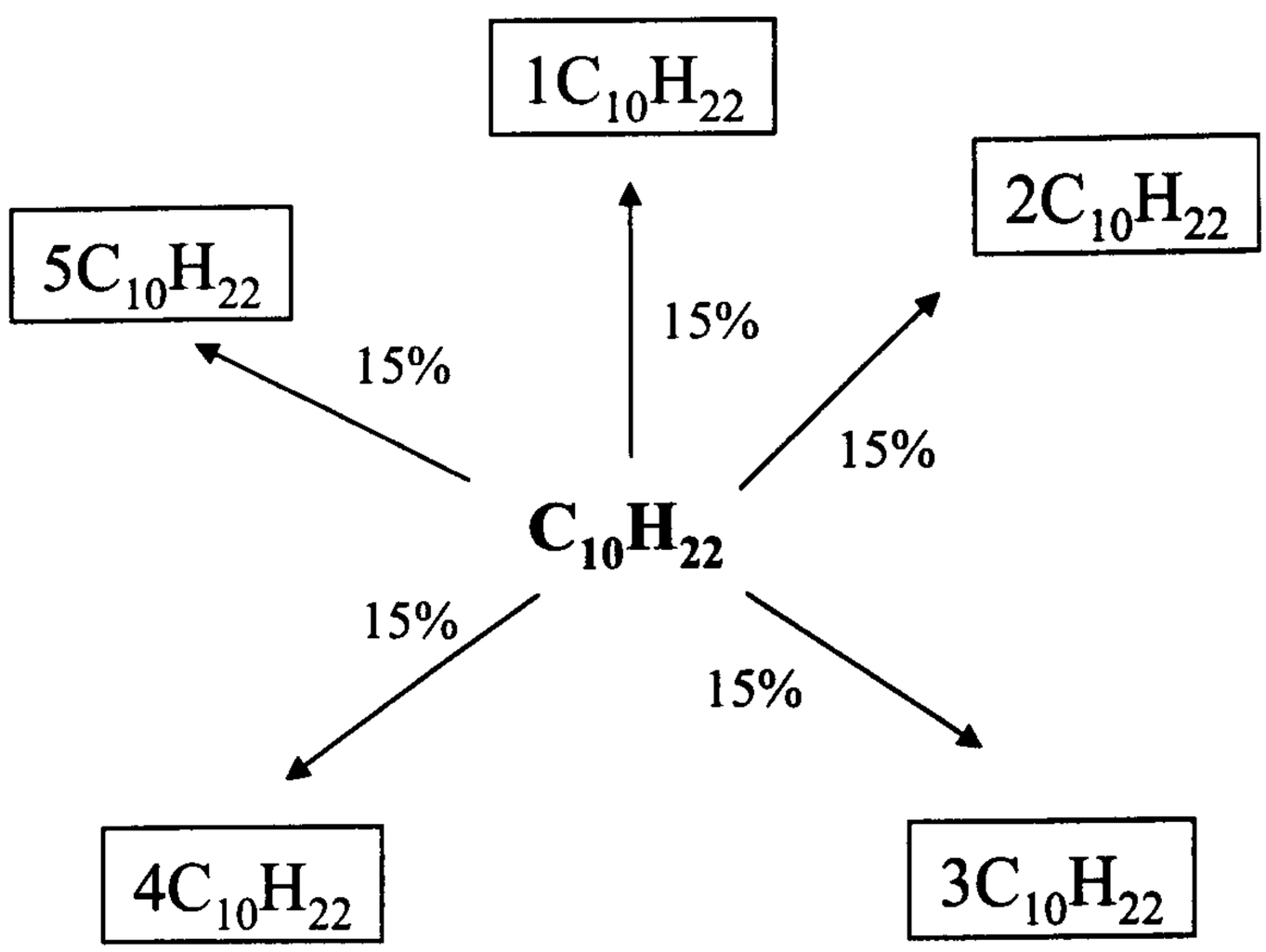


Figure 5.17: Diagram illustrating the consumption paths of the paraffin component of the kerosene mix (n – decane) and its intermediate species in a Jet Stirred Reactor (T = 1000 K, P = 10 atm, ϕ = 2.0). Species in boxes are considered in subsequent pages.

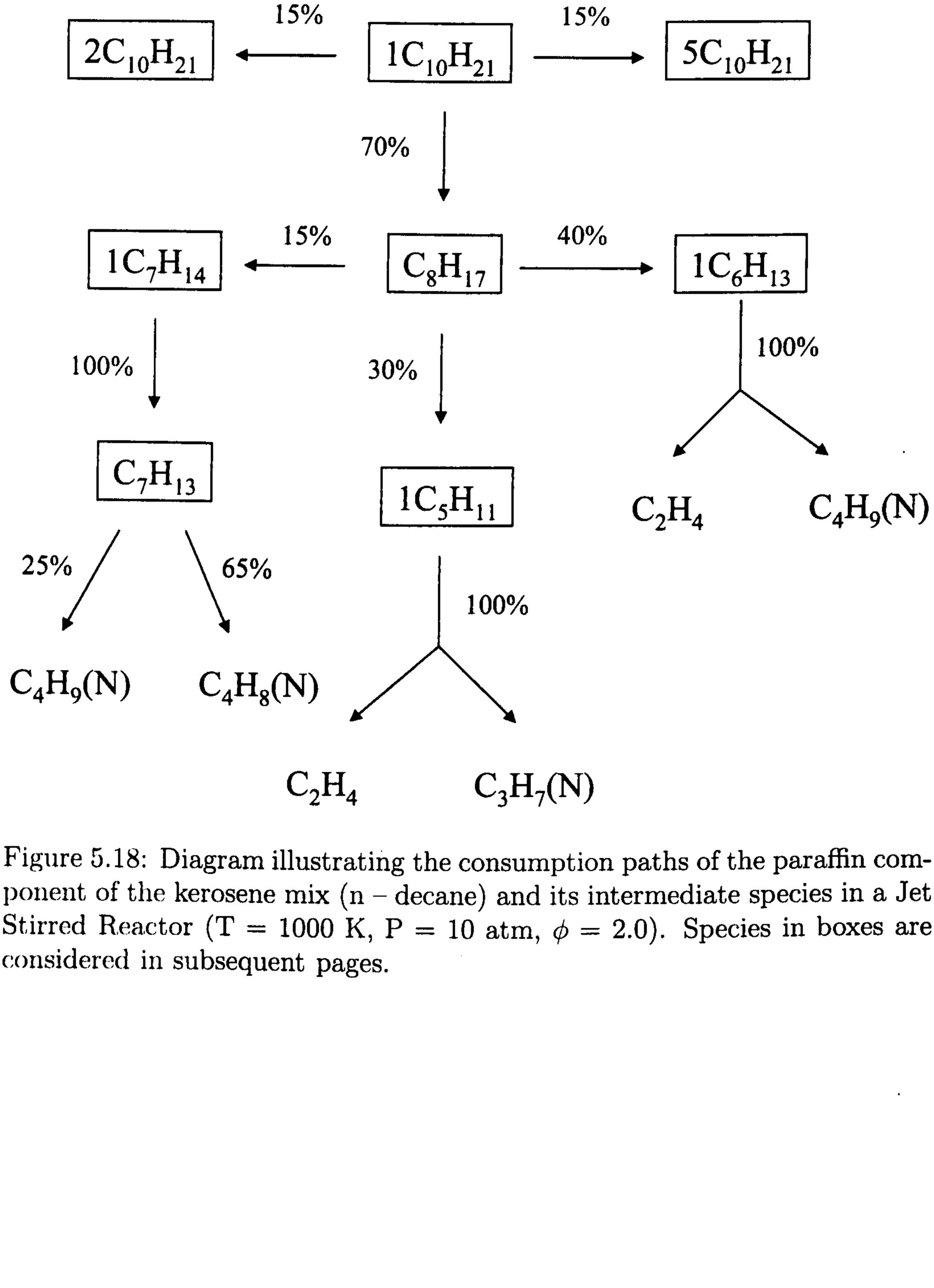


Figure 5.18: Diagram illustrating the consumption paths of the paraffin component of the kerosene mix (n – decane) and its intermediate species in a Jet Stirred Reactor (T = 1000 K, P = 10 atm, ϕ = 2.0). Species in boxes are considered in subsequent pages.

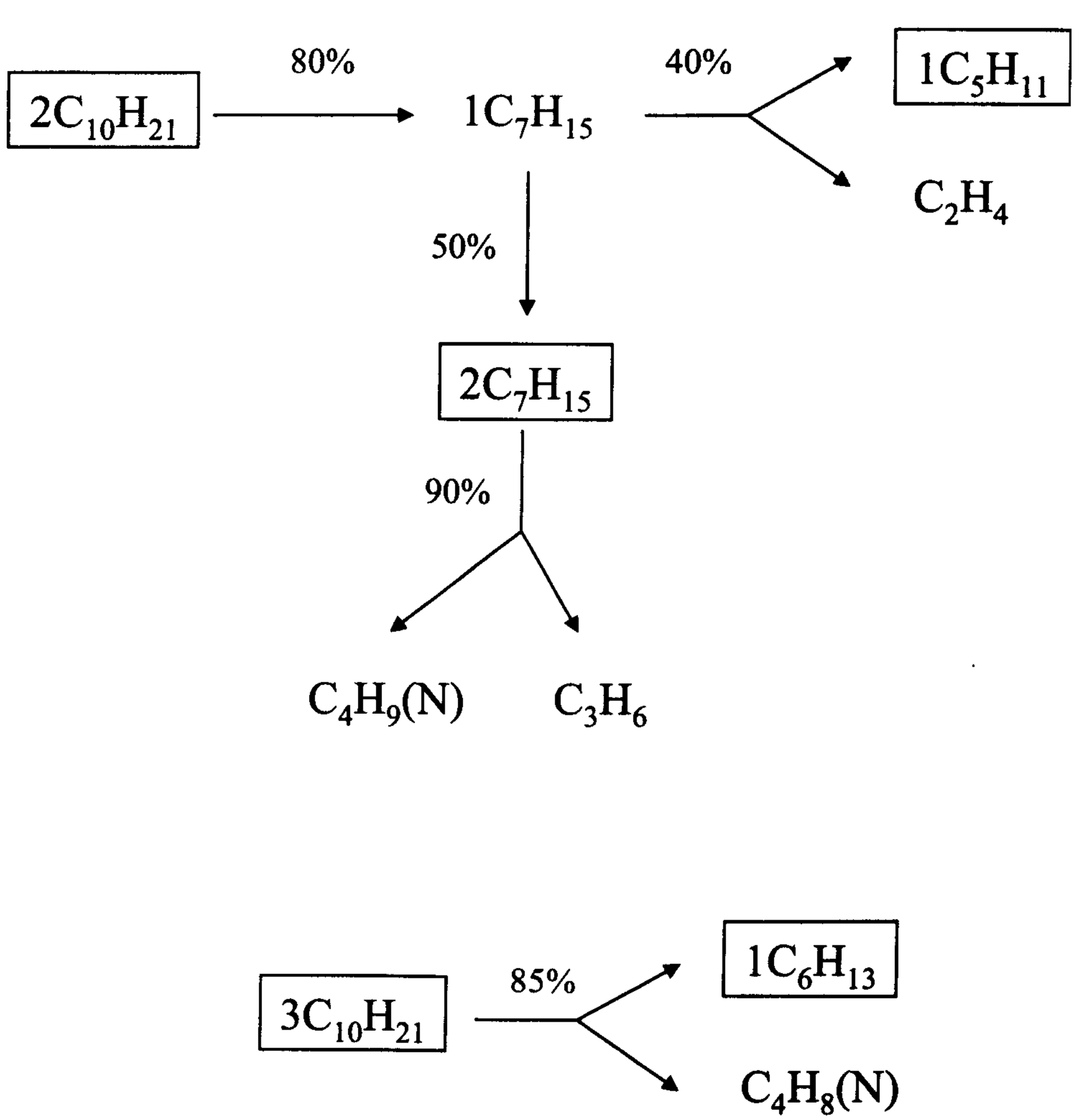


Figure 5.19: Diagram illustrating the consumption paths of the paraffin component of the kerosene mix (n – decane) and its intermediate species in a Jet Stirred Reactor (T = 1000 K, P = 10 atm, ϕ = 2.0). Species in boxes are considered in subsequent pages.

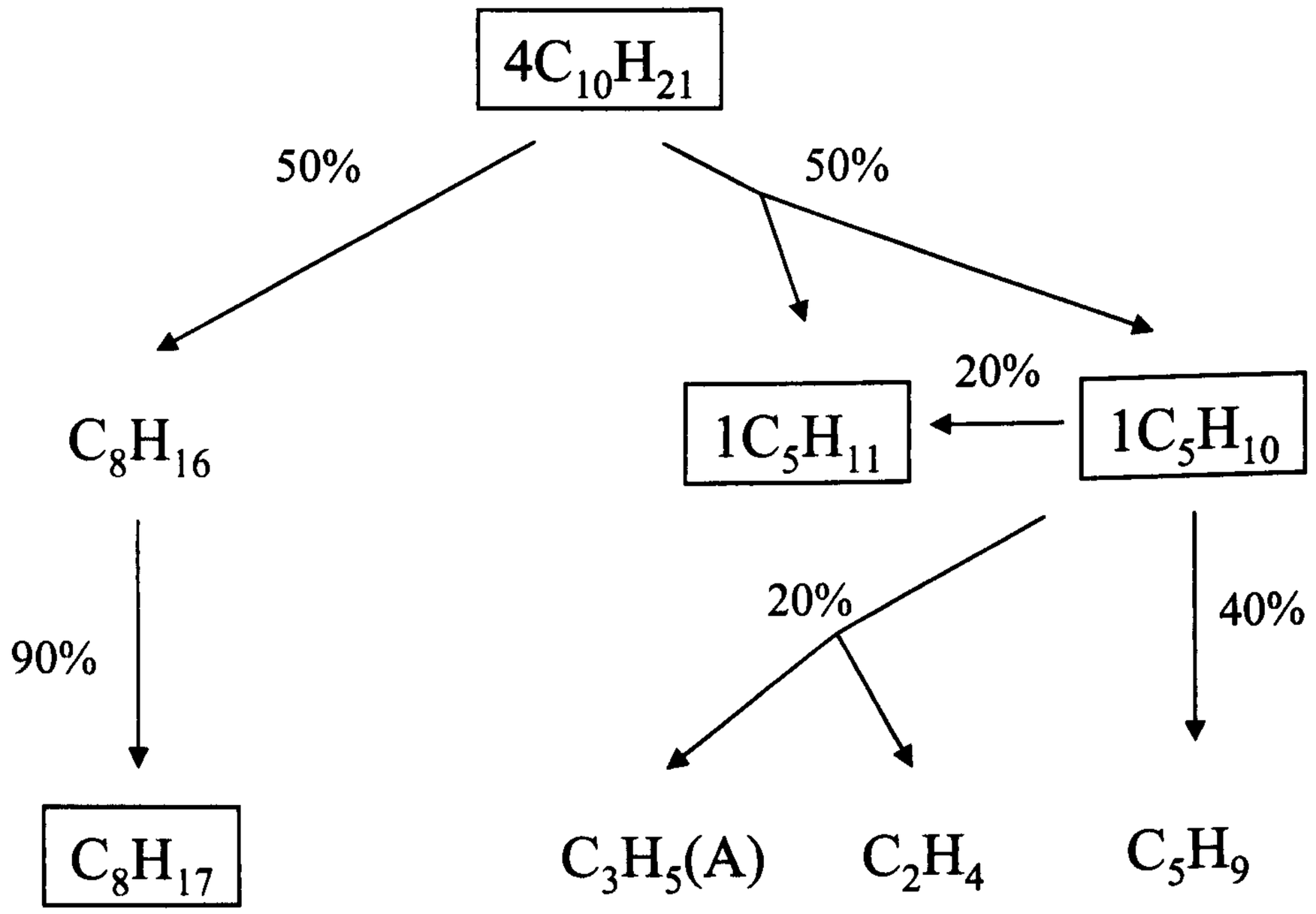


Figure 5.20: Diagram illustrating the consumption paths of the paraffin component of the kerosene mix (n – decane) and its intermediate species in a Jet Stirred Reactor (T = 1000 K, P = 10 atm, ϕ = 2.0). Species in boxes are considered in subsequent pages.

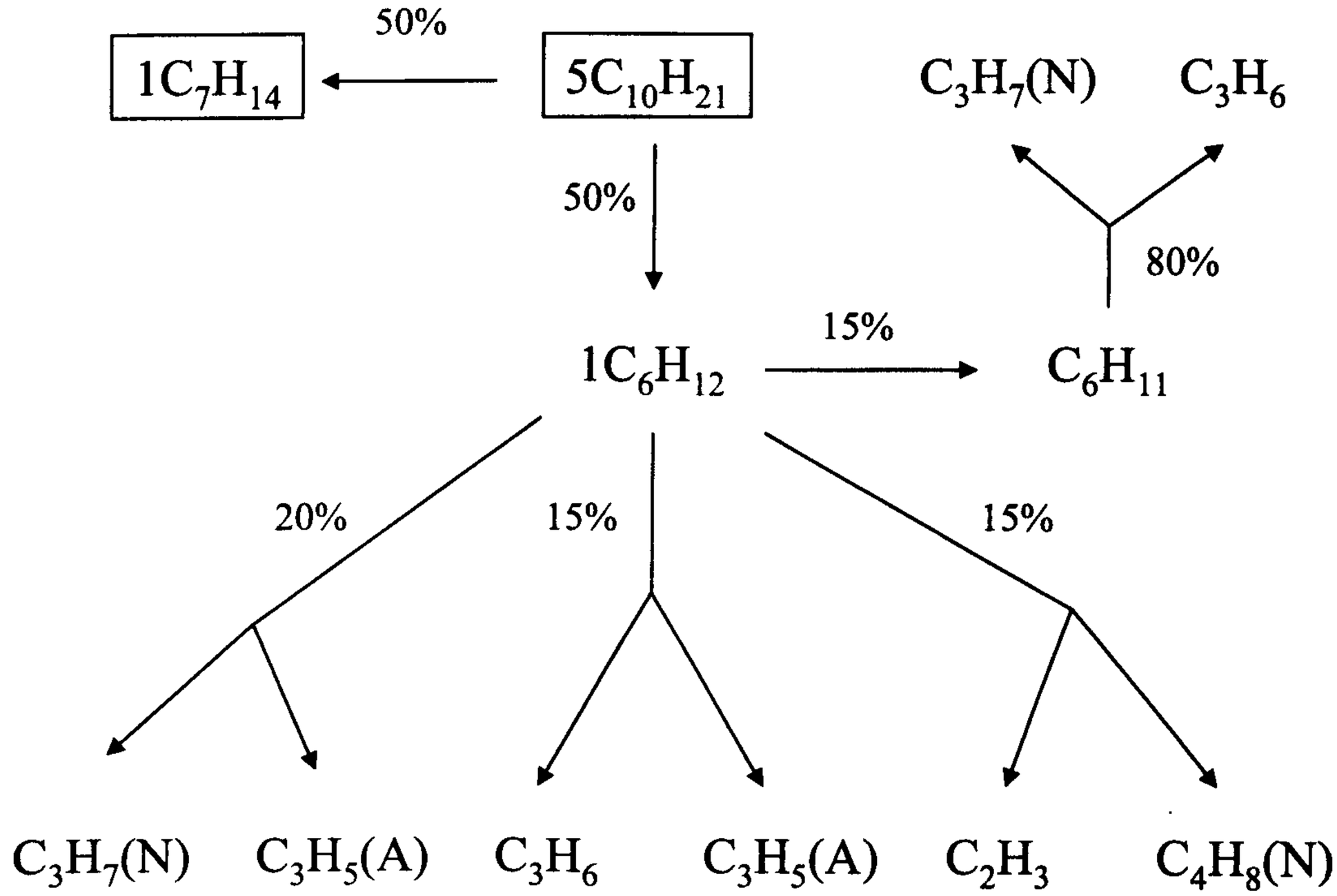


Figure 5.21: Diagram illustrating the consumption paths of the paraffin component of the kerosene mix (n – decane) and its intermediate species in a Jet Stirred Reactor (T = 1000 K, P = 10 atm, ϕ = 2.0). Species in boxes are considered in subsequent pages.

5.4 Summary

The detailed chemical mechanism has been applied to model the oxidation of a simple practical fuel blend containing a mixture of n – decane and n – propylbenzene representing the paraffin and alkyl – substituted aromatic components of kerosene respectively. The investigation was conducted under Jet Stirred Reactor conditions for a variety of stoichiometries (ϕ = 0.75, 1.0, 1.5 and 2.0) over a temperature range of 800 – 1100 K and at a pressure of 10 atm. Overall the results are encouraging, however, poor prediction for some species profile concentrations involving consumption of the alkane component are noted, probably due to detailed mechanism not considering low temperature channels in detail. The computations for the aromatic components are very encouraging when compared to the experimental data of Dagaut & Cathonnet [55].

The problem that arose in Chapter 3 regarding the inaccurate prediction of styrene has again arisen in the kerosene mix. Uncertainties in the rate parameters and fall off may need to be taken into account for reaction (1489).

$$C_9H_{12} = C_8H_9 + CH_3 \quad (1489)$$

Additionally, a reduction in the frequency factor by a factor of 3 for reaction (1195)

$$C_8H_8 + OH = C_7H_7 + CH_2O \quad (1195)$$

significantly improved the predictions for styrene concentration profiles.

The current trends for the aromatic species produced from the detailed chemical mechanism in the kerosene mix are of similar shape to that of the pure n – propylbenzene case investigated in Chapter 3. This confirms that the paraffin component of the kerosene mix, n – decane does not affect the

consumption paths of the alkyl – substituted aromatic as reported by Douté *et al.* [81], Lindstedt & Maurice [167] and Vovelle *et al.* [254].

Chapter 6

Conclusions and Future Work

6.1 Contributions of the Present Work

The main objectives of the present thesis has been to develop and validate detailed chemical kinetic models for the gas-phase combustion of propulsive fuel compounds. An understanding of the chemical complexities of such fuels, followed by the hierarchical construction of such a mechanism and the application over a broad range of combustion devices has resulted in a detailed chemical kinetic model that can qualitatively predict many aspects of the combustion chemistry of the fuels studied. The final mechanism features alkane molecules up to C_{12} and an aromatic sub – mechanism featuring MSA's and two and three ringed PAH's. The present mechanism offers an improvement over any such related detailed chemical kinetic model found in the literature. A summary of each of the major achievements is given in each of the preceding Chapters below.

6.1.1 Toluene and m – Xylene

A consolidation of the toluene sub – mechanism over a broad range of conditions has been performed follows the work of Lindstedt & Maurice [168] and Maurice [182]. A detailed sub – mechanism for m – xylene based on that of toluene was developed and introduced into the hierarchical detailed chemical kinetic mechanism. Overall the detailed chemical kinetic mechanism performed very well regarding the oxidation of the alkyl – substituted aromatic compounds. However, problems were found in the over prediction of C_6H_6 and C_7H_6O where the equivalent species concentrations would be C_7H_8 and C_8H_8O(M) for m – xylene. The dominant channels regarding the formation of these species are estimated thermal decomposition reactions. Hence, fall off parameters are not available at present. Encouragingly, these problems demonstrate consistency within the detailed chemical mechanism. In all cases concerning toluene, CH_4 species profile concentrations were consistently under predicted. This may stem from arguments relating to the cleavage of the CH_3 group from the ring as discussed by Pamidimukkala *et al.* [199] and Rao & Skinner [208].

Problems were found in some of the experimental data sets used to validate and verify the present detailed chemical kinetic mechanism. Namely, the data sets from Klotz *et al.* [148] and Emdee *et al.* [87]. Further experimental data sets are imperative in producing a detailed chemical reaction mechanism.

6.1.2 Phenylacetylene and n – Propylbenzene

The combustion of phenylacetylene was studied under Turbulent Flow Reactor conditions from Shaddix [226]. Due to the concentration profiles for some species, it was suggested that the initial conditions were incorrect, leading

to an amendment being made. The latter led to accurate predictions for the initial, intermediate and final species. The formation of PAH was also considered, with the larger structures being formed from ring – ring reactions. Additionally, the formation of other PAH structures were investigated for intermediate temperatures under different fuels and conditions in Turbulent Flow Reactors. The present work shows that without the consideration of the ring – ring reactions, it was impossible to form these PAH structures and a new area for the formation of PAH is accordingly opened since currently no information was found in the literature.

The reaction mechanism was expanded further to consider an additional alkyl – substituted aromatic compound. The choice of n – propylbenzene enables a wider selection of alkyl – substituted aromatics present in kerosene fuels. The detailed sub – mechanism was validated under Jet Stirred Reactor conditions. It was reported in the literature (Dagaut *et al.* [60] and Litzinger [174] that an isomerisation of the $2C_9H_{11}$ radical is necessary to explain the surprisingly low concentrations of propene and high concentrations of styrene. In the detailed chemical kinetic scheme used in this study, the accurate modelling of these species was possible without the use of this reaction step.

6.1.3 Naphthalene and 1 – Methylnaphthalene

The reaction mechanism was expanded further to consider the aromatic component of diesel fuels. The literature reports that the analysis of practical diesel fuel compositions suggests that an alkyl – substituted PAH is a suitable additional choice to represent the aromatic fuel component found in diesel fuels. Detailed kinetic sub – mechanisms for the oxidation of 1 – methylnaphthalene was developed and introduced into the hierarchical detailed chemical

kinetic mechanism. The chemical kinetic model was based on toluene. Additionally, naphthalene proved to be a significant intermediate in the oxidation of 1 – methylnaphthalene, hence the sub – mechanism for the oxidation of this PAH fuel compound was studied with the rate parameters being modelled upon benzene oxidation.

Overall the detailed chemical kinetic mechanism performed very well. However, problems were found in the over prediction of $C_{10}H_8$ and $C_{11}H_8O$, where the equivalent species in the toluene sub – mechanism is C_6H_6 and C_7H_6O. It was mentioned earlier that C_6H_6 and C_7H_6O were over predicted in the toluene study. Encouragingly, these problems demonstrate consistency within the detailed chemical mechanism. The dominant channels regarding the formation of these species are thermal decomposition reactions which were estimated, and fall off parameters are not available at present. Similarly, CH_4 was constantly under predicted in all of the 1 – methylnaphthalene cases, again this may stem from the arguments that still pursue regarding the cleavage of the CH_3 group from the ring as discussed by Pamidimukkala *et al.* [199] and Rao & Skinner [208].

Again, problems were found in some of the experimental data sets (Pfahl *et al.* [202] and Shaddix [226]) used to validate the present detailed chemical kinetic mechanism. Again, the further need for correct experimental data is imperative.

The oxidation of naphthalene was studied under Turbulent Flow Reactor conditions with the experimental data being obtained from Shaddix [226]. The conceptual modelling approach was to base the reaction steps on benzene, including a low temperature sub – mechanism from DiNaro *et al.* [76]. The results are most encouraging, reproducing accurately initial, intermediate and end products.

6.1.4 The Oxidation of Kerosene Fuels

A kerosene fuel mix comprising of n – decane and n – propylbenzene representing the alkane and alkyl – substituted aromatic components respectively was studied under Jet Stirred Reactor conditions. The model was validated against experimental data from Dagaut & Cathonnet [55]. Overall the model performed well, reproducing the species profile concentrations. However, further validation and verification is still required to cover ignition delay times and flame structures. Additionally, uncertainties still remain within the styrene sub – mechanism which need to be addressed.

6.2 Recommendations and Suggestions for Future Work

The present thesis demonstrates significant advances in constructing a hierarchical detailed chemical kinetic mechanism concerning the combustion of a wide range of practical propulsive fuels. However, the evolution of the detailed chemical mechanism is necessary for improvement. The following points are recommended for further development:-

- The present mechanism is clearly supported by its success in modelling a wide range of fuels, combustion devices and conditions. However, a detailed chemical mechanism is only as accurate as the experimental data used to validate and verify it. The need for precise experimental data cannot be emphasised enough. Additionally, the measurement of elementary reaction rate parameters and thermodynamic data also plays a vital role in the construction of a detailed chemical mechanism. Therefore, further validation and verification of the detailed chemical

mechanism is required with new accurate experimental data in order to produce a precise kinetic model.

- The present mechansim is able to reproduce the modelling of the combustion of a wide variety of fuels in a successful manner, for a number of different devices and conditions. Nevertheless, uncertainties still remain such as the cleavage of the CH_3 group from the ring, the consumption of the radical C_7H_7O and the breakage of the first aromatic in the C_9H_8 type structure. There is a need for additional fundamental data aimed at resolving these prevailing issues.

- The present work has demonstrated the significance of ring – ring reactions playing an important role in the formation of PAH's at intermediate temperatures. Currently, there is no information in the literature regarding this type of chemistry. Therefore, both experimental and modelling studies would be useful in understanding the chemistry of PAH formation at these intermediate temperatures. Additionally, only the formation of the three ringed PAH structures is considered. Therefore, it would be logical to consider the consumption of the three ring PAH structures.

- In the current study, it has been found that the concentration profiles for styrene were reproduced accurately for toluene and phenylacetylene fuels. However, in the study of n – propylbenzene oxidation (both pressures) styrene was initially poorly predicted. It was found that by reducing the dominant styrene consumption channel by a factor of 3, the results for this species profile was significantly improved. This highlights the fact that there are still outstanding uncertainties in the styrene sub – mechanism that need to be addressed. Ideally, the sub –

mechanism should be applied to a wide range of conditions which will help give an understanding into the consumption channels for styrene.

- Presented in this work are also sub – mechanisms for the alkane n – dodecane and the alkyl substituted aromatic, n – butylbenzene (Reactions 1794 – 1894 and 1528 – 1563 in Appendix A respectively). These fuel components offer an additional fuel mix for the alkane component present in diesel fuels and another alkyl substituted aromatic for kerosene fuels. With more experimental data available, the validation and verification of these models may be carried out.

- The kerosene fuel model proposed here performs well. However, a broader range of conditions would be required to further validate and verify the detailed chemical mechanism.

- Although the current detailed chemical mechanism for propulsion fuels can benefit from additional refinement, the logical extension of the present work is to attempt reductions in order to address practical problems in realistic combustor configurations.

References

[1] Executive Summary: Diesel Exhaust: Critical Analysis of Emissions, Exposure and Health Effects. http://www.healtheffects.org/pubs/diesum.htm, 2002.

[2] M.U. Alzueta, P. Glarborg, and K. Dam-Johansen. Experimental and Kinetic Modelling Study of the Oxidation of Benzene. *Int. J. Chem. Kin.*, 32:498, 2000.

[3] M.U. Alzueta, M. Oliva, and P. Glarborg. Parabenzoquinone Pyrolysis and Oxidation in a Flow Reactor. *Int. J. Chem. Kin.*, 30:683, 1998.

[4] I.W.C.E. Arends, R. Louw, and R. Mulder. Kinetic Study of the Thermolysis of Anisole in a Hydrogen Atmosphere. *J. Phys. Chem.*, 97:7914, 1993.

[5] D.C. Astholz, J. Durant, and J. Troe. Thermal Decomposition of Toluene and Benzyl Radicals in Shock Waves. In *18th Symposium (International) on Combustion, The Combustion Institute*, page 885, 1981.

[6] B. Atakan, A.T. Hartlieb, J. Brand, and K. Hohse-Hoinghaus. An Experimental Investigation of Premixed Fuel-Rich Low Pressure Propene/Oxygen/Argon Flames by Laser Spectroscopy and Molecu-

lar Beam Mass Spectrometry. In *27th Symposium (International) on Combustion, The Combustion Institute*, page 435, 1998.

[7] R. Atkinson, D.L. Baulch, R.A. Cox, R.F. Hampson Jr., J.A. Kerr, M.J. Rossi, and J. Troe. Evaluated Kinetic, Photochemical and Heterogeneous Data for Atmospheric Chemistry: Supplement V, IUPAC Subcommittee on Gas Kinetic Data Evaluation for Atmospheric Chemistry. *J. Phys. Chem. Ref. Data*, 26:521, 1997.

[8] R.R. Baker, R.R. Baldwin, A.R. Fuller, and R.W. Walker. Addition of n-C_4H_{10} and C_4H_8 to Slowly Reacting Mixtures of Hydrogen and Oxygen at 480°C. Part 1. Formation of Hydrocarbon Products. *Faraday Discuss.*, 71:736, 1975.

[9] P. Barbe, F. Battin-Lerclerc, and G.M. Come. Experimental and Modelling Study of Methane and Ethane Oxidation between 773 – 1573 K. *J. Chim. Phys.*, 92:1666, 1995.

[10] M. Bartels, J. Edelbuttel-EihHaus, and K. Hoyermann. The Reactions of Benzyl Radicals with Hydrogen Atoms, Oxygen Atoms, and Molecular Oxygen using EI/REMPI Mass Spectrometry. In *22nd Symposium (International) on Combustion, The Combustion Institute*, page 1041, 1989.

[11] F. Battin-Leclerc, R. Fournet, P.A. Glaude, B. Judenherc, V. Warth, G.M. Come, and G. Scacchi. Modelling of the Gas-Phase Oxidation of n – decane from 550 to 1600 K. In *28th Symposium (International) on Combustion, The Combustion Institute*, page 1597, 2000.

[12] S.L. Baughcum and R.C. Oldenborg. Measurement of the C_2(a3πu) and C_2(x1$\sum$g+) disappearance rates with O_2 from 298 – 1300 Kelvin.

In *The Chemistry of Combustion, ACS Symp. Ser.* (Ed. T.M. Sloane), volume 249, page 257, 1984.

[13] D.L. Baulch, C.J. Cobos, R.A. Cox, C. Esser, P. Frank, Th. Just, J.A. Kerr, M.J. Pilling, J. Troe, R.W. Walker, and J. Warnatz. Evaluated Data for Combustion Modelling. *J. Phys. Chem.*, 21:411, 1992.

[14] D.L. Baulch, C.J. Cobos, R.A. Cox, C. Esser, P. Frank, Th. Just, J.A. Kerr, M.J. Pilling, J. Troe, R.W. Walker, and J. Warnatz. Summary Table of Evaluated Kinetic Data for Combustion Modelling. *Comb. Flame*, 98:59, 1994.

[15] A. Bencsura, V.D. Knyazev, S.B. Xing, I.R. Slagle, and D. Gutman. Kinetics of the Thermal Decomposition of the n – propyl Radical. In *24th Symposium (International) on Combustion, The Combustion Institute*, page 629, 1992.

[16] S.W. Benson. *Thermochemical Kinetics.* John Wiley & Sons, INC., first edition, 1976.

[17] S.W. Benson. The Kinetics and Thermochemistry of Chemical Oxidation with Application to Combustion and Flames. *Prog. Energy Comb. Sci.*, 7:125, 1981.

[18] G. Bikas and N. Peters. Kinetic Modelling of n – decane Combustion and Autoignition. *Comb. Flame*, 126:1456, 2001.

[19] R.B. Bird, W.E. Stewart, and E.N. Lightfoot. *Transport Phenomena.* John Wiley & Sons, INC, first edition, 1960.

[20] J.D. Bittner and J.B. Howard. Composition Profiles and Reaction Mechanisms in a Near Sooting Premixed Benzene/Oxygen/Argon

Flame. In *18th Symposium (International) on Combustion, The Combustion Institute*, page 1105, 1981.

[21] Bockhorn. *Soot formation in combustion.* Springer–Verlag, first edition, 1994.

[22] T. Bohland, K. Heberger, F. Temps, and H. Gg. Wagner. The Reaction of CH_2 with C_6H_6. *Ber. Bursenges. Phys. Chem. Chem.*, 93:80, 1983.

[23] T. Bohland and F. Temps. Direct Determination of the Rate Constant for the Reaction $CH_2 + H \rightarrow CH + H_2$. *Ber. Bunsenges. Phys. Chem.*, 88:459, 1984.

[24] H. Bohm and H. Jander. PAH Formation in Acetylene – Benzene Pyrolysis. *Phys. Chem. Chem. Phys.*, 1:3775, 1999.

[25] U. Brand, H. Hippler, L. Lindemann, and J. Troe. C – C and C – H Bond Splits of Laser Excited Aromatic Molecules. *J. Phys. Chem.*, 94:6305, 1990.

[26] M. Braun-Unkhoff, P. Frank, and Th. Just. A Shock Tube Study of the Thermal Decomposition of Toluene and the Phenyl Radical at High Temperatures. In *22nd Symposium (International) on Combustion, The Combustion Institute*, page 1053, 1988.

[27] M. Braun-Unkhoff, P. Frank, and Th. Just. High Temperature Reactions of Benzyl Radicals. *Ber. Bursenges. Phys. Chem.*, 94:1417, 1990.

[28] K. Brezinksy, T.A. Litzinger, and I. GLassman. The High Temperature Oxidation of the Methyl Side Chain of Toluene. *Int. J. Chem. Kin.*, 16:1053, 1984.

[29] K. Brezinsky. The High Temperature Oxidation of Aromatic Hydrocarbons. *Prog. En. Comb. Sci.*, 12:1, 1986.

[30] C.T. Brooks, C.P.R. Cummins, and S.J. Peacock. Pyrolysis of Toluene Using a Static System. *Trans. Faraday Soc.*, 67:3265, 1971.

[31] L.D. Brouwer, Muller-Markgraf, and J. Troe. Thermal Decomposition of Toluene: A Comparison of Thermal and Laser – Photochemical Activation Experiments. *J. Phys. Chem.*, 92:4905, 1988.

[32] A. Burcat. ftp://ftp.technion.ac.il/pub/supported/aetdd/thermodynamics. Ideal Gas Thermochemical Database, October 2002.

[33] A. Burcat, R.C. Farmer, R.L. Epsinoza, and R.A. Matula. Comparative Ignition Delay Times for Selected Ring – Structured Hydrocarbons. *Comb. Flame*, 36:313, 1979.

[34] A. Burcat, C. Snyder, and T. Brabbs. Technical report, NASA, January 1986. Technical Memorandum 87312.

[35] R. Buth, K. Hoyermann, and G. Rohde. Mechanisms and Rates of Benzoyl Reactions: C_6H_5CHO + Cl, C_6H_5CO + O and C_6H_5CO + H. In *24th Symposium (International) on Combustion, The Combustion Institute*, page 669, 1992.

[36] P. Cadman, G.O. Thomas, and P. Butler. The Auto-Ignition of Propane at Intermediate Temperatures and High Pressuers. *Phys. Chem. Chem. Phys.*, 2:5411, 2000.

[37] H.F. Calcote and D.G. Keil. The Role of Ions in Soot Formation. *Pure and App. Chem.*, 82:815, 1990.

[38] C.V. Callahan, T.J. Held, F.L. Dryer, R. Minetti, M. Ribaucour, L.R. Sochet, T. Faravelli, P. Gaffuri, and E. Ranzi. Experimental Data and Kinetic Modelling of Primary Reference Fuel Mixtures. In *26th Symposium (International) on Combustion, The Combustion Institute*, page 739, 1996.

[39] S. Campleman. Carcinogenicity Profile: Diesel Exhaust. http://www.prop65news/pubs/p65news/issues/9701/970117.html, 2002.

[40] C.E. Canosa-Mas, H.M. Frey, and R. Walsh. Studies of Methylene Chemistry by Pulsed Laser-Induced Decomposition of Ketene. Part 1.-Ketene in the Presence of Noble Gases. *Faraday Discuss.*, 80:561, 1984.

[41] M. Cathonnet. Chemical Kinetic Modelling from 1969 to 2019. *Comb. Sci. Tech.*, 98:265, 1994.

[42] Y. Chai and L.D. Pfefferle. An Experimental Study of Benzene Oxidation at Fuel – Lean and Stoichiometric Equivalence Ratio Conditions. *Fuel*, 77:313, 1998.

[43] A. Chakir, M. Belliman, J.C. Boettner, and M. Cathonnet. Kinetic Study of n – heptane Oxidation. *Int. Journ. of Chem. Kin.*, 24:385, 1992.

[44] A. Chakir, J.C. Boettner, M. Cathonnet, and F. Gaillard. Kinetic Study of 1 – Butene Oxidation. In *22nd Symposium (International) on Combustion, The Combustion Institute*, page 873, 1988.

[45] A. Chakir, J.C. Boettner, M. Cathonnet, and F. Gaillard. Kinetic Study of n – butane Oxidation. *Comb. Sci. Tech.*, 65:207, 1988.

[46] A. Chakir, J.C. Boettner, M. Cathonnet, and F. Gaillard. Kinetic Study of n – pentane Oxidation. *Comb. Sci. Tech.*, 77:239, 1991.

[47] J.A. Cole, J.D. Bittner, J.P. Longwell, and J.B. Howard. Formation Mechanisms of Aromatic Compunds in Aliphatic Flames. *Comb. Flame*, 56:51, 1984.

[48] M.B. Colket, R.J. Hall, and M.D. Smooke. Mechanisms for Controlling Soot Formation in Diffusion Flames. Technical report.

[49] M.B. Colket and D.J. Seery. Reaction Mechanisms for Toluene Pyrolysis. In *25th Symposium (International) on Combustion, The Combustion Institute*, page 883, 1994.

[50] H.J. Curran, P. Gaffuri, W.J. Pitz, C.K. Westbrook, and W.R. Leppard. Autoignition Chemistry in a Motored Engine: An Experimental and Kinetic Modelling study. In *26th Symposium (International) on Combustion, The Combustion Institute*, page 2669, 1996.

[51] H.J. Curran, P. Gaffurl, W.J. Pitz, and C.K. Westbrook. A Comprehensive Modelling Study of n – heptane Oxidation. *Comb. Flame*, 114:149, 1998.

[52] P. Dagaut. On the Kinetics of Hydrocarbon Oxidation from Natural Gas to Kerosene and Diesel Fuel. *Phys. Chem. Chem. Phys.*, 4:2079, 2002.

[53] P. Dagaut and M. Cathonnet. Isobutene Oxidation Ignition: Experimental and Detailed Kinetic Modeling Study. *Combust. Sci. Tech.*, 137:237, 1998.

[54] P. Dagaut and M. Cathonnet. The Oxidation of 1,3-Butadiene: Experimental Results and Kinetic Modelling. *Combust. Sci. Tech.*, 140:225, 1998.

[55] P. Dagaut and M. Cathonnet. CFD4C, EU Report, Private Communication. February 2001.

[56] P. Dagaut, G. Pengloan, and A. Ristori. Oxidation, Ignition and Combustion of Toluene: Experimental and Detailed Chemical Kinetic Modelling. *Phys. Chem. Chem. Phys.*, 4:1846, 2002.

[57] P. Dagaut, M. Reuillon, and M. Cathonnet. High Pressure Oxidation of Liquid Fuels from Low to High Temperature. n – decane. *Comb. Sci. Tech.*, 103:349, 1994.

[58] P. Dagaut, M. Reuillon, M. Cathonnet, and D. Voisin. High Pressure Oxidation of Normal Decane and Kerosene in Dilute Conditions from Low to High Temperature. *J. Chim. Phys.*, 92:47, 1995.

[59] P. Dagaut, M. Reullion, J.-C. Boettner, and M. Cathonnet. Kerosene Combustion at Pressures up to 40 ATM.: Experimental Study and Detailed Chemical Kinetic Modelling. In *25th Symposium (International) on Combustion, The Combustion Institute*, page 919, 1994.

[60] P. Dagaut, A. Ristori, El Bakali, and M. Cathonnet. Experimental and Kinetic Modeling Study of the Oxidation of n – propylbenzene. *Fuel*, 81:173, 2002.

[61] P. Daguat, M. Cathonnet, and J.C. Boettnner. Kinetic Modelling of Propane Oxidation. *Comb. Sci. Tech.*, 56:23, 1987.

[62] P. Daguat, M. Cathonnet, and J.C. Boettnner. Kinetic Study of n – butane Oxidation. *Comb. Sci. Tech.*, 65:207, 1989.

[63] P. Daguat, M. Cathonnet, and J.C Boettnner. Ethylene Pyrolysis and Oxidation: A Kinetic Modelling Study. *Int. J. Chem. Kin.*, 22:641, 1990.

[64] P. Daguat, M. Cathonnet, and J.C Boettnner. Kinetics of Ethane Oxidation. *Int. J. Chem. Kin.*, 23:437, 1991.

[65] P. Daguat, M. Cathonnet, and J.C Boettnner. Methane Oxidation: Experimental and Kinetic Modelling Study. *Comb. Sci. Tech.*, 77:127, 1991.

[66] P. Daguat, M. Cathonnet, and J.C Boettnner. A Kinetic Modelling Study of Propene Oxidation in a JSR and Flame. *Comb. Sci. Tech.*, 83:167, 1992.

[67] P. Daguat, M. Cathonnet, J.C Boettnner, and F. Gaillard. Kinetic Modelling of Ethylene Oxidation. *Comb. Flame*, 71:295, 1988.

[68] A. D'Anna and A. Violi. A Kinetic Model for the Formation of Aromatic Hydrocarbons in Premixed Laminar Flames. In *27th Symposium (International) on Combustion, The Combustion Institute*, page 425, 1998.

[69] S.G. Davis and C.K. Law. Determination of and Fuel Structure Effects on Laminar Flame Speeds of C-1 to C-8 Hydrocarbons. *Comb. Sci. Tech.*, 140:427, 1998.

[70] S.G. Davis, C.K. Law, and H.Wang. Propene Pyrolysis and Oxidation Kinetics in a Flow Reactor and Laminar Flames. *Comb. Flame*, 119:375, 1999.

[71] S.G. Davis, H. Wang, K. Brezinsky, and C.K. Law. Laminar Flame Speeds and Oxidation Kinetics of Benzene – Air and Toluene – Air Flames. In *26th Symposium (International) on Combustion, The Combustion Institute*, page 1025, 1996.

[72] A.J. Dean, D.F. Davidson, and R.K. Hanson. A Shock Tube Study of Reactions of C Atoms with H_2 and O_2 Using Excimer Photolysis of C_2O_2 and C Atom Atomic Resonance Absorption Spectroscopy. *J. Phys. Chem.*, 95:183, 1991.

[73] A.M. Dean. Predictions of Pressure and Temperature Effects Upon Radical Addition and Recombination Reactions. *J. Phys. Chem.*, 89:4600, 1985.

[74] A.M. Dean and P.R. Westmoreland. Bimolecular QRRK Analysis of Methyl Radical Reactions. *Int. J. Chem. Kin.*, 19:207, 1987.

[75] J.L. Delfau, M. Bouhria, M. Reuillon, O. Sanogo, R. Akrich, and C. Vovelle. Experimental and Computational Investigation of the Structure of a Sooting Decane – O_2 – Air Flame. In *23rd Symposium (International) on Combustion, The Combustion Institute*, page 1567, 1990.

[76] J.L. DiNaro, J.B. Howard, W.H. Green, J.W. Tester, and J.W. Bozzelli. Elementary Reaction Mechanism for Benzene Oxidation in Supercritical Water. *J. Phys. Chem.*, 104:10576, 2000.

[77] G. Dixon-Lewis. Flame Structure and Flame Reaction Kinetics. I. Solution of Conservation Equations and Application to Rich Hydrogen – Oxygen Flames. *Proc. R. Soc. Lon.*, A298:495, 1967.

[78] D.W. Dockery and C.A. Pope. Acute Respiratory Effects of Particulate Air Pollution. *Annu. Rev. Public Health*, 15:107, 1994.

[79] D.W. Dockery, C.A. Pope, X. Xu, J.D. Spengler, J.H. Ware M.E. Fay, Jr. B.G. Ferris, and F.E. Speizer. Association between Air Pollution and Mortality in six U.S. Cities. *New Eng. J. Med.*, 329:1753, 1993.

[80] Ch. Dombrowsky and H.Gg. Wagner. Investigation of the $^3CH_2$ + O_2 Reaction in Shock Waves. *Ber. Bunsenges. Phys. Chem.*, 96:1048, 1992.

[81] C. Douté, J.L. Delfau, R. Akrich, and C. Vovelle. Chemical Structure of Atmospheric Pressure Premixed n – decane and Kerosene Flames. *Comb. Sci. Tech.*, 106:327, 1995.

[82] C. Douté, J.L. Delfau, and C. Vovelle. Modelling of the Structure of a Premixed n – Decane Flame. *Comb. Sci. Tech.*, 130:269, 1997.

[83] R.P. Duran, V.T. Amorebieta, and A.J. Colussi. Is the Homogeneous Thermal Dimerization of Acetylene a Free-Radical Chain Reaction? Kinetic and Thermochemical Analysis. *J. Phys. Chem.*, 92:636, 1988.

[84] T. Edwards and L.Q. Maurice. Surrogate Mixtures to Represent Complex Aviation and Rocket Fuels. *J. Prop. and Power*, 17:461, 2001.

[85] M. Eichholtz, A. Schneider, D.-V. Stucken, J.-T. Vollmer, and H.G. Wagner. The Reactions of Phenylacetylene with O(^{3}) in the Gas Phase.

In *25th Symposium (International) on Combustion, The Combustion Institute*, page 859, 1994.

[86] C. Ellis, M.S. Scott, and R.W. Walker. Addition of Toluene and Ethylbenzene to Mixtures of H_2 and O_2 at 772K: Part 2: Formation of Products and Determination of Kinetic Data for H + additive and for Other Elementary Reactions Involved. *Comb. Flame*, 132:291, 2003.

[87] J.L. Emdee, K. Brezinsky, and I. Glassman. Oxidation of o – xylene. In *23rd Symposium (International) on Combustion, The Combustion Institute*, page 77, 1990.

[88] J.L. Emdee, K. Brezinsky, and I. Glassman. High Temperature Oxidation of m – and p – xylene. *J. Phys. Chem.*, 95:1626, 1991.

[89] J.L. Emdee, K. Brezinsky, and I. Glassman. A Kinetic Model for the Oxidation of Toluene near 1200K. *J. Phys. Chem.*, 96:2151, 1992.

[90] A. Fahr and S.E. Stein. Reactions of Vinyl and Phenyl Radicals with Ethyne, Ethene and Benzene. In *22nd Symposium (International) on Combustion, The Combustion Institute*, volume 22, page 1023, 1989.

[91] S. Fahr and S.E. Stein. Gas Phase Reactions of Phenyl Radicals with Aromatic Molecules. *J. Phys. Chem.*, 92:4951, 1988.

[92] A.R. Fairbairn. The dissociation of carbon monoxide. *Proc. R. Soc. London A*, 312:207, 1969.

[93] T. Faravelli, A. Goldaniga, and E. Ranzi. The Kinetic Modelling of Soot Precursors in Ethylene Flames. In *27th Symposium (International) on Combustion, The Combustion Institute*, page 1489, 1998.

[94] P. Frank, J. Herzler, Th. Just, and C. Wahl. High Temperature Reactions of Phenyl Oxidation. In *25th Symposium (International) on Combustion, The Combustion Institute*, page 833, 194.

[95] M. Frenklach. Reaction Mechanisms of Soot Formation in Flames. *Phys. Chem. Chem. Phys.*, 4:2028, 2002.

[96] M. Frenklach and H. Wang. *Detailed Mechanism and Modelling of Soot Particle Formation in Soot Formation in Combustion: Mechanisms and Models.* Springer–Verlag, first edition, 1994.

[97] H. Freund and W.N. Olmstead. Detailed Chemical Kinetic Modelling of Butylbenzene Pyrolysis. *Int. J. Chem. Kin.*, 21:561, 1989.

[98] J.S. Gaffney, R. Atkinson, and J.N. Pitts Jr. Temperature Dependence of the Relative Rate Constants for the Reaction of $O(^3P)$ Atoms with Selected Olefins, Monoterpenes and Unsaturated Aldehydes. *J. Am. Chem. Soc.*, 97:6481, 1975.

[99] J. Gang, M.J. Pilling, and S.H. Robertson. Asymmetric Internal Rotation: Application to the 2-C_4H_9 = CH_3 + C_3H_6 Reaction. *Faraday Discuss.*, 93:1481, 1997.

[100] W.C. Gardiner, Jr. W.G. Mallard, K. Morinaga, D.L. Ripley, and B.F. Walker. Shock – Tube Study of Chemiluminescence and Heat Release in the High Temperature Oxidation of Acetylene. In *11th Symposium (International) on Combustion*, page 1151, 1966.

[101] I. Glassman. *Combustion.* Academic Press, first edition, 1977.

[102] P.A. Glaude, V. Conraud, R. Fournet, F. Battin-Leclerc, G.M. Come, G. Scacchi, P. Dagaut, and M. Cathonnet. Modelling the Oxidation of

Mixtures of Primary Reference Automobile Fuels. *Energy and Fuels*, 16:1186, 2002.

[103] E. Goodger and Ray Vere. *Aviation Fuels Technology.* MacMillan Publishers, LTD., first edition, 1985.

[104] M.A. Grela and A.J. Colussi. Kinetics and Mechanism of the Thermal Decomposition of Unsaturated Aldehydes: Benzaldehyde, 2–Butenal and 2–Furaldehyde. *J. Phys. Chem.*, 90:434, 1986.

[105] J. Griesheimer and K.H. Homann. Large Molecules, Radical Ions and Small Soot Particles in Fuel – Rich Hydrocarbon Flames. Part II. Aromatic Radicals and Intermediate PAHs in a Premixed Low Pressure Naphthalene/Oxygen/Argon Flame. In *27th Symposium (International) on Combustion, The Combustion Institute*, page 1753, 1998.

[106] H.H. Grotheer, G. Riekert, D. Walter, and T. Just. Non – Arrhenius Behaviour of the Reaction of Hydroxymethyl Radicals with Molecular Oxygen. *J. Phys. Chem.*, 92:4028, 1988.

[107] C. Gureét, M. Cathonnet, J.-C. Boettner, and F. Gaillard. Experimental Study and Modelling of Kerosene Oxidation in a Jet Stirred Flow Reactor. In *23rd Symposium (International) on Combustion, The Combustion Institute*, page 211, 1990.

[108] C.W. Hamilton and G.L. Schott. Post – Induction Kinetics in Shock Initiated H_2 – O_2 Reactions. In *11th Symposium (International) on Combustion, The Combustion Institute*, page 635, 1967.

[109] B.S. Haynes and H.G. Wagner. Soot Formation. *Prog. En. Comb. Sci.*, 7:229, 1981.

[110] Y.Z. He, W.G. Mallard, and W.J. Tsang. Kinetics of Hydrogen and Hydroxyl Radical Attack on Phenol at High Temperature. *J. Phys. Chem.*, 92:2196, 1988.

[111] T.J. Held and F.L. Dryer. An Experimental and Computational Study of Methanol Oxidation in the Intermediate- and High-Temperature Regimes. In *25th Symposium (International) on Combustion*, page 901, 1994.

[112] T.J. Held and F.L. Dryer. A Comprehensive Mechanism for Methanol Oxidation. *Int. J. Chem. Kin.*, 30(11):805, 1998.

[113] J. Herzler and P. Frank. High Temperature Reactions of Phenylacetylene. *Ber. Bursenges. Phys. Chem.*, 96:1333, 1992.

[114] J. Herzler, J.A. Manion, and W. Tsang. 1,2-Pentadiene Decomposition. *Int. J. Chem. Kin.*, 33:755, 2001.

[115] B. Heyberger, F. Battin-Lerclerc, V. Warth, R. Fournet, G.M. Côme, and G. Scacchi. Comprehensive Mechanism for the Gas Phase Oxidation of Propene. *Comb. Flame*, 126:1780, 2001.

[116] Y. Hidaka, K. Hattori, T. Okuno, T. Abe, and T. Koike K. Inami. Shock – Tube and Modelling Study of Acetylene Pyrolysis and Oxidation. *Comb. Flame*, 107:401, 1996.

[117] Y. Hidaka, T. Higashihara, N. Ninomiya, H. Oshita, and H. Kawano. Thermal Isomerization and Decomposition of 2-Butyne in Shock Waves. *J. Phys. Chem.*, 97:10977, 1993.

[118] Y. Hidaka, K. Kimura, and H. Kawano. High temperature pyrolysis of ketene in shock waves. *Comb. Flame*, 99:18, 1994.

[119] Y. Hidaka, T. Nakamura, A. Miyauchi, T. Shiraishi, and H. Kawano. Thermal Decomposition of Propyne and Allene in Shock Waves. *Int. J. Chem. Kin.*, 21:643, 1989.

[120] Y. Hidaka, T. Nakamura, H. Tanaka, K. Inami, and H. Kawano. High Temperature Pyrolysis of Methane in Shock Waves. Dissociative Recombination Reactions of Methyl Radicals and for Propyne Formation Reaction. *Int. J. Chem. Kin.*, 22:701–709, 1990.

[121] Y. Hidaka, T. Nakamura, H. Tanaka, A. Jinno, H. Kawano, and T. Higashihara. Shock Tube and Modeling Study of Propene Pyrolysis. *Int. J. Chem. Kin.*, 24:761, 1992.

[122] Y. Hidaka, T. Nishimori, K. Sato, Y. Henmi, R. Okuda, and K. Inami. Shock – Tube and Modelling Study of Ethylene Pyrolysis and Oxidation. *Comb. Flame*, 117:755, 1999.

[123] Y. Hidaka, T. Oki, and H. Kawano. Thermal Decomposition of Methanol in Shock Waves. *J. Phys. Chem.*, 93:7134, 1989.

[124] Y. Hidaka, K. Sato, Y. Henmi, H. Tanaka, and K. Inami. Shock – Tube and Modelling Study of Methane Pyrolysis and Oxidation. *Comb. Flame*, 118:340, 1999.

[125] H. Hippler, C. Reihs, and J. Troe. Elementary Steps in the Pyrolysis of Toluene and Benzyl Radicals. *Z. Phys. Chem.*, 1-16:167, 1990.

[126] H. Hippler, C. Reihs, and J. Troe. Shock Tube UV Absorption Study of the Oxidation of Benzyl Radicals. In *23rd Symposium (International) on Combustion, The Combustion Institute*, page 37, 1991.

[127] H. Hippler and J. Troe. Thermodynamic Properties of Benzyl Radicals: Enthalpy of Formation from Toluene, Benzyl Iodide, and Benzyl Dissociation Equilibria. *J. Phys. Chem.*, 94:3803, 1990.

[128] G.D. Hobson and W. Pohl. *Modern Petroleum Technology.* Applied Science Publishers LTD, fourth edition, 1984.

[129] A. Hoffmann, M. Klatt, and H. Gg. Wagner. An Investigation of the Reaction Between O(^{3}) and Toluene at High Temperatures. *Z. Phys. Chem., (Neue Folge)*, 168:1, 1990.

[130] K.-H. Homann, W. Schwanebeck, and J. Warnatz. Reaktionen des Butadiins ii. Die Reaktion mit Sauerstoffatomen. *Ber. Bunsenges. Phys. Chem.*, 79:536, 1975.

[131] K.H. Homann and H.G. Wagner. Some New Aspects of the Mechanism of Carbon Formation in Premixed Flames. In *11th Symposium (International) on Combustion, The Combustion Institute*, page 371, 1967.

[132] H. Hopf, G. Wachholz, and R. Walsh. Gas Phase Kinetics of Pyrolysis of 1-Methyl-1-cyclopropene. *Chem. Ber.*, 118:3579, 1985.

[133] C. Horn, K. Roy, P. Frank, and T. Just. Shock – Tube Study on the High Temperature Pyrolysis of Phenol. In *27th Symposium (International) on Combustion, The Combustion Institute*, page 321, 1998.

[134] C.-C. Hsu, A.M. Mebel, and M.C. Lin. Ab Initio Molecular Orbital Study of HCO+O_2 Reaction: Direct versus Indirect Abstraction Channels. *J. Chem. Phys.*, 105(6):2346, 1996.

[135] T.B. Hunter, T.A. Litzinger, H. Wang, and M. Frenklach. Ethane Oxidation at Elevated Pressures in the intermediate temperature regime: Experiments and Modelling. *Comb. Flame*, 104:505, 1996.

[136] T.B. Hunter, H. Wang, T.A. Litzinger, and M. Frenklach. The Oxidation of Methane at Elevated Pressures: Experiments and Modelling. *Comb. Flame*, 97:201, 1994.

[137] J.Y. Hwang, S.H. Chung, and W. Lee. Effects of Oxygen and Propane Addition on Soot Formation in Counterflow Ethylene Flames and the Role of C_3 Chemistry. In *27th Symposium (International) on Combustion, The Combustion Institute*, page 1531, 1998.

[138] E. Ikeda, R.S. Tranter, J.H. Kiefer, R.D. Kern, H.J. Singh, and Q. Zhang. The Pyrolysis of Methylcyclopentadiene: Isomerisation and Formation of Aromatics. In *28th Symposium (International) on Combustion, The Combustion Institute*, page 1725, 2000.

[139] A.T. Ingemarsson, J.R. Pedersen, and J.O. Olsson. Oxidation of n heptane in a Premixed Laminar Flame. *J. Phys. Chem.*, 103:8222, 1999.

[140] D.R. Jenkins, V.S. Yumlu, and D.B. Spalding. Combustion of Hydrogen and Oxygen in a Steady – Flow Adiabatic Stirred Reactor. In *11th Symposium (International) on Combustion, The Combustion Institute*, page 779, 1967.

[141] W.P. Jones and R.P. Lindstedt. Global Reaction Schemes for Hydrocarbon Combustion. *Comb. Flame*, 73:233, 1988.

[142] W.P. Jones and R.P. Lindstedt. The Calculation of the Structure of Laminar Counterflow Diffusion Flames Using a Global Reaction Mechanism. *Comb. Sci. Tech.*, 61:31, 1988.

[143] W. Juchmann, H. Latzel, D.I. Shin, G. Peiter, T. Dreier, H.-R. Volpp, J. Wolfrum, R.P. Lindstedt, and K.M. Leung. Absolute Radical Concentration Measurements and Modelling of Low Pressure $CH_4/O_2/NO$ Flames. In *27th Symposium (International) on Combustion, The Combustion Institute*, page 469, 1998.

[144] R.J. Kee, F.M. Rupley, and J.A. Miller. The CHEMKIN Thermodynamic Data Base. Technical report, Sandia National Laboratories, Report No. SAND87-8215B, 1989.

[145] R.D. Kern, H.J. Singh, and C.H. Wu. Thermal Decomposition of 1,2 Butadiene. *Int. J. Chem.*, 20:731, 1988.

[146] J.A. Kerr and A.F. Trotman-Dickenson. The Reactions of Alkyl Radicals. Part III. N-Butyl Radicals from the Photolysis of n-Valeraldehyde. *J. Chem. Soc.*, page 1602, 1960.

[147] J.H. Kiefer, L.J. Mizerka, M.R. Patel, and H.C. Wei. A Shock Tube Investigation of Major Pathways in the High Temperature Pyrolysis of Benzene. *J. Phys. Chem.*, 89:2013, 1985.

[148] S.D. Klotz, K. Brezinsky, and I. Glassman. Modelling the Combuston of Toluene – Butane Blends. In *27th Symposium (International) on Combustion, The Combustion Institute*, page 337, 1998.

[149] V.D. Knyazev, A. Bencsura, S.I. Stoliarov, and I.R. Slagle. Kinetics of the $C_2H_3 + H_2 = h + C_2H_4$ Reactions. *J. Phys. Chem.*, 100:11346, 1996.

[150] V.D. Knyazev and I.R. Slagle. Unimolecular Decomposition of n-C_4H_9 and iso-C_4H_9 Radicals. *J. Phys. Chem.*, 100:5318, 1996.

[151] M. Koch, F. Temps, and H.Gg. Wagner. Kinetics of the Reactions of $CH_2(\tilde{a}^1A_1)$ with CH_3C_2H, HCN, CO_2, N_2O and COS. *Ber. Bunsenges. Phys. Chemistry*, 94:645, 1990.

[152] K. Kohse-Hoinghaus, B. Atakan, A. Lamprecht, G.G. Alatorre, M. Kamphus, and N.N. Liu. Contributions to the Investigation of Recation Pathways in Fuel – Rich Flames. *Phys. Chem. Chem. Phys.*, 4:2056, 2002.

[153] S. Kojima. Detailed Modelling of n – butane Autoignition Chemistry. *Comb. Flame*, 99:87, 1994.

[154] C.P. Koshland. Impacts and Control of Air Toxics from Combustion. In *26th Symposium (International) on Combustion, The Combustion Institute*, page 2049, 1996.

[155] N. Kunzli, R. Kaiser, S. Medina, M. Studnicka, O. Chanel, P. Filliger, M. Herry, Jr. F. Horak, V. Puybonnieux-Texier, P. Quenel, J. Schneider, R. Seethaler, J.C. Vergnaud, and H. Sommer. Public Health Impact of Outdoor and Traffic Related Air Pollution: A European Assessment. *Lancet*, 100:795, 2000.

[156] K.K. Kuo. *Principles of Combustion.* Wiley–Interscience, first edition, 1986.

[157] A. Laskin and A. Lifshitz. Thermal Decomposition of Indene. Experimental Results and Kinetic Modelling. In *27th Symposium (International) on Combustion, The Combustion Institute*, page 313, 1998.

[158] A. Laskin and H. Wang. On Initiation Reactions of Acetylene Oxidation in Shock Tubes. A Quantum Mechanical and Kinetic Modeling Study. *Chem. Phys. Lett.*, 303:43, 1999.

[159] A. Laskin, H. Wang, and C.K. Law. Detailed Kinetic Modelling of 1,3-Butadiene Oxidation at High Temperatures. *Int. J. Chem. Kin.*, 32:589, 2000.

[160] D.R. Leslie. Diesel Emissions Evaluation for the Surface Mining Industry. http://smartmines.com/diesem.html, 2002.

[161] K.M. Leung. *Kinetic Modelling of Hydrocarbon Flames Using Detailed and Systematically Reduced Chemistry.* PhD thesis, Imperial College of Science, Technology and Medicine, England, UK, 1995.

[162] K.M. Leung and R.P. Lindstedt. Detailed Kinetic Modelling of C_1 – C_3 Alkane Diffusion Flames. *Comb. Flame*, 102:129, 1995.

[163] P.D. Lightfoot, R.A. Cox, J.N. Crowley, M. Destriau, G.D. Hayman, M.E. Jenkin, G.K. Moortgat, and F. Zabel. Organic Peroxy Radicals: Kinetics, Spectroscopy and Tropospheric Chemistry. *Atmos. Environ. Part A*, 26:1805, 1992.

[164] C.Y. Lin and M.C. Lin. Thermal Decomposition of Methyl Phenyl – Ethyl in Shock Waves: The Kinetics of Phenoxy Radical Reactions. *J. Phys Chem.*, 90:425, 1986.

[165] R.P. Lindstedt. Modelling of the Chemical Complexities of Flames. In *27th Symposium (International) on Combustion*, page 269, 1998.

[166] R.P. Lindstedt and L.Q. Maurice. Detailed Kinetic Modelling of n – Heptane Combustion. *Comb. Sci. Tech.*, 107:317, 1995.

[167] R.P. Lindstedt and L.Q. Maurice. Detailed Chemical Kinetic Modelling for Aviation Fuels. *J. of Prop. and Power.*, 120:187, 1996.

[168] R.P. Lindstedt and L.Q. Maurice. Detailed Kinetic Modelling of Toluene Combustion. *Comb. Sci. Tech.*, 120:119, 1996.

[169] R.P. Lindstedt, L.Q. Maurice, and M.P. Meyer. Thermodynamic and Kinetic Issues in the Formation and Oxidation of Aromatic Species. *Faraday Discuss.*, 119:409, 2001.

[170] R.P. Lindstedt and K.-A. Rizos. The Formation and Oxidation of Aromatics in Cylopentene and Methyl – Cyclopentadiene Mixtures. In *29th Symposium (International) on Combustion, The Combustion Institute*, page 2291, 2002.

[171] R.P. Lindstedt and G. Skevis. Detailed Modelling of Premixed Benzene Flames. *Comb. Flame*, 99:551, 1994.

[172] R.P. Lindstedt and G. Skevis. A Study of Acetylene Chemistry in Flames. *Comb. Sci. Tech.*, 125:73, 1997.

[173] R.P. Lindstedt and G. Skevis. Molecular Growth and Oxygenated Species Formation in Laminar Ethylene Flames. In *28th Symposium (International) on Combustion, The Combustion Institute*, page 1801, 2000.

[174] T.A. Litzinger. *The High Temperature Oxidation of Alkylated Aromatic Hydrocarbons.* PhD thesis, Princeton University, USA, 1985.

[175] A.C. Lloyd. Evaluated and Estimated Kinetic Data for Phase Reactions of the Hydroperoxyl Radical. *Int. J. Chem. Kin.*, 6:169, 1974.

[176] J.P. Longwell. The Formation of Polycyclic Aromatic Hydrocarbons by Combustion. In *19th Symposium (International) on Combustion*, page 1339, 1982.

[177] R. Lundgard and J. Heicklen. Pyrolysis of Vinylacetylene between 300 and 450 C. *Int. J. Chem. Kin.*, 16:125, 1984.

[178] R.K. Lyon. The Existence of Second Threshold for Combustion and its Implications to Incineration. In *23rd Symposium (International) on Combustion*, page 903, 1990.

[179] N.M. Marinov, M.J. Castaldi, C.F. Melius, and W. Tsang. Aromatic and Polycyclic Aromatic Hydrocarbon Formation in a Premixed Propane Flame. *Combust. Sci. Tech.*, 128:295, 1997.

[180] N.M. Marinov and P.C. Malte. Ethylene Oxidation in a Well Stirred Reactor. *Int. J. Chem. Kin.*, 27:957, 1995.

[181] N.M. Marinov, W.J. Pitz, C.K. Westbrook, A.M. Vincitore, M.J. Castaldi, S.M. Senkan, and C.F. Melius. Aromatic and PAH Formation in a Laminar Premixed n – butane Flame. *Comb. Flame*, 114:192, 1998.

[182] L.Q. Maurice. *Detailed Chemical Kinetic Models for Aviation Fuels.* PhD thesis, Imperial College of Science, Technology and Medicine, England, UK, 1996.

[183] L.Q. Maurice, H. Lander, T. Edwards, and W.E. Harrison. Advanced Aviation Fuels: a look ahead via a historical perspective. *Fuel*, 80:747, 2001.

[184] C.S. McEnally and L.D. Pfefferle. The Use of Carbon-13-Labelled Fuel Dopants for Identifying Naphthalene Formation Pathways in Non-Premixed Flames. In *28th Symposium (International) on Combustion, The Combustion Institute*, page 2569, 2000.

[185] A.M. Mebel, M.C. Lin, T. Yu, and K. Morokuma. Theoretical Study of Potential Energy Surface and Thermal Data Rate Constants for the $C_6H_5 + H_2$ and $C_6H_6 + H$ Reactions. *J. Phys. Chem.*, 101:3189, 1997.

[186] C.F. Melius, M.E. Colvin, N.M. Marinov, W.J. Pitz, and S.M. Senkan. Reaction Mechanisms in Aromatic Hydrocarbon Formation Involving the C_5H_5 Cyclopetadienyl Moiety. In *26th Symposium (International) on Combustion, The Combustion Institute*, page 685, 1996.

[187] M.P. Meyer. *The Application of Detailed and Systematically Reduced Chemistry to Transient Laminar Flames.* PhD thesis, Imperial College of Science, Technology and Medicine, England, UK, 2001.

[188] J.A. Miller and C.F. Melius. Kinetic and Thermodynamic Issues in the Formation of Aromatic Compounds in Flames and Aliphatic Fuels. *Comb. Flame*, 91:21, 1992.

[189] J.A. Miller, J.K. Roberts, and C.K. Westbrook. Chemical Kinetics and Combustion Modelling. *Ann. Rev. Phys. Chem.*, 41:345, 1990.

[190] R. Minetti, M. Ribaucour, M. Carlier, C. Fittschen, and L.R. Sochet. Experimental and Modelling Study of Oxidation and Autoignition of Butane at High Pressure. *Comb. Flame*, 96:201, 1994.

[191] R. Minetti, A. Roubaud, and E. Therssen. The Chemistry of Pre – Ignition of n – pentane and 1–pentane. *Comb. Flame*, 118:213, 1999.

[192] L. Mingming and J.A. Mulholland. Aromatic Hydrocarbon Growth from Indene. *Chemosphere*, 42:625, 2001.

[193] L.V. Moskaleva, A.M. Mebel, and M.C. Lin. The CH_3 + C_5H_5: A Potential Source of Benzene at High Temperatures. In *26th Symposium (International) on Combustion, The Combustion Institute*, page 521, 1996.

[194] M.F.R. Mulachy, B.G. Tucker, D.J. Williams, and J.R. Wilmhurst. Reactions of Free Radicals with Aromatic Compounds in the Gaseous Phase. III Kinetics of the Reaction of Methyl Radicals with Anisole (Methoxybenzene). *Aust. J. Chem.*, 20:1155, 1967.

[195] J.A. Mulholland, M. Lu, and D.-H. Kim. Pyrolytic Growth of Polycyclic Aromatic Hydrocarbons by Cyclopentadienyl Moieties. In *28th Symposium (International) on Combustion, The Combustion Institute*, page 2593, 2000.

[196] W. Muller-Markgraf and J. Troe. Shock Wave Study of Benzyl UV Absorption Spectra: Revised Toluene and Benzyl Decomposition Rates. In *22nd Symposium (International) on Combustion, The Combustion Institute*, page 815, 1986.

[197] W. Muller-Markgraf and J. Troe. Thermal Decomposition of Ethylbenzene, Styrene and Bromophenylethane: UV Absorption Study in Shock waves. *J. Phys. Chem.*, 92:4914, 1988.

[198] M. Nehse, J. Warnatz, and C. Chevalier. Kinetic Modelling of the Oxidation of Large Aliphatic Hydrocarbons. In *26th Symposium (International) on Combustion, The Combustion Institute*, page 773, 1996.

[199] K.M. Pamidimukkala, R.D. Kern, M.R. Patel, and H.C. Wei. High Temperature Pyrolysis of Toluene. *J. Phys. Chem.*, 91:2148, 1987.

[200] J. Peeters, W. Boullart, and K. Devriendt. $CH_4(a^4\sum^-$ and/or $X^2\pi)$ formation in the reaction between ketenyl radicals and oxygen atoms. determination of the CH yield between 405 and 960 K. *J. Phys. Chem.*, 99:3583, 1995.

[201] R.A. Perry, R. Atkinson, and J.N. Jr. Pitts. Kinetics and Mechansim of the Gas Phase Reaction of OH Radicals with Methoxybeneze and O–Cresol over the Temperature Range 299 – 435 K. *J. Phys. Chem.*, 81:1607, 1977.

[202] U. Pfahl, K. Fieweger, and G. Adomeit. Self-Ignition of Diesel-Relavent Hydrocarbon- Air Mixtures Under Engine Conditions. In *26th Symposium (International) on Combustion, The Combustion Institute*, page 781, 1996.

[203] H. Pitsch. Detailed Kinetic Reaction Mechanism for Ignition and Oxidation of 1 – Methylnaphthalene. In *26th Symposium (International) on Combustion, The Combustion Institute*, page 721, 1996.

[204] W.J. Pitz and C.K. Westbrook. Chemical Kinetics of the High Pressure Oxidation of n-Butane and its Relation to Engine Knock. *Combust. Flame*, 63:113, 1986.

[205] W.J. Pitz, C.K. Westbrook, W.M. Proscia, and F.L. Dryer. A Comprehensive Chemical Kinetic Reaction Mechanism for the Oxidation of n – butane. In *20th Symposium (International) on Combustion, The Combustion Institute*, page 831, 1984.

[206] C.J. Pope and J.A. Miller. Exploring Old and New Benzene Formation Pathways in Low Pressure Premixed Flames of Aliphatic Fuels. In *28th Symposium (International) on Combustion, The Combustion Institute*, page 1519, 2000.

[207] M.J. Rabinowitz, J. Sunderland, P.M. Patterson, and R.B. Klumm. Direct Rate Constant Measurements of H + CH_4 = CH_3 + H_2 Using the Flash – Photolysis Technique. *J. Phys. Chem.*, 95:674, 1991.

[208] V.S. Rao and G.B. Skinner. Formation of H and D Atoms in the Pyrolysis of Toluene-d_8 and Toluene-1,1,1-d_3. *J. Phys. Chem.*, 93:1864, 1989.

[209] I.A.B. Reid, C. Robinson, and D.B. Smith. Spontaneous Ignition of Methane: Measurement and Chemical Model. In *20th Symposium (International) on Combustion, The Combustion Institute*, page 1833, 1984.

[210] R.C. Reid, J.M. Prausnitz, and B.E. Poling. *The Properties of Gases and Liquids.* McGraw Hill, INC., first edition, 1987.

[211] M. Ribaucour, R. Minetti, and L.R. Sochet. Autoignition of n – pentane and 1 – pentane: Experimental Data and Kinetic Modelling. In *26th Symposium (International) on Combustion, The Combustion Institute*, page 345, 1998.

[212] H. Richter, T.G. Benish, O.A. Mazyar, W.H. Green, and J.B. Howard. Formation of PAH and their Radicals in a Nearly Sooting Premixed Benzene Flame. In *28th Symposium (International) on Combustion, The Combustion Institute*, page 2609, 2000.

[213] H. Richter, W.J. Grieco, and J.B. Howard. Formation Mechanism of Polycyclic Aromatic Hydrocarbons and Fullerenes in Premixed Benzene Flames. *Comb. Flame*, 119:1, 1999.

[214] H. Richter and J.B. Howard. Formation of Polycyclic Aromatic Hydrocarbons and their Growth to Soot – A Review of Chemical Reaction Pathways. *Prog. En. Comb. Sci.*, 26:565, 2000.

[215] H. Richter and J.B. Howard. Formation and Consumption of Single–Ring Aromatic Hydrocarbons and their Precursors in Premixed Acetylene, Ethylene and Benzene Flames. *Phys. Chem. Chem. Phys.*, 4:2038, 2002.

[216] H. Richter, O.A. Mazyar, R. Sumathi, W.H. Green, J.B. Howard, and J.W. Bozzelli. Detailed Kinetic Study of the Growth of Small Polycyclic Aromatic Hydrocarbons. 1 – Naphthyl + Ethyne. *J. Phys. Chem. A.*, 105:1561, 2001.

[217] A. Ristori, P. Dagaut, A.El. Bakali, G. Pengloan, and M. Cathonnet. Benzene Oxidation: Experimental Results in a JDR and Comprehensive Kinetic Modelling in a JSR, Shock – Tube and Flame. *Comb. Sci. Tech.*, 167:223, 2001.

[218] K.A. Rizos. *Detailed Chemical Kinetic Modelling of Homogeneous Systems.* PhD thesis, Imperial College of Science, Technology and Medicine, England, UK, 2003.

[219] D.A. Robaugh and W. Tsang. Mechanism and Rate of Hydrogen Atom Attack on Toluene at High Temperature. *J. Phys. Chem.*, 90:4159, 1986.

[220] D.A. Robaugh, W. Tsang, A. Fahr, and S.E. Stein. Ethylbenzene Pyrolysis: Benzyl C – C or C – H Bond Homolysis. *Ber. Bunsenges. Phys. Chemistry*, 90:77, 1986.

[221] J.F. Roesler and M.A. De Tessan. Aromatics and Soot Growth Enhancement by Methane Addition to Fuel Rich n – heptane Combustion in a Flow Reactor. *Comb. Sci. Tech.*, 161:245, 2000.

[222] F.D. Rossini, K.S. Pitzer, R.L. Arnett, R.M. Braun, and G.C. Pimentel. *Selected Values of Physical and Thermodynamic Properties of Hydrocarbons and Related Compounds.* Carnegie Press, Pittsburgh, first edition, 1953.

[223] R. Rota, Fiandaca R, M. Morbidelli, and S. Carra. Experimental Analysis of the Combustion of Mixtures of $C_1 - C_2$ Hydrocarbons. *Ind. Eng. Chem. Res.*, 38:897, 1999.

[224] K. Roy, M. Braun-Unkhoff, P. Frank, and Th. Just. Kinetics of the Cyclopentadiene Decay and the Recombination of Cyclopentadienyl Radicals with H-Atoms: Enthalpy of Formation of the Cyclopentadienyl Radical. *Int. J. Chem. Kinet.*, 33:821, 2001.

[225] K. Roy, C. Horn, P. Frank, V.G. Slutsky, and T. Just. High–Temperature Investigations on the Pyrolysis of Cyclopentadiene. In *27th Symposium (International) on Combustion, The Combustion Institute*, page 329, 1998.

[226] C.R. Shaddix. *An Experimental Study of the High Temperature Oxidation of 1 – Methylnaphthalene.* PhD thesis, Princeton University, USA, 1993.

[227] C.R. Shaddix, K. Brezinksy, and I. Glassman. Oxidation of 1 – Methylnaphthalene. In *24th Symposium (International) on Combustion, The Combustion Institute*, page 683, 1992.

[228] C.R. Shaddix, K. Brezinksy, and I. Glassman. Analysis of Fuel Decay Routes in the High Temperature Oxidation of 1 – Methylnaphthalene. *Comb. Flame*, 108:139, 1997.

[229] R.A. Shandross, J.P. Lovell, and J.B. Howard. Destruction of Benzene in High Temperature Flames: Chemistry of Benzene and Phenol. In *26th Symposium (International) on Combustion, The Combustion Institute*, page 711, 1996.

[230] V. Sick, F. Hildenbrand, and R.P. Lindstedt. Quantitive Laser-Based Measurements and Detailed Chemical Modelling fo Nitric Oxide Concentrations in Methane-Air Counterflow Diffusion Flames. In *27th Symposium (International) on Combustion, The Combustion Institute*, page 1401, 1998.

[231] G. Skevis. *Soot Precursor Chemistry in Laminar Premixed Flames.* PhD thesis, Imperial College of Science, Technology and Medicine, England, UK, 1996.

[232] M.W. Slack. Kinetics and Thermodynamics of the CN molecule. III. Shock Tube Measurement of CN Dissociation Rates. *J. Phys. Chem.*, 64:228, 1976.

[233] T.M. Sloane. Ignition and Flame Propagation Modelling with an Improved Methane Oxidation Mechanism. *Comb. Sci. Tech.*, 63:287, 1989.

[234] G.P. Smith, D.M. Golden, M. Frenklanch, B. Eiteneer, M. Goldenberg, C.T. Bowman, R.K. Hanson, S. Song, W.C. Gar-

diner Jr., V.V. Lissianski, and Z. Quinn. Gri–mech 3.0. http://www.me.berkeley.edu/gri_mech/version30/text30.html, 1999.

[235] L.R. Smith. Hydrocarbon Speciation. http://www.swri.org/3pubs/brochure/d08/hycarbs/hycarbs.htm, 2002.

[236] R.K. Solly and S.W. Benson. Kinetics of the Gas – Phase Reaction of Benzaldehyde with Iodine: The Heat of Formation and Stabilization Energy of the Benzoyl Radical. *J. Am. Chem. Soc.*, 93:2127, 1971.

[237] B.R. Stanmore, J.F. Briljac, and P. Gilot. The Oxidation of Soot: A Review of Experiments and Models. *Carbon*, 39:2247, 2001.

[238] D.R. Stull, E.F. Westrum Jr., and G.C. Sinke. *The Chemical Thermodynamics of Organic Compounds.* John Wiley & Sons, INC., first edition, 1969.

[239] Y. Tan, P. Dagaut, M. Cathonnet, and J.C. Boettner. Acetylene Oxidation in a JSR from 1 to 10 atm. and Comprehensive Modelling. *Comb. Sci. Tech.*, 102:21, 1994.

[240] Y. Tan, P. Dagaut, M. Cathonnet, and J.C. Boettner. Pyrolysis, Oxidation and Ignition of C_1 and C_2 Hydrocarbons: Experiments and Modelling. *J. Chim. Phys.*, 92:726, 1995.

[241] Y. Tan and P. Frank. A Detailed Comprehensive Kinetic Model for Benzene oxidation using the recent kinetic results. In *26th Symposium (International) on Combustion, The Combustion Institute*, page 677, 1996.

[242] R.S. Timonen, E. Ratajczak, D. Gutman, and A.F. Wagner. The Addition and Dissociation Reaction H + O_2 = HCO. 2. Experimental Details and Comparison with Theory. *J. Phys. Chem.*, 91:5325, 198.

[243] J. Troe. Towards a Quantitive Understanding of Elementary Combustion Reactions. In *22nd Symposium (International) on Combustion, The Combustion Institute*, page 843, 1988.

[244] W. Tsang. Pyrolysis of 2,4-Dimethylhexene-1 and the Stability of Isobutenyl Radicals. *Int. J. Chem. Kin.*, 5:929, 1973.

[245] W. Tsang. Chemical Kinetic Data Base for Combustion Chemistry. Part 3. Propane. *J. Phys. Chem. Ref. Data*, 17:887, 1988.

[246] W. Tsang. Chemical Kinetic Database for Combustion Chemistry. Part 3. Propane. *J. Phys. Chem. Ref. Data*, 17:887, 1988.

[247] W. Tsang. Chemical Kinetic Data Base for Combustion Chemistry. Part 4. Isobutane. *J. Phys. Chem. Ref. Data*, 19:1, 1990.

[248] W. Tsang. Chemical Kinetic Database for Combustion Chemistry. Part v. Propene. *J. Phys. Chem. Ref. Data*, 20:221, 1991.

[249] W. Tsang and R.F. Hampson. Chemical Kinetic Database for Combustion Chemistry. Part 1. Methane and Related Compunds. *J. Phys. Chem. Ref. Data*, 15:1087, 1986.

[250] W. Tsang and V. Mokrushin. Mechanism and Rate Constants for 1,3-Butadiene Decomposition. In *28th Symposium (International) on Combustion*, page 1717, 2000.

[251] W. Tsang and J.A. Walker. Hydrogen Atom Attack on 1 – Phenylpropene at High Temperatures. In *25th Symposium (International) on Combustion, The Combustion Institute*, page 867, 1994.

[252] C. Venkat, K. Brezinsky, and I. Glassman. High Temperature Oxidation of Aromatic Hydrocarbons. In *19th Symposium (International) on Combustion*, page 143, 1982.

[253] J.V. Volponi and M.C. Branch. Flame Structure of C_2H_2-O_2-Ar and C_2H_2-NO_2-Ar Laminar Premixed Flames. In *24th Symposium (International) on Combustion*, page 823, 1992.

[254] C. Vovelle, J.L. Delfau, and M. Reuillion. *Soot Formation in Combustion*, chapter Formation of Aromatic Hydrocarbons in Decane and Kerosene Flames at Reduced Pressure. Springer–Verlag, first edition, 1994.

[255] A.F. Wagner, I.R. Slagle, D. Sarzynski, and D. Gutman. Experimental and Theoretical Study of the $C_2H_5 + O_2$ Reaction Kinetics. *J. Phys. Chem.*, 94:1853, 1990.

[256] H. Wang and M. Frenklach. Calculations of Rate Coefficients for the Chemically Activated Reactions of Acetylene with Vinylic and Aromatic Radicals. *J. Phys. Chem.*, 98:11465, 1994.

[257] H. Wang and M. Frenklach. A Detailed Kinetic Modelling Study of Aromatics Formation in Laminar Premixed Acetylene and Ethylene Flames. *Comb. Flame*, 110:173, 1997.

[258] J. Warnatz. The Mechanism of High Temperature Combustion of Propane and Butane. *Comb. Sci. Tech.*, 34:177, 1983.

[259] J. Warnatz. Chemistry of High Temperature Combustion of Alkanes up to Octane. In *20th Symposium (International) on Combustion, The Combustion Institute*, page 845, 1984.

[260] J. Warnatz. *Combustion Chemistry*. Springer–Verlag, 1984.

[261] J. Warnatz, U. Maas, and R.W. Dibble. Combustion. ftp://reaflow.iwr.uni-heidlelberg.de/pub/mechanism_for_export/, 1996.

[262] C.K. Westbrook and F.L. Dryer. Chemical Kinetic Modelling of Hydrocarbon Combustion. *Prog. En. Comb. Sci.*, 10:1, 1984.

[263] C.K. Westbrook, W.J. Pitz, H.C. Curran, J. Boercker, and E. Kunrath. Chemical Kinetic Modelling Study of Shock Tube Ignition of Heptane Isomers. *Int. J. Chem. Kin.*, 33:868, 2001.

[264] C.K. Westbrook, M.M. Thornton, W.J. Pitz, and P.C. Malte. A Kinetic Study of Ethylene Oxidation in a Well Stirred Reactor. In *11th Symposium (International) on Combustion, The Combustion Institute*, page 863, 1988.

[265] C.K. Westbrook, J. Warantz, and W.J. Pitz. A Detailed Chemical Kinetic Reaction Mechanism for the Oxidation of Iso – Octane and n – Heptane over an Extended Temperature Range and its Application to Analysis of Engine Knock. In *22nd Symposium (International) on Combustion, The Combustion Institute*, page 893, 1988.

[266] P.R. Westmoreland, A.M. Dean, J.B. Howard, and J.P. Longwell. Forming Benzene in Flames by Chemically Activated Isomerization. *J. Phys. Chem.*, 93:8171, 1989.

[267] R.D. Wilk, N.P. Cernansky, and R.S. Cohen. The Oxidation of Propane at Low and Transition Temperatures. *Comb. Sci. Tech.*, 49:41, 1986.

[268] R.D. Wilk, N.P. Cernansky, W.J. Pitz, and C.K. Westbrook. Propene Oxidation at a Low and Intermediate Temperatures: A Detailed Chemical Kinetic Study. *Comb. Flame*, 77:145, 1989.

[269] W.Tsang. Thermal Decomposition of Cyclopentane and Related Compunds. *Int. J. Chem. Kin.*, 10:599, 1978.

[270] C.L. Yu, C. Wang, and M. Frenklach. Chemical Kinetics of Methyl Oxidation by Molecular Oxygen. *J. Phys. Chem.*, 99:14377, 1995.

[271] T. Yu and M.C. Lin. Kinetics of the $C_6H_5 + O_2$ Reaction at Low Temperatures. *J. Am. Chem. Soc.*, 116:9571, 1994.

[272] S.P. Zeppieri, S.D. Klotz, and F.L. Dryer. Modelling Concepts for Larger Carbon Number Alkanes: A Partially Reduced Skeletal Mechanism for n – decane Oxidation and Pyrolysis. In *28th Symposium (International) on Combustion, The Combustion Institute*, page 1587, 2000.

[273] X. Zhong and J.W. Bozzelli. Thermochemical and Kinetic Analysis on the Addition Reactions of H, O, OH and HO_2 with 1,3 Cyclopentadiene. *Int. J. Chem. Kin.*, 29:893, 1997.

[274] X. Zhong and J.W. Bozzelli. Thermochemical and Kinetic Analysis of the H, OH, HO_2, O and O_2 Association Reactions with Cyclopentadienyl Radical. *J. Phys. Chem.*, 102:3537, 1998.

Appendix A

Reaction Mechanism

The comprehensive reaction mechanism developed and utilised in the present work is shown in Table A.1. Reaction rates are expressed in the form:

$$k = AT^n exp(-E_a/RT) \tag{A.1}$$

where,

A = frequency factor, $(\text{kmol/m}^3)^{(1-m)}/\text{s}$, m is the order of reaction

n = temperature dependancy exponent

E_a = activation energy, kJ/mole

R = ideal gas constant, 8.314 kJ/K/mole

T = temperature, K

Unimolecular and recombination reactions generally exhibit complex pressure dependance. Troe [243] proposed a generalised expression for the fall–off behaviour of such reactions:

Fall-Off Expression

$$k = \frac{k_0 k_\infty [M]}{k_0 [M] + k_\infty} F \tag{A.2}$$

The parameter F is the broadening factor and can be mathematically described as:

Broadening Factor

$$\log F = \frac{\log F_c}{1 + \left(\log \frac{k_0[M]}{k_\infty} / N\right)^2} \tag{A.3}$$

$$N = 0.75 - 1.27 \log F_c \tag{A.4}$$

The factor F_c is temperature dependent and may be estimated through Equation A.5.

$$F_c = (1 - a) \exp\left(-\frac{T}{T^{***}}\right) + a \exp\left(-\frac{T}{T^{*}}\right) + \exp\left(-\frac{T^{**}}{T}\right) \tag{A.5}$$

Finally, in the case where the broadening factor is set as equal to unity, the Lindemann form is assumed. The reaction mechanism consists of 1896 reactions and 324 species.

Table A.1: Detailed Chemical Kinetic Mechanism

No	*Reaction*			A	n	E_a	*Ref*
1	$H + O_2$	=	$OH + O$	2.0000E+11	0.00	70.30	[162]
2	$O + H_2$	=	$OH + H$	5.1200E+01	2.67	26.30	[162]
3	$OH + H_2$	=	$H_2O + H$	1.0000E+05	1.60	13.80	[162]
4	$OH + OH$	=	$H_2O + O$	3.5700E+01	2.40	-8.84	[162]
5	$O_2 + H + M$	=	$HO_2 + M^a$	2.3000E+12	-0.80	0.00	[162]
6	$HO_2 + H$	=	$OH + OH$	1.6800E+11	0.00	3.66	[162]
7	$HO_2 + H$	=	$H_2 + O_2$	4.2700E+10	0.00	5.90	[162]
8	$HO_2 + OH$	=	$H_2O + O_2$	2.8900E+10	0.00	-2.08	[162]
9	$HO_2 + H$	=	$H_2O + O$	3.0000E+10	0.00	7.20	[162]
10	$HO_2 + O$	=	$OH + O_2$	3.1900E+10	0.00	0.00	[162]
11	$HO_2 + HO_2$	=	$H_2O_2 + O_2$	1.8600E+09	0.00	6.44	[162]
12	$H_2O_2 + H$	=	$H_2O + OH$	1.0000E+10	0.00	15.00	[162]
13	$H_2O_2 + H$	=	$HO_2 + H_2$	1.7000E+09	0.00	15.70	[162]
14	$H_2O_2 + O$	=	$HO_2 + OH$	6.6000E+08	0.00	16.60	[162]
15	$H_2O_2 + OH$	=	$H_2O + HO_2$	1.7500E+09	0.00	1.33	[7]
16	$H_2O_2 + M$	=	$OH + OH + M^b$	1.2000E+14	0.00	190.00	[162]
17	$H + H + M$	=	$H_2 + M^c$	6.5300E+11	-1.00	0.00	[162]
18	$H + H + H_2$	=	$H_2 + H_2$	9.2000E+10	-0.60	0.00	[162]
19	$H + H + H_2O$	=	$H_2 + H_2O$	6.0000E+13	-1.25	0.00	[162]
20	$H + H + CO_2$	=	$H_2 + CO_2$	5.4900E+14	-2.00	0.00	[162]
21	$H + OH + M$	=	$H_2O + M^d$	2.2000E+16	-2.00	0.00	[162]
22	$O + O + M$	=	$O_2 + M^b$	1.0000E+11	-1.00	0.00	[162]
23	$C_1 + OH$	=	$CO + H$	5.0000E+10	0.00	0.00	[172]
24	$C_1 + O_2$	=	$CO + O$	1.2000E+11	0.00	16.71	[72]
25	$C_1 + C_1 + M$	=	$C_2 + M$	1.8000E+15	-1.60	0.00	[232]
26	$CH + M$	=	$C_1 + H + M$	1.0000E+11	0.00	267.95	[173]
27	$CH + H$	=	$C_1 + H_2$	3.0000E+10	0.00	0.00	[218]
28	$CH + O$	=	$CO + H$	4.0000E+10	0.00	0.00	[162]
29	$CH + OH$	=	$C_1 + H_2O$	4.0000E+04	2.00	12.55	[172]
30	$CH + OH$	=	$CHO + H$	3.0000E+10	0.00	0.00	[162]
31	$CH + O_2$	=	$CHO + O$	7.5000E+10	0.00	0.00	[172]
32	$CH + H_2O$	=	CH_2OH	5.7300E+09	0.00	-3.15	[172]
33	$CH + CO_2$	=	$CO + CHO$	3.4000E+09	0.00	2.90	[162]
34	$^1CH_2 + M$	=	$^3CH_2 + M^e$	1.0000E+10	0.00	0.00	[162]
35	$^1CH_2 + H$	=	$CH + H_2$	7.0000E+10	0.00	0.00	[162]
36	$^1CH_2 + O$	=	$CO + H + H$	1.5000E+10	0.00	0.00	[162]
37	$^1CH_2 + O$	=	$CO + H_2$	1.5000E+10	0.00	0.00	[162]
38	$^1CH_2 + OH$	=	$CH_2O + H$	3.0000E+10	0.00	0.00	[162]
39	$^1CH_2 + H_2$	=	$CH_3 + H$	7.2300E+10	0.00	0.00	[162]
40	$^1CH_2 + O_2$	=	$CO + OH + H$	3.0000E+10	0.00	0.00	[162]
41	$^1CH_2 + CO_2$	=	$CH_2O + CO$	3.0000E+09	0.00	0.00	[162]
42	$^3CH_2 + M$	=	$C_1 + H_2 + M$	1.1480E+11	0.00	233.70	[173]
43	$^3CH_2 + H$	=	$CH + H_2$	1.1000E+11	0.00	0.00	[23]
44	$^3CH_2 + O$	=	$CO + H + H$	4.8800E+10	0.00	0.00	[200]
45	$^3CH_2 + O$	=	$CO + H_2$	3.2500E+10	0.00	0.00	[200]
46	$^3CH_2 + OH$	=	$CH + H_2O$	1.1300E+04	2.00	12.56	[162]
47	$^3CH_2 + OH$	=	$CH_2O + H$	2.5000E+10	0.00	0.00	[162]
48	$^3CH_2 + C_1$	=	$C_2H + H$	5.0000E+10	0.00	0.00	[172]
49	$^3CH_2 + CH$	=	$C_2H_2 + H$	4.0000E+10	0.00	0.00	[162]
50	$^3CH_2 + {}^3CH_2$	=	$C_2H_2 + H + H$	1.2000E+11	0.00	3.32	[162]

Table A.1, continued

No	*Reaction*			A	n	E_a	*Ref*
51	$^3CH_2 + H_2$	=	$CH_3 + H$	3.0000E+06	0.00	0.00	[162]
52	$^3CH_2 + O_2$	=	$CO + H + OH$	1.6420E+18	-3.30	12.00	[80]
53	$^3CH_2 + O_2$	=	$CO + H_2O$	2.2400E+19	-3.30	12.00	[80]
54	$^3CH_2 + O_2$	=	$CO_2 + H + H$	3.2850E+18	-3.30	12.00	[80]
55	$^3CH_2 + O_2$	=	$CO_2 + H_2$	2.6300E+18	-3.30	12.00	[80]
56	$^3CH_2 + O_2$	=	$CH_2O + O$	3.2850E+18	-3.30	12.00	[80]
57	$^3CH_2 + CO$	=	C_2H_2O	6.0300E+05	0.00	0.00	[218]
58	$^3CH_2 + CO_2$	=	$CH_2O + CO$	1.1000E+08	0.00	4.18	[162]
59	$CH_3 + M$	=	$CH + H_2 + M$	6.9000E+11	0.00	345.03	[162]
60	$CH_3 + M$	=	$^1CH_2 + H + M$	1.9000E+13	0.00	382.44	[162]
61	$CH_3 + H$	=	CH_4[f,1] $k_\infty =$	2.1000E+11	0.00	0.00	[162]
			$k_0 =$	6.3000E+17	-1.80	0.00	
62	$CH_3 + O$	=	$CH_2O + H$	8.4300E+10	0.00	0.00	[162]
63	$CH_3 + OH$	=	$^1CH_2 + H_2O$	4.0000E+10	0.00	10.47	[162]
64	$CH_3 + OH$	=	$CH_2O + H_2$	1.0240E+09	0.00	0.00	[162]
65	$CH_3 + OH$	=	$CH_2OH + H$	1.5000E+11	0.00	34.46	[162]
66	$CH_3 + OH$	=	$CH_3O + H$	5.7400E+09	-0.23	58.28	[162]
67	$CH_3 + OH$	=	CH_3OH[2] $k_\infty =$	6.0000E+10	0.00	0.00	[14]
			$k_0 =$	1.5950E+38	-8.20	0.00	
68	$CH_3 + HO_2$	=	$CH_3O + OH$	1.8000E+10	0.00	0.00	[162]
69	$CH_3 + C_1$	=	$C_2H_2 + H$	5.0000E+10	0.00	0.00	[172]
70	$CH_3 + CH$	=	$C_2H_3 + H$	3.0000E+10	0.00	0.00	[162]
71	$CH_3 + {}^1CH_2$	=	$C_2H_4 + H$	1.8000E+10	0.00	0.00	[162]
72	$CH_3 + {}^3CH_2$	=	$C_2H_4 + H$	4.0000E+10	0.00	0.00	[13]
73	$CH_3 + CH_3$	=	$C_2H_5 + H$	5.0000E+09	0.10	44.36	[13]
74	$CH_3 + CH_3$	=	C_2H_6[g,3] $k_\infty =$	3.6000E+10	0.00	0.00	[162]
			$k_0 =$	1.2700E+35	-7.00	11.55	
75	$CH_3 + O_2$	=	$CH_2O + OH$	1.8500E+09	0.00	85.01	[270]
76	$CH_3 + O_2$	=	$CH_3O + O$	1.3200E+11	0.00	131.36	[162]
77	$CH_3 + O_2$	=	CH_3OO[4] $k_\infty =$	2.0600E+06	1.10	0.00	[7]
			$k_0 =$	5.3100E+19	-3.30	0.00	
78	$CH_4 + H$	=	$CH_3 + H_2$	3.8600E+03	2.11	32.42	[207]
79	$CH_4 + O$	=	$CH_3 + OH$	9.0330E+05	1.56	35.50	[13]
80	$CH_4 + OH$	=	$CH_3 + H_2O$	1.5600E+04	1.83	11.60	[13]
81	$CH_4 + HO_2$	=	$CH_3 + H_2O_2$	9.0330E+09	0.00	103.09	[162]
82	$CH_4 + CH$	=	$C_2H_4 + H$	6.0000E+10	0.00	0.00	[162]
83	$CH_4 + {}^1CH_2$	=	$CH_3 + CH_3$	4.2700E+10	0.00	0.00	[162]
84 a	$CH_4 + O_2$	=	$CH_3 + HO_2$	3.9700E+10	0.00	238.00	[162] ♯
84 b	$CH_3 + HO_2$	=	$CH_4 + O_2$	1.0000E+10	0.00	0.00	adj. [249] ♯
85	$CO + O + M$	=	$CO_2 + M$[b]	5.3000E+07	0.00	-19.00	[162]
86	$CO + OH$	=	$CO_2 + H$	4.4000E+03	1.50	-3.10	[172]
87	$CO + HO_2$	=	$CO_2 + OH$	1.5000E+11	0.00	98.93	[162]
88	$CO + O_2$	=	$CO_2 + O$	2.5000E+09	0.00	200.00	[162]
89	$CHO + M$	=	$CO + H + M$[h]	1.8600E+14	-1.00	71.13	[242]
90	$CHO + H$	=	$CO + H_2$	9.0000E+10	0.00	0.00	[162]
91	$CHO + O$	=	$CO + OH$	3.0000E+10	0.00	0.00	[162]
92	$CHO + O$	=	$CO_2 + H$	3.0000E+10	0.00	0.00	[162]
93	$CHO + OH$	=	$CO + H_2O$	1.0000E+11	0.00	0.00	[162]
94	$CHO + CH_3$	=	$CO + CH_4$	1.2000E+11	0.00	0.00	[162]
95	$CHO + O_2$	=	$CO + HO_2$	1.2000E+07	0.81	-3.04	[134]
96	$CH_2O + M$	=	$CHO + H + M$	1.2600E+13	0.00	326.00	[162]
97	$CH_2O + H$	=	$CHO + H_2$	1.2600E+05	1.62	9.06	[14]
98	$CH_2O + O$	=	$CHO + OH$	4.1500E+08	0.57	11.56	[162]
99	$CH_2O + OH$	=	$CHO + H_2O$	3.4300E+06	1.18	-1.87	[13]
100	$CH_2O + HO_2$	=	$CHO + H_2O_2$	2.0000E+09	0.00	48.97	[162]
101	$CH_2O + CH$	=	$C_2H_2O + H$	9.4600E+10	0.00	-2.16	[162]
102	$CH_2O + CH_3$	=	$CHO + CH_4$	4.0900E+09	0.00	37.00	[162]
103	$CH_2O + O_2$	=	$CHO + HO_2$	6.0000E+10	0.00	170.00	[162]

♯ : Reaction (84a) used in Chapters 2 – 3.2 and Chapter 4, Reaction (84b) used in Chapter 3.3 and Chapter 5.

Table A.1, continued

No	*Reaction*			A	n	E_a	*Ref*
104	$CH_2OH + M$	=	$CH_2O + H + M$	4.4000E+12	0.00	125.52	[123]
105	$CH_2OH + H$	=	$CH_2O + H_2$	3.0000E+10	0.00	0.00	[162]
106	$CH_2OH + O$	=	$CH_2O + OH$	4.2200E+10	0.00	0.00	[162]
107	$CH_2OH + OH$	=	$CH_2O + H_2O$	2.4000E+10	0.00	0.00	[162]
108	$CH_2OH + O_2$	=	$CH_2O + HO_2$	4.5600E-09	5.94	-18.99	[106]
109	$CH_3O + M$	=	$CH_2O + H + M$	5.4500E+10	0.00	56.50	[162]
110	$CH_3O + CH_3OH$	=	$CH_2OH + CH_3OH$	3.0100E+08	0.00	17.04	[162]
111	$CH_3O + H$	=	$CH_2O + H_2$	2.0000E+10	0.00	0.00	[162]
112	$CH_3O + O$	=	$CH_2O + OH$	6.0000E+09	0.00	0.00	[162]
113	$CH_3O + OH$	=	$CH_2O + H_2O$	1.8000E+10	0.00	0.00	[162]
114	$CH_3O + O_2$	=	$CH_2O + HO_2$	6.6000E+07	0.00	10.88	[162]
115	$CH_3OH + M$	=	$^1CH_2 + H_2O + M$	7.0000E+12	0.00	277.99	[162]
116	$CH_3OH + M$	=	$CH_2OH + H + M$	2.0000E+14	0.00	315.89	[162]
117	$CH_3OH + H$	=	$CH_2OH + H_2$	1.4400E+10	0.00	25.50	[111]
118	$CH_3OH + H$	=	$CH_3O + H_2$	4.0000E+09	0.00	25.50	[162]
119	$CH_3OH + O$	=	$CH_2OH + OH$	3.8800E+02	2.50	12.90	[162]
120	$CH_3OH + O$	=	$CH_3O + OH$	1.0000E+10	0.00	19.59	[162]
121	$CH_3OH + OH$	=	$CH_2OH + H_2O$	3.0000E+01	2.65	-3.70	[162]
122	$CH_3OH + OH$	=	$CH_3O + H_2O$	5.3000E+00	2.65	-3.70	[162]
123	$CH_3OH + O_2$	=	$CH_2OH + HO_2$	2.0500E+10	0.00	188.00	[250]
124	$CH_3OH + HO_2$	=	$CH_2OH + H_2O_2$	3.9800E+10	0.00	81.22	[112]
125	$CH_3OH + CH_3$	=	$CH_2OH + CH_4$	3.1900E-02	3.20	30.00	[162]
126	$CH_3OO + HO_2$	=	$CH_3OOH + O_2$	2.4700E+08	0.00	-6.57	[163]
127	$CH_3OO + CH_3$	=	$CH_3O + CH_3O$	1.0000E+10	0.00	0.00	[218]
128	$CH_3OO + CH_4$	=	$CH_3OOH + CH_3$	3.0000E+09	0.00	95.00	[209]
129	$CH_3OO + CH_2O$	=	$CH_3OOH + CHO$	3.0000E+09	0.00	52.00	[218]
130	$CH_3OO + CH_3OO$	=	$CH_3O + CH_3O + O_2$	5.4800E+07	0.00	-3.49	[14]
131	CH_3OOH	=	$CH_3O + OH$	6.0000E+14	0.00	177.09	[209]
132	$C_2 + O$	=	$CO + C_1$	3.6100E+11	0.00	0.00	[92]
133	$C_2 + O_2$	=	$CO + CO$	8.9700E+09	0.00	4.10	[12]
134	$C_2H + H$	=	$C_2 + H_2$	3.6100E+10	0.00	118.25	[249]
135	$C_2H + O$	=	$CO + CH$	1.0000E+10	0.00	0.00	[162]
136	$C_2H + OH$	=	$C_2HO + H$	2.0000E+10	0.00	0.00	[162]
137	$C_2H + CH_3$	=	$C_3H_3 + H$	2.4100E+10	0.00	0.00	[162]
138	$C_2H + C_2H$	=	$C_4H + H$	1.0000E+11	0.00	0.00	[162]
139	$C_2H + H_2$	=	$C_2H_2 + H$	5.6700E+07	0.90	8.34	[162]
140	$C_2H + O_2$	=	$CO + CO + H$	9.0400E+09	0.00	-1.91	[162]
141	$C_2H + H_2O$	=	$C_2H_2O + H$	1.1400E+10	0.00	1.66	[172]
142	$C_2H + C_2H$	=	$C_2H_2 + C_2$	1.8100E+09	0.00	0.00	[249]
143	$C_2H_2 + M$	=	$C_2H + H + M$	4.2000E+13	0.00	448.00	[162]
144	$C_2H_2 + M$	=	$H_2C_2 + M$	2.5000E+12	-0.64	207.95	[158]
145	$C_2H_2 + O$	=	$CO + {}^3CH_2$	2.8930E+03	2.09	6.53	[218]
146	$C_2H_2 + O$	=	$C_2HO + H$	4.3390E+03	2.09	6.53	[218]
147	$C_2H_2 + OH$	=	$C_2H + H_2O$	3.3700E+04	2.00	58.57	[162]
148	$C_2H_2 + OH$	=	$C_2H_2O + H$	3.7500E+03	1.70	4.18	[172]
149	$C_2H_2 + O_2$	=	$C_2H + HO_2$	1.2000E+10	0.00	311.70	[162]
150	$C_2H_2 + HO_2$	=	$C_2H_2O + OH$	6.0000E+06	0.00	33.52	[249]
151	$C_2H_2 + CH$	=	$C_3H + H_2$	3.1500E+10	0.00	-0.51	[172]
152	$C_2H_2 + CH$	=	$C_3H_2 + H$	1.7850E+11	0.00	-0.51	[172]
153	$C_2H_2 + {}^1CH_2$	=	$C_3H_3 + H$	8.0000E+10	0.00	0.00	[172]
154	$C_2H_2 + {}^1CH_2$	=	$C_3H_4(B)$	8.0000E+10	0.00	0.00	[172]
155	$C_2H_2 + {}^3CH_2$	=	$C_3H_4(B)$	1.2000E+10	0.00	27.70	[162]
156	$C_2H_2 + CH_3$	=	$C_3H_4(A) + H$	9.6800E+10	0.00	117.13	[165]
157	$C_2H_2 + CH_3$	=	$C_3H_4(P) + H$	6.1900E+09	0.00	71.12	[120]
158	$C_2H_2 + CH_3$	=	$C_3H_5(A)$	2.6800E+50	-12.82	149.59	[70]
159	$C_2H_2 + CH_3$	=	$C_3H_5(S)$	1.6100E+37	-8.58	85.06	[74]
160	$C_2H_2 + C_2H$	=	$C_4H_2 + H$	1.2000E+11	0.00	0.00	[162]
161	$C_2H_2 + C_2H_2$	=	$C_4H_3(I) + H$	2.0000E+09	0.00	268.00	[162]
162	$C_2H_2 + C_2H_2$	=	$C_4H_3(N) + H$	1.0000E+09	0.00	276.14	[162]

Table A.1, continued

No	Reaction			A	n	E_a	Ref
163	$H_2C_2 + O$	=	$^3CH_2 + CO$	3.0000E+10	0.00	0.00	[158]
164	$H_2C_2 + OH$	=	$^3CH_2 + CHO$	2.0000E+10	0.00	0.00	[158]
165	$H_2C_2 + O_2$	=	$CHO + CHO$	1.0000E+10	0.00	0.00	[218]
166	$H_2C_2 + O_2$	=	$^3CH_2 + CO_2$	5.0000E+10	0.00	0.00	[158]
167	C_2H_3	=	$C_2H_2 + H^{i,5}$ $k_\infty =$	2.0000E+14	0.00	166.28	[13]
			$k_0 =$	4.1600E+38	-7.50	190.40	
168	$C_2H_3 + H$	=	$C_2H_2 + H_2$	3.0000E+10	0.00	0.00	[13]
169	$C_2H_3 + O$	=	$C_2H_2O + H$	3.0000E+10	0.00	0.00	[162]
170	$C_2H_3 + OH$	=	$C_2H_2 + H_2O$	2.0000E+10	0.00	0.00	[162]
171	$C_2H_3 + O_2$	=	$CH_2O + CHO$	1.6400E+18	-2.78	10.56	[257]
172	$C_2H_3 + O_2$	=	$C_2H_2 + HO_2$	1.6600E+11	-0.83	10.63	[173]
173	$C_2H_3 + O_2$	=	$CH_2CHO + O$	2.5000E+09	0.06	3.97	[173]
174	$C_2H_3 + O_2$	=	$CH_3CO + O$	1.5000E+08	0.00	-1.00	[172]
175	$C_2H_3 + HO_2$	=	$CH_3CO + OH$	3.0000E+10	0.00	0.00	[249]
176	$C_2H_3 + CH$	=	$C_2H_2 + {}^3CH_2$	5.0000E+10	0.00	0.00	[162]
177	$C_2H_3 + CH$	=	$C_3H_2 + H_2$	3.1500E+10	0.00	-0.51	[218]
178	$C_2H_3 + CH$	=	$C_3H_3 + H$	1.7850E+11	0.00	-0.51	[218]
179	$C_2H_3 + {}^1CH_2$	=	$C_3H_3 + H_2$	8.0000E+10	0.00	0.00	[218]
180	$C_2H_3 + {}^1CH_2$	=	$C_3H_4(B) + H$	8.0000E+10	0.00	0.00	[218]
181	$C_2H_3 + {}^3CH_2$	=	$C_3H_4(B) + H$	1.2000E+10	0.00	27.70	[218]
182	$C_2H_3 + C_2H$	=	$C_2H_2 + C_2H_2$	3.0000E+10	0.00	0.00	[162]
183	$C_2H_3 + C_2H$	=	C_4H_4	1.0000E+11	0.00	0.00	[83]
184	$C_2H_3 + C_2H_2$	=	$C_4H_4 + H$	4.6800E+09	0.00	21.70	[172]
185	$C_2H_3 + C_2H_3$	=	$C_4H_6(T)$	1.0000E+10	0.00	0.00	[162]
186	$C_2H_4 + M$	=	$C_2H_3 + H + M$	2.6000E+14	0.00	404.00	[162]
187	$C_2H_4 + H$	=	$C_2H_3 + H_2$	5.0700E+04	1.93	54.19	[149]
188	$C_2H_4 + H$	=	$C_2H_5{}^{e,6}$ $k_\infty =$	3.9740E+06	1.28	5.40	[14]
			$k_0 =$	4.7140E+12	0.00	3.16	
189	$C_2H_4 + O$	=	$CHO + CH_3$	8.1000E+03	1.88	0.76	[173]
190	$C_2H_4 + O$	=	$CH_2CHO + H$	4.7000E+03	1.88	0.76	[173]
191	$C_2H_4 + O$	=	$C_2H_2O + H_2$	6.7500E+02	1.88	0.76	[173]
192	$C_2H_4 + OH$	=	$C_2H_3 + H_2O$	2.0500E+10	0.00	24.86	[13]
193	$C_2H_4 + O_2$	=	$C_2H_3 + HO_2$	4.2200E+10	0.00	241.12	[249]
194	$C_2H_4 + HO_2$	=	$C_2H_3 + H_2O_2$	1.1200E+10	0.00	127.30	[135]
195	$C_2H_4 + HO_2$	=	$CH_3CHO + OH$	6.0300E+06	0.00	33.26	[249]
196	$C_2H_4 + HO_2$	=	$C_2H_4O + OH$	2.2300E+09	0.00	71.90	[13]
197	$C_2H_4 + CH$	=	$C_3H_3 + H_2$	3.1500E+10	0.00	-0.51	[218]
198	$C_2H_4 + CH$	=	$C_3H_4(B) + H$	1.7850E+11	0.00	-0.51	[218]
199	$C_2H_4 + {}^1CH_2$	=	$C_3H_4(B) + H_2$	8.0000E+10	0.00	0.00	[218]
200	$C_2H_4 + {}^1CH_2$	=	$C_3H_5(B) + H$	8.0000E+10	0.00	0.00	[218]
201	$C_2H_4 + {}^1CH_2$	=	C_3H_6	6.6000E+10	0.00	0.00	[162]
202	$C_2H_4 + {}^3CH_2$	=	$C_3H_5(B) + H$	1.2000E+10	0.00	27.70	[218]
203	$C_2H_4 + {}^3CH_2$	=	C_3H_6	1.8000E+07	0.00	0.00	[162]
204	$C_2H_4 + C_2H$	=	$C_4H_4 + H$	1.2100E+10	0.00	0.00	[249]
205	$C_2H_5 + O$	=	$CH_2O + CH_3$	6.6000E+10	0.00	0.00	[162]
206	$C_2H_5 + O$	=	$CH_3CHO + H$	6.6000E+10	0.00	0.00	[173]
207	$C_2H_5 + O_2$	=	$C_2H_4 + HO_2$	1.0200E+07	0.00	-9.14	[162]
208	$C_2H_5 + O_2$	=	$C_2H_5OO^7$ $k_\infty =$	2.2100E+07	0.77	-2.39	[255]
			$k_0 =$	7.1000E+36	-8.24	17.87	
209	C_2H_6	=	$C_2H_5 + H^{g,8}$ $k_\infty =$	8.8500E+20	-1.23	427.70	[162]
			$k_0 =$	4.9000E+39	-6.43	448.40	
210	$C_2H_6 + H$	=	$C_2H_5 + H_2$	1.4450E+06	1.50	31.00	[162]
211	$C_2H_6 + O$	=	$C_2H_5 + OH$	1.0000E+06	1.50	24.30	[162]
212	$C_2H_6 + OH$	=	$C_2H_5 + H_2O$	7.2260E+03	2.00	3.61	[162]
213	$C_2H_6 + O_2$	=	$C_2H_5 + HO_2$	6.0230E+10	0.00	217.00	[13]
214	$C_2H_6 + HO_2$	=	$C_2H_5 + H_2O_2$	1.3200E+10	0.00	85.64	[13]
215	$C_2H_6 + {}^1CH_2$	=	$C_2H_5 + CH_3$	1.1400E+11	0.00	0.00	[162]
216	$C_2H_6 + CH_3OO$	=	$CH_3OOH + C_2H_5$	3.0000E+08	0.00	62.50	[249]

Table A.1, continued

No	*Reaction*			A	n	E_a	*Ref*
217	$C_2O + H$	=	$CO + CH$	5.0000E+10	0.00	0.00	[162]
218	$C_2O + O$	=	$CO + CO$	5.0000E+10	0.00	0.00	[162]
219	$C_2O + OH$	=	$CO + CO + H$	2.0000E+10	0.00	0.00	[162]
220	$C_2O + O_2$	=	$CO + CO + O$	2.0000E+10	0.00	0.00	[162]
221	$C_2HO + H$	=	$^1CH_2 + CO$	1.0000E+11	0.00	0.00	[162]
222	$C_2HO + O$	=	$CO + CO + H$	9.6350E+10	0.00	0.00	[162]
223	$C_2HO + OH$	=	$C_2O + H_2O$	3.0000E+10	0.00	0.00	[162]
224	$C_2HO + CH$	=	$C_2H_2 + CO$	5.0000E+10	0.00	0.00	[162]
225	$C_2HO + {}^3CH_2$	=	$C_2H_3 + CO$	3.0000E+10	0.00	0.00	[162]
226	$C_2HO + C_2HO$	=	$C_2H_2 + CO + CO$	1.0000E+10	0.00	0.00	[162]
227	$C_2HO + O_2$	=	$CO + CO + OH$	1.0000E+10	0.00	0.00	[162]
228	$C_2HO + O_2$	=	$CO_2 + CO + H$	1.0000E+10	0.00	0.00	[162]
229	$C_2HO + C_2H_2$	=	$C_3H_3 + CO$	1.0000E+08	0.00	12.60	[162]
230	$C_2H_2O + H$	=	$CO + CH_3$	1.1100E+04	2.00	8.36	[118]
231	$C_2H_2O + H$	=	$C_2HO + H_2$	1.8000E+11	0.00	35.98	[118]
232	$C_2H_2O + O$	=	$CO_2 + {}^3CH_2$	2.0000E+10	0.00	9.60	[260]
233	$C_2H_2O + O$	=	$C_2HO + OH$	2.0000E+04	2.00	41.68	[173]
234	$C_2H_2O + OH$	=	$CH_2OH + CO$	1.0200E+10	0.00	0.00	[13]
235	$C_2H_2O + OH$	=	$C_2HO + H_2O$	1.0000E+04	2.00	12.56	[173]
236	$C_2H_2O + {}^1CH_2$	=	$C_2H_4 + CO$	1.2600E+11	0.00	0.00	[40]
237	$C_2H_2O + CH_3$	=	$C_2H_5 + CO$	9.0000E+07	0.00	0.00	[172]
238	$C_2H_2O + CH_3$	=	$C_2HO + CH_4$	7.5000E+09	0.00	54.39	[172]
239	CH_2CHO	=	CH_3CO	1.0000E+13	0.00	184.10	[173]
240	CH_2CHO	=	$C_2H_2O + H$	1.5800E+13	0.00	196.65	[173]
241	$CH_2CHO + O$	=	$C_2H_2O + OH$	1.0000E+11	0.00	0.00	[173]
242	$CH_2CHO + OH$	=	$C_2H_2O + H_2O$	1.0000E+10	0.00	0.00	[173]
243	$CH_2CHO + O_2$	=	$CH_2O + CO + OH$	1.8100E+07	0.00	0.00	[13]
244	$CH_2CHO + CH_3$	=	$C_2H_6 + CO$	6.1000E+09	0.00	0.00	[173]
245	CH_3CO	=	$CH_3 + CO$* k_∞ =	2.8000E+13	0.00	71.75	[173]
			k_0 =	6.0300E+12	0.00	58.86	
246	$CH_3CO + H$	=	$CH_3 + CHO$	2.1500E+10	0.00	0.00	[218]
247	$CH_3CO + H$	=	$C_2H_2O + H_2$	1.1500E+10	0.00	0.00	[218]
248	$CH_3CO + O$	=	$CH_3 + CO_2$	1.5440E+11	0.00	0.00	[218]
249	$CH_3CO + O$	=	$C_2H_2O + OH$	3.8600E+10	0.00	0.00	[218]
250	$CH_3CO + OH$	=	$C_2H_2O + H_2O$	1.2100E+10	0.00	0.00	[249]
251	$CH_3CO + CH_3$	=	$C_2H_6 + CO$	5.0000E+10	0.00	0.00	[172]
252	$CH_3CHO + M$	=	$CHO + CH_3 + M$	7.0800E+15	0.00	342.15	[13]
253	$CH_3CHO + H$	=	$CH_3CO + H_2$	2.1000E+06	1.16	10.09	[172]
254	$CH_3CHO + O$	=	$CH_3CO + OH$	5.0000E+09	0.00	7.50	[260]
255	$CH_3CHO + OH$	=	$CH_3CO + H_2O$	2.3000E+07	0.73	-4.66	[172]
256	$CH_3CHO + HO_2$	=	$CH_3CO + H_2O_2$	3.0000E+09	0.00	49.87	[13]
257	$CH_3CHO + {}^3CH_2$	=	$CH_3CO + CH_3$	2.5000E+09	0.00	15.89	[172]
258	$CH_3CHO + CH_3$	=	$CH_3CO + CH_4$	2.0000E-09	5.64	10.31	[13]
259	$CH_3CHO + O_2$	=	$CH_3CO + HO_2$	4.0000E+10	0.00	164.19	[172]
260	C_2H_4O	=	$CH_3 + CHO$	3.4000E+13	0.00	241.90	[135]
261	C_2H_4O	=	CH_3CHO	5.8400E+11	0.00	219.10	[135]
262	$C_2H_4O + H$	=	$CHCH_2O + H_2$	7.9000E+10	0.00	41.00	[135]
263	$C_2H_4O + OH$	=	$CHCH_2O + H_2O$	1.7800E+10	0.00	15.10	[135]
264	$C_2H_4O + HO_2$	=	$CHCH_2O + H_2O_2$	1.1200E+10	0.00	127.30	[135]
265	$C_2H_4O + CH_3$	=	$CHCH_2O + CH_4$	1.0700E+09	0.00	49.50	[135]
266	$C_2H_4O + CH_3O$	=	$CHCH_2O + CH_3OH$	1.2000E+08	0.00	28.30	[135]
267	$C_2H_4O + CH_3OO$	=	$CHCH_2O + CH_3OOH$	1.1200E+10	0.00	127.30	[135]
268	C_2H_5O	=	$CH_2O + CH_3$	1.0000E+15	0.00	90.40	[135]
269	C_2H_5O	=	$CH_3CHO + H$	2.5100E+14	0.00	97.90	[135]
270	$C_2H_5O + O_2$	=	$CH_3CHO + HO_2$	6.0300E+07	0.00	6.90	[135]

Table A.1, continued

No	*Reaction*			A	n	E_a	*Ref*
271	C_2H_4OOH	=	$C_2H_4 + HO_2$	2.0000E+13	0.00	81.60	[135]
272	C_2H_4OOH	=	$C_2H_4O + OH$	3.1600E+11	0.00	81.60	[135]
273	C_2H_5OO	=	C_2H_4OOH	2.8600E+11	0.00	125.60	[135]
274	$C_2H_5OO + HO_2$	=	$C_2H_5OOH + O_2$	1.6300E+08	0.00	-8.31	[135]
275	$C_2H_5OO + CH_4$	=	$C_2H_5OOH + CH_3$	1.1200E+10	0.00	103.20	[135]
276	$C_2H_5OO + CH_2O$	=	$C_2H_5OOH + CHO$	2.0000E+09	0.00	48.80	[135]
277	$C_2H_5OO + C_2H_4$	=	$C_2H_4O + C_2H_5O$	2.8200E+09	0.00	71.60	[135]
278	$C_2H_5OO + C_2H_4$	=	$C_2H_5OOH + C_2H_3$	1.1200E+10	0.00	127.30	[135]
279	$C_2H_5OO + C_2H_6$	=	$C_2H_5OOH + C_2H_5$	1.7000E+10	0.00	85.60	[135]
280	$C_2H_5OO + C_2H_4O$	=	$CHCH_2O + C_2H_5OOH$	1.1200E+10	0.00	127.30	[135]
281	C_2H_5OOH	=	$C_2H_5O + OH$	4.0000E+15	0.00	179.60	[135]
282	$C_2H_5OOH + CH_2OH$	=	$C_2H_5OO + CH_3OH$	3.0106E+06	0.00	10.80	[135]
283	$C_3H + O$	=	$C_2H + CO$	6.8000E+10	0.00	0.00	[162]
284	$C_3H + OH$	=	$C_2H_2 + CO$	6.8000E+10	0.00	0.00	[162]
285	$C_3H + CH$	=	$C_4H + H$	7.0000E+10	0.00	0.00	[172]
286	$C_3H + {}^1CH_2$	=	$C_4H_2 + H$	8.0000E+10	0.00	0.00	[172]
287	$C_3H + {}^3CH_2$	=	$C_4H_2 + H$	8.0000E+10	0.00	0.00	[172]
288	$C_3H + CH_3$	=	$C_4H_3(I) + H$	4.0000E+10	0.00	0.00	[172]
289	$C_3H + O_2$	=	$C_2H + CO_2$	9.0400E+09	0.00	-1.91	[218]
290	$C_3H + H_2O$	=	$C_3H_2O + H$	1.1500E+10	0.00	1.66	[172]
291	C_3H_2	=	C_3H_2L	1.0000E+13	0.00	272.00	[172]
292	$C_3H_2 + H$	=	$C_3H + H_2$	1.0000E+11	0.00	0.00	[172]
293	$C_3H_2 + O$	=	$C_2H + CO + H$	1.4000E+11	0.00	0.00	[172]
294	$C_3H_2 + OH$	=	$C_3H + H_2O$	6.0000E+10	0.00	0.00	[172]
295	$C_3H_2 + H_2O$	=	$C_3H_2O + H_2$	5.7300E+09	0.00	-3.16	[172]
296	$C_3H_2 + O_2$	=	$C_2H_2 + CO_2$	2.0000E+09	0.00	0.00	[162]
297	$C_3H_2 + O_2$	=	$C_3H_2O + O$	2.0000E+09	0.00	0.00	[218]
298	$C_3H_2 + CH$	=	$C_4H_2 + H$	7.0000E+10	0.00	0.00	[172]
299	$C_3H_2 + {}^1CH_2$	=	$C_4H_3(I) + H$	8.0000E+10	0.00	0.00	[172]
300	$C_3H_2 + {}^3CH_2$	=	$C_4H_3(I) + H$	8.0000E+10	0.00	0.00	[172]
301	$C_3H_2 + CH_3$	=	$C_4H_4 + H$	4.0000E+10	0.00	0.00	[172]
302	$C_3H_2L + H$	=	$C_3H + H_2$	1.0000E+11	0.00	0.00	[172]
303	$C_3H_2L + OH$	=	$C_3H + H_2O$	2.0000E+10	0.00	0.00	[172]
304	$C_3H_3 + H$	=	$C_3H_2L + H_2$	1.0000E+10	0.00	9.00	[172]
305	$C_3H_3 + O$	=	$C_3H_2O + H$	2.5000E+10	0.00	0.00	[218]
306	$C_3H_3 + OH$	=	$C_3H_2O + H_2$	4.0000E+09	0.00	0.00	[218]
307	$C_3H_3 + H_2O$	=	$C_3H_4O + H$	1.1500E+10	0.00	100.66	[172]
308	$C_3H_3 + O_2$	=	$C_2H_2O + CHO$	3.0000E+07	0.00	12.00	[162]
309	$C_3H_3 + CH$	=	$C_4H_3(I) + H$	7.0000E+10	0.00	0.00	[162]
310	$C_3H_3 + CH$	=	$C_4H_3(N) + H$	7.0000E+10	0.00	0.00	[162]
311	$C_3H_3 + {}^1CH_2$	=	$C_4H_4 + H$	8.0000E+10	0.00	0.00	[172]
312	$C_3H_3 + {}^3CH_2$	=	$C_4H_4 + H$	8.0000E+10	0.00	0.00	[162]
313	$C_3H_3 + C_3H_2$	=	$C_6H_4L + H$	1.0000E+10	0.00	0.00	[162]
314	$C_3H_3 + C_3H_3$	=	$C_6H_6(A)$	1.0000E+10	0.00	0.00	[162]
315	$C_3H_3 + C_3H_3$	=	$C_6H_6(B)$	1.0000E+10	0.00	0.00	[162]
316	$C_3H_3 + C_3H_3$	=	$C_6H_6(S)$	1.0000E+10	0.00	0.00	[162]
317	$C_3H_4(A) + M$	=	$C_3H_3 + H + M$	2.0000E+15	0.00	334.71	[162]
318	$C_3H_4(A) + H$	=	$C_3H_3 + H_2$	1.0000E+09	0.00	6.28	[119]
319	$C_3H_4(A) + H$	=	$C_3H_5(A)$	1.5200E+56	-13.54	112.83	[70]
320	$C_3H_4(A) + H$	=	$C_3H_5(T)$	8.5000E+09	0.00	8.37	[162]
321	$C_3H_4(A) + O$	=	$C_2H_3 + CHO$	1.1000E-05	4.61	-17.80	[162]
322	$C_3H_4(A) + OH$	=	$C_2H_2O + CH_3$	3.1200E+09	0.00	-1.66	[162]
323	$C_3H_4(A) + OH$	=	$C_3H_3 + H_2O$	1.0000E+09	0.00	6.27	[162]
324	$C_3H_4(A) + O_2$	=	$C_3H_3 + HO_2$	4.0000E+10	0.00	257.50	[162]
325	$C_3H_4(A) + CH$	=	$C_4H_4 + H$	2.7700E+11	0.00	0.00	[172]
326	$C_3H_4(A) + {}^1CH_2$	=	$C_4H_6(B)$	1.6000E+11	0.00	0.00	[172]
327	$C_3H_4(A) + {}^3CH_2$	=	$C_4H_6(B)$	1.6000E+10	0.00	0.00	[172]
328	$C_3H_4(A) + CH_3$	=	$C_3H_3 + CH_4$	2.0000E+09	0.00	32.20	[162]
329	$C_3H_4(A) + C_2H$	=	$C_3H_3 + C_2H_2$	1.0000E+10	0.00	0.00	[162]
330	$C_3H_4(A) + C_3H_3$	=	$C_6H_7(L)$	3.0000E+08	0.00	12.56	[266]
331	$C_3H_4(A) + C_3H_4(A)$	=	$C_3H_5(A) + C_3H_3$	5.0000E+11	0.00	270.88	[162]

Table A.1, continued

No	*Reaction*			A	n	E_a	*Ref*
332	$C_3H_4(B)$	=	$C_3H_4(A)$	1.5130E+14	0.00	211.00	[162]
333	$C_3H_4(B)$	=	$C_3H_4(P)$	7.0800E+13	0.00	182.96	[162]
334	$C_3H_4(P)$	=	$C_3H_4(A)$	5.1500E+60	-13.93	381.49	[70]
335	$C_3H_4(P) + H$	=	$C_3H_4(A) + H$	6.2700E+14	-0.91	42.20	[70]
336	$C_3H_4(P) + M$	=	$C_3H_3 + H + M$	4.7000E+15	0.00	334.17	[162]
337	$C_3H_4(P) + H$	=	$C_3H_3 + H_2$	1.0000E+09	0.00	6.28	[119]
338	$C_3H_4(P) + H$	=	$C_3H_5(S)$	5.8000E+09	0.00	12.98	[162]
339	$C_3H_4(P) + H$	=	$C_3H_5(T)$	6.5000E+09	0.00	8.37	[162]
340	$C_3H_4(P) + O$	=	$C_2H_3 + CHO$	3.2000E+09	0.00	8.41	[162]
341	$C_3H_4(P) + O$	=	$C_2HO + CH_3$	6.3000E+09	0.00	8.41	[162]
342	$C_3H_4(P) + O$	=	$C_2H_2O + {}^3CH_2$	6.4000E+09	0.00	8.41	[162]
343	$C_3H_4(P) + OH$	=	$C_2H_4 + CHO$	5.0000E-07	4.50	-4.19	[162]
344	$C_3H_4(P) + OH$	=	$C_3H_3 + H_2O$	3.0000E+00	3.00	0.83	[66]
345	$C_3H_4(P) + O_2$	=	$C_2HO + {}^3CH_2 + OH$	6.1538E+04	1.50	126.00	[218]
346	$C_3H_4(P) + O_2$	=	$C_3H_3 + HO_2$	5.0000E+09	0.00	213.00	[162]
347	$C_3H_4(P) + CH$	=	$C_4H_4 + H$	2.7700E+11	0.00	0.00	[172]
348	$C_3H_4(P) + {}^1CH_2$	=	$C_4H_6(B)$	1.6000E+11	0.00	0.00	[162]
349	$C_3H_4(P) + {}^3CH_2$	=	$C_4H_6(B)$	1.6000E+10	0.00	0.00	[172]
350	$C_3H_4(P) + CH_3$	=	$C_3H_3 + CH_4$	2.0000E+09	0.00	32.20	[119]
351	$C_3H_4(P) + C_2H$	=	$C_3H_3 + C_2H_2$	1.0000E+10	0.00	0.00	[162]
352	$C_3H_5(A) + H$	=	$C_3H_4(A) + H_2$	1.8100E+10	0.00	0.00	[248]
353	$C_3H_5(A) + H$	=	C_3H_6 [9] $k_\infty =$	2.0000E+11	0.00	0.00	[70]
			$k_0 =$	1.3300E+54	-12.00	24.98	
354	$C_3H_5(A) + O$	=	$C_3H_4O + H$	6.0000E+10	0.00	0.00	[248]
355	$C_3H_5(A) + OH$	=	$C_2H_2 + CH_2O + H_2$	1.5000E+10	0.00	0.00	[248]
356	$C_3H_5(A) + O_2$	=	$CH_3CO + CH_2O$	1.1900E+12	-1.01	84.27	[70]
357	$C_3H_5(A) + O_2$	=	$C_3H_4(A) + HO_2$	1.2100E+09	0.00	56.70	[248]
358	$C_3H_5(A) + O_2$	=	$C_3H_4O + OH$	8.4200E+05	0.00	-9.62	[172]
359	$C_3H_5(A) + HO_2$	=	$C_3H_5O + OH$	4.4550E+09	0.00	0.00	[218]
360	$C_3H_5(A) + HO_2$	=	$OH + C_2H_3 + CH_2O$	6.6000E+09	0.00	0.00	[70]
361	$C_3H_5(A) + CH_3$	=	$C_3H_4(A) + CH_4$	3.0000E+09	-0.32	-0.54	[162]
362	$C_3H_5(A) + C_2H_2$	=	$C_5H_6 + H$	4.0000E+10	0.00	90.00	[218]
363	$C_3H_5(A) + C_2H_3$	=	$C_3H_4(A) + C_2H_4$	2.4100E+09	0.00	0.00	[162]
364	$C_3H_5(A) + C_2H_4$	=	$C_5H_8 + H$	1.2046E+07	0.00	48.02	[248]
365	$C_3H_5(A) + C_2H_5$	=	$C_3H_4(A) + C_2H_6$	9.6000E+08	0.00	-0.54	[162]
366	$C_3H_5(A) + C_3H_5(A)$	=	$C_3H_6 + C_3H_4(A)$	8.4300E+07	0.00	-1.09	[162]
367	$C_3H_5(B)$	=	$C_3H_5(A)$	1.0000E+10	0.00	0.00	[173]
368	$C_3H_5(B) + H$	=	$C_3H_4(B) + H_2$	1.0000E+11	0.00	0.00	[173]
369	$C_3H_5(B) + O$	=	$C_2H_4 + CHO$	1.1000E+11	0.00	0.00	[173]
370	$C_3H_5(B) + O$	=	$C_3H_4(B) + OH$	3.6700E+10	0.00	0.00	[173]
371	$C_3H_5(B) + OH$	=	$C_3H_4(B) + H_2O$	2.0000E+10	0.00	0.00	[173]
372	$C_3H_5(S) + H$	=	$C_3H_4(A) + H_2$	1.8100E+10	0.00	0.00	[173]
373	$C_3H_5(S) + O$	=	$C_2H_2O + CH_3$	1.8070E+11	0.00	0.00	[162]
374	$C_3H_5(S) + O_2$	=	$CH_3CO + CH_2O$	2.1700E+09	0.00	0.00	[172]
375	$C_3H_5(S) + O_2$	=	$C_3H_4O + OH$	2.1700E+09	0.00	0.00	[172]
376	$C_3H_5(S) + CH_3$	=	$C_3H_4(A) + CH_4$	1.0000E+08	0.00	0.00	[162]
377	$C_3H_5(S) + C_2H_3$	=	$C_3H_4(A) + C_2H_4$	1.0000E+08	0.00	0.00	[162]
378	$C_3H_5(S) + C_2H_3$	=	$C_5H_8(X)$	1.0000E+10	0.00	0.00	[217]
379	$C_3H_5(S) + C_2H_5$	=	$C_3H_4(A) + C_2H_6$	1.0000E+08	0.00	0.00	[162]
380	$C_3H_5(T) + H$	=	$C_3H_4(A) + H_2$	1.8100E+10	0.00	0.00	[70]
381	$C_3H_5(T) + O$	=	$C_2HO + CH_3 + H$	1.8070E+11	0.00	0.00	[162]
382	$C_3H_5(T) + O_2$	=	$CH_3CO + CH_2O$	2.1700E+09	0.00	0.00	[172]
383	$C_3H_5(T) + O_2$	=	$C_3H_4O + OH$	2.1700E+09	0.00	0.00	[172]
384	$C_3H_5(T) + CH_3$	=	$C_3H_4(A) + CH_4$	1.0000E+08	0.00	0.00	[162]
385	$C_3H_5(T) + C_2H_3$	=	$C_3H_4(A) + C_2H_4$	1.0000E+08	0.00	0.00	[162]
386	$C_3H_5(T) + C_2H_3$	=	$C_5H_8(I)$	2.5000E+10	0.00	0.00	[53]
387	$C_3H_5(T) + C_2H_5$	=	$C_3H_4(A) + C_2H_6$	1.0000E+08	0.00	0.00	[162]
388	C_3H_6	=	$C_2H_3 + CH_3$ [10] $k_\infty =$	1.1000E+21	-1.20	408.84	[162]
389	C_3H_6	=	$C_3H_5(S) + H$	7.5900E+14	0.00	424.12	[162]
390	C_3H_6	=	$C_3H_5(T) + H$	1.4500E+15	0.00	410.56	[162]
391	$C_3H_6 + H$	=	$C_2H_4 + CH_3$	2.6000E+05	1.50	8.36	[121]
392	$C_3H_6 + H$	=	$C_3H_5(A) + H_2$	1.7280E+02	2.50	10.42	[248]
393	$C_3H_6 + H$	=	$C_3H_5(S) + H_2$	4.1000E+02	2.50	40.98	[248]

Table A.1, continued

No	*Reaction*			A	n	E_a	*Ref*
394	$C_3H_6 + H$	=	$C_3H_5(T) + H_2$	8.0360E+02	2.50	51.39	[248]
395	$C_3H_6 + H$	=	$C_3H_7(N)$	7.2300E+09	0.00	12.14	[162]
396	$C_3H_6 + O$	=	$CH_3 + CH_3 + CO$	6.9600E+04	1.57	-2.62	[162]
397	$C_3H_6 + O$	=	$C_2H_4 + CH_2O$	3.4840E+04	1.57	-2.62	[162]
398	$C_3H_6 + O$	=	$C_2H_5 + CHO$	5.2170E+04	1.57	-2.62	[162]
399	$C_3H_6 + OH$	=	$CH_3CHO + CH_3$	3.4600E+08	0.00	0.00	[205]
400	$C_3H_6 + OH$	=	$C_3H_5(A) + H_2O$	3.1000E+03	2.00	-1.25	[70]
401	$C_3H_6 + OH$	=	$C_3H_5(S) + H_2O$	4.1000E+09	0.00	28.87	[162]
402	$C_3H_6 + OH$	=	$C_3H_5(T) + H_2O$	4.1000E+09	0.00	28.87	[162]
403	$C_3H_6 + OH$	=	C_3H_6OH	2.7500E+09	0.00	-4.35	[172]
404	$C_3H_6 + O_2$	=	$C_3H_5(A) + HO_2$	1.9500E+09	0.00	163.28	[162]
405	$C_3H_6 + O_2$	=	$C_3H_5(S) + HO_2$	2.0000E+10	0.00	199.29	[162]
406	$C_3H_6 + O_2$	=	$C_3H_5(T) + HO_2$	2.0000E+10	0.00	184.22	[162]
407	$C_3H_6 + HO_2$	=	$C_3H_5(A) + H_2O_2$	9.6400E+00	2.60	58.20	[70]
408	$C_3H_6 + HO_2$	=	$C_3H_6O + OH$	1.2900E+09	0.00	62.38	[172]
409	$C_3H_6 + CH_3$	=	$C_3H_5(A) + CH_4$	2.2160E-03	3.50	23.74	[162]
410	$C_3H_6 + CH_3$	=	$C_3H_5(S) + CH_4$	8.4200E-04	3.50	48.77	[162]
411	$C_3H_6 + CH_3$	=	$C_3H_5(T) + CH_4$	1.3510E-03	3.50	53.76	[162]
412	$C_3H_6 + C_2H_5$	=	$C_3H_5(A) + C_2H_6$	2.2200E-03	3.50	27.77	[162]
413	$C_3H_6(B)$	=	C_3H_6	8.0400E+14	0.00	267.50	[173]
414	$C_3H_6(B) + H$	=	$C_3H_5(B) + H_2$	1.6200E+11	0.00	49.00	[173]
415	$C_3H_6(B) + O$	=	$C_2H_6 + CO$	6.3000E+05	1.45	-3.59	[173]
416	$C_3H_6(B) + OH$	=	$C_3H_5(B) + H_2O$	7.0400E+04	1.50	4.33	[173]
417	$C_3H_7(I)$	=	$C_2H_4 + CH_3$	2.0000E+10	0.00	123.50	[162]
418	$C_3H_7(I)$	=	$C_3H_6 + H^5$ k_∞ =	8.7600E+07	1.76	148.57	[14]
			k_0 =	2.1600E+14	0.00	118.06	
419	$C_3H_7(I) + H$	=	$C_3H_6 + H_2$	3.6100E+09	0.00	0.00	[245]
420	$C_3H_7(I) + H$	=	C_3H_8	2.0000E+10	0.00	0.00	[162]
421	$C_3H_7(I) + O$	=	$CH_3CHO + CH_3$	4.8200E+10	0.00	0.00	[245]
422	$C_3H_7(I) + O$	=	$AC_3H_6O + H$	4.8200E+10	0.00	0.00	[245]
423	$C_3H_7(I) + OH$	=	$C_3H_6 + H_2O$	2.4100E+10	0.00	0.00	[245]
424	$C_3H_7(I) + O_2$	=	$C_3H_6 + HO_2$	1.0000E+09	0.00	12.50	[162]
425	$C_3H_7(I) + O_2$	=	$C_3H_7OO(I)$	6.6200E+09	0.00	0.00	[218]
426	$C_3H_7(N)$	=	$C_2H_4 + CH_3{}^{11}$ k_∞ =	1.2300E+13	-0.10	126.37	[15]
			k_0 =	5.4000E+46	-12.00	149.65	
427	$C_3H_7(N) + H$	=	$C_3H_6 + H_2$	1.8100E+09	0.00	0.00	[245]
428	$C_3H_7(N) + H$	=	C_3H_8	2.0000E+10	0.00	0.00	[162]
429	$C_3H_7(N) + O$	=	$CH_2O + C_2H_5$	1.4000E+10	0.00	0.00	[173]
430	$C_3H_7(N) + O$	=	$PC_3H_6O + H$	8.3000E+10	0.00	0.00	[173]
431	$C_3H_7(N) + OH$	=	$C_3H_6 + H_2O$	2.4100E+10	0.00	0.00	[245]
432	$C_3H_7(N) + O_2$	=	$C_3H_6 + HO_2$	1.0000E+09	0.00	20.91	[162]
433	$C_3H_7(N) + O_2$	=	$C_3H_7OO(N)$	1.0000E+09	0.00	0.00	[267]
434	C_3H_8	=	$C_2H_5 + CH_3{}^{12}$ k_∞ =	1.1000E+17	0.00	353.00	[162]
			k_0 =	7.8280E+15	0.00	271.90	
435	$C_3H_8 + H$	=	$C_3H_7(I) + H_2$	1.0000E+11	0.00	34.90	[162]
436	$C_3H_8 + H$	=	$C_3H_7(N) + H_2$	1.3000E+11	0.00	40.60	[162]
437	$C_3H_8 + O$	=	$C_3H_7(I) + OH$	2.6000E+10	0.00	18.70	[162]
438	$C_3H_8 + O$	=	$C_3H_7(N) + OH$	3.0000E+10	0.00	24.10	[162]
439	$C_3H_8 + OH$	=	$C_3H_7(I) + H_2O$	4.7860E+05	1.40	3.55	[162]
440	$C_3H_8 + OH$	=	$C_3H_7(N) + H_2O$	5.7540E+05	1.40	3.55	[162]
441	$C_3H_8 + O_2$	=	$C_3H_7(I) + HO_2$	3.9700E+10	0.00	199.54	[245]
442	$C_3H_8 + O_2$	=	$C_3H_7(N) + HO_2$	3.9700E+10	0.00	212.85	[245]
443	$C_3H_8 + CH_3$	=	$C_3H_7(I) + CH_4$	1.5050E-03	3.46	22.90	[162]
444	$C_3H_8 + CH_3$	=	$C_3H_7(N) + CH_4$	9.0330E-04	3.65	29.90	[162]
445	C_3H_2O	=	$C_2H_2 + CO$	8.5100E+14	0.00	297.00	[162]
446	$C_3H_2O + O$	=	$C_2HO + CHO$	1.0000E+10	0.00	0.00	[162]
447	$C_3H_2O + OH$	=	$C_2H_2O + CHO$	1.0000E+10	0.00	0.00	[162]
448	C_3H_3O	=	$C_2H_3 + CO$	1.0000E+12	0.00	138.27	[172]
449	$C_3H_3O + H$	=	$C_3H_2O + H_2$	6.0000E+10	0.00	0.00	[172]
450	$C_3H_3O + O$	=	$C_3H_2O + OH$	7.8300E+10	0.00	0.00	[172]

Table A.1, continued

No	*Reaction*			A	n	E_a	*Ref*
451	C_3H_4O	=	$C_2H_3 + CHO$	1.0000E+14	0.00	422.00	[172]
452	$C_3H_4O + H$	=	$C_3H_3O + H_2$	3.9800E+10	0.00	17.58	[172]
453	$C_3H_4O + O$	=	$C_3H_3O + OH$	5.0000E+09	0.00	7.50	[172]
454	$C_3H_4O + OH$	=	$C_3H_3O + H_2O$	1.0000E+10	0.00	0.00	[172]
455	$C_3H_4O + HO_2$	=	$C_3H_3O + H_2O_2$	1.6980E+09	0.00	44.80	[172]
456	C_3H_5O	=	$C_2H_3 + CH_2O$	3.2400E+13	0.00	246.02	[172]
457	C_3H_5O	=	$C_2H_4 + CHO$	2.4500E+14	0.00	244.76	[172]
458	C_3H_5O	=	$C_2H_2O + CH_3$	1.5100E+14	0.00	250.62	[172]
459	C_3H_5O	=	PC_3H_5O	1.8400E+14	0.00	244.76	[172]
460	C_3H_5O	=	TC_3H_5O	1.8400E+14	0.00	244.76	[172]
461	AC_3H_5O	=	$C_2H_2O + CH_3$	8.0000E+13	0.00	108.78	[172]
462	PC_3H_5O	=	$C_2H_2O + CH_3$	8.0000E+13	0.00	125.52	[172]
463	TC_3H_5O	=	$C_2H_4 + CHO$	8.0000E+13	0.00	83.68	[172]
464	$TC_3H_5O + O_2$	=	$C_3H_4O + HO_2$	1.7370E+08	0.00	7.32	[172]
465	C_3H_6O	=	$CH_3CO + CH_3$	8.0000E+15	0.00	384.92	[172]
466	C_3H_6O	=	$C_3H_5O + H$	8.0000E+14	0.00	383.92	[172]
467	C_3H_6O	=	AC_3H_6O	1.0100E+14	0.00	250.62	[172]
468	C_3H_6O	=	PC_3H_6O	1.8400E+14	0.00	244.76	[172]
469	$C_3H_6O + H$	=	$C_3H_5O + H_2$	5.0000E+09	0.00	6.27	[172]
470	$C_3H_6O + O$	=	$C_3H_5O + OH$	3.0000E+10	0.00	21.75	[172]
471	$C_3H_6O + OH$	=	$C_3H_5O + H_2O$	2.0000E+10	0.00	12.80	[172]
472	$C_3H_6O + HO_2$	=	$C_3H_5O + H_2O_2$	3.2400E+08	0.00	62.34	[172]
473	$AC_3H_6O + M$	=	$CH_3CO + CH_3 + M$	2.4800E+16	0.00	340.58	[172]
474	$AC_3H_6O + H$	=	$AC_3H_5O + H_2$	2.0000E+11	0.00	37.65	[172]
475	$AC_3H_6O + O$	=	$AC_3H_5O + OH$	1.0000E+10	0.00	24.94	[172]
476	$AC_3H_6O + OH$	=	$AC_3H_5O + H_2O$	1.0200E+09	0.00	4.98	[172]
477	$AC_3H_6O + CH_3$	=	$AC_3H_5O + CH_4$	5.0000E+09	0.00	33.47	[172]
478	$PC_3H_6O + M$	=	$C_2H_5 + CHO + M$	7.2500E+16	0.00	344.76	[172]
479	$PC_3H_6O + M$	=	$CH_3CO + CH_3 + M$	4.7800E+16	0.00	351.46	[172]
480	$PC_3H_6O + H$	=	$PC_3H_5O + H_2$	1.0000E+11	0.00	37.65	[172]
481	$PC_3H_6O + H$	=	$TC_3H_5O + H_2$	1.0000E+11	0.00	37.65	[172]
482	$PC_3H_6O + O$	=	$PC_3H_5O + OH$	5.6800E+09	0.00	6.45	[172]
483	$PC_3H_6O + O$	=	$TC_3H_5O + OH$	5.6800E+09	0.00	6.45	[172]
484	$PC_3H_6O + OH$	=	$PC_3H_5O + H_2O$	1.2100E+10	0.00	0.00	[172]
485	$PC_3H_6O + OH$	=	$TC_3H_5O + H_2O$	1.2100E+10	0.00	0.00	[172]
486	$PC_3H_6O + CH_3$	=	$PC_3H_5O + CH_4$	5.0000E+09	0.00	33.47	[172]
487	$PC_3H_6O + CH_3$	=	$TC_3H_5O + CH_4$	5.0000E+09	0.00	33.47	[172]
488	C_3H_6OH	=	$C_2H_5 + CH_2O$	1.4100E+09	0.00	72.00	[172]
489	C_3H_6OH	=	$CH_3CHO + CH_3$	1.0000E+09	0.00	72.00	[172]
490	$C_3H_6OH + O_2$	=	$CH_3CHO + CH_2O + OH$	1.0000E+09	0.00	-4.60	[172]
491	$C_3H_7O(I)$	=	$CH_3CHO + CH_3$	3.9810E+14	0.00	71.96	[267]
492	$C_3H_7O(I) + O_2$	=	$AC_3H_6O + HO_2$	3.1620E+08	0.00	16.74	[267]
493	$C_3H_7O(I) + O_2$	=	$PC_3H_6O + HO_2$	3.1620E+08	0.00	16.74	[267]
494	$C_3H_7O(N)$	=	$C_2H_5 + CH_2O$	3.9810E+14	0.00	71.96	[267]
495	$C_3H_7O(N) + O_2$	=	$C_3H_6O + HO_2$	3.1620E+08	0.00	16.74	[267]
496	$C_3H_7O(N) + O_2$	=	$PC_3H_6O + HO_2$	3.1620E+08	0.00	16.74	[267]
497	C_3H_6OOH	=	$C_3H_6O + OH$	3.9810E+15	0.00	179.91	[17]
498	$C_3H_7OO(I)$	=	$CH_3CHO + CH_3O$	1.0000E+13	0.00	104.60	[267]
499	$C_3H_7OO(I) + CH_3CHO$	=	$C_3H_7OOH(I) + CH_3CO$	1.0000E+09	0.00	37.66	[267]
500	$C_3H_7OO(I) + C_3H_8$	=	$C_3H_7OOH(I) + C_3H_7(I)$	1.0000E+09	0.00	71.55	[267]
501	$C_3H_7OO(I) + C_3H_8$	=	$C_3H_7OOH(I) + C_3H_7(N)$	1.0000E+09	0.00	81.17	[267]
502	$C_3H_7OO(N)$	=	C_3H_6OOH	1.2590E+12	0.00	158.99	[267]
503	$C_3H_7OO(N) + CH_3CHO$	=	$C_3H_7OOH(N) + CH_3CO$	1.0000E+09	0.00	37.66	[267]
504	$C_3H_7OO(N) + C_3H_8$	=	$C_3H_7OOH(N) + C_3H_7(I)$	1.0000E+09	0.00	71.55	[267]
505	$C_3H_7OO(N) + C_3H_8$	=	$C_3H_7OOH(N) + C_3H_7(N)$	1.0000E+09	0.00	81.17	[267]
506	$C_3H_7OOH(I)$	=	$C_3H_7O(I) + OH$	3.9810E+15	0.00	179.91	[267]
507	$C_3H_7OOH(N)$	=	$C_3H_7O(N) + OH$	3.9810E+15	0.00	179.91	[267]
508	$C_4H + H_2$	=	$C_4H_2 + H$	4.0740E+02	2.40	0.84	[162]
509	$C_4H + C_2H_2$	=	$C_6H_2 + H$	1.2000E+11	0.00	0.00	[162]

Table A.1, continued

No	*Reaction*			A	n	E_a	*Ref*
510	C_4H_2	=	$C_4H + H$	7.8000E+14	0.00	502.40	[162]
511	$C_4H_2 + O$	=	$C_3H_2 + CO$	9.0000E+08	0.00	0.00	[162]
512	$C_4H_2 + OH$	=	$C_4H_2O + H$	6.6900E+09	0.00	-1.71	[162]
513	$C_4H_2 + CH$	=	$C_5H_2 + H$	8.0000E+10	0.00	0.00	[172]
514	$C_4H_2 + {}^1CH_2$	=	$C_5H_3(L) + H$	3.0000E+10	0.00	0.00	[162]
515	$C_4H_2 + {}^3CH_2$	=	$C_5H_3(L) + H$	1.3000E+10	0.00	18.10	[162]
516	$C_4H_2 + C_2H$	=	$C_6H_2 + H$	1.2000E+11	0.00	0.00	[162]
517	$C_4H_2 + C_2H_2$	=	$C_6H_2 + H + H$	1.5000E+11	0.00	234.50	[162]
518	$C_4H_2 + C_4H$	=	$C_8H_2 + H$	1.2000E+11	0.00	0.00	[162]
519	$C_4H_2 + C_4H_2$	=	$C_8H_2 + H + H$	1.5000E+11	0.00	234.50	[162]
520	$C_4H_3(I)$	=	$C_4H_2 + H^*$ $k_\infty =$	1.0000E+14	0.00	230.27	[162]
			$k_0 =$	2.0000E+12	0.00	200.83	
521	$C_4H_3(I)$	=	$C_4H_3(N)$	1.5000E+13	0.00	283.45	[162]
522	$C_4H_3(I) + H$	=	$C_4H_2 + H_2$	8.1300E+10	0.00	0.00	[162]
523	$C_4H_3(I) + O$	=	$C_4H_2 + OH$	2.0000E+10	0.00	0.00	[162]
524	$C_4H_3(I) + OH$	=	$C_4H_2 + H_2O$	3.0000E+10	0.00	0.00	[162]
525	$C_4H_3(I) + O_2$	=	$C_4H_2 + HO_2$	1.0000E+09	0.00	12.55	[162]
526	$C_4H_3(I) + CH$	=	$C_5H_3(L) + H$	1.6000E+11	0.00	0.00	[172]
527	$C_4H_3(I) + {}^1CH_2$	=	$C_5H_4(L) + H$	1.6000E+11	0.00	0.00	[172]
528	$C_4H_3(I) + {}^3CH_2$	=	$C_5H_4(L) + H$	1.6000E+11	0.00	0.00	[172]
529	$C_4H_3(N)$	=	$C_4H_2 + H^*$ $k_\infty =$	1.0000E+14	0.00	150.72	[162]
			$k_0 =$	1.0000E+11	0.00	125.52	
530	$C_4H_3(N) + H$	=	$C_4H_2 + H_2$	8.1300E+10	0.00	0.00	[162]
531	$C_4H_3(N) + OH$	=	$C_4H_2 + H_2O$	3.0000E+10	0.00	0.00	[162]
532	$C_4H_3(N) + CH$	=	$C_5H_3(L) + H$	1.6000E+11	0.00	0.00	[172]
533	$C_4H_3(N) + {}^1CH_2$	=	$C_5H_4(L) + H$	1.6000E+11	0.00	0.00	[172]
534	$C_4H_3(N) + {}^3CH_2$	=	$C_5H_4(L) + H$	1.6000E+11	0.00	0.00	[172]
535	$C_4H_3(N) + C_2H_2$	=	$C_6H_5(B)$	4.1200E+03	1.65	10.46	[162]
536	C_4H_4	=	$C_4H_3(I) + H$	8.6300E+09	0.00	246.86	[162]
537	$C_4H_4 + H$	=	$C_4H_3(N) + H_2$	2.0000E+04	2.00	25.17	[162]
538	$C_4H_4 + O$	=	$C_3H_4(A) + CO$	2.9500E+09	0.00	0.00	[130]
539	$C_4H_4 + OH$	=	$C_4H_3(N) + H_2O$	1.0000E+04	2.00	12.60	[162]
540	$C_4H_4 + CH$	=	C_5H_5	8.0000E+10	0.00	0.00	[172]
541	$C_4H_4 + {}^1CH_2$	=	C_5H_6	7.0000E+10	0.00	0.00	[172]
542	$C_4H_4 + {}^3CH_2$	=	C_5H_6	7.0000E+10	0.00	0.00	[172]
543	$C_4H_4 + CH_3$	=	$C_5H_7(I)$	2.5000E+10	0.00	0.00	[53]
544	$C_4H_4 + C_2H$	=	$C_4H_3(I) + C_2H_2$	3.9800E+10	0.00	0.00	[162]
545	$C_4H_4 + C_2H_3$	=	$C_6H_6 + H$	1.9000E+09	0.00	10.50	[173]
546	$C_4H_4 + C_4H_4$	=	C_8H_8	1.4800E+11	0.00	159.00	[177]
547	$C_4H_5(I)$	=	$C_4H_4 + H^*$ $k_\infty =$	1.0000E+14	0.00	209.34	[162]
			$k_0 =$	2.0000E+12	0.00	175.73	
548	$C_4H_5(I)$	=	$C_4H_5(T)$	1.5000E+13	0.00	283.45	[162]
549	$C_4H_5(I) + H$	=	$C_4H_4 + H_2$	1.0000E+11	0.00	0.00	[162]
550	$C_4H_5(I) + O$	=	$C_2H_2O + C_2H_3$	1.8070E+11	0.00	0.00	[172]
551	$C_4H_5(I) + OH$	=	$C_4H_4 + H_2O$	2.0000E+04	2.00	4.18	[162]
552	$C_4H_5(I) + O_2$	=	$CH_3CO + C_2H_2O$	4.1500E+07	0.00	10.50	[172]
553	$C_4H_5(I) + O_2$	=	$C_4H_4 + HO_2$	1.0000E+10	0.00	0.00	[218]
554	$C_4H_5(I) + CH_3$	=	$C_5H_8(X)$	4.8000E+34	-7.60	47.53	[217]
555	$C_4H_5(S)$	=	$C_4H_4 + H^*$ $k_\infty =$	1.0000E+14	0.00	209.20	[162]
			$k_0 =$	2.0000E+12	0.00	175.73	
556	$C_4H_5(S)$	=	$C_4H_5(T)$	1.5000E+13	0.00	283.45	[162]
557	$C_4H_5(S) + H$	=	$C_4H_4 + H_2$	1.0000E+11	0.00	0.00	[162]
558	$C_4H_5(S) + O$	=	$C_2H_2O + C_2H_3$	1.8070E+11	0.00	0.00	[172]
559	$C_4H_5(S) + OH$	=	$C_4H_4 + H_2O$	2.0000E+04	2.00	4.18	[162]
560	$C_4H_5(S) + O_2$	=	$C_3H_3O + CH_2O$	4.1500E+07	0.00	10.50	[172]
561	$C_4H_5(T)$	=	$C_2H_2 + C_2H_3$	1.0000E+14	0.00	183.75	[73]
562	$C_4H_5(T)$	=	$C_4H_4 + H^*$ $k_\infty =$	1.0000E+14	0.00	154.90	[162]
			$k_0 =$	1.0000E+11	0.00	125.52	
563	$C_4H_5(T) + H$	=	$C_4H_4 + H_2$	1.0000E+11	0.00	0.00	[162]
564	$C_4H_5(T) + O$	=	$C_3H_4(A) + CHO$	1.8070E+11	0.00	0.00	[172]
565	$C_4H_5(T) + OH$	=	$C_4H_4 + H_2O$	2.0000E+04	2.00	4.18	[162]

Table A.1, continued

No	*Reaction*			A	n	E_a	*Ref*
566	$C_4H_5(T) + O_2$	=	$CH_3CO + C_2H_2O$	2.0000E+09	0.00	0.00	[173]
567	$C_4H_5(T) + O_2$	=	$C_3H_4O + CHO$	5.0000E+08	0.00	0.00	[172]
568	$C_4H_5(T) + O_2$	=	$C_4H_4 + HO_2$	1.0000E+10	0.00	0.00	[218]
569	$C_4H_5(T) + O_2$	=	$C_4H_4O + OH$	5.0000E+08	0.00	0.00	[172]
570	$C_4H_5(T) + O_2$	=	$CH_2CHCHCHO + O$	3.0000E+08	0.29	0.05	[159]
571	$C_4H_5(T) + HO_2$	=	$C_3H_4(A) + CHO + OH$	8.9100E+09	0.00	0.00	[172]
572	$C_4H_5(T) + C_2H_2$	=	$C_6H_7(L)$	1.7250E+03	1.79	9.37	[162]
573	$C_4H_5(T) + C_3H_4(A)$	=	$C_7H_8 + H$	2.0000E+08	0.00	15.48	[145]
574	$C_4H_5(T) + C_3H_4(P)$	=	$C_7H_8 + H$	3.1600E+08	0.00	15.48	[47]
575	$C_4H_5(T) + C_4H_2$	=	$C_8H_6 + H$	1.0000E+10	0.00	0.00	[218]
576	$C_4H_5(T) + C_4H_4$	=	$C_8H_8 + H$	3.1600E+08	0.00	2.51	[47]
577	$C_4H_6(B)$	=	$C_2H_4 + C_2H_2$	1.4000E+15	0.00	301.80	[250]
578	$C_4H_6(B)$	=	$C_4H_6(M)$	5.2500E+12	0.00	158.00	[132]
579	$C_4H_6(B)$	=	$C_4H_6(S)$	3.0000E+13	0.00	183.00	[162]
580	$C_4H_6(B)$	=	$C_4H_6(T)$	3.0000E+13	0.00	177.00	[162]
581	$C_4H_6(F)$	=	$C_3H_3 + CH_3$	3.0000E+13	0.00	317.14	[172]
582	$C_4H_6(F)$	=	$C_4H_6(S)$	2.5000E+13	0.00	271.96	[172]
583	$C_4H_6(F) + H$	=	$C_2H_5 + C_2H_2$	6.5000E+01	2.50	4.18	[172]
584	$C_4H_6(F) + H$	=	$C_3H_4(A) + CH_3$	1.3000E+02	2.50	4.18	[172]
585	$C_4H_6(F) + O$	=	$C_3H_6 + CO$	2.0000E+10	0.00	6.94	[172]
586	$C_4H_6(M) + H$	=	$C_3H_4(P) + CH_3$	6.5000E+01	2.50	4.18	[172]
587	$C_4H_6(M) + O$	=	$C_3H_6 + CO$	6.0000E+10	0.00	7.48	[172]
588	$C_4H_6(S)$	=	$C_3H_3 + CH_3$	2.0000E+11	0.00	248.95	[172]
589	$C_4H_6(S)$	=	$C_3H_3 + CH_3$	9.3320E+87	-20.83	510.48	[250]
590	$C_4H_6(S)$	=	$C_4H_5(I) + H$	4.2000E+15	0.00	387.10	[162]
591	$C_4H_6(S)$	=	$C_4H_6(M)$	7.0000E+12	0.00	263.72	[250]
592	$C_4H_6(S) + H$	=	$C_2H_4 + C_2H_3$	4.0000E+08	0.00	0.00	[162]
593	$C_4H_6(S) + H$	=	$C_3H_4(A) + CH_3$	6.0000E+09	0.00	8.78	[172]
594	$C_4H_6(S) + H$	=	$C_4H_5(S) + H_2$	1.0000E+11	0.00	60.71	[162]
595	$C_4H_6(S) + O$	=	$C_3H_3O + CH_3$	3.5800E+09	0.00	0.00	[172]
596	$C_4H_6(S) + OH$	=	$C_4H_5(S) + H_2O$	1.6200E+10	0.00	0.00	[162]
597	$C_4H_6(S) + CH_3$	=	$C_4H_5(S) + CH_4$	7.0000E+10	0.00	25.00	[162]
598	$C_4H_6(S) + C_3H_3$	=	$C_4H_5(S) + C_3H_4(A)$	1.0000E+10	0.00	25.00	[172]
599	$C_4H_6(S) + C_3H_3$	=	$C_4H_5(S) + C_3H_4(P)$	1.0000E+10	0.00	25.00	[172]
600	$C_4H_6(T)$	=	$C_4H_5(I) + H$	4.4000E+15	0.00	397.92	[162]
601	$C_4H_6(T)$	=	$C_4H_5(T) + H$	7.0000E+14	0.00	397.46	[117]
602	$C_4H_6(T)$	=	$C_4H_6(M)$	2.1000E+13	0.00	304.29	[250]
603	$C_4H_6(T)$	=	$C_4H_6(S)$	2.1878E+75	-17.56	484.46	[250]
604	$C_4H_6(T) + H$	=	$C_2H_4 + C_2H_3$	2.0000E+10	0.00	20.92	[117]
605	$C_4H_6(T) + H$	=	$C_3H_4(A) + CH_3$	6.0000E+09	0.00	29.71	[172]
606	$C_4H_6(T) + H$	=	$C_3H_4(P) + CH_3$	6.0000E+09	0.00	29.71	[218]
607	$C_4H_6(T) + H$	=	$C_4H_5(I) + H_2$	6.6500E+02	2.53	38.69	[257]
608	$C_4H_6(T) + H$	=	$C_4H_5(T) + H_2$	6.3000E+07	0.70	25.10	[162]
609	$C_4H_6(T) + O$	=	$C_2H_2O + C_2H_4$	1.0000E+09	0.00	0.00	[218]
610	$C_4H_6(T) + O$	=	$C_3H_4(P) + CH_2O$	1.0000E+09	0.00	0.00	[218]
611	$C_4H_6(T) + O$	=	$C_4H_5(I) + OH$	4.5300E+12	-0.47	29.42	[54]
612	$C_4H_6(T) + O$	=	$C_4H_5(T) + OH$	2.2700E+12	-0.48	29.42	[54]
613	$C_4H_6(T) + O$	=	$CH_3CHCHCO + H$	1.5000E+05	1.45	-3.60	[159]
614	$C_4H_6(T) + O$	=	AC_4H_6O	6.2000E+05	1.45	-3.59	[165]
615	$C_4H_6(T) + OH$	=	$CH_3CO + C_2H_4$	2.8100E+09	0.00	-3.66	[172]
616	$C_4H_6(T) + OH$	=	$C_3H_5(A) + CH_2O$	2.8100E+09	0.00	-3.66	[172]
617	$C_4H_6(T) + OH$	=	$C_3H_4O + CH_3$	2.8100E+09	0.00	-3.66	[172]
618	$C_4H_6(T) + OH$	=	$C_4H_5(I) + H_2O$	3.1000E+03	2.00	1.80	[159]
619	$C_4H_6(T) + OH$	=	$C_4H_5(T) + H_2O$	2.0000E+04	2.00	20.93	[188]
620	$C_4H_6(T) + O_2$	=	$C_4H_5(I) + HO_2$	1.4000E+09	0.00	211.85	[54]
621	$C_4H_6(T) + O_2$	=	$C_4H_5(T) + HO_2$	4.0000E+10	0.00	242.00	[162]
622	$C_4H_6(T) + HO_2$	=	$C_3H_4O + CH_2O + H$	1.3000E+09	0.00	62.60	[172]
623	$C_4H_6(T) + C_2H_3$	=	$C_4H_5(T) + C_2H_4$	6.3100E+10	0.00	60.70	[162]
624	$C_4H_6(T) + C_2H_3$	=	$C_6H_8 + H$	5.6000E+08	0.00	6.90	[172]
625	$C_4H_6(T) + C_3H_3$	=	$C_4H_5(T) + C_3H_4(A)$	2.0000E+09	0.00	75.31	[218]
626	$C_4H_6(T) + C_3H_3$	=	$C_4H_5(T) + C_3H_4(P)$	1.0000E+10	0.00	75.31	[172]

Table A.1, continued

No	*Reaction*			A	n	E_a	*Ref*
627	$C_4H_7(I)$	=	$C_3H_4(A) + CH_3$	2.0000E+13	0.00	209.52	[244]
628	$C_4H_7(I) + HO_2$	=	$C_4H_7O(X) + OH$	4.5000E+09	0.00	0.00	[53]
629	$C_4H_7(I) + CH_3$	=	$C_5H_{10}(A)$	7.0000E+09	0.00	0.00	[53]
630	$C_4H_7(I) + CH_3OO$	=	$C_4H_7O(X) + CH_3O$	2.0000E+09	0.00	-5.02	[53]
631	$C_4H_7(I) + C_4H_7(I)$	=	$C_3H_4(A) + C_5H_{10}(A)$	5.0000E+07	0.00	26.36	[53]
632	$C_4H_7(N)$	=	$C_2H_4 + C_2H_3$	5.0000E+13	0.00	159.10	[54]
633	$C_4H_7(N)$	=	$C_4H_6(T) + H$	2.4800E+53	-12.30	217.57	[54]
634	$C_4H_7(N) + H$	=	$C_4H_6(T) + H_2$	3.1600E+09	0.00	0.00	[218]
635	$C_4H_7(N) + H$	=	$C_4H_8(N)^{j,13}$ k_∞ =	3.6000E+10	0.00	0.00	[159]
			k_0 =	3.0100E+42	-9.32	24.41	
636	$C_4H_7(N) + O$	=	$C_4H_6(T) + OH$	4.0000E+10	0.00	0.00	[218]
637	$C_4H_7(N) + OH$	=	$C_4H_6(T) + H_2O$	4.0000E+10	0.00	0.00	[218]
638	$C_4H_7(N) + O_2$	=	$C_4H_6(T) + HO_2$	1.0000E+08	0.00	0.00	[45]
639	$C_4H_7(S) + H$	=	$C_4H_6(S) + H_2$	3.1600E+09	0.00	0.00	[54]
640	$C_4H_7(S) + O$	=	$C_4H_6(S) + OH$	4.0000E+10	0.00	0.00	[54]
641	$C_4H_7(S) + OH$	=	$C_4H_6(S) + H_2O$	4.0000E+10	0.00	0.00	[54]
642	$C_4H_8(I)$	=	$C_3H_5(T) + CH_3$	3.3000E+21	-1.20	408.86	[53]
643	$C_4H_8(I)$	=	$C_4H_7(I) + H$	1.0600E+47	-9.30	437.44	[53]
644	$C_4H_8(I) + H$	=	$C_3H_6 + CH_3$	1.7200E+10	0.00	15.06	[53]
645	$C_4H_8(I) + H$	=	$C_4H_7(I) + H_2$	1.7200E+11	0.00	33.47	[53]
646	$C_4H_8(I) + O$	=	$C_3H_7(I) + CHO$	5.0000E+05	1.28	-4.51	[53]
647	$C_4H_8(I) + O$	=	$C_4H_7(I) + OH$	3.0000E+05	1.28	-4.51	[53]
648	$C_4H_8(I) + O$	=	$C_4H_8O(X)$	1.0000E+05	1.28	-4.51	[53]
649	$C_4H_8(I) + OH$	=	$C_4H_7(I) + H_2O$	6.0000E+03	2.00	-0.25	[53]
650	$C_4H_8(I) + OH$	=	$C_4H_8OH(I)$	3.4000E+20	-3.59	8.71	[53]
651	$C_4H_8(I) + O_2$	=	$C_4H_7(I) + HO_2$	1.4400E+10	0.00	161.21	[53]
652	$C_4H_8(I) + HO_2$	=	$C_4H_7(I) + H_2O_2$	3.0000E+08	0.00	59.37	[53]
653	$C_4H_8(I) + HO_2$	=	$C_4H_8O(X) + OH$	1.0200E+09	0.00	62.61	[53]
654	$C_4H_8(I) + CH_3$	=	$C_4H_7(I) + CH_4$	4.4200E-03	3.50	18.49	[53]
655	$C_4H_8(I) + CH_3$	=	$C_5H_{10}(B) + H$	1.5500E+04	1.86	59.34	[53]
656	$C_4H_8(I) + CH_3$	=	$C_5H_{11}(T)$	1.7000E+08	0.00	267.78	[53]
657	$C_4H_8(I) + CHO$	=	$C_4H_7(I) + CH_2O$	3.3000E+08	0.00	25.98	[53]
658	$C_4H_8(I) + CH_3OO$	=	$C_4H_8O(X) + CH_3O$	4.0000E+08	0.00	50.21	[53]
659	$C_4H_8(I) + C_2H_3$	=	$C_4H_7(I) + C_2H_4$	1.0000E+10	0.00	54.39	[53]
660	$C_4H_8(I) + C_3H_5(A)$	=	$C_4H_7(I) + C_3H_6$	7.9400E+08	0.00	85.77	[53]
661	$C_4H_8(I) + C_3H_5(S)$	=	$C_4H_7(I) + C_3H_6$	7.9400E+08	0.00	85.77	[53]
662	$C_4H_8(I) + C_3H_5(T)$	=	$C_4H_7(I) + C_3H_6$	7.9400E+08	0.00	85.77	[53]
663	$C_4H_8(N)$	=	$C_3H_5(A) + CH_3$	1.0000E+16	0.00	305.43	[73]
664	$C_4H_8(N) + H$	=	$C_3H_6 + CH_3$	1.7200E+10	0.00	32.06	[218]
665	$C_4H_8(N) + H$	=	$C_4H_7(N) + H_2$	1.7200E+11	0.00	88.47	[218]
666	$C_4H_8(N) + O$	=	$C_3H_7(N) + CHO$	5.0000E+05	1.28	-4.51	[218]
667	$C_4H_8(N) + O$	=	$C_4H_7(N) + OH$	3.0000E+05	1.28	-4.51	[218]
668	$C_4H_8(N) + OH$	=	$C_4H_7(N) + H_2O$	6.0000E+03	2.00	-0.25	[218]
669	$C_4H_8(N) + O_2$	=	$C_4H_7(N) + HO_2$	1.4400E+10	0.00	250.21	[218]
670	$C_4H_8(N) + HO_2$	=	$C_4H_7(N) + H_2O_2$	3.0000E+08	0.00	148.37	[218]
671	$C_4H_8(N) + CH_3$	=	$C_4H_7(N) + CH_4$	4.4200E-03	3.50	73.49	[218]
672	$C_4H_8(N) + CHO$	=	$C_4H_7(N) + CH_2O$	3.3000E+08	0.00	80.98	[218]
673	$C_4H_8(N) + C_2H_3$	=	$C_4H_7(N) + C_2H_4$	1.0000E+10	0.00	109.92	[218]
674	$C_4H_8(N) + C_3H_5(A)$	=	$C_4H_7(N) + C_3H_6$	7.9400E+08	0.00	140.77	[218]
675	$C_4H_8(N) + C_3H_5(S)$	=	$C_4H_7(N) + C_3H_6$	7.9400E+08	0.00	140.77	[218]
676	$C_4H_8(N) + C_3H_5(T)$	=	$C_4H_7(N) + C_3H_6$	7.9400E+08	0.00	140.77	[218]
677	$C_4H_8(S)$	=	$C_3H_5(S) + CH_3$	3.1600E+17	0.00	415.46	[73]
678	$C_4H_8(S)$	=	$C_4H_7(S) + H$	3.9800E+15	0.00	356.05	[73]
679	$C_4H_8(S) + H$	=	$C_3H_6 + CH_3$	1.7200E+10	0.00	32.06	[218]
680	$C_4H_8(S) + H$	=	$C_4H_7(S) + H_2$	1.7200E+11	0.00	88.47	[218]
681	$C_4H_8(S) + O$	=	$C_3H_7(I) + CHO$	5.0000E+05	1.28	-4.51	[218]
682	$C_4H_8(S) + O$	=	$C_4H_7(S) + OH$	3.0000E+05	1.28	-4.51	[218]
683	$C_4H_8(S) + OH$	=	$C_4H_7(S) + H_2O$	6.0000E+03	2.00	-0.25	[218]
684	$C_4H_8(S) + O_2$	=	$C_4H_7(S) + HO_2$	1.4400E+10	0.00	250.21	[218]

Table A.1, continued

No	*Reaction*			A	n	E_a	*Ref*
685	$C_4H_8(S) + HO_2$	=	$C_4H_7(S) + H_2O_2$	3.0000E+08	0.00	148.37	[218]
686	$C_4H_8(S) + CH_3$	=	$C_4H_7(S) + CH_4$	4.4200E-03	3.50	73.49	[218]
687	$C_4H_8(S) + CHO$	=	$C_4H_7(S) + CH_2O$	3.3000E+08	0.00	80.98	[218]
688	$C_4H_8(S) + C_2H_3$	=	$C_4H_7(S) + C_2H_4$	1.0000E+10	0.00	109.92	[218]
689	$C_4H_8(S) + C_3H_5(A)$	=	$C_4H_7(S) + C_3H_6$	7.9400E+08	0.00	140.77	[218]
690	$C_4H_8(S) + C_3H_5(S)$	=	$C_4H_7(S) + C_3H_6$	7.9400E+08	0.00	140.77	[218]
691	$C_4H_8(S) + C_3H_5(T)$	=	$C_4H_7(S) + C_3H_6$	7.9400E+08	0.00	140.77	[218]
692	$C_4H_9(I)$	=	$C_3H_6 + CH_3$	2.0000E+13	0.00	125.31	[53]
693	$C_4H_9(I)$	=	$C_4H_8(I) + H$	1.9100E+29	-5.25	166.35	[53]
694	$C_4H_9(I) + O_2$	=	$C_4H_8(I) + HO_2$	2.4000E+07	0.00	0.00	[53]
695	$C_4H_9(I) + HO_2$	=	$C_3H_7(I) + CH_2O + OH$	2.4100E+10	0.00	0.00	[53]
696	$C_4H_9(N)$	=	$C_2H_5 + C_2H_4$[14] $k_\infty =$	1.0600E+13	0.00	116.44	[150]
			$k_0 =$	1.9000E+52	-11.91	135.00	
697	$C_4H_9(N)$	=	$C_3H_6 + CH_3$	1.2600E+12	0.00	113.38	[146]
698	$C_4H_9(N)$	=	$C_4H_8(N) + H$	1.0000E+14	0.00	160.24	[73]
699	$C_4H_9(N) + H$	=	$C_4H_8(N) + H_2$	5.4000E+09	0.00	0.00	[218]
700	$C_4H_9(N) + O$	=	$C_4H_8(N) + OH$	4.1600E+11	0.00	0.00	[218]
701	$C_4H_9(N) + OH$	=	$C_4H_8(N) + H_2O$	1.8000E+10	0.00	0.00	[218]
702	$C_4H_9(N) + O_2$	=	$C_4H_8(N) + HO_2$	2.7000E+08	0.00	0.00	[8]
703	$C_4H_9(N) + CH_3$	=	$C_4H_8(N) + CH_4$	1.2600E+10	0.00	-2.49	[218]
704	$C_4H_9(S)$	=	$C_3H_6 + CH_3$[15] $k_\infty =$	2.6700E+10	1.06	129.48	[99]
			$k_0 =$	2.3000E+60	-14.30	153.80	
705	$C_4H_9(S)$	=	$C_4H_8(N) + H$	1.5800E+13	0.00	165.68	[73]
706	$C_4H_9(S)$	=	$C_4H_8(S) + H$	3.1600E+12	0.00	154.38	[73]
707	$C_4H_9(S) + H$	=	$C_4H_8(N) + H_2$	5.4000E+09	0.00	0.00	[218]
708	$C_4H_9(S) + H$	=	$C_4H_8(S) + H_2$	5.4000E+09	0.00	0.00	[218]
709	$C_4H_9(S) + O$	=	$C_4H_8(N) + OH$	4.1600E+11	0.00	0.00	[218]
710	$C_4H_9(S) + O$	=	$C_4H_8(S) + OH$	4.1600E+11	0.00	0.00	[218]
711	$C_4H_9(S) + OH$	=	$C_4H_8(N) + H_2O$	1.8000E+10	0.00	0.00	[218]
712	$C_4H_9(S) + OH$	=	$C_4H_8(S) + H_2O$	1.8000E+10	0.00	0.00	[218]
713	$C_4H_9(S) + O_2$	=	$C_4H_8(N) + HO_2$	5.1100E+07	0.00	0.00	[8]
714	$C_4H_9(S) + O_2$	=	$C_4H_8(S) + HO_2$	7.8000E+07	0.00	0.00	[8]
715	$C_4H_9(S) + CH_3$	=	$C_4H_8(N) + CH_4$	1.2600E+10	0.00	-2.49	[218]
716	$C_4H_9(S) + CH_3$	=	$C_4H_8(S) + CH_4$	1.2600E+10	0.00	-2.49	[218]
717	$C_4H_9(T)$	=	$C_3H_6 + CH_3$	3.0000E+14	0.00	193.72	[53]
718	$C_4H_9(T)$	=	$C_4H_8(I) + H$	2.9000E+51	-11.53	220.16	[53]
719	$C_4H_9(T) + H$	=	$C_4H_8(I) + H_2$	5.4000E+09	0.00	0.00	[53]
720	$C_4H_9(T) + O$	=	$AC_3H_6O + CH_3$	1.0400E+11	0.00	0.00	[53]
721	$C_4H_9(T) + O$	=	$C_4H_8(I) + OH$	4.1600E+11	0.00	0.00	[53]
722	$C_4H_9(T) + OH$	=	$C_4H_8(I) + H_2O$	1.8000E+10	0.00	0.00	[53]
723	$C_4H_9(T) + O_2$	=	$C_4H_8(I) + HO_2$	4.8000E+08	0.00	0.00	[53]
724	$C_4H_9(T) + HO_2$	=	$AC_3H_6O + CH_3 + OH$	1.8000E+10	0.00	0.00	[53]
725	$C_4H_9(T) + CH_3$	=	$C_4H_8(I) + CH_4$	1.2600E+10	0.00	-2.49	[53]
726	$C_4H_9(T) + CH_3OO$	=	$AC_3H_6O + CH_3 + CH_3O$	1.3000E+10	0.00	0.00	[247]
727	$C_4H_{10}(I)$	=	$C_3H_7(I) + CH_3$	1.1000E+26	-2.61	377.98	[247]
728	$C_4H_{10}(I) + H$	=	$C_4H_9(I) + H_2$	1.8100E+03	2.54	28.27	[247]
729	$C_4H_{10}(I) + H$	=	$C_4H_9(T) + H_2$	6.0200E+02	2.40	10.81	[247]
730	$C_4H_{10}(I) + OH$	=	$C_4H_9(I) + H_2O$	2.2900E+05	1.53	3.24	[247]
731	$C_4H_{10}(I) + OH$	=	$C_4H_9(T) + H_2O$	5.7300E+07	0.51	0.27	[247]
732	$C_4H_{10}(I) + O$	=	$C_4H_9(I) + OH$	4.2800E+02	2.50	15.25	[247]
733	$C_4H_{10}(I) + O$	=	$C_4H_9(T) + OH$	1.5600E+02	2.50	4.66	[247]
734	$C_4H_{10}(I) + HO_2$	=	$C_4H_9(I) + H_2O_2$	3.0100E+01	2.55	64.85	[247]
735	$C_4H_{10}(I) + HO_2$	=	$C_4H_9(T) + H_2O_2$	3.6100E+00	2.55	44.07	[247]
736	$C_4H_{10}(N)$	=	$C_2H_5 + C_2H_5$	2.0000E+16	0.00	340.00	[181]
737	$C_4H_{10}(N)$	=	$C_3H_7(N) + CH_3$	1.0000E+17	0.00	354.37	[73]
738	$C_4H_{10}(N)$	=	$C_4H_9(N) + H$	1.5800E+16	0.00	410.02	[73]
739	$C_4H_{10}(N)$	=	$C_4H_9(S) + H$	1.0000E+16	0.00	397.46	[73]
740	$C_4H_{10}(N) + H$	=	$C_4H_9(N) + H_2$	5.6200E+04	2.00	32.22	[204]
741	$C_4H_{10}(N) + H$	=	$C_4H_9(S) + H_2$	2.0000E+11	0.00	34.90	[153]
742	$C_4H_{10}(N) + O$	=	$C_4H_9(N) + OH$	3.0000E+10	0.00	24.00	[153]
743	$C_4H_{10}(N) + O$	=	$C_4H_9(S) + OH$	5.2000E+10	0.00	18.60	[153]

Table A.1, continued

No	*Reaction*			A	n	E_a	*Ref*
744	$C_4H_{10}(N) + OH$	=	$C_4H_9(N) + H_2O$	4.1300E+04	1.73	3.15	[153]
745	$C_4H_{10}(N) + OH$	=	$C_4H_9(S) + H_2O$	2.5700E+06	1.25	2.93	[204]
746	$C_4H_{10}(N) + O_2$	=	$C_4H_9(N) + HO_2$	2.5100E+10	0.00	205.00	[181]
747	$C_4H_{10}(N) + O_2$	=	$C_4H_9(S) + HO_2$	3.9800E+10	0.00	199.00	[181]
748	$C_4H_{10}(N) + HO_2$	=	$C_4H_9(N) + H_2O_2$	1.1200E+10	0.00	81.16	[204]
749	$C_4H_{10}(N) + HO_2$	=	$C_4H_9(S) + H_2O_2$	5.0000E+08	0.00	43.92	[175]
750	$C_4H_2O + OH$	=	$C_2H_2 + CO + CO + H$	1.0000E+12	0.00	0.00	[162]
751	C_4H_4O	=	$C_2H_2O + C_2H_2$	5.0100E+14	0.00	324.25	[172]
752	C_4H_4O	=	$C_3H_4(P) + CO$	1.7800E+15	0.00	324.25	[172]
753	$CH_3CHCHCO$	=	$C_3H_5(S) + CO$	1.0000E+14	0.00	125.60	[159]
754	$CH_2CHCHCHO$	=	$C_3H_5(A) + CO$	1.0000E+14	0.00	104.67	[159]
755	AC_4H_6O	=	$CH_3CO + C_2H_3$	1.0000E+16	0.00	284.51	[172]
756	AC_4H_6O	=	BC_4H_6O	1.3500E+15	0.00	211.70	[172]
757	BC_4H_6O	=	$C_3H_6 + CO$	1.0900E+16	0.00	305.43	[162]
758	BC_4H_6O	=	$C_4H_5(T) + OH$	5.3000E+12	0.00	203.06	[218]
759	$C_4H_7O(M) + M$	=	$C_3H_7(I) + CO + M$	8.6400E+12	0.00	60.25	[53]
760	$C_4H_7O(X)$	=	$C_3H_5(A) + CH_2O$	1.0000E+15	0.00	104.60	[53]
761	$C_4H_7O(X)$	=	$C_3H_5(T) + CH_2O$	5.0000E+15	0.00	104.60	[53]
762	$C_4H_8O(M)$	=	$C_3H_7(I) + CHO$	2.4400E+16	0.00	351.99	[53]
763	$C_4H_8O(M) + H$	=	$C_4H_7O(M) + H_2$	4.0000E+10	0.00	17.60	[53]
764	$C_4H_8O(M) + O$	=	$C_4H_7O(M) + OH$	5.0000E+09	0.00	7.50	[53]
765	$C_4H_8O(M) + OH$	=	$C_4H_7O(M) + H_2O$	3.3700E+09	0.00	-2.58	[53]
766	$C_4H_8O(M) + O_2$	=	$C_4H_7O(M) + HO_2$	3.0100E+10	0.00	163.80	[53]
767	$C_4H_8O(M) + HO_2$	=	$C_4H_7O(M) + H_2O_2$	3.0100E+09	0.00	49.89	[53]
768	$C_4H_8O(X)$	=	$C_3H_7(I) + CHO$	6.0000E+13	0.00	239.33	[53]
769	$C_4H_8O(X)$	=	$C_4H_8O(M)$	4.0000E+13	0.00	239.33	[53]
770	$C_4H_8OH(I) + O_2$	=	$O_2C_4H_9O$	3.2500E+23	-4.69	17.97	[53]
771	$O_2C_4H_9O$	=	$AC_3H_6O + CH_2O + OH$	1.0000E+16	0.00	104.60	[53]
772	$C_5H + O$	=	$C_4H + CO$	6.8000E+10	0.00	0.00	[172]
773	$C_5H + OH$	=	$C_4H_2 + CO$	6.8000E+10	0.00	0.00	[172]
774	$C_5H + O_2$	=	$C_3H + CO + CO$	3.2900E+18	-3.30	12.00	[172]
775	$C_5H_2 + H$	=	$C_5H + H_2$	1.0000E+11	0.00	0.00	[172]
776	$C_5H_2 + OH$	=	$C_4H_2 + CHO$	1.0000E+10	0.00	0.00	[172]
777	$C_5H_3(L) + H$	=	$C_5H_2 + H_2$	1.0000E+10	0.00	0.00	[162]
778	$C_5H_3(L) + H$	=	$C_5H_4(L)$	1.0000E+10	0.00	0.00	[162]
779	$C_5H_3(L) + O$	=	$C_4H_3(I) + CO$	1.0000E+11	0.00	0.00	[162]
780	$C_5H_3(L) + OH$	=	$C_5H_2 + H_2O$	1.0000E+10	0.00	0.00	[162]
781	$C_5H_3(L) + {}^1CH_2$	=	$C_6H_4L + H$	7.0000E+10	0.00	0.00	[172]
782	$C_5H_3(L) + {}^3CH_2$	=	$C_6H_4L + H$	7.0000E+10	0.00	0.00	[172]
783	$C_5H_4(L) + H$	=	$C_5H_3(L) + H_2$	1.0000E+10	0.00	0.00	[162]
784	$C_5H_4(L) + OH$	=	$C_5H_3(L) + H_2O$	1.0000E+10	0.00	83.68	[162]
785	$C_5H_4(L) + CH$	=	$C_6H_4L + H$	8.0000E+10	0.00	0.00	[172]
786	C_5H_5	=	$C_5H_5(L)$	3.9000E+11	1.00	322.58	[225]
787	$C_5H_5 + M$	=	$C_3H_3 + C_2H_2 + M$	7.1600E+66	-14.67	385.89	[138]
788	$C_5H_5 + O$	=	$C_4H_5(T) + CO$	1.0000E+11	0.00	0.00	[162]
789	$C_5H_5 + O$	=	$C_5H_4O + H$	5.8100E+10	-0.02	0.08	[274]
790	$C_5H_5 + O$	=	C_5H_5O	1.0000E+10	0.00	0.00	[162]
791	$C_5H_5 + OH$	=	$C_5H_4OH + H$	3.0000E+10	0.00	0.00	[162]
792	$C_5H_5 + OH$	=	$C_5H_5O + H$	1.3600E+48	-10.46	238.91	[274]
793	$C_5H_5 + OH$	=	C_5H_5OH	6.4900E+11	-0.85	-11.42	[274]
794	$C_5H_5 + OH$	=	$C_4H_6(T) + CO$	4.0000E+11	0.00	18.84	[217]
795	$C_5H_5 + O_2$	=	$C_5H_5O + O$	7.7300E+12	-0.73	203.93	[274]
796	$C_5H_5 + O_2$	=	C_5H_5OO	7.3100E+04	0.08	-40.04	[274]
797	$C_5H_5 + HO_2$	=	$C_5H_4O + H_2O$	1.1900E+30	-6.52	56.07	[274]
798	$C_5H_5 + HO_2$	=	$C_5H_5O + OH$	6.2700E+26	-4.69	48.74	[274]
799	$C_5H_5 + CH_3$	=	$C_5H_4CH_3 + H$	2.0000E+10	0.00	26.00	[170]
800	$C_5H_5 + C_3H_3$	=	$C_8H_7(F) + H$	2.0000E+10	0.00	42.30	[218]
801	$C_5H_5 + C_3H_5(A)$	=	$C_8H_9(F) + H$	2.0000E+10	0.00	42.30	[218]
802	$C_5H_5 + C_5H_5$	=	$C_{10}H_9F + H$	2.0000E+10	0.00	34.00	[169]
803	$C_5H_5 + C_5H_5$	=	$C_{10}H_{10}K$	1.0000E+10	0.00	0.00	[182]

Table A.1, continued

No	*Reaction*			A	n	E_a	*Ref*
804	$C_5H_5(L)$	=	$C_3H_3 + C_2H_2$	3.7000E+11	0.00	176.10	[218]
805	$C_5H_5(L) + H$	=	$C_5H_4(L) + H_2$	1.0000E+10	0.00	0.00	[162]
806	$C_5H_5(L) + H$	=	$C_5H_6(L)$	1.0000E+10	0.00	0.00	[162]
807	$C_5H_5(L) + O$	=	$C_4H_5(I) + CO$	1.0000E+11	0.00	0.00	[162]
808	$C_5H_5(L) + OH$	=	$C_5H_4(L) + H_2O$	1.0000E+10	0.00	0.00	[162]
809	$C_5H_5(L) + O_2$	=	$C_2H_3 + C_2HO + CHO$	1.0000E+09	0.00	155.00	[162]
810	C_5H_6	=	$C_5H_5 + H^*$ k_∞ =	7.6500E+19	-1.18	353.45	[224]
			k_0 =	1.0700E+77	-16.79	71.07	
811	C_5H_6	=	$C_5H_6(L)$	1.0000E+14	0.00	235.00	[162]
812	$C_5H_6 + H$	=	$C_5H_5 + H_2$	2.8000E+10	0.00	9.45	[170]
813	$C_5H_6 + H$	=	C_5H_7	2.4000E+70	-17.85	131.80	[273]
814	$C_5H_6 + O$	=	$C_5H_5 + OH$	1.8100E+10	0.00	12.87	[162]
815	$C_5H_6 + OH$	=	$C_5H_5 + H_2O$	1.1433E+06	1.18	-1.87	[218]
816	$C_5H_6 + HO_2$	=	$C_5H_5 + H_2O_2$	2.0000E+09	0.00	48.78	[162]
817	$C_5H_6(L) + H$	=	$C_5H_5(L) + H_2$	1.0000E+09	0.00	0.00	[162]
818	$C_5H_6(L) + O$	=	$C_3H_2O + C_2H_3 + H$	2.0000E+10	0.00	126.00	[162]
819	$C_5H_6(L) + OH$	=	$C_5H_5(L) + H_2O$	1.0000E+10	0.00	0.00	[162]
820	C_5H_7	=	$C_3H_4(A) + C_2H_3$	3.1600E+14	0.00	327.00	[217]
821	$C_5H_7 + H$	=	$C_5H_6 + H_2$	3.6000E+09	0.00	0.00	[2]
822	$C_5H_7 + O$	=	$C_5H_6 + OH$	1.0000E+10	0.00	0.00	[2]
823	$C_5H_7 + OH$	=	$C_5H_6 + H_2O$	2.4000E+10	0.00	0.00	[2]
824	$C_5H_7 + O_2$	=	$C_3H_4O + CH_2CHO$	4.0000E+07	0.00	20.92	[217]
825	$C_5H_7 + HO_2$	=	$C_5H_6 + H_2O_2$	2.6500E+09	0.00	0.00	[217]
826	$C_5H_7(X) + H$	=	$C_5H_8(X)$	1.0000E+11	0.00	0.00	[217]
827	$C_5H_7(X) + O$	=	$C_3H_3O + C_2H_4$	2.0000E+11	0.00	0.00	[218]
828	$C_5H_8 + H$	=	$C_5H_7 + H_2$	2.8000E+10	0.00	9.45	[170]
829	$C_5H_8 + O$	=	$C_3H_4O + C_2H_4$	5.6000E+09	0.00	-1.80	[98]
830	$C_5H_8 + O$	=	$C_5H_7 + OH$	2.7800E+08	0.00	10.49	[217]
831	$C_5H_8 + OH$	=	$C_5H_7 + H_2O$	3.4300E+06	1.18	-1.87	[170]
832	$C_5H_8 + O_2$	=	$C_5H_7 + HO_2$	1.2800E+07	0.00	104.60	[217]
833	$C_5H_8 + HO_2$	=	$C_5H_7 + H_2O_2$	1.6000E+08	0.00	71.38	[217]
834	$C_5H_8(I) + OH$	=	$C_5H_7(I) + H_2O$	2.0000E+04	2.00	20.92	[53]
835	$C_5H_8(I) + HO_2$	=	$C_5H_7(I) + H_2O_2$	2.0000E+02	2.60	58.20	[53]
836	$C_5H_8(X) + H$	=	$C_3H_5(A) + C_2H_4$	6.7000E+05	1.50	8.37	[218]
837	$C_5H_8(X) + H$	=	$C_4H_5(T) + CH_4$	1.6750E+05	1.50	8.37	[218]
838	$C_5H_8(X) + H$	=	$C_4H_6(T) + CH_3$	1.6750E+05	1.50	8.37	[218]
839	$C_5H_8(X) + H$	=	$C_5H_7(X) + H_2$	7.0000E+03	2.00	0.00	[217]
840	$C_5H_8(X) + O$	=	$C_3H_4O + C_2H_4$	4.5000E+05	1.40	-3.59	[217]
841	$C_5H_8(X) + O$	=	$CH_2O + C_4H_6(T)$	4.5000E+05	1.40	-3.59	[217]
842	$C_5H_8(X) + O$	=	$C_5H_7(X) + OH$	7.0000E+03	2.00	0.00	[218]
843	$C_5H_8(X) + OH$	=	$CH_3CHO + C_3H_5(A)$	6.0000E+09	0.00	-1.64	[217]
844	$C_5H_8(X) + OH$	=	$C_5H_7(X) + H_2O$	7.0000E+03	2.00	0.00	[217]
845	$C_5H_8(X) + O_2$	=	$C_3H_4O + CH_3CHO$	2.0000E+05	1.50	126.36	[217]
846	$C_5H_8(X) + HO_2$	=	$C_3H_4O + C_2H_4 + OH$	5.0000E+08	0.00	79.50	[217]
847	$C_5H_8(X) + HO_2$	=	$C_4H_6(T) + CH_2O + OH$	5.0000E+08	0.00	79.50	[217]
848	$C_5H_8(X) + HO_2$	=	$C_5H_7(X) + H_2O_2$	2.0000E+08	0.00	52.72	[217]
849	$C_5H_8(X) + CH_3$	=	$C_5H_7(X) + CH_4$	2.0000E+11	0.00	95.40	[217]
850	$C_5H_8(Y)$	=	C_5H_8	1.8000E+11	0.00	216.83	[114]
851	$C_5H_8(Y)$	=	$C_5H_8(X)$	2.7000E+16	0.00	340.87	[114]
852	$C_5H_9(A)$	=	$C_5H_8(I) + H$	1.2000E+08	2.50	188.28	[53]
853	$C_5H_9(A) + H$	=	$C_5H_8(I) + H_2$	3.6000E+09	0.00	0.00	[53]
854	$C_5H_9(A) + O$	=	$C_5H_8(I) + OH$	1.8000E+10	0.00	0.00	[53]
855	$C_5H_9(A) + OH$	=	$C_5H_8(I) + H_2O$	1.8000E+10	0.00	0.00	[53]
856	$C_5H_9(A) + O_2$	=	$C_5H_8(I) + HO_2$	1.0000E+08	0.00	154.81	[53]
857	$C_5H_9(A) + HO_2$	=	$C_5H_8(I) + H_2O_2$	1.0000E+09	0.00	0.00	[53]
858	$C_5H_9(A) + CH_3$	=	$C_5H_8(I) + CH_4$	1.0000E+10	0.00	0.00	[53]
859	$C_5H_9(A) + C_4H_7(I)$	=	$C_5H_8(I) + C_4H_8(I)$	4.0000E+10	0.00	0.00	[53]

Table A.1, continued

No	*Reaction*			A	n	E_a	*Ref*
860	$C_5H_9(B)$	=	$C_5H_8(I) + H$	1.2000E+08	2.50	188.28	[53]
861	$C_5H_9(B) + H$	=	$C_5H_8(I) + H_2$	3.6000E+09	0.00	0.00	[53]
862	$C_5H_9(B) + O$	=	$C_5H_8(I) + OH$	1.8000E+10	0.00	0.00	[53]
863	$C_5H_9(B) + OH$	=	$C_5H_8(I) + H_2O$	1.8000E+10	0.00	0.00	[53]
864	$C_5H_9(B) + O_2$	=	$C_5H_8(I) + HO_2$	1.0000E+08	0.00	154.81	[53]
865	$C_5H_9(B) + HO_2$	=	$C_5H_8(I) + H_2O_2$	1.0000E+09	0.00	0.00	[53]
866	$C_5H_9(B) + CH_3$	=	$C_5H_8(I) + CH_4$	1.0000E+10	0.00	0.00	[53]
867	$C_5H_9(B) + C_4H_7(I)$	=	$C_5H_8(I) + C_4H_8(I)$	4.0000E+10	0.00	0.00	[53]
868	$C_5H_{10}(A)$	=	$C_3H_5(T) + C_2H_5$	3.3000E+21	-1.20	408.86	[53]
869	$C_5H_{10}(A)$	=	$C_5H_9(A) + H$	4.0700E+18	-1.00	407.31	[53]
870	$C_5H_{10}(A)$	=	$C_5H_{10}(B)$	3.5000E+12	0.00	251.04	[53]
871	$C_5H_{10}(A) + H$	=	$C_3H_6 + C_2H_5$	1.7000E+09	0.00	12.13	[53]
872	$C_5H_{10}(A) + H$	=	$C_5H_9(A) + H_2$	1.9500E+10	0.00	18.60	[53]
873	$C_5H_{10}(A) + O$	=	$C_5H_9(A) + OH$	1.3000E+09	0.00	18.83	[53]
874	$C_5H_{10}(A) + OH$	=	$C_5H_9(A) + H_2O$	6.2700E+03	2.00	-2.27	[53]
875	$C_5H_{10}(A) + O_2$	=	$C_5H_9(A) + HO_2$	4.0000E+09	0.00	167.36	[53]
876	$C_5H_{10}(A) + HO_2$	=	$C_5H_9(A) + H_2O_2$	1.0000E+08	0.00	71.38	[53]
877	$C_5H_{10}(A) + CH_3$	=	$C_2H_4 + C_2H_4 + C_2H_5$	1.7000E+08	0.00	30.96	[53]
878	$C_5H_{10}(A) + CH_3$	=	$C_5H_9(A) + CH_4$	1.0000E+08	0.00	30.54	[53]
879	$C_5H_{10}(B)$	=	$C_5H_9(A) + H$	2.1300E+47	-9.30	437.44	[53]
880	$C_5H_{10}(B)$	=	$C_5H_9(B) + H$	1.0600E+47	-9.30	437.44	[53]
881	$C_5H_{10}(B) + H$	=	$C_5H_9(A) + H_2$	1.2900E+10	0.00	18.60	[53]
882	$C_5H_{10}(B) + H$	=	$C_5H_9(B) + H_2$	6.4500E+09	0.00	18.60	[53]
883	$C_5H_{10}(B) + O$	=	$CH_3CHO + C_3H_6$	7.2300E+02	2.34	-4.39	[53]
884	$C_5H_{10}(B) + O$	=	$C_5H_9(A) + OH$	3.5000E+08	0.70	24.62	[53]
885	$C_5H_{10}(B) + O$	=	$C_5H_9(B) + OH$	1.7500E+08	0.70	24.62	[53]
886	$C_5H_{10}(B) + OH$	=	$CH_3CHO + C_3H_7(I)$	2.0000E+07	0.00	16.74	[53]
887	$C_5H_{10}(B) + OH$	=	$C_5H_9(A) + H_2O$	9.0000E+03	2.00	-0.25	[53]
888	$C_5H_{10}(B) + OH$	=	$C_5H_9(B) + H_2O$	3.0000E+03	2.00	-0.25	[53]
889	$C_5H_{10}(B) + O_2$	=	$C_5H_9(A) + HO_2$	4.8000E+09	0.00	161.21	[53]
890	$C_5H_{10}(B) + O_2$	=	$C_5H_9(B) + HO_2$	2.4000E+09	0.00	161.21	[53]
891	$C_5H_{10}(B) + HO_2$	=	$C_5H_9(A) + H_2O_2$	3.0000E+08	0.00	59.37	[53]
892	$C_5H_{10}(B) + HO_2$	=	$C_5H_9(B) + H_2O_2$	1.5000E+08	0.00	59.37	[53]
893	$C_5H_{10}(B) + CH_3$	=	$C_5H_9(A) + CH_4$	3.2000E+08	0.00	36.82	[53]
894	$C_5H_{10}(B) + CH_3$	=	$C_5H_9(B) + CH_4$	1.6000E+08	0.00	36.82	[53]
895	$C_5H_{11}(T)$	=	$C_5H_{10}(A) + H$	1.6000E+13	0.00	150.62	[53]
896	$C_5H_{11}(T)$	=	$C_5H_{10}(B) + H$	5.3000E+12	0.00	138.07	[53]
897	$C_5H_{11}(T) + O_2$	=	$C_5H_{10}(A) + HO_2$	2.0000E+09	0.00	20.92	[53]
898	$C_5H_{11}(T) + O_2$	=	$C_5H_{10}(B) + HO_2$	4.0000E+08	0.00	20.92	[53]
899	C_5H_4O	=	$C_3H_2O + C_2H_2$	1.0000E+15	0.00	326.57	[218]
900	C_5H_4O	=	$C_4H_4 + CO$	2.5000E+11	0.00	221.90	adj. [217]
901	$C_5H_4O + H$	=	$C_4H_5(T) + CO$	9.5000E+10	0.00	23.00	est.
902	$C_5H_4O + O$	=	$C_4H_4 + CO_2$	1.0000E+10	0.00	8.37	[76]
903	C_5H_4OH	=	$C_5H_4O + H$	2.1000E+13	0.00	200.83	[162]
904	C_5H_5O	=	$C_4H_5(T) + CO$	7.5000E+11	0.00	183.68	adj. [162]
905	C_5H_5O	=	$C_5H_4O + H$	2.0000E+14	0.00	78.16	[274]
906	C_5H_5OO	=	$C_5H_4O + OH$	3.6100E+12	0.00	156.06	[274]
907	C_5H_5OO	=	$C_5H_5O + O$	2.3600E+14	0.00	245.68	[274]
908	C_5H_5OH	=	$C_5H_4OH + H$	6.0000E+14	0.00	326.10	[274]
909	C_5H_5OH	=	$C_5H_5O + H$	1.0900E+16	0.00	433.71	[274]
910	$C_5H_4CH_3$	=	$C_6H_6(F) + H$	1.0000E+14	0.00	217.00	[170]
911	$C_5H_5CH_3$	=	$CH_3 + C_5H_5$	1.5200E+84	-20.29	437.23	[138]
912	$C_5H_5CH_3 + CH_3$	=	$CH_4 + H + C_6H_6$	4.4200E-03	3.50	23.77	[138]
913	$C_6H_2 + C_2H$	=	$C_8H_2 + H$	1.2000E+11	0.00	0.00	[162]
914	$C_6H_2 + C_2H_2$	=	$C_8H_2 + H + H$	1.5000E+11	0.00	234.50	[162]
915	$C_6H_3 + H$	=	$C_6H_2 + H_2$	1.0000E+11	0.00	0.00	[162]
916	$C_6H_3 + O$	=	$C_6H_2 + OH$	2.0000E+10	0.00	0.00	[162]
917	$C_6H_3 + OH$	=	$C_6H_2 + H_2O$	2.0000E+10	0.00	0.00	[162]
918	C_6H_4	=	C_6H_4L	1.0000E+12	0.00	138.07	[162]
919	$C_6H_4 + C_3H_5(A)$	=	$C_9H_8 + H$	2.0000E+10	0.00	90.00	[]
920	$C_6H_4L + H$	=	$C_6H_3 + H_2$	1.0000E+11	0.00	0.00	[162]
921	$C_6H_4L + O$	=	$C_6H_3 + OH$	2.0000E+10	0.00	0.00	[162]
922	$C_6H_4L + OH$	=	$C_6H_3 + H_2O$	2.0000E+10	0.00	0.00	[162]

Table A.1, continued

No	*Reaction*			A	n	E_a	*Ref*
923	C_6H_5	=	$C_6H_4 + H$	3.0000E+13	0.00	372.37	[162]
924	C_6H_5	=	$C_6H_5(B)$	4.0000E+13	0.00	303.40	[162]
925	$C_6H_5 + H$	=	$C_6H_4 + H_2$	1.5000E+11	0.00	0.00	[162]
926	$C_6H_5 + H$	=	C_6H_6	7.8300E+10	0.00	0.00	[13]
927	$C_6H_5 + O$	=	$C_6H_4 + OH$	2.0000E+10	0.00	0.00	[162]
928	$C_6H_5 + OH$	=	$C_6H_4 + H_2O$	2.0000E+10	0.00	0.00	[162]
929	$C_6H_5 + HO_2$	=	$C_6H_5O + OH$	5.0000E+10	0.00	4.18	[162]
930	$C_6H_5 + O_2$	=	$C_6H_5O + O$	2.6000E+10	0.00	25.61	[94]
931	$C_6H_5 + O_2$	=	C_6H_5OO	3.0800E+09	-0.15	0.67	adj. [76]
932	$C_6H_5 + C_2H_2$	=	$C_8H_6 + H$	1.8000E+13	-0.62	73.00	[216]
933	$C_6H_5 + C_2H_2$	=	C_8H_7	2.6000E+09	0.00	42.30	adj. [169]
934	$C_6H_5 + C_2H_3$	=	C_8H_8	5.0000E+09	0.00	0.00	[182]
935	$C_6H_5 + C_2H_4$	=	$C_8H_8 + H$	2.5100E+09	0.00	25.93	[90]
936	$C_6H_5 + C_3H_3$	=	$C_9H_8(S)$	1.0000E+10	0.00	0.00	[169]
937	$C_6H_5 + C_3H_3$	=	$C_9H_8(T)$	1.0000E+10	0.00	0.00	[169]
938	$C_6H_5 + C_3H_4(A)$	=	$C_9H_9(I)$	1.0000E+10	0.00	0.00	[169]
939	$C_6H_5 + C_3H_5(A)$	=	$C_9H_9(I) + H$	1.0000E+10	0.00	0.00	[169]
940	$C_6H_5 + C_4H_3(N)$	=	$C_{10}H_8J$	1.0000E+10	0.00	0.00	[169]
941	$C_6H_5 + C_4H_4$	=	$C_{10}H_8G + H$	2.8000E+10	0.00	42.30	[169]
942	$C_6H_5 + C_4H_4$	=	$C_{10}H_8J + H$	2.8000E+10	0.00	42.30	[169]
943	$C_6H_5 + C_4H_4$	=	$C_{10}H_9B$	2.8000E+10	0.00	42.30	[169]
944	$C_6H_5 + C_4H_5(T)$	=	$C_{10}H_9M + H$	1.0000E+10	0.00	0.00	[169]
945	$C_6H_5 + C_6H_5$	=	$C_{12}H_{10}$	3.1600E+09	0.00	0.00	[182]
946	$C_6H_5(A)$	=	$C_6H_4L + H$	6.0000E+11	0.00	188.00	[162]
947	$C_6H_5(A) + H$	=	$C_6H_4L + H_2$	1.0000E+11	0.00	0.00	[162]
948	$C_6H_5(A) + O$	=	$C_6H_4L + OH$	2.0000E+10	0.00	0.00	[162]
949	$C_6H_5(A) + OH$	=	$C_6H_4L + H_2O$	2.0000E+10	0.00	0.00	[162]
950	$C_6H_5(B)$	=	$C_4H_3(I) + C_2H_2$	5.0000E+14	0.00	159.00	[162]
951	$C_6H_5(B)$	=	$C_6H_4L + H$	2.5000E+58	-13.80	208.00	[162]
952	$C_6H_5(B)$	=	$C_6H_5(A)$	1.0000E+11	0.00	0.00	[162]
953	$C_6H_5(B) + H$	=	$C_6H_4L + H_2$	1.0000E+11	0.00	0.00	[162]
954	$C_6H_5(B) + O$	=	$C_6H_4L + OH$	2.0000E+10	0.00	0.00	[162]
955	$C_6H_5(B) + OH$	=	$C_6H_4L + H_2O$	2.0000E+10	0.00	0.00	[162]
956	$C_6H_6 + H$	=	$C_6H_5 + H_2$	2.5000E+11	0.00	66.94	[162]
957	$C_6H_6 + H$	=	C_6H_7	4.0000E+10	0.00	18.04	[162]
958	$C_6H_6 + O$	=	$C_6H_5 + OH$	2.0000E+10	0.00	61.52	[162]
959	$C_6H_6 + O$	=	$C_6H_5O + H$	2.4000E+10	0.00	19.53	[76]
960	$C_6H_6 + OH$	=	$C_6H_5 + H_2O$	1.6300E+05	1.42	6.10	[162]
961	$C_6H_6 + OH$	=	$C_6H_5OH + H$	1.3200E+10	0.00	44.31	[162]
962	$C_6H_6 + O_2$	=	$C_6H_5 + HO_2$	6.3000E+10	0.00	251.04	[162]
963	$C_6H_6 + HO_2$	=	$C_6H_5 + H_2O_2$	1.5200E+08	0.00	71.40	[217]
964	$C_6H_6 + {}^1CH_2$	=	$C_7H_7 + H$	4.0000E+10	0.00	36.33	[218]
965	$C_6H_6 + CH_3$	=	$C_6H_5 + CH_4$	4.3650E-07	5.00	51.49	[162]
966	$C_6H_6 + C_2H_3$	=	$C_8H_8 + H$	7.9400E+08	0.00	26.77	[169]
967	$C_6H_6 + C_6H_5$	=	$C_{12}H_{10} + H$	2.0000E+09	0.00	16.73	[182]
968	$C_6H_6(A)$	=	$C_6H_5(A) + H$	1.4000E+15	0.00	326.60	[162]
969	$C_6H_6(A)$	=	$C_6H_6(S)$	5.4000E+11	0.00	149.66	[162]
970	$C_6H_6(A) + H$	=	$C_6H_5(A) + H_2$	1.0000E+11	0.00	0.00	[162]
971	$C_6H_6(A) + O$	=	$C_6H_5(A) + OH$	2.0000E+10	0.00	0.00	[162]
972	$C_6H_6(A) + OH$	=	$C_6H_5(A) + H_2O$	2.0000E+10	0.00	0.00	[162]
973	$C_6H_6(B)$	=	$C_6H_5(A) + H$	7.0000E+14	0.00	326.60	[162]
974	$C_6H_6(B)$	=	$C_6H_6(D)$	1.0000E+12	0.00	224.00	[162]
975	$C_6H_6(B)$	=	$C_6H_6(F)$	5.0000E+11	0.00	144.00	[162]
976	$C_6H_6(B) + H$	=	$C_6H_5(A) + H_2$	1.0000E+11	0.00	0.00	[162]
977	$C_6H_6(B) + O$	=	$C_6H_5(A) + OH$	2.0000E+10	0.00	0.00	[162]
978	$C_6H_6(B) + OH$	=	$C_6H_5(A) + H_2O$	2.0000E+10	0.00	0.00	[162]
979	$C_6H_6(D)$	=	C_6H_6	5.0000E+11	0.00	200.00	[162]
980	$C_6H_6(D) + H$	=	$C_6H_5(B) + H_2$	1.0000E+11	0.00	46.00	[162]
981	$C_6H_6(D) + O$	=	$C_6H_5(B) + OH$	2.0000E+10	0.00	0.00	[162]
982	$C_6H_6(D) + OH$	=	$C_6H_5(B) + H_2O$	2.0000E+10	0.00	12.60	[162]

Table A.1, continued

No	*Reaction*			A	n	E_a	*Ref*
983	$C_6H_6(F)$	=	C_6H_6	7.5900E+13	0.00	309.00	[162]
984	$C_6H_6(F)$	=	$C_6H_6(D)$	1.0000E+13	0.00	342.00	[162]
985	$C_6H_6(F) + H$	=	$C_6H_6 + H$	3.0000E+09	0.50	8.37	[179]
986	$C_6H_6(M)$	=	$C_6H_6(F)$	4.2600E+13	0.00	206.00	[162]
987	$C_6H_6(S)$	=	$C_6H_6(F)$	5.0000E+11	0.00	132.40	[162]
988	$C_6H_6(S)$	=	$C_6H_6(M)$	5.0000E+11	0.00	92.00	[162]
989	C_6H_7	=	$C_6H_7(L)$	3.0000E+14	0.00	209.20	[162]
990	C_6H_8	=	$C_6H_6 + H_2$	1.0000E+06	0.00	0.00	[172]
991	C_6H_8	=	$C_6H_7 + H$	5.0100E+15	0.00	303.74	[172]
992	$C_6H_3O_2 + H$	=	$C_2H_2 + C_2H_2 + CO + CO$	1.0000E+11	0.00	0.00	[76]
993	$C_6H_3O_2 + O$	=	$C_2H_2 + C_2HO + CO + CO$	1.0000E+11	0.00	0.00	[76]
994	$C_6H_3O_3$	=	$C_2H_2 + C_2HO + CO + CO$	1.0000E+12	0.00	209.00	[76]
995	$C_6H_4O_2$	=	$C_5H_4O + CO$	3.7000E+11	0.00	247.00	[76]
996	$C_6H_4O_2 + H$	=	$C_5H_5O + CO$	2.5000E+10	0.00	19.68	[76]
997	$C_6H_4O_2 + H$	=	$C_6H_3O_2 + H_2$	2.0000E+09	0.00	33.90	[76]
998	$C_6H_4O_2 + O$	=	$C_6H_3O_2 + OH$	1.4000E+10	0.00	61.55	[76]
999	$C_6H_4O_2 + O$	=	$C_6H_3O_3 + H$	1.5000E+10	0.00	18.97	[76]
1000	$C_6H_4O_2 + OH$	=	$C_6H_3O_2 + H_2O$	1.0000E+03	2.00	16.75	[76]
1001	C_6H_5O	=	$C_5H_5 + CO$	4.5000E+11	0.00	183.68	[162]
1002	$C_6H_5O + H$	=	C_6H_5OH	2.5000E+11	0.00	0.00	[76]
1003	$C_6H_5O + O$	=	$C_6H_4O_2 + H$	3.0000E+10	0.00	0.00	[76]
1004	$C_6H_5O + OH$	=	C_6H_5OOH	1.0000E+09	0.00	0.00	[76]
1005	$C_6H_5O + HO_2$	=	$C_6H_5OH + O_2$	1.2500E+10	0.00	0.00	est.
1006	C_6H_5OO	=	$C_5H_5 + CO_2$	1.6000E+08	0.00	0.00	[76]
1007	C_6H_5OO	=	$C_6H_4O_2 + H$	4.0000E+08	0.00	0.00	[76]
1008	C_6H_5OO	=	$C_6H_5O + O$	4.2700E+15	-0.70	138.28	[76]
1009	$C_6H_5OO + H$	=	C_6H_5OOH	2.5000E+11	0.00	0.00	[76]
1010	$C_6H_5OO + HO_2$	=	$C_6H_5OOH + O_2$	1.8700E+09	0.00	6.45	[76]
1011	C_6H_5OH	=	$C_5H_6 + CO$	1.0000E+12	0.00	254.41	[133]
1012	$C_6H_5OH + H$	=	$C_6H_5O + H_2$	1.1500E+11	0.00	51.92	[215]
1013	$C_6H_5OH + O$	=	$C_6H_5O + OH$	2.8100E+10	0.00	30.78	[215]
1014	$C_6H_5OH + OH$	=	$C_6H_5O + H_2O$	6.0000E+09	0.00	0.00	[217]
1015	$C_6H_5OH + HO_2$	=	$C_6H_5O + H_2O_2$	3.0000E+10	0.00	62.80	[76]
1016	$C_6H_5OH + C_5H_5$	=	$C_6H_5O + C_5H_6$	2.6700E+11	0.00	105.62	est.
1017	$C_6H_5OH + C_6H_5OO$	=	$C_6H_5OOH + C_6H_5O$	3.1600E+08	0.00	29.14	[76]
1018	$C_7H_5 + O$	=	$C_5H_4(L) + C_2HO$	2.0000E+10	0.00	0.00	est.
1019	$C_7H_5 + O$	=	$C_5H_4O + C_2H$	2.0000E+10	0.00	0.00	est.
1020	$C_7H_5 + OH$	=	$C_5H_4O + C_2H_2$	2.0000E+10	0.00	0.00	est.
1021	$C_7H_5 + O_2$	=	$C_5H_4O + C_2HO$	1.0800E+05	1.50	125.94	est. (345)
1022	$C_6H_5C + O$	=	$C_6H_5 + CO$	1.5800E+10	0.00	0.00	est. (28)
1023	$C_6H_5C + O_2$	=	$C_6H_5CO + O$	2.9700E+10	0.00	0.00	est. (31)
1024	$C_6H_5C + H_2O$	=	C_7H_7O	2.2700E+09	0.00	-3.15	est. (32)
1025	$C_6H_5C + CH_3$	=	$C_8H_7 + H$	1.8900E+10	0.00	0.00	est. (70)
1026	$C_6H_5C + CH_4$	=	$C_8H_8 + H$	2.3700E+10	0.00	0.00	est. (82)
1027	$C_7H_6 + H$	=	$C_4H_4 + C_3H_3$	6.0000E+10	0.00	61.92	[27]
1028	$C_7H_6 + H$	=	$C_5H_5 + C_2H_2$	2.0000E+10	0.00	20.00	[27]
1029	$C_7H_6 + H$	=	$C_7H_5 + H_2$	2.8000E+10	0.00	9.45	est. (812)
1030	$C_7H_6 + O$	=	$C_5H_5 + C_2HO$	2.3320E+03	2.09	6.53	est. (146)
1031	$C_7H_6 + O$	=	$C_6H_6(F) + CO$	1.5550E+03	2.09	6.53	est. (145)
1032	$C_7H_6 + O$	=	$C_7H_5 + OH$	1.8100E+10	0.00	12.87	est. (814)
1033	$C_7H_6 + OH$	=	$C_7H_5 + H_2O$	1.1433E+06	1.18	-1.87	est. (815)
1034	$C_7H_6 + HO_2$	=	$C_7H_5 + H_2O_2$	2.0000E+09	0.00	48.78	est. (816)
1035	$C_6H_5CH + H$	=	$C_6H_5C + H_2$	4.3620E+10	0.00	0.00	est. (43)
1036	$C_6H_5CH + H$	=	C_7H_7	1.0000E+11	0.00	0.00	[215]
1037	$C_6H_5CH + O$	=	C_7H_6O	1.0000E+10	0.00	0.00	est.
1038	$C_6H_5CH + OH$	=	$C_6H_5C + H_2O$	4.4810E+03	2.00	12.56	est. (46)
1039	$C_6H_5CH + OH$	=	$C_7H_6O + H$	1.1400E+10	0.00	0.00	est. (47)
1040	$C_6H_5CH + O_2$	=	$C_6H_6 + CO_2$	5.3300E+18	-3.30	12.00	est. (55)
1041	$C_6H_5CH + O_2$	=	$C_7H_6O + O$	8.0000E+18	-3.30	12.00	est. (56)
1042	$C_6H_5CH + HO_2$	=	$C_7H_7 + O_2$	1.0000E+10	0.00	0.00	est.
1043	$C_6H_5CH + {}^1CH_2$	=	C_8H_8	1.0000E+10	0.00	0.00	est.
1044	$C_6H_5CH + {}^3CH_2$	=	C_8H_8	1.0000E+10	0.00	0.00	est.

Table A.1, continued

No	*Reaction*			A	n	E_a	*Ref*
1045	$C_6H_5CH + CH_3$	=	$C_8H_8 + H$	1.0000E+10	0.00	0.00	est.
1046	$C_6H_5CH + CH_4$	=	$C_8H_9 + H$	1.0000E+10	0.00	0.00	est.
1047	$C_6H_5CH + C_2H_2$	=	$C_9H_8(T)$	3.3333E+09	0.00	0.00	est.
1048	$C_6H_5CH + C_3H_3$	=	$C_9H_6CH_2 + H$	1.0000E+10	0.00	0.00	est.
1049	C_7H_7	=	C_7H_7L	3.1600E+15	0.00	356.67	[27]
1050	$C_7H_7 + H$	=	$C_6H_5CH + H_2$	6.0300E+10	0.00	63.20	[215]
1051	$C_7H_7 + OH$	=	$C_7H_7O + H$	4.5920E+09	-0.23	58.28	est. (66)
1052	$C_7H_7 + O$	=	$C_7H_6O + H$	3.5000E+10	0.00	0.00	[126]
1053	$C_7H_7 + O$	=	$C_6H_6 + CHO$	3.5000E+10	0.00	0.00	[126]
1054	$C_7H_7 + O_2$	=	$C_7H_6O + OH$	5.2280E+03	0.20	0.00	[86]
1055	$C_7H_7 + O_2$	=	$C_7H_7OO^4$ k_∞ =	1.3000E+06	1.10	0.00	est. (77)
			k_0 =	5.3100E+19	-3.30	0.00	
1056	$C_7H_7 + O_2$	=	$C_7H_7O + O$	8.6400E+10	0.00	131.36	est. (76)
1057	$C_7H_7 + HO_2$	=	$C_7H_7O + OH$	5.0000E+09	0.00	0.00	[86]
1058	$C_7H_7 + {}^1CH_2$	=	$C_8H_8 + H$	2.4000E+11	0.00	0.00	adj. [22]
1059	$C_7H_7 + {}^3CH_2$	=	$C_8H_8 + H$	7.0000E+10	0.00	37.50	adj. [22]
1060	$C_7H_7 + CH_3$	=	$C_8H_9 + H$	3.0000E+09	0.10	44.36	est. (73)
1061	$C_7H_7 + CH_3$	=	C_8H_{10}	1.4600E+10	0.00	0.00	[169]
1062	$C_7H_7 + C_2H_2$	=	$C_9H_8 + H$	2.0000E+10	0.00	90.00	est. (362)
1063	$C_7H_7 + C_2H_2$	=	$C_9H_9(P)$	1.0000E+09	0.00	20.92	[169]
1064	$C_7H_7 + C_3H_3$	=	$C_{10}H_{10}$	3.0000E+10	0.00	0.00	[182]
1065	$C_7H_7 + C_6H_5OH$	=	$C_6H_5O + C_7H_8$	1.0500E+08	0.00	39.77	[89]
1066	$C_7H_7 + C_6H_5CH$	=	$C_8H_8 + C_6H_5$	1.0000E+10	0.00	0.00	est.
1067	$C_7H_7 + C_7H_7$	=	$C_{14}H_{14}$	2.5100E+08	0.40	0.00	[86]
1068	C_7H_7L	=	$C_4H_4 + C_3H_3$	2.0000E+15	0.00	349.78	[26]
1069	C_7H_7L	=	$C_7H_6 + H$	5.0000E+15	0.00	165.00	[26]
1070	C_7H_7P	=	$C_2H_2 + C_2H_2 + C_3H_3$	2.5000E+14	0.00	347.00	[199]
1071	C_7H_7P	=	$C_4H_3(N) + C_3H_4(P)$	2.5000E+14	0.00	408.00	[182]
1072	$C_7H_7P + O_2$	=	$OC_7H_7 + O$	2.6000E+10	0.00	25.61	est. (930)
1073	$C_7H_7P + O_2$	=	OOC_7H_7P	3.8000E+09	-0.15	0.67	est. (931)
1074	$C_7H_7P + C_2H_2$	=	$C_9H_9(F)$	1.0000E+09	0.00	20.92	[169]
1075	$C_7H_7P + C_3H_3$	=	$C_{10}H_{10}F$	3.0000E+10	0.00	0.00	[169]
1076	C_7H_8	=	$C_6H_5 + CH_3$	8.9100E+12	0.00	303.75	[199]
1077	C_7H_8	=	$C_7H_7 + H$	5.6000E+15	0.00	381.30	[182]
1078	$C_7H_8 + H$	=	$C_6H_6 + CH_3$	1.2000E+10	0.00	21.43	[219]
1079	$C_7H_8 + H$	=	$C_7H_7 + H_2$	3.9800E-01	3.44	13.05	[13]
1080	$C_7H_8 + H$	=	$C_7H_7P + H_2$	2.5000E+11	0.00	66.94	est. (956)
1081	$C_7H_8 + O$	=	$C_7H_7 + OH$	6.3000E+08	0.00	0.00	[129]
1082	$C_7H_8 + O$	=	$C_7H_7O + H$	1.5500E+10	0.00	16.63	[182]
1083	$C_7H_8 + O$	=	$OC_7H_7 + H$	3.1000E+10	0.00	16.63	[129]
1084	$C_7H_8 + O$	=	C_7H_8OA	3.1000E+09	0.00	16.63	[129]
1085	$C_7H_8 + O$	=	$C_7H_7P + OH$	1.8400E+10	0.00	61.52	est. (958)
1086	$C_7H_8 + OH$	=	$C_7H_7 + H_2O$	5.1900E+06	1.00	3.66	[13]
1087	$C_7H_8 + OH$	=	$C_7H_7O + H_2$	2.2900E+09	0.00	35.50	est. [182]
1088	$C_7H_8 + OH$	=	$HOC_7H_7 + H$	2.2900E+09	0.00	-1.50	[182]
1089	$C_7H_8 + OH$	=	$C_7H_7OH + H$	6.6000E+09	0.00	44.31	[182]
1090	$C_7H_8 + OH$	=	$C_7H_7P + H_2O$	1.5000E+05	1.42	6.10	est. (960)
1091	$C_7H_8 + O_2$	=	$C_7H_7 + HO_2$	1.8100E+09	0.00	166.28	[13]
1092	$C_7H_8 + HO_2$	=	$C_7H_7 + H_2O_2$	3.9750E+08	0.00	58.86	[14]
1093	$C_7H_8 + HO_2$	=	$C_7H_7P + H_2O_2$	5.4800E+09	0.00	120.55	[14]
1094	$C_7H_8 + CH_3$	=	$CH_4 + C_7H_7$	3.1600E+09	0.00	46.44	[182]
1095	$C_7H_8 + CH_3$	=	$C_7H_7P + CH_4$	1.0000E+10	0.00	66.94	[182]
1096	$C_7H_8 + C_2H_3$	=	$C_7H_7 + C_2H_4$	3.9800E+09	0.00	33.47	[182]
1097	$C_7H_8 + C_3H_5(A)$	=	$C_7H_7 + C_3H_6$	5.0000E+09	0.00	58.58	[182]
1098	$C_7H_8 + C_6H_5$	=	$C_6H_6 + C_7H_7$	2.1000E+09	0.00	18.42	[91]
1099	C_6H_5CO	=	$C_6H_5 + CO$	3.9800E+14	0.00	123.06	[236]
1100	$C_6H_5CO + H$	=	$C_6H_6 + CO$	3.0000E+10	0.00	0.00	[35]
1101	C_7H_6O	=	$C_6H_5CO + H$	3.9800E+15	0.00	350.20	[104]
1102	$C_7H_6O + H$	=	$C_6H_6 + CHO$	6.3000E+04	1.62	9.06	[89]
1103	$C_7H_6O + H$	=	$C_6H_5CO + H_2$	5.0000E+10	0.00	20.63	[89]
1104	$C_7H_6O + O$	=	$C_6H_6 + CO_2$	2.0000E+10	0.00	0.00	est.
1105	$C_7H_6O + O$	=	$C_6H_5CO + OH$	9.0400E+09	0.00	12.89	[89]

Table A.1, continued

No	*Reaction*			A	n	E_a	*Ref*
1106	$C_7H_6O + OH$	=	$C_6H_5CO + H_2O$	1.7100E+06	1.18	-1.87	[89]
1107	$C_7H_6O + O_2$	=	$C_6H_5CO + HO_2$	1.0200E+10	0.00	163.05	[89]
1108	$C_7H_6O + HO_2$	=	$C_6H_5CO + H_2O_2$	1.9900E+09	0.00	48.80	[182]
1109	$C_7H_6O + CH_3$	=	$C_6H_5CO + CH_4$	2.7700E+00	2.81	24.17	[89]
1110	$C_7H_6O + C_6H_5$	=	$C_6H_5CO + C_6H_6$	7.0100E+08	0.00	18.42	[89]
1111	C_7H_7O	=	$C_6H_6 + CHO$	5.0000E+12	0.00	79.00	est. [73] ♯
1112	C_7H_7O	=	$C_6H_5 + CH_2O$	2.5000E+13	0.00	135.00	est. [73]
1113	C_7H_7O	=	$C_7H_6O + H$	3.0000E+12	0.00	68.00	est.[73]
1114	$C_7H_7O + M$	=	$C_7H_6O + H + M$	2.5000E+08	0.00	0.00	[129]
1115	$C_7H_7O + H$	=	$C_7H_6O + H_2$	3.0000E+10	0.00	0.00	[182]
1116	$C_7H_7O + H$	=	C_7H_7OH	2.5300E+11	0.00	0.00	[182]
1117	$C_7H_7O + O$	=	$C_7H_6O + OH$	4.2000E+10	0.00	0.00	[182]
1118	$C_7H_7O + OH$	=	$C_7H_6O + H_2O$	2.4000E+10	0.00	0.00	[182]
1119	$C_7H_7O + O_2$	=	$C_7H_6O + HO_2$	1.0000E+10	0.00	21.00	[182]
1120	OC_7H_7	=	$C_5H_4CH_3 + CO$	4.5000E+11	0.00	183.68	est. (1001)
1121	$OC_7H_7 + H$	=	HOC_7H_7	2.5000E+11	0.00	0.00	[89]
1122	$OC_7H_7 + H_2O$	=	$HOC_7H_7 + OH$	6.8800E+09	0.36	136.19	[89]
1123	C_7H_7OA	=	$C_7H_6O + H$	3.1600E+12	0.00	87.86	[194]
1124	$C_7H_7OH + H$	=	$C_6H_6 + CH_2OH$	1.2000E+10	0.00	21.55	[89]
1125	$C_7H_7OH + H$	=	$C_7H_7O + H_2$	8.0000E+10	0.00	34.45	adj. [89]
1126	$C_7H_7OH + OH$	=	$C_7H_7O + H_2O$	5.0000E+09	0.00	0.00	[127]
1127	$C_7H_7OH + O_2$	=	$C_7H_6O + HO_2 + H$	2.0000E+11	0.00	173.30	[89]
1128	$C_7H_7OH + C_6H_5$	=	$C_7H_6O + C_6H_6 + H$	1.4000E+09	0.00	18.42	[89]
1129	$HOC_7H_7 + H$	=	$C_6H_5OH + CH_3$	1.2000E+10	0.00	21.55	[89]
1130	$HOC_7H_7 + H$	=	$OC_7H_7 + H_2$	1.1500E+11	0.00	51.91	[110]
1131	$HOC_7H_7 + C_7H_7$	=	$OC_7H_7 + C_7H_8$	1.0500E+08	0.00	39.77	[89]
1132	C_7H_8OA	=	$C_6H_5O + CH_3$	2.0000E+15	0.00	266.09	[4]
1133	$C_7H_8OA + H$	=	$C_6H_5OH + CH_3$	7.0800E+09	0.00	22.55	[4]
1134	$C_7H_8OA + O$	=	$C_7H_7OA + OH$	1.6700E+10	0.00	12.30	[151]
1135	$C_7H_8OA + OH$	=	$C_7H_7OA + H_2O$	1.2000E+09	0.00	-2.09	[201]
1136	$C_7H_8OA + CH_3$	=	$C_7H_7OA + CH_4$	5.0100E+08	0.00	43.92	[194]
1137	C_7H_7OO	=	$C_7H_6O + OH$	1.0000E+10	0.00	121.00	[182]
1138	OOC_7H_7P	=	$OC_7H_7 + O$	4.2700E+15	-0.70	138.28	est. (1008)
1139	OOC_7H_7P	=	$C_5H_4CH_3 + CO_2$	1.5060E+08	0.00	0.00	est. (1006)
1140	$C_8H_5 + H$	=	C_8H_6	2.0000E+11	0.00	0.00	est.
1141	$C_8H_5 + O_2$	=	$C_8H_5O + O$	2.2700E+10	0.00	25.61	est. (930)
1142	$C_8H_5 + O_2$	=	C_8H_5OO	1.6490E+10	-0.15	0.67	est. (931)
1143	$C_8H_5 + C_2H_2$	=	$C_{10}H_7L$	4.0000E+10	0.00	42.30	[96]
1144	$C_8H_5(S) + H$	=	C_8H_6	1.8100E+11	0.00	0.00	[182]
1145	$C_8H_5(S) + O_2$	=	$C_6H_4 + CHO + CO$	1.8800E+09	0.00	31.25	[182]
1146	$C_8H_5(S) + C_2H_2$	=	$C_{10}H_7M$	4.0000E+10	0.00	42.30	[169]
1147	C_8H_6	=	$C_6H_4 + C_2H_2$	1.0000E+14	0.00	398.70	est.
1148	$C_8H_6 + M$	=	$C_6H_5CHC + M$	1.3400E+12	-0.64	207.00	est. (144)
1149	$C_8H_6 + H$	=	$C_8H_5 + H_2$	2.5000E+11	0.00	66.94	[257]
1150	$C_8H_6 + H$	=	$C_8H_5(S) + H_2$	3.0150E+10	0.00	116.40	[182]
1151	$C_8H_6 + O$	=	$C_6H_5 + C_2HO$	2.1900E+03	2.09	6.54	est. (146)
1152	$C_8H_6 + O$	=	$C_6H_5CH + CO$	1.4600E+03	2.09	6.53	[85]
1153	$C_8H_6 + O$	=	$C_8H_5 + OH$	2.0000E+10	0.00	61.52	est. (958)
1154	$C_8H_6 + O$	=	$C_6H_5C_2O + H$	2.1900E+03	2.09	6.54	est. (146)
1155	$C_8H_6 + O$	=	$C_8H_5O + H$	2.4000E+10	0.00	19.54	est. (959)
1156	$C_8H_6 + OH$	=	$C_6H_5 + C_2H_2O$	3.7500E+03	1.70	4.18	est. (148)
1157	$C_8H_6 + OH$	=	$C_6H_6 + C_2HO$	2.4400E+00	3.02	46.34	[182]
1158	$C_8H_6 + OH$	=	$C_2H + C_6H_5OH$	3.3700E+04	2.00	58.58	est. (147)
1159	$C_8H_6 + OH$	=	$C_7H_7 + CO$	6.1000E+00	3.02	46.34	[182]
1160	$C_8H_6 + OH$	=	$C_8H_5 + H_2O$	2.1000E+10	0.00	19.10	[96]
1161	$C_8H_6 + OH$	=	$C_8H_5(S) + H_2O$	1.6850E+04	2.00	58.58	[182]
1162	$C_8H_6 + HO_2$	=	$C_2H_2O + C_6H_5O$	6.0000E+06	0.00	33.53	est. (150)
1163	$C_8H_6 + HO_2$	=	$C_8H_5 + H_2O_2$	1.0000E+10	0.00	101.00	est.
1164	$C_8H_6 + {}^1CH_2$	=	$C_9H_8(S)$	1.2000E+10	0.00	0.00	[182]
1165	$C_8H_6 + {}^3CH_2$	=	$C_9H_8(T)$	1.2000E+10	0.00	0.00	[182]
1166	$C_8H_6 + CH_3$	=	$C_9H_8(S) + H$	4.0000E+16	-2.08	132.18	[182]
1167	$C_8H_6 + CH_3$	=	$C_9H_8(T) + H$	1.6000E+15	-1.96	86.16	[182]
1168	$C_6H_5CHC + H$	=	C_8H_7	1.0750E+11	0.00	0.00	est. [158]
1169	$C_6H_5CHC + O_2$	=	$C_6H_5CH + CO_2$	2.6800E+10	0.00	0.00	est. (166)

♯ : Removed for Chapter 3.3 and Chapter 5.

Table A.1, continued

No	*Reaction*			A	n	E_a	*Ref*
1170	C_8H_7	=	$C_8H_6 + H$	1.3000E+41	-8.65	46.10	[256]
1171	$C_8H_7 + M$	=	$C_8H_6 + H + M$	2.0000E+14	0.00	166.29	[182]
1172	$C_8H_7 + H$	=	$C_8H_6 + H_2$	9.6400E+10	0.00	0.00	[182]
1173	$C_8H_7 + H$	=	C_8H_8	1.2100E+11	0.00	0.00	[182]
1174	$C_8H_7 + OH$	=	$C_8H_6 + H_2O$	2.0000E+10	0.00	0.00	[182]
1175	$C_8H_7 + OH$	=	$C_6H_5 + CH_3CO$	3.0000E+10	0.00	0.00	[182]
1176	$C_8H_7 + O$	=	$C_6H_5 + C_2H_2O$	3.0000E+10	0.00	0.00	[182]
1177	$C_8H_7 + O$	=	$C_7H_7 + CO$	3.0000E+10	0.00	0.00	[182]
1178	$C_8H_7 + O_2$	=	$C_6H_6 + C_2HO + O$	2.5000E+09	0.06	43.98	adj. [173]
1179	$C_8H_7 + O_2$	=	$C_7H_6O + CHO$	8.3900E+17	-2.78	10.56	adj. [173]
1180	$C_8H_7 + O_2$	=	$C_8H_6 + HO_2$	8.4900E+10	-0.83	10.63	adj. [173]
1181	$C_8H_7 + HO_2$	=	$C_7H_7 + CO + OH$	3.0000E+10	0.00	0.00	est.
1182	$C_8H_7 + HO_2$	=	$C_8H_6 + H_2O_2$	2.0000E+10	0.00	0.00	est.
1183	$C_8H_7 + C_2H_2$	=	$C_{10}H_9A$	4.0000E+10	0.00	42.30	[182]
1184	$C_8H_7(F)$	=	$C_8H_6 + H$	3.0000E+13	0.00	242.20	[169]
1185	$C_8H_7(P) + H$	=	C_8H_8	7.8300E+10	0.00	0.00	[182]
1186	$C_8H_7(P) + O$	=	$C_6H_5O + C_2H_2$	3.0000E+10	0.00	0.00	[182]
1187	$C_8H_7(P) + O$	=	$C_7H_7P + CO$	3.0000E+10	0.00	0.00	[182]
1188	$C_8H_7(P) + OH$	=	$C_6H_5O + C_2H_3$	3.0000E+10	0.00	0.00	[182]
1189	$C_8H_7(P) + C_2H_2$	=	$C_{10}H_9P$	4.0000E+10	0.00	42.30	[169]
1190	$C_8H_8 + H$	=	$C_8H_7 + H_2$	6.6250E+02	2.53	51.21	[182]
1191	$C_8H_8 + H$	=	$C_8H_7(P) + H_2$	2.7000E+10	0.00	40.58	[182]
1192	$C_8H_8 + O$	=	$C_6H_5 + CH_3CO$	2.5000E+03	1.88	0.76	adj. [173]
1193	$C_8H_8 + O$	=	$C_6H_6 + C_2H_2O$	3.3000E+02	1.88	0.76	adj. [173]
1194	$C_8H_8 + O$	=	$C_7H_7 + CHO$	4.2020E+03	1.88	0.76	adj. [173]
1195	$C_8H_8 + OH$	=	$C_7H_7 + CH_2O$	3.0000E+10	0.00	0.00	[182] ♯
1196	$C_8H_8 + OH$	=	$C_8H_7 + H_2O$	7.8500E+00	2.75	17.46	[182]
1197	$C_8H_8 + OH$	=	$C_8H_7(P) + H_2O$	2.1000E+10	0.00	19.10	[182]
1198	C_8H_9	=	$C_6H_5 + C_2H_4$	8.9100E+12	0.00	303.75	[182]
1199	C_8H_9	=	$C_8H_8 + H$	3.1600E+13	0.00	212.00	[197]
1200	$C_8H_9(M) + O$	=	$C_7H_8 + CHO$	3.5000E+10	0.00	0.00	est. (1053)
1201	$C_8H_9(M) + O$	=	$C_8H_8O(M) + H$	3.5000E+10	0.00	0.00	est. (1052)
1202	$C_8H_9(M) + OH$	=	$C_8H_9O(M) + H$	4.5920E+09	-0.23	58.28	est. (1051)
1203	$C_8H_9(M) + O_2$	=	$C_8H_8O(M) + OH$	5.2280E+03	0.20	0.00	est. (1054)
1204	$C_8H_9(M) + O_2$	=	$C_8H_9O(M) + O$	8.6400E+10	0.00	131.00	est. (1056)
1205	$C_8H_9(M) + HO_2$	=	$C_8H_9O(M) + OH$	5.0000E+09	0.00	0.00	est. (1057)
1206	$C_8H_9(F)$	=	$C_8H_8 + H$	3.0000E+13	0.00	172.40	[169]
1207	C_8H_{10}	=	$C_8H_9 + H$	2.5100E+15	0.00	340.00	[197]
1208	$C_8H_{10} + H$	=	$C_6H_6 + C_2H_5$	1.2000E+10	0.00	21.34	[220]
1209	$C_8H_{10} + H$	=	$C_8H_9 + H_2$	1.2600E-01	3.44	13.05	[182]
1210	$C_8H_{10} + O$	=	$C_8H_9 + OH$	2.2000E+09	0.00	15.90	[182]
1211	$C_8H_{10} + OH$	=	$C_8H_9 + H_2O$	5.0000E+08	0.00	0.00	[13]
1212	$C_8H_{10} + HO_2$	=	$C_8H_9 + H_2O_2$	2.6500E+08	0.00	47.22	[14]
1213	$C_8H_{10} + C_6H_5$	=	$C_8H_9 + C_6H_6$	5.0000E+08	0.00	0.00	[182]
1214	$C_8H_{10}(M)$	=	$C_7H_7P + CH_3$	8.9100E+12	0.00	303.75	est. (1076)
1215	$C_8H_{10}(M)$	=	$C_8H_9(M) + H$	5.6000E+15	0.00	381.30	est. (1077)
1216	$C_8H_{10}(M) + H$	=	$C_7H_8 + CH_3$	6.0000E+09	0.00	21.43	est. (1078)
1217	$C_8H_{10}(M) + H$	=	$C_8H_9(M) + H_2$	3.9800E-01	3.44	13.05	est. (1079)
1218	$C_8H_{10}(M) + O$	=	$C_5H_4CH_3 + CH_3 + CO$	4.5000E+11	0.00	183.69	est. (1001)
1219	$C_8H_{10}(M) + O$	=	$C_8H_9(M) + OH$	6.3000E+08	0.00	0.00	est. (1081)
1220	$C_8H_{10}(M) + O$	=	$C_8H_9O(M) + H$	1.5500E+10	0.00	16.63	est. (1082)
1221	$C_8H_{10}(M) + OH$	=	$C_8H_9(M) + H_2O$	5.1900E+06	1.00	3.66	est. (1086)
1222	$C_8H_{10}(M) + OH$	=	$C_8H_9O(M) + H_2$	2.2900E+09	0.00	35.00	est. (1087)
1223	$C_8H_{10}(M) + OH$	=	$HOC_7H_7 + CH_3$	2.2900E+09	0.00	-1.49	est. (1088)
1224	$C_8H_{10}(M) + OH$	=	$C_8H_9OH(M) + H$	6.6000E+09	0.00	44.31	est. (1089)
1225	$C_8H_{10}(M) + O_2$	=	$C_8H_9(M) + HO_2$	1.8100E+09	0.00	166.28	est. (1091)
1226	$C_8H_{10}(M) + HO_2$	=	$C_8H_9(M) + H_2O_2$	3.9750E+08	0.00	58.86	est. (1092)
1227	$C_8H_{10}(M) + CH_3$	=	$C_8H_9(M) + CH_4$	3.1600E+09	0.00	46.44	est. (1094)
1228	$C_6H_5C_2O + O_2$	=	$C_6H_5O + CO + CO$	1.0000E+10	0.00	0.00	est. (227)
1229	$C_6H_5C_2O + O_2$	=	$C_6H_5 + CO + CO_2$	1.0000E+10	0.00	0.00	est. (228)
1230	$C_6H_5C_2O + O_2$	=	$C_6H_5CO + CO_2$	1.1839E+10	0.00	0.00	est.

♯ : Amended to 1.0000E+10 for Chapter 3.3 and Chapter 5.

Table A.1, continued

No	*Reaction*			A	n	E_a	*Ref*
1231	C_8H_5O	=	$C_7H_5 + CO$	4.0100E+11	0.00	183.68	est. (1001)
1232	C_8H_5OO	=	$C_7H_5 + CO_2$	1.7825E+07	0.00	0.00	est. (1006)
1233	C_8H_5OO	=	$C_8H_5O + O$	3.8060E+15	-0.70	138.20	est. (1008)
1234	C_7H_7CO	=	$C_7H_7P + CO$	3.9800E+14	0.00	123.06	est. (1099)
1235	$C_7H_7CO + H$	=	$C_7H_8 + CO$	3.0000E+10	0.00	0.00	est. (1100)
1236	$C_8H_8O(M)$	=	$C_7H_7CO + H$	3.9800E+15	0.00	350.20	est. (1101)
1237	$C_8H_8O(M) + H$	=	$C_7H_8 + CHO$	6.3000E+04	1.62	9.06	est. (1102)
1238	$C_8H_8O(M) + H$	=	$C_7H_6O + CH_3$	1.2000E+10	0.00	21.43	est. (1078)
1239	$C_8H_8O(M) + H$	=	$C_7H_7CO + H_2$	5.0000E+10	0.00	20.63	est. (1103)
1240	$C_8H_8O(M) + O$	=	$C_5H_4CH_3 + CHO + CO$	2.5000E+11	0.00	189.69	est. (1001)
1241	$C_8H_8O(M) + O$	=	$OC_7H_7 + CHO$	3.1000E+10	0.00	16.63	est. (1083)
1242	$C_8H_8O(M) + O$	=	$C_7H_8 + CO_2$	2.0000E+10	0.00	0.00	est. (1104)
1243	$C_8H_8O(M) + O$	=	$C_7H_7CO + OH$	9.0400E+09	0.00	12.89	est. (1105)
1244	$C_8H_8O(M) + OH$	=	$C_7H_7CO + H_2O$	1.7100E+06	1.18	-1.87	est. (1106)
1245	$C_8H_8O(M) + O_2$	=	$C_7H_7CO + HO_2$	1.0200E+10	0.00	163.05	est. (1107)
1246	$C_8H_8O(M) + HO_2$	=	$C_7H_7CO + H_2O_2$	1.9900E+09	0.00	48.80	est. (1108)
1247	$C_8H_8O(M) + CH_3$	=	$C_7H_7CO + CH_4$	2.7700E+00	2.81	24.17	est. (1109)
1248	$C_8H_8O(M) + C_6H_5$	=	$C_7H_7CO + C_6H_6$	7.0100E+08	0.00	18.42	est. (1100)
1249	$C_8H_9O(M) + M$	=	$C_8H_8O(M) + H + M$	2.5000E+08	0.00	00.00	est. (1114)
1250	$C_8H_9O(M) + O_2$	=	$C_8H_8O(M) + HO_2$	1.0000E+10	0.00	21.00	est. (1119)
1251	$C_8H_9O(M)$	=	$C_7H_8 + CHO$	5.0000E+12	0.00	79.00	est. (1111)
1252	$C_8H_9O(M)$	=	$C_7H_7P + CH_2O$	2.5000E+13	0.00	135.00	est. (1112)
1253	$C_8H_9O(M)$	=	$C_8H_8O(M) + H$	3.0000E+12	0.00	68.00	est. (1113)
1254	$C_8H_9OH(M) + H$	=	$C_7H_8 + CH_2OH$	1.2000E+10	0.00	21.55	est. (1124)
1255	$C_8H_9OH(M) + H$	=	$C_8H_9O(M) + H_2$	8.0000E+10	0.00	34.45	est. (1125)
1256	$C_8H_9OH(M) + OH$	=	$C_8H_9O(M) + H_2O$	5.0000E+09	0.00	0.00	est. (1126)
1257	$C_8H_9OH(M) + O_2$	=	$C_8H_8O(M) + HO_2 + H$	2.0000E+11	0.00	173.30	est. (1127)
1258	$C_9H_7 + H$	=	C_9H_8	2.0000E+11	0.00	0.00	est.
1259	$C_9H_7 + O$	=	$C_8H_7(P) + CO$	4.5000E+10	0.00	0.00	est.
1260	$C_9H_7 + O$	=	$C_9H_6O + H$	5.8100E+10	-0.02	0.08	est. (789)
1261	$C_9H_7 + O$	=	C_9H_7O	7.5000E+09	0.00	0.00	[203]
1262	$C_9H_7 + OH$	=	$C_8H_7(P) + CHO$	1.0000E+11	0.00	97.00	est.
1263	$C_9H_7 + O_2$	=	$C_6H_5O + C_3H_2O$	6.2703E+05	0.00	11.00	est.
1264	$C_9H_7 + O_2$	=	$C_7H_7 + CO + CO$	2.7770E+05	0.00	11.00	est.
1265	$C_9H_7 + O_2$	=	$C_7H_6O + C_2HO$	2.7770E+05	0.00	11.00	est.
1266	$C_9H_7 + O_2$	=	$C_9H_6O + OH$	1.9325E+12	-0.73	203.93	est. (795)
1267	$C_9H_7 + O_2$	=	$C_9H_7O + O$	1.9325E+12	-0.73	203.93	est. (795)
1268	$C_9H_7 + HO_2$	=	$C_9H_6O + H_2O$	1.1900E+30	-6.52	56.07	est. (797)
1269	$C_9H_7 + HO_2$	=	$C_9H_7O + OH$	4.7000E+26	-4.69	48.74	est. (798)
1270	$C_9H_7 + {}^1CH_2$	=	$C_{10}H_9T$	1.0000E+11	0.00	0.00	[182]
1271	$C_9H_7 + {}^3CH_2$	=	$C_9H_6CH_2 + H$	5.0000E+10	0.00	0.00	adj. [169]
1272	$C_9H_7 + CH_3$	=	$C_9H_7CH_3$	2.0000E+10	0.00	0.00	[157]
1273	$C_9H_7L + O$	=	$C_6H_5 + C_2H_2 + CO$	8.2000E+10	0.00	0.00	[182]
1274	$C_9H_7L + OH$	=	$C_6H_5 + C_2H_2 + CHO$	3.5000E+10	0.00	26.00	[182]
1275	$C_9H_7L + O_2$	=	$C_6H_5 + C_2HO + CHO$	1.7000E+07	0.00	12.00	[182]
1276	$C_9H_8 + H$	=	$C_9H_7 + H_2$	2.1120E+10	0.00	9.45	est. (812)
1277	$C_9H_8 + O$	=	$C_9H_7 + OH$	1.3650E+10	0.00	12.87	est. (814)
1278	$C_9H_8 + OH$	=	$C_9H_7 + H_2O$	8.6233E+05	1.18	-1.87	est. (815)
1279	$C_9H_8 + HO_2$	=	$C_9H_7 + H_2O_2$	1.5086E+09	0.00	48.78	est. (816)
1280	$C_9H_8(S) + H$	=	$C_9H_7L + H_2$	1.2000E+11	0.00	62.84	[182]
1281	$C_9H_8(S) + O$	=	$C_8H_7 + CHO$	6.5000E-06	4.61	-17.80	[182]
1282	$C_9H_8(S) + OH$	=	$C_9H_7L + H_2O$	5.9000E+08	0.00	6.28	[182]
1283	$C_9H_8(T) + H$	=	$C_9H_7L + H_2$	1.2000E+11	0.00	62.84	[182]
1284	$C_9H_8(T) + O$	=	$C_8H_8 + CO$	1.3690E+03	2.09	6.53	[182]
1285	$C_9H_8(T) + OH$	=	$C_8H_8 + CHO$	3.0000E-07	4.50	-4.19	[182]
1286	$C_9H_8(T) + OH$	=	$C_9H_7L + H_2O$	1.8000E+00	3.00	0.84	[182]
1287	$C_9H_9(C)$	=	$C_9H_8 + H$	1.0000E+13	0.00	90.00	[182]
1288	$C_9H_9(C)$	=	$C_9H_9(P)$	1.0000E+14	0.00	334.00	[182]
1289	$C_9H_9(F)$	=	$C_9H_9(S)$	1.0000E+09	0.00	0.00	[182]
1290	$C_9H_9(I)$	=	$C_9H_8(S) + H$	1.0000E+13	0.00	138.00	[182]
1291	$C_9H_9(I)$	=	$C_9H_8(T) + H$	1.0000E+13	0.00	150.00	[182]
1292	$C_9H_9(I)$	=	$C_9H_9(N)$	1.0000E+13	0.00	17.00	[182]

Table A.1, continued

No	*Reaction*			A	n	E_a	*Ref*
1293	$C_9H_9(N)$	=	$C_9H_9(S)$	1.0000E+10	0.00	0.00	[182]
1294	$C_9H_9(P)$	=	$C_9H_8(T) + H$	1.0000E+13	0.00	137.00	[182]
1295	$C_9H_9(S)$	=	$C_9H_8 + H$	1.0000E+13	0.00	137.00	[182]
1296	C_9H_6O	=	$CO + C_2H_2 + C_6H_4$	1.0000E+15	0.00	326.57	est. (899)
1297	C_9H_6O	=	$C_8H_6 + CO$	1.8825E+11	0.00	183.68	est. (1001)
1298	$C_9H_6O + H$	=	$C_8H_7 + CO$	1.2500E+10	0.00	19.68	[218]
1299	$C_9H_6O + H$	=	$C_8H_7(P) + CO$	1.2500E+10	0.00	19.68	[218]
1300	$C_9H_6O + O$	=	$C_8H_6 + CO_2$	1.0000E+10	0.00	8.37	est. (902)
1301	C_9H_7O	=	$C_8H_7 + CO$	2.0000E+14	0.00	155.00	[203]
1302	C_9H_7O	=	$C_9H_6O + H$	2.0000E+14	0.00	242.00	est.
1303	$C_{10}H_7 + H$	=	$C_{10}H_8$	7.8300E+10	0.00	0.00	[182]
1304	$C_{10}H_7 + OH$	=	$C_{10}H_7O + H$	5.0000E+10	0.00	0.00	[182]
1305	$C_{10}H_7 + H_2$	=	$C_{10}H_8 + H$	4.4400E+01	2.43	26.29	adj. [2]
1306	$C_{10}H_7 + O_2$	=	$C_{10}H_7O + O$	2.1500E+10	0.00	25.61	est. (930)
1307	$C_{10}H_7 + O_2$	=	$C_{10}H_7OO$	2.5000E+09	-0.15	0.67	est. (931)
1308	$C_{10}H_7 + HO_2$	=	$C_{10}H_7O + OH$	4.0700E+10	0.00	4.18	est. (929)
1309	$C_{10}H_7 + C_2H_4$	=	$1C_{12}H_{10} + H$	2.0160E+09	0.00	25.93	est. (935)
1310	$C_{10}H_7L$	=	$C_{10}H_6 + H$	1.0000E+13	0.00	138.00	est. (1295)
1311	$C_{10}H_7L$	=	$C_{10}H_7$	1.0000E+10	0.00	0.00	[169]
1312	$C_{10}H_7L + H$	=	$C_{10}H_6 + H_2$	1.0000E+10	0.00	0.00	[182]
1313	$C_{10}H_7L + H$	=	$C_{10}H_8L$	1.0000E+11	0.00	0.00	[182]
1314	$C_{10}H_7L + OH$	=	$C_{10}H_6 + H_2O$	1.0000E+10	0.00	0.00	[182]
1315	$C_{10}H_7M$	=	$C_{10}H_6 + H$	1.0000E+13	0.00	141.00	[182]
1316	$C_{10}H_7M$	=	$C_{10}H_7$	1.6600E+11	0.00	68.42	[182]
1317	$C_{10}H_8 + H$	=	$C_{10}H_9$	4.0000E+10	0.00	18.04	[182]
1318	$C_{10}H_8 + H$	=	$C_{10}H_9T$	4.0000E+10	0.00	18.04	[182]
1319	$C_{10}H_8 + O$	=	$C_{10}H_7 + OH$	2.1000E+10	0.00	61.52	est. (958)
1320	$C_{10}H_8 + O$	=	$C_{10}H_7O + H$	2.5000E+10	0.00	19.54	est. (959)
1321	$C_{10}H_8 + OH$	=	$C_{10}H_7 + H_2O$	1.7000E+05	1.42	6.07	est. (960)
1322	$C_{10}H_8 + OH$	=	$C_{10}H_7OH + H$	1.0300E+10	0.00	44.31	est. (961)
1323	$C_{10}H_8 + O_2$	=	$C_{10}H_7 + HO_2$	5.0400E+10	0.00	251.04	est. (962)
1324	$C_{10}H_8 + HO_2$	=	$C_{10}H_7 + H_2O_2$	1.2160E+08	0.00	71.70	est. (963)
1325	$C_{10}H_8 + C_2H_3$	=	$1C_{12}H_{10} + H$	7.9400E+08	0.00	26.70	est. (966)
1326	$C_{10}H_8G + H$	=	$C_{10}H_9T$	2.0000E+11	0.00	0.00	[169]
1327	$C_{10}H_8J + H$	=	$C_{10}H_9T$	2.0000E+11	0.00	0.00	[169]
1328	$C_{10}H_8K$	=	$C_{10}H_8$	8.5100E+12	0.00	263.01	[182]
1329	$C_{10}H_8L + H$	=	$C_{10}H_7L + H_2$	1.0000E+10	0.00	24.00	[182]
1330	$C_{10}H_8L + OH$	=	$C_{10}H_7L + H_2O$	1.0000E+10	0.00	0.00	[182]
1331	$C_9H_6CH_2$	=	$C_{10}H_8$	8.0000E+13	0.00	305.60	[157]
1332	$C_9H_6CH_2 + H$	=	$C_{10}H_8 + H$	2.0000E+11	0.00	20.90	[157]
1333	$C_{10}H_9$	=	$C_{10}H_9A$	3.0000E+14	0.00	209.20	[182]
1334	$C_{10}H_9 + O_2$	=	$C_6H_5 + C_4H_4O + O$	1.6000E+09	0.00	31.25	[182]
1335	$C_{10}H_9A$	=	$C_{10}H_8L + H$	1.0000E+13	0.00	146.00	[182]
1336	$C_{10}H_9B$	=	$C_{10}H_8L + H$	1.0000E+13	0.00	166.00	[182]
1337	$C_{10}H_9B$	=	$C_{10}H_9L$	1.0000E+13	0.00	36.00	[169]
1338	$C_{10}H_9D$	=	$C_{10}H_8L + H$	1.0000E+13	0.00	70.00	[182]
1339	$C_{10}H_9D$	=	$C_{10}H_9$	1.0000E+10	0.00	0.00	[182]
1340	$C_{10}H_9E$	=	$C_{10}H_8L + H$	1.0000E+13	0.00	90.00	[182]
1341	$C_{10}H_9E$	=	$C_{10}H_9T$	1.0000E+10	0.00	0.00	[182]
1342	$C_{10}H_9F$	=	$C_{10}H_8 + H$	3.0000E+13	0.00	197.00	[182]
1343	$C_{10}H_9K$	=	$C_{10}H_8K + H$	1.0000E+13	0.00	210.40	[182]
1344	$C_{10}H_9L$	=	$C_{10}H_9M$	1.0000E+10	0.00	0.00	[182]
1345	$C_{10}H_9M$	=	$C_{10}H_9T$	1.0000E+10	0.00	0.00	[182]
1346	$C_{10}H_9P$	=	$C_{10}H_8L + H$	1.0000E+13	0.00	135.00	[182]
1347	$C_{10}H_9P$	=	$C_{10}H_9T$	1.0000E+10	0.00	0.00	[182]
1348	$C_{10}H_9T + O_2$	=	$C_6H_5 + C_4H_4O + O$	1.6000E+09	0.00	31.25	[182]
1349	$C_9H_6CH_3$	=	$C_9H_6CH_2 + H$	5.0000E+14	0.00	213.50	[157]
1350	$C_{10}H_{10}$	=	$C_{10}H_9D + H$	1.0000E+13	0.00	459.00	[182]
1351	$C_{10}H_{10} + H$	=	$C_{10}H_9D + H_2$	1.0000E+10	0.00	24.00	[182]
1352	$C_{10}H_{10} + O$	=	$C_{10}H_9D + OH$	1.0000E+10	0.00	31.00	[182]
1353	$C_{10}H_{10} + OH$	=	$C_{10}H_9D + H_2O$	1.0000E+10	0.00	0.00	[182]

Table A.1, continued

No	*Reaction*			A	n	E_a	*Ref*
1354	$C_{10}H_{10}F$	=	$C_{10}H_9E + H$	1.0000E+13	0.00	459.00	[182]
1355	$C_{10}H_{10}F + H$	=	$C_{10}H_9E + H_2$	1.0000E+10	0.00	23.00	[182]
1356	$C_{10}H_{10}F + O$	=	$C_{10}H_9E + OH$	1.0000E+10	0.00	31.00	[182]
1357	$C_{10}H_{10}F + OH$	=	$C_{10}H_9E + H_2O$	1.0000E+10	0.00	0.00	[182]
1358	$C_{10}H_{10}K$	=	$C_{10}H_9K + H$	1.0000E+13	0.00	266.00	[182]
1359	$C_{10}H_{10}K + H$	=	$C_{10}H_9K + H_2$	1.0000E+11	0.00	0.00	[182]
1360	$C_{10}H_{10}K + O$	=	$C_{10}H_9K + OH$	1.0000E+11	0.00	0.00	[182]
1361	$C_{10}H_{10}K + OH$	=	$C_{10}H_9K + H_2O$	1.0000E+11	0.00	0.00	[182]
1362	$C_9H_7CH_3$	=	$C_9H_6CH_3 + H$	5.0000E+15	0.00	314.00	[157]
1363	$C_{10}H_6O_2$	=	$C_9H_6O + CO$	2.9600E+11	0.00	247.00	est. (995)
1364	$C_{10}H_6O_2 + H$	=	$C_9H_7O + CO$	2.5000E+10	0.00	19.68	est. (996)
1365	$C_{10}H_7O$	=	$C_9H_7 + CO$	1.8000E+11	0.00	183.68	est. (1001)
1366	$C_{10}H_7O + H$	=	$C_{10}H_7OH$	2.0000E+11	0.00	0.00	est. (1002)
1367	$C_{10}H_7O + O$	=	$C_{10}H_6O_2 + H$	3.0000E+10	0.00	0.00	est. (1003)
1368	$C_{10}H_7OO$	=	$C_9H_7 + CO_2$	2.2720E+08	0.00	0.00	est. (1006)
1369	$C_{10}H_7OO$	=	$C_{10}H_6O_2 + H$	2.2720E+08	0.00	0.00	est. (1007)
1370	$C_{10}H_7OO$	=	$C_{10}H_7O + O$	3.5300E+15	-0.70	138.28	est. (1008)
1371	$C_{10}H_7OH$	=	$C_9H_8 + CO$	4.0350E+11	0.00	254.00	est. (1011)
1372	$C_{10}H_7OH + H$	=	$C_{10}H_7O + H_2$	9.0000E+10	0.00	51.88	est. (1012)
1373	$C_{10}H_7OH + O$	=	$C_{10}H_7O + OH$	2.2300E+10	0.00	30.76	est. (1013)
1374	$C_{10}H_7OH + OH$	=	$C_{10}H_7O + H_2O$	4.8000E+09	0.00	0.00	est. (1014)
1375	$C_{10}H_7OH + O_2$	=	$C_{10}H_7O + HO_2$	8.0000E+09	0.00	159.00	est.
1376	$C_{10}H_7OH + HO_2$	=	$C_{10}H_7O + H_2O_2$	2.4490E+10	0.00	62.80	est. (1015)
1377	$C_{10}H_7OH + C_5H_5$	=	$C_5H_6 + C_{10}H_7O$	2.6700E+11	0.00	105.62	est. (1016)
1378	$C_{11}H_9 + O$	=	$C_{11}H_8O + H$	2.8000E+10	0.00	0.00	est. (1052)
1379	$C_{11}H_9 + O$	=	$C_{10}H_8 + CHO$	2.8000E+10	0.00	0.00	est. (1053)
1380	$C_{11}H_9 + OH$	=	$C_{11}H_9O + H$	3.2100E+10	-0.23	58.28	est. (66)
1381	$C_{11}H_9 + O_2$	=	$C_{11}H_8O + OH$	4.1827E+04	0.20	0.00	est. (1054)
1382	$C_{11}H_9 + O_2$	=	$C_{11}H_9OO$ k_∞ =	1.0830E+06	1.10	0.00	est. (1055)
			k_0 =	3.7170E+19	-3.30	0.00	
1383	$C_{11}H_9 + O_2$	=	$C_{11}H_9O + O$	6.6000E+10	0.00	131.36	est. (76)
1384	$C_{11}H_9 + HO_2$	=	$C_{11}H_9O + OH$	4.0000E+09	0.00	0.00	est. (1057)
1385	$C_{11}H_9 + CH_3$	=	$C_{12}H_{11} + H$	2.4500E+08	0.10	44.36	est. (1060)
1386	$C_{11}H_9 + CH_3$	=	$C_{12}H_{12}$	1.2200E+10	0.00	0.00	est. (1061)
1387	$C_{11}H_9P$	=	$C_8H_5 + C_3H_4(P)$	2.0000E+14	0.00	408.00	est. (1071)
1388	$C_{11}H_9P$	=	$C_3H_3 + C_8H_6$	1.0000E+14	0.00	298.17	est.
1389	$C_{11}H_9P + H$	=	$C_{11}H_{10}$	7.8300E+10	0.00	0.00	est. (926)
1390	$C_{11}H_9P + H_2$	=	$C_{11}H_{10} + H$	4.4400E+01	2.43	26.29	est. (1305)
1391	$C_{11}H_9P + O_2$	=	$OC_{11}H_9 + O$	1.9575E+10	0.00	25.61	est. (930)
1392	$C_{11}H_9P + O_2$	=	$OOC_{11}H_9P$	2.5000E+09	-0.15	0.67	est. (931)
1393	$C_{11}H_{10}$	=	$C_{10}H_7 + CH_3$	7.1280E+12	0.00	303.76	est. (1076)
1394	$C_{11}H_{10}$	=	$C_{11}H_9 + H$	4.4800E+15	0.00	381.30	est. (1077)
1395	$C_{11}H_{10} + H$	=	$C_{10}H_8 + CH_3$	9.6000E+09	0.00	21.43	est. (1078)
1396	$C_{11}H_{10} + H$	=	$C_{11}H_9 + H_2$	3.1840E-01	3.44	13.05	est. (1079)
1397	$C_{11}H_{10} + O$	=	$C_{11}H_9 + OH$	5.0400E+08	0.00	0.00	est. (1081)
1398	$C_{11}H_{10} + O$	=	$C_{11}H_9P + OH$	2.0000E+10	0.00	61.52	est. (1085)
1399	$C_{11}H_{10} + O$	=	$C_{11}H_9O + H$	1.2420E+10	0.00	16.63	est. (1082)
1400	$C_{11}H_{10} + O$	=	$OC_{11}H_9 + H$	2.4000E+10	0.00	16.63	est. (1083)
1401	$C_{11}H_{10} + OH$	=	$C_{11}H_9 + H_2O$	4.1520E+06	1.00	3.66	est. (1086)
1402	$C_{11}H_{10} + OH$	=	$C_{11}H_9P + H_2O$	1.7000E+05	1.42	6.07	est. (1090)
1403	$C_{11}H_{10} + OH$	=	$C_{11}H_9O + H_2$	1.7760E+09	0.00	35.00	est. (1087)
1404	$C_{11}H_{10} + OH$	=	$HOC_{11}H_9 + H$	1.8320E+09	0.00	-1.50	est. (1088)
1405	$C_{11}H_{10} + OH$	=	$C_{11}H_{10}O + H$	5.2820E+09	0.00	44.31	est. (1089)
1406	$C_{11}H_{10} + O_2$	=	$C_{11}H_9 + HO_2$	1.2670E+09	0.00	166.28	est. (1091)
1407	$C_{11}H_{10} + O_2$	=	$C_{11}H_9P + HO_2$	5.0400E+10	0.00	251.04	est. (1323)
1408	$C_{11}H_{10} + HO_2$	=	$C_{11}H_9 + H_2O_2$	3.1800E+08	0.00	58.86	est. (1092)
1409	$C_{11}H_{10} + HO_2$	=	$C_{11}H_9P + H_2O_2$	4.3840E+09	0.00	120.55	est. (1093)
1410	$C_{11}H_{10} + CH_3$	=	$C_{11}H_9 + CH_4$	2.5280E+09	0.00	46.44	est. (1094)
1410 b	$C_{11}H_{10} + CH_3$	=	$C_{11}H_9P + CH_4$	3.1600E+09	0.00	66.94	est. (1095)
1411	$C_{11}H_{10} + C_{10}H_7$	=	$C_{11}H_9 + C_{10}H_8$	1.6800E+09	0.00	18.42	est. (1098)
1412	$C_{11}H_{10} + O$	=	$AC_{11}H_{10}O$	2.1700E+08	0.00	16.62	est. (1084)
1413	$C_{11}H_7O$	=	$C_{10}H_7 + CO$	3.1840E+14	0.00	123.06	est. (1099)
1414	$C_{11}H_7O + H$	=	$C_{10}H_8 + CO$	2.4000E+10	0.00	0.00	est. (1100)

Table A.1, continued

No	*Reaction*			A	n	E_a	*Ref*
1415	$C_{11}H_8O$	=	$C_{11}H_7O + H$	3.1840E+15	0.00	350.20	est. (1101)
1416	$C_{11}H_8O + H$	=	$C_{10}H_8 + CHO$	5.0000E+04	1.62	9.06	est. (1102)
1417	$C_{11}H_8O + H$	=	$C_{11}H_7O + H_2$	4.0000E+10	0.00	20.63	est. (1103)
1418	$C_{11}H_8O + O$	=	$C_{10}H_8 + CO_2$	1.6000E+10	0.00	0.00	est. (1104)
1419	$C_{11}H_8O + O$	=	$C_{11}H_7O + OH$	7.2320E+09	0.00	12.89	est. (1105)
1420	$C_{11}H_8O + OH$	=	$C_{11}H_7O + H_2O$	1.3680E+06	1.18	-1.87	est. (1106)
1421	$C_{11}H_8O + O_2$	=	$C_{11}H_7O + HO_2$	8.1600E+09	0.00	163.05	est. (1107)
1422	$C_{11}H_8O + HO_2$	=	$C_{11}H_7O + H_2O_2$	1.6000E+09	0.00	48.81	est. (1108)
1423	$C_{11}H_8O + CH_3$	=	$C_{11}H_7O + CH_4$	2.2160E+00	2.81	24.17	est. (1109)
1424	$C_{11}H_8O + C_{10}H_7$	=	$C_{11}H_7O + C_{10}H_8$	5.6080E+08	0.00	18.42	est. (1110)
1425	$C_{11}H_9O$	=	$C_{10}H_8 + CHO$	4.0000E+12	0.00	79.00	est. (1111)
1426	$C_{11}H_9O$	=	$C_{10}H_7 + CH_2O$	2.0000E+13	0.00	135.39	est. (1112)
1427	$C_{11}H_9O$	=	$C_{11}H_8O + H$	2.4000E+12	0.00	68.00	est. (1113)
1428	$C_{11}H_9O + M$	=	$C_{11}H_8O + H + M$	2.0000E+08	0.00	0.00	est. (1114)
1429	$C_{11}H_9O + H$	=	$C_{11}H_8O + H_2$	2.4000E+10	0.00	0.00	est. (1115)
1430	$C_{11}H_9O + H$	=	$C_{11}H_{10}O$	2.0240E+11	0.00	0.00	est. (1116)
1431	$C_{11}H_9O + O$	=	$C_{11}H_8O + OH$	3.3600E+10	0.00	0.00	est. (1117)
1432	$C_{11}H_9O + OH$	=	$C_{11}H_8O + H_2O$	1.9200E+10	0.00	0.00	est. (1118)
1433	$C_{11}H_9O + O_2$	=	$C_{11}H_8O + HO_2$	8.0000E+09	0.00	21.00	est. (1119)
1434	$OC_{11}H_9$	=	$C_9H_6CH_3 + CO$	3.3750E+11	0.00	183.74	est. (1001)
1435	$OC_{11}H_9 + H$	=	$HOC_{11}H_9$	2.0000E+11	0.00	0.00	est. (1121)
1436	$OC_{11}H_9 + H_2O$	=	$HOC_{11}H_9 + OH$	5.5040E+09	0.36	136.25	est. (1122)
1437	$AC_{11}H_9O$	=	$C_{11}H_8O + H$	2.5280E+12	0.00	87.86	est. (1123)
1438	$HOC_{11}H_9 + H$	=	$C_{10}H_7OH + CH_3$	9.6000E+09	0.00	21.55	est. (1129)
1439	$HOC_{11}H_9 + H$	=	$OC_{11}H_9 + H_2$	9.2000E+10	0.00	51.91	est. (1130)
1440	$C_{11}H_9OO$	=	$C_{11}H_8O + OH$	8.0000E+09	0.00	121.00	est. (1137)
1441	$C_{11}H_{10}O + H$	=	$C_{10}H_8 + CH_2OH$	9.6000E+09	0.00	21.55	est. (1124)
1442	$C_{11}H_{10}O + H$	=	$C_{11}H_9O + H_2$	5.6000E+10	0.00	34.00	est. (1125)
1443	$C_{11}H_{10}O + OH$	=	$C_{11}H_9O + H_2O$	4.0000E+09	0.00	0.00	est. (1126)
1444	$C_{11}H_{10}O + O_2$	=	$C_{11}H_8O + HO_2 + H$	1.4000E+10	0.00	173.30	est. (1127)
1445	$AC_{11}H_{10}O$	=	$C_{10}H_7O + CH_3$	1.6000E+15	0.00	266.10	est. (1132)
1446	$AC_{11}H_{10}O + H$	=	$C_{10}H_7OH + CH_3$	5.6640E+09	0.00	22.55	est. (1133)
1447	$AC_{11}H_{10}O + O$	=	$AC_{11}H_9O + OH$	1.3360E+10	0.00	12.30	est. (1134)
1448	$AC_{11}H_{10}O + OH$	=	$AC_{11}H_9O + H_2O$	9.6000E+08	0.00	-2.10	est. (1135)
1449	$AC_{11}H_{10}O + CH_3$	=	$AC_{11}H_9O + CH_4$	4.0080E+08	0.00	43.92	est. (1136)
1450	$OOC_{11}H_9P$	=	$OC_{11}H_9 + O$	2.9800E+15	-7.00	138.28	est. (1008)
1451	$OOC_{11}H_9P$	=	$C_9H_6CH_3 + CO_2$	1.2048E+08	0.00	0.00	est. (1139)
1452	$1C_{12}H_{10} + O$	=	$C_{10}H_7 + CH_3CO$	2.0080E+03	1.88	0.76	est. (1192)
1453	$1C_{12}H_{10} + O$	=	$C_{11}H_9 + CHO$	3.3750E+03	1.88	0.76	est. (1194)
1454	$1C_{12}H_{10} + OH$	=	$C_{11}H_9 + CH_2O$	3.3750E+03	1.88	0.76	est. (1195)
1455	$C_{12}H_{11}$	=	$1C_{12}H_{10} + H$	2.5380E+13	0.00	212.00	est. (1199)
1456	$C_{12}H_{12}$	=	$C_{12}H_{11} + H$	1.2255E+15	0.00	330.00	est. (1207)
1457	$C_{12}H_{12} + H$	=	$C_{10}H_8 + C_2H_5$	6.0000E+09	0.00	21.34	est. (1208)
1458	$C_{12}H_{12} + H$	=	$C_{12}H_{11} + H_2$	6.3000E-02	3.44	13.05	est. (1209)
1459	$C_{12}H_{12} + O$	=	$C_{12}H_{11} + OH$	1.1000E+09	0.00	15.90	est. (1210)
1460	$C_{12}H_{12} + OH$	=	$C_{12}H_{11} + H_2O$	2.5000E+08	0.00	0.00	est. (1211)
1461	$C_{12}H_{12} + HO_2$	=	$C_{12}H_{11} + H_2O_2$	1.3250E+09	0.00	47.22	est. (1212)
1462	$C_{10}H_7 + C_2H_2$	=	$AC_{12}H_8 + H$	3.5700E+21	-3.17	62.20	[215]
1463	$C_9H_7 + C_3H_3$	=	$AC_{12}H_8 + H_2$	1.5000E+10	0.00	26.00	est.
1464	$AC_{14}H_{10}$	=	$PC_{14}H_{10}$	7.4900E+11	0.00	27.19	[215]
1465	$C_8H_6 + C_6H_5$	=	$PC_{14}H_{10} + H$	2.0000E+11	0.00	40.00	est.
1466	$C_8H_6 + C_6H_5CH$	=	$AC_{14}H_{10} + {}^3CH_2$	2.0000E+10	0.00	80.00	est.
1467	$C_6H_5CH + C_6H_5CH$	=	$AC_{14}H_{10} + H_2$	1.0000E+11	0.00	0.00	est.

Table A.2: n – propylbenzene Detailed Kinetic Sub – Mechanism

No	*Reaction*			A	n	E_a	*Ref*
1468	$C_9H_{12} + H$	=	$1C_9H_{11} + H_2$	1.0100E+01	2.90	12.30	[60]
1469	$C_9H_{12} + H$	=	$2C_9H_{11} + H_2$	1.0100E+01	2.90	12.30	[60]
1470	$C_9H_{12} + H$	=	$3C_9H_{11} + H_2$	1.3000E+03	2.50	28.30	[60]
1471	$C_9H_{12} + O$	=	$1C_9H_{11} + OH$	2.6000E+10	0.00	18.70	est. (437)
1472	$C_9H_{12} + O$	=	$2C_9H_{11} + OH$	2.6000E+10	0.00	18.70	est. (437)
1473	$C_9H_{12} + O$	=	$3C_9H_{11} + OH$	3.0000E+10	0.00	24.10	est. (438)
1474	$C_9H_{12} + OH$	=	$1C_9H_{11} + H_2O$	4.7865E+05	1.40	3.56	est. (439)
1475	$C_9H_{12} + OH$	=	$2C_9H_{11} + H_2O$	4.7865E+05	1.40	3.56	est. (439)
1476	$C_9H_{12} + OH$	=	$3C_9H_{11} + H_2O$	5.7500E+05	1.40	3.56	est. (440)
1477	$C_9H_{12} + CH_3$	=	$1C_9H_{11} + CH_4$	1.2000E+09	0.00	42.40	[60]
1478	$C_9H_{12} + CH_3$	=	$2C_9H_{11} + CH_4$	1.2000E+09	0.00	42.40	[60]
1479	$C_9H_{12} + CH_3$	=	$3C_9H_{11} + CH_4$	1.0000E+10	0.00	49.00	[60]
1480	$C_9H_{12} + O_2$	=	$1C_9H_{11} + HO_2$	2.7700E+10	0.00	199.54	est. (441)
1481	$C_9H_{12} + O_2$	=	$2C_9H_{11} + HO_2$	2.7700E+10	0.00	199.54	est. (441)
1482	$C_9H_{12} + O_2$	=	$3C_9H_{11} + HO_2$	2.7700E+10	0.00	212.84	est. (442)
1483	$C_9H_{12} + HO_2$	=	$1C_9H_{11} + H_2O_2$	4.8200E+00	2.60	58.2	adj. [246]
1484	$C_9H_{12} + HO_2$	=	$2C_9H_{11} + H_2O_2$	4.8200E+00	2.60	58.2	adj. [246]
1485	$C_9H_{12} + HO_2$	=	$3C_9H_{11} + H_2O_2$	2.3800E+01	2.55	69.0	adj. [246]
1486	$C_9H_{12} + H$	=	$C_3H_7(N) + C_6H_6$	2.4000E+10	0.00	21.44	[60]
1487	C_9H_{12}	=	$C_6H_5 + C_3H_7(N)$	5.0000E+16	0.00	424.15	[60]
1488	C_9H_{12}	=	$C_7H_7 + C_2H_5$	5.0000E+16	0.00	326.75	[60]
1489	C_9H_{12}	=	$C_8H_9 + CH_3$	5.0000E+16	0.00	320.65	[60]
1490	$C_9H_{12} + C_2H_5$	=	$1C_9H_{11} + C_2H_6$	5.0100E+07	0.00	43.54	[60]
1491	$C_9H_{12} + C_2H_5$	=	$2C_9H_{11} + C_2H_6$	5.0100E+07	0.00	43.54	[60]
1492	$C_9H_{12} + C_2H_5$	=	$3C_9H_{11} + C_2H_6$	3.1600E+08	0.00	51.44	[60]
1493	$C_9H_{12} + C_2H_3$	=	$1C_9H_{11} + C_2H_4$	1.0000E+00	3.10	36.94	[60]
1494	$C_9H_{12} + C_2H_3$	=	$2C_9H_{11} + C_2H_4$	1.0000E+00	3.10	36.94	[60]
1495	$C_9H_{12} + C_2H_3$	=	$3C_9H_{11} + C_2H_4$	6.0000E-01	3.30	43.96	[60]
1496	$C_9H_{12} + C_3H_5(A)$	=	$1C_9H_{11} + C_3H_6$	7.9400E+08	0.00	67.82	[60]
1497	$C_9H_{12} + C_3H_5(A)$	=	$2C_9H_{11} + C_3H_6$	7.9400E+08	0.00	67.82	[60]
1498	$C_9H_{12} + C_3H_5(A)$	=	$3C_9H_{11} + C_3H_6$	7.9400E+08	0.00	85.84	[60]
1499	$C_9H_{12} + C_5H_5$	=	$1C_9H_{11} + C_5H_6$	7.9400E+08	0.00	67.82	[60]
1500	$C_9H_{12} + C_5H_5$	=	$2C_9H_{11} + C_5H_6$	7.9400E+08	0.00	67.82	[60]
1501	$C_9H_{12} + C_5H_5$	=	$3C_9H_{11} + C_5H_6$	7.9400E+08	0.00	85.84	[60]
1502	$C_9H_{12} + C_6H_5$	=	$1C_9H_{11} + C_6H_6$	7.9400E+08	0.00	67.82	[60]
1503	$C_9H_{12} + C_6H_5$	=	$2C_9H_{11} + C_6H_6$	7.9400E+08	0.00	67.82	[60]
1504	$C_9H_{12} + C_6H_5$	=	$3C_9H_{11} + C_6H_6$	7.9400E+08	0.00	85.84	[60]
1505	$C_9H_{12} + C_7H_7$	=	$1C_9H_{11} + C_7H_8$	7.9400E+08	0.00	67.82	[60]
1506	$C_9H_{12} + C_7H_7$	=	$2C_9H_{11} + C_7H_8$	7.9400E+08	0.00	67.82	[60]
1507	$C_9H_{12} + C_7H_7$	=	$3C_9H_{11} + C_7H_8$	7.9400E+08	0.00	85.84	[60]
1508	$1C_9H_{11}$	=	$1C_9H_{10} + H$	6.3000E+13	0.00	154.39	adj. [162]
1509	$1C_9H_{11}$	=	$C_7H_7 + C_2H_4$	2.0000E+13	0.00	149.10	est. [73]
1510	$2C_9H_{11} + H$	=	C_9H_{12}	2.0000E+10	0.00	0.00	est. (420)
1511	$2C_9H_{11}$	=	$C_8H_8 + CH_3$	2.0000E+10	0.00	123.43	adj. [162]
1512	$2C_9H_{11}$	=	$1C_9H_{10} + H$	3.1500E+13	0.00	154.39	adj. [162]
1513	$2C_9H_{11}$	=	$C_6H_6 + C_3H_5(S)$	4.0000E+13	0.00	197.75	est. [73]
1514	$2C_9H_{11}$	=	$2C_9H_{10} + H$	3.1500E+13	0.00	154.39	adj. [162]
1515	$2C_9H_{11}$	=	$C_6H_6 + C_3H_5(A)$	0.0000E+00	0.00	0.00	ommited
1516	$3C_9H_{11}$	=	$C_8H_8 + CH_3$	2.0000E+13	0.00	153.10	est. [73]
1517	$1C_9H_{10} + H$	=	$C_6H_5 + C_3H_6$	1.0000E+11	0.00	44.57	[251]
1518	$1C_9H_{10} + H$	=	$C_8H_8 + CH_3$	3.9800E+10	0.00	9.97	[251]
1519	$1C_9H_{10} + H$	=	$C_6H_6 + C_3H_5(S)$	1.5848E+11	0.00	52.35	[251]
1520	$1C_9H_{10} + H$	=	$C_9H_9(T) + H_2$	1.5848E+11	0.00	46.53	[251]
1521	$1C_9H_{10} + O$	=	$C_7H_6O + C_2H_4$	5.2300E+04	1.57	-2.63	est. (397)
1522	$1C_9H_{10} + O_2$	=	$C_9H_9(T) + HO_2$	2.0000E+10	0.00	184.10	est. (406)
1523	$2C_9H_{10} + H$	=	$C_6H_5 + C_3H_6$	1.0000E+11	0.00	44.57	est. (1517)
1524	$2C_9H_{10} + H$	=	$C_7H_7 + C_2H_4$	3.9800E+10	0.00	9.97	est. (1518)
1525	$2C_9H_{10} + H$	=	$C_6H_6 + C_3H_5(S)$	1.5848E+11	0.00	52.35	est. (1519)
1526	$2C_9H_{10} + H$	=	$3C_9H_{11}$	7.2300E+09	0.00	12.14	adj. [162]
1527	$2C_9H_{10} + O$	=	$C_8H_8 + CH_2O$	5.2300E+04	1.57	-2.63	est. (397)

Table A.3: n – butylbenzene Detailed Kinetic Sub – Mechanism

No	*Reaction*			A	n	E_a	*Ref*
1528	$C_{10}H_{14}$	=	$1C_{10}H_{13} + H$	1.0400E+16	0.00	410.02	est. (738)
1529	$C_{10}H_{14}$	=	$2C_{10}H_{13} + H$	6.6000E+15	0.00	397.46	est. (739)
1530	$C_{10}H_{14}$	=	$3C_{10}H_{13} + H$	6.6000E+15	0.00	397.46	est. (739)
1531	$C_{10}H_{14}$	=	$4C_{10}H_{13} + H$	1.0400E+16	0.00	410.02	est. (738)
1532	$C_{10}H_{14}$	=	$3C_9H_{11} + CH_3$	6.6000E+16	0.00	354.37	est. (737)
1533	$C_{10}H_{14}$	=	$C_8H_9(B) + C_2H_5$	1.3200E+16	0.00	340.00	est. (736)
1534	$C_{10}H_{14}$	=	$C_7H_7 + C_3H_7(N)$	1.0000E+15	0.00	327.00	est.
1535	$C_{10}H_{14} + H$	=	$1C_{10}H_{13} + H_2$	3.7092E+04	2.00	32.21	est. (740)
1536	$C_{10}H_{14} + H$	=	$2C_{10}H_{13} + H_2$	1.3200E+11	0.00	34.90	est. (741)
1537	$C_{10}H_{14} + H$	=	$3C_{10}H_{13} + H_2$	1.3200E+11	0.00	34.90	est. (741)
1538	$C_{10}H_{14} + H$	=	$4C_{10}H_{13} + H_2$	3.7092E+04	2.00	32.21	est. (738)
1539	$C_{10}H_{14} + OH$	=	$1C_{10}H_{13} + H_2O$	2.7258E+04	1.73	3.15	est. (744)
1540	$C_{10}H_{14} + OH$	=	$2C_{10}H_{13} + H_2O$	1.6962E+06	1.25	2.92	est. (745)
1541	$C_{10}H_{14} + OH$	=	$3C_{10}H_{13} + H_2O$	1.6962E+06	1.25	2.92	est. (745)
1542	$C_{10}H_{14} + OH$	=	$4C_{10}H_{13} + H_2O$	2.7258E+04	1.73	3.15	est. (744)
1543	$C_{10}H_{14} + O$	=	$1C_{10}H_{13} + OH$	1.9800E+10	0.00	24.00	est. (742)
1544	$C_{10}H_{14} + O$	=	$2C_{10}H_{13} + OH$	3.4320E+10	0.00	18.60	est. (743)
1545	$C_{10}H_{14} + O$	=	$3C_{10}H_{13} + OH$	3.4320E+10	0.00	18.60	est. (743)
1546	$C_{10}H_{14} + O$	=	$4C_{10}H_{13} + OH$	1.9800E+10	0.00	24.00	est. (742)
1547	$C_{10}H_{14} + HO_2$	=	$1C_{10}H_{13} + H_2O_2$	7.3920E+09	0.00	81.16	est. (748)
1548	$C_{10}H_{14} + HO_2$	=	$2C_{10}H_{13} + H_2O_2$	3.3000E+08	0.00	43.92	est. (749)
1549	$C_{10}H_{14} + HO_2$	=	$3C_{10}H_{13} + H_2O_2$	3.3000E+08	0.00	43.92	est. (749)
1550	$C_{10}H_{14} + HO_2$	=	$4C_{10}H_{13} + H_2O_2$	7.3920E+09	0.00	81.16	est. (748)
1551	$C_{10}H_{14} + O_2$	=	$1C_{10}H_{13} + HO_2$	1.6566E+10	0.00	205.00	est. (746)
1552	$C_{10}H_{14} + O_2$	=	$2C_{10}H_{13} + HO_2$	2.6268E+10	0.00	199.00	est. (747)
1553	$C_{10}H_{14} + O_2$	=	$3C_{10}H_{13} + HO_2$	2.6268E+10	0.00	199.00	est. (747)
1554	$C_{10}H_{14} + O_2$	=	$4C_{10}H_{13} + HO_2$	1.6566E+10	0.00	205.00	est. (746)
1555	$C_{10}H_{14} + CH_3$	=	$1C_{10}H_{13} + CH_4$	1.7160E+09	0.00	48.00	adj. [153]
1556	$C_{10}H_{14} + CH_3$	=	$2C_{10}H_{13} + CH_4$	2.6400E+08	0.00	40.00	adj. [153]
1557	$C_{10}H_{14} + CH_3$	=	$3C_{10}H_{13} + CH_4$	2.6400E+08	0.00	40.00	adj. [153]
1558	$C_{10}H_{14} + CH_3$	=	$4C_{10}H_{13} + CH_4$	1.7160E+09	0.00	48.00	adj. [153]
1559	$1C_9H_{10} + CH_3$	=	$2C_{10}H_{13}$	1.6600E+08	0.00	30.98	[97]
1560	$C_8H_9(B) + C_2H_4$	=	$4C_{10}H_{13}$	2.4100E+46	-11.67	120.57	[97]
1561	$C_8H_8 + H$	=	$C_8H_9(B)^{e,6}$ k_∞ =	2.6220E+06	1.28	5.40	est. (188)
			k_0 =	2.3574E+12	0.00	3.16	
1562	$C_8H_8 + C_2H_5$	=	$1C_{10}H_{13}$	6.0000E+07	0.00	18.84	[97]
1563	$C_7H_7 + C_3H_6$	=	$3C_{10}H_{13}$	6.0000E+07	0.00	31.99	[97]

Table A.4: n – decane and do – decane Detailed Kinetic Sub Mechanism

No	*Reaction*			A	n	E_a	*Ref*
1564	$C_{10}H_{22}$	=	$C_9H_{18} + CH_4$	3.5000E+17	0.00	339.00	est.
1565	$C_{10}H_{22}$	=	$1C_7H_{15} + C_3H_7(N)$	2.1900E+14	0.00	283.90	[167]
1566	$C_{10}H_{22}$	=	$1C_5H_{11} + 1C_5H_{11}$	2.1900E+14	0.00	283.90	[167]
1567	$C_{10}H_{22}$	=	$1C_6H_{13} + C_4H_9(N)$	7.8500E+14	0.00	283.90	[167]
1568	$C_{10}H_{22}$	=	$1C_{10}H_{21} + H$	8.0000E+14	0.00	424.00	[167]
1569	$C_{10}H_{22}$	=	$2C_{10}H_{21} + H$	8.0000E+14	0.00	424.00	[167]
1570	$C_{10}H_{22}$	=	$3C_{10}H_{21} + H$	8.0000E+14	0.00	424.00	[167]
1571	$C_{10}H_{22}$	=	$4C_{10}H_{21} + H$	8.0000E+14	0.00	424.00	[167]
1572	$C_{10}H_{22}$	=	$5C_{10}H_{21} + H$	8.0000E+14	0.00	424.00	[167]
1573	$C_{10}H_{22} + H$	=	$1C_{10}H_{21} + H_2$	4.7000E+04	2.00	32.20	[167]
1574	$C_{10}H_{22} + H$	=	$2C_{10}H_{21} + H_2$	1.5000E+04	2.00	20.92	[167]
1575	$C_{10}H_{22} + H$	=	$3C_{10}H_{21} + H_2$	1.5000E+04	2.00	20.92	[167]
1576	$C_{10}H_{22} + H$	=	$4C_{10}H_{21} + H_2$	1.5000E+04	2.00	20.92	[167]
1577	$C_{10}H_{22} + H$	=	$5C_{10}H_{21} + H_2$	1.5000E+04	2.00	20.92	[167]
1578	$C_{10}H_{22} + OH$	=	$1C_{10}H_{21} + H_2O$	4.4000E+06	0.97	6.65	[167]
1579	$C_{10}H_{22} + OH$	=	$2C_{10}H_{21} + H_2O$	1.9600E+04	1.61	0.00	[167]
1580	$C_{10}H_{22} + OH$	=	$3C_{10}H_{21} + H_2O$	1.9600E+04	1.61	0.00	[167]
1581	$C_{10}H_{22} + OH$	=	$4C_{10}H_{21} + H_2O$	1.9600E+04	1.61	0.00	[167]
1582	$C_{10}H_{22} + OH$	=	$5C_{10}H_{21} + H_2O$	1.9600E+04	1.61	0.00	[167]
1583	$C_{10}H_{22} + O$	=	$1C_{10}H_{21} + OH$	1.9200E+03	2.40	6.65	[167]
1584	$C_{10}H_{22} + O$	=	$2C_{10}H_{21} + OH$	5.3300E+02	2.50	20.92	[167]
1585	$C_{10}H_{22} + O$	=	$3C_{10}H_{21} + OH$	5.3300E+02	2.50	20.92	[167]
1586	$C_{10}H_{22} + O$	=	$4C_{10}H_{21} + OH$	5.3300E+02	2.50	20.92	[167]
1587	$C_{10}H_{22} + O$	=	$5C_{10}H_{21} + OH$	5.3300E+02	2.50	20.92	[167]
1588	$C_{10}H_{22} + CH_3$	=	$1C_{10}H_{21} + CH_4$	2.5000E+09	0.00	48.53	[167]
1589	$C_{10}H_{22} + CH_3$	=	$2C_{10}H_{21} + CH_4$	1.3300E+09	0.00	39.75	[167]
1590	$C_{10}H_{22} + CH_3$	=	$3C_{10}H_{21} + CH_4$	1.3300E+09	0.00	39.75	[167]
1591	$C_{10}H_{22} + CH_3$	=	$4C_{10}H_{21} + CH_4$	1.3300E+09	0.00	39.75	[167]
1592	$C_{10}H_{22} + CH_3$	=	$5C_{10}H_{21} + CH_4$	1.3300E+09	0.00	39.75	[167]
1593	$C_{10}H_{22} + O_2$	=	$1C_{10}H_{21} + HO_2$	2.0900E+10	0.00	218.12	[167]
1594	$C_{10}H_{22} + O_2$	=	$2C_{10}H_{21} + HO_2$	3.3000E+10	0.00	204.00	[167]
1595	$C_{10}H_{22} + O_2$	=	$3C_{10}H_{21} + HO_2$	3.3000E+10	0.00	204.00	[167]
1596	$C_{10}H_{22} + O_2$	=	$4C_{10}H_{21} + HO_2$	3.3000E+10	0.00	204.00	[167]
1597	$C_{10}H_{22} + O_2$	=	$5C_{10}H_{21} + HO_2$	3.3000E+10	0.00	204.00	[167]
1598	$C_{10}H_{22} + HO_2$	=	$1C_{10}H_{21} + H_2O_2$	1.8700E+09	0.00	81.20	[18]
1599	$C_{10}H_{22} + HO_2$	=	$2C_{10}H_{21} + H_2O_2$	4.2000E+09	0.00	71.20	[18]
1600	$C_{10}H_{22} + HO_2$	=	$3C_{10}H_{21} + H_2O_2$	4.2000E+09	0.00	71.20	[18]
1601	$C_{10}H_{22} + HO_2$	=	$4C_{10}H_{21} + H_2O_2$	4.2000E+09	0.00	71.20	[18]
1602	$C_{10}H_{22} + HO_2$	=	$5C_{10}H_{21} + H_2O_2$	4.2000E+09	0.00	71.20	[18]
1603	$C_{10}H_{21}O_2$	=	$C_9H_{18} + CH_2O + OH$	2.0000E+12	0.00	94.20	[18]
1604	$C_{10}H_{21}O_2$	=	$C_{10}H_{20} + HO_2$	3.0000E+12	0.00	100.00	[18]
1605	$C_{10}H_{21}OO$	=	$C_{10}H_{21}O_2$	3.0000E+12	0.00	100.00	[18]
1606	$1C_{10}H_{21}$	=	$C_8H_{17} + C_2H_4$	3.3000E+13	0.00	121.00	[167]
1607	$2C_{10}H_{21}$	=	$1C_7H_{15} + C_3H_6$	3.3000E+13	0.00	110.00	[167]
1608	$3C_{10}H_{21}$	=	$1C_6H_{13} + C_4H_8(N)$	3.3000E+13	0.00	110.00	[167]
1609	$4C_{10}H_{21}$	=	$1C_5H_{11} + 1C_5H_{10}$	3.3000E+13	0.00	107.00	[167]
1610	$4C_{10}H_{21}$	=	$C_8H_{16} + C_2H_5$	3.3000E+13	0.00	121.00	[167]
1611	$5C_{10}H_{21}$	=	$C_4H_9(N) + 1C_6H_{12}$	3.3000E+13	0.00	108.00	[167]
1612	$5C_{10}H_{21}$	=	$C_3H_7(N) + 1C_7H_{14}$	3.3000E+13	0.00	121.00	[167]
1613	$1C_{10}H_{21}$	=	$4C_{10}H_{21}$	2.0000E+11	0.00	84.00	[167]
1614	$3C_{10}H_{21}$	=	$5C_{10}H_{21}$	2.0000E+11	0.00	84.00	[167]
1615	$1C_{10}H_{21}$	=	$5C_{10}H_{21}$	2.0000E+11	0.00	84.00	[167]
1616	$2C_{10}H_{21}$	=	$5C_{10}H_{21}$	2.0000E+11	0.00	84.00	[167]
1617	$3C_{10}H_{21}$	=	$4C_{10}H_{21}$	2.0000E+11	0.00	84.00	[167]
1618	$2C_{10}H_{21}$	=	$4C_{10}H_{21}$	2.0000E+11	0.00	84.00	[167]
1619	$1C_{10}H_{21}$	=	$C_{10}H_{20} + H$	1.0000E+13	0.00	169.11	est. (1691)
1620	$1C_{10}H_{21} + O_2$	=	$C_{10}H_{20} + HO_2$	5.0000E+08	0.00	14.65	[18]
1621	$2C_{10}H_{21} + O_2$	=	$C_{10}H_{20} + HO_2$	5.0000E+08	0.00	14.65	[18]
1622	$3C_{10}H_{21} + O_2$	=	$C_{10}H_{20} + HO_2$	5.0000E+08	0.00	14.65	[18]
1623	$4C_{10}H_{21} + O_2$	=	$C_{10}H_{20} + HO_2$	5.0000E+08	0.00	14.65	[18]
1624	$5C_{10}H_{21} + O_2$	=	$C_{10}H_{20} + HO_2$	5.0000E+08	0.00	14.65	[18]
1625	$1C_{10}H_{21} + HO_2$	=	$C_9H_{19} + CH_2O + OH$	2.0000E+10	0.00	0.00	est.
1626	$2C_{10}H_{21} + HO_2$	=	$C_8H_{17} + C_2H_4O + OH$	2.0000E+10	0.00	0.00	est.

Table A.4, continued

No	*Reaction*			A	n	E_a	*Ref*
1627	$1C_{10}H_{21} + O_2$	=	$C_{10}H_{21}OO$	4.0000E+08	0.00	0.00	[18]
1628	$2C_{10}H_{21} + O_2$	=	$C_{10}H_{21}OO$	4.0000E+08	0.00	0.00	[18]
1629	$3C_{10}H_{21} + O_2$	=	$C_{10}H_{21}OO$	4.0000E+08	0.00	0.00	[18]
1630	$4C_{10}H_{21} + O_2$	=	$C_{10}H_{21}OO$	4.0000E+08	0.00	0.00	[18]
1631	$5C_{10}H_{21} + O_2$	=	$C_{10}H_{21}OO$	4.0000E+08	0.00	0.00	[18]
1632	$C_{10}H_{20} + O$	=	$C_9H_{18} + CH_2O$	3.6220E+03	1.88	0.76	est. (189)
1633	$C_{10}H_{20} + O$	=	$C_9H_{19} + CHO$	3.6220E+03	1.88	0.76	est. (189)
1634	$C_{10}H_{20} + O$	=	$C_{10}H_{19} + OH$	4.0000E+10	0.00	16.74	est. (1714)
1635	$C_{10}H_{20} + H$	=	$C_{10}H_{19} + H_2$	8.0000E+10	0.00	14.23	est. (1711)
1636	$C_{10}H_{20} + OH$	=	$C_{10}H_{19} + H_2O$	2.0000E+10	0.00	10.88	est. (1717)
1637	$C_{10}H_{20} + CH_3$	=	$C_{10}H_{19} + CH_4$	2.0000E+08	0.00	28.47	est. (1720)
1638	$C_{10}H_{20} + HO_2$	=	$C_{10}H_{19} + H_2O_2$	5.0000E+09	0.00	0.00	est. (1723)
1639	$C_{10}H_{19}$	=	$C_2H_3 + C_8H_{16}$	2.0000E+13	0.00	245.00	est.
1640	C_8H_{17}	=	$1C_7H_{14} + CH_3$	7.9400E+13	0.00	138.07	[265]
1641	C_8H_{17}	=	$1C_5H_{11} + C_3H_6$	1.5800E+13	0.00	118.41	[265]
1642	C_8H_{17}	=	$C_4H_9(N) + C_4H_8(N)$	5.0100E+12	0.00	121.75	[265]
1643	C_8H_{17}	=	$C_8H_{16} + H$	2.0000E+13	0.00	158.99	[182]
1644	C_8H_{17}	=	$1C_5H_{10} + C_3H_7(N)$	5.0100E+12	0.00	121.75	[265]
1645	C_8H_{17}	=	$1C_6H_{13} + C_2H_4$	2.5100E+13	0.00	120.50	[265]
1646	$C_8H_{17} + O_2$	=	$C_8H_{16} + HO_2$	4.0000E+09	0.00	8.37	[182]
1647	C_8H_{16}	=	$1C_5H_{11} + C_3H_5(A)$	2.0000E+15	0.00	297.48	[265]
1648	C_8H_{16}	=	$C_4H_9(N) + C_4H_7(N)$	1.0000E+16	0.00	342.25	[265]
1649	$C_8H_{16} + O$	=	$1C_6H_{13} + C_2H_3O$	1.0000E+08	0.00	0.00	[265]
1650	$C_8H_{16} + O$	=	$1C_7H_{15} + CHO$	1.0000E+08	0.00	0.00	[265]
1651	$C_8H_{16} + OH$	=	$1C_6H_{13} + C_2H_4O$	1.0000E+08	0.00	0.00	[265]
1652	$C_8H_{16} + OH$	=	$1C_7H_{15} + CH_2O$	1.0000E+08	0.00	0.00	[265]
1653	$C_8H_{14} + H$	=	$4C_8H_{13} + H_2$	6.2000E+10	0.00	14.24	est. (1711)
1654	$C_8H_{14} + O$	=	$4C_8H_{13} + OH$	3.1000E+10	0.00	16.75	est. (1714)
1655	$C_8H_{14} + OH$	=	$4C_8H_{13} + H_2O$	1.5000E+10	0.00	10.89	est. (1717)
1656	$C_8H_{14} + CH_3$	=	$4C_8H_{13} + CH_4$	1.5000E+08	0.00	28.48	est. (1720)
1657	$C_8H_{14} + HO_2$	=	$4C_8H_{13} + H_2O_2$	3.8000E+09	0.00	0.00	est. (1723)
1658	$4C_8H_{13}$	=	$C_4H_7(N) + C_4H_6(T)$	2.5200E+16	0.00	297.63	est. (1707)
1659	C_7H_{16}	=	$1C_7H_{15} + H$	1.0000E+15	0.00	418.60	[43]
1660	C_7H_{16}	=	$2C_7H_{15} + H$	1.0000E+15	0.00	418.60	[43]
1661	C_7H_{16}	=	$3C_7H_{15} + H$	1.0000E+15	0.00	418.60	[43]
1662	C_7H_{16}	=	$4C_7H_{15} + H$	1.0000E+15	0.00	418.60	[43]
1663	C_7H_{16}	=	$C_3H_7(N) + C_4H_9(N)$	2.5000E+13	0.00	261.90	[182]
1664	C_7H_{16}	=	$C_2H_5 + 1C_5H_{11}$	1.2500E+13	0.00	261.90	[182]
1665	C_7H_{16}	=	$1C_6H_{13} + CH_3$	4.1750E+12	0.00	261.90	[182]
1666	$C_7H_{16} + H$	=	$1C_7H_{15} + H_2$	5.6200E+04	2.00	32.23	[43]
1667	$C_7H_{16} + H$	=	$2C_7H_{15} + H_2$	1.8200E+04	2.00	20.93	[43]
1668	$C_7H_{16} + H$	=	$3C_7H_{15} + H_2$	1.8200E+04	2.00	20.93	[43]
1669	$C_7H_{16} + H$	=	$4C_7H_{15} + H_2$	9.0000E+03	2.00	20.93	[43]
1670	$C_7H_{16} + O$	=	$1C_7H_{15} + OH$	2.3000E+03	2.40	6.66	[43]
1671	$C_7H_{16} + O$	=	$2C_7H_{15} + OH$	6.4000E+02	2.50	20.93	[43]
1672	$C_7H_{16} + O$	=	$3C_7H_{15} + OH$	6.4000E+02	2.50	20.93	[43]
1673	$C_7H_{16} + O$	=	$4C_7H_{15} + OH$	3.2000E+02	2.50	20.93	[43]
1674	$C_7H_{16} + OH$	=	$1C_7H_{15} + H_2O$	5.2500E+06	0.97	6.66	[43]
1675	$C_7H_{16} + OH$	=	$2C_7H_{15} + H_2O$	2.3500E+04	1.61	0.00	[43]
1676	$C_7H_{16} + OH$	=	$3C_7H_{15} + H_2O$	2.3500E+04	1.61	0.00	[43]
1677	$C_7H_{16} + OH$	=	$4C_7H_{15} + H_2O$	1.1750E+04	1.61	0.00	[43]
1678	$C_7H_{16} + CH_3$	=	$1C_7H_{15} + CH_4$	3.0000E+09	0.00	48.56	[43]
1679	$C_7H_{16} + CH_3$	=	$2C_7H_{15} + CH_4$	1.6000E+09	0.00	39.77	[43]
1680	$C_7H_{16} + CH_3$	=	$3C_7H_{15} + CH_4$	1.6000E+09	0.00	39.77	[43]
1681	$C_7H_{16} + CH_3$	=	$4C_7H_{15} + CH_4$	8.0000E+08	0.00	39.77	[43]
1682	$C_7H_{16} + O_2$	=	$1C_7H_{15} + HO_2$	2.5100E+10	0.00	205.11	[43]
1683	$C_7H_{16} + O_2$	=	$2C_7H_{15} + HO_2$	3.9800E+10	0.00	199.25	[43]
1684	$C_7H_{16} + O_2$	=	$3C_7H_{15} + HO_2$	4.0000E+10	0.00	199.25	[43]
1685	$C_7H_{16} + O_2$	=	$4C_7H_{15} + HO_2$	2.0000E+10	0.00	199.25	[43]
1686	$1C_7H_{15}$	=	$C_2H_4 + 1C_5H_{11}$	2.5200E+13	0.00	120.56	[265]
1687	$2C_7H_{15}$	=	$C_3H_6 + C_4H_9(N)$	1.6000E+13	0.00	118.46	[265]
1688	$3C_7H_{15}$	=	$C_3H_7(N) + C_4H_8(N)$	5.0000E+12	0.00	121.81	[265]
1689	$3C_7H_{15}$	=	$1C_6H_{12} + CH_3$	8.0000E+12	0.00	138.14	[265]
1690	$4C_7H_{15}$	=	$1C_5H_{10} + C_2H_5$	1.0800E+13	0.00	117.21	[265]

Table A.4, continued

No	Reaction			A	n	E_a	Ref
1691	$1C_7H_{15}$	=	$1C_7H_{14} + H$	1.0000E+13	0.00	169.11	[43]
1692	$2C_7H_{15}$	=	$1C_7H_{14} + H$	1.0000E+13	0.00	169.11	[43]
1693	$2C_7H_{15}$	=	$2C_7H_{14} + H$	1.0000E+13	0.00	169.11	[43]
1694	$3C_7H_{15}$	=	$2C_7H_{14} + H$	1.0000E+13	0.00	169.11	[43]
1695	$3C_7H_{15}$	=	$3C_7H_{14} + H$	1.0000E+13	0.00	169.11	[43]
1696	$4C_7H_{15}$	=	$3C_7H_{14} + H$	1.0000E+13	0.00	169.11	[43]
1697	$1C_7H_{15}$	=	$2C_7H_{15}$	2.0000E+11	0.00	46.46	[43]
1698	$1C_7H_{15}$	=	$3C_7H_{15}$	2.0000E+11	0.00	75.77	[43]
1699	$1C_7H_{15}$	=	$4C_7H_{15}$	2.0000E+11	0.00	83.72	[43]
1700	$2C_7H_{15}$	=	$3C_7H_{15}$	2.0000E+11	0.00	83.72	[43]
1701	$1C_7H_{15} + O_2$	=	$1C_7H_{14} + HO_2$	1.0000E+09	0.00	8.37	[43]
1702	$2C_7H_{15} + O_2$	=	$1C_7H_{14} + HO_2$	1.0000E+09	0.00	18.84	[43]
1703	$2C_7H_{15} + O_2$	=	$2C_7H_{14} + HO_2$	2.0000E+09	0.00	17.79	[43]
1704	$3C_7H_{15} + O_2$	=	$2C_7H_{14} + HO_2$	2.0000E+09	0.00	17.79	[43]
1705	$3C_7H_{15} + O_2$	=	$3C_7H_{14} + HO_2$	2.0000E+09	0.00	17.79	[43]
1706	$4C_7H_{15} + O_2$	=	$3C_7H_{14} + HO_2$	4.0000E+09	0.00	17.79	[43]
1707	$1C_7H_{14}$	=	$C_3H_5(A) + C_4H_9(N)$	2.5200E+16	0.00	297.63	[43]
1708	$2C_7H_{14}$	=	$C_3H_7(N) + C_4H_7(N)$	1.6000E+16	0.00	290.09	[265]
1709	$3C_7H_{14}$	=	$C_2H_5 + C_5H_9$	3.6000E+15	0.00	297.21	[43]
1710	$3C_7H_{14}$	=	$C_6H_{11} + CH_3$	5.3000E+16	0.00	305.58	[43]
1711	$1C_7H_{14} + H$	=	$C_7H_{13} + H_2$	8.0000E+10	0.00	14.23	[43]
1712	$2C_7H_{14} + H$	=	$C_7H_{13} + H_2$	1.6000E+11	0.00	14.23	[43]
1713	$3C_7H_{14} + H$	=	$C_7H_{13} + H_2$	1.6000E+11	0.00	14.23	[43]
1714	$1C_7H_{14} + O$	=	$C_7H_{13} + OH$	4.0000E+10	0.00	16.74	[43]
1715	$2C_7H_{14} + O$	=	$C_7H_{13} + OH$	8.0000E+10	0.00	16.74	[43]
1716	$3C_7H_{14} + O$	=	$C_7H_{13} + OH$	8.0000E+10	0.00	16.74	[43]
1717	$1C_7H_{14} + OH$	=	$C_7H_{13} + H_2O$	2.0000E+10	0.00	10.88	[43]
1718	$2C_7H_{14} + OH$	=	$C_7H_{13} + H_2O$	4.0000E+10	0.00	10.88	[43]
1719	$3C_7H_{14} + OH$	=	$C_7H_{13} + H_2O$	4.0000E+10	0.00	10.88	[43]
1720	$1C_7H_{14} + CH_3$	=	$C_7H_{13} + CH_4$	2.0000E+08	0.00	28.47	[43]
1721	$2C_7H_{14} + CH_3$	=	$C_7H_{13} + CH_4$	4.0000E+08	0.00	28.47	[182]
1722	$3C_7H_{14} + CH_3$	=	$C_7H_{13} + CH_4$	4.0800E+08	0.00	28.47	[43]
1723	$1C_7H_{14} + HO_2$	=	$C_7H_{13} + H_2O_2$	5.0000E+09	0.00	0.00	[43]
1724	$2C_7H_{14} + HO_2$	=	$C_7H_{13} + H_2O_2$	5.0000E+09	0.00	0.00	[43]
1725	$3C_7H_{14} + HO_2$	=	$C_7H_{13} + H_2O_2$	5.0000E+09	0.00	0.00	[43]
1726	$1C_7H_{14} + O$	=	$C_2H_3 + 1C_5H_{10} + OH$	2.8200E+10	0.00	21.77	[43]
1727	$1C_7H_{14} + O$	=	$C_3H_5(A) + C_4H_8(N) + OH$	2.8200E+10	0.00	21.77	[43]
1728	$1C_7H_{14} + O$	=	$C_4H_7(N) + C_3H_6 + OH$	2.8200E+10	0.00	21.77	[43]
1729	$1C_7H_{14} + O$	=	$C_5H_9 + C_2H_4 + OH$	5.0000E+10	0.00	32.86	[43]
1730	$2C_7H_{14} + O$	=	$t\text{-}C_3H_5 + C_4H_8(N) + OH$	2.8200E+10	0.00	21.77	[43]
1731	$2C_7H_{14} + O$	=	$C_4H_7(N) + C_3H_6 + OH$	2.8200E+10	0.00	21.77	[43]
1732	$2C_7H_{14} + O$	=	$C_5H_9 + C_2H_4 + OH$	5.0000E+10	0.00	32.86	[43]
1733	$3C_7H_{14} + O$	=	$C_4H_7(N) + C_3H_6 + OH$	2.8200E+10	0.00	21.77	[43]
1734	$3C_7H_{14} + O$	=	$C_5H_9 + C_2H_4 + OH$	5.0000E+10	0.00	32.86	[43]
1735	$1C_7H_{14} + OH$	=	$C_2H_3 + 1C_5H_{10} + H_2O$	1.2900E+06	1.25	2.93	[43]
1736	$1C_7H_{14} + OH$	=	$C_3H_5(A) + C_4H_8(N) + H_2O$	1.2900E+06	1.25	2.93	[43]
1737	$1C_7H_{14} + OH$	=	$C_4H_7(N) + C_3H_6 + H_2O$	1.2900E+06	1.25	2.93	[43]
1738	$1C_7H_{14} + OH$	=	$C_5H_9 + C_2H_4 + H_2O$	4.2700E+06	1.05	7.58	[43]
1739	$2C_7H_{14} + OH$	=	$C_3H_5(A) + C_4H_8(N) + H_2O$	1.1600E+06	1.25	2.93	[43]
1740	$2C_7H_{14} + OH$	=	$C_4H_7(N) + C_3H_6 + H_2O$	1.1600E+06	1.25	2.93	[43]
1741	$2C_7H_{14} + OH$	=	$C_5H_9 + C_2H_4 + H_2O$	4.2700E+06	1.05	7.58	[43]
1742	$3C_7H_{14} + OH$	=	$C_4H_7(N) + C_3H_6 + H_2O$	1.1600E+06	1.25	2.93	[43]
1743	$3C_7H_{14} + OH$	=	$C_5H_9 + C_2H_4 + H_2O$	4.2700E+06	1.05	2.93	[43]
1744	C_7H_{13}	=	$C_3H_5(A) + C_4H_8(N)$	2.5200E+13	0.00	125.58	[43]
1745	C_7H_{13}	=	$C_3H_4(A) + C_4H_9(N)$	1.0000E+13	0.00	125.58	[43]
1746	C_7H_{13}	=	$C_4H_6(S) + C_3H_7(N)$	1.0000E+13	0.00	133.95	[265]
1747	$1C_6H_{13}$	=	$2C_6H_{13}$	2.0000E+11	0.00	75.77	[43]
1748	$1C_6H_{13}$	=	$C_2H_4 + C_4H_9(N)$	2.5200E+13	0.00	120.56	[265]
1749	$2C_6H_{13}$	=	$C_3H_7(N) + C_3H_6$	1.6000E+13	0.00	118.46	[265]
1750	$1C_6H_{12}$	=	$C_3H_7(N) + C_3H_5(A)$	7.9400E+15	0.00	297.64	[269]
1751	$1C_6H_{12}$	=	$C_3H_6 + C_3H_6$	3.9800E+12	0.00	241.41	[269]
1752	$1C_6H_{12} + H$	=	$C_6H_{11} + H_2$	5.0000E+09	0.00	14.23	[182]
1753	$1C_6H_{12} + O$	=	$C_6H_{11} + OH$	4.0000E+10	0.00	16.74	[43]
1754	$1C_6H_{12} + OH$	=	$C_6H_{11} + H_2O$	2.0000E+09	0.00	10.88	[182]
1755	$1C_6H_{12} + CH_3$	=	$C_6H_{11} + CH_4$	2.0000E+08	0.00	28.46	[43]
1756	$1C_6H_{12} + HO_2$	=	$C_6H_{11} + H_2O_2$	1.0000E+08	0.00	71.41	[43]

Table A.4, continued

No	*Reaction*			A	n	E_a	*Ref*
1757	$1C_6H_{12} + O$	=	$C_2H_3 + C_4H_8(N) + OH$	2.8200E+10	0.00	21.77	[43]
1758	$1C_6H_{12} + O$	=	$C_3H_5(A) + C_3H_6 + OH$	2.8200E+10	0.00	21.77	[43]
1759	$1C_6H_{12} + O$	=	$C_4H_7(N) + C_2H_4 + OH$	5.0100E+10	0.00	32.86	[43]
1760	$1C_6H_{12} + O$	=	$CHO + 1C_5H_{11}$	1.0000E+08	0.00	0.00	[43]
1761	$1C_6H_{12} + O$	=	$CH_3 + CO + C_4H_9(N)$	1.0000E+08	0.00	0.00	[43]
1762	$1C_6H_{12} + OH$	=	$C_2H_3 + C_4H_8(N) + H_2O$	2.1700E+05	1.25	2.93	[43]
1763	$1C_6H_{12} + OH$	=	$C_3H_5(A) + C_3H_6 + H_2O$	2.1700E+05	1.25	2.93	[43]
1764	$1C_6H_{12} + OH$	=	$C_4H_7(N) + C_2H_4 + H_2O$	7.1700E+05	1.05	7.58	[43]
1765	$1C_6H_{12} + OH$	=	$CH_2O + 1C_5H_{11}$	1.0000E+08	0.00	0.00	[43]
1766	$1C_6H_{12} + OH$	=	$C_2H_4O + C_4H_9(N)$	1.0000E+08	0.00	0.00	[43]
1767	C_6H_{11}	=	$C_3H_6 + C_3H_5(A)$	5.0400E+13	0.00	125.58	[43]
1768	C_6H_{11}	=	$C_2H_5 + 1,3\text{-}C_4H_6$	5.0000E+12	0.00	133.89	[43]
1769	$1C_5H_{11}$	=	$C_3H_7(N) + C_2H_4$	3.2000E+13	0.00	118.83	[182]
1770	$1C_5H_{11}$	=	$1C_5H_{10} + H$	1.3000E+13	0.00	161.50	[182]
1771	$1C_5H_{10}$	=	$C_2H_5 + C_3H_5(A)$	1.0000E+16	0.00	298.88	[269]
1772	$1C_5H_{10}$	=	$C_3H_6 + C_2H_4$	3.1600E+12	0.00	238.00	[269]
1773	$1C_5H_{10} + H$	=	$C_5H_9 + H_2$	2.8000E+10	0.00	16.74	[265]
1774	$1C_5H_{10} + O$	=	$C_5H_9 + OH$	2.5400E+02	2.56	-4.73	[182]
1775	$1C_5H_{10} + O$	=	$C_4H_9(N) + CHO$	1.0000E+08	0.00	0.00	[182]
1776	$1C_5H_{10} + O$	=	$C_3H_7(N) + C_2H_3O$	1.0000E+08	0.00	0.00	[182]
1777	$1C_5H_{10} + O$	=	$C_4H_8(N) + CH_2O$	8.5100E+09	0.00	0.00	[182]
1778	$1C_5H_{10} + O$	=	$C_2H_4O + C_3H_6$	8.5100E+09	0.00	0.00	[265]
1779	$1C_5H_{10} + O$	=	$C_3H_5(S) + C_2H_4 + OH$	2.0000E+10	0.00	29.30	[182]
1780	$1C_5H_{10} + O$	=	$C_3H_6 + C_2H_3 + OH$	1.0000E+10	0.00	29.30	[182]
1781	$1C_5H_{10} + OH$	=	$C_5H_9 + H_2O$	6.8000E+10	0.00	12.81	[182]
1782	$1C_5H_{10} + OH$	=	$C_4H_9(N) + CH_2O$	1.0000E+08	0.00	0.00	[182]
1783	$1C_5H_{10} + OH$	=	$C_3H_7(N) + C_2H_4O$	1.0000E+08	0.00	0.00	[182]
1784	$1C_5H_{10} + OH$	=	$C_3H_5(S) + C_2H_4 + H_2O$	2.0000E+06	1.20	0.50	[182]
1785	$1C_5H_{10} + OH$	=	$C_3H_6 + C_2H_3 + H_2O$	1.0000E+06	1.20	0.50	[182]
1786	$1C_5H_{10} + O_2$	=	$C_5H_9 + HO_2$	4.0000E+09	0.00	167.44	[182]
1787	$1C_5H_{10} + CH_3$	=	$C_5H_9 + CH_4$	1.0000E+08	0.00	30.56	[182]
1788	C_5H_9	=	$C_3H_5(A) + C_2H_4$	2.5000E+13	0.00	125.52	[265]
1789	C_5H_9	=	$C_2H_3 + C_3H_6$	2.5000E+13	0.00	125.52	[265]
1790	C_5H_9	=	$C_4H_6(S) + CH_3$	1.0000E+13	0.00	133.89	[182]
1791	$C_2H_5 + HO_2$	=	$C_2H_5O + OH$	3.0000E+10	0.00	0.00	[218]
1792	$C_2H_5 + HO_2$	=	$C_2H_4 + H_2O_2$	3.0000E+08	0.00	0.00	[249]
1793	$C_2H_5 + HO_2$	=	$C_2H_6 + O_2$	3.0000E+08	0.00	0.00	[249]
1794	$C_{12}H_{26}$	=	$C_9H_{19} + C_3H_7(N)$	7.5800E+14	0.00	354.40	est.
1795	$C_{12}H_{26}$	=	$C_8H_{17} + C_4H_9(N)$	7.5800E+14	0.00	340.50	est.
1796	$C_{12}H_{26}$	=	$1C_7H_{15} + 1C_5H_{11}$	7.5800E+14	0.00	340.50	est.
1797	$C_{12}H_{26}$	=	$1C_6H_{13} + 1C_6H_{13}$	7.5800E+14	0.00	340.90	est.
1798	$C_{12}H_{26}$	=	$1C_{12}H_{25} + H$	8.0000E+14	0.00	393.30	est.
1799	$C_{12}H_{26}$	=	$2C_{12}H_{25} + H$	8.0000E+14	0.00	408.90	est.
1800	$C_{12}H_{26}$	=	$3C_{12}H_{25} + H$	8.0000E+14	0.00	408.90	est.
1801	$C_{12}H_{26}$	=	$4C_{12}H_{25} + H$	8.0000E+14	0.00	408.90	est.
1802	$C_{12}H_{26}$	=	$5C_{12}H_{25} + H$	8.0000E+14	0.00	408.90	est.
1803	$C_{12}H_{26}$	=	$6C_{12}H_{25} + H$	8.0000E+14	0.00	408.90	est.
1804	$C_{12}H_{26} + H$	=	$1C_{12}H_{25} + H_2$	4.4900E+04	2.00	32.20	est. (1572)
1805	$C_{12}H_{26} + H$	=	$2C_{12}H_{25} + H_2$	1.4300E+04	2.00	20.92	est. (1573)
1806	$C_{12}H_{26} + H$	=	$3C_{12}H_{25} + H_2$	1.4300E+04	2.00	20.92	est. (1574)
1807	$C_{12}H_{26} + H$	=	$4C_{12}H_{25} + H_2$	1.4300E+04	2.00	20.92	est. (1575)
1808	$C_{12}H_{26} + H$	=	$5C_{12}H_{25} + H_2$	1.4300E+04	2.00	20.92	est. (1576)
1809	$C_{12}H_{26} + H$	=	$6C_{12}H_{25} + H_2$	1.4300E+04	2.00	20.92	est. (1576)
1810	$C_{12}H_{26} + OH$	=	$1C_{12}H_{25} + H_2O$	4.2000E+06	0.97	6.65	est. (1577)
1811	$C_{12}H_{26} + OH$	=	$2C_{12}H_{25} + H_2O$	1.8700E+04	1.61	0.00	est. (1578)
1812	$C_{12}H_{26} + OH$	=	$3C_{12}H_{25} + H_2O$	1.8700E+04	1.61	0.00	est. (1579)
1813	$C_{12}H_{26} + OH$	=	$4C_{12}H_{25} + H_2O$	1.8700E+04	1.61	0.00	est. (1580)
1814	$C_{12}H_{26} + OH$	=	$5C_{12}H_{25} + H_2O$	1.8700E+04	1.61	0.00	est. (1581)
1815	$C_{12}H_{26} + OH$	=	$6C_{12}H_{25} + H_2O$	1.8700E+04	1.61	0.00	est. (1581)
1816	$C_{12}H_{26} + O$	=	$1C_{12}H_{25} + OH$	1.8700E+03	2.40	6.65	est. (1582)
1817	$C_{12}H_{26} + O$	=	$2C_{12}H_{25} + OH$	5.0900E+02	2.50	20.92	est. (1583)
1818	$C_{12}H_{26} + O$	=	$3C_{12}H_{25} + OH$	5.0900E+02	2.50	20.92	est. (1584)

Table A.4, continued

No	*Reaction*			A	n	E_a	*Ref*
1819	$C_{12}H_{26} + O$	=	$4C_{12}H_{25} + OH$	5.0900E+02	2.50	20.92	est. (1585)
1820	$C_{12}H_{26} + O$	=	$5C_{12}H_{25} + OH$	5.0900E+02	2.50	20.92	est. (1586)
1821	$C_{12}H_{26} + O$	=	$6C_{12}H_{25} + OH$	5.0900E+02	2.50	20.92	est. (1586)
1822	$C_{12}H_{26} + O$	=	$1C_{12}H_{25} + OH$	1.8700E+03	2.40	6.65	est. (1582)
1823	$C_{12}H_{26} + O$	=	$2C_{12}H_{25} + OH$	5.0900E+02	2.50	20.92	est. (1583)
1824	$C_{12}H_{26} + O$	=	$3C_{12}H_{25} + OH$	5.0900E+02	2.50	20.92	est. (1584)
1825	$C_{12}H_{26} + O$	=	$4C_{12}H_{25} + OH$	5.0900E+02	2.50	20.92	est. (1585)
1826	$C_{12}H_{26} + O$	=	$5C_{12}H_{25} + OH$	5.0900E+02	2.50	20.92	est. (1586)
1827	$C_{12}H_{26} + O$	=	$6C_{12}H_{25} + OH$	5.0900E+02	2.50	20.92	est. (1586)
1828	$C_{12}H_{26} + CH_3$	=	$1C_{12}H_{25} + CH_4$	2.3900E+09	0.00	48.53	est. (1587)
1829	$C_{12}H_{26} + CH_3$	=	$2C_{12}H_{25} + CH_4$	1.2700E+09	0.00	39.75	est. (1588)
1830	$C_{12}H_{26} + CH_3$	=	$3C_{12}H_{25} + CH_4$	1.2700E+09	0.00	39.75	est. (1589)
1831	$C_{12}H_{26} + CH_3$	=	$4C_{12}H_{25} + CH_4$	1.2700E+09	0.00	39.75	est. (1590)
1832	$C_{12}H_{26} + CH_3$	=	$5C_{12}H_{25} + CH_4$	1.2700E+09	0.00	39.75	est. (1591)
1833	$C_{12}H_{26} + CH_3$	=	$6C_{12}H_{25} + CH_4$	1.2700E+09	0.00	39.75	est. (1591)
1834	$C_{12}H_{26} + HO_2$	=	$1C_{12}H_{25} + H_2O_2$	1.0000E+10	0.00	81.20	est. (1598)
1835	$C_{12}H_{26} + HO_2$	=	$2C_{12}H_{25} + H_2O_2$	1.0000E+10	0.00	72.00	est. (1599)
1836	$C_{12}H_{26} + HO_2$	=	$3C_{12}H_{25} + H_2O_2$	1.0000E+10	0.00	72.00	est. (1600)
1837	$C_{12}H_{26} + HO_2$	=	$4C_{12}H_{25} + H_2O_2$	1.0000E+10	0.00	72.00	est. (1601)
1838	$C_{12}H_{26} + HO_2$	=	$5C_{12}H_{25} + H_2O_2$	1.0000E+10	0.00	72.00	est. (1602)
1839	$C_{12}H_{26} + HO_2$	=	$6C_{12}H_{25} + H_2O_2$	1.0000E+10	0.00	72.00	est. (1602)
1840	$C_{12}H_{26} + O_2$	=	$1C_{12}H_{25} + HO_2$	2.0900E+10	0.00	217.80	est. (1592)
1841	$C_{12}H_{26} + O_2$	=	$2C_{12}H_{25} + HO_2$	3.1500E+10	0.00	203.40	est. (1593)
1842	$C_{12}H_{26} + O_2$	=	$3C_{12}H_{25} + HO_2$	3.1500E+10	0.00	203.40	est. (1594)
1843	$C_{12}H_{26} + O_2$	=	$4C_{12}H_{25} + HO_2$	3.1500E+10	0.00	203.40	est. (1595)
1844	$C_{12}H_{26} + O_2$	=	$5C_{12}H_{25} + HO_2$	3.1500E+10	0.00	203.40	est. (1596)
1845	$C_{12}H_{26} + O_2$	=	$6C_{12}H_{25} + HO_2$	3.1500E+10	0.00	203.40	est. (1596)
1846	$1C_{12}H_{25}$	=	$C_2H_4 + 1C_{10}H_{21}$	2.1000E+13	0.00	110.25	est.
1847	$2C_{12}H_{25}$	=	$C_3H_6 + C_9H_{19}$	2.1000E+13	0.00	83.40	est.
1848	$3C_{12}H_{25}$	=	$C_4H_8(N) + C_8H_{17}$	2.1000E+13	0.00	83.14	est.
1849	$4C_{12}H_{25}$	=	$C_2H_4 + 1C_{10}H_{21}$	2.1000E+13	0.00	82.60	est.
1850	$4C_{12}H_{25}$	=	$1C_5H_{10} + 1C_7H_{15}$	2.1000E+13	0.00	82.60	est.
1851	$5C_{12}H_{25}$	=	$C_3H_7(N) + C_9H_{18}$	2.1000E+13	0.00	83.30	est.
1852	$5C_{12}H_{25}$	=	$1C_6H_{12} + 1C_6H_{13}$	2.1000E+13	0.00	83.30	est.
1853	$6C_{12}H_{25}$	=	$1C_5H_{11} + 1C_7H_{14}$	2.1000E+13	0.00	83.30	est.
1854	$6C_{12}H_{25}$	=	$C_4H_9(N) + C_8H_{16}$	2.1000E+13	0.00	83.30	est.
1855	$1C_{12}H_{25}$	=	$2C_{12}H_{25}$	2.0000E+11	0.00	84.00	est. (1604)
1856	$1C_{12}H_{25}$	=	$4C_{12}H_{25}$	2.0000E+11	0.00	84.00	est. (1604)
1857	$1C_{12}H_{25}$	=	$5C_{12}H_{25}$	2.0000E+11	0.00	84.00	est. (1604)
1858	$1C_{12}H_{25}$	=	$6C_{12}H_{25}$	2.0000E+11	0.00	84.00	est. (1604)
1859	$2C_{12}H_{25}$	=	$3C_{12}H_{25}$	2.0000E+11	0.00	84.00	est. (1604)
1860	$2C_{12}H_{25}$	=	$5C_{12}H_{25}$	2.0000E+11	0.00	84.00	est. (1604)
1861	$2C_{12}H_{25}$	=	$6C_{12}H_{25}$	2.0000E+11	0.00	84.00	est. (1604)
1862	$3C_{12}H_{25}$	=	$4C_{12}H_{25}$	2.0000E+11	0.00	84.00	est. (1604)
1863	$3C_{12}H_{25}$	=	$6C_{12}H_{25}$	2.0000E+11	0.00	84.00	est. (1604)
1864	$4C_{12}H_{25}$	=	$5C_{12}H_{25}$	2.0000E+11	0.00	84.00	est. (1604)
1865	$5C_{12}H_{25}$	=	$6C_{12}H_{25}$	2.0000E+11	0.00	84.00	est. (1604)
1866	C_9H_{19}	=	$C_9H_{18} + H$	2.0000E+13	0.00	211.80	est.
1867	C_9H_{19}	=	$C_8H_{16} + CH_3$	3.3000E+13	0.00	121.00	[18]
1868	C_9H_{19}	=	$C_7H_{16} + C_2H_3$	3.3000E+13	0.00	121.00	[18]
1869	$C_9H_{19} + O_2$	=	$C_9H_{18} + HO_2$	5.0000E+08	0.00	14.65	est. (1620)
1870	$C_9H_{19} + O_2$	=	$C_8H_{16} + CH_2O + OH$	2.0000E+08	0.00	0.00	est.
1871	C_9H_{18}	=	$C_3H_5(A) + 1C_6H_{13}$	2.0000E+16	0.00	229.90	est.
1872	C_9H_{18}	=	$C_4H_7(N) + 1C_5H_{11}$	2.0000E+16	0.00	229.90	est.
1873	C_9H_{18}	=	$C_5H_9 + C_4H_9(N)$	2.0000E+16	0.00	229.90	est.
1874	C_9H_{18}	=	$C_6H_{11} + C_3H_7(N)$	2.0000E+16	0.00	229.90	est.
1875	$C_9H_{18} + O$	=	$C_9H_{17} + OH$	1.0000E+08	0.00	0.00	est.
1876	$C_9H_{18} + OH$	=	$C_9H_{17} + H_2O$	1.0000E+08	0.00	0.00	est.
1877	$C_9H_{18} + H$	=	$C_9H_{17} + H_2$	1.0000E+08	0.00	0.00	est.
1878	$C_9H_{18} + HO_2$	=	$C_9H_{17} + H_2O_2$	1.0000E+08	0.00	0.00	est.
1879	$C_9H_{18} + H$	=	$2C_9H_{17} + H_2$	6.2000E+10	0.00	14.24	est. (1711)
1880	$C_9H_{18} + O$	=	$2C_9H_{17} + OH$	3.1000E+10	0.00	16.75	est. (1714)

Table A.4, continued

No	*Reaction*			A	n	E_a	*Ref*
1881	$C_9H_{18} + OH$	=	$2C_9H_{17} + H_2O$	1.5000E+10	0.00	10.89	est. (1717)
1882	$C_9H_{18} + CH_3$	=	$2C_9H_{17} + CH_4$	1.5000E+08	0.00	28.48	est. (1720)
1883	$C_9H_{18} + HO_2$	=	$2C_9H_{17} + H_2O_2$	3.8000E+09	0.00	0.00	est. (1723)
1884	C_9H_{17}	=	$C_7H_{13} + C_2H_4$	2.5200E+13	0.00	92.85	est.
1885	C_9H_{17}	=	$C_6H_{11} + C_3H_6$	2.5200E+13	0.00	74.00	est.
1886	C_9H_{17}	=	$C_5H_9 + C_4H_8(N)$	2.5200E+13	0.00	81.84	est.
1887	C_9H_{17}	=	$C_8H_{14} + CH_3$	2.5200E+13	0.00	140.30	est.
1888	$2C_9H_{17}$	=	$1C_7H_{14} + C_2H_3$	2.0000E+13	0.00	119.78	est. [73]
1889	$2C_9H_{17} + O_2$	=	$C_8H_{14} + CH_2O + OH$ [7] k_∞	1.0500E+06	0.77	-2.39	est. (208)
			k_0 =	7.1000E+36	-8.24	17.87	
1890	$1C_5H_{10} + HO_2$	=	$C_5H_9 + H_2O_2$	9.6400E+00	2.60	58.20	est. (407)
1891	$1C_5H_{10} + HO_2$	=	$OH + C_2H_4O + C_3H_6$	9.5500E+08	0.00	59.40	est.
1892	$1C_6H_{12} + HO_2$	=	$C_6H_{11} + H_2O_2$	9.6400E+00	2.60	58.20	est. (407)
1893	$1C_6H_{12} + HO_2$	=	$OH + PC_3H_6O + C_3H_6$	8.1300E+08	0.00	58.30	est.
1894	$1C_6H_{13}$	=	$1C_6H_{12} + H$	1.5000E+13	0.00	158.30	est.

Enhanced Collision Efficiencies:

M^a: $N_2 = 0.4$; $O_2 = 0.35$; $CO = 0.7$; $CO_2 = 1.5$; $H_2O = 6.5$.

M^b: $H_2 = 2.5$; $CO = 1.9$; $CO_2 = 3.8$; $H_2O = 6.5$.

M^c: $H_2 = 0.0$; $CO_2 = 0.0$; $H_2O = 0.0$.

M^d: $H_2O = 6.5$; $O_2 = 2.5$; $CO = 2.0$; $CO_2 = 5.0$; $H_2 = 3.0$.

M^e: $H_2O = 4.0$; $N_2 = 0.36$; $CO = 0.36$; $CO_2 = 0.36$; $CH_4 = 0.7$; $C_2H_2 = 5.0$; $C_2H_4 = 1.4$; $C_2H_6 = 2.2$.

M^f: $H_2 = 2.0$; $O_2 = 1.5$; $CO = 1.5$; $H_2O = 6.0$; $CO_2 = 3.0$.

M^g: $H_2O = 5.7$; $H_2 = 1.1$; $CO = 1.9$; $CO_2 = 3.3$; $O_2 = 1.9$; $N_2 = 1.6$.

M^h: $H_2O = 6.5$; $H_2 = 1.89$; $CO = 2.5$; $CO_2 = 2.5$.

M^i: $H_2O = 5.0$; $CO = 2.0$; $CO_2 = 3.0$; $H_2 = 2.0$; $O_2 = 1.5$.

M^j: $H_2 = 2.0$; $H_2O = 6.0$; $CH_4 = 2.0$; $CO = 1.5$; $CO_2 = 2.0$; $C_2H_6 = 3.0$; $AR = 0.7$.

Fall-off parameters for pressure dependent reactions:

^1F_C = 0.63exp(-T/3315.0)+ 0.37exp(-T/61.0)

^2F_C = 0.18exp(-T/200.0)+ 0.82exp(-T/1438.0)

^3F_C = 0.38exp(-T/73.0) + 0.62exp(-T/1180.0)

^4F_C = 0.27

^5F_C = 0.35

^6F_C = 0.24exp(-T/40.0)+ 0.76exp(-T/1025.0)

^7F_C = 0.58exp(-T/1250.0)+ 0.42exp(-T/183.0)

^8F_C = exp(-T/3371.0)+ 47.6exp(-16182.0/T)

^9F_C = exp(-T/1097.0)+ exp(6860.0/T)

$^{10}F_C = \log(k/k_\infty)$ = -0.1155 + 8.842E-4*T - 1.591E-6*T^2 + 2.874E-10*T^3 $^{11}F_C$ = 2.17exp(-T/251.0)+ exp(-1185.0/T)

$^{12}F_C$ = 0.76exp(-T/38.0)+ 0.24exp(-T/1946.0)

$^{13}F_C$ = exp(-T/1314.0)+ exp(50000.0/T)

$^{14}F_C$ = 0.19exp(205.0/T)+ 15300.0exp(-10578.0/T)

$^{15}F_C$ = 1.01exp(-T/206.0)+ 0.196exp(-278.0/T)

* Reaction in the Lindemann form.

Appendix B

Thermodynamic Data

The thermodynamic data of the species considered in the present thesis, are essential for the calculation of the enthalpy of the mixture and the reaction equilibrium constants.

$$K_p = \exp\left(\frac{\Delta S^0}{R} - \frac{\Delta H^0}{RT}\right) \tag{B.1}$$

The thermodynamic data are commonly expressed in the form of polynomials, often referred to as JANAF polynomials, are shown in Equations B.2-B.4. The data for each species is represented by fourteen coefficients (a_1 - a_7), corresponding to temperature ranges above 1000 K (first set of seven coefficients) and below 1000 K (second set of seven coefficients).

The JANAF polynomials for the species considered in the current mechanism are grouped in Table B.1. The structure of each species, with the enthalpy and the entropy at 298 K is shown in Table B.1.

Heat Capacity

$$\frac{C_p}{R} = a_1 + a_2T + a_3T^2 + a_4T^3 + a_5T^4 \tag{B.2}$$

Enthalpy

$$\frac{H}{RT} = a_1 + \frac{a_2T}{2} + \frac{a_3T^2}{3} + \frac{a_4T^3}{4} + \frac{a_5T^4}{5} + \frac{a_6}{T} \tag{B.3}$$

Entropy

$$\frac{S}{R} = a_1ln(T) + a_2T + \frac{a_3T^2}{2} + \frac{a_4T^3}{3} + \frac{a_5T^4}{4} + a_7 \tag{B.4}$$

Table B.1: Thermodynamic Data

H				
0.25000000E+01	0.00000000E+00	0.00000000E+00	0.00000000E+00	0.00000000E+00
0.25471627E+05	-0.46011763E+00	0.25000000E+01	0.00000000E+00	0.00000000E+00
0.00000000E+00	0.00000000E+00	0.25471627E+05	-0.46011762E+00	
OH				
0.28827305E+01	0.10139743E-02	-0.22768771E-06	0.21746837E-10	-0.51263053E-15
0.38868879E+04	0.55957122E+01	0.36372659E+01	0.18509105E-03	-0.16761646E-05
0.23872027E-08	-0.84314418E-12	0.36067817E+04	0.13588605E+01	
O				
0.25420597E+01	-0.27550619E-04	-0.31028033E-08	0.45510674E-11	-0.43680515E-15
0.29230803E+05	0.49203081E+01	0.29464288E+01	-0.16381665E-02	0.24210317E-05
-0.16028432E-08	0.38906963E-12	0.29147644E+05	0.29639949E+01	
HO_2				
0.41722659E+01	0.18812098E-02	-0.34629297E-06	0.19468516E-10	0.17609153E-15
0.61818851E+02	0.29577974E+01	0.43017880E+01	-0.47490201E-02	0.21157953E-04
-0.24275961E-07	0.92920670E-11	0.29480876E+03	0.37167010E+01	
H_2				
0.29914234E+01	0.70006441E-03	-0.56338287E-07	-0.92315782E-11	0.15827518E-14
-0.83503399E+03	-0.13551102E+01	0.32981243E+01	0.82494417E-03	-0.81430153E-06
-0.94754343E-10	0.41348722E-12	-0.10125209E+04	-0.32940941E+01	
H_2O				
0.26721456E+01	0.30562929E-02	-0.87302601E-06	0.12009964E-09	-0.63916179E-14
-0.29899209E+05	0.68628168E+01	0.33868425E+01	0.34749825E-02	-0.63546963E-05
0.69685813E-08	-0.25065884E-11	-0.30208113E+05	0.25902328E+01	
H_2O_2				
0.45731667E+01	0.43361363E-02	-0.14746888E-05	0.23489037E-09	-0.14316536E-13
-0.18006961E+05	0.50113696E+00	0.33887536E+01	0.65692260E-02	-0.14850126E-06
-0.46258055E-08	0.24715147E-11	-0.17663147E+05	0.67853631E+01	
O_2				
0.36975782E+01	0.61351969E-03	-0.12588419E-06	0.17752815E-10	-0.11364353E-14
-0.12339302E+04	0.31891656E+01	0.32129364E+01	0.11274863E-02	-0.57561505E-06
0.13138772E-08	-0.87685539E-12	-0.10052490E+04	0.60347376E+01	
C_1				
0.26055830E+01	-0.19593434E-03	0.10673722E-06	-0.16423940E-10	0.81870580E-15
0.85411742E+05	0.41923868E+01	0.25542395E+01	-0.32153772E-03	0.73379223E-06
-0.73223487E-09	0.26652144E-12	0.85442681E+05	0.45313085E+01	
C_2				
0.37913706E+01	0.51650473E-03	-0.25486960E-07	-0.82263554E-11	0.10086168E-14
0.99023059E+05	0.28151802E+01	0.86470550E+00	0.39353120E-01	-0.11981818E-03
0.13908103E-06	-0.55205503E-10	0.98731303E+05	0.11530141E+02	
CO				
0.30250781E+01	0.14426885E-02	-0.56308278E-06	0.10185813E-09	-0.69109515E-14
-0.14268349E+05	0.61082177E+01	0.32624516E+01	0.15119408E-02	-0.38817552E-05
0.55819442E-08	-0.24749512E-11	-0.14310539E+05	0.48488969E+01	
CO_2				
0.44536228E+01	0.31401687E-02	-0.12784105E-05	0.23939967E-09	-0.16690332E-13
-0.48966961E+05	-0.95539588E+00	0.22757246E+01	0.99220723E-02	-0.10409113E-04
0.68666868E-08	-0.21172801E-11	-0.48373141E+05	0.10188488E+02	
CH				
0.25209062E+01	0.17653726E-02	-0.46147581E-06	0.59288567E-10	-0.33473209E-14
0.71134082E+05	0.74053223E+01	0.34898166E+01	0.32383554E-03	-0.16889906E-05
0.31621733E-08	-0.14060907E-11	0.70799939E+05	0.20840111E+01	
CHO				
0.35572712E+01	0.33455728E-02	-0.13350060E-05	0.24705726E-09	-0.17138509E-13
0.39163245E+04	0.55522995E+01	0.28983297E+01	0.61991466E-02	-0.96230842E-05
0.10898249E-07	-0.45748852E-11	0.41599219E+04	0.89836139E+01	
$^1CH_2$				
0.35528886E+01	0.20667882E-02	-0.19141160E-06	-0.11046734E-09	0.20213496E-13
0.49849754E+05	0.16865700E+01	0.39712651E+01	-0.16990887E-03	0.10253688E-05
0.24925508E-08	-0.19812663E-11	0.49893676E+05	0.57532072E-01	
$^3CH_2$				
0.36364078E+01	0.19330566E-02	-0.16870163E-06	-0.10098994E-09	0.18082558E-13
0.45341339E+05	0.21565606E+01	0.37622371E+01	0.11598191E-02	0.24895854E-06
0.88008356E-09	-0.73324354E-12	0.45367906E+05	0.17125776E+01	

Table B.1, continued

CH_2O				
0.31694807E+01	0.61932742E-02	-0.22505981E-05	0.36598245E-09	-0.22015410E-13
-0.14478425E+05	0.60423533E+01	0.47937036E+01	-0.99081518E-02	0.37321459E-04
-0.37927902E-07	0.13177015E-10	-0.14308955E+05	0.60288702E+00	
CH_3				
0.28440516E+01	0.61379741E-02	-0.22303452E-05	0.37851608E-09	-0.24521590E-13
0.16437808E+05	0.54526973E+01	0.24304428E+01	0.11124099E-01	-0.16802203E-04
0.16218287E-07	-0.58649526E-11	0.16423781E+05	0.67897939E+01	
CH_2OH				
0.46776733E+01	0.65608772E-02	-0.22636864E-05	0.35530469E-09	-0.20842959E-13
-0.28928048E+04	0.48041879E+00	0.38644027E+01	0.55913161E-02	0.59514635E-05
-0.10477176E-07	0.43793199E-11	-0.25050493E+04	0.54710652E+01	
CH_3O				
0.37707996E+01	0.78714974E-02	-0.26563839E-05	0.39444314E-09	-0.21126164E-13
0.12783252E+03	0.29295749E+01	0.21062040E+01	0.72165951E-02	0.53384719E-05
-0.73776363E-08	0.20756105E-11	0.97860107E+03	0.13152177E+02	
CH_3OO				
0.66812963E 01	0.80057271E-02	-0.27188507E-05	0.40631365E-09	-0.21927725E-13
0.52621851E 03	-0.99423847E 01	0.20986490E 01	0.15786357E-01	0.75683261E-07
-0.11274587E-07	0.56665133E-11	0.20695879E 04	0.15007068E 02	
CH_4				
0.16834788E+01	0.10237235E-01	-0.38751286E-05	0.67855849E-09	-0.45034231E-13
-0.10080787E+05	0.96233949E+01	0.77874148E+00	0.17476683E-01	-0.27834090E-04
0.30497080E-07	-0.12239307E-10	-0.98252285E+04	0.13722195E+02	
CH_3OH				
0.36012593E+01	0.10243223E-01	-0.35999217E-05	0.57251951E-09	-0.33912719E-13
-0.25997155E+05	0.47056025E+01	0.57153948E+01	-0.15230920E-01	0.65244182E-04
-0.71080873E-07	0.26135383E-10	-0.25642765E+05	-0.15040970E+01	
CH_3OOH				
0.61600316E+01	0.10239957E-01	-0.36101507E-05	0.57550301E-09	-0.34178147E-13
-0.17654526E+05	-0.61911544E+01	0.49652507E+01	0.92343510E-03	0.34455956E-04
-0.44469600E-07	0.17456120E-10	-0.16726970E+05	0.29880275E+01	
C_2O				
0.51512722E+01	0.23726722E-02	-0.76135971E-06	0.11706415E-09	-0.70257804E-14
0.33241888E+05	-0.22183135E+01	0.28648610E+01	0.11990216E-01	-0.18362448E-04
0.15769739E-07	-0.53897452E-11	0.33749932E+05	0.88867772E+01	
C_2H				
0.36646060E+01	0.38218694E-02	-0.13650743E-05	0.21324828E-09	-0.12309430E-13
0.67297055E+05	0.39134973E+01	0.29018020E+01	0.13285982E-01	-0.28050886E-04
0.28930184E-07	-0.10744742E-10	0.67190326E+05	0.61723506E+01	
C_2HO				
0.42603635E+01	0.48274243E-02	-0.16661974E-05	0.26140685E-09	-0.15325901E-13
0.17880484E+05	0.39788463E+01	0.27659287E+01	0.14174259E-01	-0.23260615E-04
0.21573491E-07	-0.75853929E-11	0.18085633E+05	0.10540898E+02	
C_2H_2				
0.44367704E+01	0.53760391E-02	-0.19128167E-05	0.32863789E-09	-0.21567095E-13
0.25667664E+05	-0.28003383E+01	0.20135622E+01	0.15190446E-01	-0.16163189E-04
0.90789918E-08	-0.19127460E-11	0.26124443E+05	0.88053779E+01	
H_2C_2				
0.42780340E+01	0.47562804E-02	-0.16301009E-05	0.25462806E-09	-0.14886379E-13
0.48316688E+05	0.64023701E+00	0.32815483E+01	0.69764791E-02	-0.23855244E-05
-0.12104432E-08	0.98189545E-12	0.48621794E+05	0.59203910E+01	
C_2H_2O				
0.60388174E+01	0.58048405E-02	-0.19209538E-05	0.27944846E-09	-0.14588675E-13
-0.85834023E+04	-0.76575813E+01	0.29749708E+01	0.12118712E-01	-0.23450457E-05
-0.64666850E-08	0.39056492E-11	-0.76326367E+04	0.86735525E+01	
C_2H_3				
0.59334679E+01	0.40177456E-02	-0.39667395E-06	-0.14412665E-09	0.23786435E-13
0.33854346E+05	-0.85303125E+01	0.24592764E+01	0.73714764E-02	0.21098729E-05
-0.13216421E-08	-0.11847838E-11	0.35352250E+05	0.11556202E+02	
CH_3CO				
0.59447731E+01	0.78667205E-02	-0.28865882E-05	0.47270875E-09	-0.28599861E-13
-0.37873075E+04	-0.50136751E+01	0.41634257E+01	-0.23261610E-03	0.34267820E-04
-0.44105227E-07	0.17275612E-10	-0.26574529E+04	0.73468280E+01	

Table B.1, continued

CH_2CHO				
0.59756699E+01	0.81305914E-02	-0.27436245E-05	0.40703041E-09	-0.21760171E-13
0.49032178E+03	-0.50320879E+01	0.34090624E+01	0.10738574E-01	0.18914925E-05
0.71585831E-08	0.28673851E-11	0.15214766E+04	0.95714535E+01	
$CHCH_2O$				
0.48131470E+00	0.20711914E-01	-0.12693155E-04	0.34579642E-08	-0.35399703E-12
0.15648642E+05	0.34629876E+02	0.10854772E+01	0.12845259E-01	0.24138660E-05
-0.44642672E-08	-0.29381916E-12	0.15910655E+05	0.33395312E+02	
C_2H_4				
0.35284188E+01	0.11485184E-01	-0.44183853E-05	0.78446005E-09	-0.52668485E-13
0.44282886E+04	0.22303891E+01	-0.86148798E+00	0.27961628E-01	-0.33886772E-04
0.27851522E-07	-0.97378789E-11	0.55730459E+04	0.24211487E+02	
CH_3CHO				
0.54041108E+01	0.11723059E-01	-0.42263137E-05	0.68372451E-09	-0.40984863E-13
-0.22593122E+05	-0.34807917E+01	0.47294595E+01	-0.31932858E-02	0.47534921E-04
-0.57458611E-07	0.21931112E-10	-0.21572878E+05	0.41030159E+01	
C_2H_4O				
0.54887641E+01	0.12046190E-01	-0.43336931E-05	0.70028311E-09	-0.41949088E-13
-0.91804251E+04	-0.70799605E+01	0.37590532E+01	-0.94412180E-02	0.80309721E-04
-0.10080788E-06	0.40039921E-10	-0.75608143E+04	0.78497475E+01	
C_2H_5				
0.42878814E+01	0.12433893E-01	-0.44139119E-05	0.70654102E-09	-0.42035136E-13
0.12056455E+05	0.84602583E+00	0.43058580E+01	-0.41833638E-02	0.49707270E-04
-0.59905874E-07	0.23048478E-10	0.12841714E+05	0.47100236E+01	
C_2H_5O				
0.60114346E+01	0.12165219E-01	-0.40449604E-05	0.59076588E-09	-0.30969595E-13
-0.49366992E+04	-0.67901798E+01	0.17302504E+01	0.16908489E-01	0.39996221E-05
-0.13711180E-07	0.57643603E-11	-0.32922483E+04	0.17336115E+02	
C_2H_5OO				
8.05957692E+00	1.52921019E-02	-5.54442603E-06	9.00496195E-10	-5.41302799E-14
-7.31028500E+03	-1.59992904E+01	5.21694144E+00	1.24160003E-04	6.15529492E-05
-7.94505636E-08	3.12101317E-11	-5.41455775E+03	4.22381533E+00	
C_2H_4OOH				
9.74660000E+00	0.01084240E+00	-3.13022000E-06	3.83694000E-10	-1.60474000E-14
-3.94819063E+02	-2.07656245E+01	2.10863000E+00	0.03341860E+00	-2.66198000E-05
1.03835000E-08	-1.41770000E-12	1.56528996E+03	1.81813376E+01	
C_2H_5OOH				
8.11695000E+00	0.02202100E+00	-9.45634000E-06	1.82565000E-09	-1.29627000E-13
-1.56095534E+04	-3.53065721E+00	2.16432000E+00	0.03722840E+00	-2.24491000E-05
5.87162000E-09	-3.70193000E-13	-1.38390827E+04	2.75891189E+01	
C_2H_6				
0.48259382E+01	0.13840429E-01	-0.45572588E-05	0.67249672E-09	-0.35981614E-13
-0.12717793E+05	-0.52395067E+01	0.14625387E+01	0.15494667E-01	0.57805073E-05
-0.12578319E-07	0.45862671E-11	-0.11239176E+05	0.14432295E+02	
C_3H				
0.34671283E+01	0.62969122E-02	-0.22708676E-05	0.36749291E-09	-0.22034692E-13
0.80801495E+05	0.53527629E+01	0.24726647E+01	0.85316627E-02	-0.63505996E-05
0.56681332E-08	-0.24832298E-11	0.81205573E+05	0.10875808E+02	
C_3H_2				
0.62476406E+01	0.56755154E-02	-0.19541329E-05	0.31686787E-09	-0.19722328E-13
0.54930960E+05	-0.96791278E+01	0.36613541E+01	0.89364130E-02	0.35404269E-05
-0.11072967E-07	0.52009416E-11	0.55858605E+05	0.46695742E+01	
C_3H_2L				
0.62476406E+01	0.56755154E-02	-0.19541329E-05	0.31686787E-09	-0.19722328E-13
0.70900772E+05	-0.63712327E+01	0.36613541E+01	0.89364130E-02	0.35404269E-05
-0.11072967E-07	0.52009416E-11	0.71828416E+05	0.79774693E+01	
C_3H_2O				
0.73427625E+01	*0.12067202E-01*	-0.55529699E-05	0.11293460E-08	-0.83762953E-13
0.10395715E+05	-0.10092804E+02	*0.16316510E+01*	0.27150964E-01	-0.19877387E-04
0.69551387E-08	-0.95779851E-12	0.12058104E+05	*0.19713200E+02*	
C_3H_3				
0.66416953E+01	0.80859651E-02	-0.28479238E-05	0.45353447E-09	-0.26888535E-13
0.38979395E+05	-0.10400071E+02	0.18283782E+01	0.23784171E-01	-0.21923663E-04
0.10007755E-07	-0.13902579E-11	0.40186308E+05	0.13844912E+02	

Table B.1, continued

C_3H_3O				
-0.10468154E+02	0.55926446E-01	-0.43825050E-04	0.15212914E-07	-0.19412007E-11
0.10792313E+05	0.83799606E+02	-0.48203077E+01	0.72770886E-01	-0.12882854E-03
0.11082336E-06	-0.35040429E-10	0.77740146E+04	0.46847744E+02	
C_3H_4(A)				
0.63168722E+01	0.11133728E-01	-0.39629378E-05	0.63564238E-09	-0.37875540E-13
0.20117495E+05	-0.10995766E+02	0.26130445E+01	0.12122575E-01	0.18539880E-04
-0.34525149E-07	0.15335079E-10	0.21541567E+05	0.10226139E+02	
C_3H_4(B)				
0.66999931E+01	0.10357372E-01	-0.34551167E-05	0.50652949E-09	-0.26682276E-13
0.30199051E+05	-0.13378770E+02	-0.24621047E-01	0.23197215E-01	-0.18474357E-05
-0.15927593E-07	0.86846155E-11	0.32334137E+05	0.22729762E+02	
C_3H_4(P)				
0.60252400E+01	0.11336542E-01	-0.40223391E-05	0.64376063E-09	-0.38299635E-13
0.19620942E+05	-0.86043785E+01	0.26803869E+01	0.15799651E-01	0.25070596E-05
-0.13657623E-07	0.66154285E-11	0.20802374E+05	0.98769351E+01	
C_3H_4O				
0.48353180E+01	0.19772601E-01	-0.10426628E-04	0.26525803E-08	-0.26278207E-12
-0.11557837E+05	0.18853144E+01	0.11529584E+01	0.28040214E-01	-0.15072153E-04
0.15905842E-08	0.84930371E-12	-0.10417694E+05	0.21453279E+02	
C_3H_5(A)				
0.09651539E+02	0.08075596E-01	-0.07965424E-05	-0.04650696E-08	0.08603281E-12
0.15300955E+05	-0.02837848E+03	0.02276486E+02	0.01985564E+00	0.11238421E-05
-0.10145757E-07	0.03441342E-10	0.01789496E+06	0.12214139E+02	
C_3H_5(B)				
0.58332834E+01	0.12053083E-01	-0.45275706E-05	0.77268597E-09	-0.49209084E-13
0.26693604E+05	-0.75762634E+01	-0.13750135E+01	0.33668146E-01	-0.30147869E-04
0.15517156E-07	-0.35801507E-11	0.28654535E+05	0.29379906E+02	
C_3H_5(S)				
0.09209764E+02	0.07871412E-01	-0.07724522E-05	-0.04497357E-08	0.08377272E-12
0.02853967E+06	-0.02383444E+03	0.03161863E+02	0.15180997E-01	0.02722659E-04
-0.05177112E-07	0.05435286E-12	0.03095547E+06	0.10468980E+02	
C_3H_5(T)				
0.09101018E+02	0.07964167E-01	-0.07884945E-05	-0.04562036E-08	0.08529212E-12
0.02670680E+06	-0.02301634E+03	0.03385811E+02	0.14045337E-01	0.03204127E-04
-0.03824120E-07	-0.09053742E-11	0.02909066E+06	0.09755734E+02	
C_3H_5O				
0.91206991E+01	0.12196117E-01	-0.42929777E-05	0.12616892E-08	-0.15705367E-12
0.91765012E+04	-0.22071447E+02	0.70599393E+00	0.25629797E-01	0.71080411E-05
-0.29693495E-07	0.14360721E-10	0.11909268E+05	0.23610039E+02	
AC_3H_5O				
0.72554278E+01	0.15458520E-01	-0.55798138E-05	0.90356727E-09	-0.54203987E-13
-0.52833268E+04	-0.11180177E+02	0.39944373E+01	0.40814746E-02	0.52034636E-04
-0.70009530E-07	0.27882479E-10	-0.33976925E+04	0.10569296E+02	
PC_3H_5O				
0.30445698E+01	0.23236429E-01	-0.86317936E-05	0.14799550E-08	-0.96860829E-13
-0.61787211E+04	0.13122302E+02	0.67368294E+01	-0.26945299E-02	0.49927017E-04
-0.50025808E-07	0.15011503E-10	-0.65703366E+04	-0.23398732E+01	
TC_3H_5O				
0.30445698E+01	0.23236429E-01	-0.86317936E-05	0.14799550E-08	-0.96860829E-13
-0.18787211E+04	0.13122302E+02	0.67368294E+01	-0.26945299E-02	0.49927017E-04
-0.50025808E-07	0.15011503E-10	-0.28703366E+04	-0.23398732E+01	
C_3H_6				
0.67213974E 01	0.14931757E-01	-0.49652353E-05	0.72510753E-09	-0.38001476E-13
-0.92453149E 03	-0.12155617E 02	0.14575157E 01	0.21142263E-01	0.40468012E-05
-0.16319003E-07	0.70475153E-11	0.10740208E 04	0.17399460E 02	
C_3H_6(B)				
0.58450527E+01	0.12029104E-01	-0.45115135E-05	0.76846424E-09	-0.48833377E-13
0.36199324E+04	-0.94565125E+01	-0.13128302E+01	0.33271749E-01	-0.29288560E-04
0.14753097E-07	-0.33411952E-11	0.55778149E+04	0.27295834E+02	
C_3H_6O				
0.86900558E 01	0.16020987E-01	-0.53971753E-05	0.79941542E-09	-0.42656366E-13
-0.15420691E 05	-0.22485016E 02	0.48733836E 00	0.28519690E-01	0.30096162E-05
-0.22652642E-07	0.10706728E-10	-0.12556434E 05	0.22605270E 02	

Table B.1, continued

AC_3H_6O				
0.72975991E+01	0.17566207E-01	-0.63170456E-05	0.10203086E-08	-0.61094016E-13
-0.29817680E+05	-0.12756981E+02	0.55557943E+01	-0.28365428E-02	0.70568945E-04
-0.87810488E-07	0.34028266E-10	-0.28113337E+05	0.23226600E+01	
PC_3H_6O				
0.33137982E+01	0.26619606E-01	-0.10475596E-04	0.18815334E-08	-0.12761310E-12
-0.25459603E+05	0.96608447E+01	0.76044596E+01	-0.86403564E-02	0.73930097E-04
-0.79687398E-07	0.28004927E-10	-0.25489789E+05	-0.67643691E+01	
C_3H_7(I)				
0.65294638E 01	0.17193288E-01	-0.57153220E-05	0.83408080E-09	-0.43663532E-13
0.77179102E 04	-0.91399021E 01	0.14461584E 01	0.20988975E-01	0.77172672E-05
-0.18481391E-07	0.71269024E-11	0.98206094E 04	0.20108200E 02	
C_3H_7(N)				
0.77026987E 01	0.16044203E-01	-0.52833220E-05	0.76298590E-09	-0.39392284E-13
0.82984336E 04	-0.15480180E 02	0.10515518E 01	0.25991980E-01	0.23800540E-05
-0.19609569E-07	0.93732470E-11	0.10631863E 05	0.21122559E 02	
C_3H_7O(I)				
5.91439000E+00	0.01846630E+00	-4.98451000E-06	6.40412000E-10	-3.20232000E-14
-1.66797208E+04	-1.46724157E+01	-2.22399000E+00	0.04403710E+00	-2.67359000E-05
7.96277000E-10	4.22750000E-12	-1.49671484E+04	2.57335809E+01	
C_3H_7O(N)				
0.84124958E+01	0.19520193E-01	-0.71317071E-05	0.12393621E-08	-0.82483889E-13
-0.87750718E+04	-0.18293360E+02	0.91452571E+00	0.33601264E-01	-0.12282254E-04
-0.10739947E-08	0.72924952E-12	-0.61847956E+04	0.22563171E+02	
C_3H_6OH				
0.87109009E+01	0.20803801E-01	-0.73841230E-05	0.11817484E-08	-0.70349614E-13
-0.13443662E+05	-0.18900965E+02	0.52779942E+01	0.80866061E-03	0.82154818E-04
-0.10848818E-06	0.43488690E-10	-0.11153823E+05	0.57052684E+01	
C_3H_7OO(I)				
1.29559000E+01	0.01098820E+00	-1.76802000E-06	1.60542000E-13	1.61298000E-14
-2.17793474E+04	-5.01676340E+01	-2.30776000E+00	0.06011690E+00	-7.36773000E-05
5.77586000E-08	-1.96759000E-11	-1.76114813E+04	2.77661282E+01	
C_3H_7OO(N)				
4.37086000E+00	0.02486060E+00	-8.90963000E-06	1.53903000E-09	-1.01327000E-13
-1.61560158E+04	-2.17260156E+00	-1.12969000E+00	0.05171790E+00	-5.83115000E-05
4.62978770E-08	-1.66124000E-11	-1.55043287E+04	2.28756317E+01	
C_3H_6OOH				
1.04261000E+01	0.01986670E+00	-7.57865000E-06	1.39283000E-09	-9.78846000E-14
-7.00601038E+03	-2.35589652E+01	2.48084000E+00	0.04244040E+00	-3.70179000E-05
2.45427000E-08	-8.47681000E-12	-4.64619947E+03	1.78489795E+01	
C_3H_8				
0.75252171E+01	0.18890340E-01	-0.62839244E-05	0.91793728E-09	-0.48124099E-13
-0.16464547E+05	-0.17843903E+02	0.89692080E+00	0.26689861E-01	0.54314251E-05
-0.21260007E-07	0.92433301E-11	-0.13954918E+05	0.19355331E+02	
C_3H_7OOH(I)				
8.62986000E+00	0.02400270E+00	-7.67920000E+00	1.15165000E-09	-6.59811000E-14
-2.81140584E+04	-1.27886356E+01	-0.72388600E+00	0.06342950E+00	-7.17611000E-05
5.20421000E-08	-1.70164000E-11	-2.64456077E+04	3.17130241E+01	
C_3H_7OOH(N)				
1.06984000E+01	0.02197610E+00	-8.27900000E-06	1.45810000E-09	-9.77969000E-14
-2.70831806E+04	-2.53658958E+01	0.45972700E+00	0.05496020E+00	-5.60910000E-05
4.00601000E-08	-1.36525000E-11	-2.43387836E+04	2.68035941E+01	
C_4H				
0.62428318E+01	0.61936825E-02	-0.20859315E-05	0.30822034E-09	-0.16364825E-13
0.94300187E+05	-0.72108059E+01	0.50232468E+01	0.70923753E-02	-0.60737619E-08
-0.22757522E-08	0.80869941E-12	0.94858125E+05	-0.69425940E-01	
C_4H_2				
0.86670035E+01	0.67166371E-02	-0.23544995E-05	0.37383079E-09	-0.22118914E-13
0.52878439E+05	-0.21114205E+02	-0.39518508E+00	0.51955813E-01	-0.91786616E-04
0.80523929E-07	-0.26917088E-10	0.54473214E+05	0.20969101E+02	
C_4H_2O				
0.10268878E+02	0.04896164E-01	-0.04885080E-05	-0.02708566E-08	0.05107013E-12
0.02346902E+06	-0.02815985E+03	0.04810971E+02	0.13139988E-01	0.09865073E-05
-0.06120720E-07	0.16400028E-11	0.02545803E+06	0.02113424E+02	

Table B.1, continued

C_4H_3(I)				
0.84874201E+01	0.86908937E-02	-0.28544437E-05	0.41200798E-09	-0.21301093E-13
0.54044069E+05	-0.19018509E+02	0.35539713E+01	0.19461986E-01	-0.48102484E-05
-0.97301225E-08	0.62390535E-11	0.55527377E+05	0.70829868E+01	
C_4H_3(N)				
0.10752738E+02	0.05381153E-01	-0.05549637E-05	-0.03052266E-08	0.05761740E-12
0.05881419E+06	-0.03163025E+03	0.04153881E+02	0.01726287E+00	-0.02389374E-05
-0.10187000E-07	0.04340504E-10	0.06098070E+06	0.04136506E+02	
C_4H_4				
0.88921490E+01	0.10908850E-01	-0.35949597E-05	0.51934190E-09	-0.26808921E-13
0.29966522E+05	-0.21726944E+02	0.21403370E+01	0.24605047E-01	-0.36391657E-05
-0.15304014E-07	0.88964608E-11	0.32056170E+05	0.14282477E+02	
C_4H_4O				
0.16174722E+01	0.37716053E-01	-0.23935409E-04	0.72674178E-08	-0.84449082E-12
0.17129492E+04	0.13399043E+02	-0.33123374E+01	0.54107033E-01	-0.48252157E-04
0.26132914E-07	-0.68544311E-11	0.30042001E+04	0.38434387E+02	
C_4H_5(I)				
0.72559180E 01	0.17141310E-01	-0.74350450E-05	0.16410520E-08	-0.15360780E-12
0.36339860E 05	-0.13420580E 02	0.10251400E 02	-0.25627670E-01	0.10715090E-03
-0.11090190E-06	0.37550050E-10	0.37128550E 05	-0.20574530E 02	
C_4H_5(S)				
0.40734210E 01	0.24907370E-01	-0.13229540E-04	0.34159060E-08	-0.34874460E-12
0.33975420E 05	0.43252930E 01	-0.19509230E 01	0.53281440E-01	-0.65306770E-04
0.46994220E-07	-0.14204880E-10	0.35048460E 05	0.32542460E 02	
C_4H_5(T)				
0.72559180E 01	0.17141310E-01	-0.74350450E-05	0.16410520E-08	-0.15360780E-12
0.40227410E 05	-0.12422830E 02	-0.20329280E 01	0.53630530E-01	-0.63382690E-04
0.40641440E-07	-0.10398020E-10	0.42219650E 05	0.32787830E 02	
$CH_3CHCHCO$				
7.20816000E+00	0.01974410E+00	-8.03095000E-06	1.54947000E-09	-1.12589000E-13
1.49335189E+03	-9.84439589E+00	-0.04646880E+00	0.04464570E+00	-4.14281000E-05
2.23551000E-08	-5.10438000E-12	3.22651472E+03	2.63785173E+01	
$CH_2CHCHCHO$				
9.08201000E+00	0.01599680E+00	-5.71687000E-06	1.04776000E-09	-7.65010000E-14
9.53163434E+03	-1.67260364E+01	4.22772000E+00	0.02276020E+00	-1.76272000E-06
-7.77497000E-09	3.00788000E-12	1.12749806E+04	1.02355507E+01	
C_4H_6(B)				
0.77061882E+01	0.15477240E-01	-0.22161657E-05	-0.17662189E-08	0.57283106E-12
0.25267377E+05	-0.15592457E+02	-0.19918253E+02	0.17644100E+00	-0.35904226E-03
0.33266232E-06	-0.11036895E-09	0.29933167E+05	0.10893895E+03	
C_4H_6(F)				
0.80465832E+01	0.16485251E-01	-0.55222272E-05	0.81235929E-09	-0.42950784E-13
0.16201305E+05	-0.18017740E+02	0.31971083E+01	0.20255916E-01	0.65101922E-05
-0.16584423E-07	0.64002822E-11	0.18215203E+05	0.99088230E+01	
C_4H_6(M)				
0.80465832E+01	0.16485251E-01	-0.55222272E-05	0.81235929E-09	-0.42950784E-13
0.13701305E+05	-0.18017740E+02	0.31971083E+01	0.20255916E-01	0.65101922E-05
-0.16584423E-07	0.64002822E-11	0.15715203E+05	0.99088230E+01	
C_4H_6(S)				
0.17815570E 02	-0.42575020E-02	0.10511850E-04	-0.44738440E-08	0.58481380E-12
0.12673420E 05	-0.69826620E 02	0.10234670E 01	0.34959190E-01	-0.22009050E-04
0.69422720E-08	-0.78791870E-12	0.18117990E 05	0.19750660E 02	
C_4H_6(T)				
0.71309430E 01	0.20640080E-01	-0.93239060E-05	0.21473070E-08	-0.20613610E-12
0.96126540E 04	-0.14172220E 02	-0.25309000E 01	0.53879690E-01	-0.51739330E-04
0.25107200E-07	-0.43247260E-11	0.11876910E 05	0.33913880E 02	
AC_4H_6O				
0.81249151E+01	0.22126706E-01	-0.94601701E-05	0.18463787E-08	-0.13361886E-12
-0.28950586E+04	-0.12988613E+02	0.65807557E+00	0.45671389E-01	-0.39022765E-04
0.19641071E-07	-0.44435727E-11	-0.93304871E+03	0.24973042E+02	
BC_4H_6O				
0.81249151E+01	0.22126706E-01	-0.94601701E-05	0.18463787E-08	-0.13361886E-12
-0.16010285E+05	-0.12988613E+02	0.65807557E+00	0.45671389E-01	-0.39022765E-04
0.19641071E-07	-0.44435727E-11	-0.14048275E+05	0.24973042E+02	

Table B.1, continued

C_4H_7(I)				
0.90657617E+01	0.19477743E-01	-0.73385554E-05	0.12863733E-08	-0.85601393E-13
0.10187905E+05	-0.24022063E+02	-0.34391326E+01	0.67889035E-01	-0.92118162E-04
0.75423011E-07	-0.25411345E-10	0.13278011E+05	0.37956421E+02	
C_4H_7(N)				
0.11184356E+02	0.14457868E-01	-0.44852630E-05	0.73693834E-09	-0.48752824E-13
0.17987671E+05	-0.32095703E+02	0.21544552E+01	0.21568453E-01	0.29077822E-04
-0.54719830E-07	0.23710092E-10	0.21387008E+05	0.18934394E+02	
C_4H_7(S)				
0.42197530E 01	0.28824510E-01	-0.13992130E-04	0.33407180E-08	-0.32264270E-12
0.12662950E 05	0.32531110E 01	-0.21523140E+01	0.55474240E-01	-0.62267150E-04
0.45930560E-07	-0.14922970E-10	0.14074430E 05	0.34211030E 02	
C_4H_7O(M)				
0.10201164E+02	0.20773985E-01	-0.78691839E-05	0.13913117E-08	-0.93376086E-13
0.12268093E+04	-0.26399888E+02	0.45826315E+01	0.19154338E-01	0.27729464E-04
-0.45646819E-07	0.18456024E-10	0.38386017E+04	0.72739076E+01	
C_4H_7O(X)				
0.10201164E+02	0.20773985E-01	-0.78691839E-05	0.13913117E-08	-0.93376086E-13
0.12268093E+04	-0.26399888E+02	0.45826315E+01	0.19154338E-01	0.27729464E-04
-0.45646819E-07	0.18456024E-10	0.38386017E+04	0.72739076E+01	
C_4H_8(I)				
0.44609470E+01	0.29611487E-01	-0.13077129E-04	0.26571934E-08	-0.20134713E-12
-0.50066758E+04	0.10803180E+01	0.26471405E+01	0.25902957E-01	0.81985354E-05
-0.22193259E-07	0.88958580E-11	-0.40373069E+04	0.12689550E+02	
C_4H_8(N)				
0.20535841E+01	0.34350507E-01	-0.15883197E-04	0.33089662E-08	-0.25361045E-12
-0.21397231E+04	0.15556360E+02	0.11811380E+01	0.30853380E-01	0.50865247E-05
-0.24654888E-07	0.11110193E-10	-0.17904004E+04	0.21075639E+02	
C_4H_8(S)				
0.11097383E+01	0.35542578E-01	-0.16481703E-04	0.34412202E-08	-0.26411468E-12
-0.26507607E+04	0.19366680E+02	0.24108791E+01	0.25147773E-01	0.98473047E-05
-0.22716758E-07	0.86585895E-11	-0.27758694E+04	0.14097700E+02	
C_4H_8O(M)				
6.58851000E+00	3.06657000E-02	-1.37822000E-05	2.73418000E-09	-1.97934000E-13
-2.97125499E+04	-5.50469103E+00	1.03169000E+00	4.28083000E-02	-2.18245000E-05
4.17674000E-09	-5.77108000E-14	-2.79349478E+04	2.42431025E+01	
C_4H_8O(X)				
0.12941058E+02	0.19981990E-01	-0.75877303E-05	0.13521897E-08	-0.91405872E-13
-0.21867511E+05	-0.45899493E+02	-0.14293192E+01	0.50569206E-01	-0.18756927E-04
-0.14736866E-07	0.10838963E-10	-0.17231486E+05	0.30995365E+02	
C_4H_9(I)				
9.43040607E+00	2.34271349E-02	-8.53599182E-06	1.39748355E-09	-8.44057456E-14
2.14214862E+03	-2.42207994E+01	3.54885235E+00	1.78747638E-02	5.00782825E-05
-7.94475071E-08	3.35802354E-11	4.74011588E+03	1.11849382E+01	
C_4H_9(N)				
9.18975615E+00	2.36322267E-02	-8.64270985E-06	1.42770515E-09	-8.70203716E-14
3.37702909E+03	-2.15600560E+01	5.82430540E+00	5.50309080E-03	7.49300330E-05
-1.02085943E-07	4.13484714E-11	5.54078049E+03	2.17609509E+00	
C_4H_9(S)				
0.88057265E+01	0.23630381E-01	-0.84564737E-05	0.13612584E-08	-0.81313232E-13
0.37941169E+04	-0.19996770E+02	0.46457042E+01	0.79313214E-02	0.70027013E-04
-0.95973349E-07	0.38628890E-10	0.62341181E+04	0.79642808E+01	
C_4H_9(T)				
6.63074656E+00	2.59353745E-02	-9.37163111E-06	1.51845890E-09	-9.11190863E-14
2.00861323E+03	-9.20581440E+00	6.87327133E+00	-1.85146306E-02	1.30560116E-04
-1.50832755E-07	5.65358282E-11	4.10958938E+03	2.30016604E-01	
C_4H_8OH(I)				
7.37014000E+00	0.03128650E+00	-1.35602000E-05	2.69870000E-09	-1.97930000E-13
-1.82435272E+04	-7.44862060E+00	-0.00684524E+00	0.05327470E+00	-3.87130000E-05
1.61902000E-08	-3.06998000E-12	-1.62748403E+04	3.03188340E+01	
$O_2C_4H_9O$				
1.33582000E+01	2.90148000E-02	-1.07482000E-05	1.83665000E-09	-1.17392000E-13
-3.56868203E+04	-3.51695449E+01	1.82318000E+00	6.02283000E-02	-3.93916000E-05
1.20365000E-08	-1.18284000E-12	-3.25476232E+04	2.44861624E+01	

Table B.1, continued

$C_4H_{10}(I)$				
0.10854125E 02	0.23317061E-01	-0.77685427E-05	0.11348074E-08	-0.59397203E-13
-0.21728570E 05	-0.35915939E 02	0.54559016E 00	0.37825324E-01	0.56197796E-05
-0.30570963E-07	0.14058456E-10	-0.18034047E 05	0.21129608E 02	
$C_4H_{10}(N)$				
0.10525002E 02	0.23590874E-01	-0.78538906E-05	0.11456114E-08	-0.59930956E-13
-0.20495137E 05	-0.32192017E 02	0.15764151E 01	0.34589723E-01	0.69701609E-05
-0.28163637E-07	0.12375117E-10	-0.17147004E 05	0.17872742E 02	
C_5H				
0.86957493E+01	0.60543008E-02	-0.20160105E-05	0.28928926E-09	-0.14700995E-13
0.90310687E+05	-0.21029110E+02	0.16348248E+01	0.25095381E-01	-0.12066364E-04
-0.10465111E-07	0.88099883E-11	0.92124875E+05	0.15135100E+02	
C_5H_2				
0.11329175E+02	0.74240565E-02	-0.26281887E-05	0.40825410E-09	-0.23013326E-13
0.78787062E+05	-0.36184340E+02	0.30623217E+01	0.27099982E-01	-0.10091697E-04
-0.12727451E-07	0.91672191E-11	0.81149687E+05	0.70842413E+01	
$C_5H_3(L)$				
0.10296658E+02	0.10470124E-01	-0.37746103E-05	0.61077326E-09	-0.36621089E-13
0.63439389E+05	-0.27338507E+02	0.15946538E+01	0.43378369E-01	-0.56253789E-04
0.41304029E-07	-0.12456939E-10	0.65491079E+05	0.15644812E+02	
$C_5H_4(L)$				
0.91465524E+01	0.12847056E-01	-0.32463853E-05	0.39700433E-09	-0.19573305E-13
0.48925483E+05	-0.20999841E+02	0.17646776E+01	0.45425568E-01	-0.58400827E-04
0.43937642E-07	-0.13555336E-10	0.50224909E+05	0.13861447E+02	
C_5H_4O				
0.78759394E+01	0.21847971E-01	-0.97307748E-05	0.19727830E-08	-0.14729530E-12
-0.22396951E+04	-0.19478951E+02	-0.30239186E+01	0.52338127E-01	-0.44466007E-04
0.22263462E-07	-0.52930564E-11	0.94996960E+03	0.37214970E+02	
C_5H_5				
0.10844072E+02	0.15392831E-01	-0.55630422E-05	0.90189440E-09	-0.54156619E-13
0.26950886E+05	-0.35254983E+02	-0.95902849E+00	0.31396777E-01	0.26724050E-04
-0.68942183E-07	0.33301983E-10	0.30779441E+05	0.29072780E+02	
$C_5H_5(L)$				
0.94095519E+01	0.13173708E-01	-0.40061435E-05	0.59642775E-09	-0.35402340E-13
0.43967887E+05	-0.21271166E+02	0.22059680E+01	0.39193876E-01	-0.40875017E-04
0.25229634E-07	-0.65871791E-11	0.45603065E+05	0.14330572E+02	
C_5H_4OH				
0.82749834E+01	0.25455624E-01	-0.11891672E-04	0.20921516E-08	-0.16007544E-13
0.65311050E+04	-0.18165775E+02	-0.75077271E+01	0.86810358E-01	-0.99664867E-04
0.56890869E-07	-0.12613540E-10	0.97140107E+04	0.58272274E+02	
C_5H_5O				
0.73219724E+01	0.26217271E-01	-0.10394357E-04	0.69805534E-09	0.30307525E-12
0.86725078E+04	-0.13395977E+02	-0.91274900E+01	0.89092843E-01	-0.98929631E-04
0.55164946E-07	-0.12054646E-10	0.12050769E+05	0.66558670E+02	
C_5H_5OO				
1.14805000E+01	2.25948000E-02	-9.51644000E-06	1.83251000E-09	-1.31169000E-13
1.62102820E+04	-3.21849683E+01	-4.58515000E+00	7.73026000E-02	-8.07651000E-05
4.43467000E-08	-9.92770000E-12	2.00023440E+04	4.79868764E+01	
C_5H_6				
0.99757848E+01	0.18905543E-01	-0.68411461E-05	0.11099340E-08	-0.66680236E-13
0.11081693E+05	-0.32209454E+02	0.86108957E+00	0.14804031E-01	0.72108895E-04
-0.11338055E-06	0.48689972E-10	0.14801755E+05	0.21353453E+02	
$C_5H_6(L)$				
0.18941353E+02	0.85102411E-02	-0.14014643E-05	0.00000000E+00	0.00000000E+00
0.23852123E+05	-0.77403470E+02	-0.56457147E+00	0.48115796E-01	-0.23131123E-04
0.00000000E+00	0.00000000E+00	0.30647513E+05	0.28139042E+02	
C_5H_5OH				
9.82793000E+00	2.35754000E-02	-9.71203000E-06	1.81889000E-09	-1.27086000E-13
-9.36197969E+03	-2.69588354E+01	-3.88538000E+00	6.34038000E-02	-4.97493000E-05
1.76587000E-08	-1.94281000E-12	-5.81392072E+03	4.31335835E+01	
C_5H_7				
0.12785659E+02	0.16457862E-01	-0.48399641E-05	0.73814083E-09	-0.46000369E-13
0.13869296E+05	-0.44346243E+02	-0.27323095E+01	0.40890569E-01	0.16006014E-04
-0.56085466E-07	0.26970736E-10	0.19024806E+05	0.40179407E+02	

Table B.1, continued

C_5H_7(I)				
7.17295000E+00	2.74828000E-02	-1.25234000E-05	2.51195000E-09	-1.83816000E-13
3.43404120E+04	-8.47072535E+00	2.70639000E+00	3.76025000E-02	-1.95473000E-05
3.85395000E-09	-6.81935000E-14	3.57297975E+04	1.52991891E+01	
C_5H_7(X)				
0.18941353E+02	0.85102411E-02	-0.14014643E-05	0.00000000E+00	0.00000000E+00
0.18109184E+05	-0.78403470E+02	-0.56457147E+00	0.48115796E-01	-0.23131123E-04
0.00000000E+00	0.00000000E+00	0.24904574E+05	0.27439042E+02	
C_5H_8				
0.77244792E+01	0.28322316E-01	-0.11545236E-04	0.21540815E-08	-0.15054178E-12
-0.78261573E+03	-0.19769698E+02	0.26898140E+01	0.20954550E-02	0.11303687E-03
-0.15408070E-06	0.62763658E-10	0.23139663E+04	0.15294056E+02	
C_5H_8(I)				
0.10991663E+02	0.22439484E-01	-0.81159626E-05	0.13948336E-08	-0.92194080E-13
0.40581428E+04	-0.32980170E+02	-0.36106649E+01	0.74856698E-01	-0.83303221E-04
0.52256651E-07	-0.13581639E-10	0.74967178E+04	0.39483975E+02	
C_5H_8(X)				
0.19403114E+02	0.96325407E-02	-0.15683147E-05	0.00000000E+00	0.00000000E+00
0.20635571E+03	-0.80798713E+02	-0.30882087E+00	0.48355898E-01	-0.22284758E-04
0.00000000E+00	0.00000000E+00	0.72982329E+04	0.26828785E+02	
C_5H_8(Y)				
1.11022000E+01	2.28513000E-02	-8.98032000E-06	1.61660000E-09	-1.09797000E-13
1.22104780E+04	-3.18752809E+01	9.34603000E-02	5.29732000E-02	-4.12327000E-05
1.86634000E-08	-3.97959000E-12	1.54213197E+04	2.54598704E+01	
C_5H_9(A)				
1.04022000E+01	2.41043000E-02	-7.91174000E-06	1.22229000E-09	-7.19975000E-14
7.30885155E+03	-2.84631187E+01	-7.06449000E-01	5.67071000E-02	-3.95469000E-05
1.18621000E-08	-5.42788000E-13	1.00953595E+04	2.80585844E+01	
C_5H_9(B)				
1.04022000E+01	2.41043000E-02	-7.91174000E-06	1.22229000E-09	-7.19975000E-14
7.30885155E+03	-2.86555652E+01	-7.06449000E-01	5.67071000E-02	-3.95469000E-05
1.18621000E-08	-5.42788000E-13	1.00953595E+04	2.78661379E+01	
C_5H_{10}(A)				
0.10169614E+02	0.29142736E-01	-0.11304015E-04	0.20426202E-08	-0.13964602E-12
-0.97185802E+04	-0.27826511E+02	0.15343285E+01	0.40535723E-01	0.26841152E-05
-0.27784359E-07	0.12941501E-10	-0.66019829E+04	0.20108917E+02	
C_5H_{10}(B)				
0.86980441E+01	0.30551374E-01	-0.11746424E-04	0.21071085E-08	-0.14329275E-12
-0.99867755E+04	-0.19723898E+02	0.12618252E+01	0.39178857E-01	0.31182431E-05
-0.25702067E-07	0.11609951E-10	-0.72175421E+04	0.21915280E+02	
C_5H_{11}(T)				
0.67232314E 01	0.36074004E-01	-0.14425089E-04	0.26385814E-08	-0.18130546E-12
-0.66929018E 03	-0.68507985E 01	0.18160004E 01	0.25384068E-01	0.46807718E-04
-0.70666410E-07	0.27488045E-10	0.19643507E 04	0.24638344E 02	
C_6H_2				
0.12532801E+02	0.87766321E-02	-0.31329616E-05	0.50371820E-09	-0.30071921E-13
0.79784338E+05	-0.38858580E+02	-0.54109216E+00	0.74532628E-01	-0.13578252E-03
0.12226630E-06	-0.41825207E-10	0.82115132E+05	0.21882710E+02	
C_6H_3				
0.12761181E+02	0.10385573E-01	-0.34791929E-05	0.51097326E-09	-0.26909651E-13
0.74777062E+05	-0.38917450E+02	0.50070896E+01	0.26928518E-01	-0.59198655E-05
-0.15272335E-07	0.94083101E-11	0.77132000E+05	0.22256212E+01	
$C_6H_3O_2$				
0.11714051E+02	0.22368333E-01	-0.87467425E-05	0.16844693E-08	-0.12537519E-12
0.12842145E+05	-0.33979273E+02	0.94789958E-01	0.52498885E-01	-0.32214180E-04
0.46879378E-08	0.18273026E-11	0.16077207E+05	0.26397580E+02	
$C_6H_3O_3$				
0.11714051E+02	0.22368333E-01	-0.87467425E-05	0.16844693E-08	-0.12537519E-12
-0.13760712E+05	-0.33979273E+02	0.94789958E-01	0.52498885E-01	-0.32214180E-04
0.46879378E-08	0.18273026E-11	-0.10525651E+05	0.26397580E+02	
C_6H_4				
0.10582770E+02	0.15914908E-01	-0.58202018E-05	0.95108725E-09	-0.57425956E-13
0.52834650E+05	-0.32571269E+02	0.28042240E+00	0.26170563E-01	0.29996638E-04
-0.63979566E-07	0.29103081E-10	0.56470786E+05	0.24784179E+02	

Table B.1, continued

C_6H_4L				
0.17183117E+02	0.66487658E-02	-0.12416263E-05	0.14697448E-09	-0.91398013E-14
0.55076954E+05	-0.64435183E+02	0.19323139E+01	0.39032183E-01	-0.69227109E-05
-0.27093357E-07	0.15730252E-10	0.59691948E+05	0.16516023E+02	
$C_6H_4O_2$				
0.11714051E+02	0.22368333E-01	-0.87467425E-05	0.16844693E-08	-0.12537519E-12
-0.19796139E+05	-0.33979273E+02	0.94789958E-01	0.52498885E-01	-0.32214180E-04
0.46879378E-08	0.18273026E-11	-0.16561077E+05	0.26397580E+02	
C_6H_5				
0.11433509E+02	0.17014805E-01	-0.58358992E-05	0.88020347E-09	-0.47983644E-13
0.34541625E+05	-0.38578339E+02	-0.22878075E+01	0.42416330E-01	-0.17666744E-05
-0.31422520E-07	0.16505464E-10	0.38870789E+05	0.35398270E+02	
$C_6H_5(A)$				
0.13411768E+02	0.14720221E-01	-0.50817705E-05	0.79886354E-09	-0.46950844E-13
0.59503716E+05	-0.42652032E+02	0.77929707E+00	0.54372126E-01	-0.47873814E-04
0.16187164E-07	0.33735744E-12	0.62650312E+05	0.21128592E+02	
$C_6H_5(B)$				
0.13411768E+02	0.14720221E-01	-0.50817705E-05	0.79886354E-09	-0.46950844E-13
0.66050312E+05	-0.41652032E+02	0.77929707E+00	0.54372126E-01	-0.47873814E-04
0.16187164E-07	0.33735744E-12	0.68596908E+05	0.22128592E+02	
C_6H_5O				
0.13833984E 02	0.17618403E-01	-0.60696257E-05	0.91988173E-09	-0.50449181E-13
-0.69212549E 03	-0.50392990E 02	-0.18219433E 01	0.48122510E-01	-0.46792302E-05
-0.34018594E-07	0.18649637E-10	0.42429180E 04	0.33526199E 02	
C_6H_5OO				
0.13245706E+02	0.22882751E-01	-0.94618800E-05	0.19371947E-08	-0.15135284E-12
0.12626493E+05	-0.41416844E+02	-0.97590288E+00	0.62119843E-01	-0.47723103E-04
0.17150270E-07	-0.21186880E-11	0.16573495E+05	0.32136878E+02	
C_6H_6				
0.12910740E+02	0.17232966E-01	-0.50242106E-05	0.58934968E-09	-0.19475212E-13
0.36645117E+04	-0.50026993E+02	-0.31380119E+01	0.47231030E-01	-0.29622079E-05
-0.32628190E-07	0.17186919E-10	0.88900312E+04	0.36575729E+02	
$C_6H_6(A)$				
0.13411768E+02	0.14720221E-01	-0.50817705E-05	0.79886354E-09	-0.46950844E-13
0.43917676E+05	-0.41652032E+02	0.77929707E+00	0.54372126E-01	-0.47873814E-04
0.16187164E-07	0.33735744E-12	0.47064288E+05	0.22128592E+02	
$C_6H_6(B)$				
0.13411768E+02	0.14720221E-01	-0.50817705E-05	0.79886354E-09	-0.46950844E-13
0.44417676E+05	-0.41652032E+02	0.77929707E+00	0.54372126E-01	-0.47873814E-04
0.16187164E-07	0.33735744E-12	0.47564288E+05	0.22128592E+02	
$C_6H_6(D)$				
0.13411768E+02	0.14720221E-01	-0.50817705E-05	0.79886354E-09	-0.46950844E-13
0.34835236E+05	-0.42652032E+02	0.77929707E+00	0.54372126E-01	-0.47873814E-04
0.16187164E-07	0.33735744E-12	0.37981848E+05	0.21128592E+02	
$C_6H_6(F)$				
0.13411768E+02	0.14720221E-01	-0.50817705E-05	0.79886354E-09	-0.46950844E-13
0.20846783E+05	-0.46451032E+02	0.77929707E+00	0.54372126E-01	-0.47873814E-04
0.16187164E-07	0.33735744E-12	0.23993395E+05	0.17329458E+02	
$C_6H_6(M)$				
0.13411768E+02	0.14720221E-01	-0.50817705E-05	0.79886354E-09	-0.46950844E-13
0.34835236E+05	-0.46451032E+02	0.77929707E+00	0.54372126E-01	-0.47873814E-04
0.16187164E-07	0.33735744E-12	0.37981848E+05	0.17329458E+02	
$C_6H_6(S)$				
0.13411768E+02	0.14720221E-01	-0.50817705E-05	0.79886354E-09	-0.46950844E-13
0.42134058E+05	-0.42652032E+02	0.77929707E+00	0.54372126E-01	-0.47873814E-04
0.16187164E-07	0.33735744E-12	0.45280670E+05	0.21128592E+02	
C_6H_5OH				
0.14943568E+02	0.18317845E-01	-0.61606479E-05	0.91048524E-09	-0.48410806E-13
-0.18386828E+05	-0.56096741E+02	-0.16677656E+01	0.52091170E-01	-0.67895007E-05
-0.36257116E-07	0.20586241E-10	-0.13287539E+05	0.32421951E+02	
C_6H_5OOH				
0.14917584E+02	0.23788571E-01	-0.94469171E-05	0.18964860E-08	-0.14478335E-12
-0.61700302E+04	-0.51578972E+02	-0.47238694E+01	0.85935761E-01	-0.81948755E-04
0.38915954E-07	-0.71680488E-11	-0.12851064E+04	0.47619104E+02	

Table B.1, continued

C_6H_7				
0.12801758E+02	0.21924749E-01	-0.79713001E-05	0.12972935E-08	-0.78100416E-13
0.17889539E+05	-0.45804341E+02	-0.10303140E+00	0.34393354E-01	0.39788466E-04
-0.85116612E-07	0.39012224E-10	0.22425515E+05	0.26022350E+02	
C_6H_7(L)				
0.13532274E+02	0.21389740E-01	-0.86673463E-05	0.16190540E-08	-0.11331597E-12
0.40693867E+05	-0.43202858E+02	-0.29128010E+01	0.75948097E-01	-0.81558552E-04
0.48383356E-07	-0.12099709E-10	0.44863027E+05	0.39691467E+02	
$C_5H_4CH_3$				
3.10980000E+00	0.04390870E+00	-2.52118000E-05	6.89967000E-09	-7.30437000E-13
2.16797341E+04	6.40658286E+00	-0.59153000E+01	0.07101713E+00	-4.16800000E-05
-5.66878006E-09	1.02333000E-11	2.35893842E+04	5.13239841E+01	
C_6H_8				
0.11779870E+02	0.25519980E-01	-0.92666947E-05	0.15068122E-08	-0.90658701E-13
0.65486686E+04	-0.41618805E+02	0.17265319E+01	0.14887612E-01	0.94809230E-04
-0.14083394E-06	0.58859873E-10	0.11021297E+05	0.19130886E+02	
$C_5H_5CH_3$				
0.16399698E+02	0.18988824E-01	-0.60996114E-05	0.95861755E-09	-0.59364731E-13
0.48834021E+04	-0.65341031E+02	-0.35829269E+01	0.78077845E-01	-0.73143499E-04
0.33645368E-07	-0.48086229E-11	0.10447644E+05	0.37418709E+02	
C_7H_5				
-0.25877289E+02	0.11646476E+00	-0.87117420E-04	0.28873247E-07	-0.35003265E-11
0.70325651E+05	0.15948605E+03	-0.22098993E+02	0.20414677E+00	-0.37352796E-03
0.32017644E-06	-0.99853313E-10	0.64621256E+05	0.11589723E+03	
C_6H_5C				
0.13411768E+02	0.14720221E-01	-0.50817705E-05	0.79886354E-09	-0.46950844E-13
0.829068400+05	-0.44902032E+02	0.77929707E+00	0.54372126E-01	-0.47873814E-04
0.16187164E-07	0.33735744E-12	0.860531700+05	0.18870992E+02	
C_6H_5CO				
1.76223084E+01	1.60979487E-02	-5.58040273E-06	8.74961227E-10	-5.11367998E-14
4.62690108E+03	-6.76753115E+01	-0.24315751E+01	0.68883315E-01	-0.71578368E-04
0.47745015E-07	-0.13654692E-10	0.11290687E+05	0.38843224E+02	
C_7H_6				
0.98222523E+01	0.33532158E-01	-0.18960140E-04	0.51221400E-08	-0.52916027E-12
0.39350844E+05	-0.23534618E+02	0.10617721E+01	0.60266692E-01	-0.48446786E-04
0.18895387E-07	-0.27898133E-11	0.41581770E+05	0.20963522E+02	
C_6H_5CH				
0.14943568E+02	0.18317845E-01	-0.61606479E-05	0.91048524E-09	-0.48410806E-13
0.488624260+05	-0.55778711E+02	-0.16677656E+01	0.52091170E-01	-0.67895007E-05
-0.36257116E-07	0.20586241E-10	5.39792429E+04	0.32731046E+02	
C_7H_6O				
0.13650737E+02	0.25680419E-01	-0.10466729E-04	0.19413430E-08	-0.13483792E-12
-0.11019744E+05	-0.47965796E+02	-0.31627334E+01	0.66369245E-01	-0.34816353E-04
-0.62999377E-08	0.85807101E-11	-0.61169349E+04	0.40231735E+02	
C_7H_7				
0.44194999E+01	0.44936005E-01	-0.25128857E-04	0.67524586E-08	-0.70487436E-12
0.22388117E+05	0.59883118E-01	0.28736699E+01	0.19180268E-01	0.68807836E-04
-0.91760405E-07	0.31172908E-10	0.23752270E+05	0.14393669E+02	
C_7H_7L				
0.14859274E+02	0.20012869E-01	-0.65044005E-05	0.87259461E-09	-0.24558031E-13
4.96436965E+04	-0.54048538E+02	-0.49989891E+00	0.70203640E-01	-0.69530965E-04
0.36911000E-07	-0.78679745E-11	5.34754207E+04	0.23319450E+02	
C_7H_7P				
0.61164446E+01	0.37172936E-01	-0.17377082E-04	0.38637173E-08	-0.33652253E-12
0.32063559E+05	-0.52912521E+01	-0.30223730E+01	0.58008973E-01	-0.23549926E-04
-0.77298736E-08	0.57327021E-11	0.34526535E+05	0.42435081E+02	
C_7H_7O				
-0.93710709E+00	0.63711032E-01	-0.39299259E-04	0.11217669E-07	-0.12150759E-11
0.11671887E+05	0.31596107E+02	-0.19170570E+01	0.64069577E-01	-0.35999619E-04
0.71819772E-08	0.14239142E-12	0.12110132E+05	0.37362877E+02	
OC_7H_7				
0.20294542E+02	0.16513433E-01	-0.47580565E-05	0.45180912E-09	-0.11270264E-14
-0.74899214E+04	-0.86606987E+02	-0.29244521E+01	0.72308660E-01	-0.52679799E-04
0.18029228E-07	-0.22330289E-11	-0.14259766E+03	0.36648621E+02	

Table B.1, continued

C_7H_7OA				
0.67097492E+01	0.48694473E-01	-0.27823204E-04	0.78128171E-08	-0.86293505E-12
0.49669780E+04	-0.10103596E+02	-0.33987746E+01	0.76359227E-01	-0.54388864E-04
0.18070734E-07	-0.21114070E-11	0.77835742E+04	0.42234520E+02	
C_7H_7OO				
-0.93281174E+00	0.65896519E-01	-0.39371462E-04	0.10397939E-07	-0.10142513E-11
0.11800492E+05	0.34893871E+02	-0.22901354E+01	0.74780665E-01	-0.57139834E-04
0.24316888E-07	-0.46916273E-11	0.11894288E+05	0.40549713E+02	
OOC_7H_7P				
0.19196302E+02	0.31294353E-01	-0.11452624E-04	0.20944079E-08	-0.15138942E-12
0.82063937E+04	-0.76888449E+02	-0.67796676E+01	0.99132130E-01	-0.77043901E-04
0.31111080E-07	-0.54388908E-11	0.15930566E+05	0.59154706E+02	
C_7H_8				
0.12940034E+02	0.26691287E-01	-0.96838505E-05	0.15738629E-08	-0.94663601E-13
-0.69764908E+03	-0.46728785E+02	0.16152663E+01	0.21099438E-01	0.85366018E-04
-0.13261066E-06	0.55956604E-10	0.40756300E+04	0.20282210E+02	
C_7H_8OA				
0.67097492E+01	0.48694473E-01	-0.27823204E-04	0.78128171E-08	-0.86293505E-12
-0.13702736E+05	-0.10103596E+02	-0.33987746E+01	0.76359227E-01	-0.54388864E-04
0.18070734E-07	-0.21114070E-11	-0.10886140E+05	0.42234520E+02	
C_7H_7OH				
1.84559079E+01	2.22510477E-02	-7.62434516E-06	1.18587731E-09	-6.89131821E-14
-2.14701621E+04	-7.36645670E+01	-3.90996428E+00	7.51258327E-02	-5.54992358E-05
2.09665376E-08	-3.21729662E-12	-1.37964122E+04	4.61826228E+01	
HOC_7H_7				
0.15932987E+02	0.27011160E-01	-0.99448722E-05	0.16296689E-08	-0.98513298E-13
-0.23592065E+05	-0.59732841E+02	0.42258267E+00	0.45551636E-01	0.32012513E-04
-0.81121959E-07	0.37665658E-10	-0.18202621E+05	0.26032903E+02	
C_8H_2				
0.17007524E+02	0.93656848E-02	-0.30485718E-05	0.47653534E-09	-0.29169032E-13
0.10628021E+06	-0.59224564E+02	0.12470437E+01	0.78392526E-01	-0.12416148E-03
0.98381697E-07	-0.30063943E-10	0.10942891E+06	0.16048227E+02	
C_8H_5				
-0.25877289E+02	0.11646476E+00	-0.87117420E-04	0.28873247E-07	-0.35003265E-11
0.73093461E+05	0.15948605E+03	-0.22098993E+02	0.20414677E+00	-0.37352796E-03
0.32017644E-06	-0.99853313E-10	0.67389086E+05	0.11589723E+03	
$C_8H_5(S)$				
-0.18226665E+02	0.98105334E-01	-0.71376540E-04	0.23047990E-07	-0.27072450E-11
0.70338272E+05	0.12116527E+03	-0.10600960E+02	0.12687966E+00	-0.19579499E-03
0.15129409E-06	-0.42934854E-10	0.65782034E+05	0.69241891E+02	
C_8H_5O				
-0.93281174E+00	0.65896519E-01	-0.39371462E-04	0.10397939E-07	-0.10142513E-11
3.05316083E+04	0.34911564E+02	-0.22901354E+01	0.74780665E-01	-0.57139834E-04
0.24316888E-07	-0.46916273E-11	3.06253876E+04	0.40549713E+02	
$C_6H_5C_2O$				
0.20618816E+02	0.35127148E-01	-0.11830690E-04	0.18073995E-08	-0.10553787E-12
0.25660497E+05	-0.62079517E+02	-0.58980299E+01	0.10341065E+00	-0.76758084E-04
0.29731117E-07	-0.48860931E-11	0.33701971E+05	0.77152836E+02	
C_8H_5OO				
0.72644663E+01	0.64415999E-01	-0.40800824E-04	0.12573261E-07	-0.14875518E-11
0.469593922+05	-0.10363039E+02	-0.17338693E+00	0.81105933E-01	-0.52993211E-04
0.15621797E-07	-0.15957625E-11	0.49374248E+05	0.29398981E+02	
C_8H_6				
0.63306952E+01	0.42378012E-01	-0.23660930E-04	0.63243646E-08	-0.65648718E-12
0.33083576E+05	-0.90218239E+01	-0.53688774E+01	0.86102039E-01	-0.85647887E-04
0.45469992E-07	-0.98395866E-11	0.35633689E+05	0.48312672E+02	
C_6H_5CHC				
0.19091084E+02	0.20300338E-01	-0.49055789E-05	-0.35590797E-09	0.19770557E-12
0.49628926E+05	-0.78016373E+02	-0.37720504E+01	0.75885393E-01	-0.52863394E-04
0.16847499E-07	-0.17698074E-11	0.56778117E+05	0.43053817E+02	
C_8H_7				
0.95205498E+01	0.40670000E-01	-0.20274416E-04	0.48689093E-08-	0.45740218E-12
0.43069902E+05	-0.26648735E+02	-0.46888218E+01	0.81018507E-01	-0.61910330E-04
0.23259584E-07	-0.33512908E-11	0.46964366E+05	0.46568810E+02	

Table B.1, continued

C_8H_7(F)				
0.19091084E+02	0.20300338E-01	-0.49055789E-05	-0.35590797E-09	0.19770557E-12
0.26016494E+05	-0.75737373E+02	-0.37720504E+01	0.75885393E-01	-0.52863394E-04
0.16847499E-07	-0.17698074E-11	0.33165690E+05	0.45346817E+02	
C_8H_7(P)				
0.19091084E+02	0.20300338E-01	-0.49055789E-05	-0.35590797E-09	0.19770557E-12
0.38798926E+05	-0.75737373E+02	-0.37720504E+01	0.75885393E-01	-0.52863394E-04
0.16847499E-07	-0.17698074E-11	0.45948117E+05	0.45346817E+02	
C_7H_7CO				
1.26038000E+01	3.33593000E-02	-1.44002000E-05	2.78057000E-09	-1.98701000E-13
2.58669379E+03	-3.55117704E+01	1.10174000E-01	6.12662000E-02	-3.77800000E-05
1.46302000E-08	-3.78725000E-12	6.67543875E+03	3.15214011E+01	
C_8H_8				
0.57468890E+01	0.48250760E-01	-0.25794920E-04	0.65860550E-08	-0.65297670E-12
0.13434980E+05	-0.60621620E+01	0.11784510E+01	0.35972650E-01	0.63202020E-04
-0.12341850E-06	0.57205890E-10	0.15406210E+05	0.22145280E+02	
C_8H_8O(M)				
1.33854000E+01	3.53266000E-02	-1.50672000E-05	2.87426000E-09	-2.02717000E-13
-1.51760183E+04	-4.28055694E+01	-4.37384000E+00	8.47585000E-02	-6.27872000E-05
2.06700000E-08	-1.91568000E-12	-1.03324041E+04	4.87953419E+01	
C_8H_9				
0.71588910E 01	0.48848290E-01	-0.25544540E-04	0.64046460E-08	-0.62730240E-12
0.13474790E 05	-0.12686970E 02	-0.82283280E 01	0.10714390E 00	-0.11722610E-03
0.76758390E-07	-0.22156920E-10	0.16992210E 05	0.63080510E 02	
C_8H_9(F)				
0.71588910E 01	0.48848290E-01	-0.25544540E-04	0.64046460E-08	-0.62730240E-12
0.18404509E 05	-0.12686970E 02	-0.82283280E 01	0.10714390E 00	-0.11722610E-03
0.76758390E-07	-0.22156920E-10	0.21921930E 05	0.63080510E 02	
C_8H_9(M)				
1.40904000E+01	3.34162000E-02	-1.36208000E-05	2.48172000E-09	-1.67811000E-13
1.47022475E+04	-4.87057111E+01	8.98762000E-01	4.11473000E-02	3.81527000E-05
-7.00591000E-08	2.61632000E-11	1.96395049E+04	2.63985665E+01	
C_8H_9O(M)				
1.20596000E+01	4.21281000E-02	-1.84653000E-05	3.55112000E-09	-2.51153000E-13
3.33124997E+03	-3.37400371E+01	-2.10428000E+00	7.44752000E-02	-4.21088000E-05
9.14138000E-09	-2.09407000E-13	7.79683244E+03	4.17013732E+01	
C_8H_{10}				
0.38789780E 01	0.58100590E-01	-0.31963800E-04	0.84489930E-08	-0.86948250E-12
-0.50249220E 03	0.38370990E 01	-0.72668450E 01	0.10030890E 00	-0.96517150E-04
0.55659080E-07	-0.14533700E-10	0.19872900E 04	0.58577460E 02	
C_8H_{10}(M)				
0.15268401E 02	0.34433573E-01	-0.13685810E-04	0.21177802E-08	-0.11564062E-12
-0.61602461E 04	-0.59529587E 02	-0.16422014E 01	0.58058664E-01	0.55675910E-05
-0.45693085E-07	0.21727536E-10	0.10412372E 03	0.34509140E 02	
C_8H_9OH(M)				
1.64879000E+01	3.47428000E-02	-1.38802000E-05	2.52034000E-09	-1.71391000E-13
-2.46619117E+04	-5.86702285E+01	-6.26716000E-01	6.41014000E-02	-1.85925000E-05
-1.03598000E-08	5.18900000E-12	-1.85078723E+04	3.55041828E+01	
C_9H_6O				
0.96623449E+01	0.53666491E-01	-0.25417114E-04	0.53300617E-08	-0.41042373E-12
1.53026445E+04	-2.65172482E+01	-0.27220635E+01	0.90556584E-01	-0.64442655E-04
0.22269356E-07	-0.28298546E-11	1.84993395E+04	0.36548115E+02	
C_9H_7				
0.18554959E+02	0.25035076E-01	-0.91457509E-05	0.14934838E-08	-0.90133030E-13
0.25721156E+05	-0.76300347E+02	-0.26698729E+01	0.62177216E-01	0.15067018E-04
-0.79645699E-07	0.40918972E-10	0.32386969E+05	0.37861193E+02	
C_9H_7L				
0.65095673E+01	0.63953526E-01	-0.38239246E-04	0.10942234E-07	-0.12007314E-11
0.58874355E+05	-0.11384365E+02	-0.10330565E+01	0.86296454E-01	-0.63314656E-04
0.23692641E-07	-0.36760152E-11	0.60911453E+05	0.27281731E+02	
C_9H_7O				
0.64210854E+01	0.64163864E-01	-0.38415004E-04	0.11003850E-07	-0.12084466E-11
0.10845017E+05	-0.14263958E+02	-0.12375939E+01	0.87553047E-01	-0.65906068E-04
0.25852191E-07	-0.42962066E-11	0.12878259E+05	0.24819180E+02	

Table B.1, continued

C_9H_8				
0.17318671E+02	0.28982768E-01	-0.10605059E-04	0.17334553E-08	-0.10467919E-12
0.11151429E+05	-0.71555323E+02	-0.68190289E+00	0.41658733E-01	0.70741234E-04
-0.13430875E-06	0.59915845E-10	0.17705036E+05	0.29781396E+02	
C_9H_8(S)				
0.65095673E+01	0.63953526E-01	-0.38239246E-04	0.10942234E-07	-0.12007314E-11
0.29786072E+05	-0.11384365E+02	-0.10330565E+01	0.86296454E-01	-0.63314656E-04
0.23692641E-07	-0.36760152E-11	0.31823168E+05	0.27281731E+02	
C_9H_8(T)				
0.61635380E+01	0.64800575E-01	-0.38971957E-04	0.11208408E-07	-0.12352123E-11
0.30968227E+05	-0.91820068E+01	-0.12068161E+01	0.87362073E-01	-0.65509172E-04
0.25519633E-07	-0.42003471E-11	0.32918797E+05	0.28408627E+02	
C_9H_9(C)				
0.63778563E+01	0.64488344E-01	-0.38863003E-04	0.11196405E-07	-0.12342460E-11
0.29844754E+05	-0.79087715E+01	-0.19958377E-01	0.80526829E-01	-0.52920732E-04
0.16153127E-07	-0.17739016E-11	0.31777998E+05	0.25758848E+02	
C_9H_9(F)				
0.63778563E+01	0.64488344E-01	-0.38863003E-04	0.11196405E-07	-0.12342460E-11
0.37915477E+05	-0.79087715E+01	-0.19958377E-01	0.80526829E-01	-0.52920732E-04
0.16153127E-07	-0.17739016E-11	0.39848723E+05	0.25758848E+02	
C_9H_9(I)				
0.63778563E+01	0.64488344E-01	-0.38863003E-04	0.11196405E-07	-0.12342460E-11
0.39311918E+05	-0.79087715E+01	-0.19958377E-01	0.80526829E-01	-0.52920732E-04
0.16153127E-07	-0.17739016E-11	0.41245164E+05	0.25758848E+02	
C_9H_9(N)				
0.61302528E+01	0.64880349E-01	-0.39039340E-04	0.11232336E-07	-0.12382503E-11
0.41447309E+05	-0.35904160E+01	-0.13012929E+01	0.87944902E-01	-0.66716180E-04
0.26528754E-07	-0.44908213E-11	0.43398613E+05	0.34233109E+02	
C_9H_9(P)				
0.63778563E+01	0.64488344E-01	-0.38863003E-04	0.11196405E-07	-0.12342460E-11
0.40309031E+05	-0.79087715E+01	-0.19958377E-01	0.80526829E-01	-0.52920732E-04
0.16153127E-07	-0.17739016E-11	0.42242277E+05	0.25758848E+02	
C_9H_9(S)				
0.64646387E+01	0.64067192E-01	-0.38341088E-04	0.10980433E-07	-0.12058170E-11
0.24235473E+05	-0.15099373E+02	-0.11953660E+01	0.87286167E-01	-0.65343927E-04
0.25376810E-07	-0.41583087E-11	0.26278357E+05	0.24035862E+02	
$C_{10}H_6$				
0.13678861E+02	0.34992404E-01	-0.15291209E-04	0.30199132E-08	-0.22002695E-12
0.57626840E+05	-0.44705902E+02	0.35246079E+01	0.60800310E-01	-0.37046779E-04
0.90492041E-08	-0.14741740E-12	0.60607137E+05	0.84791813E+01	
$C_{10}H_6O_2$				
0.22727753E+02	0.43812073E-01	-0.17862083E-04	0.32897970E-08	-0.22638566E-12
-0.64286992E+04	-9.48827156E+01	-0.49985988E+01	0.11278945E+00	-0.72481576E-04
0.11138080E-07	0.52180972E-11	1.90028483E+03	0.50861947E+02	
$C_{10}H_7$				
0.12082234E+02	0.40327162E-01	-0.18103172E-04	0.36466918E-08	-0.26948368E-12
0.41458590E+05	-0.39890186E+02	-0.21620619E+01	0.74107781E-01	-0.44805129E-04
0.11957607E-07	-0.14147860E-11	0.45864543E+05	0.35592331E+02	
$C_{10}H_7L$				
0.20179207E+02	0.29670304E-01	-0.11986855E-04	0.22532105E-08	-0.15916158E-12
0.65061531E+05	-0.80279839E+02	-0.27711501E+01	0.98102115E-01	-0.93714450E-04
0.50875709E-07	-0.12535519E-10	0.71358156E+05	0.37574230E+02	
$C_{10}H_7M$				
0.65410190E+01	0.53486425E-01	-0.29065039E-04	0.74644158E-08	-0.74340073E-12
0.68869992E+05	-0.52155113E+01	-0.10437305E+01	0.67275584E-01	-0.30733951E-04
-0.58702049E-09	0.27725385E-11	0.71426141E+05	0.36028225E+02	
$C_{10}H_7O$				
0.64573956E+01	0.53688969E-01	-0.29238150E-04	0.75265669E-08	-0.75136674E-12
0.88888809E+04	-0.76713142E+01	-0.10527838E+01	0.67329355E-01	-0.30843101E-04
-0.49683690E-09	0.27467763E-11	0.11420077E+05	0.33169201E+02	
$C_{10}H_7OO$				
1.94198000E+01	3.44120000E-02	-1.41794000E-05	2.75337000E-09	-2.00551000E-13
1.78603581E+04	-7.36370390E+01	-4.40270000E+00	1.03367000E-01	-8.54871000E-05
3.36537000E-08	-4.80820000E-12	2.41710387E+04	4.84736134E+01	

Table B.1, continued

$C_{10}H_8$				
0.19726501E+02	0.28167639E-01	-0.96896429E-05	0.14654855E-08	-0.80134955E-13
0.85581797E+04	-0.86036400E+02	-0.46547480E+01	0.74611127E-01	-0.53069607E-05
-0.54125859E-07	0.29066527E-10	0.16325324E+05	0.45018630E+02	
$C_{10}H_8G$				
0.19726501E+02	0.28167639E-01	-0.96896429E-05	0.14654855E-08	-0.80134955E-13
0.37803781E+05	-0.86036400E+02	-0.46547480E+01	0.74611127E-01	-0.53069607E-05
-0.54125859E-07	0.29066527E-10	0.45570926E+05	0.45018630E+02	
$C_{10}H_8J$				
0.19726501E+02	*0.28167639E-01*	-0.96896429E-05	0.14654855E-08	-0.80134955E-13
0.37322689E+05	-0.86036400E*+02*	*-0.46547480E+01*	*0.*74611127E-01	-0.53069607E-05
-0.54125859E-07	0.29066527E-10	0.45089833E+05	*0.45018630E+02*	
$C_{10}H_8K$				
0.11772461E+02	0.57660352E-01	-0.30821095E-04	0.75626927E-08	-0.70893232E-12
0.32469912E+05	-0.40646545E+02	-0.44647784E+01	0.11770219E+00	-0.11535290E-03
0.60753699E-07	-0.13172704E-10	0.36058523E+05	0.39126045E+02	
$C_{10}H_8L$				
0.20179207E+02	0.29670304E-01	-0.11986855E-04	0.22532105E-08	-0.15916158E-12
0.36023766E+05	-0.80279839E+02	-0.27711501E+01	0.98102115E-01	-0.93714450E-04
0.50875709E-07	-0.12535519E-10	0.42320391E+05	0.37574230E+02	
$C_9H_6CH_2$				
0.19196302E+02	0.31294353E-01	-0.11452624E-04	0.20944079E-08	-0.15138942E-12
0.22725338E+05	-0.82727289E+02	-0.67796676E+01	0.99132130E-01	-0.77043901E-04
0.31111080E-07	-0.54388908E-11	0.30449510E+05	0.53315855E+02	
$C_{10}H_7OH$				
2.08930252E+01	3.10560066E-02	-1.14407562E-05	1.87872866E-09	-1.13823881E-13
-1.35886443E+04	-8.88597101E+01	-2.08768263E+00	7.68099506E-02	-1.53593023E-05
-4.04657632E-08	2.33759779E-11	-6.29056385E+03	3.43331051E+01	
$C_{10}H_9$				
0.68115206E+01	0.65562524E-01	-0.41825122E-04	0.12954322E-07	-0.15378892E-11
0.33704418E+05	-0.17856285E+02	-0.42732394E+00	0.82983948E-01	-0.57861042E-04
0.20382418E-07	-0.31126404E-11	0.36035789E+05	0.20662096E+02	
$C_{10}H_9A$				
0.66120329E+01	0.63693613E-01	-0.38005401E-04	0.10854013E-07	-0.11889092E-11
0.48451477E+05	-0.85609169E+01	-0.12000567E+01	0.87316290E-01	-0.65407883E-04
0.25431104E-07	-0.41740856E-11	0.50539168E+05	0.31368935E+02	
$C_{10}H_9B$				
0.72644663E+01	0.64415999E-01	-0.40800824E-04	0.12573261E-07	-0.14875518E-11
0.44031582E+05	-0.10033039E+02	0.67291107E+01	0.65731078E-01	-0.41942687E-04
0.12989477E-07	-0.15416270E-11	0.45676203E+05	-0.10065762E+02	
$C_{10}H_9D$				
0.86939049E+01	0.55521198E-01	-0.26573391E-04	0.56274336E-08	-0.43778685E-12
0.57101551E+05	-0.16647057E+02	-0.36075311E+01	0.95335580E-01	-0.72291477E-04
0.27238373E-07	-0.38435700E-11	0.60013586E+05	0.45020737E+02	
$C_{10}H_9E$				
0.10033731E+02	0.52762281E-01	-0.24639734E-04	0.50493378E-08	-0.37425426E-12
0.54185570E+05	-0.25021866E+02	-0.26096890E+01	0.89858010E-01	-0.62988067E-04
0.21048692E-07	-0.24775707E-11	0.57484742E+05	0.39586952E+02	
$C_{10}H_9F$				
0.11772461E+02	0.57660352E-01	-0.30821095E-04	0.75626927E-08	-0.70893232E-12
0.57391734E+05	-0.40646545E+02	-0.44647784E+01	0.11770219E+00	-0.11535290E-03
0.60753699E-07	-0.13172704E-10	0.36924531E+05	0.39126045E+02	
$C_{10}H_9K$				
0.11772461E+02	0.57660352E-01	-0.30821095E-04	0.75626927E-08	-0.70893232E-12
0.57391734E+05	-0.40646545E+02	-0.44647784E+01	0.11770219E+00	-0.11535290E-03
0.60753699E-07	-0.13172704E-10	0.36924531E+05	0.39126045E+02	
$C_{10}H_9L$				
0.72644663E+01	0.64415999E-01	-0.40800824E-04	0.12573261E-07	-0.14875518E-11
0.49005121E+05	-0.10033039E+02	-0.17338693E+00	0.81105933E-01	-0.52993211E-04
0.15621797E-07	-0.15957625E-11	0.51421648E+05	0.29762981E+02	
$C_{10}H_9M$				
0.72644663E+01	0.64415999E-01	-0.40800824E-04	0.12573261E-07	-0.14875518E-11
0.48644285E+05	-0.10033039E+02	-0.17338693E+00	0.81105933E-01	-0.52993211E-04
0.15621797E-07	-0.15957625E-11	0.51054797E+05	0.29762981E+02	

Table B.1, continued

$C_{10}H_9P$				
0.96623449E+01	0.53666491E-01	-0.25417114E-04	0.53300617E-08	-0.41042373E-12
0.48876445E+05	-0.23922482E+02	-0.27220635E+01	0.90556584E-01	-0.64442655E-04
0.22269356E-07	-0.28298546E-11	0.52073395E+05	0.39207115E+02	
$C_{10}H_9T$				
0.61069269E+01	0.64933605E-01	-0.39081573E-04	0.11246288E-07	-0.12398898E-11
0.27354137E+05	-0.13169773E+02	-0.12790513E+01	0.87806582E-01	-0.66427318E-04
0.26285688E-07	-0.44205243E-11	0.29295166E+05	0.24432716E+02	
$C_9H_6CH_3$				
0.19196302E+02	0.31294353E-01	-0.11452624E-04	0.20944079E-08	-0.15138942E-12
0.21249827E+05	-0.82021862E+02	-0.67796676E+01	0.99132130E-01	-0.77043901E-04
0.31111080E-07	-0.54388908E-11	0.28973999E+05	0.54021292E+02	
$C_{10}H_{10}$				
0.86939049E+01	0.55521198E-01	-0.26573391E-04	0.56274336E-08	-0.43778685E-12
0.28114301E+05	-0.16647057E+02	-0.36075311E+01	0.95335580E-01	-0.72291477E-04
0.27238373E-07	-0.38435700E-11	0.31026338E+05	0.45020737E+02	
$C_{10}H_{10}F$				
0.10033731E+02	0.52762281E-01	-0.24639734E-04	0.50493378E-08	-0.37425426E-12
0.25138184E+05	-0.25021866E+02	-0.26096890E+01	0.89858010E-01	-0.62988067E-04
0.21048692E-07	-0.24775707E-11	0.28437354E+05	0.39586952E+02	
$C_{10}H_{10}K$				
0.11772461E+02	0.57660352E-01	-0.30821095E-04	0.75626927E-08	-0.70893232E-12
0.25217086E+05	-0.40646545E+02	-0.44647784E+01	0.11770219E+00	-0.11535290E-03
0.60753699E-07	-0.13172704E-10	0.28805697E+05	0.39126045E+02	
$C_9H_7CH_3$				
0.19196302E+02	0.31294353E-01	-0.11452624E-04	0.20944079E-08	-0.15138942E-12
0.82063937E+04	-0.76888449E+02	-0.67796676E+01	0.99132130E-01	-0.77043901E-04
0.31111080E-07	-0.54388908E-11	0.15930566E+05	0.59154706E+02	
$C_{11}H_7O$				
0.27231269E+02	0.26040644E-01	-0.10377854E-04	0.18715858E-08	-0.12636018E-12
0.81121090E+04	-0.12050997E+03	-0.31465258E+01	0.10679716E+00	-0.10968916E-03
0.69037351E-07	-0.18363943E-10	0.18071491E+05	0.40402345E+02	
$C_{11}H_8O$				
0.21204625E+02	0.40753532E-01	-0.17960043E-04	0.35348363E-08	-0.25728495E-12
-0.64059942E+04	-0.87076491E+02	-0.44640862E+01	0.10410496E+00	-0.54663804E-04
-0.13750550E-07	0.16040985E-10	0.88328263E+03	0.46924361E+02	
$C_{11}H_9$				
0.23571720E+02	0.29080150E-01	-0.94253200E-05	0.14375044E-08	-0.86432991E-13
0.21835987E+05	-0.10355592E+03	-0.55627434E+01	0.10663281E+00	-0.86584861E-04
0.36316999E-07	-0.62652074E-11	0.30429877E+05	0.48643127E+02	
$C_{11}H_9P$				
0.23571720E+02	0.29080150E-01	-0.94253200E-05	0.14375044E-08	-0.86432991E-13
0.31963483E+05	-0.10355592E+03	-0.55627434E+01	0.10663281E+00	-0.86584861E-04
0.36316999E-07	-0.62652074E-11	0.40557373E+05	0.48643127E+02	
$C_{11}H_9O$				
0.23571720E+02	0.29080150E-01	-0.94253200E-05	0.14375044E-08	-0.86432991E-13
0.11781769E+05	-0.10355592E+03	-0.55627434E+01	0.10663281E+00	-0.86584861E-04
0.36316999E-07	-0.62652074E-11	0.20375631E+05	0.48643127E+02	
$OC_{11}H_9$				
0.23571720E+02	0.29080150E-01	-0.94253200E-05	0.14375044E-08	-0.86432991E-13
-0.72797280E+03	-0.10355592E+03	-0.55627434E+01	0.10663281E+00	-0.86584861E-04
0.36316999E-07	-0.62652074E-11	0.78658888E+04	0.48643127E+02	
$AC_{11}H_9O$				
0.23571720E+02	0.29080150E-01	-0.94253200E-05	0.14375044E-08	-0.86432991E-13
0.76891553E+04	-0.10355592E+03	-0.55627434E+01	0.10663281E+00	-0.86584861E-04
0.36316999E-07	-0.62652074E-11	0.16283017E+05	0.48643127E+02	
$OOC_{11}H_9P$				
0.72920350E 01	0.92502000E-01	-0.51686410E-04	0.13627090E-07	-0.13811480E-11
2.73164660E 04	-1.27437380E 01	-0.13889580E 02	0.17209840E 00	-0.17006600E-03
0.96018880E-07	-0.23732530E-10	0.31998940E 05	0.90588360E 02	
$C_{11}H_{10}$				
0.20618816E+02	0.35127148E-01	-0.11830690E-04	0.18073995E-08	-0.10553787E-12
0.37591297E+04	-0.87356517E+02	-0.58980299E+01	0.10341065E+00	-0.76758084E-04
0.29731117E-07	-0.48860931E-11	0.11751871E+05	0.51882836E+02	

Table B.1, continued

$C_{11}H_{10}O$				
0.22727753E+02	0.43812073E-01	-0.17862083E-04	0.32897970E-08	-0.22638566E-12
-0.14723957E+05	-0.93448156E+02	-0.49985988E+01	0.11278945E+00	-0.72481576E-04
0.11138080E-07	0.52180972E-11	-0.63307633E+04	0.52433847E+02	
$AC_{11}H_{10}O$				
0.22727753E+02	0.43812073E-01	-0.17862083E-04	0.32897970E-08	-0.22638566E-12
-0.11238992E+05	-0.93448156E+02	-0.49985988E+01	0.11278945E+00	-0.72481576E-04
0.11138080E-07	0.52180972E-11	-0.28457983E+04	0.52433847E+02	
$HOC_{11}H_9$				
0.23571720E+02	0.29080150E-01	-0.94253200E-05	0.14375044E-08	-0.86432991E-13
-0.18046832E+05	-0.10355592E+03	-0.55627434E+01	0.10663281E+00	-0.86584861E-04
0.36316999E-07	-0.62652074E-11	-0.94529708E+04	0.48643127E+02	
$C_{12}H_{10}$				
0.24289017E 02	0.34006648E-01	-0.11722408E-04	0.17729298E-08	-0.96812532E-13
0.10287000E 05	-0.10802374E 03	-0.40739527E 01	0.86973310E-01	-0.42353613E-05
-0.64564460E-07	0.34150169E-10	0.19405965E 05	0.44741348E 02	
$1C_{12}H_{10}$				
2.36421335E+01	3.60544766E-02	-1.31138294E-05	2.13119639E-09	-1.28115416E-13
1.46625473E+04	-1.02784235E+02	-1.19668570E+00	7.06115758E-02	4.27863652E-05
-1.21989834E-07	5.83744402E-11	2.29191651E+04	3.30370914E+01	
$C_{12}H_{11}$				
2.45873044E+01	3.73929821E-02	-1.36001742E-05	2.21047875E-09	-1.32883841E-13
1.49850894E+04	-1.05426141E+02	-1.14973681E+00	7.78725206E-02	2.87023997E-05
-1.08719393E-07	5.37519164E-11	2.33370112E+04	3.42336399E+01	
$C_{12}H_{12}$				
2.53697727E+01	4.04594180E-02	-1.49784208E-05	2.46402471E-09	-1.49382751E-13
-8.20299732E+02	-1.14459910E+02	1.98405802E-02	6.20844325E-02	7.79624479E-05
-1.55438421E-07	6.85371120E-11	8.47514808E+03	2.80182938E+01	
$C_{14}H_{14}$				
0.72920350E 01	0.92502000E-01	-0.51686410E-04	0.13627090E-07	-0.13811480E-11
0.10316730E 05	-0.11327380E 02	-0.13889580E 02	0.17209840E 00	-0.17006600E-03
0.96018880E-07	-0.23732530E-10	0.15032340E 05	0.92707360E 02	
AR				
0.25000000E+01	0.00000000E+00	0.00000000E+00	0.00000000E+00	0.00000000E+00
-0.74537502E 03	0.43660006E 01	0.25000000E+01	0.00000000E+00	0.00000000E+00
0.00000000E+00	0.00000000E+00	-0.74537502E 03	0.43660006E 01	
NE				
0.25000000E 01	0.00000000E+00	0.00000000E+00	0.00000000E+00	0.00000000E+00
-0.74537500E 03	0.33553227E 01	0.25000000E 01	0.00000000E+00	0.00000000E+00
0.00000000E+00	0.00000000E+00	-0.74537498E 03	0.33553227E 01	
N_2				
0.29266400E+01	0.14879767E-02	-0.56847608E-06	0.10097038E-09	-0.67533513E-14
-0.92279767E+03	0.59805279E+01	0.32986769E+01	0.14082404E-02	-0.39632223E-05
0.56415153E-08	-0.24448549E-11	-0.10208999E+04	0.39503722E+01	
$AC_{12}H_8$				
1.93183637E+01	3.90205238E-02	-1.63352587E-05	3.10041991E-09	-2.19199281E-13
2.15445149E+04	-8.32372261E+01	-2.81264181E+00	7.04681002E-02	3.15341955E-05
-1.05176189E-07	5.08713845E-11	2.88462829E+04	3.75755975E+01	
$AC_{14}H_{10}$				
0.26567127E+02	0.39790904E-01	-0.14577610E-04	0.23850396E-08	-0.14413090E-12
0.14850923E+05	-0.12283160E+03	-0.15665980E+01	0.69536302E-01	0.78609880E-04
-0.17056214E-06	0.78003880E-10	0.24656643E+05	0.33282196E+02	
$PC_{14}H_{10}$				
0.26602474E+02	0.39769744E-01	-0.14572026E-04	0.23843296E-08	-0.14409548E-12
0.12132838E+05	-0.12266672E+03	-0.33646717E+01	0.85073271E-01	0.37531110E-04
-0.12664499E-06	0.61445705E-10	0.22019878E+05	0.40596218E+02	
C_9H_{12}				
2.35608000E+01	0.02668650E+00	-6.95019000E-06	7.47373000E-10	-4.29661000E-14
-1.01777000E+04	-1.00614900E+02	-1.59527000E+00	0.06990600E+00	4.89570000E-06
-5.78932000E-08	2.85139000E-11	-1.62220000E+03	3.64360000E+01	
$1C_9H_{11}$				
2.27377700E+01	0.03124470E+00	-1.26214000E-05	2.66750000E-09	-2.28703000E-13
6.54159400E+03	-9.73310770E+01	-1.47412000E+00	6.87621000E-02	8.17269000E-06
-6.17700000E-08	3.01092000E-11	1.51220940E+04	3.58219710E+01	

Table B.1, continued

$2C_9H_{11}$				
2.27377700E+01	0.03124470E+00	-1.26214000E-05	2.66750000E-09	-2.28703000E-13
1.34347000E+04	-9.66090770E+01	-1.47412000E+00	6.87621000E-02	8.17269000E-06
-6.17700000E-08	3.01092000E-11	2.19813150E+04	3.65449710E+01	
$3C_9H_{11}$				
2.27377700E+01	0.03124470E+00	-1.26214000E-05	2.66750000E-09	-2.28703000E-13
1.40364000E+04	-9.66090770E+01	-1.47412000E+00	6.87621000E-02	8.17269000E-06
-6.17700000E-08	3.01092000E-11	2.25837600E+04	3.65449710E+01	
$1C_9H_{10}$				
2.80789000E+01	0.01428560E+00	-1.5427000E-06	1.16379000E-10	-3.52139000E-14
1.26115410E+03	-1.26742300E+02	-2.5830800E+00	0.07596300E+00	-2.60832000E-05
-2.15095000E-08	1.46560000E-11	1.1732790E+04	3.91389000E+01	
$2C_9H_{10}$				
2.80789000E+01	0.01428560E+00	-1.5427000E-06	1.16379000E-10	-3.52139000E-14
1.26115410E+03	-1.26742300E+02	-2.5830800E+00	0.07596300E+00	-2.60832000E-05
-2.15095000E-08	1.46560000E-11	1.1732790E+04	3.91389000E+01	
C_9H_9(T)				
0.63778563E+01	0.64488344E-01	-0.38863003E-04	0.11196405E-07	-0.12342460E-11
0.40309031E+05	-0.79087715E+01	-0.19958377E-01	0.80526829E-01	-0.52920732E-04
0.16153127E-07	-0.17739016E-11	0.42242277E+05	0.25758848E+02	
$C_{10}H_{14}$				
2.02595000E+01	4.11181000E-02	-1.37704000E-05	2.24242000E-09	-1.43670000E-13
-1.14682291E+04	-7.95128196E+01	-4.39881000E+00	1.04898000E-01	-7.28383000E-05
2.63543000E-08	-4.03424000E-12	-4.26042512E+03	4.95101506E+01	
$1C_{10}H_{13}$				
2.04104000E+01	3.89946000E-02	-1.40301000E-05	2.66069000E-09	-1.94897000E-13
6.31928981E+03	-7.99242362E+01	-3.72223000E+00	9.81115000E-02	-6.02300000E-05
1.40447000E-08	-3.01157000E-14	1.34144777E+04	4.69252508E+01	
$2C_{10}H_{13}$				
2.10876000E+01	3.60228000E-02	-1.13184000E-05	1.71689000E-09	-1.03397000E-13
1.21509529E+04	-8.06482463E+01	-1.94657000E+00	8.72062000E-02	-4.11697000E-05
-4.58607000E-11	3.71335000E-12	1.92211945E+04	4.18418099E+01	
$3C_{10}H_{13}$				
2.10876000E+01	3.60228000E-02	-1.13184000E-05	1.71689000E-09	-1.03397000E-13
1.21509529E+04	-8.06482463E+01	-1.94657000E+00	8.72062000E-02	-4.11697000E-05
-4.58607000E-11	3.71335000E-12	1.92211945E+04	4.18418099E+01	
$4C_{10}H_{13}$				
2.04104000E+01	3.89946000E-02	-1.40301000E-05	2.66069000E-09	-1.94897000E-13
1.32191695E+04	-7.73323382E+01	-3.72223000E+00	9.81115000E-02	-6.02300000E-05
1.40447000E-08	-3.01157000E-14	2.03143574E+04	4.95171488E+01	
C_8H_9(B)				
1.76812000E+01	2.22669000E-02	-5.22086000E-06	6.13378000E-10	-3.04408000E-14
2.01399197E+04	-6.57808452E+01	-4.08336000E+00	7.85843000E-02	-5.32283000E-05
1.49665000E-08	-6.76053000E-13	2.62891016E+04	4.76267581E+01	
C_5H_9				
0.37042289E+01	0.39042108E-01	-0.18223191E-04	0.38031742E-08	-0.29095449E-12
0.17857311E+05	0.11002142E+02	0.37042289E+01	0.39042108E-01	-0.18223191E-04
0.38031742E-08	-0.29095449E-12	0.17857311E+05	0.11002142E+02	
$1C_5H_{10}$				
-0.26194715E+00	0.52521653E-01	-0.27921931E-04	0.52903104E-08	0.22517016E-12
-0.46336323E+04	0.28551981E+02	-0.26194715E+00	0.52521653E-01	-0.27921931E-04
0.52903104E-08	0.22517016E-12	-0.46336323E+04	0.28551981E+02	
$1C_5H_{11}$				
0.32912431E+01	0.45529757E-01	-0.21101181E-04	0.43925299E-08	-0.33570976E-12
0.26192629E+04	0.13674364E+02	0.32912431E+01	0.45529757E-01	-0.21101181E-04
0.43925299E-08	-0.33570976E-12	0.26192629E+04	0.13674364E+02	
C_6H_{11}				
0.24938654E+02	0.13258801E-01	-0.23302223E-05	0.00000000E+00	0.00000000E+00
0.51145941E+04	-0.10690338E+03	0.63802451E+00	0.56209452E-01	-0.23047424E-04
0.00000000E+00	0.00000000E+00	0.14624427E+05	0.28133981E+02	
$1C_6H_{12}$				
0.18663635E+02	0.20971451E-01	-0.31082809E-05	-0.68651618E-09	0.16023608E-12
-0.13590895E+05	-0.70915860E+02	0.19686203E+01	0.47656231E-01	0.66015373E-05
-0.37148173E-07	0.16922463E-10	-0.77118789E+04	0.20859230E+02	-0.50138854E+04

Table B.1, continued

$1C_6H_{13}$				
0.12759770E 02	0.37134279E-01	-0.14256110E-04	0.25052556E-08	-0.16459707E-12
-0.35693750E 04	-0.36999527E 02	0.23062353E 01	0.50200045E-01	0.79387773E-05
-0.41260655E-07	0.18794369E-10	0.10269711E 03	0.20896637E 02	0.30188548E 04
$2C_6H_{13}$				
0.24056369E+03	-0.16540524E+01	0.41218125E-02	-0.38506450E-05	0.11862751E-08
-0.18510320E+05	-0.98342773E+03	0.24056369E+03	-0.16540524E+01	0.41218125E-02
-0.38506450E-05	0.11862751E-08	-0.18510320E+05	-0.98342773E+03	
C_7H_{13}				
0.20154745E+02	2.94825740E-02	-1.00547928E-05	1.55779043E-09	-9.02420561E-14
5.28806957E+03	-7.55263310E+01	-5.42049681E-01	7.60738062E-02	-4.99213653E-05
1.70382432E-08	-2.39883209E-12	1.26846066E+04	3.63048921E+01	
$1C_7H_{14}$				
0.13952881E+02	0.41712158E-01	-0.16157950E-04	0.29187538E-08	-0.19958112E-12
-0.14853311E+05	-0.43649205E+02	0.19140427E+01	0.58601697E-01	0.16939333E-05
-0.38140418E-07	0.18157007E-10	-0.10616395E+05	0.22793909E+02	
$2C_7H_{14}$				
0.32385807E+01	0.62326781E-01	-0.29207546E-04	0.61119079E-08	-0.46836433E-12
-0.12588305E+05	0.17598330E+02	0.32385807E+01	0.62326781E-01	-0.29207546E-04
0.61119079E-08	-0.46836433E-12	-0.12588305E+05	0.17598330E+02	
$3C_7H_{14}$				
0.32385807E+01	0.62326781E-01	-0.29207546E-04	0.61119079E-08	-0.46836433E-12
-0.12588305E+05	0.17598330E+02	0.32385807E+01	0.62326781E-01	-0.29207546E-04
0.61119079E-08	-0.46836433E-12	-0.12588305E+05	0.17598330E+02	
$1C_7H_{15}$				
0.12660566E+02	0.47893065E-01	-0.19735835E-04	0.37298693E-08	-0.26299814E-12
-0.64258434E+04	-0.34510489E+02	0.10280414E+02	0.70155356E-03	0.15955135E-03
-0.20959318E-06	0.83344532E-10	-0.36030731E+04	-0.10315257E+02	
$2C_7H_{15}$				
0.66495419E+00	0.77137977E-01	-0.44929548E-04	0.12854724E-07	-0.14434085E-11
-0.31296282E+04	0.28957718E+02	0.66495419E+00	0.77137977E-01	-0.44929548E-04
0.12854724E-07	-0.14434085E-11	-0.31296282E+04	0.28957718E+02	
$3C_7H_{15}$				
0.66495419E+00	0.77137977E-01	-0.44929548E-04	0.12854724E-07	-0.14434085E-11
-0.31296282E+04	0.28957718E+02	0.66495419E+00	0.77137977E-01	-0.44929548E-04
0.12854724E-07	-0.14434085E-11	-0.31296282E+04	0.28957718E+02	
$4C_7H_{15}$				
0.66495419E+00	0.77137977E-01	-0.44929548E-04	0.12854724E-07	-0.14434085E-11
-0.31296282E+04	0.28957718E+02	0.66495419E+00	0.77137977E-01	-0.44929548E-04
0.12854724E-07	-0.14434085E-11	-0.31296282E+04	0.28957718E+02	
C_7H_{16}				
-0.23626566E+01	0.89415804E-01	-0.56126759E-04	0.17017969E-07	-0.19792464E-11
-0.25392135E+05	0.40574043E+02	-0.23626566E+01	0.89415804E-01	-0.56126759E-04
0.17017969E-07	-0.19792464E-11	-0.25392135E+05	0.40574043E+02	
$4C_8H_{13}$				
0.20831284E 02	0.38294513E-01	-0.12417870E-04	0.17957589E-08	-0.93705913E-13
2.39923141E 04	-6.98409051E 01	0.26075478E 01	0.64282537E-01	0.92502323E-05
-0.51046708E-07	0.23316557E-10	3.05134527E 04	3.08468656E 01	
C_8H_{14}				
0.20831284E 02	0.38294513E-01	-0.12417870E-04	0.17957589E-08	-0.93705913E-13
-6.10173141E 03	-1.11109051E 02	0.26075478E 01	0.64282537E-01	0.92502323E-05
-0.51046708E-07	0.23316557E-10	0.42734527E 03	-1.01884656E 01	
C_8H_{16}				
0.20831284E 02	0.38294513E-01	-0.12417870E-04	0.17957589E-08	-0.93705913E-13
-0.20133141E 05	-0.79240051E 02	0.26075478E 01	0.64282537E-01	0.92502323E-05
-0.51046708E-07	0.23316557E-10	-0.13597527E 05	0.21584656E 02	-0.99738727E 04
C_8H_{17}				
0.17027115E 02	0.49380627E-01	-0.19069470E-04	0.33672309E-08	-0.22210039E-12
-0.10763527E 05	-0.56252975E 02	0.26141319E 01	0.67607820E-01	0.11190068E-04
-0.56412340E-07	0.25483921E-10	-0.57469414E 04	0.23451477E 02	-0.19628570E 04
$C_{10}H_{19}$				
2.47482587E+01	5.14076858E-02	-1.95828774E-05	3.47928330E-09	-2.34079322E-13
-1.20167044E+04	-9.35125879E+01	-2.43834540E+01	2.82492767E-01	-4.99496066E-04
4.71514086E-07	-1.70502072E-10	-1.41157149E+03	1.41304170E+02	

Table B.1, continued

$C_{10}H_{20}$				
2.39013980E+01	5.38878964E-02	-2.01285612E-05	3.52665091E-09	-2.34996859E-13
-2.85617759E+04	-9.25811186E+01	2.73154321E+00	7.88862849E-02	2.51641756E-05
-8.52509662E-08	3.92427894E-11	-2.06898473E+04	2.57333929E+01	
$1C_{10}H_{21}$				
0.21322128E 02	0.61573524E-01	-0.23849483E-04	0.42209116E-08	-0.27889307E-12
-0.17967809E 05	-0.75656952E 02	0.29391508E 01	0.84870219E-01	0.14858843E-04
-0.72042951E-07	0.32363209E-10	-0.11598363E 05	0.25938156E 02	-0.69445689E 04
$2C_{10}H_{21}$				
0.13470533E+02	0.80290854E-01	-0.39518403E-04	0.97089403E-08	-0.96419151E-12
-0.15685746E+05	-0.33952385E+02	0.29079616E+00	0.10640167E+00	-0.45561803E-04
-0.35957344E-08	0.54528122E-11	-0.11504166E+05	0.36831581E+02	
$3C_{10}H_{21}$				
0.13470533E+02	0.80290854E-01	-0.39518403E-04	0.97089403E-08	-0.96419151E-12
-0.15685746E+05	-0.33952385E+02	0.29079616E+00	0.10640167E+00	-0.45561803E-04
-0.35957344E-08	0.54528122E-11	-0.11504166E+05	0.36831581E+02	
$4C_{10}H_{21}$				
0.13470533E+02	0.80290854E-01	-0.39518403E-04	0.97089403E-08	-0.96419151E-12
-0.15685746E+05	-0.33952385E+02	0.29079616E+00	0.10640167E+00	-0.45561803E-04
-0.35957344E-08	0.54528122E-11	-0.11504166E+05	0.36831581E+02	
$5C_{10}H_{21}$				
0.13470533E+02	0.80290854E-01	-0.39518403E-04	0.97089403E-08	-0.96419151E-12
-0.15685746E+05	-0.33952385E+02	0.29079616E+00	0.10640167E+00	-0.45561803E-04
-0.35957344E-08	0.54528122E-11	-0.11504166E+05	0.36831581E+02	
$C_{10}H_{21}OO$				
0.21322128E 02	0.61573524E-01	-0.23849483E-04	0.42209116E-08	-0.27889307E-12
-0.34326809E 05	-0.69766952E 02	0.29391508E 01	0.84870219E-01	0.14858843E-04
-0.72042951E-07	0.32363209E-10	-0.27955363E 05	0.31892256E 02	
$C_{10}H_{21}O_2$				
0.14116570E+02	0.78702390E-01	-0.38137303E-04	0.92046113E-08	-0.89854003E-12
-0.24961109E+05	-0.28566538E+02	0.56013346E-01	0.10784968E+00	-0.48558370E-04
-0.10920577E-08	0.47324675E-11	-0.20627523E+05	0.46538103E+02	
$C_{10}H_{22}$				
0.14116570E+02	0.78702390E-01	-0.38137303E-04	0.92046113E-08	-0.89854003E-12
-0.38875109E+05	-0.40076538E+02	0.56013346E-01	0.10784968E+00	-0.48558370E-04
-0.10920577E-08	0.47324675E-11	-0.34466523E+05	0.35138103E+02	
C_9H_{17}				
2.10867922E+01	4.61782938E-02	-1.72507130E-05	3.02355150E-09	-2.01567606E-13
3.27938951E+01	-7.58751351E+01	4.36832491E+00	5.77776115E-02	4.89429265E-05
-1.04595584E-07	4.61873643E-11	6.51405343E+03	1.91916207E+01	
$2C_9H_{17}$				
2.10867922E+01	4.61782938E-02	-1.72507130E-05	3.02355150E-09	-2.01567606E-13
3.27938951E+01	-7.58751351E+01	4.36832491E+00	5.77776115E-02	4.89429265E-05
-1.04595584E-07	4.61873643E-11	6.51405343E+03	1.91916207E+01	
C_9H_{18}				
1.53793000E+01	5.61292000E-02	-1.98147000E-05	3.23022000E-09	-2.01192000E-13
-2.06309000E+04	-4.56273000E+01	5.26230000E-01	8.78248000E-02	-2.39189000E-05
-2.41905000E-08	1.44519000E-11	-1.63330000E+04	3.28075000E+01	
C_9H_{19}				
0.19195267E+02	0.55439249E-01	-0.21436601E-04	0.37885144E-08	-0.25002987E-12
-0.14373711E+05	-0.66069458E+02	0.27452002E+01	0.76430142E-01	0.12624764E-04
-0.63882226E-07	0.28818781E-10	-0.86689141E+04	0.24831818E+02	
$1C_{12}H_{25}$				
0.22393200E+02	0.78112400E-01	-0.30867100E-04	0.57177200E-08	-0.40015200E-12
-0.25730414E+05	-0.75649764E+02	-0.26173200E+01	0.14965400E+00	-0.10838700E-03
0.45326300E-07	-0.86613400E-11	-0.18900635E+05	0.53197575E+02	
$2C_{12}H_{25}$				
0.25979400E+02	0.73765100E-01	-0.29004100E-04	0.52184100E-08	-0.35054300E-12
-0.25737432E+05	-0.97216017E+02	-0.29531700E+01	0.15169800E+00	-0.11101100E-03
0.46357800E-07	-0.87104100E-11	-0.17048552E+05	0.54090483E+02	
$3C_{12}H_{25}$				
0.25979400E+02	0.73765100E-01	-0.29004100E-04	0.52184100E-08	-0.35054300E-12
-0.25737432E+05	-0.97216017E+02	-0.29531700E+01	0.15169800E+00	-0.11101100E-03
0.46357800E-07	-0.87104100E-11	-0.17048552E+05	0.54090483E+02	

Table B.1, continued

$4C_{12}H_{25}$				
0.25979400E+02	0.73765100E-01	-0.29004100E-04	0.52184100E-08	-0.35054300E-12
-0.25737432E+05	-0.97216017E+02	-0.29531700E+01	0.15169800E+00	-0.11101100E-03
0.46357800E-07	-0.87104100E-11	-0.17048552E+05	0.54090483E+02	
$5C_{12}H_{25}$				
0.25979400E+02	0.73765100E-01	-0.29004100E-04	0.52184100E-08	-0.35054300E-12
-0.25737432E+05	-0.97216017E+02	-0.29531700E+01	0.15169800E+00	-0.11101100E-03
0.46357800E-07	-0.87104100E-11	-0.17048552E+05	0.54090483E+02	
$6C_{12}H_{25}$				
0.25979400E+02	0.73765100E-01	-0.29004100E-04	0.52184100E-08	-0.35054300E-12
-0.25737432E+05	-0.97216017E+02	-0.29531700E+01	0.15169800E+00	-0.11101100E-03
0.46357800E-07	-0.87104100E-11	-0.17048552E+05	0.54090483E+02	
$C_{12}H_{26}$				
0.37018793E+02	0.55472149E-01	-0.19207955E-04	0.30817557E-08	-0.18480062E-12
-0.52698446E+05	-0.16145350E+03	0.21326448E+02	-0.38639400E-01	0.39947611E-03
-0.50668110E-06	0.20069788E-09	-0.42247505E+05	-0.48584830E+02	

Appendix C

Species Structure

Table C.1: Species Structure and Thermodynamic Data.

Specie	Structure	Hf^0 [kJ/mol]	S^0 [J/(mole*K)]	Reference
H	H	217.96	114.58	[162]
OH	OH	38.97	183.58	[162]
O	O	249.18	160.92	[162]
HO_2	HO_2	12.54	229.07	[162]
H_2	H_2	0.00	130.57	[162]
H_2O	H_2O	-241.83	188.68	[162]
H_2O_2	H_2O_2	-136.10	232.84	[162]
O_2	O_2	0.00	205.01	[162]
C_1	C	716.62	158.08	[33]
C_2	CC	830.79	199.38	[33]
CO	CO	-110.53	197.52	[162]
CO_2	CO_2	-393.53	213.70	[162]

Table C.1, continued

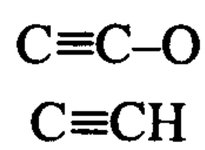
Specie	Structure	Hf^0 [kJ/mol]	S^0 [J/(mole*K)]	Reference
CH	CH	597.31	183.01	[33]
CHO	HC=O	43.50	224.50	[162]
$CH_2(S)$	$^1CH_2$	424.70	188.68	[33]
$CH_2(T)$	$^3CH_3$	386.96	195.45	[162]
CH_2O	CH_2=O	-108.57	218.73	[33]
CH_3	CH_3	145.68	194.02	[162]
CH_2OH	CH_2–OH	-8.90	243.87	[162]
CH_3O	CH_3–O	16.29	228.45	[162]
CH_3OO	CH_3–OO	28.07	262.57	[218]
CH_4	CH_4	-74.89	186.03	[162]
CH_3OH	CH_3–OH	-200.93	239.77	[162]
CH_3OOH	CH_3–OOH	-124.55	272.05	[218]
C_2O	C≡C–O	291.01	233.57	[33]
C_2H	C≡CH	569.08	213.26	[33]
C_2HO	CH_2=C=O	161.06	246.63	[162]
C_2H_2	HC≡CH	226.75	200.88	[162]
H_2C_2	C=CH_2	414.75	220.98	[33]
C_2H_2O	CH_2=C=O	-51.87	241.77	[131]
C_2H_3	HC=CH_2	302.86	231.48	[131]
CH_3CO	CH_3–C=O	-10.00	267.40	[33]
CH_2CHO	CH_2–CHO	25.32	268.92	[33]
$CHCH_2O$	CH_2=CH–O	139.81	361.44	[33]
C_2H_4	CH_2=CH_2	52.45	219.13	[162]
CH_3CHO	CH_3–CHO	-166.18	263.90	[33]
C_2H_4O		-52.63	242.83	[33]
C_2H_5	CH_2–CH_3	118.64	247.07	[33]
C_2H_5O	CH_3–CH_2–O	-16.75	268.54	[218]
C_2H_5OO	CH_3–CH_2–OO	-28.71	299.93	[33]
C_2H_4OOH	CH_3–CH–OOH	28.78	324.74	[218]

Table C.1, continued

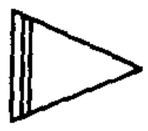
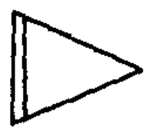
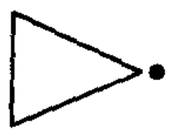
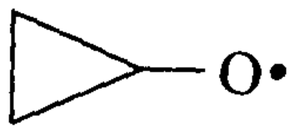
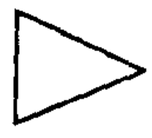
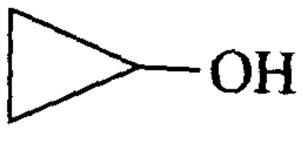
Specie	Structure	Hf ^{0} [kJ/mol]	S^0 [J/(mole*K)]	Reference
C_2H_5OOH	CH_3–CH_2–OOH	-97.50	416.26	[218]
C_2H_6	CH_3–CH_3	-83.86	228.93	[162]
C_3H	C–C≡CH	684.03	226.70	[33]
C_3H_2		476.87	234.96	[161]
C_3H_2L	HC–C≡CH	609.65	262.46	[172]
C_3H_2O	HC≡C–CHO	112.96	301.60	[162]
C_3H_3	HC≡C–CH_2	345.96	253.25	[162]
C_3H_3O	CH_2=CH–C=O	71.78	301.46	[172]
C_3H_4(A)	CH_2=C=CH_2	190.89	243.38	[33]
C_3H_4(B)		276.96	243.57	[33]
C_3H_4(P)	HC≡C–CH_3	185.41	248.25	[33]
C_3H_4O	CH_2=CH–CHO	-74.48	297.01	[172]
C_3H_5(A)	CH_2–CH=CH_2	161.67	258.29	[162]
C_3H_5(B)		245.28	252.50	[173]
C_3H_5(S)	CH_3–CH=CH	270.91	275.04	[162]
C_3H_5(T)	CH_3–C=CH_2	255.60	277.16	[162]
C_3H_5O		110.31	293.91	[182]
AC_3H_5O	CH_3–CO–CH_2	-14.06	301.71	[33]
PC_3H_5O	CH_3–CH_2–CO	-36.02	307.97	[33]
TC_3H_5O	CH_2–CH_2–CHO	-5.26	307.97	[182]
C_3H_6	CH_3–CH=CH_2	20.40	266.48	[33]
C_3H_6(B)		53.48	237.40	[173]
C_3H_6O		-92.76	281.30	[182]
AC_3H_6O	CH_3–CO–CH_3	-217.14	295.60	[33]

Table C.1, continued

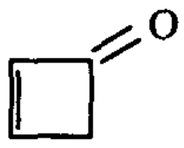
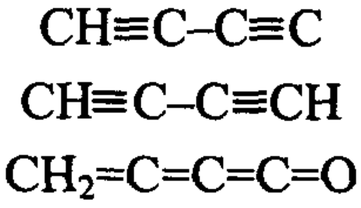
Specie	Structure	Hf ^{0} [kJ/mol]	S^0 [J/(mole*K)]	Reference
PC_3H_6O	$CH_3–CH_2–CHO$	-192.04	304.45	[33]
$C_3H_7(I)$	$CH_3–\dot{C}H–CH_3$	93.27	289.28	[33]
$C_3H_7(N)$	$CH_3–CH_2–\dot{C}H_2$	100.48	289.41	[33]
$C_3H_7O(I)$	$CH_3–\underset{\displaystyle O\bullet}{\underset{\vert}{CH}}–CH_3$	-115.62	207.97	[218]
$C_3H_7O(N)$	$CH_3–CH_2–CH_2–O$	-37.66	309.55	[33]
C_3H_6OH	$CH_3–\dot{C}H–CH_2–OH$	-74.94	322.51	[173]
$C_3H_7OO(I)$	$CH_3–\underset{\displaystyle OO\bullet}{\underset{\vert}{CH}}–CH_3$	-134.48	247.19	[218]
$C_3H_7OO(N)$	$CH_3–CH_2–CH_2–OO$	-116.19	246.41	[218]
C_3H_6OOH	$CH_3–\dot{C}H–CH_2–OOH$	-19.16	359.04	[218]
C_3H_8	$CH_3–CH_2–CH_3$	-103.86	270.12	[33]
$C_3H_7OOH(I)$	$CH_3–\underset{\displaystyle OOH}{\underset{\vert}{CH}}–CH_3$	-202.72	363.57	[218]
$C_3H_7OOH(N)$	$CH_3–CH_2–CH_2–OOH$	-184.43	362.79	[218]
C_4H	$CH{\equiv}C–C{\equiv}C$	803.67	254.76	[162]
C_4H_2	$CH{\equiv}C–C{\equiv}CH$	465.57	255.92	[162]
C_4H_2O	$CH_2{=}C{=}C{=}C{=}O$	228.40	277.94	[182]
$C_4H_3(I)$	$CH{\equiv}C–C{=}CH_2$	477.15	273.05	[162]
$C_4H_3(N)$	$CH{\equiv}C–CH{=}\dot{C}H$	523.49	273.14	[162]
C_4H_4	$CH_2{=}CH–C{\equiv}CH$	280.41	278.76	[162]
C_4H_4O		33.60	280.69	[173]
$C_4H_5(I)$	$CH_2{=}\dot{C}–CH{=}CH_2$	330.81	283.05	[33]
$C_4H_5(S)$	$CH_3–CH{=}\dot{C}{=}CH$	302.15	289.26	[33]
$C_4H_5(T)$	$CH_2{=}CH–\dot{C}H{=}CH$	361.75	288.59	[172]
$CH_3CHCHCO$	$CH_3–CH{=}CH–\dot{C}{=}O$	40.49	313.98	[218]
$CH_2CHCHCHO$	$CH_2–CH{=}CH–\dot{C}HO$	112.37	340.56	[218]
$C_4H_6(B)$		243.33	289.46	[162]

Table C.1, continued

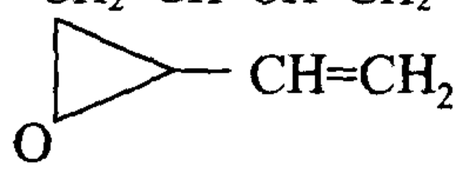
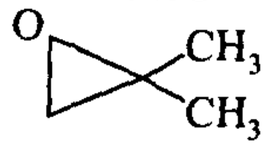
Specie	Structure	Hf ^{0} [kJ/mol]	S^0 [J/(mole*K)]	Reference
C_4H_6(F)	$CH{\equiv}C{-}CH_2{-}CH_3$	167.07	285.29	[182]
C_4H_6(M)	$CH_3{-}C{\equiv}C{-}CH_3$	146.28	285.29	[33]
C_4H_6(S)	$CH_3{-}CH{=}C{=}CH_2$	164.57	291.66	[33]
C_4H_6(T)	$CH_2{=}CH{-}CH{=}CH_2$	108.96	278.24	[33]
AC_4H_6O		8.17	338.91	[182]
BC_4H_6O	$CH_2{=}CH{-}CH{=}CH{-}OH$	-100.86	338.91	[182]
C_4H_7(I)	$CH_2{-}C(CH_3){=}CH_2$	121.31	291.98	[33]
C_4H_7(N)	$CH_2{=}CH{-}CH_2{-}CH_2$	192.43	320.01	[33]
C_4H_7(S)	$CH_2{-}CH{=}CH{-}CH_3$	128.28	300.06	[33]
C_4H_7O(M)	$CH_3{-}CH(CO){-}CH_3$	51.69	332.18	[33]
C_4H_7O(X)	$CH_2{-}CH(CHO){-}CH_3$	51.69	332.18	[33]
C_4H_8(I)	$CH_3{-}C(CH_3){=}CH_2$	-17.17	296.60	[33]
C_4H_8(N)	$CH_2{=}CH{-}CH_2{-}CH_3$	-0.55	307.75	[33]
C_4H_8(S)	$CH_3{-}CH{=}CH{-}CH_3$	-7.43	295.81	[33]
C_4H_8O(M)	$CH_3{-}CH(CHO){-}CH_3$	-215.42	332.18	[218]
C_4H_8O(X)		-129.71	307.45	[33]
C_4H_9(I)	$CH_2{-}CH(CH_3){-}CH_3$	57.30	318.58	[33]
C_4H_9(N)	$CH_2{-}CH_2{-}CH_2{-}CH_3$	66.51	328.45	[33]
C_4H_9(S)	$CH_3{-}CH(CH_3){-}CH_3$	69.98	325.35	[33]
C_4H_9(T)	$CH_3{-}C(CH_3)_2{-}CH_3$	51.68	319.65	[33]
C_4H_8OH(I)	$CH_3{-}CH(CH_2){-}CH_2{-}OH$	-118.24	370.58	[218]

Table C.1, continued

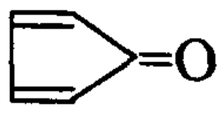
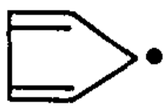
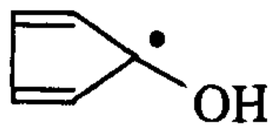
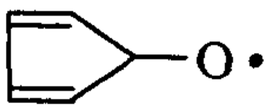
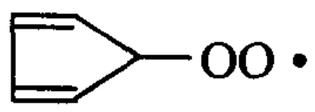
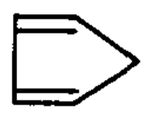
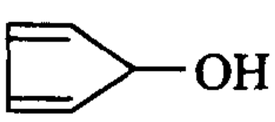
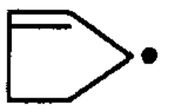
Specie	Structure	Hf ^{0} [kJ/mol]	S^0 [J/(mole*K)]	Reference
$O_2C_4H_9O$	$CH_3–\underset{\displaystyle CH_2–OO\bullet}{\overset{\displaystyle \vert}{CH}}–CH_2–OH$	-246.54	425.47	[218]
$C_4H_{10}(I)$	$CH_3–\underset{\displaystyle CH_3}{\overset{\displaystyle \vert}{CH}}–CH_3$	-134.65	295.29	[33]
$C_4H_{10}(N)$	$CH_3–CH_2–CH_2–CH_3$	-125.78	309.67	[33]
C_5H	$C=C=C=C=CH$	778.21	260.36	[33]
C_5H_2	$CH=C=C=C=CH$	691.35	266.58	[33]
$C_5H_3(L)$	$CH\ \ C–CH–C\equiv CH$	560.95	295.13	[172]
$C_5H_4(L)$	$CH_2=C=CH–C\equiv CH$	435.09	292.81	[182]
C_5H_4O		16.81	280.97	[162]
C_5H_5		8.17	338.91	[33]
$C_5H_5(L)$	$CH_2=C=CH–CH=CH$	396.46	307.39	[218]
C_5H_4OH		87.78	311.11	[162]
C_5H_5O		104.06	309.10	[162]
C_5H_5OO		178.24	346.58	[274]
C_5H_6		134.28	274.09	[33]
$C_5H_6(L)$	$CH_3–C\equiv C–CH=CH_2$	269.47	317.87	[182]
C_5H_5OH		-37.92	314.56	[274]
C_5H_7		166.85	308.18	[33]
$C_5H_7(I)$	$CH_2=\underset{\displaystyle CH_2}{\overset{\displaystyle \vert}{C}}–CH=CH_2$	316.27	341.61	[218]
$C_5H_7(X)$	$CH_2–CH=CH–CH=CH_2$	221.72	312.05	[33]

Table C.1, continued

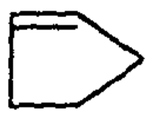
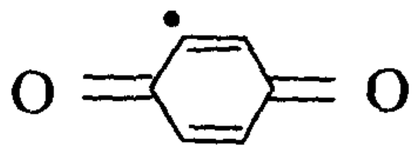
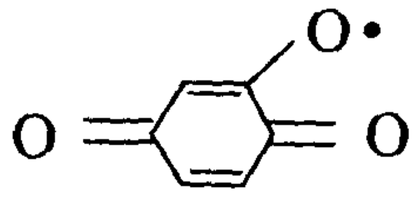
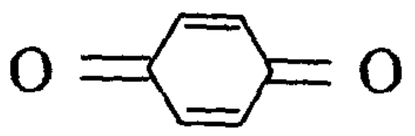
Specie	Structure	Hf ^{0} [kJ/mol]	S^0 [J/(mole*K)]	Reference
C_5H_8		32.68	291.20	[33]
$C_5H_8(I)$	$CH_2=C(CH_3)-CH=CH_2$	75.71	315.56	[33]
$C_5H_8(X)$	$CH_3-CH=CH-CH=CH_2$	76.12	320.00	[33]
$C_5H_8(Y)$	$CH_2=C=CH-CH_2-CH_3$	145.26	333.42	[218]
$C_5H_9(A)$	$CH_2=C(CH_3)-CH-CH_3$	100.40	326.57	[218]
$C_5H_9(B)$	$CH_2=C(CH_2)-CH_2-CH_3$	100.40	324.97	[218]
$C_5H_{10}(A)$	$CH_2=C(CH_3)-CH_2-CH_3$	-36.33	339.45	[218]
$C_5H_{10}(B)$	$CH_3-C(CH_3)=CH-CH_3$	-42.56	338.49	[218]
$C_5H_{11}(T)$	$CH_3-C(CH_3)-CH_2-CH_3$	32.58	366.29	[218]
C_6H_2	$CH\equiv C-C\equiv C-C\equiv CH$	700.76	299.11	[162]
C_6H_3	$CH\equiv C-C=CH-C\equiv CH$	662.97	319.23	[162]
$C_6H_3O_2$		151.00	342.51	[215]
$C_6H_3O_3$		-70.17	342.51	[215]
C_6H_4		481.11	291.03	[162]
C_6H_4L	$CH\equiv C-CH=CH-C\equiv CH$	514.58	321.25	[162]
$C_6H_4O_2$		-120.35	342.51	
C_6H_5		332.58	288.34	[215]
$C_6H_5(A)$	$CH\equiv C-CH-CH_2-C\equiv CH$	539.63	330.80	[215]

Table C.1, continued

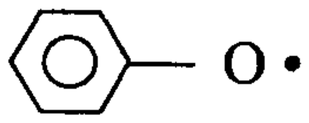
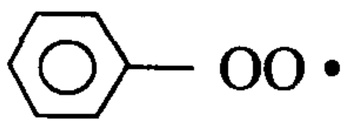
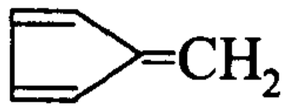
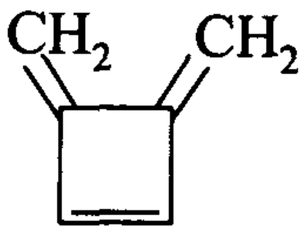
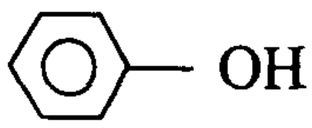
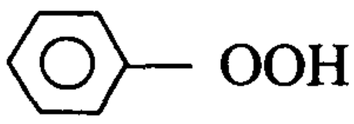
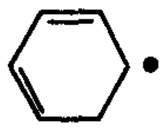
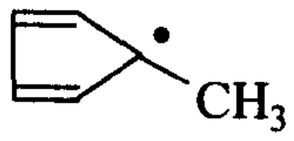
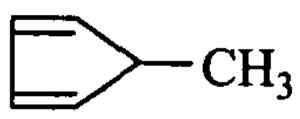
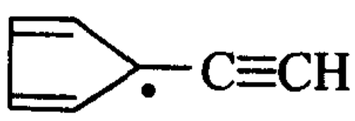
Specie	Structure	Hf ^{0} [kJ/mol]	S^0 [J/(mole*K)]	Reference
C_6H_5(B)	CH≡C–CH=CH–CH=CH	589.07	339.11	[162]
C_6H_5O		47.69	307.74	[162]
C_6H_5OO		155.07	358.47	[76]
C_6H_6		82.88	269.27	[162]
C_6H_6(A)	CH≡C–CH_2–CH_2–C≡CH	410.05	339.11	[162]
C_6H_6(B)	CH_2=C=CH–CH_2–C≡CH	414.20	339.11	[162]
C_6H_6(D)	CH_2=CH–CH=CH–C≡CH	334.53	330.80	[162]
C_6H_6(F)		218.23	299.21	[162]
C_6H_6(M)		334.53	299.21	[162]
C_6H_6(S)	CH_2=C=CH–CH=C=CH_2	395.22	330.8	[162]
C_6H_5OH		-96.38	314.79	[162]
C_6H_5OOH		3.93	357.55	[76]
C_6H_7		200.56	305.76	[162]
C_6H_7(L)	CH_2=CH–CH=CH–CH=CH	388.57	353.43	[162]
$C_5H_4CH_3$		204.57	306.84	[253]
C_6H_8		106.27	303.35	[33]
$C_5H_5CH_3$		101.97	310.22	[138]
C_7H_5		535.33	306.57	est. [16]

Table C.1, continued

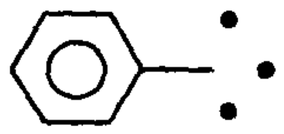
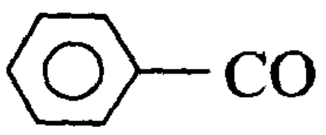
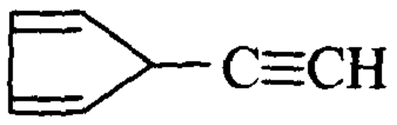
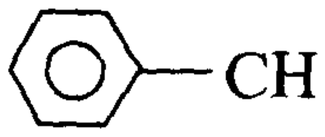
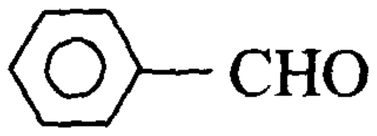
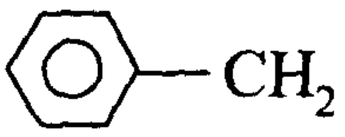
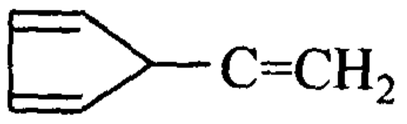
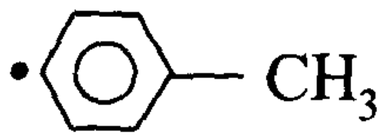
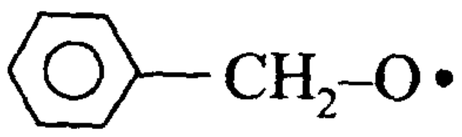
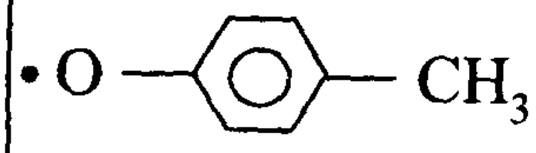
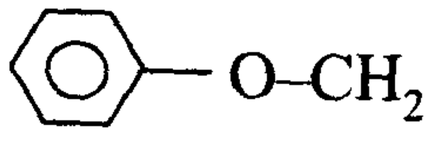
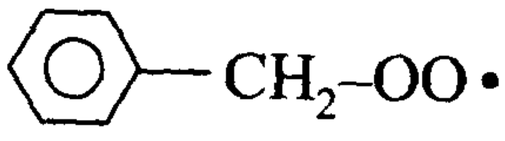
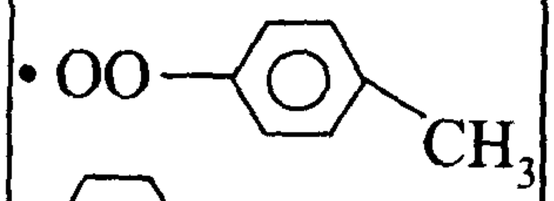
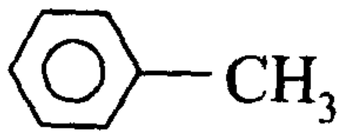
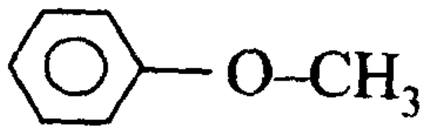
Specie	Structure	Hf ^{0} [kJ/mol]	S^0 [J/(mole*K)]	Reference
C_6H_5C		734.20	312.03	est. [16]
C_6H_5CO		108.75	355.28	[89]
C_7H_6		367.33	357.35	[27]
C_6H_5CH		462.86	317.36	[85]
C_7H_6O		-36.81	335.94	[89]
C_7H_7		215.34	322.48	[27]
C_7H_7L		422.53	321.04	[27]
C_7H_7P		299.14	344.20	[182]
C_7H_7O		117.06	365.80	[182]
OC_7H_7		14.68	327.16	[89]
C_7H_7OA		80.77	360.55	[182]
C_7H_7OO		117.01	394.54	[182]
OOC_7H_7P		147.08	390.04	est. [16]
C_7H_8		49.98	320.11	[33]
C_7H_8OA		-74.44	360.55	[182]

Table C.1, continued

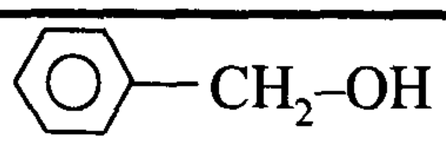
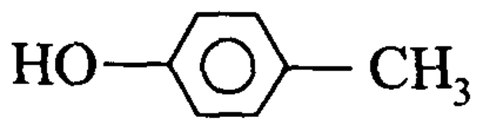
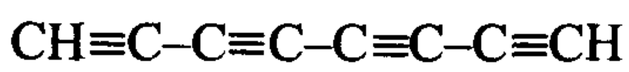
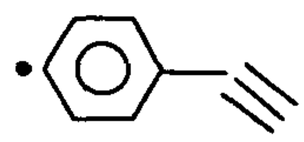
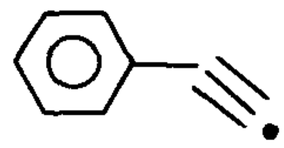
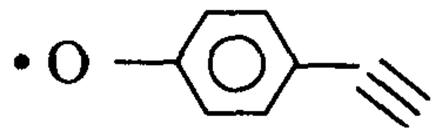
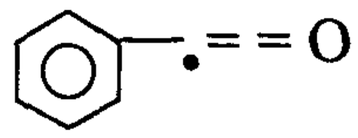
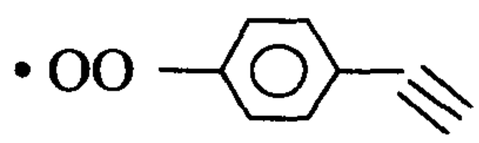
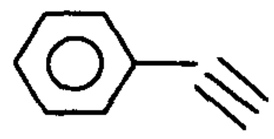
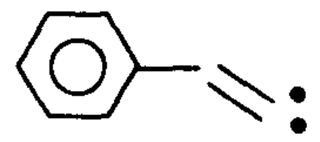
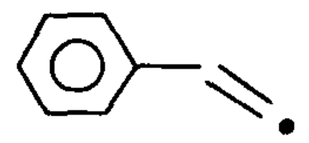
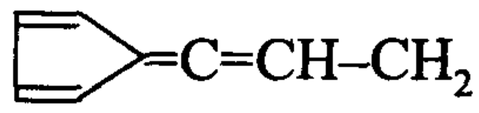
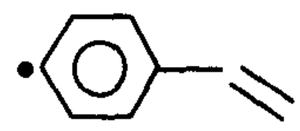
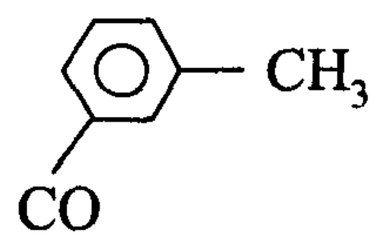
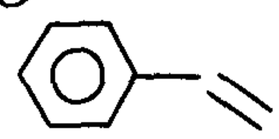
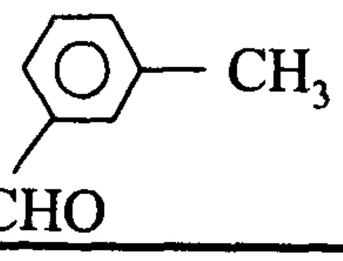
Specie	Structure	Hf ^{0} [kJ/mol]	S^0 [J/(mole*K)]	Reference
C_7H_7OH		-100.39	365.89	[89]
OHC_7H_7		-132.30	355.79	[89]
C_8H_2		934.21	347.60	[33]
C_8H_5		558.34	306.57	[182]
C_8H_5(S)		555.43	326.02	[182]
C_8H_5O		272.74	394.54	est. [16]
$C_6H_5C_2O$		298.59	592.05	est. [16]
C_8H_5OO		436.37	418.71	est. [16]
C_8H_6		309.16	332.25	[182]
C_6H_5CHC		487.11	348.98	est. [16]
C_8H_7		404.58	344.60	[182]
C_8H_7(F)		290.80	368.05	[169]
C_8H_7(P)		397.07	368.05	[182]
C_7H_7CO		75.84	406.14	est. [16]
C_8H_8		147.12	344.27	[89]
C_8H_8O(M)		-69.72	386.81	est. [16]

Table C.1, continued

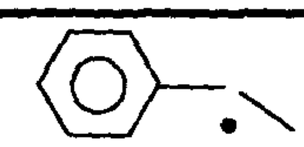
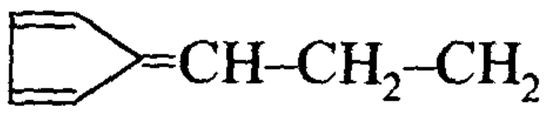
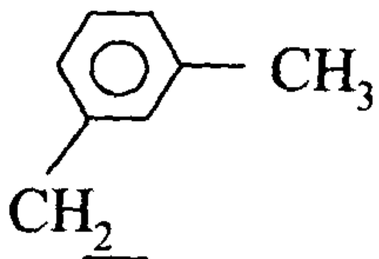
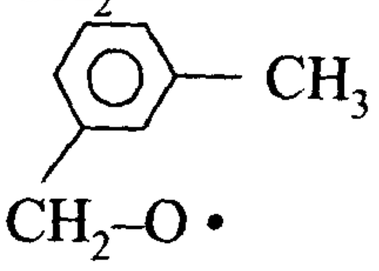
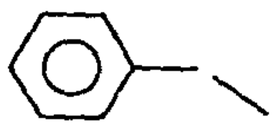
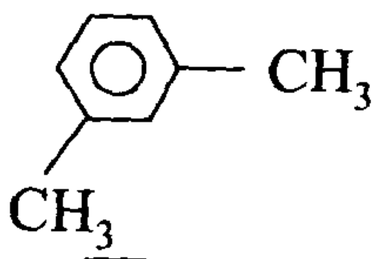
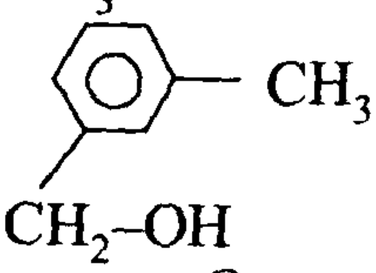
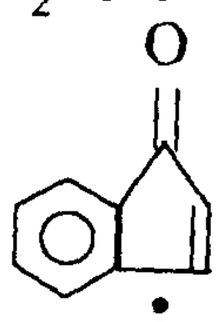
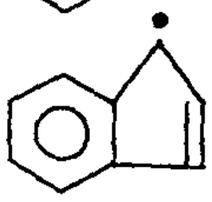
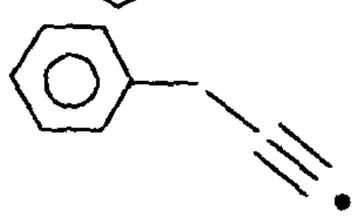
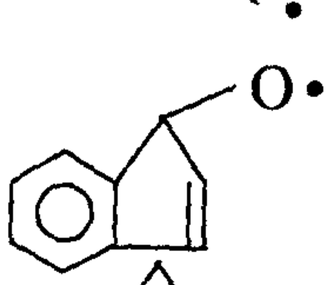
Specie	Structure	Hf ^{0} [kJ/mol]	S^0 [J/(mole*K)]	Reference
C_8H_9		153.01	362.15	[182]
C_8H_9(F)		194.00	362.15	[169]
C_8H_9(M)		182.45	373.36	est. [16]
C_8H_9O(M)		84.16	416.67	est. [16]
C_8H_{10}		29.32	359.55	[89]
C_8H_{10}(M)		17.97	352.02	[33]
C_8H_9OH(M)		-133.27	416.77	est. [33]
C_9H_6O		176.11	377.08	est. [33]
C_9H_7		285.56	342.75	[182]
C_9H_7L		531.44	369.99	[182]
C_9H_7O		131.89	342.14	est. [33]
C_9H_8		164.10	335.76	[33]

Table C.1, continued

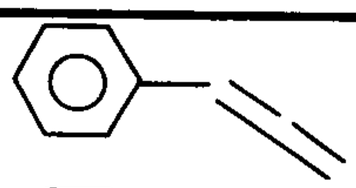
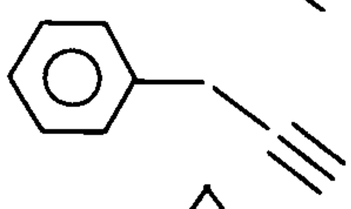
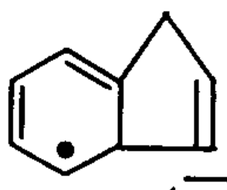
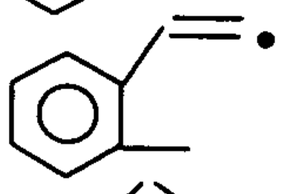
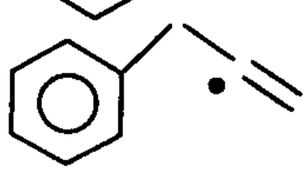
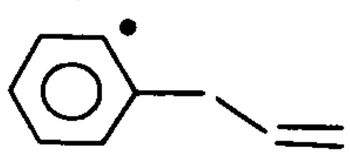
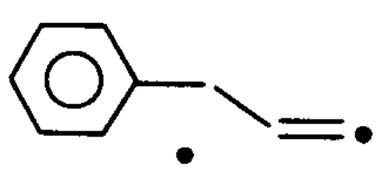
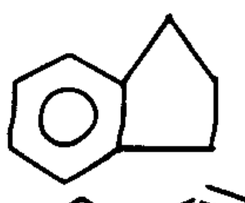
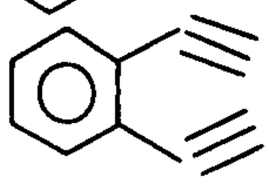
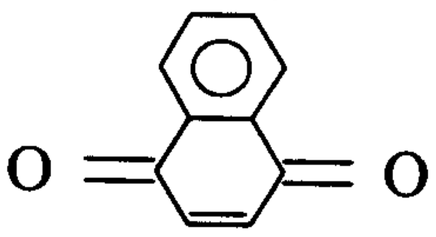
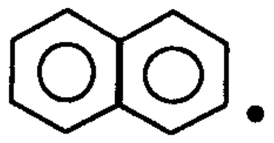
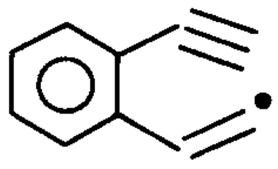
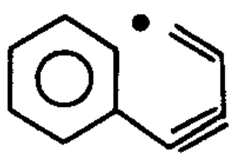
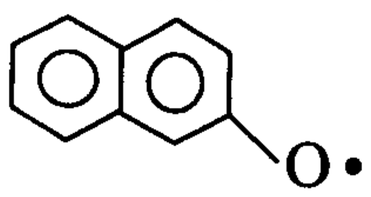
Specie	Structure	Hf^0 [kJ/mol]	S^0 [J/(mole*K)]	Reference
$C_9H_8(S)$		289.60	369.99	[182]
$C_9H_8(T)$		298.54	373.09	[182]
$C_9H_9(C)$		290.25	394.34	[182]
$C_9H_9(F)$		357.35	394.34	[182]
$C_9H_9(I)$		368.96	394.34	[182]
$C_9H_9(N)$		385.58	418.11	[182]
$C_9H_9(P)$		377.25	394.34	[182]
$C_9H_9(S)$		243.34	337.14	[182]
$C_{10}H_6$		532.49	375.06	*[182]*
$C_{10}H_6O_2$		39.93	439.69	est. [16]
$C_{10}H_7$		400.22	361.42	[182]
$C_{10}H_7L$		616.53	393.12	[182]
$C_{10}H_7M$		613.83	405.43	[182]
$C_{10}H_7O$		114.93	381.33	[182]

Table C.1, continued

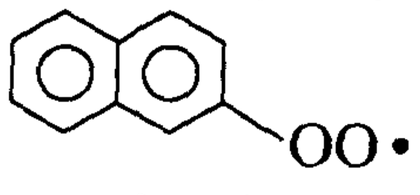
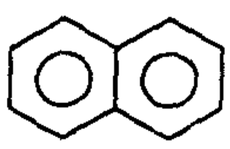
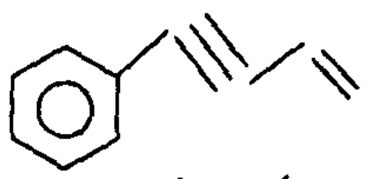
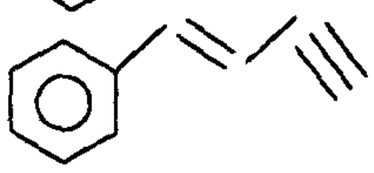
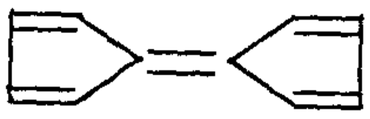
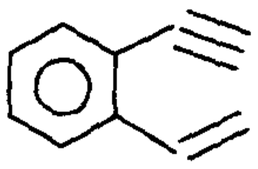
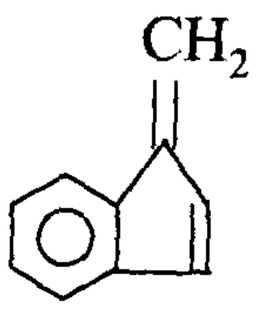
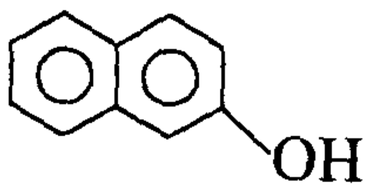
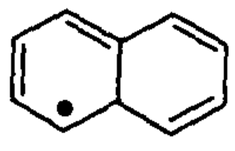
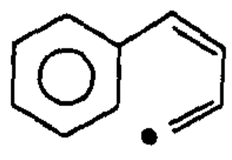
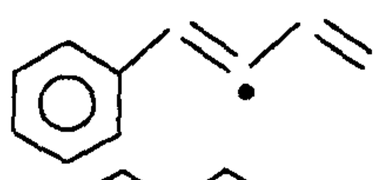
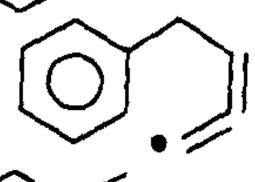
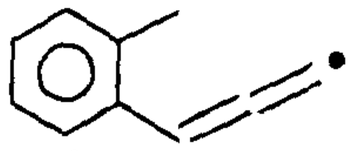
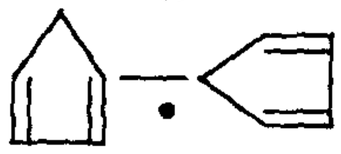
Specie	Structure	ΔHf^0 [kJ/mol]	S^0 [J/(mole*K)]	Reference
$C_{10}H_7OO$		222.47	421.40	est. [16]
$C_{10}H_8$		150.57	333.21	[33]
$C_{10}H_8G$		393.72	333.21	[182]
$C_{10}H_8J$		389.72	333.21	[182]
$C_{10}H_8K$		324.66	367.08	[182]
$C_{10}H_8L$		375.11	393.12	[182]
$C_9H_6CH_2$		267.79	341.50	[157]
$C_{10}H_7OH$		-30.81	368.60	[182]
$C_{10}H_9$		325.25	337.22	[182]
$C_{10}H_9A$		445.04	397.94	[182]
$C_{10}H_9B$		417.81	383.33	[182]
$C_{10}H_9D$		520.33	414.87	[182]
$C_{10}H_9E$		500.35	406.39	[182]
$C_{10}H_9F$		331.86	367.08	[169]

Table C.1, continued

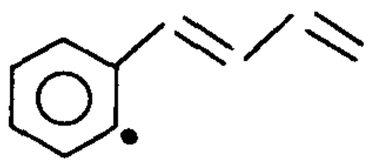
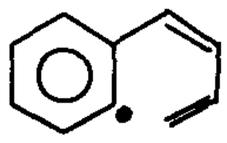
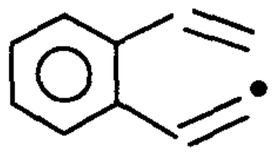
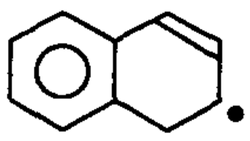
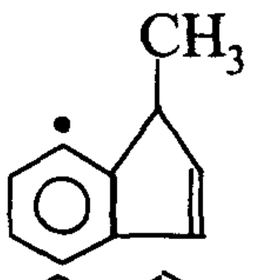
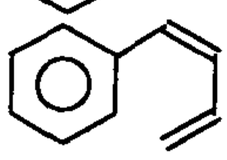
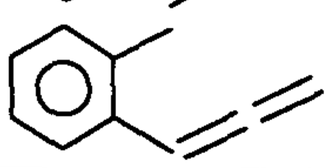
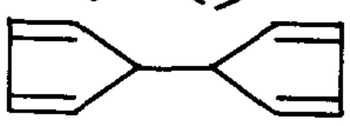
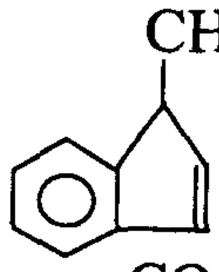
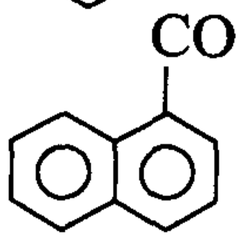
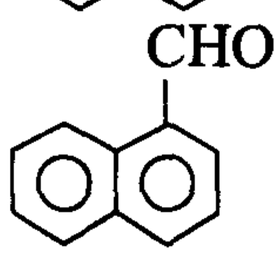
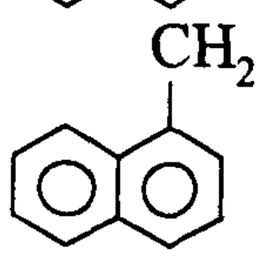
Specie	Structure	Hf ^{0} [kJ/mol]	S^0 [J/(mole*K)]	Reference
$C_{10}H_9K$		331.86	367.08	[182]
$C_{10}H_9L$		453.39	421.73	[182]
$C_{10}H_9M$		450.34	421.73	[182]
$C_{10}H_9P$		455.25	399.19	[182]
$C_{10}H_9T$		268.34	337.43	[182]
$C_9H_6CH_3$		255.52	347.36	[157]
$C_{10}H_{10}$		279.33	414.87	[182]
$C_{10}H_{10}F$		258.85	406.39	[182]
$C_{10}H_{10}K$		264.36	367.08	[182]
$C_9H_7CH_3$		147.08	390.04	[157]
$C_{11}H_7O$		174.89	415.73	[33]
$C_{11}H_8O$		30.54	415.68	[33]
$C_{11}H_9$		272.79	375.72	[33]

Table C.1, continued

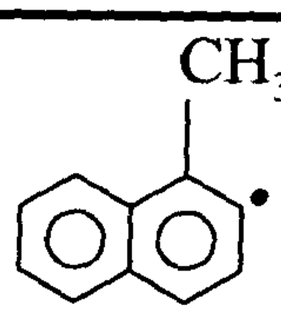
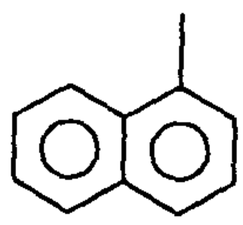
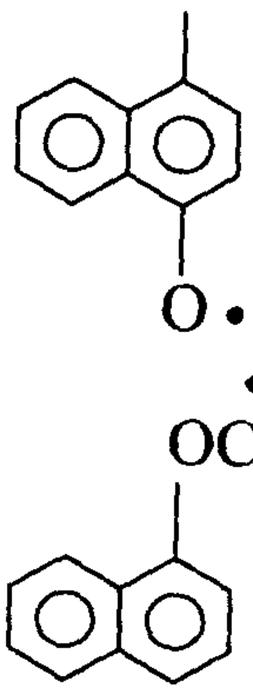
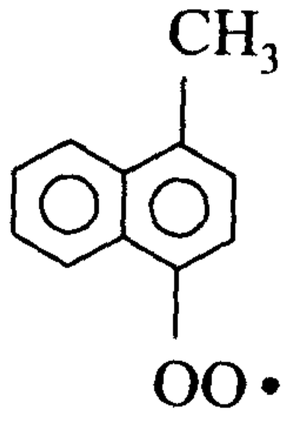
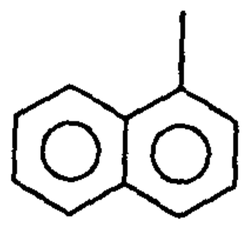
Specie	Structure	Hf ^{0} [kJ/mol]	S^0 [J/(mole*K)]	Reference
$C_{11}H_9P$		356.99	375.72	est. [16]
$C_{11}H_9O$		189.20	375.72	est. [16]
$OC_{11}H_9$		85.20	375.72	est. [16]
$AC_{11}H_9O$		155.18	375.72	est. [16]
$OOC_{11}H_9P$		284.16	465.52	est. [16]
$C_{11}H_{10}$		116.10	381.96	[33]

Table C.1, continued

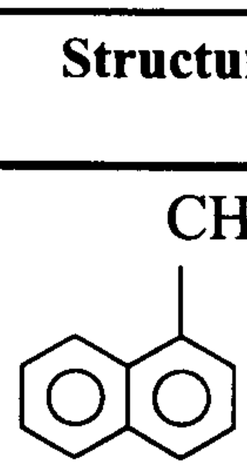
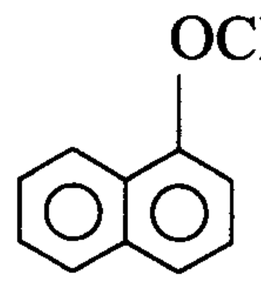
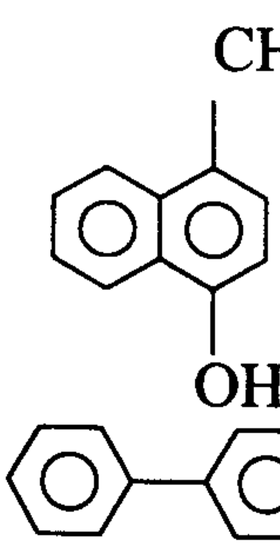
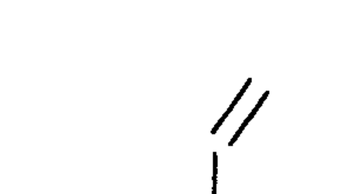
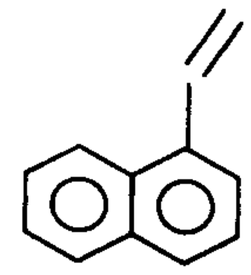
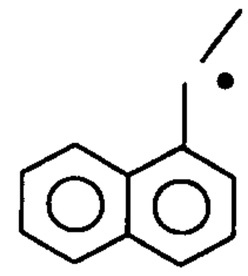
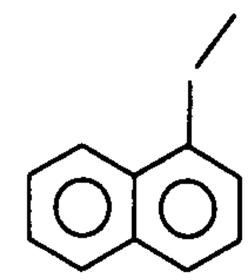
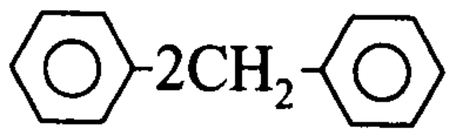
Specie	Structure	Hf^0 [kJ/mol]	S^0 [J/(mole*K)]	Reference
$C_{11}H_{10}O$		-28.49	452.76	est. [16]
$AC_{11}H_{10}O$		0.48	452.76	est. [16]
$HOC_{11}H_9$		-58.78	375.72	est. [16]
$C_{12}H_{10}$		182.11	388.75	[33]
$1C_{12}H_{10}$		215.02	400.74	[33]
$C_{12}H_{11}$		220.45	426.59	[33]
$C_{12}H_{12}$		96.86	406.2	[33]
$C_{14}H_{14}$		143.10	483.13	[33]

Table C.1, continued

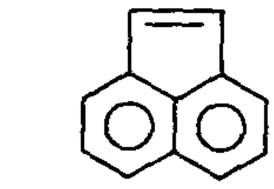
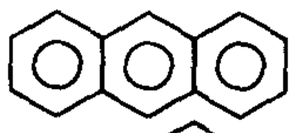
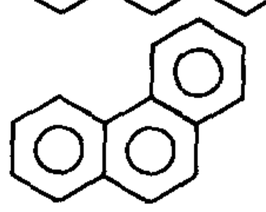
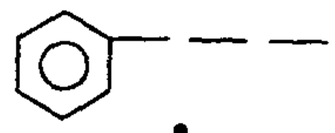
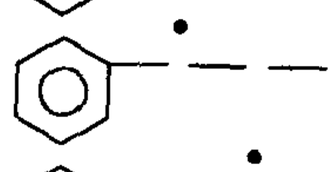
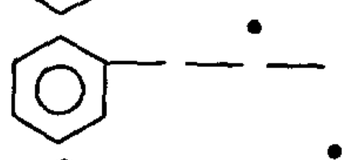
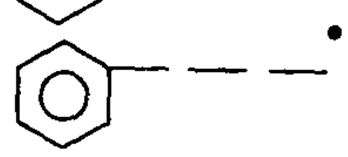
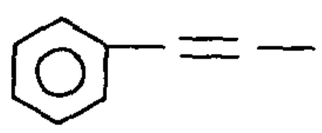
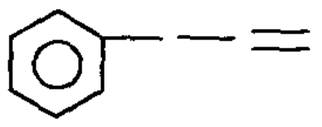
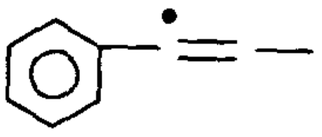
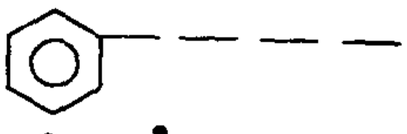
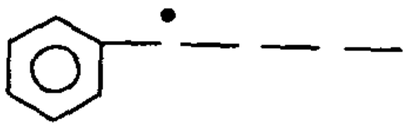
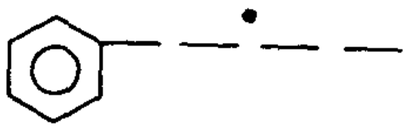
Specie	Structure	Hf ^{0} [kJ/mol]	S^{0} [J/(mole*K)]	Reference
$AC_{12}H_8$		259.66	358.53	[215]
$AC_{14}H_{10}$		230.05	392.57	[215]
$PC_{14}H_{10}$		207.05	394.49	[215]
C_9H_{12}		7.89	398.59	[60]
$1C_9H_{11}$		147.16	397.34	[60]
$2C_9H_{11}$		204.19	403.35	[60]
$3C_9H_{11}$		209.20	403.35	[60]
$1C_9H_{10}$		121.99	380.28	[238]
$2C_9H_{10}$		116.98	380.28	[238]
$C_9H_9(T)$		377.26	394.34	est. [16]
$C_{10}H_{14}$		-12.52	438.14	[97]
$1C_{10}H_{13}$		134.34	435.70	[97]
$2C_{10}H_{13}$		184.17	456.59	[97]

Table C.1, continued

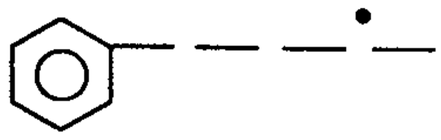
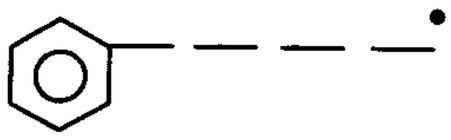
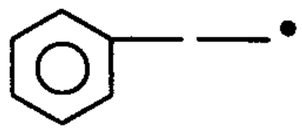
Specie	Structure	ΔHf^0 [kJ/mol]	S^0 [J/(mole*K)]	Reference
$3C_{10}H_{13}$		184.17	456.59	[97]
$4C_{10}H_{13}$		191.70	457.25	[97]
C_8H_9(B)		252.34	364.62	[97]
C_5H_9	$CH_3CH_2CHCHCH_2$	170.16	358.56	[182]
$1C_5H_{10}$	$CH_2CH\text{-}2(CH_2)CH_3$	-21.27	345.78	[33]
$1C_5H_{11}$	$CH_3\text{-}3(CH_2)CH_2$	45.89	368.06	[33]
C_6H_{11}	$CH_2CH\text{-}3(CH_2)CH_2$	142.22	394.88	[33]
$1C_6H_{12}$	$CH_2CH\text{-}3(CH_2)CH_3$	-41.71	384.73	[33]
$1C_6H_{13}$	$CH_3\text{-}4(CH_2)CH_2$	25.08	407.56	[182]
$2C_6H_{13}$	$CH_3\text{-}3(CH_2)CHCH_2$	75.32	378.84	[182]
C_7H_{13}	$CH_2\text{-}4(CH_2)CHCH_2$	128.81	447.42	[182]
$1C_7H_{14}$	$CH_2CH\text{-}4(CH_2)CH_3$	-62.32	423.48	[33]
$2C_7H_{14}$	$CH_2CHCH\text{-}3(CH2)CH_3$	-75.67	443.79	[182]
$3C_7H_{14}$	$CH_3CH_2CHCH\text{-}2(CH2)CH_3$	-75.67	443.79	[182]
$1C_7H_{15}$	$CH_3\text{-}5(CH_2)CH_2$	4.37	447.81	[33]
$2C_7H_{15}$	$CH_3\text{-}4(CH_2)CHCH_3$	1.01	447.70	[182]
$3C_7H_{15}$	$CH_3\text{-}3(CH_2)CHCH_2CH_3$	1.01	447.70	[182]
$4C_7H_{15}$	$CH_3\text{-}2(CH_2)CH\text{-}2(CH_2)CH_3$	1.01	447.70	[182]
n-C_7H_{16}	$CH_3\text{-}5(CH_2)CH_3$	-187.80	427.45	[33]
$4C_8H_{13}$	$CH_2CHCH_2CH2\text{-}(CH_2)CHCH_2$	283.84	539.28	est. [16]
C_8H_{14}	$CH_2CH\text{-}4(CH_2)CHCH_2$	33.61	198.11	est. [16]
C_8H_{16}	$CH_2CH\text{-}5(CH_2)CH_3$	-82.93	462.28	[33]
C_8H_{17}	$CH_3\text{-}6(CH_2)CH_2$	-16.35	486.71	[33]
$C_{10}H_{19}$	$CH_2CHCH\text{-}6(CH_2)CH_3$	256.29	561.71	[33]
$C_{10}H_{20}$	$CH_2CH\text{-}7(CH_2)CH_3$	-135.52	542.45	[33]
$1C_{10}H_{21}$	$CH_3\text{-}8(CH_2)CH_2$	-57.78	565.87	[182]

Table C.1, continued

Specie	Structure	Hf^0 [kJ/mol]	S^0 [J/(mole*K)]	Reference
$2C_{10}H_{21}$	CH_3-7(CH_2)$CHCH_3$	-59.03	566.62	[182]
$3C_{10}H_{21}$	CH_3-6(CH_2)$CHCH_2CH_3$	-59.03	566.61	[182]
$4C_{10}H_{21}$	CH_2-5(CH_2)CH-2(CH_2)CH_3	-59.03	566.61	[182]
$5C_{10}H_{21}$	CH_3-4(CH_2)CH-3(CH_2)CH_3	-59.03	566.61	[182]
$C_{10}H_{21}OO$	CH_2OO-8(CH_2)CH_3	-193.76	615.37	est. [16]
$C_{10}H_{21}O_2$	CHOOH-8(CH_2)CH_3	-135.13	683.84	est. [16]
n-$C_{10}H_{22}$	CH_3-8(CH_2)CH_3	-250.16	544.07	[182]
C_9H_{17}	CH_2CH-6(CH_2)CH_2	88.44	520.21	[33]
$2C_9H_{17}$	CH_2C-6(CH_2)CH_3	88.44	520.21	[33]
C_9H_{18}	CH_2CH-6(CH_2)CH_3	-104.61	504.91	[33]
C_9H_{19}	CH_2CH-7(CH_2)CH_3	-37.07	526.29	[33]
$1C_{12}H_{25}$	CH_2-10(CH_2)CH_3	-115.62	652.26	est. [16]
$2C_{12}H_{25}$	CH_3CH-9(CH_2)CH_3	-100.47	647.95	est. [16]
$3C_{12}H_{25}$	CH_3CH_2CH-8(CH_2)CH_3	-100.47	647.95	est. [16]
$4C_{12}H_{25}$	$CH_3CH_2CH_2CH$-7(CH_2)CH_3	-100.47	647.95	est. [16]
$5C_{12}H_{25}$	CH_3-3(CH_2)CH-6(CH_2)CH_3	-100.47	647.95	est. [16]
$6C_{12}H_{25}$	CH_3-4(CH_2)CH-8(CH_3)CH_3	-100.47	647.95	est. [16]
$C_{12}H_{26}$	CH_3-10(CH_2)CH_3	-290.90	624.07	[33]

BABL.
LONDON.
UNIV.